AD 6856666

AGARD CONFERENCE PROCEEDINGS No. 37

AGARD CP No. 37

AGARD

ADVISORY GROUP FOR AEROSPACE RESEARCH & DEVELOPMENT

7 RUE ANCELLE 92 NEUILLY SUR SEINE FRANCE

Scatter Propagation of Radio Waves

PART 2

★

AUGUST 1968

NORTH ATLANTIC TREATY ORGANIZATION

Reproduced by the CLEARINGHOUSE for Federal Scientific & Technical Information Springfield Va. 22151

AGARD Conference Proceedings No. 37

NORTH ATLANTIC TREATY ORGANIZATION

ADVISORY GROUP FOR AEROSPACE RESEARCH AND DEVELOPMENT

(ORGANISATION DU TRAITE DE L'ATLANTIQUE NORD)

SCATTER PROPAGATION OF RADIO WAVES

Published in Two Parts

PART 2

Papers presented at the XIVth Symposium of the Electromagnetic Wave Propagation Committee of the Avionics Panel of AGARD, held at Sandefjord, Norway, 19th - 23rd August 1968.

CONTENTS

PART 2

SESSION 5 - AURORAL SCATTER AND VHF FORWARD SCATTER — Paper

AURORAL SCATTER
by P.A.Forsyth — 34

A NOTE ON A PARTICULAR TYPE OF SCATTERING ECHOES OBSERVED AT HIGH LATITUDES
by Kristen Folkestad — 35

FIELD-ALIGNED IONIZATION SCATTER GEOMETRY
by George H.Millman — 36

DISCUSSION — 37

REVIEW OF VHF FORWARD SCATTER
by Richard C.Kirby — 38

ELECTROMAGNETIC SCATTERING FROM A PLASMA SLAB HAVING LARGE SCALE, RANDOM ELECTRON DENSITY FLUCTUATIONS
by Adolf R.Hochstim and Charles P.Martens — 39

CONTROLLABILITY ASPECTS OF SCATTER PROPAGATION OF RADIO WAVES
by M.Z.von Krzywoblocki — 40

VHF IONOSPHERIC SCATTER PROPAGATION VIA THE EQUATORIAL ELECTROJET
by Carlos A.Romero, Alberto A.Gíesecke, Jr and Oscar Pérez — 41

MICROWAVE SCATTERING FROM SPHERICAL ELECTRON CLOUDS
by N.W.Rosenberg, M.M.Klein and G.Anderson — 42

STOCHASTIC THEORY OF THE SCATTERING OF ELECTROMAGNETIC WAVES FROM A RANDOM MEDIUM
by C.M.Tchen — 43

DISCUSSION — 44

SESSION 6 - TRANSEQUATORIAL PROPAGATION AND F-REGION SCATTER

A REVIEW OF VHF TRANSEQUATORIAL PROPAGATION
by D.L.Nielson — 45

THE IMPORTANCE OF HORIZONTAL F-REGION DRIFTS TO TRANSEQUATORIAL VHF PROPAGATION
by D.L.Nielson — 46

ETUDE D'UNE PROPAGATION TRANSEQUATORIALE EN DEHORS DU GRAND CERCLE EN PERIODE D'OCCURRENCE DE F DIFFUS
par M.Crochet et P.Broche — 47

Paper

RAY TRACING OVER A TRANSEQUATORIAL PATH
by N.C.Gerson 48

TRANSEQUATORIAL PROPAGATION IMPLICATIONS OF EQUATORIAL VERTICAL DRIFT MEASUREMENTS
by Robert Cohen and J.P.McClure 49

DISCUSSION 50

F-REGION SCATTER
by Robert Cohen 51

RADIO-DOPPLER OBSERVATIONS OF THE IONOSPHERE NEAR THE MAGNETIC EQUATOR
by Kenneth Davies and Norman J.F.Chang 52

JOINT PROBABILITY DENSITY OF SIGNAL FADING AT SPACED RECEIVERS
by T.J.Elkins 53

SATELLITE SCINTILLATION AT HIGH LATITUDES
by Jon Frihagen 54

HF RADAR SIGNATURES OF TRAVELING IONOSPHERIC IRREGULARITIES 3D RAY-TRACING SIMULATION
by T.M.Georges and Judith J.Stephenson 55

NATURE OF F-REGION IRREGULARITIES INFERRED FROM OBLIQUE REFLECTION MEASUREMENTS
by L.C.Humphrey, C.R.Roberts and R.Mather 56

DISCUSSION 57

SESSION 7 - F-REGION SCATTER

BACKSCATTER OBSERVATIONS FROM DISTANT FIELD-ALIGNED IRREGULARITIES
by H.Kopka and H.G.Möller 58

RESEARCH ON FIELD-ALIGNED PROPAGATION OF HF RADIOWAVES USING ALOUETTE 2 TOPSIDE SOUNDER DATA AND DIGITAL RAY-TRACING TECHNIQUES
by Jayaram Ramasastry, Edward J.Walsh and John R.Herman 59

DISCUSSION 60

AURORAL SCATTER

by

P.A.Forsyth

Centre for Radio Science
University of Western Ontario
London, Canada

SUMMARY

The evidence regarding the nature of radio aurora, particularly that relating to the scattering mechanism is reviewed. Much evidence is found which supports the hypothesis that the radio waves are scattered from electron density gradients produced by propagating ion-acoustic waves in the auroral ionization. Such waves could be generated by the auroral electrojet. Nevertheless there is another large body of evidence which cannot be explained by the existence of ion-acoustic waves. It is concluded that this evidence relates to occasions on which the radio waves are weakly scattered from electron density gradients randomly distributed throughout the auroral ionization. It is possible also that strong scattering sometimes occurs for radio frequencies near the bottom of the VHF band.

AURORAL SCATTER

P. A. Forsyth

1. INTRODUCTION

Any attempt to discuss the scattering of radio waves by auroral ionization is faced with a number of pitfalls. A large amount of experimental evidence has been accumulated in the last twenty years, and it is quite impossible to provide a comprehensive summary in a convenient form. Calling attention to any part of this evidence as being more significant than the rest presupposes a model of the scattering process which is being tested against the evidence. The most important model of this kind to emerge in recent years is that derived from the work of Farley[1] in which it is suggested that ion-acoustic waves in the auroral ionization, generated by the auroral electrojet, provide the ionization gradients which are detected as radio aurora. While too early for a definitive assessment it seems likely that this model may well join a growing list of previous models, each of which has successfully explained the characteristics of certain examples of radio aurora but failed to explain other examples.

In what follows, evidence which seems to bear on the ion-acoustic wave model is surveyed and the expected characteristics of the scattered signals are then compared with those that are observed.

2. THE EXPERIMENTAL EVIDENCE

2.1 Aspect Sensitivity

From the earliest investigations it has been obvious that radio echoes from aurora tend to arise in regions where the radio waves are nearly perpendicularly incident upon the lines of force of the earth's magnetic field. For an observing station in middle latitudes in the Northern Hemisphere these regions are near the northern horizon. At first it was assumed that the echoes arose by specular reflection from greatly elongated columns of ionization aligned with the magnetic field and, indeed an early analysis (Chapman[2]) undertook to predict the regions of the earth from which auroral radar echoes could be obtained. For a station located within a few hundred kilometres of the auroral zone the specular condition cannot be fulfilled and echoes would not be expected. In fact echoes are observed more frequently from stations near the auroral zone than from stations at lower latitudes, indicating that precise perpendicularity is not required. Nevertheless a strong geometrical dependence is present. For a given station the number of echoes observed increases as perpendicularity is approached. The term "aspect angle" is used to denote the angle between the direction of the ray from the radar station to the echoing region and the direction of the earth's magnetic field in the echoing region. The dependence of echo strength or echo occurrence on this aspect angle is called "aspect sensitivity". One of the most systematic attempts to determine the aspect sensitivity of radio aurora was carried out during the International Geophysical Year by McDiarmid and McNamara[3], using two radars to observe a region of the auroral zone simultaneously from the north and from the south. They concluded that for aspect angles between 95° and 110° the average variation of echo strength with angle was about 1 dB per degree for a frequency near 50 MHz. Generally, the evidence seems to suggest increasing aspect sensitivity with increasing frequency and as the aspect angle approaches 90° (Leadabrand, Larson and Hodges[4]).

While most VHF and UHF radar observations seem to indicate the high aspect sensitivity described in the preceding paragraph, somewhat different results have been derived from bistatic VHF radio systems. Collins and Forsyth[5] identified three, or possibly four, distinct types of radio aurora of which two showed varying degrees of aspect sensitivity but the remainder (their A_3 and S events) showed a relative lack of aspect sensitivity. The number of these VHF bistatic "circuits" that have been used in Canada for studies of radio aurora is now approaching forty. Figure 1 shows a representative group of the paths used. For only two of these paths does the aspect angle actually reach 90°. For the rest, minimum aspect angles range from 91° to 105°. The circuits have been operated at various times over the past twelve years but all have yielded an abundant harvest of auroral reflections.

2.2 Other Geometrical Considerations

In addition to aspect sensitivity, other effects seem to occur. One of these that is particularly puzzling has been tentatively interpreted as an elevation-angle effect but may actually be more appropriately interpreted as evidence of ion-acoustic waves. The situation can best be described in terms of a concrete example. At Saskatoon the distribution of auroral radar echoes in range and azimuth at both 56 and 106 MHz has been determined several times (see, for example, Currie, Forsyth and Vawter[6]). Such distributions show, in addition to aspect sensitivity, a general concentration near the auroral zone. However two areas having similar aspect angles and located at similar distances from the centre of the auroral zone can be compared. For example this condition prevails for a comparison of an area about 400 km due north of Saskatoon with one that is 800 km away from Saskatoon in a direction 60° east of north. The number of echoes received from the latter region is much greater than that received from the former in spite of the rapid decrease in radar sensitivity with distance. Since the more distant region is viewed at a lower elevation angle the effect might be due to elevation angle alone.

In searching for an explanation some authors have suggested absorption but this mechanism seems hardly likely to be completely responsible for the effect. Another, more promising suggestion has recurred several times and was made most recently by Unwin[7]. Refraction in the ionosphere may become important at low elevation angles under auroral conditions and the result would be to improve the effective aspect angle at low elevation angles. It may also be suggested that the Saskatoon data are typical and certainly for these data the more distant area is also characterized by a smaller angle between the direction of observation and the average direction of flow of the auroral electrojet. This in turn should lead to an increased probability of observation of ion-acoustic waves.

Yet another effect has to do only with the radar parameters and the disposition of the auroral ionization. Several specific cases have been discussed by Forsyth[8], but one example will serve to illustrate the nature of this "observational" effect. Consider a large number of scatterers disposed in a region extending many kilometres in the east-west direction but only about one kilometre in the north-south direction (similar in shape to an auroral arc). Let this distribution be observed by a radar having a fairly wide antenna beam width (say 20°) and a fairly short pulse length (say 20 microseconds). Such a radar will obtain much stronger echo when the array of scatterers is located to the north of the radar than when the same array of scatterers is located to the east of the radar, simply because in the first case a larger number of scatterers can contribute simultaneously to the echo. Any observational verification of the effect would give a better understanding of the nature of the auroral scatterers. This verification has not yet been obtained.

2.3 Height of the Scattering Region

In principle the determination of the height of the echoing region by radar is straightforward. It is only necessary to determine the elevation of the target as viewed from the radar and the range to the target in order to determine geometrically the height of the target above the (curved) surface of the earth. Unfortunately, the ranges are so great and the elevation angles so small that even at UHF (above 300 MHz) the achievable antenna

beamwidths are too broad to permit accuracy of measurement. At lower frequencies the problem is more difficult and corrections should be made for refraction.

A number of radio-auroral heights have been reported but unfortunately many of these were derived, not by the direct measurement described above, but by assuming that echoes could be produced only where the aspect angle is precisely 90°. In the Northern Hemisphere satisfactory height determinations seem to have been made at VHF by Harang and Troim[9], and by Currie, Forsyth and Vawter[6]. In the Southern Hemisphere, Unwin and Gadsden[10] and Unwin[11] were able to take advantage of an elevated site to make precise measurements. All of these investigations indicated that the auroral echoes originated in a remarkably well-defined range of heights near but probably above the 100 km level. At higher frequencies, Lockwood[12] and Leadabrand[13] found that most of the echoes were produced in the 100-105 km height region.

It seems that the scattering is produced predominantly at heights corresponding closely with the heights of maximum luminosity in auroral forms. It is also clear that the range of heights over which the scattering occurs is more limited than is the corresponding range for luminosity. It is interesting to note that the lower part of the visible auroral form, possibly the most luminous part, is also thought to be the approximate location of the auroral electrojet.

A possible exception to this uniformity of height is provided by the A_3 and S echoes of Collins and Forsyth[5]. Only indirect evidence is available but this evidence, recently confirmed by Collins and Maynard[14], suggests that the scattering region responsible for these events is located well below the 100 km level, probably at about 85 km.

2.4 Motions in Radio Aurora

A number of studies of motions of auroral echoes with time have been made, but more important for our present purpose is the relatively large number of direct measurements of the frequency spectrum of the scattered radiation. Starting with Bowles[15] and McNamara[16], many investigations have found that the returned signal is spread in frequency and often shifted by amounts which are proportional to the radar frequency (suggestive of Doppler shifts) corresponding to random speeds of about 500 m sec^{-1}. The ordered velocities found by the spectrum analysis correspond reasonably to that found for the echoing regions by measuring the rate-of-change of range. It must be added, however, that most of the early measurements of frequency spectrum did not have sufficient resolution to be able to detect modest concentrations of energy which might have been present at frequencies corresponding to acoustic velocities.

2.5 Frequency Dependence

A number of earlier investigations used two frequencies in an attempt to establish the frequency dependence of the auroral reflections. About all that was accomplished was to establish the extreme variability of the phenomenon. As soon as three or more frequencies were used it was possible to see that not only was the frequency dependence variable but that it was inconsistent with any simple description of the scattering process. Four exactly scaled bistatic systems with wide transmitter-receiver separations (860 km) were used by Forsyth and Vogan[17]. Another four scaled bistatic systems with much smaller transmitter-receiver separations (so that the scattering was nearly backscatter) were used at frequencies ranging from 42 to 104 MHz by Lyon and Forsyth[18]. The widest frequency range used seems to be that of Leadabrand, Larson and Hodges[4] which included six frequencies between 50 and 3000 MHz. Unfortunately it was not possible to use exactly scaled systems over so wide a frequency range and in the absence of precise knowledge of the volume of the echoing region there is a substantial uncertainty regarding the derived frequency dependence.

The results of all these investigations seem to indicate that, while on occasion the frequency dependence is well behaved, such that the scattering cross-section is approximately independent of frequency, there are other occasions when the cross-section decreases rapidly but non-uniformly with frequency. Some typical frequency dependence results taken at four frequencies and at 3.75 minute intervals by Lyon and Forsyth[18] are shown in Figure 2.

3. THE SCATTERING PROCESS

While much necessary information has been provided by other types of measurements, the most important clues to the nature of the scattering process in radio aurora seem to be contained in the frequency dependence measurements and in the detailed measurements of the frequency spectrum of the scattered radiation. Dealing first with the frequency dependence, it is usual to discuss the scattering cross-section of the radio aurora,

$$\sigma_r = \frac{P_r}{P_t} \frac{64\Pi^3}{G_r G_t \lambda^2} \quad (R^4) , \tag{1}$$

where

σ_r = radar cross-section

P_r = received power

P_t = transmitted power

R = range to scatterer

G_r = receiving antenna gain

G_t = transmitting antenna gain

λ = operating wavelength of the radar.

This cross-section is related to the scattering coefficient (the power scattered per unit solid angle per unit incident power density) σ_s by a constant

$$\sigma_r = 4\Pi\sigma_s \tag{2}$$

and for our purposes we need not differentiate between them.

Until quite recently it was assumed that the evidence of frequency spread in the scattered signal was a clear indication that the scattering region was made up of a large number of scatterers in random relative motion and, most importantly, distributed randomly in space. As a result, several attempts to develop a model of the scattering region were made, all based on the random distribution of scatterers. The best known of these is that produced by Booker[19] who assumed that all scattering in radio aurora was weak scattering and took place at gradients of electron density (gradients of index of refraction) which were randomly distributed in space. The term weak scattering is used to indicate a situation where only a small fraction of the incident power is scattered at any particular gradient. Booker avoided a precise description of individual scatterers and characterized the scattering region by the spatial auto-correlation function of its electron density variation. This auto-correlation function was assumed to have a Gaussian form which again implies no order in the spatial distribution of the scattering gradients. Such a distribution will produce a scattered signal at any given frequency which varies in amplitude with scattering geometry (particularly if the auto-correlation function is non isotropic) and with the correlation length (or lengths), but at any instant in time the relationship between cross-section and wavelength will be given by

$$\sigma = \sigma_0 \exp(-K/\lambda^2) . \tag{3}$$

Somewhat later, Moorcroft[20,21] used a different description of the region, describing each scatterer as a cloud of electrons having a Gaussian electron density variation (a gaussoid):

$$N = N_0 \exp\{-[(x^2 + y^2)/a^2 + y^2/c^2]\} , \tag{4}$$

where N is the electron density (m^{-3}), x , y and z are spatial co-ordinates, and a and c are size parameters of the cloud. While this description seems at first glance to be more restrictive than that used by Booker, for weak scattering it can be used in a way that is formally similar to the Booker model provided the gaussoids are assumed to be randomly distributed. The major advantage is that this model can be extended to include strong scattering when the peak electron densities in some of the gaussoids are assumed to approach the value for critical reflection given by

$$N = 4\Pi/\lambda^2 r_e \, . \qquad (5)$$

where λ is the radio wavelength and r_e the classical electron radius. Because the inclusion of strong scattering introduces a strong frequency dependence in one part of the frequency range, leaving higher frequencies unaffected, it is no longer possible to specify the frequency dependence simply. In fact one might expect to encounter a variation of cross-section with frequency like that shown in Figure 3. In that figure the region marked (c) corresponds to weak scattering for the whole region and the frequency dependence is that given by Equation (3). The region marked (a) corresponds to critical reflection when most of the scatterers are opaque to the incident radiation. The actual frequency dependence in this region is dependent upon the distribution of sizes of scatterers and the distribution of the peak electron densities. The region marked (b) corresponds to the transition from weak to strong scattering and was assumed to be the most characteristic feature of the model. In practice one might expect the transition region to sweep through the region of observation, moving to higher frequencies with increasing intensity of ionization and to lower frequencies as the aurora becomes weaker. As long as random spatial distributions only were being considered the curve of Figure 3 was thought to be a unique indication of strong scattering and the observation of such frequency dependence curves (like some of those in Figure 2) was considered to be clear evidence of the operation of strong (critical) reflection in the lower part of the VHF band (electron densities approaching 10^7 cm^{-3}).

Moorcroft[22] has re-examined the experimental frequency dependence curves in more detail in an effort to see if the introduction of complex size distributions in the scatterers could account for these curves using only weak scattering. In fact he concludes that not only is this impossible but that it seems physically unreasonable to explain all of the curves using only a combination of weak and strong scattering. In the end he chooses to question the assumption of random distribution because most of the peculiarities of the observed frequency dependence curves could be explained by a model which permits some ordered array of scatterers. Indeed once this is accepted there is no longer any need to include strong scattering to account for the frequency dependence curves. This is more clearly seen when it is recalled that any distribution of electron density gradients may be represented by a series of spatial Fourier components of different wavelengths, phases and amplitudes. A radar measurement at a given frequency and along a given line-of-sight merely responds to the appropriate spatial Fourier component along that line-of-sight (for backscatter, the appropriate Fourier component has a wavelength which is just one half of the radio wavelength). The spatial Fourier "spectrum" is just reproduced in the spectrum representing the scattering cross-section as a function of frequency. The assumption of random spatial distribution corresponds to a flat Fourier spectrum and the assumption of "order" corresponds to the presence of peaks in the Fourier spectrum.

It is interesting to note that although strong scattering seems no longer to be needed for an explanation of radio aurora there is independent evidence that it should be included. Rocket measurements of auroral electron densities have revealed rapid spatial fluctuations with peak values apparently in excess of 10^6 cm^{-3} (McNamara[23]).

Once it is decided that some order must be accepted in the spatial distribution of electron density gradients to account for the characteristics of radio aurora then it seems reasonable to look for some type of wave motion in the auroral ionization. The leading contender is clearly the two-stream instability mechanism which gives rise to ion-acoustic waves (Farley[1]). This mechanism has been very successful in explaining the observed

characteristics of VHF scattering from the equatorial ionosphere. The suggestion as applied to the aurora is that ion-acoustic waves are generated whenever the auroral electrojet current exceeds a threshold value. When this threshold is passed, energy is transferred from the streaming electrons to the plasma waves which propagate with wavefronts parallel to the magnetic field lines and with the propagation vector generally parallel to the electron velocity vector. As the electron velocity increases above the threshold value two things can happen: waves can be propagated at larger and larger angles to the electron velocity vector (though still mostly perpendicular to the magnetic field) and the lower limit of the generated wavelengths decreases.

There is a striking correspondence between the expected characteristics of the ion-acoustic waves and the observed characteristics summarized earlier. Indeed it may be recalled that the auroral electrojet is thought to flow at a fairly well-defined height near the lower border of visual forms and although it may flow in almost any direction (in response to the orientation of the auroral forms), it tends to flow generally in the east-west direction. These characteristics too are consistent with the observations.

4. FURTHER EXPERIMENTAL EVIDENCE

In view of the weight of evidence which appears to be consistent with the existence of ion-acoustic waves it is worthwhile to look specifically for those characteristics which should be unique to ion-acoustic waves. Here, the evidence is not as conclusive as might be hoped.

The most direct evidence of ion-acoustic waves should be found in close study of the frequency spectrum and spatial correlation of the scattered signals. For example, although echoes might be expected more often when the line-of-sight to the aurora makes a small angle with the direction of the electrojet, there should be no variation of the magnitude of the Doppler shift with direction of viewing. It should always correspond to the phase velocity of the ion-acoustic waves. Correlation studies with spaced antennas should reveal drift velocities which are consistent with group velocities of the ion-acoustic waves.

Leadabrand[24] studied the variation of Doppler shift with azimuth and concluded that, although the Doppler shift was too high and too dependent on azimuth to indicate scattering from ion-acoustic waves alone, nevertheless there was evidence for the existence of ion-acoustic waves.

Two other experiments have been concluded recently. Palmer[25] studied the spatial correlation of the radio-auroral reflections and found two basically different types of event. In one type of event the signals showed a typical fading rate of 15 Hz and an east-to-west drift of the amplitude patterns which was consistent with the expected group velocity of 420 m sec^{-1}, as indeed were most of the other characteristics of this type of event. The second type of event exhibited a fading spectrum which extended beyond 100 Hz and drift velocities in the range of 0.5 to 10 km sec^{-1}. The characteristics of this type of event seemed to be quite inconsistent with scattering from ion-acoustic waves.

Another, as yet unpublished, experiment by Hofstee has measured the frequency spectrum simultaneously with two radio systems looking at the same region from directions which differ by 17^{o}. For both systems the radio waves were incident nearly perpendicularly on the magnetic field in the echoing region. The rapid and apparently independent variation of the spectra observed with these systems is indicated by a few successive spectra in Figure 4. Here again the conclusion is that on some occasions the spectra are entirely consistent with the presence of ion-acoustic waves but on other occasions they are quite inconsistent with that interpretation. While the volumes of the ionosphere viewed by the two systems are not quite identical it seems very difficult to explain the large difference seen on the two systems without introducing a very sharp angular dependence for the scattering cross-section, which suggests an ordered structure existing over a considerable volume of the auroral ionization.

5. CONCLUSION

While various models of radio aurora have been proposed from time to time over the last 20 years the important features of them all can be included in only three mechanisms:

(a) Weak scattering from randomly distributed gradients in electron density.

(b) Strong scattering from randomly distributed clouds of ionization.

(c) Weak scattering from ordered arrays of gradients in electron density produced in turn by propagating ion-acoustic waves.

With regard to mechanism (b) the radio evidence is no longer considered to be conclusive, though rocket evidence suggests that it probably operates for the lower part of the VHF radio spectrum. While many authors have tried to choose between mechanisms (a) and (c), the existing evidence points to the operation of both and much work is still required to delineate the respective conditions under which each is predominant.

REFERENCES

1. Farley, D.T. — *A Plasma Instability Resulting in Field Aligned Irregularities in the Ionosphere.* Journal of Geophysical Research, Vol.68, 1963, p.6083.

2. Chapman, S. — *The Geometry of Radio Echoes from Aurorae.* Journal of Atmospheric and Terrestrial Physics, Vol.3, 1952, p.1.

3. McDiarmid, D.R. McNamara, A.G. — *VHF Radio Aurora: Simultaneous Observation of Auroral Ionization by Two Separated Radars.* Canadian Journal of Physics, Vol.45, 1967, p.3009.

4. Leadabrand, R.L. et al. — *Preliminary Results on the Wavelength Dependence and Aspect Sensitivity of Radar Auroral Echoes Between 50 and 3000 MHz.* Journal of Geophysical Research, Vol.72, 1967, p.3877.

5. Collins, C. Forsyth, P.A. — *A Bistatic Radio Investigation of Auroral Ionization.* Journal of Atmospheric and Terrestrial Physics, Vol.13, 1959, p.315.

6. Currie, B.W. et al. — *Radio Reflections from Aurora.* Journal of Geophysical Research, Vol.58, 1953, p.179.

7. Unwin, R.S. — *The Importance of Refraction in the Troposphere and Ionosphere in Determining the Aspect Sensitivity and Height of the Radio Aurora.* Journal of Geophysical Research, Vol.71, 1966, p.3677.

8. Forsyth, P.A. — *On the Geometry of Radio Reflections from Aurora.* Canadian Journal of Physics, Vol.38, 1960, p.593.

9. Harang, L. Troim, J. — *Studies of Auroral Echoes - I.* Planetary and Space Science, Vol.5, 1961, p.33.

10. Unwin, R.S. Gadsden, M. — *Determination of Auroral Height by Radar.* Nature, Vol.180, 1957, p.1496.

11. Unwin, R.S. — *Studies of the Upper Atmosphere from Invercargill, New Zealand: Part I - Characteristics of Auroral Radar Echoes at 55 Mc/sec.* Annales de Géophysique, Vol.15, 1959, p.377.

12. Lockwood, G.E.K. — *Determination of Radar Auroral Heights with the Prince Albert Radar.* Canadian Journal of Physics, Vol.39, 1961, p.1725.

13. Leadabrand, R.L. — *Electromagnetic Measurements of Auroras.* Auroral Phenomena, edited by Martin Watt, Stanford University Press, 1965, p.99.

14. Collins, C.
Maynard, L.A. — *Simultaneous VHF Riometer and Forward-Scatter Observations of the Disturbed Lower Ionosphere.* Advanced Study Institute on Ionospheric Radio Communications in the Arctic, Finse, Norway, April 1967.

15. Bowles, K.L. — *Doppler Shifted Radio Echoes from Aurorae.* Journal of Geophysical Research, Vol.59, 1954, p.553.

16. McNamara, A.G. — *Double-doppler Radar Investigation of Aurora.* Journal of Geophysical Research, Vol.60, 1955, p.257.

17. Forsyth, P.A.
Vogan, E.L. — *The Frequency Dependence of Radio Reflections from Aurora.* Journal of Atmospheric and Terrestrial Physics, Vol.10, 1957, p.215.

18. Lyon, G.F.
Forsyth, P.A. — *Radio-Auroral Reflection Mechanisms.* Canadian Journal of Physics, Vol.40, 1962, p.749.

19. Booker, H.G. — *A Theory of Scattering by Nonisotropic Irregularities with Application to Radar Reflections from the Aurora.* Journal of Atmospheric and Terrestrial Physics, Vol.8, 1956, p.204.

20. Moorcroft, D.R. — *Models of Auroral Ionization. Part I: Auroral Ionization Models and their Radio-Reflection Characteristics.* Canadian Journal of Physics, Vol.39, 1961, p.677.

21. Moorcroft, D.R. — *Models of Auroral Ionization. Part II: Applications to Radio Observations of Aurora.* Canadian Journal of Physics, Vol.39, 1961, p.695.

22. Moorcroft, D.R. — *The Interpretation of the Frequency Dependence of Radio Aurora.* Planetary and Space Science, Vol.14, 1966, p.269.

23. McNamara, A.G. — Private Communication, 1967.

24. Leadabrand, R.L. — *A Comparison of Radar Auroral Reflection Data with Acoustic Wave Theory.* Radio Science, Vol.69D, 1965, p.959.

25. Palmer, F.H. — *VHF Studies of the Lower Ionosphere.* Ph.D. Thesis, University of Western Ontario, London, Canada, 1967.

26. Forsyth, P.A. — *Reflection Mechanisms for Radio Aurora.* Planetary and Space Science, Vol.10, 1963, p.179.

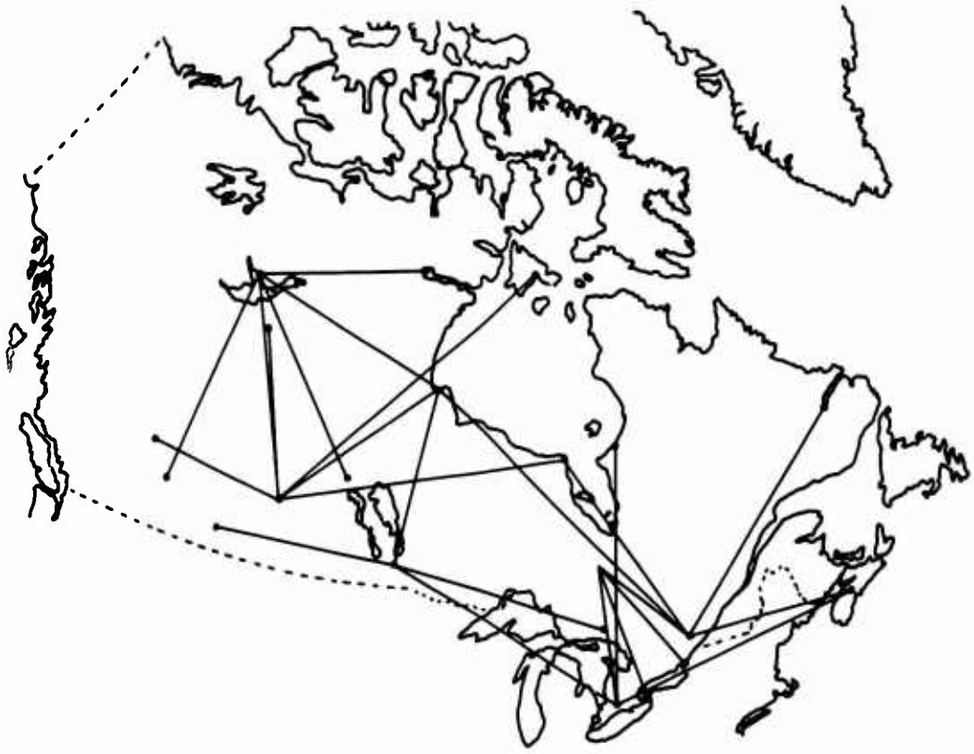


Fig.1. A representative group of bistatic scatter paths used in Canada to investigate radio aurora

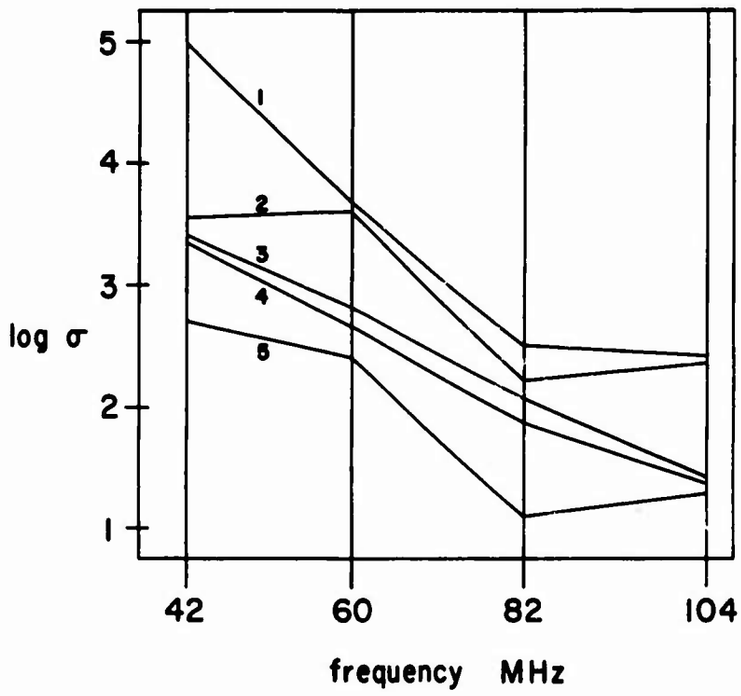


Fig.2. Relative scattering cross-sections observed by Lyon and Forsyth (Ref.18) at four frequencies simultaneously. The five sets of results were taken consecutively at 3.75 minute intervals and are displaced vertically in order to prevent overlapping

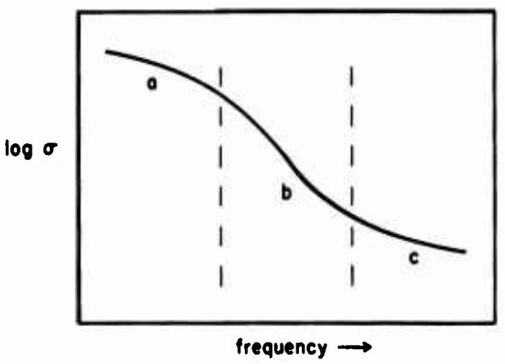


Fig.3. Idealized variation of total cross-section with frequency for a situation involving both strong and weak scattering

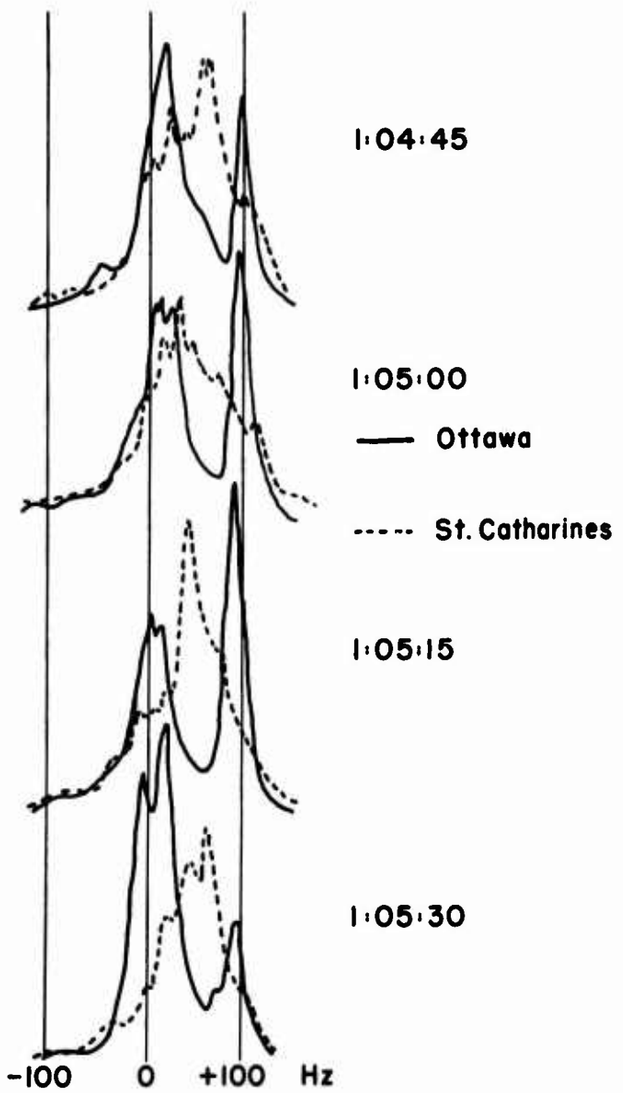


Fig.4. Four examples of frequency spectra observed simultaneously by two radio systems which view a common region from slightly different directions. Successive spectra were separated in time by 15 seconds

A NOTE ON A PARTICULAR TYPE OF SCATTERING ECHOES OBSERVED AT HIGH LATITUDES

by

Kristen Folkestad

Forsvarets Forskningsinstitutt
Norwegian Defence Research Establishment
P.O. Box 25 - N-2007 Kjeller, Norway

SUMMARY

This report is concerned with a particular group of backscatter traces recorded in swept frequency oblique soundings at high latitudes. Characteristic echo properties are displayed. Results of attempts to interpret the measured returns are given. The explanation offered is in terms of aspect sensitive scattering from irregularities located in spatially limited regions of enhanced ionization density to the north of the sounding site.

A NOTE ON A PARTICULAR TYPE OF SCATTERING ECHOES OBSERVED AT HIGH LATITUDES

Kristen Folkestad

1. INTRODUCTION

For a three-year period from the autumn of 1963 the Norwegian Defence Research Establishment operated a Granger step frequency sounder at Andøya (69°N, 16°E) in Northern Norway. Backscatter measurements were conducted in four directions, three of which were in the range 10° to 70° west, the fourth one pointing southward approximately at right angles to the auroral belt.

On the southern path the backscatter observations essentially consist of one- and two-hop ground-scatter modes. The recordings on the three other circuits, which all traverse the auroral zone at various angles of incidence, contain more complex echo-structures. This is particularly true for the path orientated in the most northerly direction. For this circuit the greater part of the backscatter findings cannot be explained in terms of simple ground-scatter mechanisms.

In the various returns observed there are both unique forms and echo-formations exhibiting a fairly high rate of recurrence. In the following treatment a special category of echoes repeatedly recorded is considered.

2. ECHO CHARACTERISTICS

A typical sample of the echoes concerned is displayed in Figure 1. Except from the vertical incidence traces visible at the bottom left-hand corner, three distinct echo-forms may be distinguished: the ground-scatter component extending in frequency up to 16 MHz and covering the virtual range 5-600 to 1600 km, another sloping echo at apparent distances from 1500 to about 2000 km and finally an essentially constant range trace detected at frequencies from about 5 to 21 MHz.

This last-mentioned component, in particular, represents a frequently recorded echo. An analysis of this type of return has revealed the following characteristics:

(i) Its rate of occurrence is highest in the winter months and it is predominantly observed on the polar paths.

(ii) Its upper cut-off frequency is usually in the range 16 to 22 MHz.

(iii) Variations in the minimum virtual range are normally less than 2-300 km.

Figure 2 shows the diurnal variation in the occurrence pattern based on two month's data in 1964. It is found that the echo essentially occurs at day-time hours. It is most frequently reported from 0800 to 1400 UT. It may appear as a single component in a backscatter ionogram or simultaneous with other scatter-forms as in the situation depicted in Figure 1.

3. METHOD OF INTERPRETATION

In an attempt to explain the propagational mechanisms responsible for the returns displayed in Figure 1 some model computations were made. A digital computer was employed in the calculations. The ray-tracing procedure was based on the use of Snell's law in a spherically stratified ionosphere. Figure 3 shows the model used.

A bounded lamina of increased electron density was introduced, specified by the angles α_1 and α_2 and the vertical boundaries h_1 and h_2. The variation of the additional electron density in the vertical direction was described by a cosine-square law. For the refractive index the simple form $n^2 = 1 - X$ was used.

Although neglected in the expression for the refractive index, the magnetic field was taken into account. The field was computed at the point where the rays enter the ionosphere and the projection of the field into the great-circle plane of emission was determined. Whenever, in the process of computation, the angle between the wave-normal and the field projection deviated by less than a small amount δ from 90^o, the apparent path was printed out. Using the projection of the magnetic field, instead of the real field, led to computational simplifications and was considered to be a fairly good approximation at the latitudes and bearings considered. The electron distributions employed in the ray calculations are shown in Figure 4. In this figure the solid line represents the real height/density profile derived from the vertical ionogram taken at Tromsø at 1200 UT.

It appeared that, in using this distribution, no additional electron content would give apparent echo-ranges which even approximately agreed with the measured traces. A single F-layer model represented by the broken line in Figure 4 was therefore adopted for the further computations.

4. RESULTS

Measured and computed echo-forms are shown in Figure 5. The computations refer to a bearing of 10^o west of north with slab parameters specified in the figure. In drawing the computed results the following assumptions were made:

(i) Field-aligned irregularities occur in the slab of enhanced electron density and extend upwards to the peak of the F-layer.

(ii) Detectable scattering is obtained from the irregularities only where the wave normals deviate by less than 2^o from normal incidence on the field lines.

Comparing computed and observed returns brings out the following features:

(a) The discrepancy between the computed and the measured ground-scatter components indicates that the applied electron distribution only approximately represents the regions of the ionosphere explored.

(b) The experimental trace with constant minimum range fits the computed direct scatter returns fairly well.

(c) A general agreement is demonstrated between the model computations and the observed echo-structure above the constant range trace from 9 to 12 MHz. This leads to the conclusion that the measured component actually results from scattering taking place after normal 1 hop F-layer propagation (including ground-reflection).

5. DISCUSSION

It may be noted that backscatter forms similar to those reported in this work have been observed by other workers concerned with soundings at high latitudes[1,2]. Bates[3]

has published the results of an analysis of echoes of this category recorded in Alaska. His method of analysis is based on standard transmission curves and an irregularity model in the form of a vertical intense ionization sheet located several hundred kilometres to the north of the sounding site. Bates finds that composite modes, involving both F-layer reflection and scattering from field-aligned irregularities are important in explaining some of his observed long-range traces.

A serious problem encountered in computations of the type performed here is a lack of adequate expressions for the scattering cross-sections determining the amounts of returned energy. Of the many modes that may be constructed as possibilities for potential returns, it is obvious empirically that just a few yield signal strengths above the receiver threshold level.

Additional problems are related to the absorption suffered by the exploring waves in the lower ionosphere, the antenna radiation patterns and their variation with frequency and the gradients in the electron density in the sounding direction.

It is known that the minimum virtual ranges of ground-scatter echoes are determined by the mechanism of time-focusing. The role played by time-focusing in measurements involving scattering from irregularities in the ionosphere is open to discussion.

It appears that with the assumptions which have to be made in estimating the active modes of return, the results arrived at will necessarily be of a somewhat qualitative nature.

Conclusions which may be drawn from the present treatment, consistent with the findings of Bates[3], are summarized thus:

(a) A group of backscatter signals frequently observed in soundings below 20 – 25 MHz at high latitudes is explainable in terms of aspect sensitive scattering from field-aligned irregularities at E- and F-layer heights.

(b) The scattering centres are confined to spatially restricted regions inside the polar cap.

(c) At the height of the E-layer the irregularities are imbedded in an Es cloud whose ionization is strong enough to bring about the refraction needed for the backscatter process.

ACKNOWLEDGEMENTS

The work reported upon in this paper has been sponsored in part by Cambridge Research Laboratories, OAR, through the European Office, Aerospace Research, United States Air Force, under Contract AF 61(052)-835.

REFERENCES

1. Bates, H.F. *Computed HF Auroral Backscatter Traces for Various Distances.* Scientific Report, UAG R-174, University of Alaska, 1966.

2. Bates, H.F. *Result of the HF Forward and Backscatter Program.* Final Report, UAG R-178, University of Alaska, 1966.

3. Bates, H.F. *Some Effects of Dense Es Cloud on High-Latitude HF Backscatter Observations.* Journal of Geophysical Research, Vol.70, 1965, p.23.

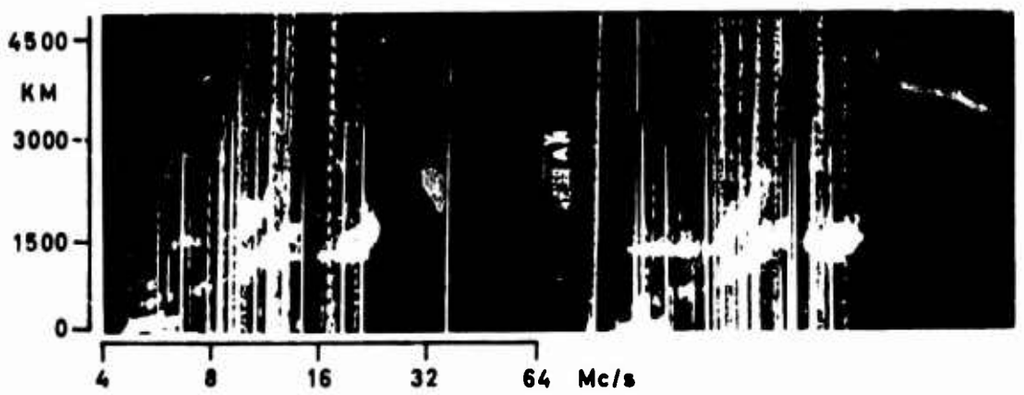


Fig. 1 Frequently observed echoes

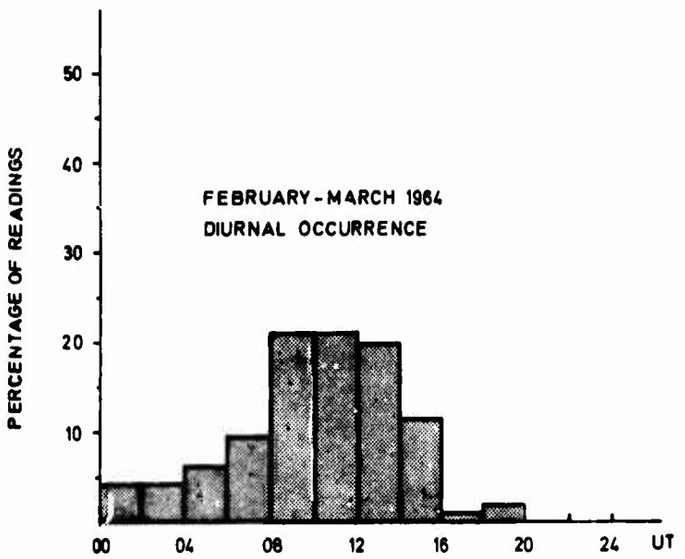


Fig. 2 Diurnal occurrence pattern of constant range trace

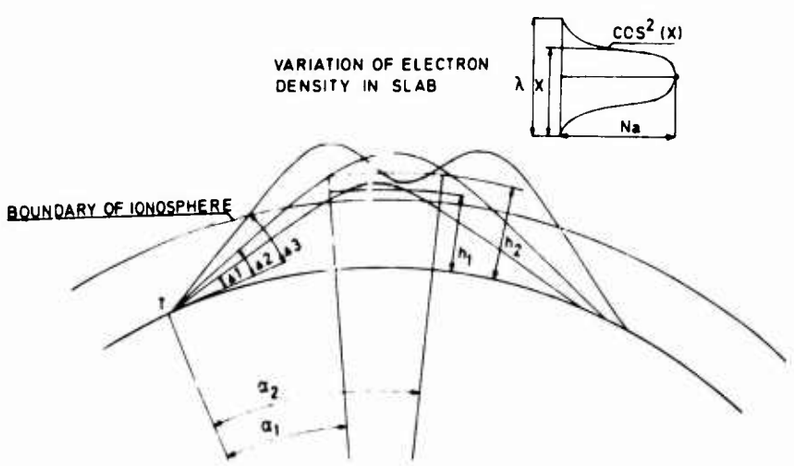


Fig. 3 Model used in ray-tracing

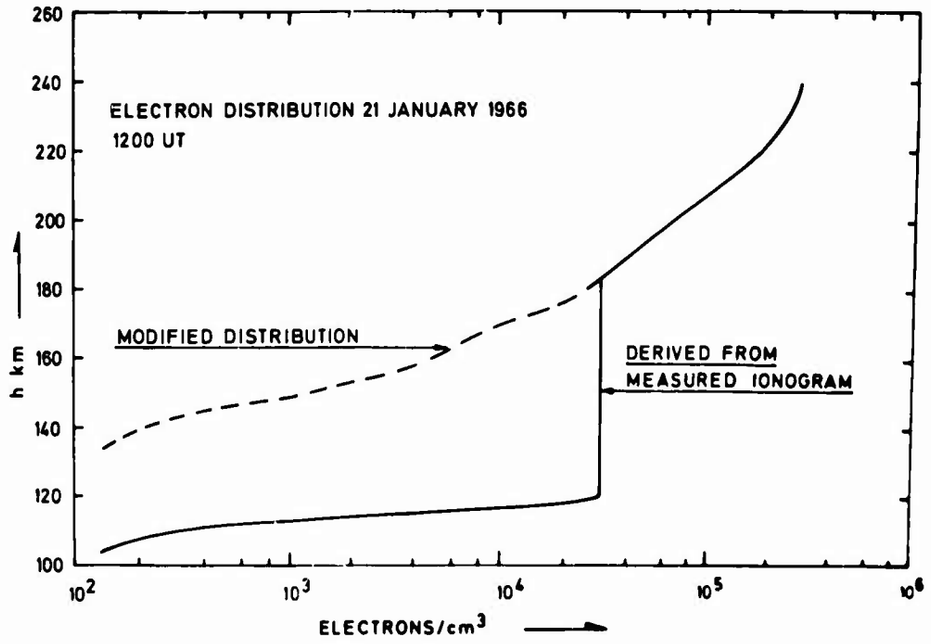


Fig. 4 Electron distributions applied in computations

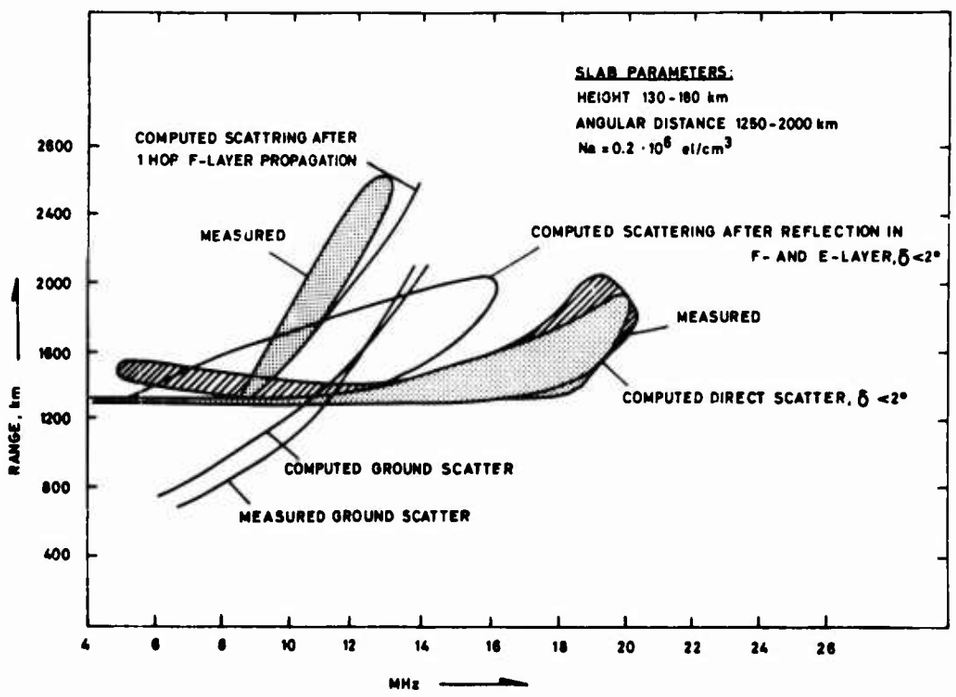


Fig. 5 Display of measured and computed backscatter traces

FIELD-ALIGNED IONIZATION SCATTER GEOMETRY

by

George H. Millman

General Electric Company
Syracuse, New York, USA

SUMMARY

Experimental studies of the characteristics of radio wave backscatter and forward scatter from magnetic field-aligned ionization have been performed for many years.

In this paper, an evaluation is made of theoretical and graphical methods for calculating (i) the orientation of the magnetic field for backscatter reflections and (ii) the locus of points on the earth's surface for the reception of the forward scatter mode.

The theoretical methods which are considered involve the assumption that the earth's magnetic field can be approximated by (i) the field of a magnetic dipole located at the earth's center and (ii) the combination of a dipole field and an irregular field, i.e., a series of spherical harmonics. The graphical technique utilizes ground-observed magnetic data scaled from isomagnetic maps.

Computations for both the backscatter and forward scatter modes of propagation are presented for two locations in the Northern Hemisphere.

FIELD-ALIGNED IONIZATION SCATTER GEOMETRY

George H.Millman

1. INTRODUCTION

Radio waves incident on magnetic field-aligned ionization, such as prevalent in the auroral region, are scattered back in the direction of the radiating source when the direction of propagation is approximately perpendicular to the lines of force of the earth's magnetic field (Leadabrand et al.[1]).

In addition to the perpendicularity requirement for radar-auroral reflections, it is necessary that this geometric configuration take place in regions of high auroral activity and at ionospheric altitudes of 80 km and above.

Anomalous radar echoes which possessed many of the characteristics of echoes from the aurora and which appeared to originate in regions of space where the perpendicular restriction is satisfied have been detected at low latitudes at frequencies of 32 and 140 MHz (Dyce et al.[2]) and 50 MHz (Bowles et al.[3]).

When the direction of propagation makes an angle of other than 90° with the magnetic lines of force, the incident radiation undergoes forward scattering.

Experimental evidence of an ionospheric forward scatter mode of propagation associated with the earth's magnetic field has been reported by Heritage et al.[4], the observations being conducted at a frequency of 200 MHz.

In this paper, an evaluation is made of various computational techniques for determining (i) the magnetic field geometry for backscatter reflections and (ii) the locations on the earth's surface for the reception of magnetic field forward scatter.

A graphical technique is discussed which utilizes ground-observed magnetic data scaled from isomagnetic maps. The theoretical methods which are also considered are (i) the dipole method, which is based on the supposition that the earth's magnetic field can be approximated by the field of a magnetic dipole located at the earth's center and (ii) the spherical harmonic method, which assumes that the earth's main field can be represented by a regular or simple dipole field and an irregular field.

This paper is, in essence, a modification and extension of the material appearing in an earlier publication (Millman[5]) on the orientation of the earth's magnetic field.

2. THEORETICAL CONSIDERATIONS

2.1 Backscatter Propagation

In the study of radar-auroral reflections, it is often desirable to determine the orientation of the lines of force of the earth's magnetic field for any geographic location, antenna azimuth bearing, elevation angle, and reflection height above the earth's surface.

It can be shown that the propagation angle θ, i.e., the angle between the direction of the magnetic lines of force and the direction of electromagnetic propagation, can be expressed by the relationship[5]

$$\theta = \cos^{-1} [-\cos e \sin I - \sin e \cos I \cos (\gamma - D) , \quad (1)$$

where I and D are the magnetic inclination and declination angles, respectively. These parameters specify the direction of the total magnetic intensity vector in space.

The angle γ which is the geographic azimuth bearing of the observer's location measured with respect to the sub-ionospheric point, i.e., the location on the earth's surface directly beneath the particular point in space, is defined by Millman[6] as

$$\gamma = \tan^{-1} \left[\frac{\sin (\lambda_R - \lambda_P) \cos \phi_R}{\sin \phi_R \cos \phi_P - \cos \phi_R \sin \phi_P \cos (\lambda_R - \lambda_P)} \right] , \quad (2)$$

where ϕ and λ are the geographic latitude and east longitude, respectively. The subscripts, R and P, refer to the transmission (or radar) site and the reflection point, respectively.

The angle e, which is the angle between the ray path and the zenith at the point of reflection, is given by

$$e = \sin^{-1} \left[\frac{r_0}{r_0 + h} \cos E \right] , \quad (3)$$

where r_0 is the radius of the earth, E is the elevation angle of the antenna beam and h is the height above the earth's surface.

The graphical technique employed in evaluating θ in this study is as follows: The parameters I and D have been scaled in 2.5^o and 5.0^o latitude and longitude steps over the whole earth's surface from the epoch 1955 isogonic and isoclinic maps issued by the US Navy Hydrographic Office and the Canadian Department of Mines and Technical Surveys. The ground-observed magnetic data obtained from these maps are stored in matrix form in an IBM 7094 digital computer. Linear interpolation is used for determining the values of the magnetic field elements at other geographic locations.

For propagation through the ionosphere, the angles I and D at the sub-ionospheric point are assumed to be invariant at all heights.

According to the 1955 magnetic charts, the geographic positions of the north and south dip-poles, which are dependent upon local surface anomalies and irregularities, are approximately 73.5^o N, 101.1^oW and 67.6^oS, 144.0^oE, respectively.

The dipole method is based on the assumption that the earth's magnetic field can be approximated by a magnetic dipole having geomagnetic poles at 78.6^oN, 70.1^oW and 78.6^oS, 109.9^oE (Vestine et al.[7]).

For this case, the inclination, or magnetic dip, which specifies the direction of the total magnetic intensity vector with respect to the horizon and is measured positive in the downward direction, is given by Chapman[8] as

$$I = \tan^{-1} [2 \tan \psi_P] , \quad (4)$$

where ψ is the geomagnetic latitude.

A simple transformation for expressing ψ_P in terms of geographic coordinates is given by Millman[5],

$$\psi_P = \sin^{-1} [\cos (\lambda_M - \lambda_P) \cos \phi_M \cos \phi_P + \sin \phi_M \sin \phi_P] , \quad (5)$$

where the subscript M refers to the geomagnetic pole.

The magnetic declination angle, which specifies the direction of the geomagnetic pole and is measured positive in a clockwise direction from geographic north, can be defined by the function[6]

$$D = \tan^{-1}\left[\frac{\sin(\lambda_M - \lambda_P)\cos\phi_M}{\cos\phi_P \sin\phi_M - \cos(\lambda_M - \lambda_P)\sin\phi_P \cos\phi_M}\right]. \tag{6}$$

It is of interest to note that, for the dipole model approximation, the inclination and declination are invariant with altitude.

Due to local magnetic anomalies on the earth's surface, there are large discrepancies and widespread departures from a simple dipole field. To take this into account, the earth's main field, i.e., the magnetic field which excludes such phenomena as magnetic disturbances and diurnal variations, can be represented by a regular or dipole field and an irregular field. A magnetic potential function for the main field over the earth's surface can be expressed in terms of a series of spherical harmonics (Chapman and Bartels[9]) such as

$$V = \sum_{n=0}^{\infty}\sum_{m=0}^{n}\frac{r_0^{n+1}}{r^{n+1}}\left[g_{nm}\cos(m\lambda) + h_{nm}\sin(m\lambda)\right]P_n^m(\cos\phi'), \tag{7}$$

where r is the distance from the center of the earth, ϕ' is the geographic colatitude, $p_n^m(\cos\phi')$ are the associated Legendre functions of degree n and order m and g_{nm} and h_{nm} are the coefficients of the spherical harmonic expansion.

It should be noted that the first-degree harmonic terms in Equation (7), i.e., terms with $n = 1$ and $m = 0$, reduce to that of a dipole potential.

In practice, the magnetic potential is not a measurable quantity. The quantities which are measured are namely X, the northward horizontal component, Y, the eastward horizontal component, and Z, the downward vertical component of the total magnetic intensity, which are defined in terms of the magnetic potential by

$$X = \frac{1}{r}\frac{\partial V}{\partial \phi'} \tag{8}$$

$$Y = -\frac{1}{r\sin\phi'}\frac{\partial V}{\partial \lambda} \tag{9}$$

$$Z = \frac{\partial V}{\partial r}. \tag{10}$$

By definition, the magnetic inclination and declination angles are related to components of the total magnetic intensity by

$$I = \tan^{-1}\left[\frac{Z}{(X^2 + Y^2)^{\frac{1}{2}}}\right] \tag{11}$$

$$D = \tan^{-1}\left[\frac{Y}{X}\right]. \tag{12}$$

It should be evident from Equations (7) through (12) that, for the spherical harmonic-magnetic field model, the parameters I and D are altitude dependent.

In this analysis, the set of 48 spherical harmonic coefficients derived by Jensen and Cain[10] for epoch 1960 was used to specify the magnetic potential function defined by Equation (7). This function, in turn, was employed in the evaluation of I and D (Equations (11) and (12)).

2.2 Forward Scatter Propagation

When the direction of propagation is not orthogonal to the field-aligned ionization, the radiation undergoes forward scattering. The location on the surface of the earth to which the scattered radiation is directed can be readily determined for both the graphical and theoretical methods.

In order to facilitate the analysis, it is assumed that the radiation is oriented in the directions which satisfy the condition of specular reflection, i.e., the angle of incidence to the ionization column is equal to the angle of reflection. This assumption was also the basis of the mathematical development of the forward scatter problem proposed by Leadabrand and Yabroff[11]. As shown in Figure 1, this condition requires that

$$\cos\theta = -\cos\theta_r , \tag{13}$$

where $(\pi - \theta_r)$ is the propagation angle formed by the reflected ray and the magnetic field line of force.

It follows from Equation (1) that the geographic azimuth angle of the receiver location, as measured at the point of reflection projected on the earth's surface, γ_r, can be expressed by the function

$$\gamma_r = \cos^{-1}\left[\frac{-\cos\theta - \cos e_r \sin I}{\sin e_r \cos I}\right] + D , \tag{14}$$

where the subscript, r, refers to the reflected ray. It should be evident that, for a given magnetic field-transmission path, the unknown parameters in this relationship are γ_r and e_r.

Referring to Figure 2, it can be shown from the law of cosines that the geographic latitude of the receiver location is given by

$$\phi_r = \sin^{-1}\left[\sin\phi_p \cos\beta_r + \cos\phi_p \sin\beta_r \cos\gamma_r\right] \tag{15}$$

while, from the law of sines, the geographic longitude becomes

$$\lambda_r = \lambda_p + \sin^{-1}\left[\frac{\sin\beta_r \sin\gamma_r}{\cos\phi_r}\right] . \tag{16}$$

The angle β_r is the angle at the center of the earth between the radial lines to the receiver location and to the reflection point projected on the earth's surface. According to Figure 1, β_r can be defined in terms of the angle e_r by the relationship

$$\beta_r = \sin^{-1}\left[\frac{r_0 + h}{r_0} \sin e_r\right] - e_r . \tag{17}$$

It follows from Equation (14) that the minimum value which e_r can attain is expressed by

$$(e_r)_{min} = \left|\frac{\pi}{2} - (\theta + I)\right| , \tag{18}$$

for the condition in which $\gamma_r = D$. This implies that minimum e_r occurs when the scattered radiation is in the direction of the magnetic field at the point of reflection in the ionization column. For the theoretical dipole method, this direction coincides with the geomagnetic longitude as measured at the reflection point.

According to Figure 1, the maximum value of e_r is given by

$$(e_r)_{max} = \sin^{-1}\left[\frac{r_0}{r_0 + h}\right]. \tag{19}$$

This relationship applies for the condition of tangency of the scattered ray at the earth's surface.

According to Figure 1, the elevation angle of the reflected ray at the receiver location E_r, is simply

$$E_r = \cos^{-1}\left[\frac{r_0 + h}{r_0} \sin e_r\right] \tag{20}$$

The azimuth bearing of the reflection point, A_r, as measured at the receiver site, is obtained from the spherical triangle in Figure 2 containing the geographic north pole, and is given by

$$A_r = -\sin^{-1}\left[\frac{\cos\phi_p \sin\gamma_r}{\cos\phi_r}\right]. \tag{21}$$

A procedure for computing the location of the scattered points on the earth's surface is to assume different values of e_r between $(e_r)_{min}$ and $(e_r)_{max}$. The angles β_r, calculated from Equation (17) and γ_r from Equation (14), of which there are two solutions, are then utilized in Equations (15) and (16) to obtain the geographical coordinates of the intersection points.

It should be noted that the solution to the forward scatter propagation problem requires that, as in the backscatter case, the following parameters be known: (i) the geographic coordinates of the transmitter site, (ii) the azimuth and elevation angles of the transmitted radiation, and (iii) the height at which reflection with the field-aligned ionization takes place.

It should be evident that there exists more than one solution, i.e., receiver locations, which would satisfy the condition of specular reflection, defined by Equation (13). It can be shown that instead of one reflected beam there is actually a cone of reflection, the apex of which is at the point of reflection and the axis of which is parallel to the direction of the magnetic field at the reflection point. Thus, for a given antenna beam orientation in space, the intersection of the cone of reflection with the earth's surface determines the loci of points on the earth to which the ray will be reflected. It is found that the loci of the intersection of the reflected beam and the earth's surface is a smooth curve which is symmetrical about the direction of the magnetic field as specified at the reflection point.

3. COMPARISON OF METHODS

The calculations of the backscatter and forward scatter magnetic field geometry presented in this study were performed for two locations in the northern hemisphere: Seattle, Washington (47.5°N, 122.0°W) and Boston, Massachusetts (42.3°N, 71.0°W).

Figure 3 is a plot of the propagation angle at 100 km altitude as viewed from Seattle. It is seen that the graphical and spherical harmonic methods give results which are, for the most part, identical. Minimum propagation angle for the two methods is attained at a geographic bearing angle which coincides approximately with the direction of the magnetic declination of 22.5°E (A = +22.5°). The propagation angle for the dipole method, on the other hand, is a minimum in the direction of geomagnetic north (A = +15.2°).

According to Figure 4, for observations at Seattle in the direction of geographic north ($A = 0^{o}$) and at an altitude of 80 km, the propagation angle is a minimum at an elevation angle of about 4^{o} for the dipole method and about 5^{o} for the graphical and spherical harmonic methods. As the altitude is increased, the elevation angle at which minimum propagation angle occurs increases slightly. For a fixed elevation angle, the propagation angle increases markedly with altitude. The dipole computations in the direction $A = 0$ are always less than the corresponding results obtained with the graphical and spherical harmonic methods. However, as shown in Figure 3, the reverse could take place at bearing angles oriented in an easterly direction.

Figure 5 is a range-azimuth plot of the contours of perpendicularity with the magnetic field, the calculations being based on a minimum altitude of 80 km. It is seen that, in the northerly direction from Seattle, orthogonality occurs at the greatest ranges with the dipole method.

A sample calculation of the forward scatter propagation mode is illustrated in Figure 6. It is assumed that the transmissions originated at Seattle at different azimuth-elevation orientations and that the reflections from field-aligned ionization took place at an altitude of 100 km. It is evident that the loci of points on the earth's surface to which the scattered radiation is directed form a smooth symmetrical curve, the ends being the tangency points of the scattered ray with the earth. A comparison of the data presented in Figure 6 reveals that, in general, there is a wide discrepancy in the results obtained with the dipole method.

The magnetic field calculations as viewed from Boston are presented in Figures 7 through 10. It is seen that minimum propagation angle exists in the direction of the dipole ($A = -14.7^{o}$) and the magnetic declination of 15.0^{o}W ($A = -15.0^{o}$) for both the graphical and spherical harmonic methods. With regard to the dipole method, the minimum angle coincides with the geomagnetic north direction ($A = 0.3^{o}$), the results being similar to that exhibited in the Seattle data.

According to Figures 7 and 8, there is a difference of about 0.5^{o} between the propagation angles determined for Boston by the graphical and spherical harmonic methods as compared to a difference of less than 0.1^{o} for the Seattle computations.

Figure 9 discloses that the contours of the perpendicular aspect angle determined by the dipole method encompass a greater spatial extent than those calculated by the other two methods. Similar results were obtained for Seattle, as shown in Figure 5.

An interesting feature of Figure 10, not readily evident in the Seattle data of Figure 6, is the slight oscillation in the middle of the loci of the scattered points on the earth's surface as derived by the dipole method. An explanation for the lack of the presence of this characteristic in the graphical and spherical harmonic data is not available at this time.

4. CONCLUSIONS

The geometry of backscatter and forward scatter reflections from columnar ionization aligned along the earth's magnetic lines of force can be resolved by graphical and theoretical, i.e., dipole and spherical harmonic, methods.

The graphical technique employs magnetic data observed at the earth's surface and yields results which are comparable to those obtained with the spherical harmonic method. The latter is based on the assumption that the earth's magnetic field can be represented by a regular or dipole field and an irregular field.

The graphical method is slightly in error because of the fact that the ground-observed magnetic inclination and declination data are assumed to be invariant with altitude. The

tedious task of scaling the magnetic data from the isomagnetic maps whenever they are revised, and the excessive storage-computer requirement of the matrix type-scaled data, makes the graphical approach somewhat less desirable.

The accuracy of the spherical harmonic technique can be readily improved by the use of recently available coefficients such as derived by Hendricks and Cain[12].

The dipole method is not the optimum one to be employed in geometric studies involving the orientation of the earth's magnetic field at ionospheric heights. However, at great distances from the earth's surface, this technique should suffice, since the earth's magnetic field theoretically approaches the regular centered-dipole field.

ACKNOWLEDGEMENT

I am grateful to E. A. Karpinski for the programming of the dipole and spherical harmonic methods on the digital computer.

REFERENCES

1. Leadabrand, R.L., et al. — *Simultaneous Very High Frequency and Ultra High Frequency Observations of the Aurora at Fraserburgh, Scotland.* Journal of Geophysical Research, Vo.70, 1965, pp.4235-4284.

2. Dyce, R.B., et al. — *Aurora-Like Radar Echoes Observed from 17° Latitude.* Journal of Geophysical Research, Vol.64, 1959, pp.1815-1818.

3. Bowles, K.L., et al. — *Radio Echoes from Field-Aligned Ionization Above the Magnetic Equator and Their Resemblance to Auroral Echoes.* Journal of Geophysical Research, Vol.65, 1960, pp.1853-1855.

4. Heritage, J.L. et al. — *Evidence for a 200Mc/s Ionospheric Forward Scatter Mode Associated with the Earth's Magnetic Field.* Journal of Geophysical Research, Vol.64, 1959, pp.1235-1241.

5. Millman, G.H. — *The Geometry of the Earth's Magnetic Field at Ionospheric Heights.* Journal of Geophysical Research, Vol.64, 1959, pp.717-726.

6. Millman, G.H. — *The Geometry of Radar-Auroral Reflections.* General Electric Technical Information Series Report R58EMH3, March 1958.

7. Vestine, E.H., et al. — *The Geomagnetic Field, its Description and Analysis.* Carnegie Institute, Washington, Publication 580, 1947.

8. Chapman, S. — *The Earth's Magnetism.* Methuen, London, 1951.

9. Chapman, S., Bartels, J. — *Geomagnetism.* Vols.I and II, Oxford University Press, 1940.

10. Jensen, D.C., Cain, J.C. — *An Interim Geomagnetic Field.* Journal of Geophysical Research, Vol.67, 1962, pp.3568-3569.

11. Leadabrand, R.L., Yabroff, I. — *The Geometry of Auroral Communications.* Transactions, Institute of Radio Engineers, Antennas and Propagation, AP-6, 1958, pp.80-87.

12. Hendricks, S.J., Cain, J.C. — *Magnetic Field Data for Trapped-Particle Evaluations.* Journal of Geophysical Research, Vol.71, 1966, pp.346-347.

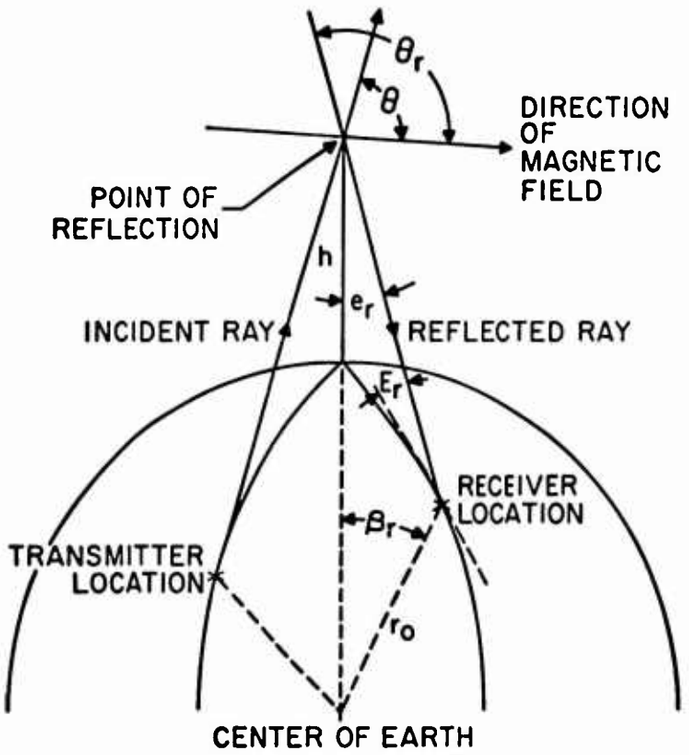


Fig. 1 Auroral scattering geometry

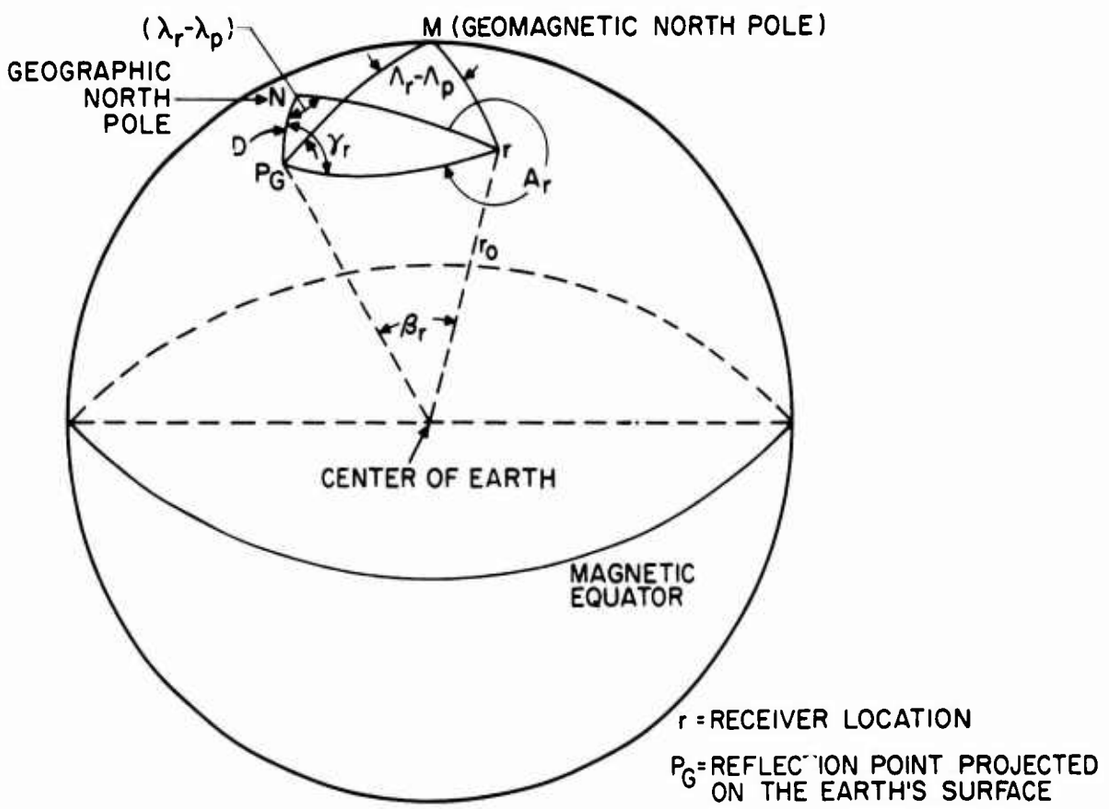


Fig. 2 Spherical geometric relations

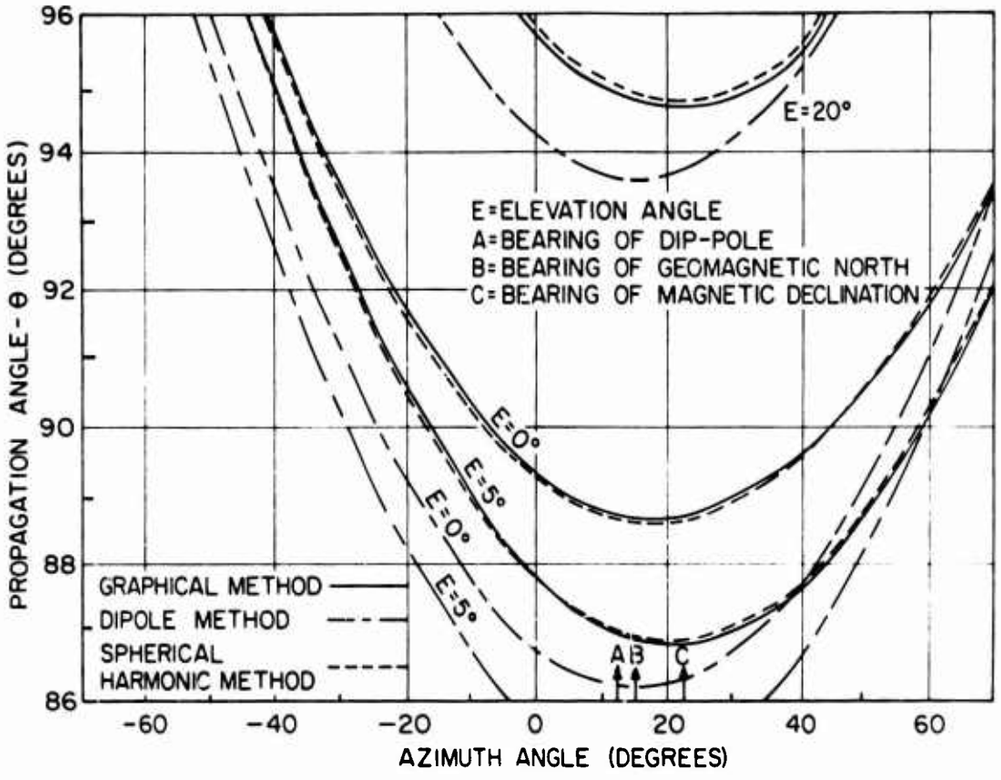


Fig. 3 Propagation angle at 100 km as viewed from Seattle

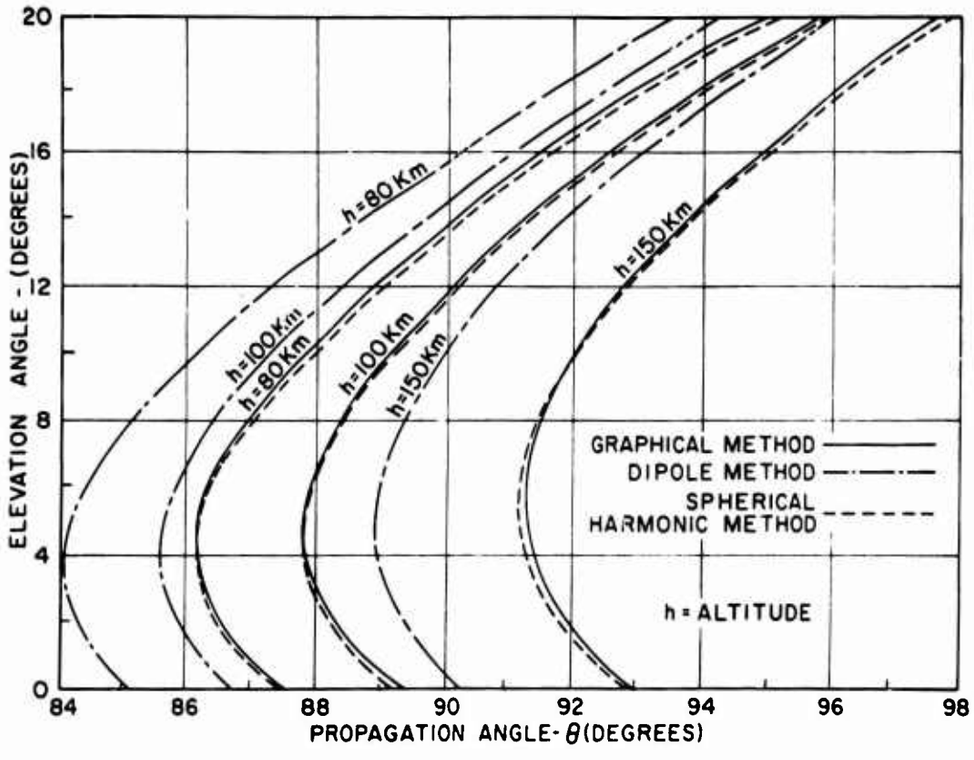


Fig. 4 Propagation angle as viewed from Seattle along the direction of geographic north ($A = 0^{o}$)

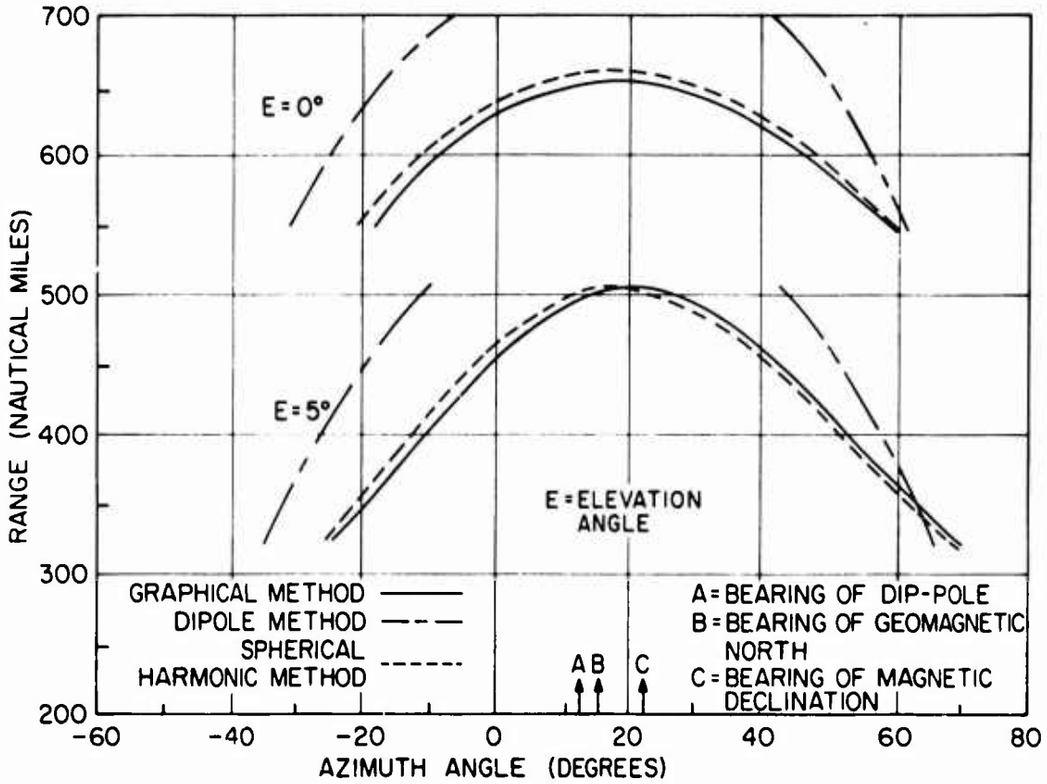


Fig. 5 Contours of perpendicularity with the magnetic field as viewed from Seattle

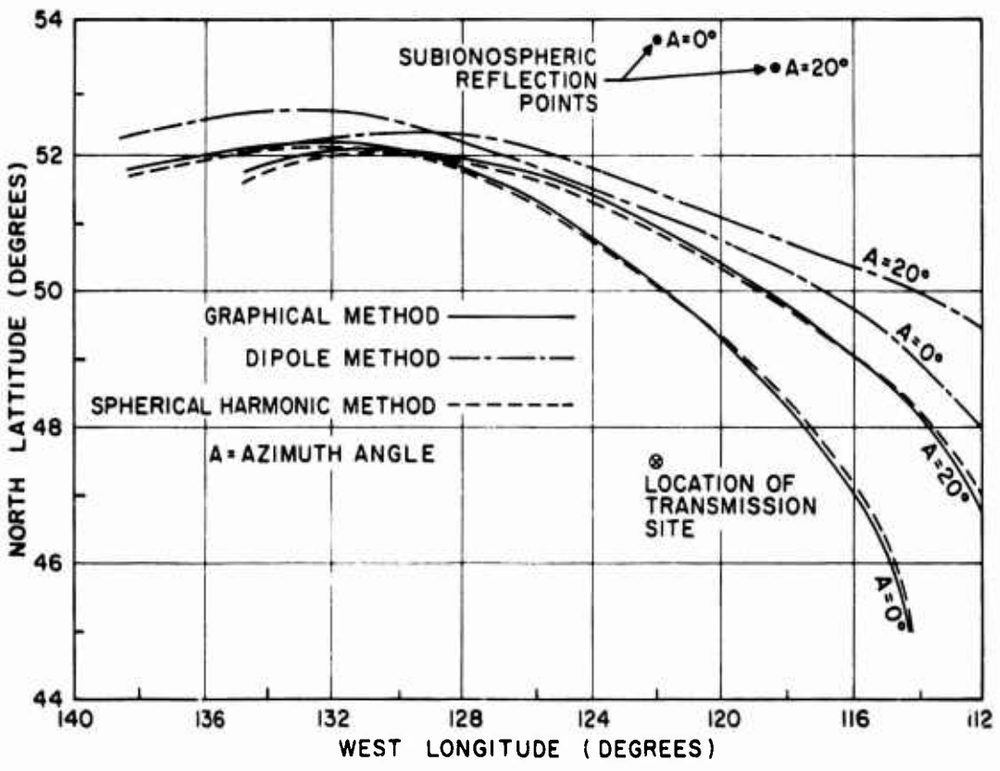


Fig. 6 Loci of receiving locations for transmissions originating at Seattle at 5° elevation angle and specularly reflected from field-aligned ionization at 100 km

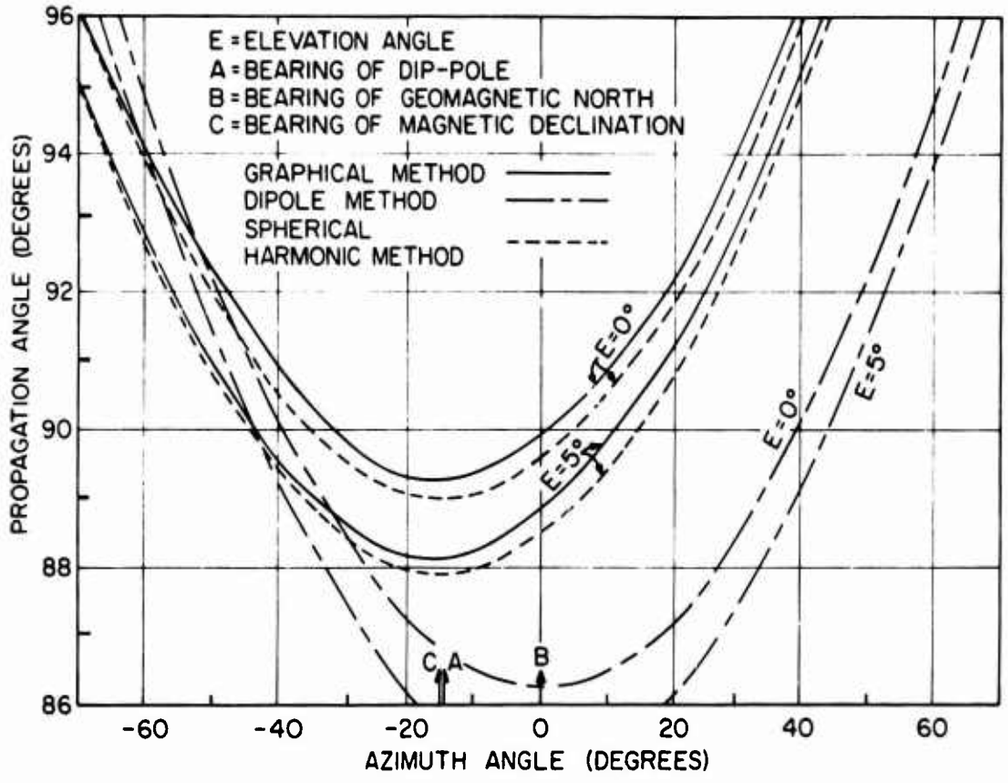


Fig. 7 Propagation angle at 100 km as viewed from Boston

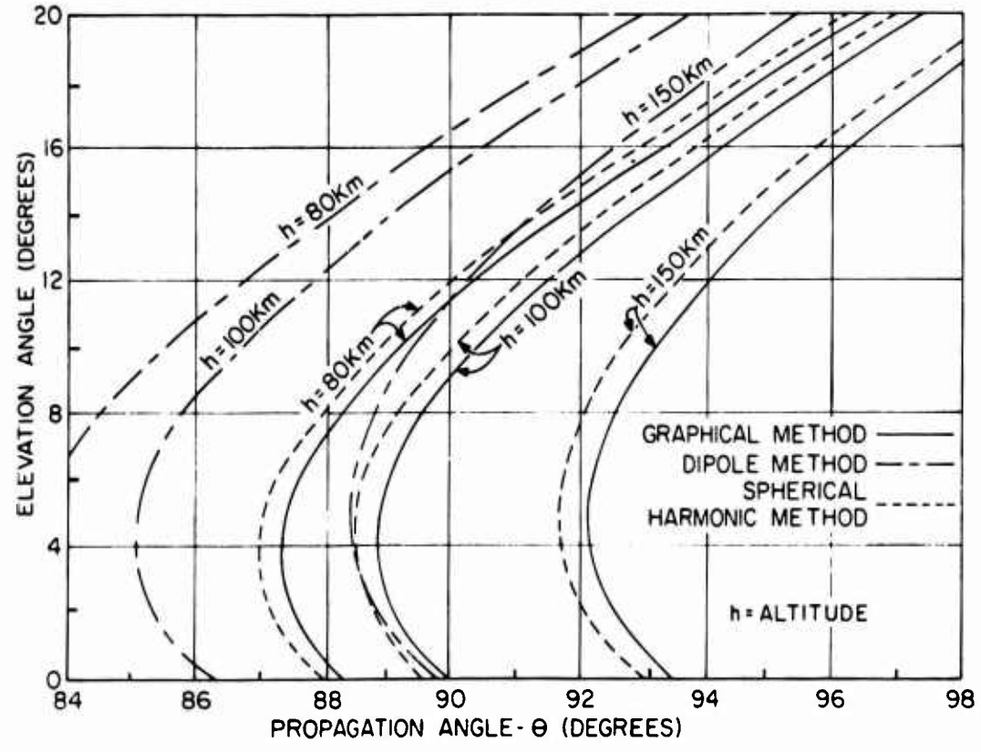


Fig. 8 Propagation angle as viewed from Boston along the direction of geographic north ($A = 0^{o}$)

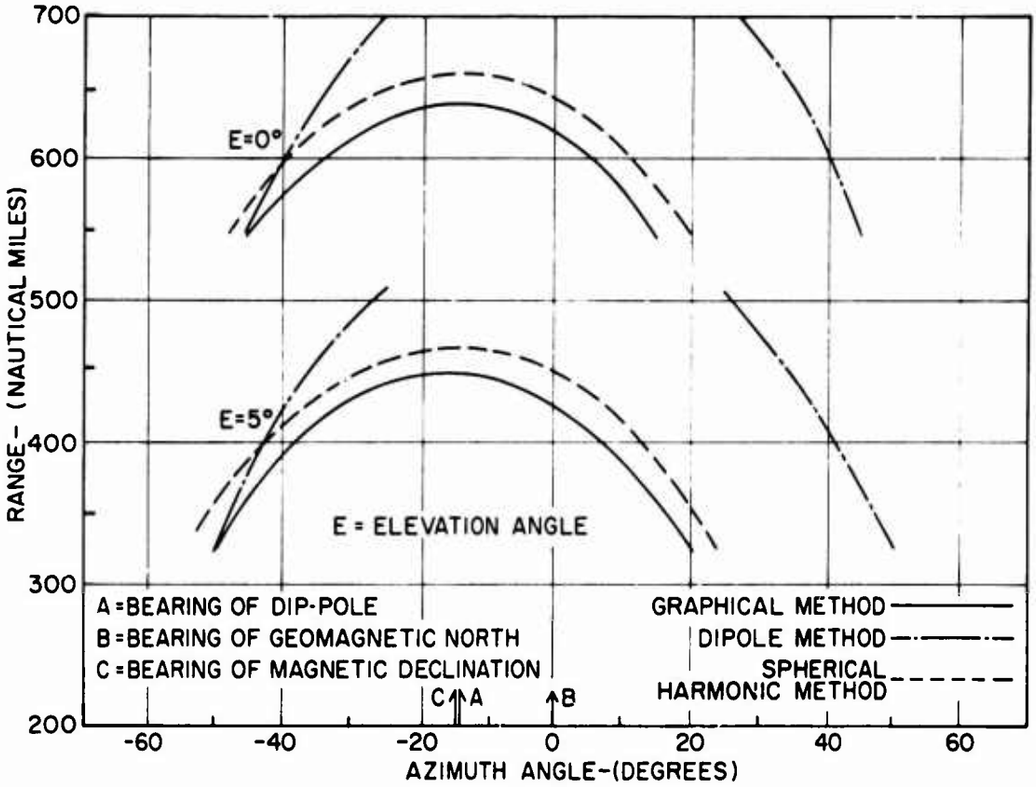


Fig. 9 Contours of perpendicularity with the magnetic field as viewed from Boston

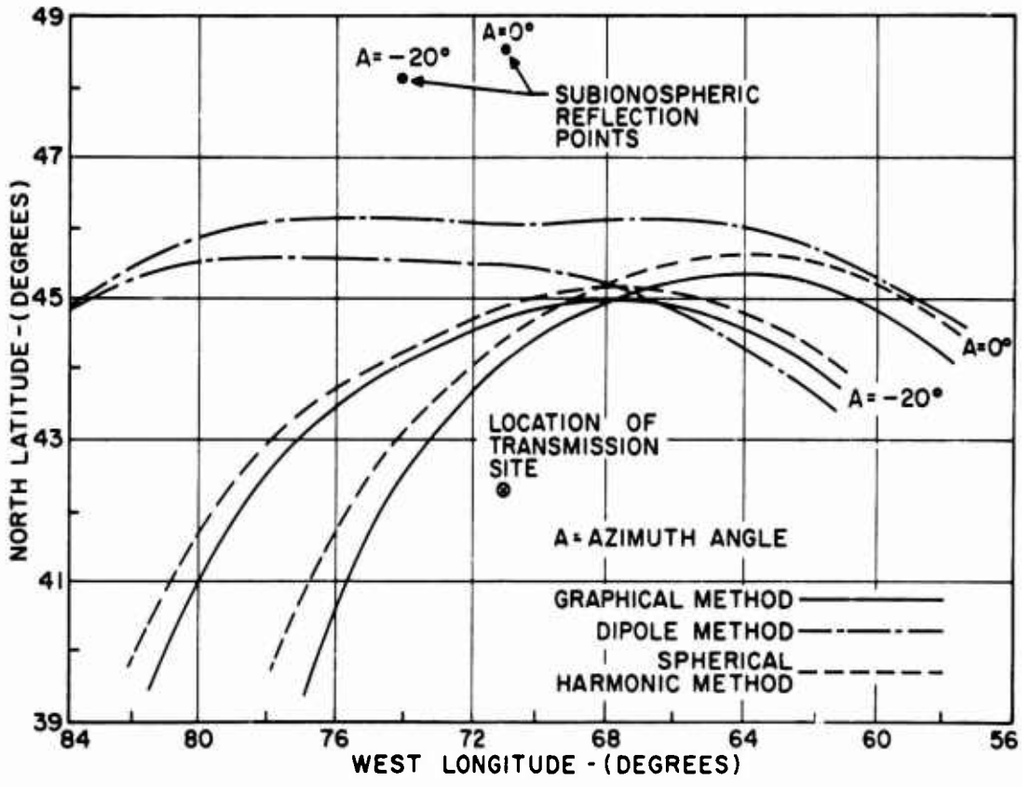


Fig. 10 Loci of receiving locations for transmissions originating at Boston at 5^{o} elevation angle and specularly reflected from field-aligned ionization at 100 km

DISCUSSION ON THE PAPERS PRESENTED IN SESSION V (AURORAL SCATTER).

Discussion on Paper 34, "Auroral scatter", by P.A.Forsyth.

Dr G.H.Millman: What is the scattering cross-section dependency with aspect angle and frequency? How do your results compare with the measurements by the Stanford Research Institute?

Professor P.A.Forsyth: As indicated in the paper, McDiarmid and McNamara found an aspect sensitivity radiation of about 1 dB per degree of aspect angle at a frequency of 50 MHz. Regarding the frequency dependence at cross-sections I would refer you to the summary provided by Morrcroft (1966). As he points out, the variability of the dependence means that averages may not be too meaningful, but he does show typical results. (For complete references, see my paper.)

Dr F.Ramasastry: Are you aware of any recent auroral electrojet measurements? If so, will you please comment on them or give some information?

Professor P.A.Forsyth: Although I am aware of a number of investigations using rockets and ground-based measurements including those of Anger (University of Calgary) I am not sufficiently familiar with them to comment on the validity of any specific measurement.

Dr L.C.Humphrey: Are the reported cross-sections based on a beam-filled or point-scatterer situation?

Professor P.A.Forsyth: The cross-sections are based simply on the radar equation in the form given as Equation (1) of the paper. The results of Palmer suggest that there are marked rapid changes in the extent to which the beam is filled by auroral scatterers during a typical event.

Dr R.Cohen: I should like to ask Professor Forsyth the following questions:

(a) What was the percentage modulation on the electron concentration as measured from rockets by McNamara? What was the variation of electron temperature?

(b) Would you give us further details on the second kind of events observed by Palmer on the oblique-scatter circuit.

I should also like to comment that your auroral-zone measurements are quite consistent with the picture now evolving of the physics of the irregularities in the equatorial electrojet. We pointed out some time ago (Journal of Geophysical Research, Vol.65, 1960, p.1853) that we would expect the irregularity phenomena in the auroral case to resemble those in the equatorial electrojet. The spectral characteristics of your stronger signals correspond to those we would associate at the equator with the strong irregularities resulting from the two-stream plasma instability, and the spectra of the coexistent weaker signals have characteristics similar to the electrojet echoes obtained simultaneously from weaker irregularities. The latter are ascribed by Dr.Balsley as due to "plasma turbulence", since they seem to arise from shears of electron velocity. These irregularities apparently move at the electron drift velocity; hence, echoes from them are good indicators of that velocity.

Professor P.A.Forsyth: I believe that the fluctuations reported by the rocket experiment amount to a few percent, say 10%, of the background. I have no information on the electron temperature at this time, but McNamara may know more about this. To answer your second question, the type of event referred to is one with high fading rate and high apparent drift velocities. These are the predominant characteristics, but Palmer and Moorcroft intend to publish this work shortly. In the meantime, Palmer's original thesis is available as Report HA-9 from the Centre for Radio Science, University of Western Ontario. Your last comment is almost certainly correct for the strong echoes with a single narrow displaced

spectral component. For the others, unfortunately, the measured characteristics are not a unique test of the mechanism.

Discussion on Paper 35, "A note on a particular type of scattering echoes observed at high latitudes", by K.Folkestad.

Dr G.H.Millman: Mr Folkestad, since the maximum occurrence of echoes appeared in the daytime, is there any evidence that the auroral echoes were actually due to sporadic-E?

Mr K.Folkestad: The slab of enhanced ionization introduced into our model may be considered as constituting an Es structure.

Discussion on Paper 36, "Field aligned ionization scatter geometry", by G.H.Millman.

Dr N.C.Gerson: Dr Millman, what model was employed for your spherical harmonics calculations? Whose coefficients were employed? The Jensen and Cain coefficients are deficient at high geomagnetic latitude because of the paucity of stations on which the coefficients are based.

Dr G.H.Millman: The 48 coefficients derived by Jensen and Cain were used in the spherical harmonic calculations. A study is now being conducted for the evaluation of the backscatter and forward scatter geometry, using spherical harmonic coefficients derived by the many workers in the field.

REVIEW OF VHF FORWARD SCATTER

by

Richard C. Kirby

Institute for Telecommunication Sciences
ESSA Research Laboratories
Environmental Science Services Administration
Boulder, Colorado, USA

SUMMARY

This review of "VHF Forward Scatter" presents mainly a *description* of the *continuous propagation* observed at oblique incidence throughout the world, in the frequency range 25 to 110 MHz, scattered from irregularities in electron density in the 70-90 km height range, and from meteoric ionization. Observations have been largely made over 1000 to 2000 km path lengths in the Northern and Southern hemispheres and near the equator, using pulsed and continuous wave transmissions. Some attention is drawn to extra modes of propagation, primarily from the E-region at low latitudes and aurora at high latitudes. Absorption effects, particularly in connection with Polar Cap absorption events, are mentioned.

REVIEW OF VHF FORWARD SCATTER

Richard ' .irby

1. INTRODUCTION

VHF forward scatter was used for reliable communication for more than a decade, for major point-to-point trunks across the Atlantic, across the Pacific. and between NATO points from Northern to Southern Europe. The transoceanic trunks are now supplanted by satellite and cable services, and the NATO circuits have been discontinued for administrative reasons. Some communication experiments continue, including the use for civil circuits, which emphasize low power systems with simple antennas for teleprinter communication.

2. SURVEY OF PROPAGATION CHARACTERISTICS

Serious experiments in this field were first inspired (Bailey et al.[1]) by application of the Booker-Gordon[2] theory of tropospheric scattering to a model of the E-region conceived of as having irregularities as suggested by the work of Eckersley[3] in 1932.

Observations in mid-USA at 50 MHz (Bailey et al.[4]) using 30 kW of power and 6°-beam antennas, established the continuous observability of scattering from weakly defined strata in the 70- to 90-km height range rather than the E-region, and also revealed the important additional component of a virtual continuum of overlapping echoes from meteor reflections. Meteoric ionization was concluded responsible for much, if not most, of the night-time signal. The root-mean-square scattering loss was typically 80 to 110 dB relative to perfect reflection from the ionosphere. Studies begun almost at the same time at high latitudes in Canada and Alaska showed even stronger continuous scattering and additional auroral echoes.

At a given hour of the day, typical standard deviations of the hourly mean scatter loss through a month were 3 to 6 dB. A diurnal minimum in early evening was characteristic year round. At mid-latitudes a broad daytime maximum was seen in summer, and a pronounced midday maximum in winter - these comprise the semi-annual daytime maxima to which Gregory[5] draws attention in his review. At high latitudes, a summer maximum was observed. In mid-USA, continuous recording for a number of years suggested a small solar cycle dependence, a change of the order of 3 dB being observed in the daytime values. The maximum was phased better with geomagnetic K than with sunspot number.

3. STRUCTURE OF RECEIVED SIGNAL

Some comments are now made on the time structure and spectrum of the received signal, from fading observations and pulse reception. Fading characteristics of the signals for all paths were comparable, except for occurrence of special events such as auroral and other extra modes. Rayleigh distributed fading is observed, with a fading rate at 50 MHz of 0.5 to 2 Hz, with recognizable bursts of meteor reflections superimposed every few seconds on the continuously fluctuating background. At mid-latitudes at night, when meteor reflections appear to dominate, a characteristic amplitude distribution is observed corresponding to a calculation by Wheelon[6].

One insight into the structure of the scattering medium is given by the range-time records (Fig.1) obtained by Carpenter and Ochs[7]. Their experiment was instrumented primarily to study individual meteor-trail characteristics, using 3-μsec pulses and a 60°-beam antenna over a 1400-km path in mid-USA. Here we see a rather diffuse D-region echo, with weak stratification, and subsequent meteor bursts. It is well to remember the broad antenna beams. The horizontal angular spectrum could easily provide the 30-μsec delay observed in these figures, even if the D-region scattering were from a thin horizontal stratum. Carpenter and Ochs put the height range at 65 to 85 km. Earlier range-time records by Pineo[8] using 40-μsec pulses and narrow-beam antennas, identified the height of the leading edge at 75 to 85 km, but did not show the diffuse echo of Carpenter and Ochs. The early pulse measurements of Pineo showed a stronger stratum at heights often lower than 75 km during summer and winter days, but 85-km echoes occurred at all times. Kirby's[9] extreme range observation from Newfoundland to the Azores confirmed an 85-km average height, and also demonstrated the absence of well defined diurnal and seasonal maxima where heights below 85 km were cut off by earth curvature. Bowles[10], working at 41 MHz at vertical incidence, received echoes from several strata in the 55-85 km height range.

Attention is now drawn, as in Gregory's review[5], to the partial reflection data obtained in the lower HF range. Gregory[11] compiled height data at 2.3 MHz over a number of months, showing backscatter from several strata in the 55-90 km range - with greater echo strength and persistence at the higher heights. The echoes at lower heights showed diurnal variation similar to that observed by Pineo.

Gregory has drawn attention to possible significant correlations between VHF scatter observations and the semi-annual maximum electron density below 85 km. In his paper on mesospheric electron densities, Gregory[12] points out that the VHF scatter signal must respond to the winter increase in electron density, and that the winter daytime VHF scatter maximum is statistically very pronounced. But the VHF scatter echo is also highly dependent on the degree of irregularity. Earlier attempts (Blair[13]) to correlate day-by-day scatter with absorption, as indicated by attenuation at 5 MHz, showed no correlation. Belrose[14] noted that even though, at Ottawa, summer electron densities below 90 km were greater than during winter, the winter echo amplitudes were greater, and more low lying echoes, i.e., near 55 km, were scaled - he concluded greater winter irregularity was responsible. Gregory's data at 2.3 MHz was obtained at a wavenumber corresponding to the $\lambda/(4\pi)$ scale size of about 10 m, while Pineo's scale size was about 2.5 m, and Bowles[10] at 41 MHz was about 0.6 m.

4. WAVELENGTH DEPENDENCE AND ANGULAR SPECTRUM

Wavelength dependence and angular spectrum are the key indicators of the spectrum of irregularities. Under the usual assumption of single isotropic scattering at an average angle θ, observations of frequency dependence or angle dependence serve to evaluate the spectrum of sizes of irregularities. This is because of the filtering action of the scattering process, which selects or emphasizes the sizes of irregularities having wavenumbers equal to

$$K = \frac{4}{\lambda} \sin \frac{\theta}{2}, \qquad (1)$$

where θ is the angle through which the wave is scattered.

4.1 Frequency Dependence

One of the most convincing pieces of evidence for turbulence has come out of the frequency-dependence results. Simultaneous observations were made (Blair et al.[15]) using antennas carefully scaled in all their dimensions proportional to wavelength, so as to illuminate an identical scattering volume at five frequencies from 30 to 108 MHz.

The measurements gave the quite unambiguous result that the received power almost always obeyed a nearly perfect power law in its dependence on frequency, i.e.

$$\frac{P_r}{P_t} \propto f^{-m} ,$$

where P_r and P_t represent the received and transmitted powers respectively, f is frequency, and m the exponent of the power law.

Thus, $S(K) = K^{-(m-2)}$, the power 2 allowing for the effect of change of antenna aperture with frequency.

Values of m averaged 8, with a standard deviation of about ±1, including systematic diurnal and seasonal variation. The strict power law was obeyed even for short samples of data, say the median for 5 minutes. The only departures occurred during sudden ionospheric disturbances (SID) when absorption affected the lowest frequencies.

Incidentally, it was concluded from the frequency-dependence observations that normal absorption occurs *above* the scatter region. Had the wave traversed the absorbing region, the 30-MHz signal would have suffered 3 to 4 dB normal midday attenuation, causing a marked departure from the strict power law for the scattering. But the power law remained in effect day and night and, indeed, with the higher values of m being observed during the day, as opposed to an absorption effect. During solar flares, absorption became evident at the lower frequencies and the power law was ruined.

It is most plausible that the diurnal and seasonal variation of m represents changing relative roles of meteors and irregularities due to turbulence. This idea is strengthened by a simultaneous set of observations which used broad beam antennas, admitting a much larger component of meteoric reflections. With the broad-beam antenna system, m was systematically lower, by 0.5 to 1, than the values obtained for the narrow beam system. Incidentally, much greater attenuation during SID's was observed using the broad-beam antennas.

The exponents were somewhat higher than given by theories for the turbulence inertial range, but were much smaller than for the dissipation range.

4.2 Angular Spectrum

Angular spectrum, as has been indicated by relation (1), is also closely related to the frequency dependence and spectrum of scale sizes.

Hagfors[16] has measured directly the complex spatial correlation coefficient for the downcoming scattered signal, using a method whereby it was possible, in principle, to separate the two main signal components of the VHF forward scatter signal. From the Fourier transform of the correlation coefficient he obtained the angular power spectrum, from which he deduced a value of 9 for the exponent of the wavenumber K. It was concluded that the spectrum of electronic irregularities in the wavenumber region near 1/3 m^{-1} is given by

$$S(K) = \frac{1}{K^9} .$$

Hagfors's value is somewhat higher than is given by the frequency-dependence results, which he attributes to more effective separation of the two signal components by his analysis. He concludes also that for the rather high latitude path from Kjeller-Troms ø that the contribution of meteor bursts to the total scattered power is rather small.

Bowles[13], in mid-USA, observed D-scatter at 41 MHz at vertical incidence with intensity corresponding to a 7th power law.

There were three other kinds of angular spectrum observations made, only one of which was quantitative. Pineo[17], using pulse observations at spaced stations along the great circle, deduced a 6th power angular dependence. He found, in another series of observations in mid-USA, using three CW transmissions aimed along the great circle and 7° either side, that the off-path (meteoric) contributions were dominant for about two-thirds of the day.

Observations at Boulder (Cottony[18]), using a pencil-beam rapid-scanning antenna, gave pictures such as Figure 2. Here an electronic scanning antenna, of one-degree horizontal beamwidth, scans the scattering volume to illustrate angular power spectrum directly. In the upper frame, we see the situation where the scattering volume is illuminated by a 6°-beam transmitting antenna. The receiver scans over about 80° of azimuth. In the lower frame the situation of broad-beam illumination by the transmitter is shown. These films integrate several minutes of reception at 20 scans per second. While the records were unfortunately not suitable for quantitative determination of angular spectrum, they did illustrate a very broad angular response consistent with a much smaller exponent than 9. Of course these observations include a strong meteoric component - one sees the systematic evening shift to the south of the great circle for this East-West path. It would, of course, be useful to separate by pulse modulation the angular spectra for the various height ranges and signal components.

5. GEOGRAPHICAL DEPENDENCE

So far we have discussed mainly mid-latitude VHF scatter, based on data obtained mostly in mid-USA and to some extent in the Arctic. Other mid-latitude and low-latitude observations were made, as well as equatorial and Arctic studies. Fortunately many of these used nearly identical techniques, so that some direct comparisons are possible.

5.1 Mid-latitudes and Low Latitudes

Goerke[19], studying paths at 50 MHz from England to Spain and Libya to Italy, found the scatter intensity and diurnal and seasonal variation in good agreement with simultaneous observations on mid-USA paths. While Isted[20] had earlier reported much weaker scatter, and meteoric-dependent distributions, Goerke showed the discrepancy was related to antenna patterns and path geometry. The Italy-Libya path at geomagnetic latitude 39°N, showed 4-5 dB weaker scattering compared to mid-USA - a trend later confirmed by low-latitude Western Pacific observations by Bain[21] (in preparation). Bain's studies within 10° of the geomagnetic equator found, along with weaker D-region scattering, field-aligned ionization at E-region height giving echo strength sensitive to the intensity of the horizontal field component. Propagation via the field-aligned ionization usually dominated, and communication capability was enhanced by use of appropriate antenna beams. Bateman et al.[22] had reported such scattering earlier, and Bowles et al.[23] described it in some detail from his near-equatorial observations. Bain[24] pointed out that while the SWF's and magnetic disturbances caused severe attenuation of the E-region field-aligned echoes, the D-scatter was unaffected during such times.

5.2 Equatorial Latitudes

Near the equator, a most comprehensive picture of VHF forward scatter is given by Cohen and Bowles[25]. During the IGY they set up several 50-MHz paths near and across the geomagnetic equator, instrumented much like the USA paths, to study scatter from the D- and E-regions; one long path was instrumented to study F-scatter. They identified D-region scattering comparable to that observed at temperate latitudes, perhaps somewhat stronger except right on the equator. But very strong scatter from the E-region almost always dominated. During the day, very intense scattering was continuously observed from the equatorial electrojet, usually 30 dB or more stronger than the usual D-scatter. At night, scatter from E irregularities, with some but not strict aspect sensitivity was observed.

They characterized the weakest VHF scatter signals near the equator as comparable to the strongest observed at temperate latitudes, and drew attention to their utility for communication. F-scatter was observed at night over the long path, though some 20 to 30 dB weaker than the E-scatter.

Flock and Balsley[26] recently studied the D-scatter with the high-power 50-MHz vertical-incidence radar. The scatter height was measured at 75 km, with a stratum present most of the daylight hours. An observation of fading rate, corresponding to that observed by Bowles[10] at 41 MHz at vertical incidence in Illinois, showed the same order of fading rate as observed at oblique incidence. Bowles's interpretation was that the principal component of turbulence velocity must be horizontal.

5.3 Auroral and Polar Latitudes

Studies at high latitudes, including auroral or polar behavior, have been from the beginning perhaps the most interesting.

It was early realized that auroral absorption events caused no observable attenuation of VHF scatter signals. Rather, generally strong scattering at 50 MHz correlated with periods of high attenuation observed at HF. This was observed in the first recordings (Bailey, et al.[4]) and was also reported by NDRE (Ref.27) in Norway.

However, Polar Cap Absorption (PCA) events, associated with solar proton influx, markedly affect high-latitude scatter propagation. In general absorption occurs by day and enhancement by night. Bailey[28] has used the VHF behavior during PCA's, simultaneous with riometer data, to provide one of the major sources of data on solar protons. Information is obtained on the influx of solar protons in the energy range 500 MeV down to 0.1 MeV, corresponding to the calculated cut-off energies for geomagnetic latitudes for the paths studied. This study has also shed additional light on the scatter, absorption, ionization and recombination processes at levels from 90 km down to 40 or 50 km in the Arctic.

From any of the transmission equations for scatter (Wheelon[29]) the scatter strength varies as the ambient, or as the average gradient, of electron density, independently of frequency. Thus, if the electron density is increased, as during a PCA event - or at lower latitudes during a solar flare - the signal intensity should increase. If, on the other hand, much of the abnormal ionization extends to heights below the main scattering level, absorption will occur - proportional to electron density but having about inverse square frequency dependence. Thus, for SID's, we have the observation of enhancement at the higher frequencies with corresponding attenuation at the lower (Blair et al.[15]). When PCA's occur during daytime the low-lying electron density may be great and the effect of absorption dominates. At night, when electron attachment occurs, the effect of enhanced scatter dominates. By using two frequencies and riometers these effects have been separated. The principal advantage of using the VHF scatter is its immunity to the auroral absorption at higher heights, which can affect the riometer. Also the night-time enhancements are observed with high sensitivity. Bailey has estimated daytime scattering heights at 70 to 75 km and night-time heights near 85 km, but direct height observations have not been made at high latitudes. Bailey[30] has more recently interpreted the scatter results to determine relativistic electron precipitation during events not explainable as proton events.

Now Forsyth[31] has classified a number of types of distinguishable *more intense* scatter echoes or events. He used broad-beam antennas and low power (100 watts). The system was sensitive mainly to enhanced scattering events rather than the continuous signal. Two distinct classes of echoes from field-aligned irregularities were observable at night, associated with aurora. The first is highly aspect-sensitive and rapidly fading. The second is less-aspect sensitive, so that it is seen at higher latitudes and more frequently. A third class of night-time echoes, called A3, seems to be common with an identified class of daytime scattering events. Forsyth attributes these echoes to

scattering from isotropic inhomogeneities of scale sizes of the order of meters, in the 70- to 90-km region, which contain peak electron densities of the order of 10^6 electron cm^{-3}.

Collins and Maynard[32], comparing simultaneous riometer and forward-scatter observations during high-latitude disturbances, have correlated strong scattering, particularly the A3 scattering, with absorption events.

6. COMMUNICATIONS APPLICATIONS

It remains to discuss communications applications and some outstanding research questions.

The continuity and character of the scatter signal make applications for reliable communication quite feasible.

The role once visualized for VHF scatter, i.e., to provide for reliable major trunk circuits as typified by the trans-Atlantic, trans-Pacific, and NATO European systems, has clearly been supplanted by cable developments and satellite services.

However, there seems a clear application for a few *teleprinter* circuits in remote areas, in the 1000-km to 2000-km range, where cables or satellites might not be economical. Indeed in any teleprinter application in this distance range where HF might be considered, VHF might be substituted with rewards in reliability and economy.

The Joint Technical Advisory Committee[33] summarized communication characteristics. The signal strength statistics are now well known for paths representative of most parts of the world. At 50 MHz, for example, 1-kW power and small antenna systems should provide at least 10 dB signal-to-noise ratio for a 100-Hz band during 99% of the hours in a year when the limiting noise is galactic. Frequency dependence of signal-to-noise ratio is given by an inverse 5th power, which allows for noise diminution with frequency. For practical purposes, the fading may be regarded as Rayleigh distributed, with a fading rate of about 1 Hz at 50 MHz. Meteor echoes and auroral signals produce multipath delays of the order of a few milliseconds relative to the first-arriving component. The signal strengths are sufficient to provide reliable teleprinter service. The signal is strong enough for telephony usually only in the daytime, except at the equator.

Only two really unique design problems are involved. The first concerns Doppler-shifted meteor echoes. The rapidly expanding trail can produce strong echoes, Doppler-shifted up to several kHz at 50 MHz, sufficient to cause errors in FSK systems using discriminators. To avoid this problem, operational systems use *dual narrow-band* filters, separated by at least 4 kHz. Other techniques have also been developed[34].

The second problem is long-delayed multipath echoes, from ground backscatter propagated by the F-region. Delays of 40 ms and greater are possible. The simplest protection is to use a frequency sufficiently high so that F-propagation rarely, if ever, occurs - say 50 MHz. Other special modulation techniques have been successful, but are more complicated.

The SHAPE Technical Centre work (Bartholomé[35]) has made it clear that 1 kW per teleprinter channel is more than sufficient, with present technology, for highly reliable 24-hour commercial service. Other digital coding developments of the past decade offer the possibility of further reductions of required power. One should consider 300 watts per 50-band channel a reasonable goal with presently available techniques. Bartholomé's work is further indication of the promise for low-power systems. He has developed two systems, one using the continuous ionospheric scatter and the other using intermittent meteor bursts - both tested over a 1000-km path between the Netherlands and the south of France, at frequencies near 40 MHz. These systems use ARQ, a synchronous system for error

detection and automatic feedback correction. The ARQ is linked with the diversity selection system. The system uses speeded-up transmission - with error detection and correction operative principally during the signal fades. By a 10% speed-up (90% duty cycle) the system maintains its regular information rate while recycling during the 10% of the time at the lowest part of the amplitude distribution of the fades. The meteor system operates in a similar way, though with a speed-up factor of 40, and duty cycle of 2.5%. Simple Yagi antenna systems are used. With 5 kW power for 4 teleprinter channels, an error rate of less than 1 per 3000 characters is maintained for 99.9% of the hours in a year. This application deserves some attention.

The Japanese have reported to CCIR[36] an experimental commercial circuit from Japan to Formosa, using 38 to 48 MHz. Ground backscatter has been encountered at the lower frequency. An experimental commercial circuit operated for a time between the Netherlands PTT and Italy.

7. RESEARCH

Low-power continuous digital communication at teleprinter speeds is a very attractive application, justifying further development for regions of the world where this may prove more economical than alternatives for 1000- to 2000-km links.

On the other hand, promising scientific use of VHF forward scatter lies in studies of the meteorology of the D-region. It would be especially valuable to extend the partial reflection work upward in frequency to embrace the scale sizes which have been observed at oblique incidence at VHF. Future measurements of angular dependence and wavelength dependence should carefully resolve the components at various heights, and should permit separation of the meteor echoes from scattering by irregularities.

Direct height measurements are needed. In high latitudes, especially, direct height observations would aid interpretation of the polar cap absorption events.

REFERENCES

1. Bailey, D.K., et al. — *A New Kind of Radio Propagation at Very High Frequencies Observable over Long Distances.* Physics Review, Vol.86, 1952, pp.141-145.

2. Booker, H.G.
Gordon, W.E. — *A Theory of Radio Scattering in the Troposphere.* Proceedings, Institute of Radio Engineers, Vol.28, April 1950, pp.401-412.

3. Eckersley, T.L. — *Studies in Radio Transmission.* Institution of Electrical Engineers, Vol.71, Sept.1932, pp.405-459.

4. Bailey, D.K., et al. — *Radio Transmission at VHF by Scattering and Other Processes in the Lower Ionosphere.* Proceedings, Institute of Radio Engineers, Vol.43, 1955, pp.1181-1231.

5. Gregory, J.B. — *A Review of Partial Reflections.* AGARD Proceedings, Sandfjord, Norway, 1968. (A paper in this volume.)

6. Wheelon, A.D. — *The Amplitude Distribution for Radio Signals Reflected from Meteor Trails.* Journal of Research, National Bureau of Standards, Vol.64D, Sept.-Oct.1960, pp.449-453.

7. Carpenter, R.J.
Ochs, G.R.
High Resolution Pulse Measurements of Meteor-Burst Propagation at 41 Mc/s over a 1295 km Path. Journal of Research, National Bureau of Standards, Vol.66D (Radio Propagation), No.3, 1962, 249-263.

8. Pineo, V.C.
Oblique-Incidence Measurements of the Heights at which Ionospheric Scattering of VHF Radio Waves Occurs. Journal of Geophysical Research, Vol.61, 1956, pp.165-169.

9. Kirby, R.C.
Extreme Useful Range of VHF Transmission by Scattering from the Lower Ionosphere. Institute of Radio Engineers National Convention Record, Part 1, 1958, pp.112-120.

10. Bowles, K.L.
Incoherent Scattering by Free Electrons as a Technique for Studying the Ionosphere and Exosphere: Some Observations and Theoretical Considerations. Journal of Research, National Bureau of Standards, Vol.65D (Radio Propagation), No.1, 1961, pp.1-14.

11. Gregory, J.B.
The Relation of Forward Scattering of Very High Frequency Radio Waves to Partial Reflection of Medium Frequency Waves at Vertical Incidence. Journal of Geophysical Research, Vol.62, 1957, pp.383-389.

12. Gregory, J.B.
Mesospheric Electron Densities at 43°S. Proceedings of the Conference on Ground-Based Radio Wave Propagation Studies of the Lower Ionosphere, Ottawa, Canada, 1967, pp.125-151.

13. Blair, J.C.
Private communication, 1961.

14. Belrose, J.S., et al.
A Critical Review of the Partial Reflection Experiment. Proceedings of the Conference on Ground-Based Radio Wave Propagation Studies of the Lower Ionosphere, Ottawa, Canada, 1967, pp.125-151.

15. Blair, J.C., et al.
Frequency Dependence of D-region Scattering at VHF. Journal of Research, National Bureau of Standards, Vol.65D (Radio Propagation), No.3, Sept.-Oct.1961, pp.249-263.

16. Hagfors, T.
On the Forward Scattering of Radio Waves in the Lower Ionosphere. Journal of Research, National Bureau of Standards, Vol.66D (Radio Propagation), No.4, 1962, pp.409-418.

17. Pineo, V.C.
Off Path Propagation at VHF. Proceedings, Institute of Radio Engineers, Vol.46, May 1958, p.922.

18. Cottony, H.V.
Wilson, A.C.
A High Resolution Rapid-Scan Antenna. Journal of Research, National Bureau of Standards, Vol.65D, 1961, pp.101-110.

19. Goerke, V.H.
Remmler, O.D.
VHF Ionospheric Scatter System Loss Measurements, European-Mediterranean Area. National Bureau of Standards, Technical Note 230, 1964.

20. Isted, G.A.
Analysis of Gibraltar-United Kingdom Ionospheric Scatter Signal Recordings. Proceedings, Institution of Electrical Engineers, Vol.104, Part B, 1958, p.2523.

21. Bain, Walter, F. — *Fourth Annual Report Long Range Data Analysis Program for the Pacific Ionospheric Scatter Communication Systems.* Vol.1 of 2. (In preparation.)

22. Bateman, R., et al. — *IGY Observations of F-layer Scatter in the Far East.* Journal of Geophysical Research, Vol.64, 1959, pp.403-405.

23. Bowles, K.L., et al. — *Radio Echoes from Field-Aligned Ionization above the Magnetic Equator and their Resemblance to Auroral Echoes.* Journal of Geophysical Research, Vol.65, 1960, pp.1853-1855.

24. Bain, Walter F. — *Solar Induced Effects on VHF Ionospheric Propagation at Low Magnetic Latitudes.* AGARDograph 59, pp.185-192, Pergamon Press, 1963.

25. Cohen, R.
Bowles, K.L. — *Ionospheric VHF Scattering near the Magnetic Equator during the International Geophysical Year.* Journal of Research, National Bureau of Standards, Vol.67D (Radio Propagation), No.5, 1963, pp.459-480.

26. Flock, W.L.
Balsley, B.B. — *VHF Radar Returns from the D-region of the Equatorial Ionosphere.* Journal of Geophysical Research, Vol.72, No.21, 1967, pp.5537-5541.

27. Ekre, H., et al. — *A Study of Ionospheric VHF Forward Scattering in High Latitudes.* Norwegian Defense Research Establishment, NDRE Report 27, 1958.

28. Bailey, D.K. — *Polar Cap Absorption.* Planetary Space Science, Vol.12, 1964, pp.495-541.

29. Wheelon, A.D. — *Relation of Turbulence Theory to Ionospheric Forward Scatter Propagation Experiments.* Journal of Research, National Bureau of Standards, Vol.64D, 1960, pp.301-309.

30. Bailey, D.K., et al. — *Characteristics of Precipitated Electrons Inferred from Ionospheric Forward Scatter.* Journal of Geophysical Research, Vol.71, 1966, pp.5179-5182.

31. Forsyth, P.A. — *VHF Forward Scatter.* Proceedings of the Conference on Ground-Based Radio Wave Propagation Studies of the Lower Ionosphere, Ottawa, Canada, December 1967.

32. Collins, C.
Maynard, L.A. — *Simultaneous VHF Riometer and Forward-Scatter Observations of the Disturbed Lower Ionosphere.* In "Ionospheric Radio Communications", NATO Institute on Ionospheric Radio Communications in the Arctic, Proceedings, edited by Kristen Folkestad, Plenum Press, New York, 1967, pp.155-164.

33. Joint Technical Advisory Committee — *Radio Transmission by Ionospheric and Tropospheric Scatter.* Proceedings, Institute of Radio Engineers, Vol.48, 1960, pp.4-44.

34. Koch, J.W. — *Factors Affecting Modulation Techniques for VHF Scatter Systems.* Institute of Radio Engineers, Transactions, Communication Systems, CS-7, 1959, pp.77-92.

35. Bartholomé, P.J. *Survey of Ionospheric and Meteor Scatter Communications.* In "Ionospheric Radio Communications", NATO Institute on Ionospheric Radio Communications in the Arctic, Proceedings, edited by Kristen Folkestad, Plenum Press, New York, 1967, pp.143-154.

36. *Echo Signals in the Ionospheric Scatter Circuit between Japan and Taiwan.* Doc. VI/51-E of the CCIR Interim Meetings, 1968, Boulder, Colorado (document submitted by Japan).

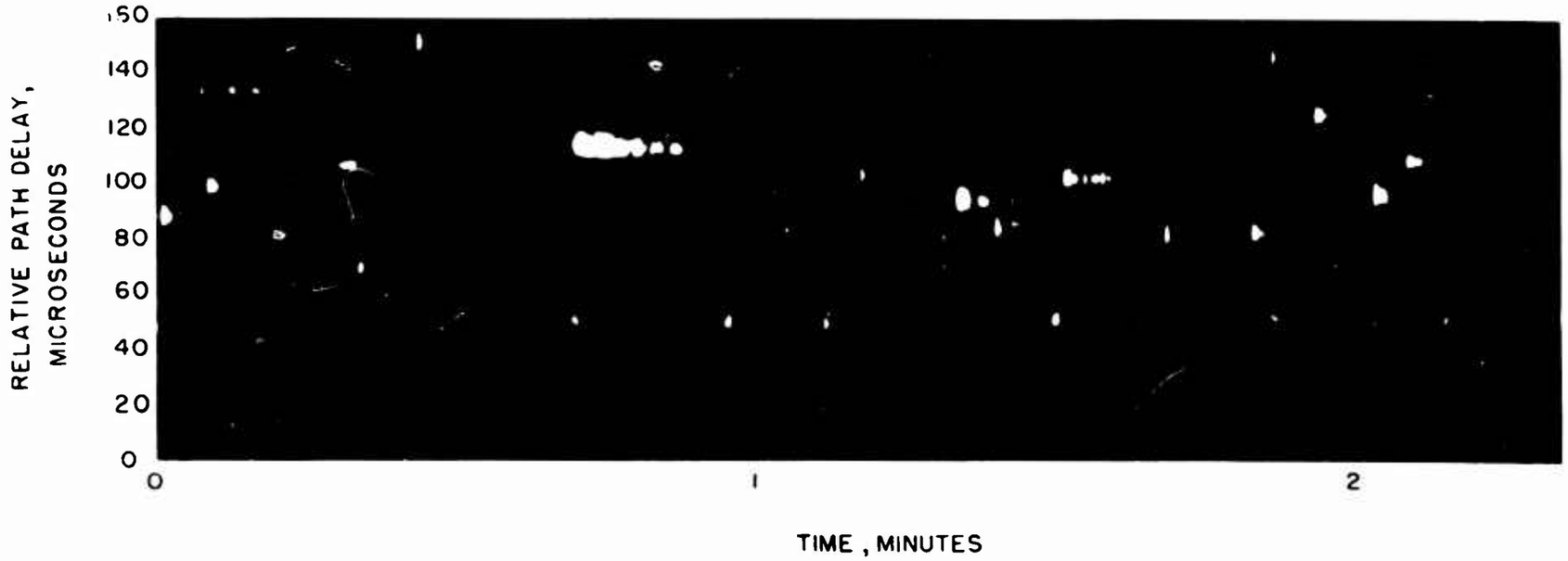


Fig. 1 Sample of record showing ionospheric scatter signal.

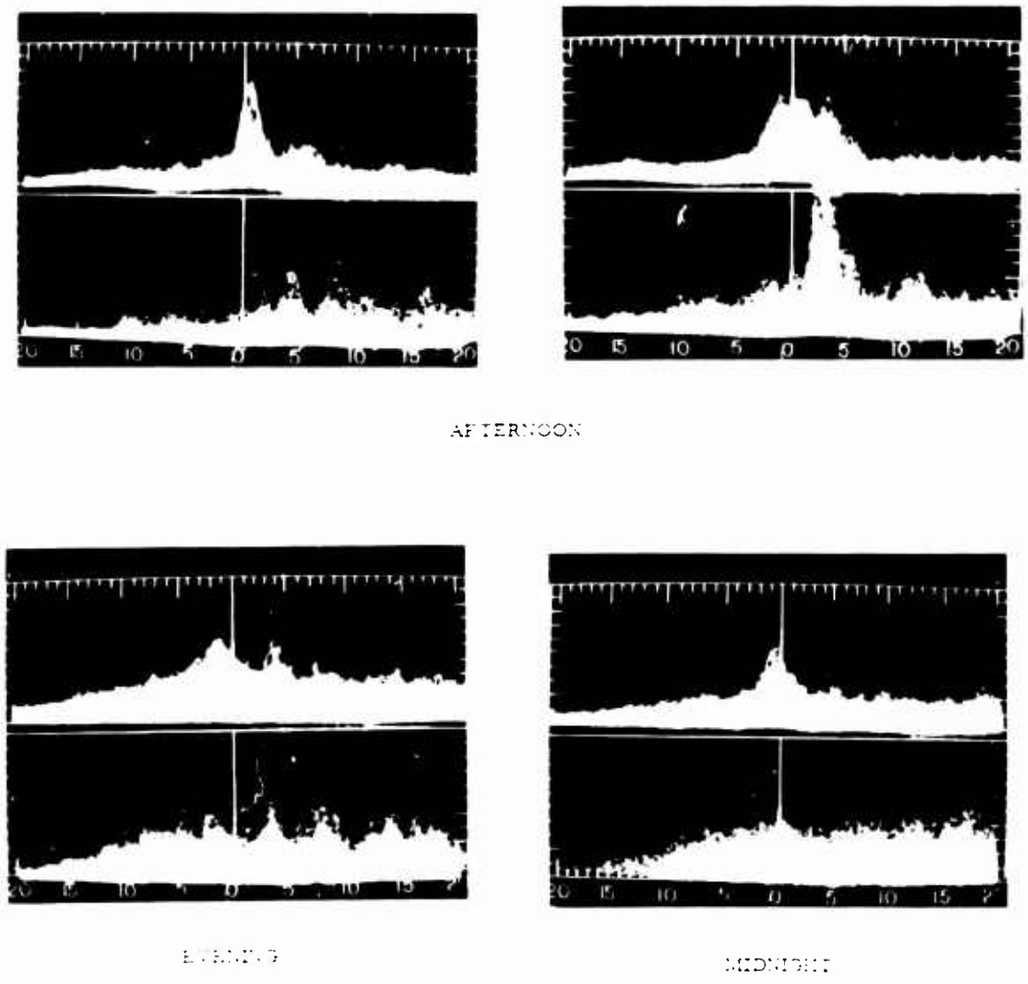


Fig. 2 Angle of arrival characteristics observed with scanning antenna, one-minute photographic integration of signal amplitude versus azimuth relative to great-circle bearing to transmitter; scanning at receiver by $1\frac{1}{2}^{o}$ beam; upper trace for narrow (6^{o}) beam transmitting, lower trace for broad beam (60^{o}) transmitting; frequency 40 Mc/s, East-West 1295 km path

ELECTROMAGNETIC SCATTERING FROM A PLASMA SLAB HAVING LARGE SCALE, RANDOM ELECTRON DENSITY FLUCTUATIONS

by

Adolf R. Hochstim* and Charles P. Martens

Institute for Defense Analyses,
Arlington, Virginia, USA

* Present address: Wayne State University, Detroit, Michigan, USA

SUMMARY

Calculations are made of the energy reflected when a plane electromagnetic wave is incident normally upon a plane parallel plasma slab having random amplitude, step-function fluctuations of electron density. A statistical averaging method and the first-order Born approximation are used to obtain an expression for the component of the mean reflection coefficient which is due to the random fluctuations. This expression is evaluated for exponential and uniform distributions of the step-function lengths in the case of an underdense, collisionless plasma having large scale fluctuations of electron density. The results are compared with those obtained using the first-order Born approximation, evaluated by means of the power spectrum of the fluctuations, and with the exact calculations from a computer model of the scattering by a random slab. It is shown that, for these cases when the correlation length is large (i.e., few correlation lengths in a slab) the first Born approximation using the power spectrum method deviates appreciably from an exact calculation. The statistical averaging method, or equivalently the use of the correlation function, gives improved results over the power spectrum method.

ELECTROMAGNETIC SCATTERING FROM A PLASMA SLAB HAVING LARGE SCALE, RANDOM ELECTRON DENSITY FLUCTUATIONS

Adolf R. Hochstim and Charles P. Martens

1. INTRODUCTION

In this paper, the authors consider the problem of determining the reflection coefficient using the first-order Born approximation when a plane electromagnetic wave is normally incident upon a plane parallel, random plasma slab. We write the total electron density as

$$N_e(x) = \langle N_e \rangle + N_e'(x) \ ,$$

where the angular brackets indicate the average value over an ensemble of slabs and N_e' is the random component of N_e. We can also write N_e in terms of a normalized fluctuating component, $\eta'(x)$, where

$$\eta'(x) = \frac{N_e'(x)}{\langle N_e \rangle} \ ,$$

so that

$$N_e(x) = \langle N_e \rangle [1 + \eta'(x)] \ .$$

It will always be assumed in this paper that $\langle N_e \rangle$ is constant throughout the slab and that there are no collisions.

If E_0 and E_R are respectively the amplitudes of the waves which are incident upon, and reflected from, the plamsa slab, then the reflection coefficient is defined to be

$$R = E_R E_R^* / E_0 E_0^* \ .$$

The mean reflection coefficient, averaged over an ensemble of random slabs, can be written as

$$\langle R \rangle = R_0 + \langle R' \rangle \ ,$$

where R_0 is the component due to the homogeneous slab and $\langle R' \rangle$ is due to the random fluctuations in electron density.

2. FIRST BORN APPROXIMATION EXPRESSION FOR $\langle R' \rangle$

Let the plasma slab be divided into n regions (Fig.1) and let the fluctuating component of the total electron density be constant in each of these regions (since the unperturbed slab is homogeneous, the total electron density is also constant in each region).

The i^{th} region is of length l_i and extends from x_{i-1} to x_i, where

$$x_j = \sum_{i=1}^{j} l_i \ .$$

Since the slab is of thickness d ,

$$d = x_n = \sum_{i=1}^{n} l_i \ .$$

η_i' and k_i are the normalized fluctuating electron density and wavenumber of the i^{th} region, respectively.

Using the first-order Born approximation, the reflection coefficient R can be calculated for a slab, assuming for the moment that η_j', l_j (j = 1, 2, ..., n) and n are fixed. This expression can then be averaged over all possible values which the η_j', l_j and n can assume to give $\langle R'^{(B1)} \rangle$, which is the first-order Born approximation to $\langle R' \rangle$. The authors have derived[1] this expression as

$$\langle R'^{(B1)} \rangle = \frac{1}{4}\left(\frac{\omega_p}{\omega}\right)^4 \left\{ \frac{1}{4}\left\langle (\eta_1')^2 + (\eta_n')^2 - 2\eta_1'\eta_n' \cos 2k_j d \right\rangle + \frac{1}{4}\left\langle \sum_{j=1}^{n-1} (\alpha_j)^2 \right\rangle + \langle S_1 \rangle + \langle S_2 \rangle \right\} \ , \tag{1}$$

where

$$S_1 = \frac{1}{2}\sum_{j=1}^{n-1} \alpha_j \left[\eta_1' \cos 2k_0 x_j - \eta_n' \cos 2k_0 (d - x_j) \right] \tag{2}$$

$$S_2 = \frac{1}{4}\sum_{\substack{j=1 \\ j \neq r}}^{n-1} \sum_{r=1}^{n-1} \alpha_j \alpha_r e^{i 2k_0 (x_j - x_r)} \ . \tag{3}$$

ω_p = root mean square plasma frequency = $\sqrt{(4\pi e^2 \langle N_e \rangle / m_e}$

ω, k_0 = angular frequency and wavenumber of incident radiation, respectively.

$\alpha_j = \eta_{j+1}' - \eta_j'$

3. EVALUATION OF $\langle R'^{(B1)} \rangle$ FOR RANDOM AMPLITUDES FLUCTUATION USING STATISTICAL AVERAGING

In this section we evaluate Equation (1) for $\langle R'^{(B1)} \rangle$, using the assumption that the amplitudes of the electron concentrations η_j' (j = 1, 2, ..., n) are independent, identically distributed random variables. We also assume that the l_j are independent and identically distributed and that the distribution of the amplitudes is independent of the distribution of the widths (see Figure 2). Since the η_j' are independent, averaging over the distribution of η' gives

$$\langle \eta_i' \eta_j' \rangle_\eta = \zeta^2 \delta_{ij} \ , \qquad i, j = 1, 2, \ldots, n) \ , \tag{4}$$

where δ_{ij} has the usual meaning

$$\delta_{ij} \begin{cases} = 0 & \text{for } i \neq j \\ = 1 & \text{for } i = j \end{cases}$$

and $$\zeta^2 = \langle (\eta')^2 \rangle \quad . \tag{5}$$

In terms of the probability density for η', $P'(\eta')$, the average over $(\eta_1')^2$ means

$$\zeta^2 = \langle (\eta_1')^2 \rangle_\eta = \int_{-\infty}^{\infty} P'(\eta')(\eta')^2 \, d\eta' \; ; \tag{6}$$

The limits of integration in reality extend from the lowest to the highest fluctuation.

We proceed to evaluate various quantities. First,

$$\left\langle (\eta_1')^2 + (\eta_n')^2 - 2\eta_1' \eta_n' \cos 2k_0 d \right\rangle_\eta = 2\zeta^2 \quad . \tag{7}$$

Averaging over the distribution of η' and l

$$\left\langle \sum_{j=1}^{n-1} (\alpha_j)^2 \right\rangle_{\eta,\, l} = 2(\langle n \rangle_l - 1)\zeta^2 \quad . \tag{8}$$

From Equation (2), with $\alpha_j = \eta_{j+1}' - \eta_j'$, and using Equation (4),

$$\langle S_1 \rangle_\eta = \tfrac{1}{2}\left[- \langle (\eta_1')^2 \rangle_\eta \cos 2k_0 x_1 - \langle (\eta_n')^2 \rangle_\eta \cos 2k_0 (d - x_{n-1}) \right] \quad , \tag{9}$$

where the only contributions to the sum result from the $j = 1$ and $j = n-1$ terms.

Equation (9) can be written as

$$\langle S_1 \rangle_\eta = - \tfrac{1}{2} \zeta^2 [\cos 2k_0 l_1 + \cos 2k_0 l_n] \quad . \tag{10}$$

Averaging over the distribution of widths gives

$$\left.\begin{aligned} \langle S_1 \rangle_{\eta, l} &= - \tfrac{1}{2}\zeta^2 [\langle \cos 2k_0 l_1 \rangle_l + \langle \cos 2k_0 l_n \rangle_l] \\ &= - \tfrac{1}{2}\zeta^2 [2 \langle \cos 2k_0 l_j \rangle_l] = - \zeta^2 W_1 \; . \end{aligned}\right\} \tag{11}$$

where

$$W_1 \equiv \langle \cos (2k_0 l_j) \rangle = \int_0^d P(l) \cos (2k_0 l) \, dl \quad . \tag{12}$$

From Equation (3),

$$S_2 = \frac{1}{4} \sum_{j=1}^{n-1} \sum_{\substack{r=1 \\ (j \neq r)}}^{n-1} \alpha_j \alpha_r \cos 2k_0 (x_j - x_r) \quad .$$

Since

$$\langle \alpha_j \alpha_r \rangle_\eta = \left\langle \eta_{j+1}' \eta_{r+1}' - \eta_{j+1}' \eta_r' - \eta_j' \eta_{r+1}' + \eta_j' \eta_r' \right\rangle \quad , \tag{13}$$

the only contributions to $\langle S_2 \rangle_\eta$ will come from the terms containing $\eta_j' \eta_{r+1}'$ when $r = j - 1$ and terms $\eta_{j+1}' \eta_r'$ when $r = j + 1$. Summing the slanting row which is parallel to, and immediately adjacent to, the principal diagonal lines of the

$$C_{jr} = \alpha_j \alpha_r \cos [2k_0 (x_j - x_r)]$$

matrix, since $C_{jr} = C_{rj}$, gives

$$\left.\begin{aligned} \langle S_2 \rangle_\eta &= \frac{1}{4}\, 2 \sum_{j=2}^{\eta=j} \langle \alpha_j \alpha_{j-1} \rangle_\eta \cos 2k_0 (x_j - x_{j-1}) \\ &= -\frac{1}{2}\,\delta^2 \sum_{j=2}^{\eta=j} \cos 2k_0 l_j \end{aligned}\right\} \tag{14}$$

and

$$\langle S_2 \rangle_{\eta, l} = -\frac{1}{2}\,\delta^2 \sum_{j=2}^{\eta=j} \langle \cos 2k_0 l_j \rangle_l = -\tfrac{1}{4}\zeta^2 (\langle n \rangle_l - 2) W_1 \quad . \tag{15}$$

Substituting Equations (7), (8), (11), and (15) into Equation (1), with $\langle n \rangle_l = d/\langle l \rangle$, gives

$$\left\langle R'^{(B1)} \right\rangle_{\eta, l} = \frac{1}{8}\left(\frac{\omega_p}{\omega}\right)^4 \zeta^2 \frac{d}{\langle l \rangle}\left\{1 - W_1\right\} \quad . \tag{16}$$

Since $-1 \leq W_1 \leq 1$, the maximum contribution to the mean reflection coefficient due to the random fluctuations is

$$\left\langle R'^{(B1)} \right\rangle^{\max}_{\eta, l} = \frac{1}{4}\left(\frac{\omega_p}{\omega}\right)^4 \zeta^2 \frac{d}{\langle l \rangle} \quad , \tag{17}$$

which is independent of the distribution of widths.

4. RELATIONSHIP BETWEEN STATISTICAL AVERAGING AND POWER SPECTRUM METHODS

An alternative and widely used method (see also Reference 1) of calculating $\langle R'^{(B1)} \rangle$ utilizes the power spectrum of the electron density fluctuations, $\Phi(\kappa)$. The result, when $d/l \gg 1$, is

$$\left\langle R'^{(B1)} \right\rangle = \frac{k_0^2}{4}\left(\frac{\omega_p}{\omega}\right)^4 \zeta^2 d\, \Phi(2k_0) \quad . \tag{18}$$

In order to relate the expressions (16) and (18), we calculate $\langle R'^{(B1)} \rangle$ using each for the case when

$$P(l) = \left\{\begin{aligned} &\frac{e^{-l/\bar{l}}}{\bar{l}(1 - e^{-d/\bar{l}})} \quad , && 0 \leq l \leq d \\ &0 \quad , && d < l \quad . \end{aligned}\right. \tag{19}$$

When $d/\bar{l} \gg 1$, then $\langle l \rangle \simeq \bar{l}$ and

$$P(l) \simeq \frac{1}{\bar{l}} e^{-l/\bar{l}} \quad . \tag{20}$$

Under these conditions

$$\Phi(\kappa) = \frac{2\bar{l}}{1 + (\kappa \bar{l})^2} \tag{21}$$

giving, from Equation (18),

$$\langle R'^{(B1)} \rangle = \frac{k_0^2}{2}\left(\frac{\omega_p}{\omega}\right)^4 \frac{\zeta^2 d\bar{l}}{1+(2k_0\bar{l})^2} \quad . \tag{22}$$

Using Equation (2) in Equation (17) gives, for W_1 ,

$$W_1 \simeq \frac{1}{1+(2k_0\bar{l})^2} \tag{23}$$

which, when substituted into Equation (16), gives Equation (22). Thus, the power spectrum and statistical averaging methods give equivalent results when $d/\bar{l} \gg 1$.

A method somewhat similar to the use of the power spectrum is to substitute $\zeta^2 Q_2(\tau)$ for $\langle \eta'(x)\eta'(x+\tau)\rangle$ directly into the expression for $\langle R'^{(B1)}\rangle$, where $Q_2(\tau)$ is the two-point correlation function and integration is carried out over the range $0 < x < d$. The correlation function corresponding to the power spectrum (21) is (the correlation length $a = \bar{l}$)

$$Q_2(\tau) = e^{-|\tau|/\bar{l}}$$

and, when this function is used in the above procedure, the result for $\langle R'^{(B1)}\rangle$ is

$$\langle R'^{(B1)}\rangle = \left(\frac{\omega_p^2}{2k_0c^2}\right)^2 \zeta^2 \left\{ \frac{2\gamma d}{\gamma^2+(2k_0)^2} - \frac{2[\gamma^2-(2k_0)^2]}{[\gamma^2+(2k_0)^2]^2} + \right.$$

$$\left. + 2e^{-\gamma d}\, \frac{[\gamma^2-(2k_0)^2]\cos(2k_0 d) - 4\gamma k_0 \sin(2k_0 d)}{[\gamma^2+(2k_0)^2]^2} \right\} \tag{23a}$$

where $\gamma = 1/\bar{l}$. This expression represents an improvement over Equation (22), and reduces in the limit of $d/\bar{l} \gg 1$ to the latter. For the cases studied in Figures 3 and 4, Equation (23a) and Equation (16) gave the same result.

5. DISCUSSION OF RESULTS

In order to study the usefulness of Equation (16) under conditions when Equation (18) would not be expected to be valid, calculations were made for the case when $\omega_p/\omega = 0.05$, $\nu/\omega = 0.0$ and $d/\langle l\rangle = 2.0$, i.e., for an underdense, collisionless plasma having large scale fluctuations in electron density. Calculations were made using the exponential distribution of lengths (Equation (19)), and a uniform distribution

$$P(l) = \begin{cases} 1/d \ , & 0 \leq l \leq d \\ 0 \ , & d < l \ . \end{cases} \tag{24}$$

The latter gives a power spectrum

$$\Phi(\kappa) = d\left[\frac{\sin \kappa d/2}{\kappa d/2}\right]^2 \quad . \tag{25}$$

In both cases the slab thickness was $d = 2\langle l\rangle$ and the incident wavenumber was $kd = 200\pi$. Figures 3 and 4 show the comparison of $\langle R'^{(B1)}\rangle$ calculated using Equations (16) and (18) (with the appropriate power spectra). Also shown are the exact values of $\langle R'\rangle$ calculated using the method of computer modeling of the electromagnetic scattering by a random plasma slab[1]. The figures show that in both cases the statistical averaging method (or equivalently using the correlation function) gives improved results over the power spectrum method.

In fact, the latter method gives $\langle R'^{(B1)} \rangle = 0$ for the case in which the uniform distribution of lengths was used, whereas both of the other methods give finite results.

Compared to the corresponding cases with a small correlation length ($d \gg a$), in which the agreement with the first Born approximation for an underdense plasma and small fluctuations was very good[1], we see that, with a large correlation length (e.g., $a = d/2$), the first Born approximation using the power spectrum method deviates appreciably. An improvement can be obtained in the first Born approximation by using the corresponding correlation function.

ACKNOWLEDGMENT

This research was supported by the Advanced Research Projects Agency through Project DEFENDER.

REFERENCES

1. Hochstim, A.R., Martens, C.P., *Electromagnetic Scattering from Random Plasma Slabs.* Proceedings of the Symposium on Turbulence of Fluids and Plasmas, MRI Symposia Series, Vol. 18 (to be published by Polytechnic Press, Brooklyn, NY).

2. Booker, H.G., *Radio Scattering in the Lower Ionosphere.* Journal of Geophysical Research, Vol. 64, 1959, p. 2164.

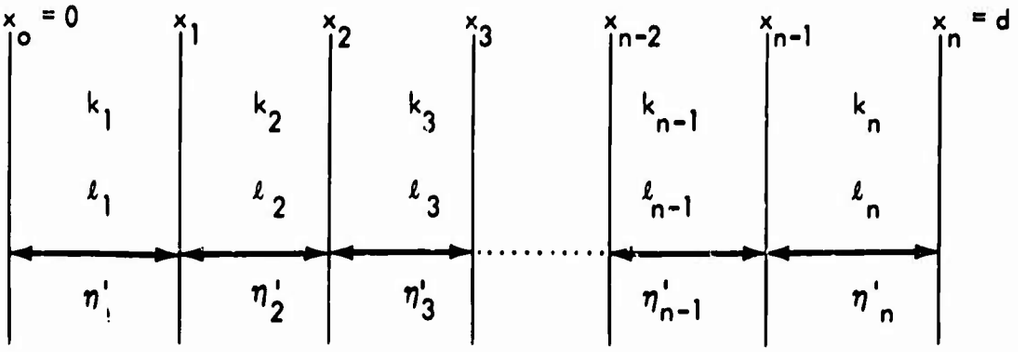
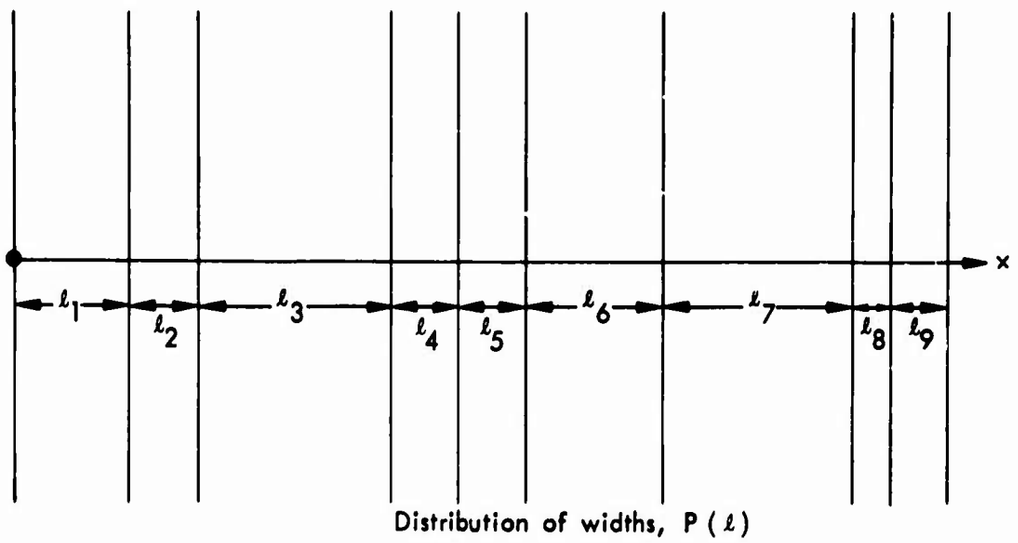


Fig. 1 Plasma slab



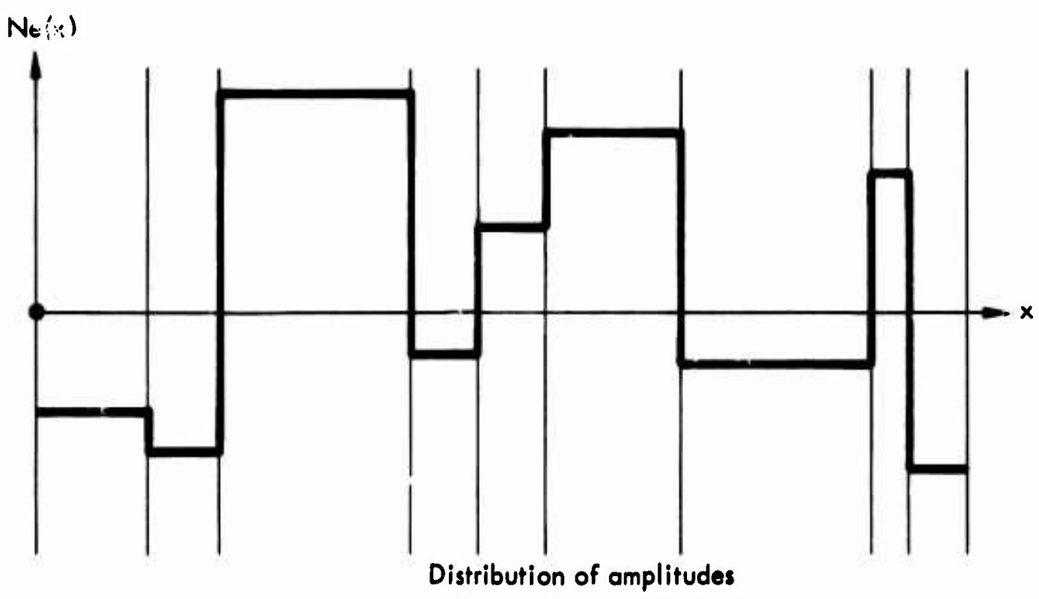


Fig. 2 Step function-shape random amplitude profile of electron concentration, illustrated for the case of nine fluctuation regions

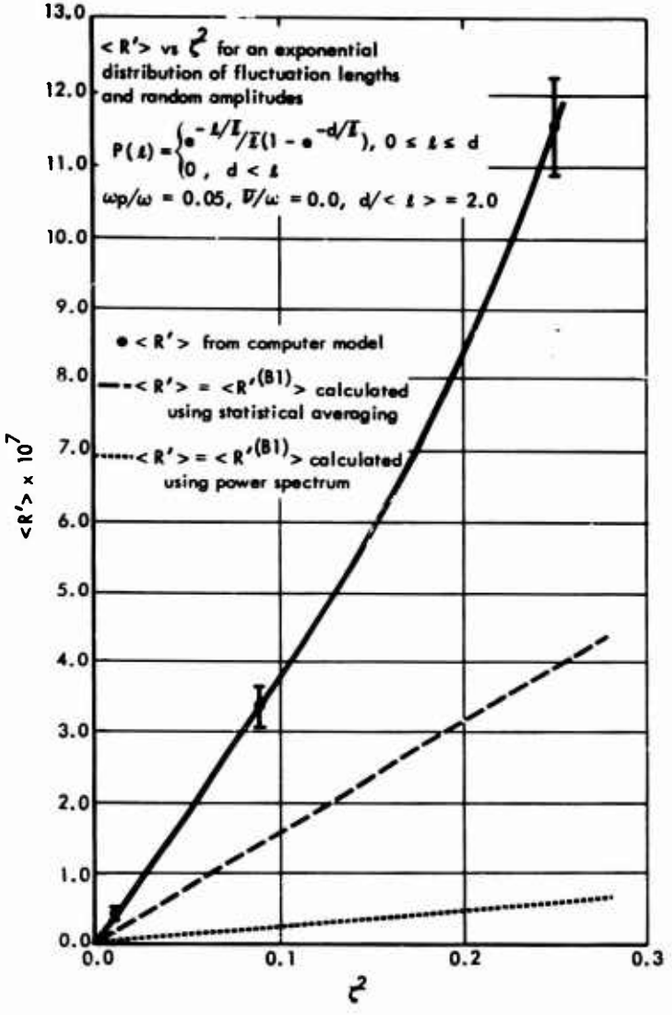


Fig.3 ⟨R′⟩ versus ζ^2 for an exponential distribution of fluctuation lengths and random amplitudes

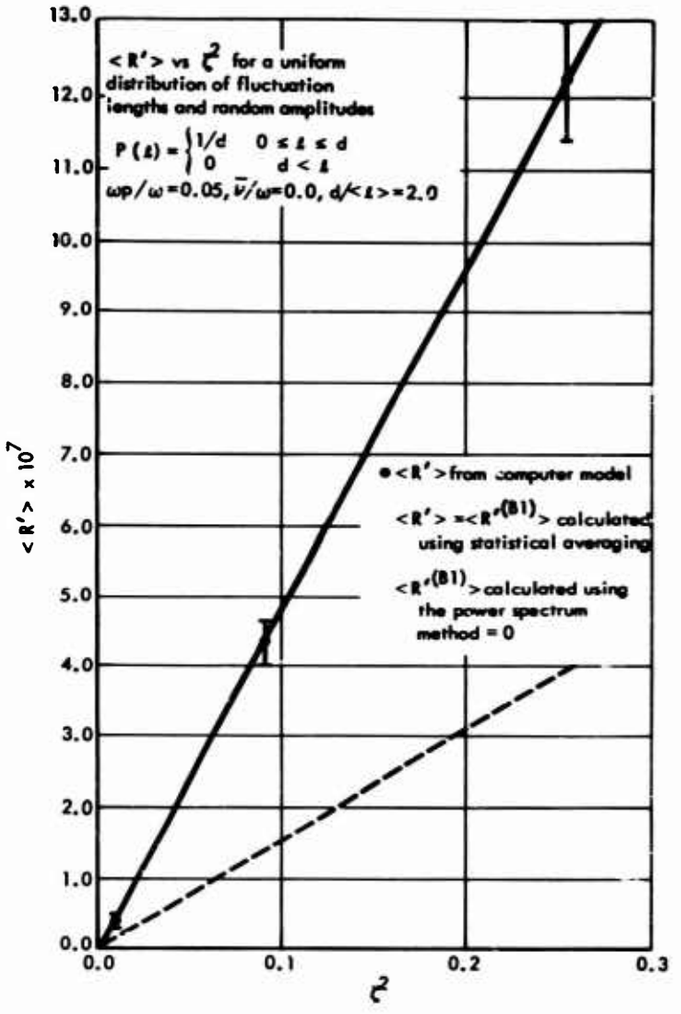


Fig.4 ⟨R′⟩ versus ζ^2 for a uniform distribution of fluctuation lengths and random amplitudes

CONTROLLABILITY ASPECTS OF SCATTER PROPAGATION OF RADIO WAVES

by

M. Z. von Krzywoblocki

Michigan State University, USA

SUMMARY

In the first part the author discusses the main aspects of the statistical theory of the locally isotropic turbulence in the Kolmogorov formulation and in the second he presents the main formalism (equations) of the scattering of electromagnetic waves due to turbulence. The next part contains the scattering of electromagnetic waves in a plasma. The main aspects of the mathematical formalism are presented as briefly as possible on an example of a scattering of transverse waves in a plasma. An analogous procedure is applicable to many other types of scattering in plasma: scattering by incoherent, coherent, Langmuir, low-frequency fluctuations, etc. The next part briefly presents the main aspects of the scatter propagation on very high frequencies due to irregularities in the D-region, F-scatter, tropospheric and ground scatter, etc., and on low and very low frequencies. The presently used techniques of selecting the optimum working frequencies (FOT) for various types of scatter propagation of radio waves are usually based on some kind of statistical approach. Is it possible to propose a formalism which is mathematically stronger than the one presently available which would allow one to select the FOT in various kinds of scatter propagation? The author attempts to answer this question in as simple a manner as possible, avoiding the heavy and deep mathematical formalism and restricting himself to presenting only the final results. At first, the author briefly presents the fundamentals of the optimization theory emphasizing the control functions and the functional which must be optimized. As the control functions given in certain definite regions one may choose the frequency, the amplitude, and the wave vector (or the energy) of the incident wave (sent from the earth or satellite or any other stations moving or being at rest somewhere, including the moon), one or more of them. This review shows that these functions are sufficient for such purposes. Next, the author proposes the following scheme of the controllability of the scatter propagation (the example given below is only for illustrative purposes; some other criteria may be chosen, as well). Given the Maxwell system describing the scatter propagation phenomenon and the expression for the scattering cross-section in the scattering volume in the form of an integral, the problem is to solve the Maxwell system under the restrictive condition that the scattering cross-section should be the minimum. The chosen control functions (the characteristic parametric variables of the sending station) are varied so that the solution of the system furnishes the sought optimum of the integral. This gives the optimum values of the parametric variables of the sending station and allows one to control the scatter propagation of radio waves.

CONTROLLABILITY ASPECTS OF SCATTER PROPAGATION OF RADIO WAVES

M. Z. von Krzywoblocki

1. STATISTICAL THEORY OF ISOTROPIC TURBULENCE

1.1 General Remarks

The statistical theory of isotropic turbulence in incompressible media, originated by Taylor[1], developed by von Kármán[2], and von Kármán and Howarth[3], was systematized by Robertson[4] with the use of certain elementary results of the theory of invariant groups. The theory of the locally isotropic turbulence in incompressible media was originated and developed by Kolmogorov (described by Batchelor[5], Chandrasekhar[6], etc.). One can also mention the work of Loitsianskij[7] referring to the invariant disturbance moment in a homogeneous isotropic, turbulent flow of an incompressible, viscous fluid. Coburn[8] furnished a method for the construction of independent scalars in various types of homogeneous turbulence in incompressible fluids. The mathematical fundamentals of the statistical theory of turbulence in incompressible fluids were constructed by Kampé de Fériet[9] (the existence proof of the second-order-correlation tensor for homogeneous turbulence in incompressible fluids). There is also the work on homogeneous turbulence by Batchelor[5].

The first approach to the theory of turbulence (not a statistical theory of isotropic turbulence) of a compressible medium was probably that proposed by Keller and Friedman[10] in 1924. The basic statistical theory of isotropic turbulence in compressible media was developed years later by von Krzywoblocki[11]: the invariant theory of isotropic turbulence, locally isotropic turbulence, decay of turbulence in terms of vorticity, isotropic turbulence in magnetohydrodynamics of a compressible medium, locally isotropic turbulence in magnetohydrodynamics, independent scalars, turbulence in rarefied gases, proof of the existence of the second-order-correlation tensor for homogeneous turbulence in compressible fluids, etc.

1.2 Isotropic Turbulence Theory in Incompressible Fluids

In accordance with the notation used in previous papers, we denote all the quantities referring to the point P by u_i, i, p, etc., and those referring to the point P' by primes u_i', i', p', etc. As usual, it is assumed that the magnitudes at the point P are independent of the variations of the coordinates (x_k') of P' and vice versa. We introduce the following correlation functions:

$$\left.\begin{aligned} &u_1,\ u_1' \quad \text{velocity components parallel to } PP' = r; \\ &u_2,\ u_2' \quad \text{velocity components perpendicular to } PP'; \\ &\overline{u_1 u_1'} = \overline{u^2} f(r,t); \qquad \overline{u_2 u_2'} = \overline{u^2} g(r,t); \quad \text{etc.} \end{aligned}\right\} \tag{1}$$

The fundamental equation for the propagation of the velocity correlation function is derived from the equation of the conservation of momentum and is known as the Kármán-Howarth equation.

1.3 Locally Isotropic Turbulence

The main results of the Kolmogorov theory of locally isotropic turbulence are the following. Assume three points in the domain in question, P, P', P''; all the variables referring to the point P' are denoted by primes u_i', p', etc; those referring to the point P'' by double primes, etc. It is assumed that the variables at P are independent of the variations of x_k' and x_k'', and vice versa. The following vectors are used:

$$PP' = \xi(r) ; \qquad PP'' = \eta(r_2) ; \qquad P'P'' = \tau(r_3) \tag{2}$$

$$|PP'| = r ; \qquad |PP''| = r_2 ; \qquad |P'P''| = r_3 . \tag{3}$$

Let suffixes "d" and "n" denote components parallel and perpendicular to PP', respectively, and let us introduce symbols

$$B_{dd}(r) = \overline{(u_d' - u_d)^2} ; \qquad B_{nn}(r) = \overline{(u_n' - u_n)^2} . \tag{4}$$

The mean rate of dissipation of energy per unit mass of the fluid due to viscosity is

$$\epsilon = \nu \tfrac{15}{2} B_{dd,rr}(0) , \tag{5}$$

where ν is the kinematic viscosity. When the flow Reynolds number is very large, the amount of energy dissipated through viscosity by all except the very smallest eddies is infinitesimal compared with the amount of energy passed on to the next smaller set of eddies. Most of the sets of eddies pass on to their neighbors, in the direction of decreasing size, the same amount of energy in unit time equal to the energy dissipation. The motion due to the larger eddies should therefore be determined statistically by the quantity ϵ. The motion of the smaller set of eddies is determined by ϵ and ν, since these eddies dissipate through viscosity some of the energy they receive from their larger neighbors. The Kolmogorov first similarity hypothesis states that in locally isotropic turbulence the probability distributions defining the turbulence are uniquely determined by the quantities ϵ and ν (small eddies). The second Kolmogorov similarity hypothesis states that, if the spatial separation PP', PP'', etc. and their difference $P'P''$, etc., are large in magnitude compared with η, the resulting probability distribution defining the turbulence depends only on ϵ (large eddies). In 1962 Kolmogorov modified[12] his theory. Kumar[13], using the idea of the Kolmogorov modified theory, proposed the structure functions for velocity, temperature and pressure fields and Silverman[14] applied Oboukhov's[15] turbulent mixing theory to the radio scattering.

2. SCATTERING DUE TO TURBULENCE

2.1 Refractive Index

Tatarski[16] uses the concept of the locally isotropic turbulence and proposes the following form of the refractive index function, n, of the atmosphere:

$$n = C_n^2 r^{2/3} , \quad \text{for} \quad l_0 \ll r ; \qquad n = C_n^2 l_0^{2/3} (r/l_0)^2 , \quad \text{for} \quad r \ll l_0 , \tag{6}$$

$$C_n^2 = a^2 l_0^{4/3} M^2 , \qquad \text{where } a \text{ is a numerical constant} , \tag{7}$$

$$M = -79 \times 10^{-6} p T^{-2} (1 + 15{,}500\, q T^{-1}) \times \left[\frac{dT}{dz} + \gamma_a - 7800 (1 + 15{,}500\, q T^{-1})^{-1} \frac{dq}{dz} \right] , \tag{8}$$

where the symbols denote: l_0 = the geometrical dimensions of the smallest fluctuations occuring in the fluid, p = static pressure, T = temperature, z = altitude, $\gamma_a = 0.98^{\circ}/100\,m$ = the adiabatic temperature gradient, i.e., a rising elementary volume of air cools at 0.98° for 100m of elevation, q = specific humidity or the concentration of water vapor in the air, i.e., the ratio of the mass of water vapor to the mass of moist

air in a unit altitude. The refractive index of a medium, being defined as the ratio of the velocity of a wave in free space to its phase velocity in a medium, is $n = cu^{-1} = kc\omega^{-1}$, where $u = \omega k^{-1}$, k = wavenumber, and c = the velocity of light, and depends obviously upon the frequency ω. Assuming, for simplicity, that the dielectric is isotropic, the dielectric tensor reduces to a dielectric scalar κ. The square of the refractive index is equal to the dielectric scalar, $n^2 = \kappa$. Paul[17] obtained results different from those given in Equations (6) to (8), using new ideas and the approach of Kolmogorov[12] and Oboukhov[15]. Namely, the structure function of the refractive index can be written as

$$D(r) = C(X)\,\bar{N}\bar{\epsilon}^{-1/3} r^{2/3} (Lr^{-1})^{-k'} , \tag{9}$$

where $C(X)$ depends upon the macrostructure of the flow, k' is a universal constant, $\bar{N}$ is the rate at which the energy is dissipated in the smallest eddies and which is constant in the region which is small in comparison with the external scale L, $\bar{\epsilon}$ is the energy dissipation rate in the turbulent flow. For $-2/3 < k' < 4/3$, the structure turbulent function (9) implies that the one-dimensional spectral density at wavenumber k of the field has the form

$$E(k) = C_\delta k^{-(5/3+k')} , \tag{10}$$

$$C_\delta = \tfrac{1}{2}\Gamma(5/3+k')C(X) \sin\left(\frac{1}{3}+\frac{k'}{2}\right) \bar{N}\bar{\epsilon}^{-1/3} L^{-k'} . \tag{11}$$

2.2 Maxwell's Equations

We use the following symbols: (a) electric field: $\mathbf{E}$ = electric vector field intensity, κ = dielectric coefficient, $\mathbf{D} = \kappa\mathbf{E}$ = displacement vector field; (b) magnetic field: $\mathbf{H}$ = magnetic vector field, μ = permeability of the medium, $\mathbf{B} = \mu\mathbf{H}$ = magnetic induction; (c) current and charge: $\mathbf{J}$ = electric current density vector, σ = density of electric charge. The Maxwell Equations are

$$\text{(a)}\quad \operatorname{curl}\mathbf{H} = \frac{1}{c}\frac{\partial \mathbf{D}}{\partial t} + \frac{4\pi}{c}\mathbf{j}\,; \qquad \operatorname{div}\mathbf{B} = 0 \tag{12}$$

$$\text{(b)}\quad \operatorname{curl}\mathbf{E} = \frac{1}{c}\frac{\partial \mathbf{B}}{\partial t}\,; \qquad \operatorname{div}\mathbf{D} = 4\pi\sigma . \tag{13}$$

In our particular present case we assume $\mu = 1$, $\sigma = \mathbf{J}$ = conductivity = 0, κ is time independent. After a few operations, the system (12), (13), takes the form

$$\nabla^2\mathbf{E} + \operatorname{grad}(\mathbf{E}\cdot\operatorname{grad}\log_e\kappa) - \frac{1}{c^2}\kappa\frac{\partial^2\mathbf{E}}{\partial t^2} = 0 . \tag{14}$$

With

$$\mathbf{E} = \mathbf{E}_1 \exp(-i\omega t), \qquad k_1 = \omega c^{-1}, \; = \text{wavenumber} , \tag{15}$$

Equation (14) takes the form

$$\mathbf{E}_1 + \operatorname{grad}(\mathbf{E}_1\cdot\operatorname{grad}\log_e\kappa) + k_1^2\kappa\mathbf{E}_1 = 0 . \tag{16}$$

2.3 Formulation of the Problem and Solution

We formulate the problem in the following way. Consider a plane, monochromatic, electromagnetic wave incident upon a volume V of a turbulent medium (air or interstellar gas). Inside the volume V there is a turbulent mixing and irregular refractive index fluctuation which cause the scattering of the incident wave. The problem is to describe the characteristic features and properties of the scattering phenomenon. The total amplitude vector function $\mathbf{E}_1$ is decomposed into the amplitude of the electric vector of the incident

plane wave, $\mathbf{E}_{1i}$, and of the scattered wave, $\mathbf{E}_{1s}$, i.e., $\mathbf{E}_1 = \mathbf{E}_{1i} + \mathbf{E}_{1s}$, with the condition that the vector $\mathbf{E}_{1i}$ satisfies the equation

$$\nabla^2 \mathbf{E}_{1i} + k_1^2 \mathbf{E}_{1i} = 0 . \tag{17}$$

With $\kappa = n^2 = (1+n_1)^2$, the equation for $\mathbf{E}_{1s}$ has the form

$$\mathbf{E}_{1s} + k_1^2 [(2n_1 + n_1^2)\mathbf{E}_{1i} + (1+n_1)^2 \mathbf{E}_{1s}] + 2\,\mathrm{grad}\,[\mathbf{E}_{1i} \cdot \mathrm{grad}\,\log_e (1+n_1) + \mathbf{E}_{1s} \cdot \mathrm{grad}\,(1+n_1)] = 0 . \tag{18}$$

Tatarski[16] applies the expansion for $\log_e (1+n)$, assumes that

$$\mathbf{E}_{1s} = \mathbf{E}_1^{(1)} + \mathbf{E}_1^{(2)} + \ldots , \quad \mathbf{E}_1^{(1)} \sim n_1^2 ,$$

reformulates (18) with the assumption that the small perturbation technique is valid and obtains the equation for $\mathbf{E}_1^{(1)}$, which supposedly is small with respect to $\mathbf{E}_{1i}$. von Krzywoblocki[18] associates with (18) the equation of the Fredholm type and proposes a solution by means of the method of successive approximations of integral equations. A solution for $\mathbf{E}_{1s}$ depends primarily upon the parameters k_1, κ. The magnetic field is calculated in the similar way and again depends primarily upon k_1, κ. The intensity of scattering, i.e., the rate of energy flow in the scattering field (the density of flow of the scattered energy) is given by

$$\mathbf{S} = c(8\pi)^{-1} \Re e\,(\mathbf{E}_1 \times \mathbf{H}_1^{\star}) , \tag{19}$$

where $\mathbf{H}_1^{\star}$ is the conjugate and $\Re$ denotes the real part, with the terms referring to the incident wave excluded from $\mathbf{E}_1$. The density of the energy flow in a given direction $\mathbf{m}$ is equal to $\mathbf{S} \cdot \mathbf{m}$, and is denoted by S_m. With σ denoting the effective cross-section for scattering into the solid angle $d\Omega$ in the direction characterized by the unit vector $\mathbf{m}$, one obtains

$$d\sigma = 8\pi (cE_{0i})^{-2} \bar{S}_m r^2 d\Omega , \tag{20}$$

where E_{0i} is a part of the solution of (17) given by

$$\mathbf{E}_{1i} = \mathbf{E}_{0i} \exp (i\boldsymbol{l}_1 \cdot \mathbf{r}) ; \quad \mathbf{E}_{0i} = \text{constant} , \tag{21}$$

and $\boldsymbol{l}_1$ denotes the unit vector in the direction of the propagation of the incident plane wave, $\mathbf{r}$ is the observation vector, i.e., a vector from the origin of the coordinate system, usually Cartesian or any other orthogonal, to a point located inside the volume V where the scattering occurs. Usually the vector $\mathbf{r}$ is very large. The turbulence existing inside the volume V causes S_m to be a turbulent variable, Equation (19), and consequently $\bar{S}_m$ denotes the mean value of a turbulent variable, taken according to the rules of the theory of turbulence. The review first presented shows that the solutions depend upon the following parameters: $k_1 = \omega c^{-1}$, $\kappa = n^2$, and n is given by Equation (6) and discussed in the Section 2.1.

3. SCATTERING OF ELECTROMAGNETIC WAVES IN PLASMA

In a plasma different oscillations interact with one another during the process of propagation and this interaction leads to different processes of wave scattering and transformation in the plasma. The probabilities of such processes of scattering are determined by the level of the fluctuations in the plasma. Electromagnetic waves which propagate in a plasma may be scattered by thermal fluctuations. A spectrum of the fluctuations is characterized not only by the main maximum at low frequencies, but also by maxima at frequencies associated with the natural oscillations of the plasma. Due to this a combination (Raman) scattering may occur, accompanied by a change in the scattered wave frequency by an amount equal to the natural frequency of the plasma oscillations. It may

be accompanied by the incoherent scattering of the electromagnetic waves associated with the small changes in the frequencies. Also the interaction of the propagating waves with the fluctuating oscillations leads to mutual transformations of the waves. The intensities of the Raman scattering and of the wave scattering are determined by the magnitude of the fluctuations. The electromagnetic field in the plasma is usually governed by the system of kinetic equations for each species of particles, which constitute the plasma:

$$\mathbf{F}_t + \mathbf{v}\frac{\partial \mathbf{F}}{\partial \mathbf{r}} + \mathbf{m}^{-1}\mathbf{e}(\mathbf{E} + \mathbf{c}^{-1}\mathbf{v}\times\mathbf{H})\frac{\partial \mathbf{F}}{\partial \mathbf{v}} = 0 , \tag{22}$$

and the system of Maxwell's equations

$$\text{curl}\,\mathbf{E} = -\frac{1}{c}\frac{\partial \mathbf{H}}{\partial t}; \qquad \text{div}\,\mathbf{E} = 4\pi(\rho + \rho_0) \tag{23}$$

$$\text{curl}\,\mathbf{H} = -\frac{1}{c}\frac{\partial \mathbf{E}}{\partial t} + \frac{4\pi}{c}(\mathbf{j} + \mathbf{j}_0); \qquad \text{div}\,\mathbf{H} = 0 , \tag{24}$$

where ρ_0, $\mathbf{j}_0$ are the densities of the external charges and currents and ρ, $\mathbf{j}$ the densities of the induced charges and currents. This system may be simplified and reduced to the form

$$\text{curl curl}\,\mathbf{E} + c^{-2}\hat{\epsilon}\frac{\partial^2 \mathbf{E}}{\partial t^2} = 0 , \tag{25}$$

where $\hat{\epsilon}$ is the dielectric tensor of the plasma. The total electric field is $\mathbf{E}_t = \mathbf{E}_0 + \mathbf{E} + \mathbf{E}'$, where $\mathbf{E}_0$ is the field of the incident wave, $\mathbf{E}$ the fluctuation field, $\mathbf{E}'$ the field of the scattered waves. The field of the scattered waves is determined from

$$\text{curl curl}\,\mathbf{E}' + c^{-2}\hat{\epsilon}\frac{\partial^2 \mathbf{E}'}{\partial t^2} = -4\pi c^{-2}\frac{\partial \mathbf{J}}{\partial t} , \tag{26}$$

where $\mathbf{J}$ is the current due to the field $\mathbf{E}_0$ and $\mathbf{E}$. Let the incident wave be a plane monochromatic wave

$$\mathbf{E}_0(r,t) = \mathbf{E}_0 \exp[i(\mathbf{k}\cdot\mathbf{r}) - i\omega t] . \tag{27}$$

Consider, for illustrative purposes, the scattering of transverse waves in a plasma $[(\mathbf{k}\cdot\mathbf{E}_0) = 0, (\mathbf{k}\cdot\mathbf{E}') = 0]$. Having the expression for the current $\mathbf{J}$, we find the scattering intensity in the frequency range $d\omega'$ and the element of a solid angle $d\Omega'$:

$$dI = Vc(16\pi^2)^{-1}e^2m^{-2}c^{-4}(\omega'\omega^{-1})^2(\epsilon(\omega'))E_{0\perp}^2\langle\delta n^2\rangle_{\mathbf{q},\Delta\omega}\,d\omega'd\Omega' , \tag{28}$$

where

V = scattering volume

e = charge

m = mass of particle

$E_{0\perp}$ = component of E_0 at right angles to the vector $\mathbf{k}'$

$\epsilon(\omega') = 1 - \Omega^2\omega'^{-2}$

ω' = frequency of the scattered wave

$\mathbf{k}'$ = wave vector of the scattered wave

$k'^2 = (\omega'c^{-1})^2\epsilon(\omega')\Omega = (4\pi e^2 n_0 m^{-1})^{1/2}$, Langmuir frequency

n_0 = particle density

$\langle \delta n^2 \rangle_{\mathbf{q}, \Delta\omega}$ = so-called correlator of the density fluctuations where $\mathbf{q} = \mathbf{k}' - \mathbf{k}$, $\Delta\omega = \omega' - \omega$.

If the incident wave is unpolarized, then the mean value of the square of the field

$$E_{0\perp}^2 = \tfrac{1}{2}(1 + \cos^2\theta) E_0^2 ,$$

where θ is the scattering angle, i.e., the angle between the vectors $\mathbf{k}$ and $\mathbf{k}'$. Dividing the scattering dI (Equation (28)) by the flux density of the incident wave's energy,

$$S_0 (8\pi)^{-1} c [\epsilon(\omega)]^{1/2} E_0^2 ,$$

and the magnitude of the scattering volume, V, we find the scattering cross-section or the scattering coefficient $d\Sigma = (S_0 V)^{-1} dI$. In a similar way we may find the scattering coefficients in other cases of wave scattering and transformation of electromagnetic waves in a magnetoactive plasma: scattering and transformation of electromagnetic waves by incoherent fluctuations (fluctuations of the electron density); scattering and transformation of electromagnetic waves by coherent fluctuations (collective fluctuations); scattering and transformation of electromagnetic waves by Langmuir fluctuations (high-frequency fluctuations; the refractive index of the fluctuation Langmuir oscillation is much larger than unity, whereas the refractive indices of the incident and scattered waves are of the order of unity); scattering and transformation of electromagnetic waves by low-frequency fluctuations (Raman scattering can be produced by low-frequency magnetic-sound and Alfvén fluctuations); scattering and transformation of Langmuir waves in a magnetoactive plasma by incoherent fluctuations, and by coherent fluctuations; transformation of low frequency waves by Langmuir fluctuations in a magnetoactive plasma, etc.

4. SCATTER PROPAGATION ON VERY HIGH AND VERY LOW FREQUENCIES

4.1 Scatter Propagation on Very High Frequencies

Concerning the scatter propagation on very high frequencies, one may obtain practical information from collections of data on ionospheric radio propagation like those produced by Davies[21]. Ionospheric transmission of VHF (very high frequencies) is more the result of scattering of waves by irregularities in the electron density distribution in the ionosphere than the result of a gradual refraction. If sufficient and strong high transmitter powers are applied, then the net scattering due to electrons (quasi-incoherent scatter) can be determined. Reference 21 lists the following sources of the irregularities in the ionosphere: irregularities due to turbulent mixing in the D-region, ionized trails due to passing meteors, spread-F irregularities, sporadic E and individual electrons. The main advantages of VHF propagation given in Reference 21 are the low signal strengths, inefficiency of the scattering mechanism, rapid fading, limited ground range (~2000 km), and mutual interference between channels normally independent, etc. For illustrative purposes we quote below some formulas in particular cases of scattering[21]. The geometry of the forward scatter from the irregularities in the D-region is governed by the formula

$$p_a = p_t r_0^{-2} l^{-2} b A_r \operatorname{cosec}(\gamma/2) S(K) , \qquad (29)$$

where

p_a = available power from a receiving antenna

p_t = power radiated from the sending antenna in the direction of a volume "V" of the ionosphere illuminated by the transmitter

r_0 = electron radius (2.8×10^{-15} m)

l = distance from "V" to the receiving station

b = thickness of the scattering volume

A_r = effective area of the receiving antenna

γ = angle through which the scattering takes place

S(K) = spectrum of turbulent irregularities

and

$$K = 4\pi\lambda^{-1} \sin(\gamma/2) , \tag{30}$$

where λ is the wavelength. The formula (29) applies when the single scattering is the dominant mechanism (i.e., the amplitude of the twice-scattered wave is negligible) and for isotropic irregularities. The formulas emphasize the joint frequency-distance dependence of the received power which is characteristic of scatter propagation, and shows that the spectrum of irregularities is the basic description of the turbulent electron density variations. In the case of turbulent mixing Davies[21] recommends

$$S(K) = K^{-n}(dN/dh)^2 , \tag{31}$$

where dN/dh is the electron density gradient. The relationship of the system loss to the frequency f and the geometry of the propagation path is given by

$$p_t p_a^{-1} \sim l^2 f^{n_s} (\sin\gamma/2)^{n_s - 1} , \tag{32}$$

where $n_s = n + 2$, is the frequency exponent for an antenna whose gain is constant with respect to frequency. The formula (32) allows for the frequency dependence of A_r, since the gain of the antenna increases as the square of the frequency. A reflection from a meteor trail is governed by the transmission equation in terms of the scattering cross-section:

$$p_r p_t^{-1} = g_t g_r \lambda^2 (16\pi^2 R^4)^{-1} \sigma , \tag{33}$$

where g_t, g_r are, respectively, the power gains of the transmitting and receiving antennas relative to an isotropic radiator in free space, λ is the wavelength in meters, R the distance from transmitter to the trail in meters, σ is the scattering cross-section of the trail in square meters[21],

$$\sigma = [(R\lambda/2)^{1/2} r_e q]^2 \exp(-32\pi^2 Dt\lambda^{-2}) , \tag{34}$$

where $r_e = 2.8178 \times 10^{-15}$m is the classical radius of the electron, q the electron line density of the trail in electrons/m, D the diffusion coefficient in m^2/s, and t is the time in seconds. Let us remember that the wavelength λ appears in (33). Davies[21] discusses various other cases: long wavelength reflections from high-density trails, short wavelength reflections from low-density trails, other aspects of reflections from meteor ionization, apparent location of trails, diurnal and monthly variations, equatorial F-scatter, auroral scatter, etc. An individual electron has a cross-section for the scattering of electromagnetic waves and the existance of incoherent scatter was demonstrated in 1958 (Ref. 21). For more details see Reference 21. Here we give only the result, i.e., the power p_r received from a distance R is

$$p_r = p_t a \sigma c \tau \eta_r^2 \eta_s^2 \eta_A (8\pi R^2)^{-1} , \tag{35}$$

where a is the antenna aperture area, σ the cross section per unit volume, c the velocity of light, τ the pulse duration in seconds, and η_r, η_s, η_A are coefficients to correct the aperture for the effects of resistance losses, sidelobes and tapered feed, respectively.

4.2 Propagation of Low and Very Low Frequency Waves

The propagation of the electromagnetic waves at low and very low frequencies is presented very well in Reference 21.

5. CONTROLLABILITY

5.1 Optimization

Before we explain the concept of controllability we have to present the concept of optimization, and we begin with ordinary differential equations. Assume that a dynamic, physical system is described by a system of ordinary differential equations in a vector form $dx/dt = f(x;u)$, where $x = (x^1(t), x^2(t), \ldots, x^i(t))$, $f = (f^1(x;u), f^2(x,u), \ldots,)$, $u = (u^1(t), u^2(t), \ldots, u^r(t))$, the $x(t)$ being the dependent variables, t the independent variable and the $u^r(t)$ being the control functions, which are bounded. The system in question satisfies two-point boundary conditions, i.e., the trajectory must pass through two given points, $x_0(t \equiv t_0)$ and $x_1(t \equiv t_1)$. Moreover, there is given a functional of the form

$$J = \int_{t_0}^{t_1} f^0(x(t), u(t))\, dt = \min, \qquad \delta J = 0, \tag{36}$$

and the optimization principle can be formulated as follows: "In the space $X(t)$ there are given two points, x_0 and x_1. Among all the admissible control functions which allow one to transfer a point x from x_0 to x_1 along the sought trajectory, find the one which makes the functional (36) a minimum". To solve the problem one may use the calculus of variations, Pontryagin's maximum principle, the steepest descent technique or any other from many available techniques. The final calculations are usually done on a digital computer. As the control functions one may use any dependent variable appearing in the system in question, including the boundary conditions. The controls must be contained in a certain finite and bounded "admissible" domain. Concerning the optimization techniques for partial differential systems, the question is much more complicated. The calculus of variations was never generalized to the field of partial differential equations as a whole, only to some partial differential equations. The Pontryagin principle was never formally generalized to partial differential equations, and no proof of this procedure was ever presented. Using numerical techniques one can apply optimization procedures to partial differential systems in the following manner: Given, a partial differential system which has to satisfy two-curve boundary conditions. Moreover, there is given a functional which has to be optimized. The control functions are located in a certain bounded sub-domain on a certain surface or hypersurface (in a multi-dimensional space), on which we construct a grid of n points. For each point we know the value of the control functions, which we insert into the system and solve it with the prescribed boundary conditions. Next, we calculate the functional (to be optimized) with the use of the functions found. Repeating this procedure n times we obtain an approximate solution of the optimized two-curve boundary value problem for a partial differential system.

5.2 Controllability. Fundamental System

For simplicity, we propose a scheme for the controllability of the scattering phenomenon in a few particular cases. The schemes may obviously be generalized and extended to other particular cases, already discussed. The starting point for the solution of a scattering problem is the Maxwell system[23],

$$\nabla \times \mathbf{E} = \partial \mathbf{B}/\partial t; \qquad \nabla \cdot \mathbf{D} = \rho; \qquad \nabla \times \mathbf{H} = \mathbf{D}_t + \mathbf{J}; \qquad \nabla \cdot \mathbf{B} = 0, \tag{37}$$

where

$\mathbf{E}$ = electric field intensity

$\mathbf{H}$ = magnetic field intensity

$\mathbf{D}$ = displacement vector

$\mathbf{B}$ = magnetic induction

$\mathbf{J}$ = current density

ρ = charge density.

Assuming the time convention $\exp(i\omega t)$ we obtain

$$\nabla \times \mathbf{E} = -i\omega \mathbf{B}\,; \quad \nabla \cdot \mathbf{D} = \rho\,; \quad \nabla \times \mathbf{H} = i\omega \mathbf{D} + \mathbf{J}\,; \quad \nabla \cdot \mathbf{B} = 0\,. \tag{38}$$

In a homogeneous charge-free region with inductive capacities μ and ϵ and conductivity σ, each of these quantities must satisfy the vector Helmholtz equation

$$\nabla \times \nabla \times \mathbf{F} = k^2 \mathbf{F}\,; \quad k^2 = \omega^2 \mu\epsilon - i\omega\mu\sigma\,, \tag{39}$$

where $\mathbf{F} = \mathbf{E}$ or $\mathbf{H}$. The solution of the scattering problem consists of finding the solution of Equation (39) which satisfies the boundary conditions on the surface of the scatterer and at infinity. For a scatterer of finite conductivity in free space, the field vectors inside and outside the scatterer are respectively $(\mathbf{E}_i, \mathbf{H}_i)$ and $(\mathbf{E}_0, \mathbf{H}_0)$. The boundary conditions at every point of the surface are given in terms of two vector and scalar products,

$$\mathbf{n} \times (\mathbf{E}_i - \mathbf{E}_0) = 0\,; \quad \mathbf{n}(\mathbf{D}_i - \mathbf{D}_0) = 0\,; \quad \mathbf{n} \times (\mathbf{H}_i - \mathbf{H}_0) = 0\,; \quad \mathbf{n}(\mathbf{B}_i - \mathbf{B}_0) = 0\,, \tag{40}$$

$\mathbf{n}$ being the unit normal to the surface, taken outward. If the conductivity of the scatterer is infinite (as for metallic scatterers in radar problems) the fields inside the scatterer are zero and equations (40) reduce to

$$\mathbf{n} \times \mathbf{E}_0 = 0\,; \quad \mathbf{n} \cdot \mathbf{B} = 0\,. \tag{41}$$

The condition at infinity for a scalar wave function Ψ is usually stated in the form

$$\lim_{R \to \infty} R\left(\frac{\partial \Psi}{\partial R} + ik\Psi\right) = 0\,. \tag{42}$$

For perfectly conducting scatterers in free space, as well as for dielectric bodies or briefly for a homogeneous, charge-free, current-free isotropic medium, the Hertz vectors are

$$\mathbf{B} = i\omega\mu\epsilon \nabla \times \boldsymbol{\pi}\,; \quad \mathbf{E} = k^2 \boldsymbol{\pi} - \nabla\Phi\,, \quad \text{where } \Phi \text{ is arbitrary}\,, \tag{43}$$

with μ = constant; since $\nabla \cdot \mathbf{E} = 0$ and $\nabla \cdot \mathbf{H} = 0$ in a charge free region, with $\Phi = -\nabla \cdot \boldsymbol{\pi}$ one obtains the equation

$$(\nabla^2 + k^2)\boldsymbol{\pi} = 0\,. \tag{44}$$

For waves in a homogeneous, charge-free medium one can express a completely general electromagnetic field in terms of two independent scalar functions (u,v):

$$\mathbf{E} = \nabla \times \nabla \times \boldsymbol{\pi} - i\omega\mu \nabla \times \boldsymbol{\pi}^\star\,; \quad \mathbf{H} = \nabla \times \nabla \times \boldsymbol{\pi}^\star + i\omega\mathbf{E} \nabla \times \boldsymbol{\pi}\,, \tag{45}$$

$$\left.\begin{aligned} \boldsymbol{\pi} &= \mathbf{u}\mathbf{a} \quad \text{(a)} \\ \boldsymbol{\pi}^\star &= \mathbf{v}\mathbf{a} \quad \text{(b)} \\ \nabla^2\Psi + k^2\Psi &= 0 \quad \text{(c)} \end{aligned}\right\} \tag{46}$$

where the scalar functions u, v, satisfy Equation (46(c)). Equation (46(c)) can be solved by the Bergman linear integral operator technique as in Reference 11, satisfying the superimposed boundary conditions on the surface of the scattering body and at infinity. But Equation (46(c)) must be solved jointly with a functional to be optimized, discussed below. In this joint system one has to choose certain variables to be the control functions which may vary in certain bounded domains.

5.3 Functionals

5.3.1 Geometrical Optics

We now discuss a few functionals and the possible control functions which may be used in various kinds of scatter propagation. When the surface of a scatterer is smooth and large compared to the wavelength, the method of geometrical or ray optics is frequently used to calculate the scattered field. The geometrical optical scattering from curved surfaces for arbitrary incident waves has been proposed by Fock[24]. The method begins with the specification of the scatterer surface of the specular reflection point in terms of the generalized curvilinear coordinates, u^i, with the metric $dS^2 = g_{ij}du^i du^j$, $(i,j = 1,2)$. The phase of the incident field at the scatterer is expressed as $\Phi = 2\pi p(u^1,u^2)\lambda^{-1}$; the relative components of the incident field vector, along the incident Poynting vector V and the corresponding scattered vector U are

$$V = \nabla p(u^1,u^2); \qquad U = V - 2n(n \cdot V), \tag{47}$$

where n denotes the unit normal at the point (u^1,u^2). The area of the cone of reflected rays at a distance R from the scatterer is given by the determinant Σ_R, of the components of the tensor T^{β}_{α}, which includes the tensor g_{ij}, the curvature tensor of the surface, and the partial derivatives of $p(u^1,u^2)$. The field intensities at distance R from the scatterer are given by the formulas[23,24]

$$E^S = [E^i - 2n(E^i \times n)]\,(\Sigma_0\Sigma_R^{-1})\exp(-ikR); \tag{48}$$

$$H^S \cdot S = [H^i - 2n(n \cdot H^i)]\,(\Sigma_0\Sigma_R^{-1})\exp(-ikR); \tag{49}$$

where E^S, H^S are the intensities of the scattered fields, S the area of the scatterer, E^i, H^i the intensities of the incident fields, Σ_0 is the determinant Σ_R for $R = 0$, and the factor k was given in Section 5.2. As the functionals to be maximized we may choose (48) and (49), and as a control function the factor "k". Then Equation (46) has to be solved so as to satisfy the boundary conditions on the surface of the scatterer and at infinity, with the additional condition that Equations (48) and (49) have to be maximized and with "k" being the control function.

5.3.2 Physical Optics

The use of the physical optics for the solution of the scattering problem is presented thoroughly in Reference 23 and other sources. Without going into all the details we present the final results. For scatterers of large characteristics dimensions, the result of energy flow considerations shows that the surface current distribution for the incident field, J^i, may be chosen in the form given below, and the scattered field, $H^S|_p$ at a point "p" is

$$J^i = n \times H^i; \qquad H^S|_p = (4\pi)^{-1}\iint_S \phi J\, dS; \qquad \phi = R^{-1}\exp(-ikR). \tag{50}$$

Choosing the parameter k as the control function, we solve Equation (46) under the condition that (50) is the optimum. Application of the variational method to the scattering of radio waves is discussed in Reference 23.

5.3.3 Radar Cross-Section and Power

The control functions may be chosen in forms of the radar cross-sections or the power. Suppose that R denotes the distance from the current element on the surface element, dS, to a point in the +y-direction, with the wave moving in the direction of negative y. If the distant point has the coordinates $(0, y_0, 0)$, and the incident electric field intensity has the form

$$E^i = E^0 \exp(iky) , \tag{51}$$

we construct the variable

$$U = \iint_S E^0 \cdot J \exp(iky)\, dS . \tag{52}$$

Then the ratio of a plane wave power density to the corresponding power density in the scattered field, which ratio we may optimize, is[23]

$$\frac{|W^r|}{|W^i|} = \frac{|E^0 \cdot E^s|^2}{|E^0|} = \frac{k^4 U^2}{(4\pi)^2 \omega^2 \epsilon^2 y_0^2 |E^0|^4} . \tag{53}$$

One can optimize the radar cross-section

$$\sigma = [4\pi\omega^2\epsilon^2 |E^0|^4]^{-1} k^4 U^2 , \tag{54}$$

or, in terms of the wavelength,

$$\sigma = [\lambda^2 |E^0|^4]^{-1} (\mu\epsilon^{-1}) \pi U^2 . \tag{55}$$

One can use the formula (33) for the transmission, cited by Davies[21] to optimize η_r with λ chosen to be the control function, or the formula (29) to optimize p_a with K Equation (30)) chosen to be a control function[21].

5.3.4 Turbulence Scattering

In the scattering due to turbulence, discussed in the Section 2, one may optimize the effective cross-section for the scattering (Equation (20)).

5.3.5 Scattering Angle

Equation (29) refers to the geometry of the forward scatter from the irregularities in the D-region. The value of the power available from a receiving antenna, p_a, can be controlled by means of the angle γ through which the scattering takes place and which is the angle contained between the center line of the emitting cone from emitting antenna and the center line of the receiving cone having its base in the scattering volume V of the ionosphere illuminated by the transmitter and its apex in the receiving antenna. The smaller the angle γ, the larger the value of p_a in Equation (29). Irregularities in the D-region, where the scattering may occur, are produced by the action of turbulence, wind shears, etc. on the electron distribution in the height range between 70 and 90 km. These irregularities in electron density result in corresponding fluctuations in refractive index (Ref. 21, p. 344). An elegant derivation of the Appleton formula for the complex refractive index of a medium such as the ionosphere is given in Reference 21. The index can be controlled up to a certain degree by means of the emitted wave. By controlling the refractive index one may be able to control the angle γ inside a certain bounded domain.

REFERENCES

1. Taylor, G.I.
   (1) *Statistical Theory of Turbulence.* Proceedings, Royal Society, London, Series A, Vol.151, 1935, p.421.
   (2) *Statistical Theory of Isotropic Turbulence.* Journal of the Aeronautical Sciences, Vol.4, 1937, p.313.
   (3) *The Spectrum of Turbulence.* Proceedings, Royal Society, London, Series A, Vol.164, 1938, p.476-490.

2. Kármán von, Th.
   (1) *The Fundamentals of the Statistical Theory of Turbulence.* Journal of the Aeronautical Sciences, Vol.4, No.4, February 1937, pp.131-138.
   (2) *On the Statistical Theory of Turbulence.* Proceedings, National Academy of Sciences, USA, Vol.23, 1937, p.98.

3. Kármán von, Th., Howarth, L. *On the Statistical Theory of Isotropic Turbulence.* Proceedings, Royal Society, London, Series A, Vol.164, 1938, p.192.

4. Robertson, H.P. *The Invariant Theory of Isotropic Turbulence.* Proceedings, Cambridge Philosophical Society, Vol.36, 1940, p.209.

5. Batchelor, G.K.
   (1) *Kolmogorov's Theory of Locally Isotropic Turbulence.* Proceedings, Cambridge Philosophical Society, Vol.43, 1947, pp.533-559.
   (2) *Recent Developments on Turbulence Research.* General Lecture, 7th International Congress of Applied Mechanics, London, 1948, pp.27-56.
   (3) *The Theory of Homogenous Turbulence.* Cambridge Monographs on Mechanics and Applied Mathematics, Cambridge University Press, 1953.

6. Chandrasekhar, S. *Turbulence – A Physical Theory of Astrophysical Interest.* The Astrophysical Journal, Vol.110, November 1949, pp.329-339.

7. Loitsianskij, L.G. *Same Basic Laws of Isotropic Turbulent Flow.* Central Aero-Hydrodynamical Institute, Moscow, Report 440, 1939. Also: NACA TM 1079, September 1945, (Translation).

8. Coburn, N. *The "Independent Scalars" in Homogeneous Turbulence.* American Journal of Mathematics, Vol.74, No.2, April 1952, pp.296-306.

9. Kampé de Fériet, J.
   (1) *Les Fonctions aléatoires stationnaires et la théorie de la turbulence homogene.* Annales, Société Scientifique de Bruxelles, Vol.59, 1939, pp.145-194.
   (2) *Sur un problème d'algèbre abstraite posé par le définition de la moyenne dans la theorie de la turbulence.* Annales, Société Scientifique de Bruxelles, Vol.63, 1939, pp.156-172.
   (3) *Fonctions aléatoires définies sur un groupe abstraite.* Comptes Rendus, Académie des Sciences, Paris, Vol.225, 1947, p.37.
   (4) *Sur une représentation des fonctions aléatoires.* Comptes Rendus, Académie des Sciences, Paris, Vol.225, 1947, p.428.

(5) *Analyse harmonique des fonctions aléatoires stationnaires d'ordre deux définies sur un groupe abelien localement compact.* Comptes, Rendus, Académie, des Sciences, Paris, Vol.226, 1948, p.868.

(6) *Fonctions aléatoires stationnaires et groupes de transformations dans un espace abstrait.* Collogue International de Calcul de Probabilitiés, Lyon, 1948 (published Paris 1950), pp.67-73.

(7) *Le tenseur spectral de la turbulence homogene non isotrope.* General Lecture, 7th International Congress Applied Mechanics, London, 1948, pp.6-26.

(8) *Spectral tensor of homogeneous turbulence.* Proceedings, Naval Ordnance Laboratories Aeroballistic Research Symposium, Washington, DC, 1949, pp.1-31.

(9) *Sur l'analyse harmonique des fonctions à carré moyen fini.* Proceedings, International Congress of Mathematicians, Cambridge, Mass., 1950, Vol.1, pp.457-458.

(10) *Sur l'analyse spectrale d'une fonction stationnaire en moyenne.* Collogue International de Mechanique des Fluides, Poiters, Mai 1950. Published in Publications Scientifiques et Techniques du Ministère de l'Air, Vol.251, pp.317-335.

(11) *Mathematical Methods Used in the Statistical Theory of Turbulence: Harmonic Analysis.* Lecture Series No.1. Institute for Fluid Dynamics and Applied Mathematics, University of Maryland, 1951.

(12) *Autocorrelation Function of a Truncated Function.* Bulletin, American Mathematical Society, Vol.57, 1951, p.129.

(13) *Introduction to the Statistical Theory of Turbulence, Parts I to IV.* Journal, Society for Industrial and Applied Mathematics, Vol.2, No.1, 3, and 4; Vol.3, No.2, March 1954, pp.1-9, September 1954, pp.143-174, December 1954, pp.244-271, June 1955, pp.90-117.

10. Keller, L., Friedmann, A. *Differential-Gleichungen fuer die turbulente Bewegung einer kompressibelen Fluessigkeit.* Proceedings, First International Congress of Applied Mechanics, 1924, pp.395-405.

11. von Krzywoblocki, M.Z.

(1) *On the Invariant Theory of Isotropic Turbulence in Compressible Fluids.* Technical Report, Naval Ordnance Laboratory, White Oak, Maryland, 1949.

(2) *On the Fundamentals of Kinematics of Statistical Theories of Turbulence in Compressible Fluids.* Proceedings of the First Midwestern Conference on Fluid Dynamics, May 1950, University of Illinois. Published by Edwards Brothers, Ann Arbor, Michigan, September 1951, pp.66-80.

(3) *On the Generalized Fundamental Equations of Isotropic Turbulence in Compressible Fluids and in Hypersonics.* Proceedings of the First US Congress on Applied Mechanics, Chicago, June 1951. Published by American Society of Mechanical Engineers, New York, December 1952, pp.827-835.

(4) *On the Foundations of Certain Theories of Turbulence.* Journal of the Franklin Institute, Vol.252, November 1951, pp.409-412.

(5) *On Locally Isotropic Turbulence in Compressible Fluids.* Proceedings of the Second Midwestern Conference on Fluid Mechanics, The Ohio State University Press, September 1952, pp. 35-47.

(6) *On the Equations of the Decay of Isotropic Turbulence in Compressible Fluid.* Journal of the Physical Society of Japan, Vol. 7, May-June 1952, pp. 299-300.

(7) *On the Invariants in the Turbulence in Compressible Viscous Fluids.* Proceedings of the 1952 Heat Transfer and Fluid Mechanics Institute, University of California, Los Angeles, California, 1952, pp. 65-71. Also: Journal of the Franklin Institute, Vol. 254, October 1952, pp. 317-322.

(8) *On the Equations of the Decay of Isotropic Turbulence in Magneto-Hydrodynamics.* Journal of the Physical Society of Japan, Vol. 7, September-October 1952, pp. 511-512.

(9) *On the Equations of Isotropic Turbulence in Magneto-Hydrodynamics of a Compressible Medium.* Acta Physica Austriaca, Vol. VI, 1952, pp. 157-166.

(10) *On the Decay of Turbulence in Compressible Fluids in Terms of Vorticity.* Proceedings of the Third Midwestern Conference on Fluid Mechanics, The University of Minnesota Press, June 1953, pp. 413-425.

(11) *On the Fundamentals of Locally Isotropic Turbulence in Magneto-Hydrodynamics of a Compressible Medium.* Acta Physica Austriaca, Vol. VI, 1953, pp. 250-256.

(12) *The "Independent Scalars" in Homogeneous Turbulence in Compressible Media.* Journal of the Physical Society of Japan, Vol. 8, November-December 1953, pp. 745-747.

(13) *The Turbulence Theory in Compressible Fluids.* Proceedings, VIII International Congress of Theoretical Applied Mechanics, Istanbul, Turkey, September 1952.

(14) *On Turbulence in Rarefied Gases.* Proceedings of the Second US National Congress of Applied Mechanics. Published by American Society of Mechanical Engineers, New York, June 1954, pp. 677-685.

(15) *Sur la turbulence spatialement homogène d'un fluide compressible.* Proceedings, 80-e Congrés des Sociétés Savantes, Lille, France, May 31 - June 4, 1955. Published by Gauthier-Villars, Paris, November 1955, pp. 367-376.

(16) *Sur la turbulence spatialement homogène d'un fluid compressible.* Thèse, L'Université de Lille, Imprimerie du SDIT, Paris, 1956, p. 54.

(17) *Sur la turbulence spatialement homogène d'un fluid compressible,* avec preface de J. Kampé de Fériet. Publications Scientifiques et Techniques du Ministère de l'Air. No. 314, 1956.

12. Kolmogorov, A.N. — Journal of Fluid Mechanics, Vol. 13, 1962, p. 82.

13. Kumar, P. — *Studies in the Statistical Theory of Turbulence and Gas Dynamics.* PhD Thesis, Delhi University, 1962.

14. Silverman, R.A. — *Turbulent Mixing Theory Applied to Radio Scattering.* Journal of Applied Physics, Vol. 27, 1956, p. 699.

15. Oboukhov, A.M. — Izvest Akademiya Nauk SSSR, Geograficheskaya i Geofizicheskaya, Vol.13, 1949, p.58.

16. Tatarski, V.I. — *Wave Propagation in a Turbulent Medium*. McGraw-Hill, New York, 196i (translated from the Russian by R.A.Silverman).

17. Paul, Yash — *Scattering of Radio Waves in a Locally Isotropic Turbulent Medium.* Tensor (New Series), Vol.17, March 1966, pp.165-168.

18. von Krzywoblocki, M.Z. — *Scattering and Attenuation of Electromagnetic Waves in a Turbulent Medium.* Research Report, R-61-40, Martin Marietta Corp., Aerospace Division, Denver 1, Colorado, December 1961, II + 77 pp. Also: Proceedings, Vibrations Problems, Polish Academy of Sciences, Institute of Basic Technical Problems, Vol.3, No.4(13), 1962, pp.245-281.

19. Akhiezer, A.I., et al. — *Collective Oscillations in a Plasma.* Translated from the Russian by H.S.H.Massey, edited by R.J.Tayler, Massachusetts Institute of Technology Press, 1967.

20. Sitenko, A.G., Kirochin, Yu.A. — *Scattering and Transformation of Waves in a Magnetoactive Plasma.* Soviet Physics USPEKHI, Vol.9, November-December 1966, pp.430-447.

21. Davies, K. — *Ionospheric Radio Propagation.* National Bureau of Standards Monograph 80, April 1, 1965.

22. Pontryagin, L.S., et al. — *The Mathematical Theory of Optimal Processes.* Translated by K.N.Trirogoff, edited by L.W.Neustadt, Interscience Publishers, 1962.

23. Mentzer, J.R. — *Scattering and Diffraction of Radio Waves.* Pergamon Press, New York, 1955.

24. Fock, V.A. — (1) *Diffraction of Radio Waves Around the Earth's Surface.* Journal of Physics, USSR, 1945, Vol.9, pp.225-226.

(2) *Generalization of the Reflection formulae to the Case of Reflection of an Arbitrary Wave from a Surface of Arbitrary Form.* Zhurnal Eksperimentalnoi i Teoreticheskoi Fiziki, 1950, Vol.20, p.961.

VHF IONOSPHERIC SCATTER PROPAGATION VIA THE EQUATORIAL ELECTROJET

by

Carlos A. Romero*, Alberto A. Gíesecke, Jr.** and Major EP Oscar Pérez†

*Jicamarca Radar Observatory

**Instituto Geofisico del Perú

†Jefatura de Transmisiones, Peruvian Army

SUMMARY

Results are presented of a statistical analysis of VHF ionospheric forward scatter signals propagated via the equatorial electrojet. Continuous data were obtained from November 1966 through June 1967 during moderate sunspot activity (sunspot numbers ranged from 50 to 100). Comparison of these data with those obtained by Cohen and Bowles[2], during the International Geophysical Year shows that the influence of the solar cycle is very small. During the period of this study, as in the IGY, the signal levels propagated by forward scatter at the magnetic equator are considerably higher than those for similar paths at temperate latitudes. The daily variation of signal intensity attains its maximum level during daytime hours, associated with minimum fading rate (about 20 Hz). A secondary maximum occurs during the night-time hours, associated with a higher fading rate (about 50 Hz). The relative minima in the daily variation occur at times of reversal in the direction of flow of the electrojet. A statistical study of these times thus provides the seasonal variation of the morning and evening reversal times. The effects on the VHF scatter signals of magnetic storms, sudden ionospheric disturbances and of the total solar eclipse of November 12, 1966, are also studied.

VHF IONOSPHERIC SCATTER PROPAGATION VIA THE EQUATORIAL ELECTROJET*

Carlos A. Romero, Alberto A. Giesecke, Jr. and Major EP Oscar Pérez

1. INTRODUCTION

This paper is a preliminary report on experiments in VHF forward scatter propagation via the equatorial electrojet, between the cities of Lima and Juliaca, Peru. The ultimate objective of these experiments was to employ this mode of propagation for telecommunications.

The first VHF ionospheric scatter propagation experiments were carried out in 1953 by National Bureau of Standards (NBS) scientists, directed by Bailey, Bateman and Kirby[1], who made a detailed study of this propagation over various circuits in North America. Ionospheric propagation by forward scatter at VHF differs completely from propagation by ionospheric refraction, since frequencies are used that exceed the 'maximum usable frequency' (MUF) for F_2 -layer propagation; such VHF signals almost completely penetrate the ionosphere, except for a very small fraction that is scattered by ionospheric irregularities. The VHF circuit typically utilized as a reference is the NBS Cedar Rapids-Sterling circuit. This circuit employed a transmitter-receiver separation of 1200 km and the signal was scattered primarily in the D-and E-regions.

During the International Geophysical Year (1958), VHF scatter experiments were conducted by NBS near the magnetic equator in South America, providing information concerning ionospheric scatter in equatorial regions. Cohen and Bowles[2] showed that the scattered signals over equatorial paths were usually about 30 dB stronger than signals obtained by Bailey et al.[1] in temperate latitudes. These signals were attributed to irregularities in the E-region associated with the equatorial electrojet. Such irregularities also produce the configurations on ionograms identified as "Equatorial Sporadic-E" and "Equatorial Slant Sporadic-E". The strong signals obtained during daytime at the magnetic equator have a time variation related to the time variations in the horizontal component of the magnetic field. Certain physical aspects of the phenomena associated with the electrojet were discussed by Cohen and Bowles[3].

Because of these IGY results, equatorial scatter propagation appeared to be an economic and reliable propagation mechanism to exploit for telecommunications, at least during daytime hours. The feasibility of this utilization would depend upon maintaining sufficiently strong scattered signal intensities throughout the solar cycle. The experiment which is described herein was originally planned for the period of minimum solar activity, during which it was supposed that the most adverse scattering conditions would be encountered. However, because of various delays, the beginning of the experimental period was not until October 1966.

The equatorial IGY observations coincided with the period of maximum solar activity (sunspot numbers from 180 to 200), while the observations described here were conducted during a period of sunspot numbers of 50 to 100, corresponding to moderate solar activity. The results reported here may be compared to the IGY results, keeping in mind certain correction factors arising from differences in circuit parameters (distance, antenna gain, transmitter power).

---

*A coöperative project of the Aeronomy Laboratory, ESSA Research Laboratories, Environmental Science Services Administration, Boulder, Colorado, and the Instituto Geofisico del Perú, Lima, Perú.

2. CHARACTERISTICS OF THE EXPERIMENT

The experiment was done in a similar fashion to that of Cohen and Bowles[2]. That experiment, in turn, was similar to that of Bailey, Bateman and Kirby[1].

Figure 1 shows the location of the transmitting and receiving stations, the position of the magnetic equator, and a horizontal projection of the antenna beams. The experimental technique consisted of transmitting a 47.3 MHz continuous wave (CW) signal from Lima (12° 02.6′W; 77° 02.5′S), recording at Juliaca (15° 29.5′S; 70° 08.1′W) the variations in signal strength as well as the fading rate of the signal. The antennas were designed so that the intersection of the vertical beams would be at a point 100 km high, so that the variations in signal characteristics could be related to changes within the ionospheric volume so defined. The transmitted power was of the order of 900 watts. The received signal was passed through an integrator (having a 12-second time constant) and recorded on paper tape at a speed of 3 inches per hour. The same process was used for recording the fading rate of the signal. The receiving system was calibrated daily with a signal generator, and absolute values of antenna voltages were scaled from the recordings. Median signal levels were determined (in decibels above 1 microvolt) for each 15-minute interval. The signal levels are referred to an antenna voltage matched to a resistive impedance of 50 ohms. Table I shows the comparative characteristics of the Lima-Juliaca circuit and the Arequipa-Trujillo (IGY) circuit.

3. INSTRUMENTATION

3.1 Antennas.

Eight-element Yagi antennas were used, having a gain of 12 dB above a dipole. These antennas were placed at a height of 11 m above the ground, in order to obtain the desired beam intersection at a height of 100 km. During the data reduction, for purposes of comparison, since the reference Arequipa-Trujillo circuit employed rhombic antennas with 18 dB gain, the Lima-Juliaca signal has been compensated by + 6 dB, assuming that the nominal gains of both kinds of antennas were always realized.

3.2 Transmitter

The transmitter (designed by Harding and Whittaker[4] was similar to those used in the NBS experiments, with an output of 3 kW. The signal levels encountered were sufficiently high so that the transmitted power was reduced to 880 watts. For purposes of data analysis and comparison with the circuits in former experiments, wherein the reference transmitter power was 30 kW, the signal was compensated by + 15.3 dB. (For the Arequipa-Trujillo circuit, the transmitted power was 2 kW, so that in the analysis of signal strength the signal was compensated by 12 dB for making comparisons with results over the Cedar Rapids-Sterling circuit.)

3.3 Receiver.

A receiver (designed by the Ionosphere Research Section of NBS (Ref.5)) was employed. This receiver was designed for flexible application to many VHF radio propagation experiments. An IF band width of 300 Hz was selected for the present application. The local oscillator is very stable (5 Hz per day variation in 50 MHz). The receiver response to the input signal is logarithmic, with a dynamic range of 100 dB. The 0 dB reference level used in the analysis of signal strength is 1 microvolt on an open circuit, relative to an antenna of 50 ohm impedance. The AGC voltage resulting from the signal received was integrated (using a 12-second time constant) and plotted as a function of time. The transmission was interrupted for 2 minutes at 15-minute intervals, permitting the external noise level (principally cosmic noise) to be recorded. This noise level is useful for evaluating the operation of the system.

3.4 FADING-RATE METER.

A "fading-rate" meter (originally developed for radio propagation experiments by B. Balsley[6]), was used in the last stages of the Arequipa-Trujillo experiment. This instrument provides a continuous record of the fading rate of radio signals. Fading rate is defined as the number of times per second that the envelope of the signal crosses, with a positive slope, the average level of the signal. It is designed to function with the received IF signal as an input, and employs a 12-second time constant in the AGC stage. In this experiment, a dynamic range from 0 to 100 Hz was used. The instrument was calibrated each day with a sinusoidal reference signal.

4. ANALYSIS OF SIGNALS RECEIVED

The recorded data on signal strengths and fading rates were analyzed as follows:

4.1 Analysis of the Received Signal Strength.

The signal strength records were reduced by obtaining median values tabulated in decibels for each 15-minute interval. Noise levels were also tabulated at 15-minute intervals. These two tabulations provided the basis for a study of signal strength and signal/noise ratio.

4.2 Analysis of the Fading Rate Recordings.

In a similar fashion, median fading-rate recordings tabulated in Hz were scaled for each 15-minute period. Such information was not scaled from the noise record. Although the experiment was conducted from October 1966 through August 1967, data has been analyzed only for the period November 1966 through June 1967. Records corresponding to the remaining months are sporadic, with useful data being available for less than 50% of each month. Data for the period analyzed are more than 90% useful.

5. CHARACTERISTICS OF THE RECEIVED SIGNALS

5.1 Signal Intensity.

Figure 2(a) shows a typical record during a quiet day. The highest signal levels occur from 08 through 17 hours, and remain at a relatively constant value during that period. The minimum intensities appear at 0700 and 1930 hours, approximately. These times are interpreted as coinciding with those when the electrojet reverses its direction of flow. This interpretation results from some radar studies by B. Balsley[7], who identified the electrojet reversal by the frequency shift of the backscatter echoes. He found that the electrojet current flows in a West to East direction during the daytime, and from East to West during night hours. The intensity of the signal appears to depend upon the electron drift velocity and the electron density.

The minimum signal levels in Figure 2(a) thus correspond to the moment when the electron drift velocity of the electrojet becomes zero, just before changing direction. On the same record one observes that after 20 hours the signal level rises in intensity, reaching a relative maximum between 21 and 01 hours. This behavior is typical, so that on a normal day there are two relative minima, corresponding to the times when the electrojet reverses, and two relative maxima. One relative maximum occurs during the daytime, and usually has a higher level than the night-time relative maximum.

Besides the change with time in the amplitude of the signal, there is also a time variation in the form of the trace. Figure 2(a) is characterized by a thick trace between 08 and 17 hours, a thin trace between 17 and 18 hours, and a trace (referred to as 'meteoric') with rapid changes or spikes during the time of reversal of the electrojet. The sharp rises

in signal level on the meteoric trace result from ionization produced by meteors. One also notes a mixture of the various traces at other hours. Figure 2(c) shows a typical recording of the signal on a disturbed day. From 1230 to 1330 hours the signal level is very low; this is the result of a sudden ionospheric disturbance (SID). During the SID, when the signal level is at a minimum, only the meteoric signal component is evident. Usually, other components of the signal are so strong that the relatively weak meteoric component is too small to be identified.

5.2 Fading Rate.

Figure 2(b) shows a fading rate recording during a normal day; as can be noted by comparison with Figure 2(a), the fading rate is low when the signal level is high; during the period of strong daytime signals, the fading rate is of the order of 20 Hz. High fading rates occur during the reversals of the electrojet flow, during which the fading rate at times approaches 100 Hz. Figure 2(d) also shows that, during the SID, when the signal levels are low, the fading rate increases to large values. Since the measured fading rate corresponds to the sum of signal plus noise, the fading rates obtained at low signal levels result principally from the noise; hence they can be disregarded.

6. STATISTICAL ANALYSIS OF THE SIGNALS RECEIVED

6.1 Monthly Median Values of Signal Intensity.

Figure 3 shows the monthly median values of signal intensity for each of the eight months of data analyzed. These values of signal intensity which are referred to dB above 1 microvolt, have been appropriately compensated for purposes of comparison with the IGY results obtained over the Arequipa-Trujillo circuit. This +25 dB compensation takes into account differences in antennas, transmitted power, and path distance. The right-hand scale of ordinates refers to the signal attenuation in decibels relative to a signal propagated with inverse-distance attenuation. This scale is useful for comparison purposes, since it directly compensates for the several factors mentioned above.

We note that the maximum signal intensity is attained during daytime hours (08-16), of order 25 to 30 dB referred to 1 microvolt or of order -70 dB referred to inverse-distance attenuation. We also see that there were two relative minima each day, near the times of sunrise and sunset. These minima are interpreted as occurring at times when the electrojet flow reverses direction. Note that the evening relative minimum is more pronounced than the one in the morning. This difference is attributed to the fact that, during the morning reversal the contribution of the ionization due to meteors is much higher than during the evening reversal. Also note that around 22 hours there is a rise (of order 5 dB) in signal level.

6.2 Monthly Percentiles of Signal Intensity.

Figure 4 shows the values of monthly percentiles of signal strength for the eight months analyzed. The percentiles shown refer to signals which are present during 10%, 50% and 90% of the time. One notes that, although the shapes of these curves differ for the various percentiles, the times of maxima and minima coincide.

6.3 Median Monthly Values of Fading Rate.

In Figure 5 are shown the monthly median values of fading rate. The fading-rate minima correspond to times of highest signal intensity, and are of order 20 Hz. The fading rate is a maximum near sunset and sunrise, the actual times (following Balsley[7]) indicating the reversal of flow of the electrojet. The fading rate corresponding to signals during nighttime hours is of the order of 50 Hz.

6.4 Monthly Percentiles of the Signal-to-Noise Ratio.

Figure 6 shows percentiles of the signal-to-noise ratio. Again, the signal has been compensated by the +25 dB referred to previously. The signal-to-noise ratio during daytime is of the order of 52 dB, and during night-time of order 35 dB. We again note the two relative minima corresponding to periods of electrojet reversal.

6.5 Monthly Median Values of Noise Level.

Figure 7 shows the monthly median values of noise level as obtained from samples at fifteen-minute intervals for the two-minute periods during which the transmitter was off the air. In this case, at 47.3 MHz, the noise arises mainly from cosmic sources. As can be seen from the curves, the daily variation in noise intensity is not regular. This would be expected for cosmic noise, since from day to day the daily variation shifts 4 minutes, corresponding to the difference between the solar and the sidereal day. Also, the antenna is not pointed toward the galactic plane, but is directed at an angle of 10 degrees above the horizon. Note that the noise level never exceeds -20 dB, nor is it ever lower than about -27 dB.

7. EFFECT OF MAGNETIC STORMS, SUDDEN IONOSPHERIC DISTURBANCES AND SOLAR ECLIPSES

The intensity of the scattered signal is related to the horizontal component (H) of the earth's magnetic field[3]. The H component consists of two contributions, H_0, of internal origin, and ΔH, of external origin ($H = H_c + \Delta H$). ΔH is the magnetic field generated by the currents that flow in the ionosphere, the electrojet being the most important of these. Consequently, ΔH is indicative of electrojet effects resulting from solar disturbances and other solar-activity phenomena.

Figure 8 shows the scattered signal intensity received at Juliaca on a quiet day, together with the record of total magnetic field intensity at Jicamarca. (In this case one can consider the record as being that of H, since Jicamarca is at the magnetic equator.) The maximum signal intensity during daylight hours coincides with the maximum of H; between 15 and 18 hours there is a slight hump in H and a corresponding hump in signal intensity. This correlation disappears during night-time; for example, there is an increase in signal level at 22 hours without any noticeable increase in the value of H.

Figure 9 shows the record of signal intensity, together with the Jicamarca magnetogram, corresponding to a disturbed day. During this day, effects of both a magnetic storm and an SID are evident; between 1230 and 1330 hours there is a sudden decrease in the magnetic field strength corresponding to an almost total disappearance of the scattered signal. Also, there is often a correlation between drops in signal level and of H. It has been found[3] that this correlation exists only over a certain range of values for H. The limits of this range of H can be described as a threshold identified by H_t and a saturation value H_s. The value H_t is associated with the time when the propagation by the electrojet is established at the beginning of each morning. H_s is defined as the value of H above which there is no further variation of signal intensity with H.

In general, variations of the magnetic field corresponding to a K-index higher than 7 result in the complete disappearance of the signal. For K-indices lower than 5, during daytime hours, changes in signal level are barely noticeable.

Figure 10 shows the effect on scatter propagation of the total solar eclipse of 12 November 1966; this eclipse was total at the point of intersection (at a height of 100 km) of the two antenna beams, although the region of totality covered only part of the scattering volume. In Figure 10(a) is plotted the intensity of the signal on the day of the eclipse, together with the median value of signal intensity as measured during 24 control days. Half the control days preceded the eclipse, the other half followed it, and this control period permits an estimation of the effect of the eclipse on the received signal

intensity. It appears that the signal intensity dropped some 19 dB at the time of the eclipse maximum. The graph also shows the times during the eclipse (A, B, C, A′, B′, C′) of appearance and occultation of some active areas on the sun's surface.

Figure 10(a) also shows the effect of the eclipse on the top frequency of the sporadic-E (foEs), as measured at Jicamarca. In Figure 10(b), the scattered signal intensity during the eclipse day is plotted, along with the H component recorded at Huancayo and the difference between the H measured at Huancayo (Dip: 2^{o}) and that measured at Bogatá, Colombia (Dip: 18^{o}). This was done (following Cohen and Bowles[3]) to remove the internal component of H , and thus to work only with the external component ΔH. A more detailed analysis[8] of the eclipse effect on this scatter propagation has been presented, and is being prepared for publication.

8. SEASONAL VARIATIONS

Figure 11(a) shows, for certain times of day, the values of signal intensity that exist 10%, 50% and 90% of the time during the eight months of data analyzed. This analysis was done for midnight (0000) and noon (1200), corresponding to times of relative maxima, as well as for the time intervals 0530-0700 and 1900-2030 hours, which correspond to the relative minima associated with times of reversal of flow of the electrojet. As can be noted from the graph for midnight (0000), the signals for each of the percentiles are a minimum for the March equinox (autumn), maximum for the December solstice (summer), and approach another peak during the June solstice (winter). No data are available for the September equinox (spring). The same trend is noted in the graphs for the morning minimum (0530-0700) and the evening minimum (1900-2030). The graph for the signal levels at noon is completely different, with no appreciable seasonal change for the 10% and 50% percentiles. For the noon 90% percentile, the variation is different from that observed at other times, with a minimum signal intensity in December and no noticeable difference in signal intensity between March and June.

Figure 11(b) shows the seasonal variation in the times of occurrence of the morning and evening reversals in direction of flow of the electrojet. Note that the morning reversal takes place earliest during summer and winter, and latest during autumn; whereas the evening reversal occurs later in summer than it does in winter.

9. COMPARISON BETWEEN DATA OBTAINED IN THE CIRCUITS AREQUIPA-TRUJILLO AND LIMA-JULIACA

As mentioned in the Introduction of this paper, one of the principal objectives of the experiment was to compare the data obtained with the results of the previous Arequipa-Trujillo experiment, which took place during sunspot maximum. This comparison was to study the influence of the solar cycle on the performance of an equatorial VHF forward scatter circuit. Figure 12 is a graph of solar activity during cycles 19 and 20, and shows the periods during which the equatorial experiments were carried out. Note that the earlier experiment coincided with sunspot numbers between 180 and 200, whereas the latter experiment, during the early part of cycle 20, coincided with sunspot numbers between 50 and 100.

Figure 13 shows the values of the monthly median signal intensity levels obtained[2] with the Arequipa-Trujillo circuit for comparison with those obtained with the Lima-Juliaca circuit. Figure 14 is based on the maximum values of signal intensity during daytime hours throughout the months of operation. One observes that the signal intensity over the Arequipa-Trujillo circuit is somewhat higher than that for the Lima-Juliaca circuit; this difference is approximately 4 dB, on the average. For the night hours, and during the periods of electrojet reversal, the values for the Lima-Juliaca circuit are somewhat higher. Considering that the sunspot numbers during the Arequipa-Trujillo experiment were appreciably higher than during the Lima-Juliaca experiment, we conclude that an equatorial VHF forward scatter circuit is rather insensitive to solar-cycle influence.

10. CONCLUSIONS

(i) The daily variation of the signal intensity has a maximum during daytime hours, order 27 dB above 1 microvolt. (This corresponds to -70 dB when referred to inverse-distance attenuation.) A secondary maximum of order 10 dB occurs during night-time hours. (This corresponds to -87 dB when referred to inverse-distance attenuation.) The minima which occur in the daily variation are at the times of reversal of the electrojet's direction of flow. The fading rate of the signal is a minimum during daytime hours, of order 20 Hz, increasing to 50 Hz at night-time, with relative maxima during the periods of electrojet reversal.

(ii) Even during the minimum of a sunspot cycle and during medium solar activity, the signal level propagated by forward scatter at the magnetic equator is considerably higher than at temperate latitudes. The influence of the solar cycle is very small.

(iii) A definite seasonal variation has been observed, especially for the night-time maximum, and for the morning and evening minima. For the minima, the signal intensity is lowest during the March (autumn) equinox and higher during the December (summer) and June (winter) solstices. Nevertheless, the signal intensity during daytime, which is of greatest importance from the point of view of communications, does not show an appreciable seasonal variation for the 10 and 50% percentiles. For the 90% percentile, there is an inverse seasonal effect, since the minimum is during the December (summer) solstice.

(iv) A seasonal variation has been observed for the times when the reversals in direction of flow of the electrojet occur. The morning reversal is latest in March and April, and the evening reversal is latest during February.

(v) Magnetic storms and sudden ionospheric disturbances sometimes affect the signal intensity adversely, in contrast with performance at temperate latitudes, where disturbances have no appreciable net effect on the scattered signal intensity.

(vi) A total solar eclipse reduces the intensity of the VHF signals scattered by irregularities in the equatorial electrojet.

(vii) The high daytime level of signal intensity, practically independent of solar cycle, suggests the possibility of exploiting VHF scatter propagation for equatorial communication circuits. Use of the weaker, faster fading night-time signals for telecommunications may also be feasible, at least for telegraphy.

ACKNOWLEDGEMENTS

These experiments were conducted thanks to the auspices of the Jicamarca Radar Observatory, the Jefatura de Transmisiones of the Peruvian Army, and the Instituto Geofísico del Perú.

We also wish to thank the following persons for their help at various stages of the experiment:

Drs. Robert Cohen, Donald T. Farley, Jr., Tor Hagfors, Ben B. Balsley and Ronald Woodman, and John L. Green of the Jicamarca Radar Observatory for their advice, suggestions and encouragement: Generals Pedro Puente Revilla, Ricardo Jáuregui Revilla, Colonels Edulfo Canales Marcos, Jorge Estrada and Fernando Salgado, and Lieut. Col. Juan Barreda Delgado, for their support and assistance on behalf of the Jefatura de Transmisiones of the Peruvian Army.

The project was carried out under the direct leadership of Ing. Carlos A. Romero, jointly with Major EP Augusto Llanos Oliveros, Alvaro Santiváñez Villalobos and Oscar Pérez Rodríguez, who successively held the post of Chief of the Division of Research and Development of the

Jefatura de Transmisiones of the Peruvian Army. The personnel actively participating in the operation included Messrs. Rómulo Gómez Sierra, Douglas Llense, Antonio Arévalo and Sergeants First Class Percy Ponce, Arístides Aparcana, Percy Iturry and Sergeant Second Class Abrahán Gilbonio.

REFERENCES

1. Bailey, D.K., et al. — *Radio Transmission at VHF by Scattering and Other Processes in the Lower Ionosphere.* Proceedings, Institute of Radio Engineers, Vol.43, 1955, pp.1181-1231

2. Cohen, R. Bowles, K.L. — *Ionospheric VHF Scattering near the Magnetic Equator during the International Geophysical Year.* Journal of Research, National Bureau of Standards, D, Radio Propagation, Vol.67D, 1963, pp.459-480.

3. Cohen, R. Bowles, K.L. — *The Association of Plane-Wave Electron-Density Irregularities with the Equatorial Electrojet.* Journal of Geophysical Research, Vol.68, 1963, pp.2503-2525.

4. Harding, W.B. Whittaker, D.C. — *A 3 kW VHF Transmitter for Radio Propagation Studies.* Unpublished NBS Report, 1957.

5. Sulser, P.G. Bowles, K.L. — *A VHF Laboratory Receiver for Radio Propagation Studies.* Unpublished NBS Report, 1956.

6. Balsley, B.B. — *A Device to Continuously Record the Rate of Fading of an Ionospherically Propagated Signal.* Unpublished NBS Report, 1959.

7. Balsley, B.B., — *Evidence of the Night-Time Current Reversal in the Equatorial Electrojet.* Annales de Géophysique, Vol.22, 1966, pp.460-462.

8. Romero, C., — *Effect of the Solar Total Eclipse of November 12, 1966 on the Behavior of VHF Ionospheric Forward Scatter Propagation in the Equatorial Electrojet.* Paper presented at the Solar Eclipse Symposium, São José dos Campos, Brazil, February 1968.

TABLE I

	Lima-Juliaca	*Arequipa-Trujillo*
Frequency	47.3 MHz	49.92 MHz
Coordinates of the transmitter location	Lima 12° 02.6W 77° 02.5S	Arequipa 16° 44′ S, 71°52S
Coordinates of the receiver location	Juliaca 15° 29.5′ S 70° 08.1′ W	Trujillo 8° 06′ S 79° 04.5′ W
Coordinates of the path midpoint	13° 46.2 S 73° 37.2 W	12° 21.0 S 79° 04.5 W
Magnetic latitude of the path mid-point (dip)	-0.8°	+2°
Path length along earth's surface	838 km	1230 km
Antenna beamwidth in the horizontal plane	38°	6°
Antenna elevation angle	10°	4.7°
Transmitted power	880 watts	2 kW
Attenuation in decibels relative to inverse-distance transmission	-70 dB	-94 dB
Date of commencement	October 1966	December 1957
Date of termination	August 1967	November 1958

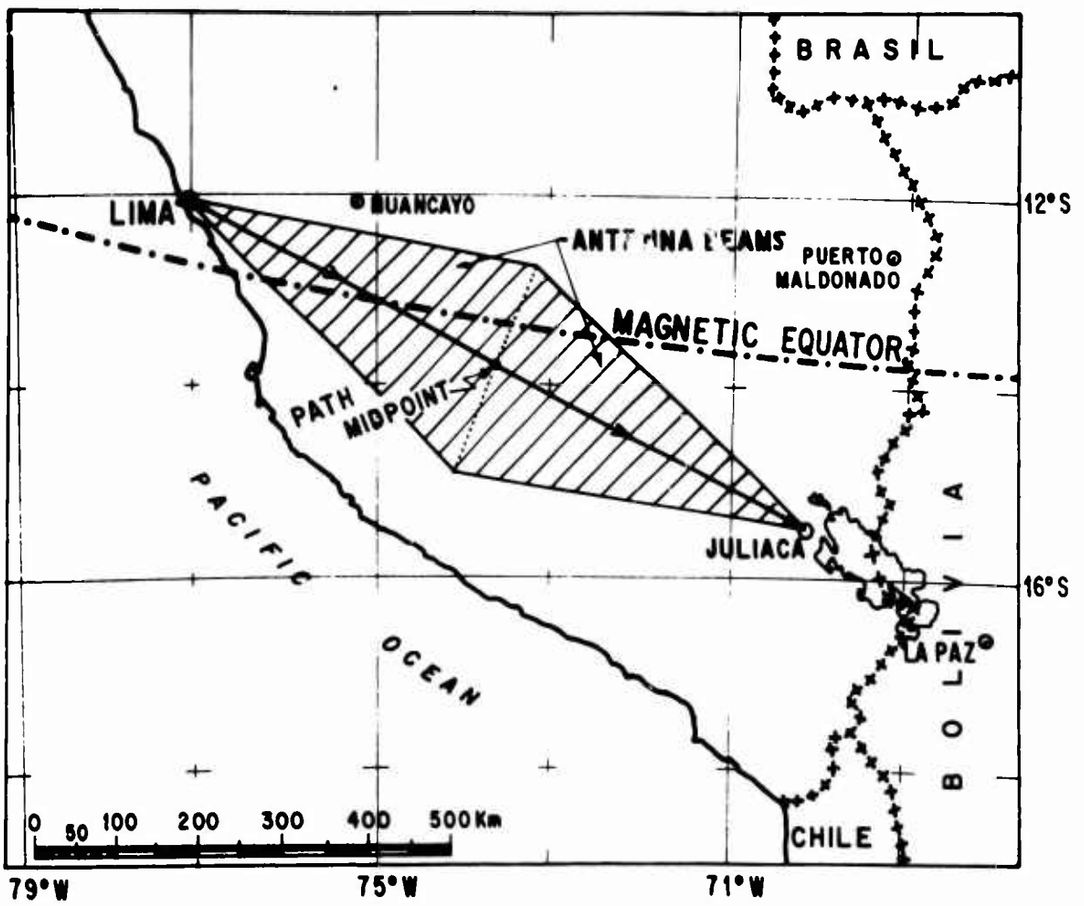


Fig. 1. Map showing the experimental circuit for VHF forward scatter propagation between the cities of Lima and Juliaca.

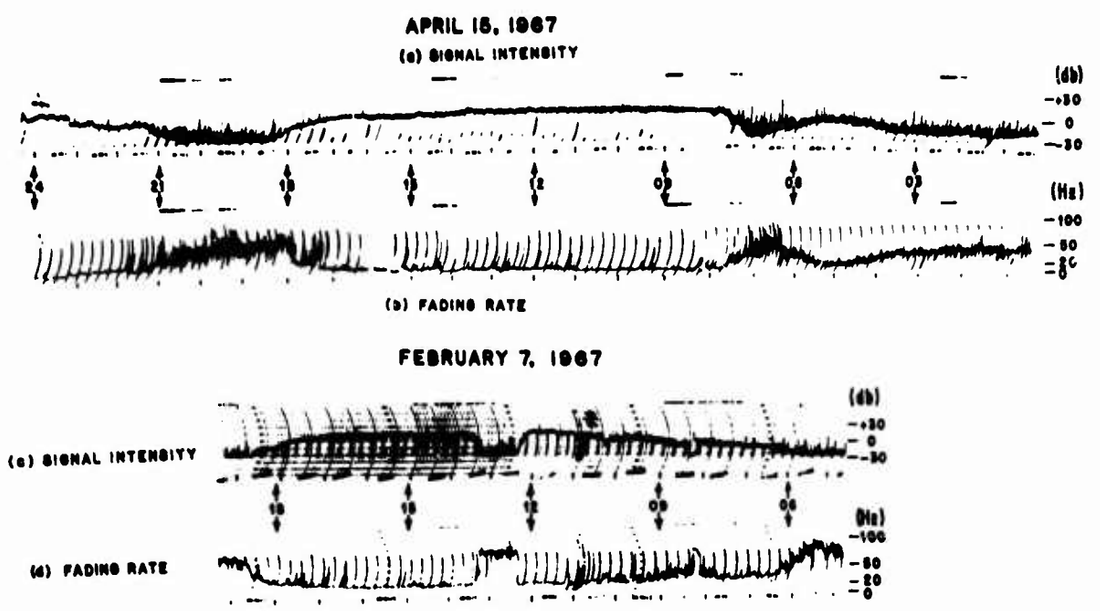


Fig. 2. Typical records of signal intensity and fading rate for a quiet day and for a disturbed day. Times shown are 75°W.

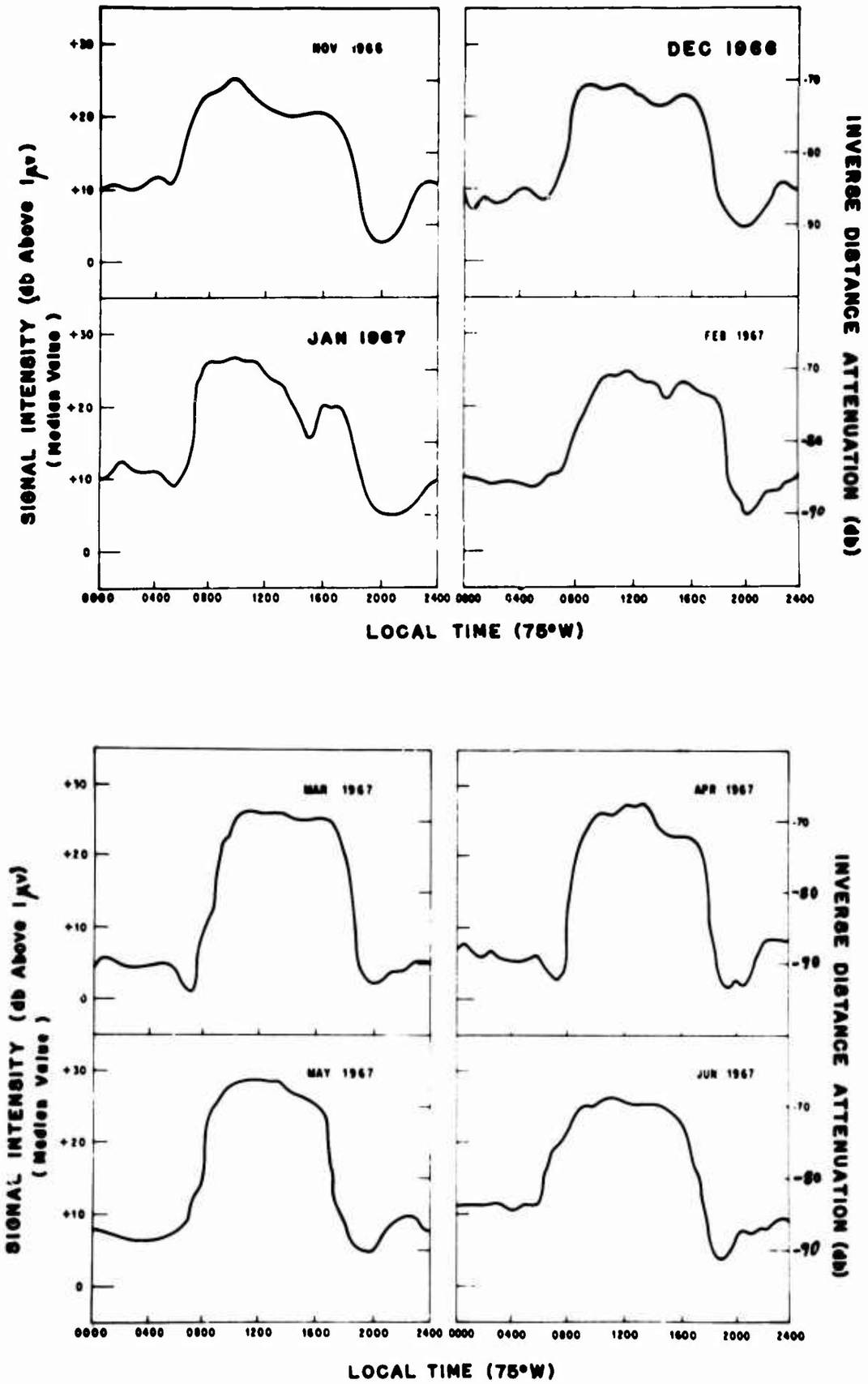


Fig.3. Monthly median values of received signal intensity.

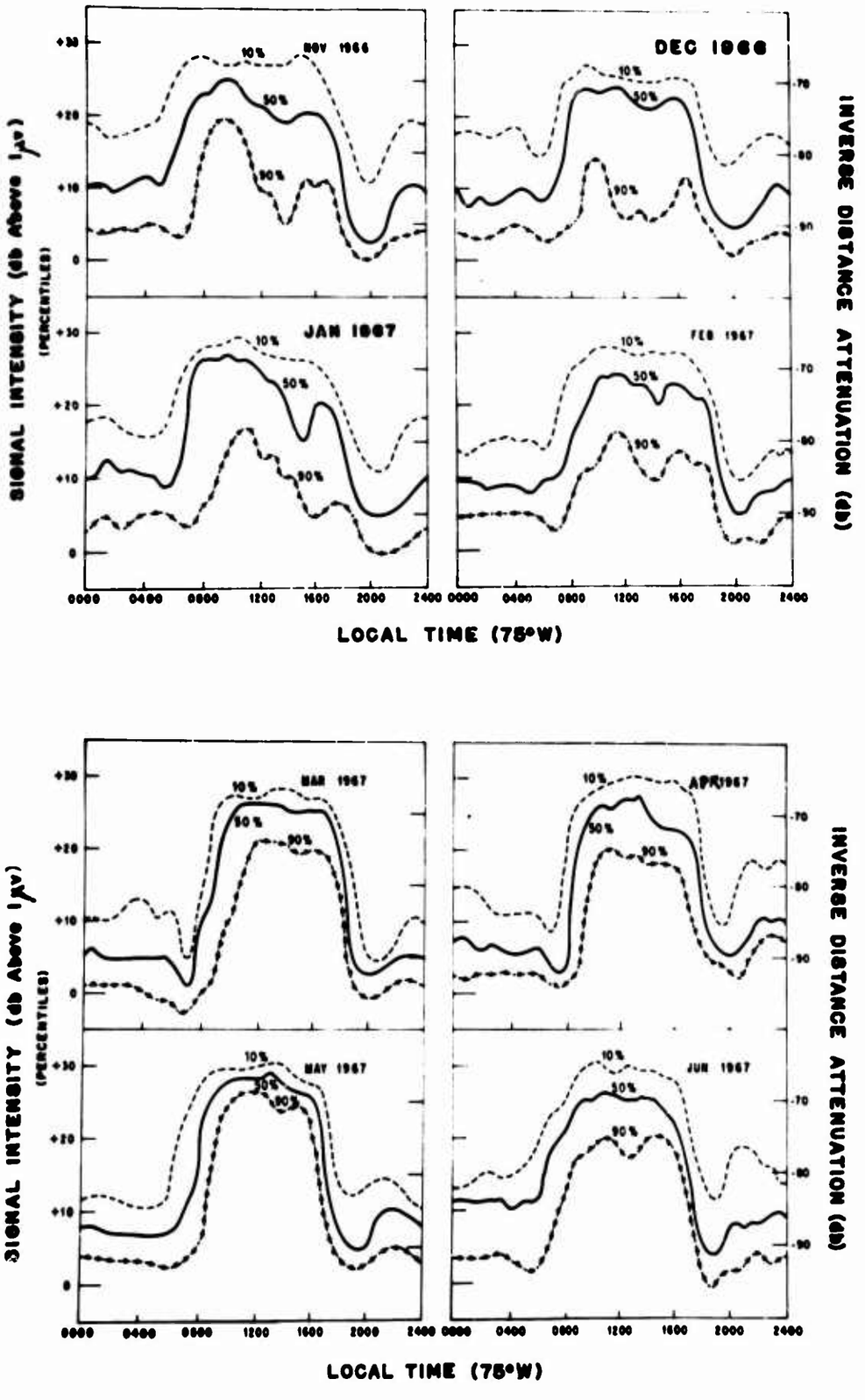


Fig. 4. Monthly percentiles of received signal intensity.

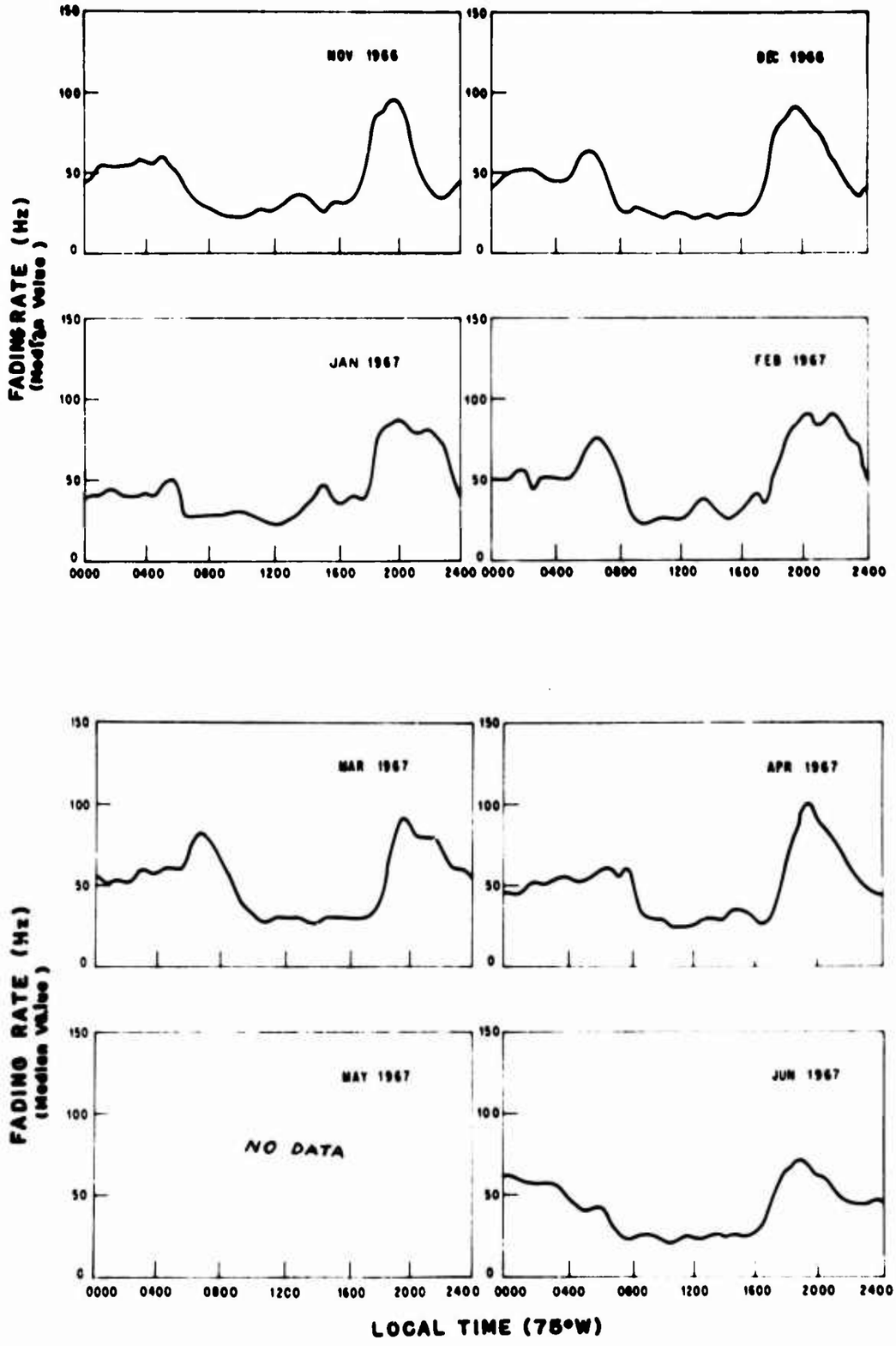


Fig. 5. Monthly median values of fading rate.

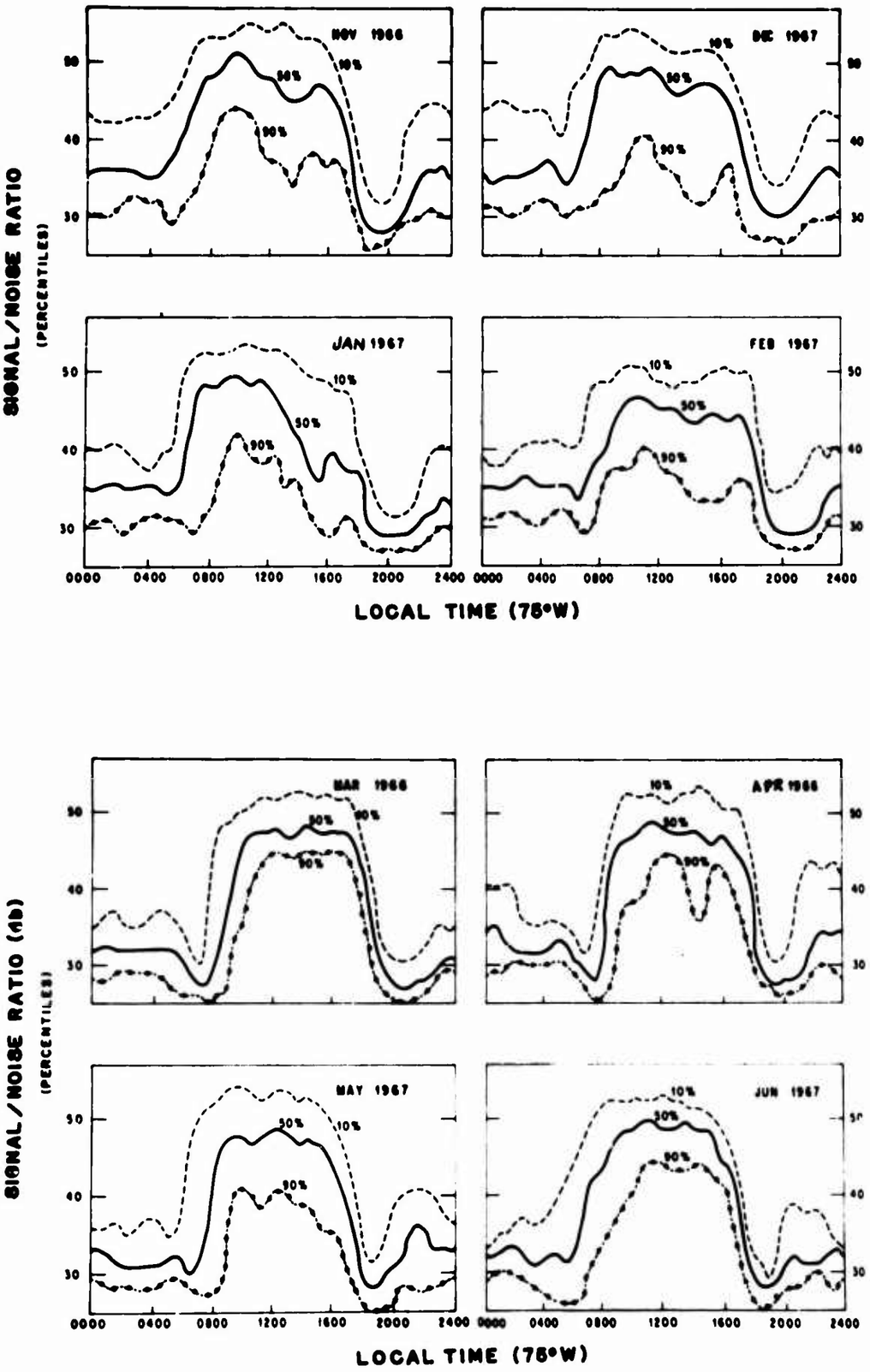


Fig.6. Monthly percentiles of signal-to-noise ratio.

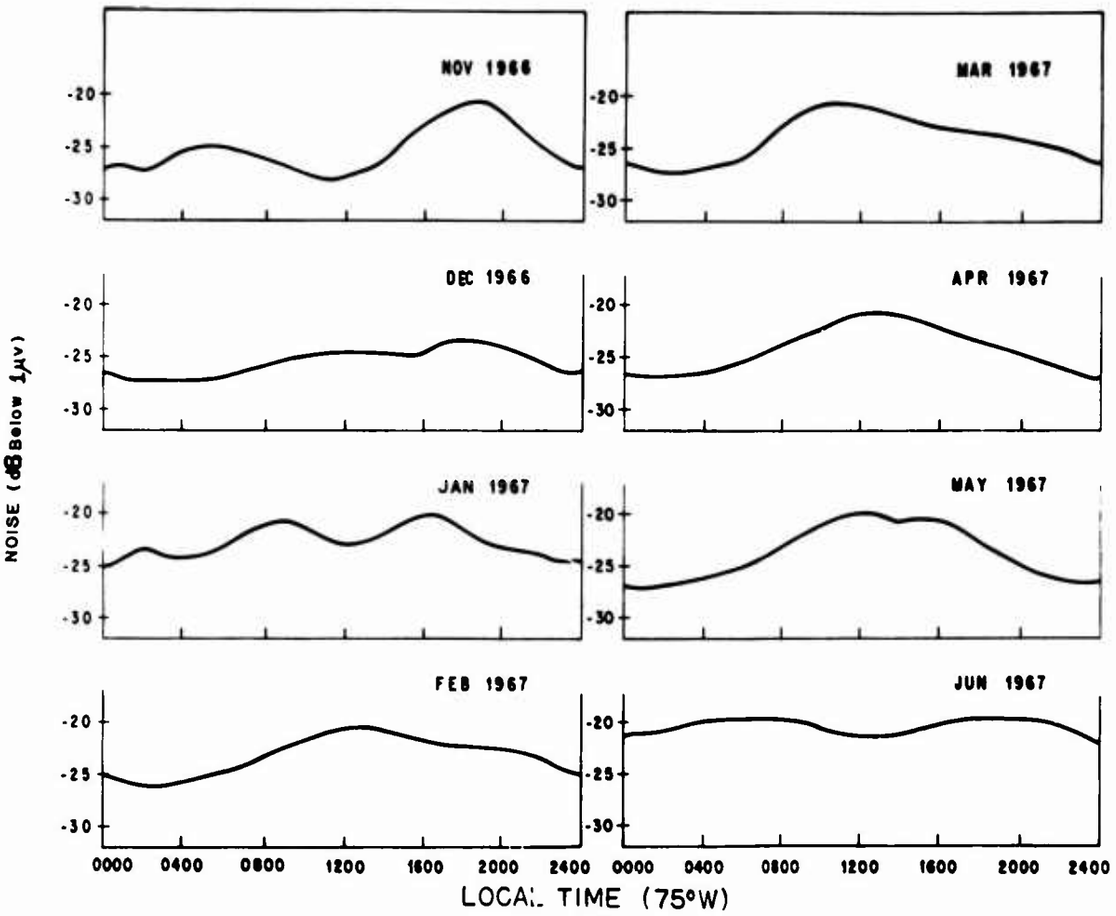


Fig.7. Monthly median values of noise level.

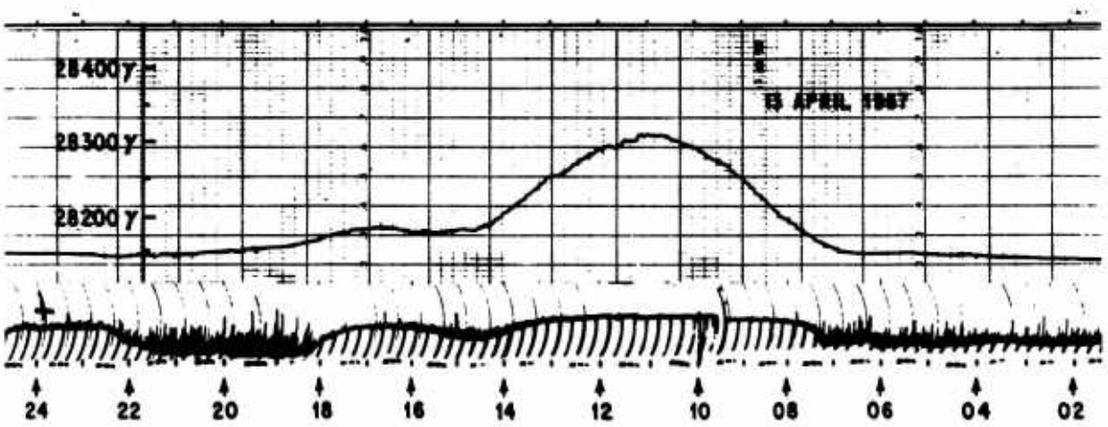


Fig.8. Record of the scattered signal intensity received at Juliaca on a quiet day, together with the total magnetic field intensity recorded at Jicamarca. Times shown are 75°W.

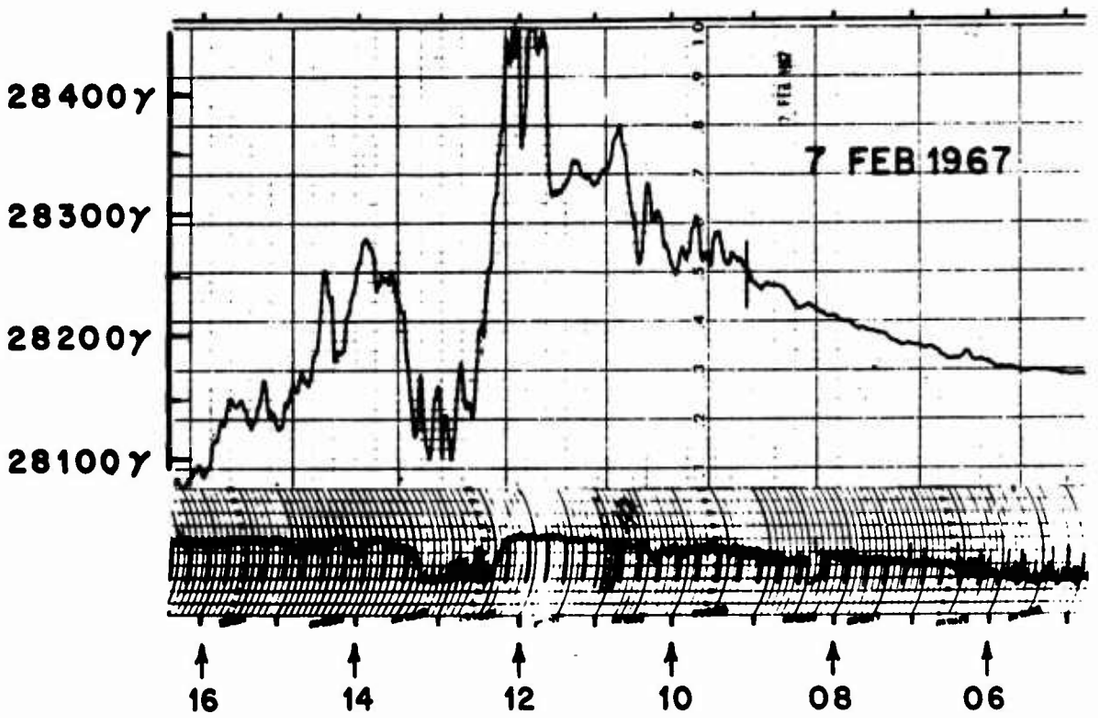
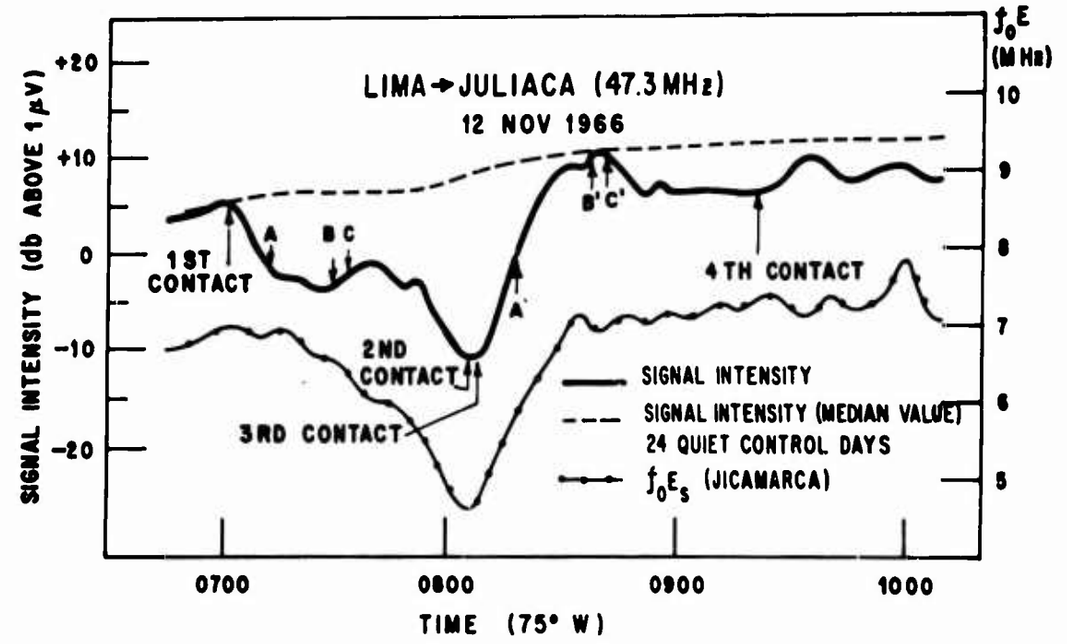


Fig.9. Record of the scattered signal intensity received at Juliaca during a disturbed day, together with the total magnetic field intensity recorded at Jicamarca. Times shown are 75°W.



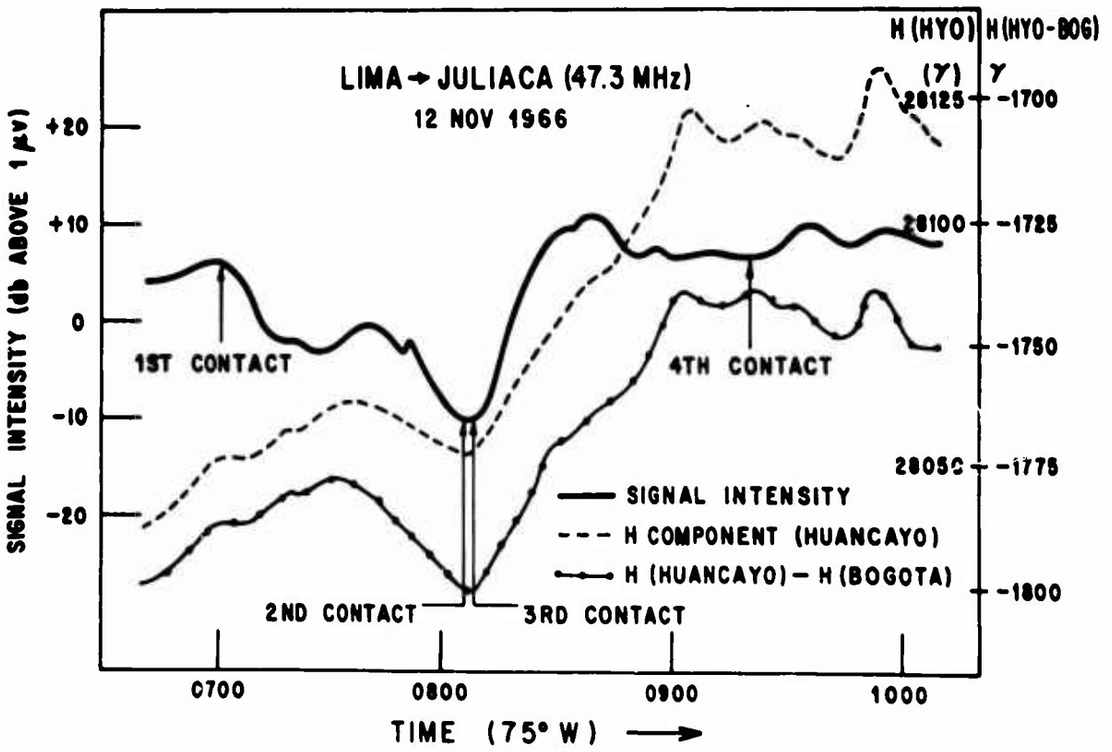


Fig. 10. Effect of the total solar eclipse of 12 November 1966 on the scattered signal intensity and other parameters.

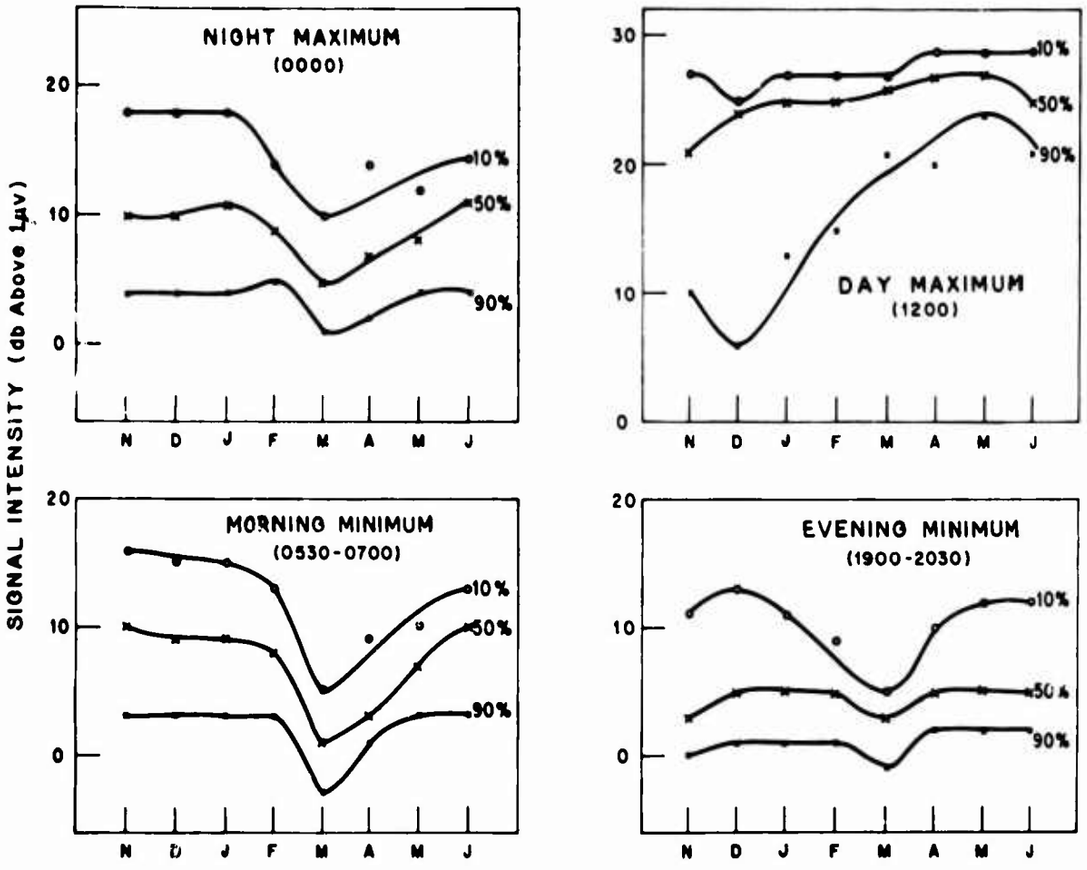


Fig. 11. (a) Seasonal variation of the scattered signal intensity during times of the night-time and daytime relative maxima and during the time intervals of the morning and evening relative minima. Times shown are 75°W.

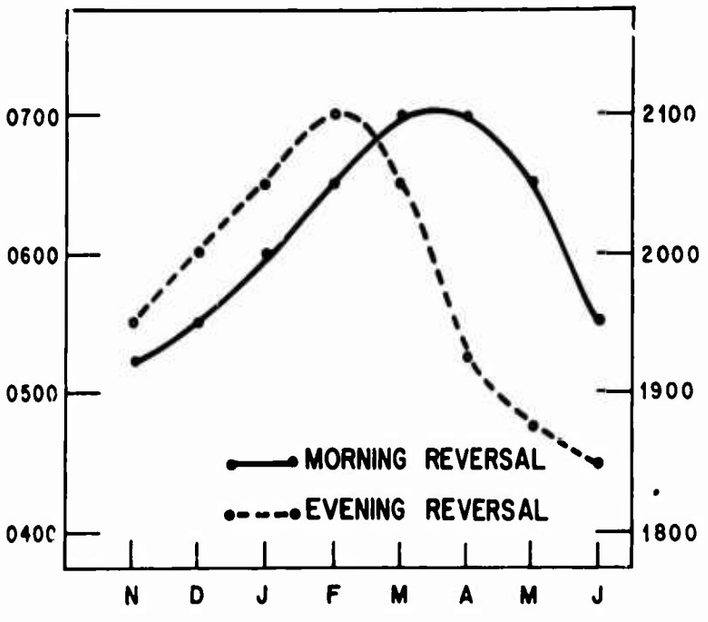


Fig. 11. (b) Seasonal variation of the times of the morning and evening reversals of the electrojet. Times shown are 75°W.

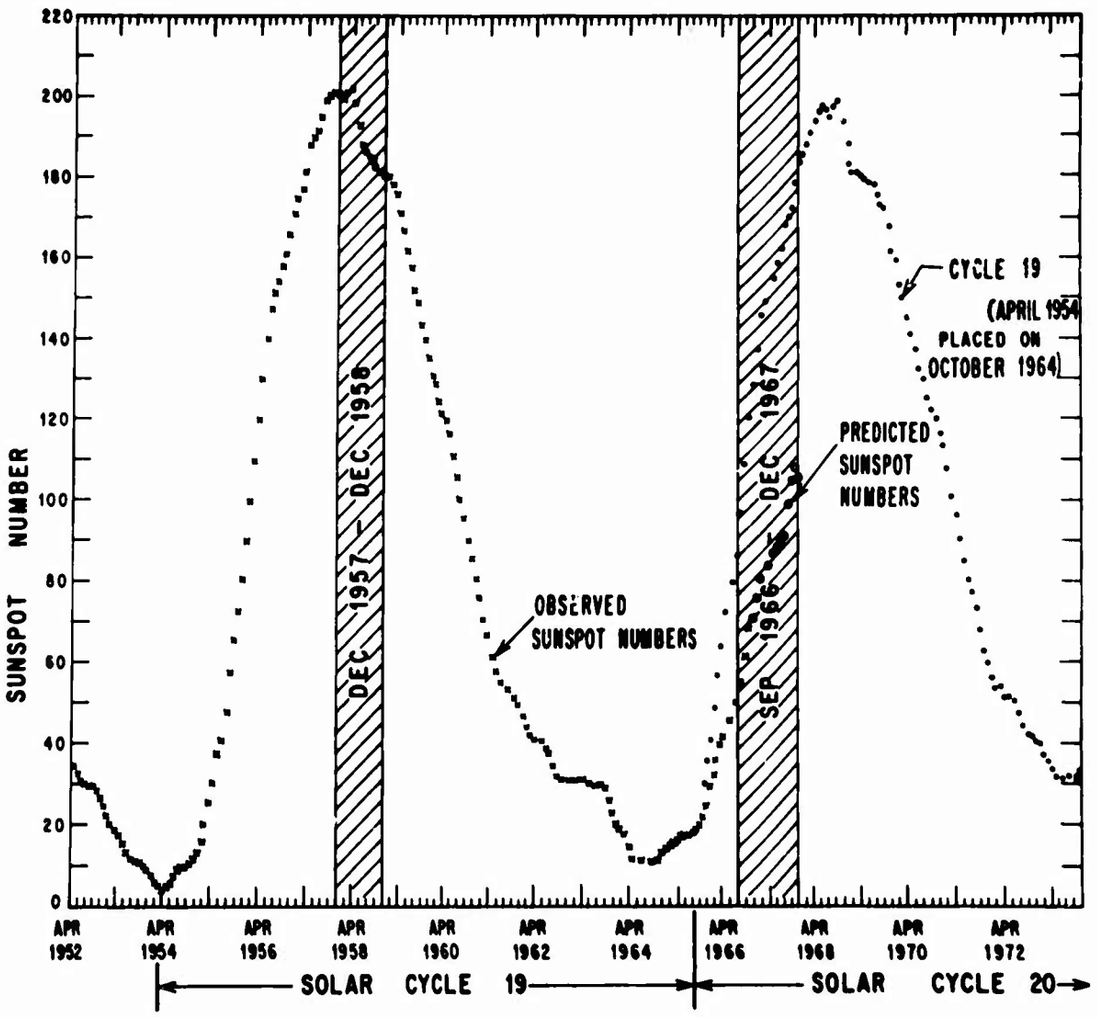


Fig. 12. Sunspot numbers for solar cycles 19 and 20, with the periods of operation of the Arequipa-Trujillo and Lima-Juliaca circuits indicated by shading.

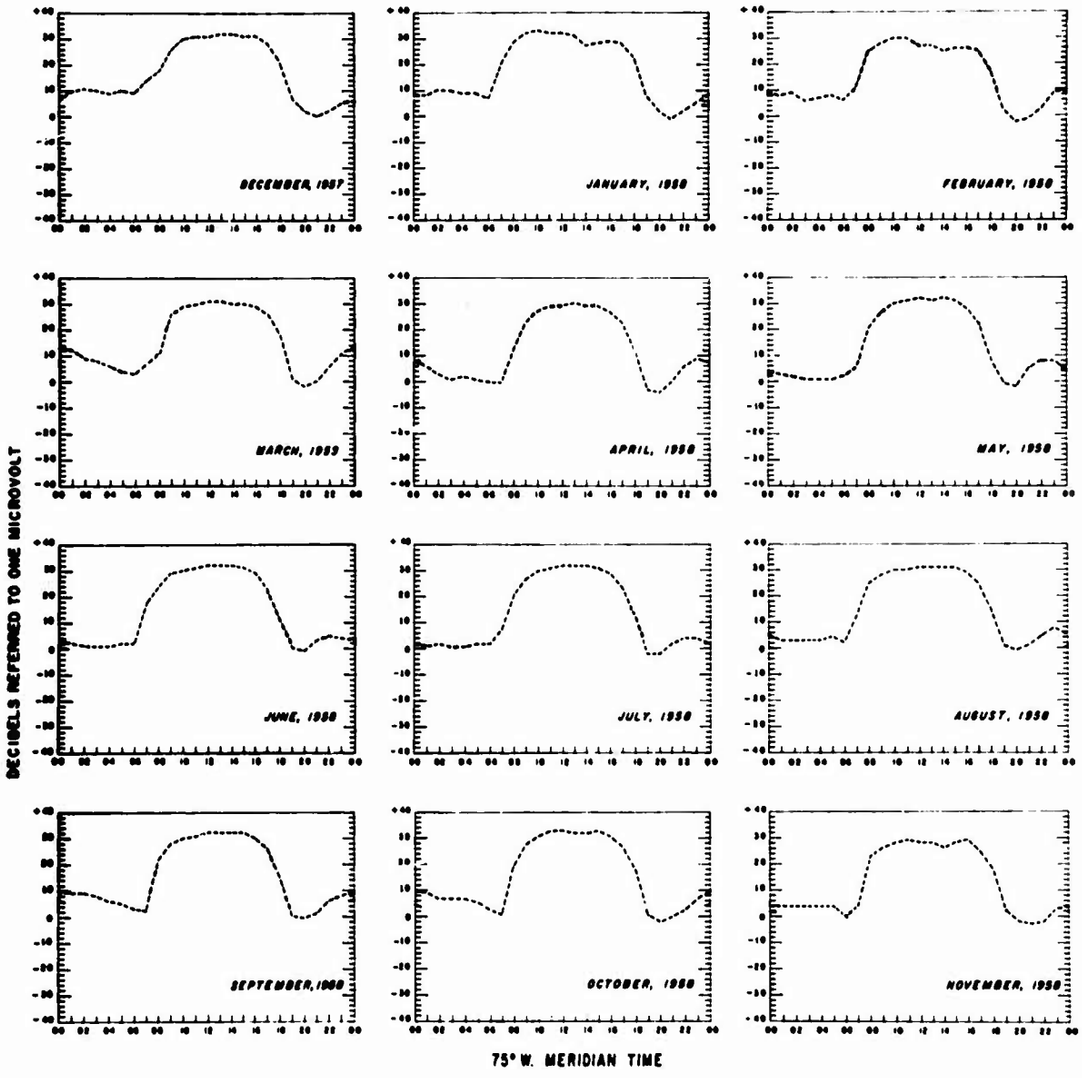


Fig. 13. Monthly median values of the scattered signal intensity for the Arequipa-Trujillo circuit during the International Geophysical Year (1958).

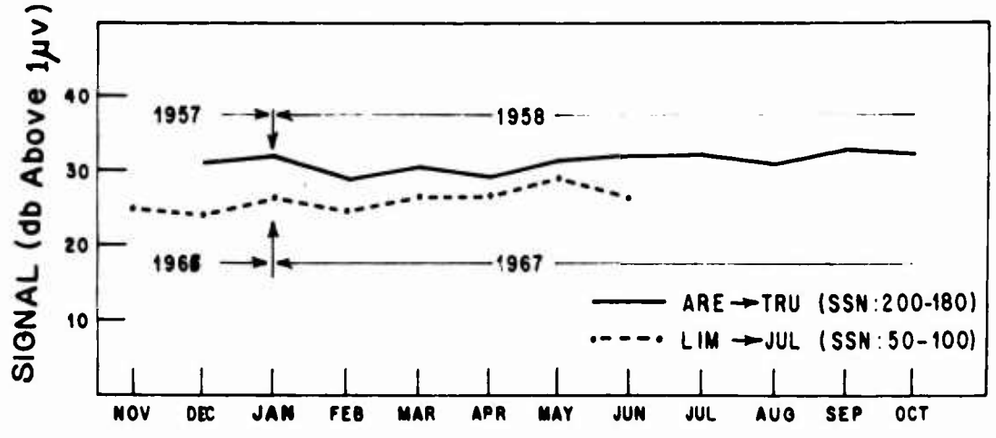


Fig. 14. Scattered signal intensity values for the daytime maximum for the Arequipa-Trujillo (1958) and Lima-Juliaca (1967) circuits.

MICROWAVE SCATTERING FROM SPHERICAL ELECTRON CLOUDS

by

N. W. Rosenberg*, M. M. Klein* and G. Anderson†

*Air Force Cambridge Research Laboratories,
Bedford, Mass., USA

†Harvard College Observatory,
Cambridge, Mass., USA

SUMMARY

The scattering of radio waves by a spherical electron cloud with a Gaussian distribution of electron density has been treated numerically by ray optics methods. In the case of no magnetic field, it is found that a hard or highly overdense sphere may be replaced by a conducting sphere of radius equal to the critical radius. This approximation is inaccurate for a soft or slightly overdense sphere. It is also found that, in forward scatter, all spheres have essentially the same cross-section. The effect of a magnetic field is found to be negligible in forward scattering and effective in backscatter only for soft spheres. The orientation of the field is similarly important in backscatter only for soft spheres. The extraordinary ray yields a cross-section generally typical of a hard sphere, provided the gyromagnetic ratio is not too small.

NOTATION

b	impact parameter
c	velocity of light
f	cyclic frequency
H_e	earth's magnetic field
r	radial coordinate
t	time
x	coordinate along direction of propagation
X	ratio of plasma electron density to critical density
Y	gyromagnetic ratio
z	coordinate in magnetic meridian plane normal to propagation direction
α	angle between wave normal and horizontal
θ	scattering angle
θ_p	angle between horizontal and earth's magnetic field
σ	scattering cross-section
μ	index of refraction
ω	circular frequency ($= 2\pi f$)

Subscripts

cr	critical
eff	effective
G	Gaussian
L	longitudinal component
o	center-point value
T	transverse component

MICROWAVE SCATTERING FROM SPHERICAL ELECTRON CLOUDS

N. W. Rosenberg, M. M. Klein and G. Anderson

1. INTRODUCTION

For the past several years, the Air Force Cambridge Research Laboratories have been engaged in studies of the atmosphere by means of barium clouds released at high altitudes. Optical studies show the development of a spherical neutral cloud during the first few seconds of the expansion. Subsequently, however, due to the rapid diffusion along the magnetic field, the ion clouds formed from the neutral cloud becomes ellipsoidal in shape with the major axis aligned along the magnetic field. The growth of the ion and neutral clouds in a typical barium release is shown in Figure 1. The cloud, which is several kilometers in extent, is overdense to radar frequencies in the range 3-30 MHz.

To help in the understanding and interpretation of experimental data, we are conducting a theoretical study of the scattering of electromagnetic waves incident upon an electron cloud. In view of the small wavelength (10-100 meters) compared to the cloud size, the method of geometrical optics may be employed. The scattering is described in terms of the deformation of neighbouring rays as they pass through the electron cloud. To obtain the ray paths, we have utilized the first-order differential equations developed by Haselgrove[1] for ray propagation in the presence of a magnetic field. These equations are particularly well suited for solution by high speed digital computers. For simplicity, we shall assume the cloud is spherical in shape and, as indicated by diffusion theory, has a Gaussian distribution of electron density in the radial direction. In addition, we shall, in view of the small values of the ratio of collision frequency to incident frequency obtaining within the cloud, neglect absorption in our calculations.

2. ANALYSIS

We consider a ray initially a distance b from the z axis and deflected through an angle θ as it emerges from the cloud (Figure 2). The equations of Haselgrove describing the ray path are

$$\frac{dx}{dt} = \frac{c}{\mu^2}\left(\mu \sin\alpha - \frac{\partial\mu}{\partial\alpha}\cos\alpha\right) \tag{1}$$

$$\frac{dz}{dt} = \frac{c}{\mu^2}\left(\mu \cos\alpha + \frac{\partial\mu}{\partial\alpha}\sin\alpha\right) \tag{2}$$

$$\frac{d\alpha}{dt} = \frac{c}{\mu^2}\left(\cos\alpha\,\frac{\partial\mu}{\partial x} - \sin\alpha\,\frac{\partial\mu}{\partial z}\right), \tag{3}$$

where μ is the index of refraction, c the velocity of light, and α the angle the wave normal makes with the horizontal at a given point in the cloud. The factor c obviously has no effect upon the geometry of the ray and may be conveniently absorbed in the time factor t. The index of refraction is given by the Appleton-Hartree equation[2] which, for the case of no absorption, has the form

$$\mu^2 = 1 - \frac{2X(1-X)}{2(1-X) - Y_T^2 \pm \sqrt{[Y_T^4 + 4Y_L^2 (1-X)^2]}}, \tag{4}$$

where $X = \omega_N^2 / \omega^2$, ω_N and ω are the plasma and incident frequencies, and Y_T and Y_L are the transverse and longitudinal components of the gyromagnetic ratio Y,

$$\left.\begin{aligned} Y_L &= Y \cos \theta_p , \\ Y_T &= Y \sin \theta_p , \end{aligned}\right\} \tag{5}$$

and θ_p is the angle between the direction of propagation and the earth's magnetic field H_e.

If the incident rays are confined to the magnetic meridian plane, i.e., the plane containing the direction of propagation and the direction of the magnetic field, then no lateral deviations occur. Outside the magnetic meridian plane, lateral deviations do occur, but numerical solutions indicate these deviations to be small[3].

The electron density distribution within the cloud is assumed spherically symmetric and to have the Gaussian form

$$\frac{N}{N_0} = \exp\left(-\frac{r^2}{r_G^2}\right), \tag{6}$$

where r_G is the Gaussian radius, N the electron density, and the subscript zero refers to the centerpoint value. We may write Equation (6) as

$$\frac{N}{N_{cr}} = \frac{\omega_N^2}{\omega^2} = X = \exp\left[-\frac{(r^2 - r_{cr}^2)}{r_G^2}\right], \tag{7}$$

where the subscript cr refers to critical value. The differential cross-section σ for neighboring rays having impact parameters b and $b + \Delta b$ and scattered into the angle θ with angular spread $\Delta\theta$ is (see Figure 2)

$$\sigma = \frac{4\pi b \Delta b}{\Delta\theta \sin \theta} . \tag{8}$$

The meridian angle does not enter into Equation(8) since we are neglecting lateral deviations.

The ray paths were obtained by numerical integration of the Haselgrove equations on an IBM 7094 computer, utilizing a Runge-Kutta technique. Because of the rapid change of direction in the turning point region, refined sub-divisions had to be employed here to insure sufficient accuracy. Step sizes limited to 0.5^o, 0.25^o, and 0.125^o turning were compared and the asymptotic solution for scatter angle was estimated by extrapolation to zero step size. The calculations were made for several values of the critical radius, frequencies of 3 and 30 MHz and several orientations of the magnetic field. The Gaussian radius r_G was taken as the unit of length and the earth's magnetic field H_e as 0.36 gauss.

3. RESULTS AND DISCUSSION

3.1 No Magnetic Field

The variation of scattering cross-section σ with scattering angle θ for the case of no magnetic field is presented in Figure 3, where we have plotted log r_{eff} against scattering angle for several values of r_{cr}, where r_{eff} is the radius of a conducting sphere which has the cross-section σ. For the higher values of the critical radius, the effective radius is almost constant over a fairly wide range of backward scattering angles. As the critical radius decreases, the effective radius decreases very rapidly and the region of constant effective radius becomes very small. Since, as the critical radius decreases, the depth of penetration into the plasma increases, it is convenient to use the critical radius as a measure of the "hardness" of the sphere. Then our calculations show that, except for the region of forward scatter, a "hard" sphere may be replaced by a conducting sphere whose radius is equal to the critical radius. Such an approximation is indicated by our results to be inaccurate for a "soft" sphere. It is also interesting to note that the curves for different critical radii approach each other in the region of forward scatter. This is not surprising since here the rays penetrate only the outer edge of the sphere, where the electron density and its gradient are small and do not differ significantly for different critical radii. The angular deflection of a ray in this region accordingly depends principally upon its location and very little on the critical radius of the sphere. Therefore, all spheres will have the same cross-section in the forward direction, whose value will depend upon the cut-off radius where the electron density is considered to have a negligible effect upon the index of refraction.

The relation between r_{eff} and r_{cr} may be more explicitly exhibited by normalizing r_{eff} with respect to r_{cr}. A plot of r_{eff}/r_{cr} against scattering angle with r_{cr} as parameter, in Figure 4, shows the curves crossing each other at a scattering angle of about 105° near $r_{eff} = r_{cr}$. Hence, in the scattering region near 105°, a conducting sphere of radius equal to the critical radius is equivalent to our Gaussian sphere. Since r_{eff} decreases very rapidly with r_{cr} and becomes very close to r_{cr} for large r_{cr}, it is of interest to see whether a simple exponential law may give accurately the relation between r_{eff} and r_{cr} in backscatter. A plot of log $(1-(r_{eff}/r_{cr}))$ against r_{cr} can indeed be fitted with reasonable accuracy by a straight line whose equation

$$1 - \frac{r_{eff}}{r_{cr}} = \exp\,(-1.20\, r_{cr}) \qquad (9)$$

is a convenient representation of the data in the backscatter region. Although Equation (9) is an empirical relation, its limiting form for small r_{cr},

$$r_{eff} = 1.20\, r_{cr}^2 , \qquad (10)$$

may be derived directly from Equation (8) with the constant 1.20 replaced by unity.

3.2 Effect of a Magnetic Field

The variation of effective radius with scattering angle is shown in Figures 5 and 6 for the case where the magnetic field is at 135° to the horizontal and for frequencies of 3 MHz and 30 MHz respectively. We note that the extraordinary ray exhibits a substantially higher cross-section in the backscatter region than the corresponding ordinary ray. This is in agreement with the fact that the extraordinary ray has a lower critical electron density than the ordinary ray, penetrating less deeply into the plasma. It, therefore, has the characteristics of a hard sphere with its relatively small variation of cross-section in the backscatter region. This result is, of course, more pronounced for the lower frequency. Because of difficulties in calculation, the curves for the ordinary ray are not complete in the backscatter region. The difficulty appears to be due to the lining up of the ray with the magnetic field when it starts to turn significantly in the

deep part of the plasma. In longitudinal propagation, however, the index of refraction stays substantially away from zero so long as the ray has not reached the critical density. The turning of the ray is therefore slowed down and it becomes difficult to obtain results in the backscatter region, no matter how small an impact parameter is chosen.

A comparison of the cross-sections for field and no-field cases is shown in Figure 7, where we have plotted the results for the extraordinary ray and the zero-field case for $r_{cr} = 0.125$ and 0.5. The effect of the magnetic field is most pronounced at the lower frequency and the smaller r_{cr}. As the critical radius increases, the effect of the magnetic field becomes very small at $r_{cr} = 0.5$ for the higher frequency. In all cases, the magnetic field has a negligible effect for a considerable range of forward scattering angles. It therefore appears that, except for frequencies not much higher than the gyromagnetic frequency, the effect of the magnetic field is negligible when the critical radius is greater than 0.5.

Calculations of the scattering cross-section for various directions of the magnetic field indicate that the effect of the field orientation becomes negligible at some value of the critical radius between 0.5 and 1.0. For a frequency of 30 MHz the required value is about 0.5, while for 3 MHz it is close to unity. The effect of the field direction upon the scattering for a very soft sphere is shown in Figure 9, where we have plotted the scattering for the extraordinary ray at a frequency of 30 MHz and for a critical radius of 0.125 against θ_p for several scattering angles. The orientation is quite significant in the backscatter region but its effect decreases rapidly and becomes negligible below about 90^o. In general, the orientation of the field is negligible for forward scattering in all cases and is significant in backscattering only for soft spheres.

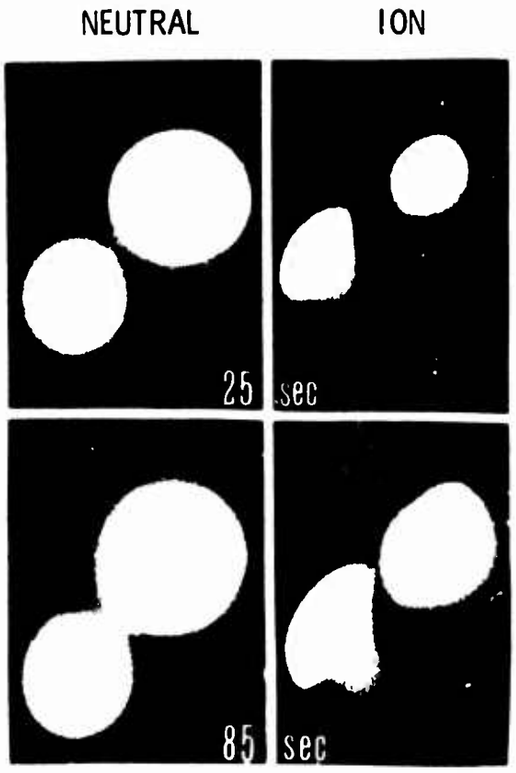
Some typical ray paths for a critical radius of 0.5 and a field orientation of 135^o are shown in Figures 10 and 11 for the extraordinary ray and in Figure 12 for the ordinary ray. In Figures 10 and 11, we note the increased effect of the magnetic field as the incident frequency is decreased from 30 to 3 MHz, exhibited principally through the downward bending of the rays with small impact parameter and the shift of the turning point away from the critical density surface $X = 1$. Figure 12 shows the greater depth of penetration of the ordinary ray and the requirement of a very small impact parameter to obtain rays in the backscatter region.

REFERENCES

1. Haselgrove, J. — *Ray Theory and a New Method for Ray Tracing.* Physical Society, London, Report of Conference on the Physics of the Ionosphere, 1955, pp. 355-364.

2. Kelso, J. — *Radio Ray Propagation in the Ionosphere.* McGraw-Hill, New York, Chapter 4, 1964.

3. Kelso, J. — *Radio Ray Propagation in the Ionosphere.* McGraw-Hill, New York, Chapter 6, 1964.



BA RELEASES 4 OCT 67

ION FILTER	4554A ± 10A
NEUT FILTER	5535A ± 20A
LOWER CLOUD	185 km
UPPER CLOUD	225 km

Fig. 1 Growth of neutral and ion clouds in a typical barium release

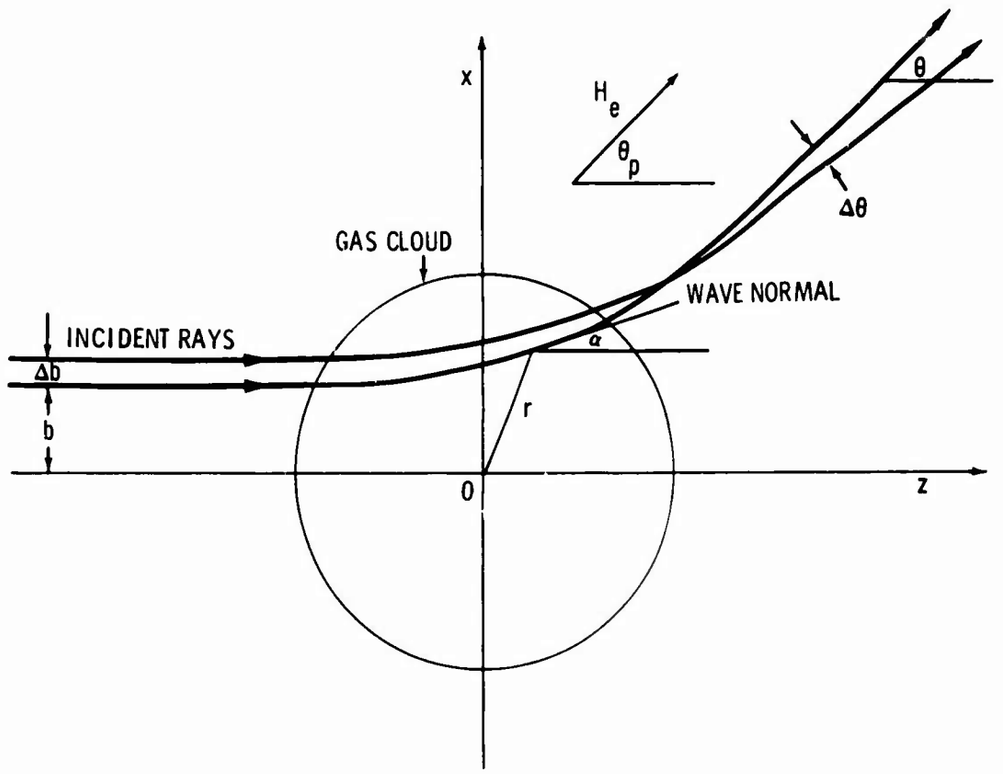


Fig. 2 Sketch showing geometry of ray path and magnetic field

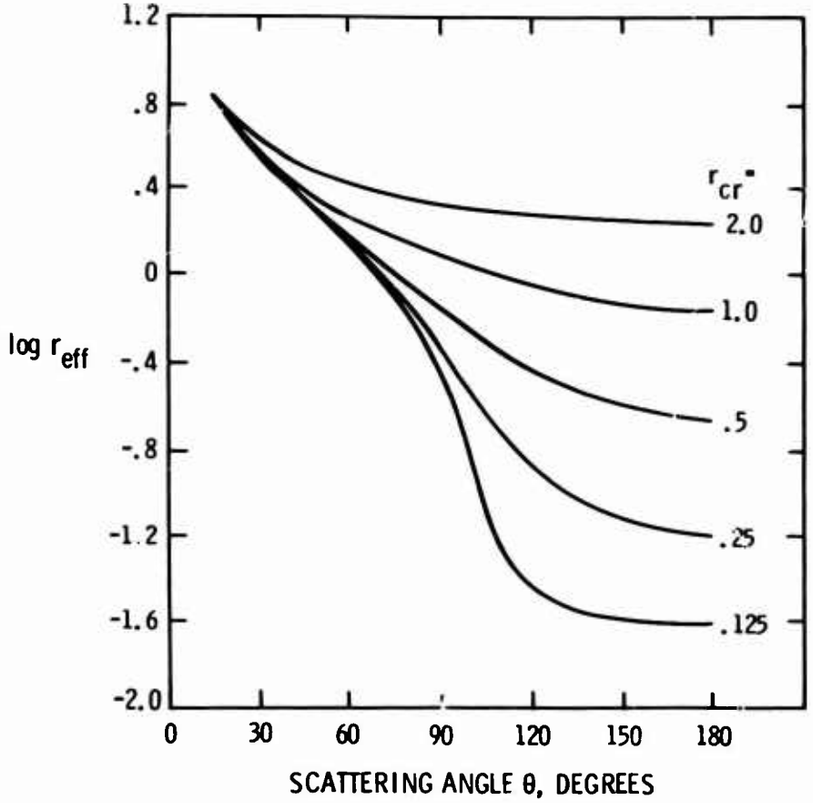


Fig. 3 Scattering for no-field case; log r_{eff} plotted as a function of scattering angle

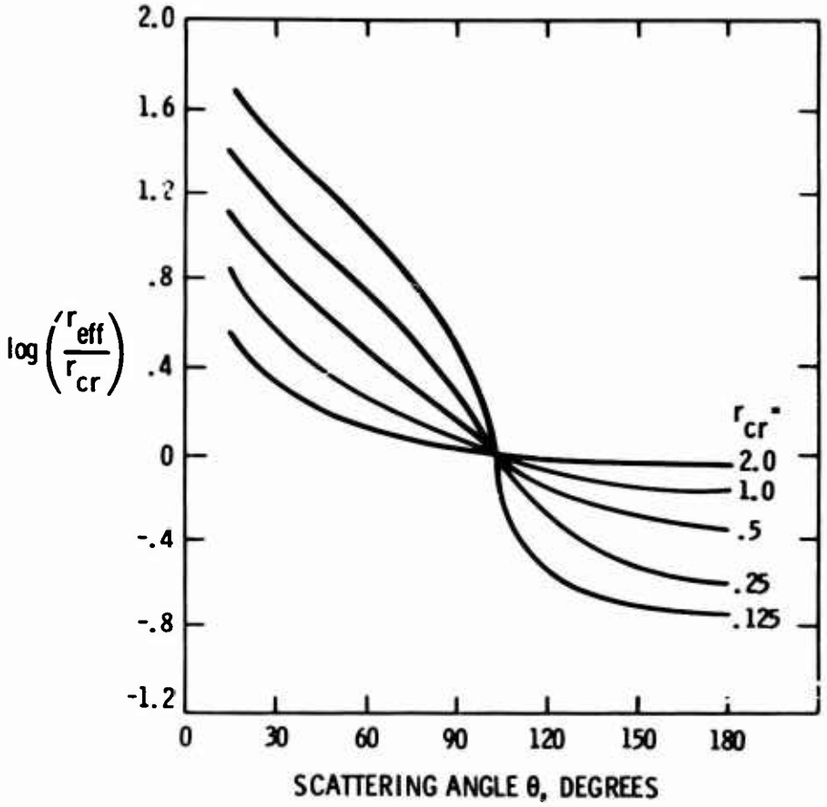


Fig. 4 Scattering for no-field case; log (r_{eff}/r_{cr}) plotted as a function of scattering angle

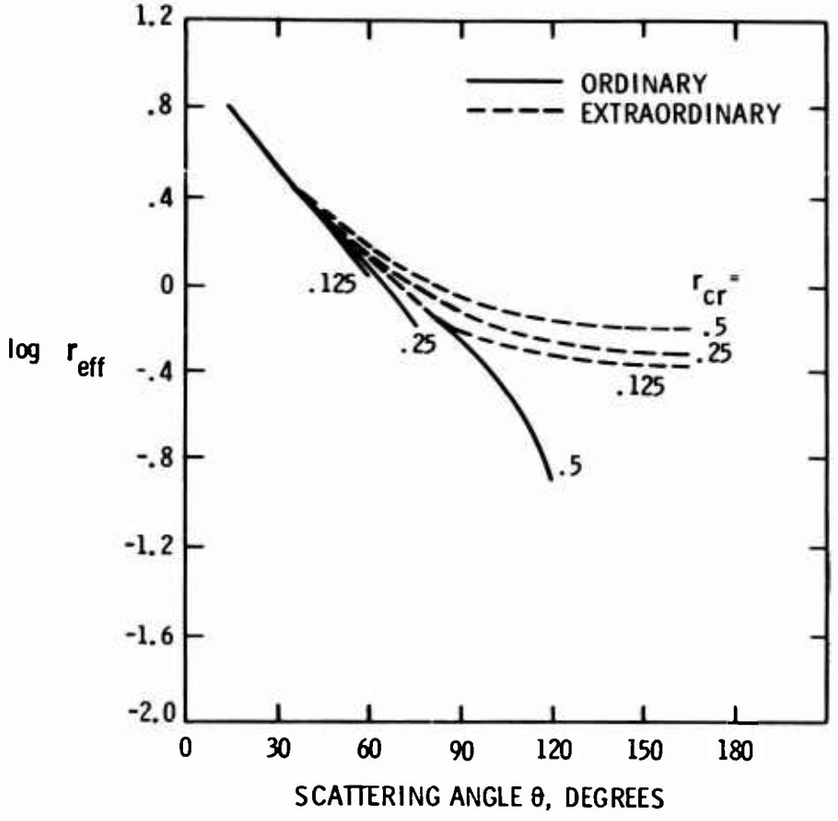


Fig. 5 Scattering in presence of magnetic field; r_{eff} plotted as a function of scattering angle.
$\theta_p = 135^o$, f = 3 MHz

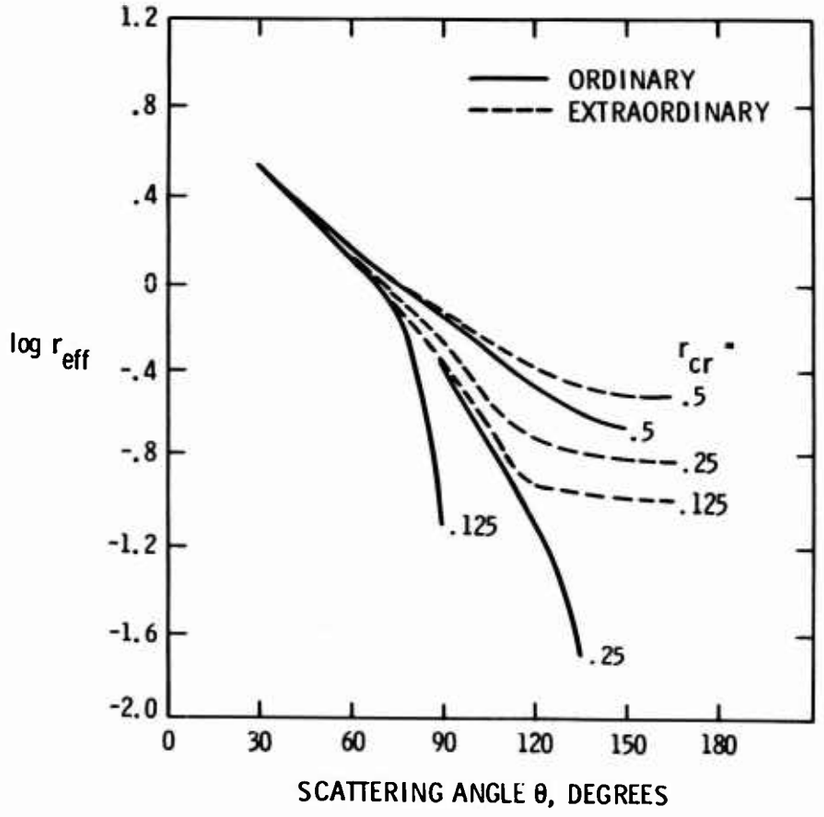


Fig. 6 Scattering in presence of magnetic field; log r_{eff} plotted as a function of scattering angle;
$\theta_p = 135^o$, f = 30 MHz

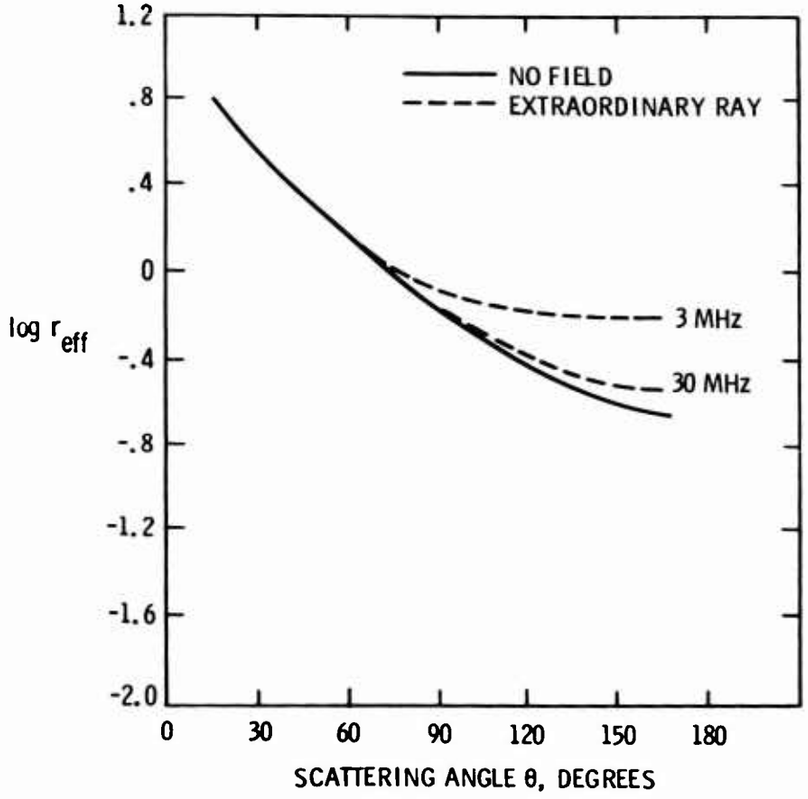


Fig. 7 Effect of magnetic field upon scattering for extraordinary ray; $\theta_p = 135^o$, $r_{cr} = 0.5$

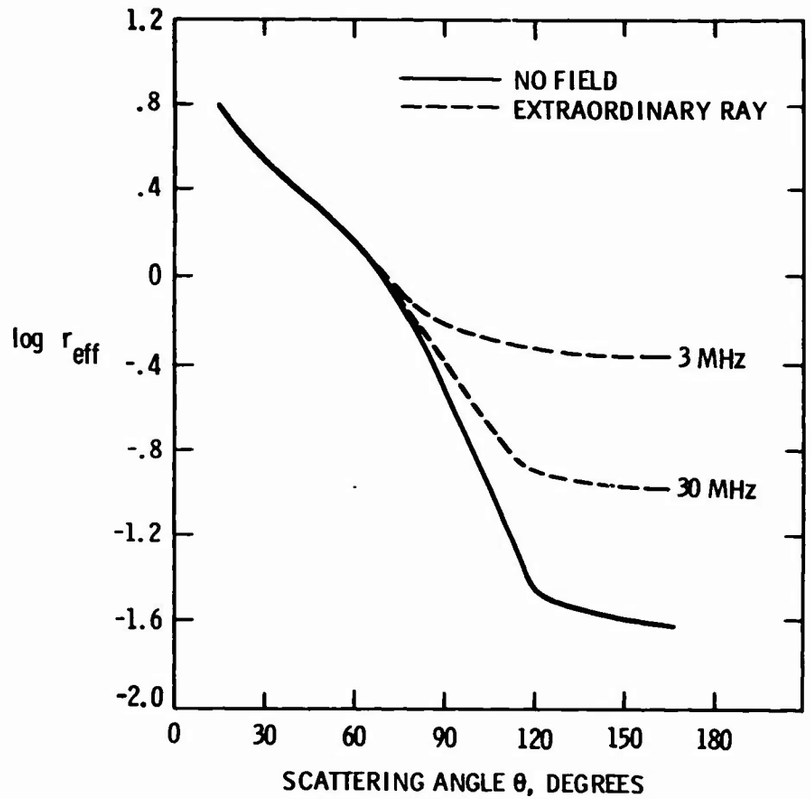


Fig. 8 Effect of magnetic field upon scattering for extraordinary ray; $\theta_p = 135^o$, $r_{cr} = 0.125$

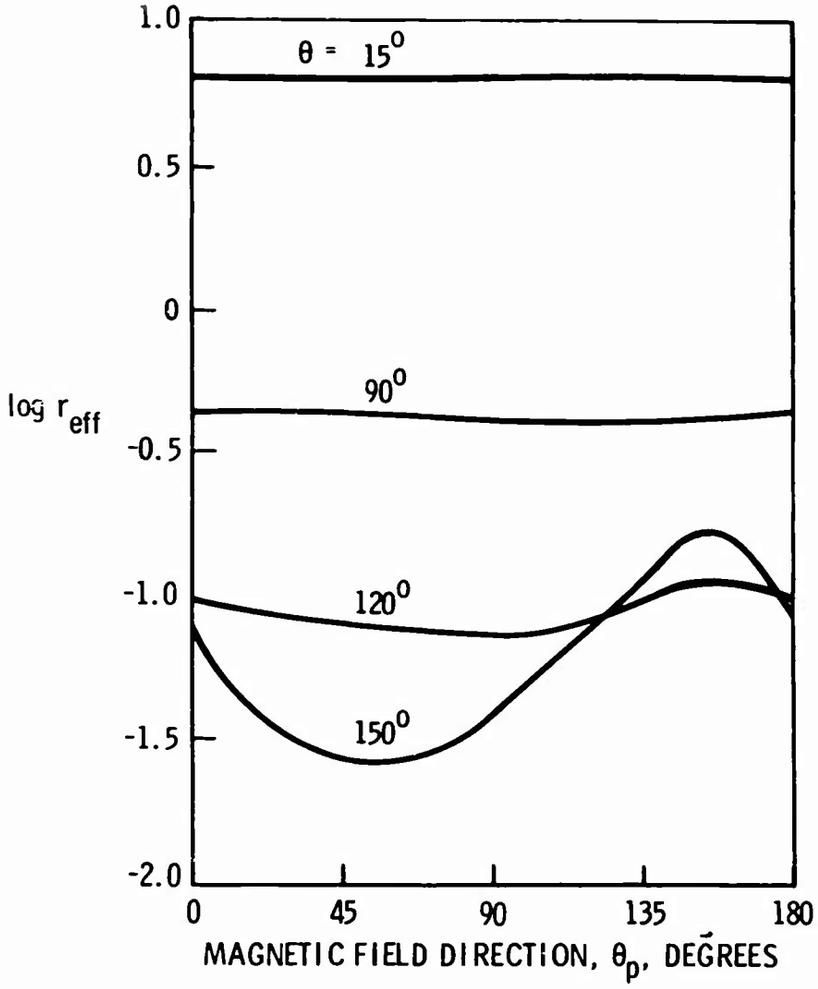


Fig. 9 Effect of orientation of magnetic field upon scattering for extraordinary ray; f = 30 MHz , r_{cr} = 0.125

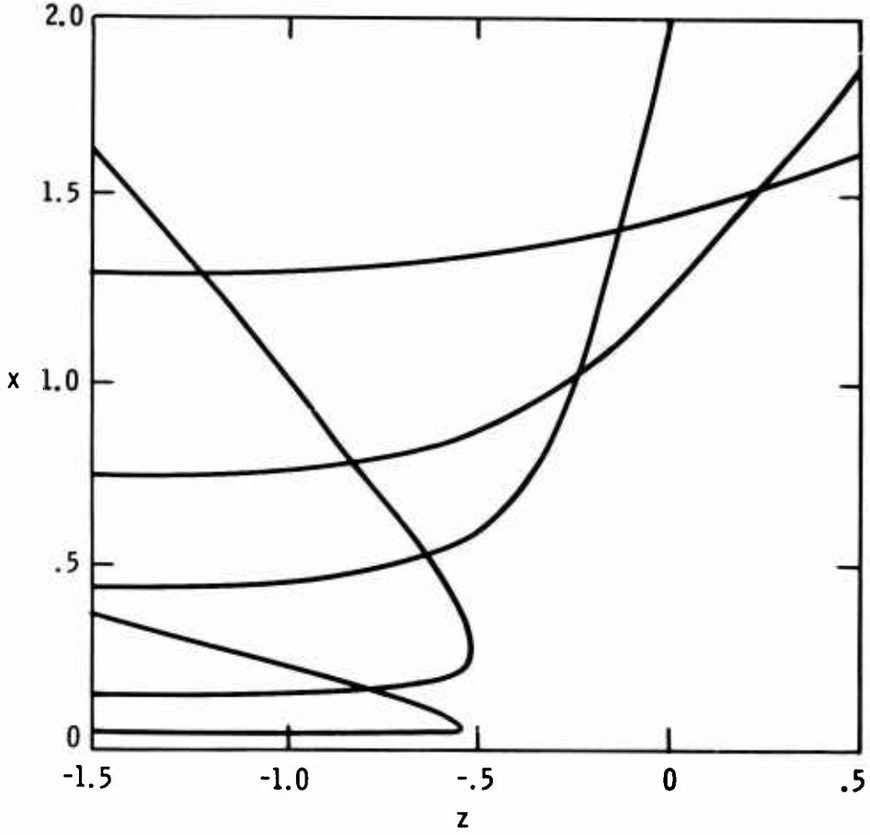


Fig. 10 Ray paths for extraordinary ray; r_{cr} = 0.5 , f = 30 MHz , $\theta_p = 135^o$

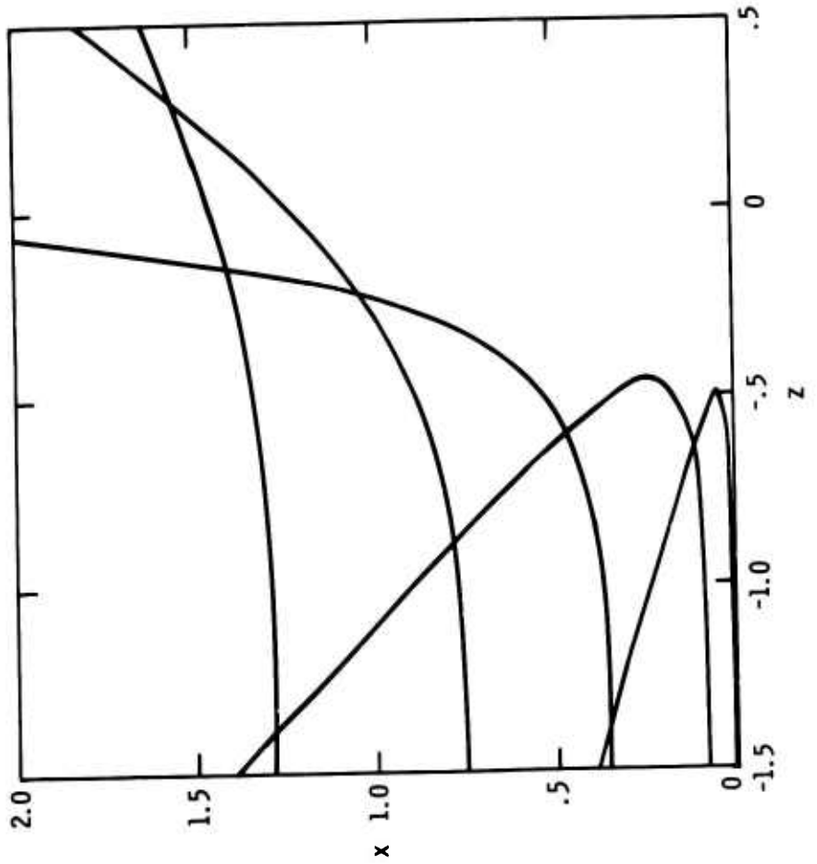


Fig. 12 Ray paths for ordinary ray; $r_{cr} = 0.5$, $f = 30$ MHz , $\theta_p = 135^o$

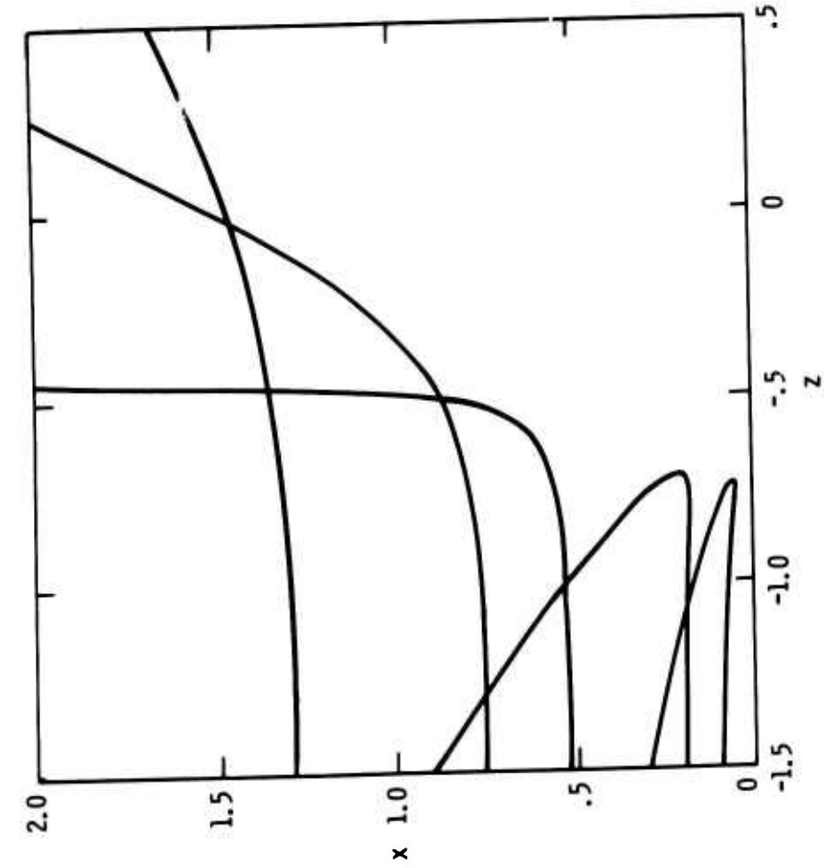


Fig. 11 Ray paths for extraordinary ray; $r_{cr} = 0.5$, $f = 3$ MHz , $\theta_p = 135^o$

STOCHASTIC THEORY OF THE SCATTERING OF ELECTROMAGNETIC WAVES FROM A RANDOM MEDIUM

by

C.M. Tchen

The City College of the City University of New York,
New York, USA

SUMMARY

The wave propagation and scattering in a random medium is studied by means of a wave equation which includes the effect of a random plasma motion, as well as the presence of a random density. The wave equation is derived from the coupled Maxwell equations and hydrodynamic equations. The second-degree differential equation of wave propagation is transformed into a simple one-dimensional model equation which is solved exactly. The spectrum of the scattered power and the spectral functions of density and velocity are obtained.

STOCHASTIC THEORY OF THE SCATTERING OF ELECTROMAGNETIC WAVES FROM A RANDOM MEDIUM

C.M. Tchen

1. INTRODUCTION

In recent years the problem of wave propagation and scattering in a random medium has attracted much interest. The characteristic feature of the fundamental equation of propagation is the presence of a stochastic term, representing the random refractive index originated from the variable density of the random medium. However, in all those investigations the motion of the plasma in the medium has been assumed to present no effect on the scattering, as its inclusion would couple the Maxwell equations to the hydrodynamic equations, posing a much more complex scheme. The stochastic equation of propagation without turbulent motion was studied several years ago by a formal method of perturbations[1,2]. Although the validity of the method has been investigated by comparison with the exact solution of a simple one-dimensional model equation[3,4], the comparison between the equation of propagation (second-degree differential equation) and the model equation (first-degree) cannot be justified.

The principle aim of the present paper is to include the effect of the plasma motion, together with the presence of a variable density of the random medium. To this end, we derive an equation of propagation from the coupled Maxwell equations and the hydrodynamic equations. The differential equation of second degree is valid in a medium with a moving plasma and a random density. The differential equation is solved by means of an exact method through a transformation into a model equation, using the assumption of local homogeneity.

2. EQUATION OF PROPAGATION OF ELECTROMAGNETIC WAVES WITH THE EFFECT OF PLASMA MOTION AND VARIABLE DENSITY IN THE RANDOM MEDIUM

The basis of the propagation of electromagnetic waves is the system of Maxwell equations of fields, coupled to the hydrodynamic equations for the motion of electrons. The Maxwell equations are

$$\text{curl } \mathbf{E} = -\frac{1}{c}\frac{\partial \mathbf{B}}{\partial t} \tag{1a}$$

$$\text{curl } \mathbf{B} = \frac{\mu\epsilon_0}{c}\frac{\partial \mathbf{E}}{\partial t} \quad \frac{4\pi\mu}{c}\mathbf{j} \tag{1b}$$

$$\mathbf{j} = -e\mathbf{N}\mathbf{u} + \sigma\left(\mathbf{E} + \frac{\mathbf{u}\times\mathbf{B}}{c}\right) \tag{1c}$$

$$\epsilon_0 \,\text{div}\,\mathbf{E} = -4\pi e(N - N_0) \tag{1d}$$

$$\text{div}\,\mathbf{B} = 0\ . \tag{1e}$$

The hydrodynamic equations consist of the equation of continuity and the equations of momentum:

$$\frac{\partial N}{\partial t} + \frac{\partial}{\partial x}(Nu) = 0 \tag{2a}$$

$$\frac{\partial}{\partial t}(Nu_i) + \frac{\partial}{\partial x_j}(Nu_i u_j) = -\frac{Ne}{m}\left(E + \frac{u \times B}{c}\right)_i - \nu N u_i \ . \tag{2b}$$

The usual notation is used: $\vec{E}$ and $\vec{B}$ are the electric and magnetic fields, N and $\vec{u}$ are the number density and the velocity of electrons, N_0 is the constant background number density, and $\vec{j}$ is the electric current. Furthermore, the constant properties are the collision frequency ν, the permeability μ, the dielectric constant ϵ_0, the speed of light c, the charge e and the electron mass m. The pressure is neglected in the momentum equations, as the sound effect is not considered in the propagation of electromagnetic wave.

We formulate curl curl $\vec{E}$ from the first of the Maxwell equations, and substitute for curl $\vec{B}$ from the second equation, by making use of the momentum equations, to obtain

$$\nabla^2 E_i - \frac{\mu\epsilon_0}{c^2}\frac{\partial^2 E_i}{\partial t^2} - \frac{4\pi\mu\sigma}{c^2}\frac{\partial E_i}{\partial t} - \frac{\partial^2 E_j}{\partial x_i \partial x_j} - \frac{\omega_p^2}{c^2}\mu E_i = \frac{4\pi e\mu\nu}{c^2} N u_i + \frac{4\pi e\mu}{c^2}\frac{\partial}{\partial x_j}(N u_i u_j) \tag{3}$$

where

$$\omega_p = (4\pi e^2 N/m)^{\frac{1}{2}} \tag{4}$$

is the plasma frequency. The right-hand side of the foregoing equation represents a collision by molecular motions and a nonlinear dissipation by turbulence. The latter term can be approximated by

$$\frac{4\pi e\mu}{c^2} N_0 \mu_j \frac{\partial u_i}{\partial x_j} \ , \tag{5}$$

neglecting the compressibility effect there. According to the mixing length concept of turbulence, the product $u_i u_j$ can be regarded as responsible for a turbulent stress, and hence a turbulent viscosity, which may be assumed quasi-stationary and quasi-linear. To this effect, we shall express u_i of the collision term and the turbulent dissipation term in terms of E_i by means of a linearized momentum equation. When we assume that $\vec{E}$ varies as $\exp(-i\omega t)$, neglect div $\vec{E}$ and terms in $\vec{u} \times \vec{B}/c$, and take $\mu = 1$, $\epsilon_0 = 1$, Equation (3) is simplified as follows:

$$\nabla^2 E_i + \frac{\omega^2}{c^2}\left\{1 - \frac{\omega_p^2}{\omega^2}\left[1 - \frac{i\nu}{\omega}\left(1 + \frac{4\pi\sigma}{\nu}\frac{\omega^2}{\omega_p^2}\right)\right]\right\} E_i = -\frac{\omega_{p0}^2}{c^2}\frac{i}{\omega} u_j \frac{\partial E_i}{\partial x_j} \tag{6}$$

where

$$\omega_{p0}^2 = 4\pi e^2 N_0/m \ . \tag{7}$$

In order to simplify further the differential equation (6), we consider the one-dimensional representation, and neglect the molecular collision and conductivity as compared to the turbulent dissipation, reducing (6) to

$$E'' + K_0^2 [1 - 2n(x)]E = -2ik_0 v E' \ , \tag{3}$$

where the prime indicates a differentiation with respect to x, n is a dimensionless density fluctuation

$$2n = \frac{4\pi e^2}{mc^2 k_0^2} (N - N_0) \tag{9}$$

k_0 is a wavenumber

$$k_0^2 = \frac{\omega^2 - \omega_{p0}^2}{c^2} \tag{10}$$

and

$$v = \frac{1}{2} \frac{1}{k_0 \omega} \frac{\omega_{p0}^2}{c^2} u \tag{11}$$

is a dimensionless velocity.

Equation (8) is the fundamental equation of wave propagation, which we shall use to investigate the statistical behaviour. The left-hand side has the usual structure of wave propagation, with a refractive index dependent on the random density. The right-hand side represents the effect of the plasma motion which causes a turbulent dissipation. If the plasma is supposed at rest, the right-hand side vanishes and (8) reduces to the classical equation of propagation of electromagnetic waves in a random medium.

3. STATISTICAL STUDY OF THE WAVE EQUATION WITH RANDOM DENSITY AND VELOCITY

The equation of propagation (8) can be rewritten in the form

$$E'' + P(x)E' + R(x)E = 0 , \tag{12}$$

with $$P = 2ik_0 v, \qquad R = k_0^2(1-n) , \tag{13}$$

and, by a change of variables

$$E = Q \exp\left[-\tfrac{1}{2}\int_0^x dx' P(x')\right] , \tag{14}$$

is transformed to

$$Q'' + M^2 Q = 0 , \tag{15}$$

where $$M^2 = R - \tfrac{1}{4}P^2 - \tfrac{1}{2}P' , \tag{16}$$

with its real part

$$\begin{aligned} M_1^2 &= R - \tfrac{1}{4}P^2 \\ &= k_0^2(1 - 2n + v^2) \\ &= [k_0(1-n)]^2 + k_0^2(v^2 - n^2) . \end{aligned} \tag{17}$$

An estimate of the last term shows that

$$k_0^2(v^2 - n^2) \sim \frac{k_0^2}{4}\left(\frac{\omega_{p0}}{k_0 c}\right)^4 \left[\left(\frac{k_0 u}{\omega}\right)^2 - \left(\frac{N - N_0}{N_0}\right)^2\right] \tag{18}$$

is negligible, in view of the small value of ω_{p0}/k_0c for small ω_{p0}/ω, and of the approximately comparable magnitude of the velocity and density fluctuations. Hence we can write an approximate value of M_1 as

$$M_1 = k_0(1-n) \quad . \tag{19}$$

If we multiply (15) by Q^*, where the star denotes the complex conjugate part, and add a similar complex conjugate equation, we find

$$QQ^{*\prime\prime} + Q^*Q^{\prime\prime} + 2M_1^2 QQ^* = 0 \tag{20}$$

which, upon taking a statistical average, simplifies to

$$\langle Q'Q'^* \rangle = \langle M_1^2 QQ^* \rangle \tag{21}$$

if we assume a locally homogeneous medium, and therefore

$$\frac{d^2}{dx^2} \langle QQ^* \rangle = 0 \quad , \tag{22}$$

as is the case with many problems of diffusion by turbulence. It is to be remarked that in the locally homogeneous medium we must keep the inequality

$$\frac{d}{dx} \langle QQ^* \rangle \neq 0 \quad , \tag{23}$$

which determines the wave attenuation.

The same result (21) is more easily obtained from the approximate equation, called the model equation

$$Q' = iM_1Q \quad , \tag{24}$$

Therefore we conclude that, in a statistically homogeneous medium and for the purpose concerned, the behaviour of correlations contained in (15) can be equivalently investigated by the simplified equation (24), with M_1 given by (19). The model equation (8) then yields the solution

$$Q = Ae^{ik_0x} \exp\left[-ik_0 \int_0^x dx' n(x')\right] \quad , \tag{25}$$

which gives, following (14),

$$E = Ae^{ik_0x} \exp\left\{-ik_0 \int_0^x dx' [n(x') + v(x')]\right\} \quad , \tag{26}$$

where A is a constant.

In order to calculate the statistical average, we consider the random variables

$$\eta = \int_0^x dx' n(x') \tag{27}$$

and

$$\zeta = \int_0^x dx' v(x') \tag{28}$$

to assume normal probability densities

$$p(\eta) = \frac{1}{\sqrt{(2\pi \langle \eta^2 \rangle}} \exp\left(-\eta^2/2\langle\eta^2\rangle\right) \tag{29}$$

$$q(\zeta) = \frac{1}{\sqrt{(2\pi \langle \zeta^2 \rangle}} \exp\left(-\zeta^2/2\langle\zeta^2\rangle\right) \tag{30}$$

with

$$\int_{-\infty}^{\infty} d\eta\, p = 1 , \qquad \int_{-\infty}^{\infty} d\zeta\, q = 1 . \tag{31}$$

It follows that

$$\begin{aligned} \langle E \rangle &= A e^{ik_0 x} \langle \exp\{-ik_0(\eta + \zeta)\}\rangle \\ &= A e^{ik_0 x} \int_{-\infty}^{\infty} d\eta \int_{-\infty}^{\infty} d\zeta\, p(\eta) q(\zeta) \exp\left[-ik_0(\eta + \zeta)\right] \\ &= A e^{ik_0 x} \exp\left[-\tfrac{1}{2} k_0^2 \langle \eta^2 + \zeta^2 \rangle\right] . \end{aligned} \tag{32}$$

We calculate

$$\begin{aligned} \langle \eta^2 \rangle &= \int_0^x dx' \int_0^x dx'' \langle n(x')n(x'')\rangle \\ &= 2 \int_0^x d\xi \int_{\xi}^x dx' \langle n(x')n(x' + \xi)\rangle \\ &= 2 \int_0^x d\xi\, (x - \xi) \langle n(0)n(\xi)\rangle . \end{aligned} \tag{33}$$

We note that the correlation $\langle n(x')n(x' + \xi)\rangle$ depends on ξ only, and is independent of position, in view of the statistical homogeneity of the medium. The correlation $\langle n(0)n(\xi)\rangle$ has a length scale l_n which may be much smaller than x. In such a case we may approximate

$$\langle n^2 \rangle l_n = \int_0^{\infty} d\xi \langle n(0)n(\xi)\rangle \tag{34}$$

and

$$\langle \eta^2 \rangle = 2 \langle n^2 \rangle l_n x . \tag{35}$$

Similarly the velocity correlation has a length scale l_v which may also be much smaller than x. Then

$$\langle v^2 \rangle l_v = \int_0^{\infty} d\xi \langle v(0)v(\xi)\rangle \tag{36}$$

and

$$\langle \zeta^2 \rangle = 2 \langle v^2 \rangle l_v x . \tag{37}$$

On the other hand, if the correlation lengths are much longer than x, i.e. near the origin of the wave source, then

$$\begin{aligned} \langle \eta^2 \rangle &= \langle n^2 \rangle x^2 \\ \langle \zeta^2 \rangle &= \langle v^2 \rangle x^2 \ . \end{aligned} \tag{38}$$

Upon substituting the results (35), (37) and (38) into (32), we find

$$\begin{aligned} \langle E \rangle &= A e^{ik_0 x} \exp\left[-k_0^2(\langle n^2 \rangle l_n + \langle v^2 \rangle l_v)x\right] \\ &= A e^{ik'x} \ , \quad \text{for large } x \ , \end{aligned} \tag{39a}$$

where

$$k' = k_0 + ik_1 \ , \qquad k_1 = k_0^2(\langle n^2 \rangle l_n + \langle v^2 \rangle l_v) \tag{39b}$$

and

$$\langle E \rangle = A e^{ik_0 x} \exp\left[-\tfrac{1}{2}k_0^2(\langle n^2 \rangle + \langle v^2 \rangle)x^2\right] \tag{40}$$

for small x.

The field fluctuation can be defined by

$$\tilde{E} = E - \langle E \rangle \tag{41}$$

and the power of field fluctuation can be calculated on the basis of (39a) and (40) and we find

$$\langle \tilde{E}\tilde{E}^* \rangle = A^2(1 - e^{-2k_1 x}) \tag{42a}$$

$$= 2A^2 k_1 x \ , \quad \text{if} \quad k_1 x \ll 1 \tag{42b}$$

$$= 2A^2 k_0^2(\langle n^2 \rangle l_n + \langle v^2 \rangle l_v)x \ , \quad \text{for} \quad x \gg l_n \ , \ l_v \tag{42b}$$

or

$$\langle \tilde{E}\tilde{E}^* \rangle = 2A^2 k_0^2(\langle n^2 \rangle + \langle v^2 \rangle)x^2 \ , \quad \text{for} \quad x \ll l_n \ , \ l_v \ . \tag{42c}$$

The results (42) indicate that the wave which is propagated in a turbulent medium suffers attenuation along the x direction, and is scattered and partly converted into the energy of the field fluctuations, through the correlations of density and velocity fluctuations of the medium. If weak, the attenuation (42b) is proportional to the density correlation, as is well known from the first Born approximation valid for a plasma at rest. The result (42a) includes, in addition, the effect of the velocity correlation, and is not restricted to a weak attenuation.

4. SPECTRUM OF THE SCATTERED POWER

The results (35) and (37) obtained under the first Born approximation and the Gaussian distributions are identical to those of the diffusion of electric fields by a random walk

model, where $\langle n^2 \rangle l_n$ and $\langle v^2 \rangle l_v$ are the equivalent coefficients of diffusion of η and ζ in the position space. Therefore we expect that the power attenuation (42b) calculated on this basis refers strictly to a stochastic process instead of a turbulent one. However, in this stochastic propagation of waves, the decay factor k_1 depends on the correlation functions of density and velocity fluctuations.

In order to illustrate the stochastic nature of the propagation, we calculate the coefficient of correlation

$$R(r) = \frac{\langle E(x)E^*(x+r) \rangle}{\langle EE^* \rangle} \tag{43a}$$

$$= e^{-k_1 r} \cos k_0 r \tag{43a}$$

whence, by means of a Fourier inversion, the spectrum

$$H(k) = \frac{H_0}{2\pi} \frac{k_1}{k_1^2 + (k+k_0)^2} \tag{43b}$$

$$\simeq \frac{H_0}{2\pi} k_1 (k+k_0)^{-2}$$

as $k_1^2 \ll (k+k_0)^2$. Here

$$\int_0^\infty H(k)\, dk = \tfrac{1}{2} \langle EE^* \rangle = \tfrac{1}{2} H_0 .$$

For large k , the spectrum (15b) reduces to

$$H(k) = \frac{H_0}{2\pi} k_1 k^{-2} . \tag{43c}$$

The k^{-2} power law is to be expected in random processes.

5. SPECTRAL FUNCTIONS OF DENSITY AND VELOCITY FLUCTUATIONS

The power attenuation (42), the correlation of electric field fluctuations (43a), and the spectrum of the scattered power (43b) or (43c) all depend on the turbulent diffusive property, which in turn depends on the correlation functions or the spectral functions of density and velocity fluctuations. The diffusive property is characterized by the scale length k_1^{-1} . For its determination we shall investigate the spectral functions. To this end, we add to the Navier-Stokes equations of motion the following diffusion equation of electrons:

$$\frac{dN}{dt} = \lambda \nabla^2 N , \tag{44}$$

where λ is the coefficient of molecular diffusion. By means of the cascade method of approximation[5], we derive the equations of spectral functions F aand G , for velocity and density fluctuations respectively, in an equilibrium turbulence

$$(\nu + \nu_k) R_0 = \epsilon \tag{45}$$

$$(\lambda + \nu_k) J_0 = \eta , \tag{46}$$

where ϵ and η are the rates of dissipation, R_0 and J_0 are the vorticity functions

$$R_0(k) = 2\int_0^k dk\, k^2 F\,, \qquad J_0(k) = 2\int_0^k dk\, k^2 G \tag{47}$$

$$\epsilon = \nu R_0(k=\infty)\,, \qquad \eta = \lambda J_0(k=\infty)\,. \tag{48}$$

Further

$$\nu_k = R_0^{-\frac{1}{2}} \int_k^\infty dk\, F \tag{49}$$

is an eddy viscosity.

We assume that the electrons form a dilute suspension of particles in a turbulent fluid which is kept in its inertial regime, with a spectrum

$$F = \epsilon^{2/3} k^{-5/3} \tag{50}$$

found as a solution of (45), in agreement with the power law of the Kolmogoroff theory[6]. Under this turbulent régime, the electron diffuses, giving a spectrum governed by (46), rewritten in the form

$$J_0 = \frac{\eta}{\lambda + \nu_k} \tag{51}$$

or, after differentiation,

$$2k^2 G = -\frac{\eta}{(\lambda + \nu_k)^2}\,\frac{d\nu_k}{dk}\,. \tag{42}$$

Two cases will be considered: (a) First, we consider the case of the diffusion of electrons in an inertial régime of the turbulent fluid, occuring when $\lambda >> \nu$, and $\lambda >> \nu_k$. The solution of (52) is

$$G = \frac{\eta\epsilon^{1/3}}{\lambda^2} k^{-13/3}\,. \tag{53a}$$

(b) Second, we consider the equipartition between the velocity and density spectra, with $\lambda \sim \nu$, $\eta \sim \epsilon$. Then the solution of (46) in the inertial range is

$$G = \eta\epsilon^{-1/3} k^{-5/3}\,, \tag{53b}$$

having the power of the Kolmogoroff law. The results (50) and (53) are written with unspecified numerical constants.

It is to be remarked that a spectral function can be written as the Fourier transform in the k-space of the correlation function $\langle n^2\rangle l_n$ or $\langle v^2\rangle l_v$, which, however, can be approximated by F and G respectively, if $kl_n << 1$ and $kl_v << 1$. Under such circumstances, we have

$$\begin{aligned} \vec{k}_1 &= k_0^2[\langle n^2\rangle l_n + \langle v^2\rangle l_v] \\ &\simeq k_0^2[\alpha F(k) + \beta G(k)] \end{aligned} \tag{54}$$

reducing (43b) to

$$H(k) = \frac{H_0}{2\pi k^2} k_1$$

$$= \frac{1}{2\pi} (\alpha F + \beta G) \quad . \tag{55}$$

Here α and β are the coefficients relating the dimensional and dimensionless density and velocity, respectively,

$$\alpha = \frac{2\pi e^2}{mc^2 k_0^2} \quad , \qquad \beta = \frac{1}{2k_0 \omega} \frac{\omega_{p0}^2}{c^2} \quad . \tag{56}$$

The formula (55) indicates that the scattering spectrum reproduces the velocity and the density spectra F and G . In practice, since the electrons diffuse passively in the turbulent fluid without being able to maintain an inertial régime with a large Reynolds number, the case (a) with the spectrum (53a) is generally found, contrarily to the customary assumption of a Kolmogoroff power law for the density spectrum. The formula (43c) and (55) are the two special cases of (43b). The former refers to a random medium with fine grain ($k \gg k_0$) , reducing (43a), to

$$R(r) = e^{-k_1 r} \quad , \tag{57}$$

a correlation belonging to a random walk process. The latter, formula (55), refers to a coarse grain medium ($k \ll k_0$) , so that the scattering spectrum H(k) measures directly the spectra of density and velocity fluctuations.

REFERENCES

1. Bourret, R.C. — *Stochastically Perturbed Fields with Applications to Wave Propagation in Random Media.* Nuovo Cimento, Vol.26, 1962, pp.1-31.

2. Tatarskii, V.I. Gertsenshtein, M.E. — *Propagation of Waves in a Medium with Strong Fluctuations of the Refractive Index.* Soviet Physics, JETP, Vol.17, 1963, pp.458-463.

3. Frisch, U. — *Propagation D'ondes dans un Milieu Aléatoire Unidimensionnel, Comptes Rendus*, Vol.261, 1965, pp.55-57.

4. Bassanini, P. — *Wave Propagation in a One-Dimensional Random Medium, Radio Science*, Vol.2 (New Series), 1967, pp.429-436.

5. Tchen, C.M. — *Spectrum of Turbulence as Generated by Gravity in the Upper Atmosphere.* To be published.

6. Kolmogoroff, A.N. — *Local Structure of Turbulence.* Comptes Rendus, Académie des Sciences, URSS, Vol.30, 1941, p.301.

DISCUSSION ON THE PAPERS PRESENTED IN SESSION V (VHF FORWARD SCATTER).

Discussion on Paper 38, "Review of VHF forward scatter", by R.C.Kirby.

Mr W.G.Burrows: Whilst I appreciate, Mr Kirby, that no quantitative information is obtainable from the film recordings of beam distortion versus time shown in your Figure 1, they are of considerable interest to me. Would you therefore elaborate on the essential details of the system employed to obtain these results?

Mr R.C.Kirby: A CW transmitter illuminated the scattering volume with a narrow beam antenna (6^{o}) near 40 MHz, and a second transmitter at a closely adjacent frequency illuminated the scattering volume with a broad beam (55^{o}) antenna. At the receiver, a 1^{o} beam scanned $\pm 25^{o}$ of azimuth about the path midpoint, at 20 scans per second. The films represent integration of several minutes of scanning, amplitude versus azimuth - the upper half of each frame scans the narrow beam illumination, the lower half scans the broad beam illumination. The 1^{o} scanning beam was formed by 25 broadside Yagi antennas with electronic phase shifting.

Discussion on Paper 40, "Controllability aspects of scatter propagation of radio waves", by M.Z.v.Krzywoblocki.

Dr A.Wasiljeff: Professor v Krzywoblocki, do you use calculus of variations or direct methods (like the method of steepest descent) to obtain the optimum on the computer?

Professor M.Z.v.Krzywoblocki: All possible methods are used; calculus of variations, Pontryagin's principle, Bellman's programming, steepest descent, various algoritms were proposed, etc.

Discussion on Paper 41, "VHF ionospheric scatter propagation by the equatorial electrojet", by C.A.Romero, A.A.Giesecke and O.Pérez (presented by R.Cohen).

Dr K.Davies: Dr Cohen, what causes the seasonal variations in time of occurrence of the morning and evening minima of signal strength?

Dr R.Cohen: According to the interpretation of Dr.Balsley, the signal strength scattered by weak irregularities in the equatorial electrojet is a measure of the absolute value of the electron drift velocity, and hence of the absolute value of the East-West electric field. The morning and evening minima in signal strength thus are manifestations of the fact that the electric field is near zero, i.e., that the electric field is reversing. This electric field is really the "S_q", or dynamo field, and results from winds of the neutral atmosphere. The seasonal variations in times of occurrence of the field reversal thus depend on the sources of these winds, which can be tidal and/or zonal in origin. Also, seasonal variations in ionospheric conductivity need to be taken into account.

Discussion on Paper 43, "Stochastic theory of the multiple scattering of electromagnetic waves from a turbulent plasma", by C.M.Tchen.

Professor M.Z.v.Krzywoblocki: There was in the past an attempt to generalize Kilmogorov's theory of turbulence to compressible fluids, where there were derived formulas for the velocity, density and temperature.

Professor C.M.Tchen: In order to get down to solutions giving the various spectral functions, as an extension of the Kolmogorov theory, one has to resort to empirical methods (e.g., mixing lengths, dimensional and similitude considerations, Heisenberg's hypothesis of eddy viscosities) which become arbitrary and diffuse when the number of variables in-

creases. I have also attempted an extension using a "cascade approximation method" (C.M. Tchen, *A Cascade Theory of Turbulence*, Proceedings of the Symposium on Advanced Problems in Fluid Mechanics, Tarda, Poland, 1967, Fluid Mechanics Transactions). However, the problem encountered in the present paper is much simpler. I treated the electrons as a dilute suspension of particles in a neutral incompressible fluid. Therefore my spectral theory is based on an incompressible diffusion equation for electrons, and the Navier-Stokes equations for the incompressible fluid. These enabled me to find a particular solution of the density spectrum of electrons as different from the Kolmogorov law, when the diffusion coefficient is larger than the kinematic viscosity, as in the case with electrons at a higher temperature than the neutral fluid. Therefore the theory cannot be considered as a theory of compressible turbulence. But it serves as a step towards that direction, because the compressible turbulence is based on the Riemann system of equations, somewhat similar to those used in the present paper.

Dr K. Cohen: Perhaps Professors Hochstim and Tchen could explain why a multiple scattering approach is pertinent to scatter propagation in the ionosphere, or even in the troposphere. Somehow, the theoretical approaches using Born's first approximation have worked all right up to now, as far as we know, and there is no reason to suspect that other than single scattering is occurring.

Dr A.R. Hochstim: Multiple scattering should be important when the first Born approximation is not valid. The detailed criteria for the validity of the first Born approximation were given by Salpeter and Treiman (Journal of Geophysical Research, Vol.69, 1964, p.869) and we have numerically confirmed their results. The multiple scattering may be important for frequencies near the plasma frequency and for large fluctuations in the electron density. Furthermore, the effect may be more significant for phase shifts and depolarization than for backscattering power.

Professor C.M. Tchen: My calculations (formula (14a) of Paper 3) show that the Born approximation is not valid when the parameter $k_0 L$ ceases to be small. Here k_0 has been defined as the wavenumber of the scattered wave, and L is the turbulent scale defined in the paper. This factor increases with increasing plasma density, with intensity of turbulent fluctuations, and when the frequency of the incident wave approaches the plasma frequency of the medium.

Dr A. Wasiljeff: The Krassilnikov-Norton-autocorrelation functions of the dielectric constant are used in tropospheric scatter theories because of the Oboukhov-Kolmogorov law of the corresponding spectrum. If Professor Tchen is right, there is no physical justification for using these correlation functions.

Professor C.M. Tchen: It is a paradox in the classical theory of the scattering spectrum (or correlation function) that one neglects the fluid motion and confines oneself to density fluctuations on the one hand, and on the other hand one imposes on this density spectrum the Oboukhov-Kolmogorov law, which was derived and is valid for the velocity fluctuations only. In order to lift this paradox, I have extended the Kolmogorov theory to include the density fluctuations of suspended electrons diffusing in a neutral fluid, and I have found that the density spectrum is in general different from the Kolmogorov law. The empirical law of Booker-Gordon, based on the random walk type of stochastic process with a random variable unspecified by hydrodynamics, seems more acceptable in principle. Its k^{-4} law is also closer to my density spectrum $k^{-13/3}$.

A REVIEW OF VHF TRANSEQUATORIAL PROPAGATION

by

D. L. Nielson

Stanford Research Institute
Menlo Park, California, 94025
USA

SUMMARY

An examination is made of both published and unpublished literature concerning VHF propagation over transequatorial paths. At least two classes of propagation appear to exist; their demarcation is given in terms of the possible reflection mechanism, the signal characteristics, and the distance of the terminals from the magnetic equator. Propagation of one class uses refraction from the horizontal gradients of electron density that are regular diurnal characteristics of the equatorial ionosphere. A second class is required to explain the propagation of frequencies above about 60MHz. This class is characteristic of 4000- to 6000-km paths and is due to both normal refraction and a low-loss reflection mechanism that is not yet completely defined. Signal characteristics for this second class of propagation are documented, and three possible mechanisms are discussed.

A REVIEW OF VHF TRANSEQUATORIAL PROPAGATION

D. L. Nielson

1. DEFINITION

In the following discussion transequatorial propagation is defined as the category of ionospheric propagation over a path that is more or less bisected by the magnetic equator, using frequencies that are substantially larger than those used in conventional shortwave ratio. This definition requires that the propagation of these high frequencies must critically depend upon the *trans*equatorial ionosphere, thus excluding many low-latitude transmissions whose basic frequency support or signal strength is not unusual. (In that sense this paper is not a review of equatorial propagation.) Notice that this definition does not specify the reflection mechanism; indeed in some instances this mechanism is not yet understood. But, after a full solar cycle of intermittent investigations, several characteristics of this propagation have become rather clear, and in this paper a working hypothesis for two types of VHF transequatorial propagation is proposed. For each type, the signal characteristics are reviewed, and the possible reflection mechanisms are examined. To the extent that the author injects some of his own ideas and calculations, this is not a review paper in the strict sense. But let us begin with a general review of the subject, and outline in broad terms the nature of this type of propagation in the context of experimental observations.

2. BACKGROUND

The first mention of transequatorial propagation appeared in reports from radio amateurs who described unusually long-range contacts at VHF (Refs. 1-4). These contacts occurred in the late evening and were most prevalent during the equinoctial months. Southworth assembled a comprehensive review of the reporting of transequatorial propagation by radio amateurs through 1959 (Ref. 5), but many amateurs have carried on an active interest to the present. Some of the most consistent and comprehensive monitoring has been conducted by Kingan[6]. His observations of Hawaiian television stations over a two-year period, while suffering from the problem of station shut-down about midnight, still offer the best evidence of the seasonal dependence and rate of occurrence collected to date. The results shown in Figures 1 and 2 are calculated from his data. The various amateur accounts correctly identified the equinoctial dependence of transequatorial propagation, as well as two types of such propagation: one characterized by slow fading rates and occurring from late afternoon to early evening, and a second suffering very rapid fades and being strictly nocturnal.

Observations of transequatorial propagation have been made on all the continents, but principally they have involved southern hemisphere monitoring of northern hemisphere transmitters. Obviously available to the listeners, in addition to amateur transmitters, have been the powerful television and FM radio broadcast stations that appeared during the 1950's. In late 1956, fixed-frequency (46-MHz) backscatter equipment was operated by Stanford University from a site in the Virgin Islands. Unusually long-range backscatter echoes observed there by Villard et al.[7] prompted their suggestion of ionosphere-to-ionosphere (F2F2) reflections from the large horizontal gradients of the equatorial anomaly. This suggestion has received much support (and correctly so) for one class of transequatorial propagation.

Observations of similar long-range backscatter echoes on 21 MHz in Japan led Obayahsi to postulate an exospheric field-guided mode of HF and VHF propagation wherein the radio wave becomes trapped between field-aligned irregularities[8]. High signal strengths and severe fading were characteristics of these returns. Obayashi's hypothesis was later tested by Dueño on 40 MHz, with negative results[9]. Similar attempts to observe exospheric ducting at HF have met with limited success[10,11].

The IGY program conducted in South America by the US National Bureau of Standards (now the Environmental Science Services Administration) established a number of 50-MHz ionospheric scatter links in the vicinity of the magnetic equator[12-14]. While most of the work there centered around E-region scatter, one 2600-km path was suitably situated for F-region scatter in the vicinity of the magnetic equator. Although some signal enhancements were observed between sunset and midnight, there was still a substantial reflection loss - a loss that was not characteristic of other longer-range transequatorial circuits. A similar but nontransequatorial case of F-region scatter with enhanced signal strength was observed with similar equipment in the Far East[15,16].

Meanwhile, attention was being directed to the specific subject of transequatorial propagation. In Australia[17,18] interest centered mainly in monitoring Korean, Russian, and Japanese television and FM stations. Afternoon and evening peaks in occurrence, as well as equinoctial dependence, were observed. In 1962 Washburn et al.[19] conducted a multifrequency (30 to 75 MHz) experiment between Panama and Chile (magnetic conjugates) and observed unusually large signal strengths relative to scatter, as well as both the rapid and the slow fading characteristics mentioned earlier.

Further investigations were conducted in the mid-Pacific and the Far East. An oblique-incidence sounder circuit operating between Kauai and Rarotonga during the summer of 1962 showed a remarkable regularity of VHF propagation up to 64 MHz (Ref. 20). These terminals are both magnetic and geographic conjugates and a rate of occurrence unequaled before or since was observed. These VHF sounder observations were also rather unique in that the VHF propagation continued throughout the night (like spread F) instead of normally ceasing about midnight. In a recent investigation, Bowen et al.[21] used multiple-frequency (34, 45, 54, and 77 MHz) CW transmissions on two conjugate paths in the Far East to acquire more detailed signal characteristics and to test the aspect sensitivity of the propagation path to the magnetic equator. On a north-south path between Okinawa and Darwin, all the transmitted frequencies were observed, whereas the path from Okinawa to the Fiji Islands rarely carried frequencies higher than 45 MHz. Both rapid and slow fading signals were observed at each location, however. Bowen et al. suggested that 80 MHz may be an upper frequency limit and that the higher-frequency rapid-fade signals are due to a "field-guided" ray path. A year-long experiment at 32, 48, and 72 MHz between Darwin and Yamagawa was reported in the Japanese literature[22]. As might be expected, the presence of the 32-MHz signal correlated well with adequate f_0F2 vaules (>8 MHz) at Manila. The higher-frequency data did not, however, correlate well with the presence of spread F at Manila. Signal strengths were often at free-space values during the equinoctial months, even at 72 MHz. The occurrence data for 48 and 74 MHz agree well with the data of Kingan shown in Figure 1. A recent experiment conducted by the author on the Rarotonga-Oahu path used pulse and CW signals to reveal the origin of transequatorial propagation. Doppler spectra indicated that frequencies up to at least 90 MHz could be reflected from large moving irregularities in the equatorial F region[23]. Few reviews of transequatorial propagation have appeared in the literature; one such article is by McCue and Fyfe[24].

From the above summary of observations, it is difficult to postulate a single self-consistent reflection mechanism. Yet the criterion for forming a given class of propagation should be the basic reflection mechanism from which the wave receives its frequency support. The traditional classification by fading rate, when used alone, is without merit, since any HF/VHF frequency traversing the ionosphere under spread-F conditions will be likely to acquire an appreciable scatter-like component. Certainly there are two classes of signal characteristics, but, more important, there may be two

entirely different reflection mechanisms, not necessarily corresponding to the two signal classes. One is fairly conventional ionospheric refraction from the pronounced horizontal gradients of electron density near the magnetic equator. Unfortunately, there is still no genuine understanding of the second reflection mechanism - low-loss and scatter-like - that characterizes many transequatorial observations. In Figure 3 these two classes are shown geometrically related to the equatorial phenomena that are important in their demarcation. As mentioned at the outset, low-latitude paths whose transmission characteristics do not appear to be abnormal are not included in this review other than for comparison purposes. This excludes E- and F-region scatter circuits within about 1500 km of the magnetic equator.

To compensate for the incomplete knowledge of the specific mechanisms involved, there is some merit in a subordinate categorization of paths based upon the distance of their terminals from the dip equator: a group of longer paths whose propagation must depend on more or less normal ionospheric F-region refraction and relatively few ray paths, and a group of intermediate-length paths whose propagation may additionally involve a scatter-like reflection or guidance mechanism capable of low reflection loss. In either case, signal levels may approach free-space values.

3. CLASS I - REFRACTION AS THE PRINCIPAL TRANSEQUATORIAL PROPAGATION MECHANISM

3.1 General

For this class of propagation, irregularities in the vicinity of the equator are excluded as the *principal* mechanism for reflection (including scatter or guiding) Since refraction is the principal mechanism, signals in this class not only have a large coherent component in the absence of irregularities but also maintain large signal levels in the presence of irregularities, since the reflection is, in the main, total. Because the night-time equatorial-F region is usually composed of irregularities, definition of meaningful geographic boundaries for this type of propagation is difficult. One might begin by placing the terminals sufficiently far apart that their horizon rays intersect at altitudes greater than about 700 km. These limits place the terminals above about $\pm 27^{\circ}$ magnetic latitude (about 3000 km from the dip equator).

Perhaps a better way of defining the above boundary is to say that VHF signals of this class *must* rely upon the equatorial anomaly[25-30]. The anomaly is the nonuniform electron density distribution that occurs in the vicinity of the magnetic equator. (Having received considerable attention in the post-Alouette satellite time period, this phenomenon may be losing its classification as anomalous[31]. The rise of the equatorial F region associated with this anomaly is now generally believed to be due to electrodynamic drift. This drift, together with diffusion along the magnetic field lines, produces the F-region ionization density depletion over the magnetic equator and the simultaneous ionization density increase from ± 10 to $\pm 20^{\circ}$ magnetic latitude. It is in these regions of increase that the earth's highest normal values of ionospheric electron density are found. The ionospheric predictions from the US Institute for Telecommunication Sciences (ITS), now based upon a modified magnetic dip angle, clearly illustrate this redistribution. Using the ITS estimates, one may predict the likelihood of such propagation over a given path. If the anomaly is critical to this class of propagation, then observations and predictions should indicate that such propagation occurs in the late afternoon as well as the early evening. This is the case for the longer paths[7, 9, 17, 33].

Many authors[7, 12, 24, 28, 30] have suggested that the F2F2 mode is responsible for most of the above-30-MHz propagation. Gibson-Wilde[28] attempted to relate the equinoctial prominences to the shape of the equatorial anomaly. He commented specifically upon the relationship between the latitude separation in the electron density peaks and the possibility of the F2F2 mode. It is unfortunate that most experiments have not had access to transequatorial electron density profiles, so that ray-tracing studies could verify the highest propagating frequencies. One limited attempt was made by the author[20].

3.2 Virtual Geometry for Magnetically Symmetric Ionosphere and Propagation Path

Rough estimates of the required ionospheric tilts, the height and location of the virtual reflection, and the resulting secant factor may be obtained by using the virtual ray path illustrated in Figure 4. A north-south path that is symmetric about the dip equator is assumed, a case that may be justifiable only near the equinox. Simple geometry sets the following conditions:

$$\cos(\theta_p + 2\alpha) = \frac{R}{R+h}\cos\Delta$$

$$\theta = 2(\theta_p + \alpha) - \Delta$$

$$\sec\phi_{eff} = \csc(\theta_p + \alpha),$$

where

θ_p = latitude of the virtual reflection

θ = latitude of the terminal

α = tilt angle

h = virtual height of reflection

Δ = angle of departure

$\sec\phi_{eff}$ = secant factor.

These conditions are shown graphically in Figure 5 where, to limit the variables involved, we set $\Delta = 0^o$, thereby obtaining the maximum secant factors. (For a more reasonable take-off angle of 4^o, the results of Figure 5 change as follows: θ_p increases about 0.5^o; the secant factor decreases 1 to 10%; and θ, the latitude of the terminal, decreases by about 3^o.) The necessary combination of virtual height, tilt angle, and latitude of reflection is shown in Figure 5(a). The latitudes of the terminals shown in Figure 5(b) give path lengths of from 5000 to 9000 km, using reasonable virtual reflection heights of from 370 to 520 km. The secant factor and height of the ray at perigee are given in Figures 5(c) and (d), respectively. Estimates of h, α, and θ_p may be found from either predictions or observations[26, 34]. For example, if we assume the latitude of the virtual reflection point to be near the latitude of the electron density peaks of the equatorial anomaly, then the March 1967 ITS predictions given in Table I may be of use. (See also Reference 26.)

To illustrate, if θ_p is taken as 12^o, and a virtual height of 400 km is assumed, then a layer tilt of 4^o is required. These conditions specify a latitude for the terminal of not more than 32^o and a secant factor of about 3.6. Thus, to support 45MHz, a critical frequency somewhere in the vicinity of 13MHz is required. The maximum frequency determined in this manner is only a first-order estimate, since knowledge of the entire vertical electron density profile along the path is obviously needed.

One might be tempted to look at the large potential secant factors and conclude that even 90 to 100 MHz propagation would be possible if the conditions were just right. However, these same conditions would also require the latitudes of the reflection points and the terminal locations to be unreasonably small. Furthermore, for circuits within 25^o magnetic latitude, nearly all the observations of frequencies above about 60 MHz occur on nights when the flutter fading is high, indicating a dependence on a spread condition in the ionosphere rather than (or in addition to) a particular shape of electron density contours[21, 23]. Examination of the curves of Figure 5 with reasonable values of θ_p, α, and h_p in mind shows that frequencies greater than about 60 to

65 MHz (depending on the available plasma frequencies) will not usually propagate via this mechanism. In addition, the signal strength at the higher frequencies decreases more than would be indicated by total reflection. Hence these higher frequencies are judged not to belong to this class.

3.3 Predicted Latitude Dependence

Since there had been no studies or measurements of the latitudinal variation of the maximum propagating frequency, it seemed worthwhile to use the ITS predictions, together with an elementary form of ray tracing[35], to estimate the maximum frequency. Figure 6 shows the two important F-region parameters for an equinoctial month along the Rarotonga-Oahu path. The equatorial anomaly is evident in both the critical frequency and the layer height. The propagation results are given in Figure 7, in the form of ionograms for paths of varying length whose terminals are geographic (and magnetic-dip) conjugates. The ray-tracing method makes a first-order correction for horizontal gradients and tilts, but the available accuracy does not encourage sharp distinction between the F2F2 ray and the long-delay 1F2 rays shown.

3.4 Signal Characteristics

The signal characteristics of this class of propagation are (i) low signal loss, on the order of free-space values, (ii) little time dispersion, only one or two modes propagating at a given frequency (ignoring magneto-ionic components), and (iii) a normally low fading rate or, more descriptively, a small Doppler spread. A typical spectrum is shown in Figure 8(a). The proper conditions for this mode may exist from mid-afternoon until nearly midnight. Voice transmissions are often undistorted, but the multipath problem usually renders wider-bandwidth signals unusable. Thus the signals observed under this classification can be reasonably well understood. In general, they may be investigated by using "normal" ionospheric ray paths, with the possibility of some scatter being introduced during times when the equatorial F region is in a spread-F condition. The question of whether another mechanism is needed to explain transequatorial VHF propagation above 50 to 60 MHz is now considered.

4. CLASS II - TRANSEQUATORIAL PROPAGATION BY OTHER THAN NORMAL REFRACTION

4.1 General

The propagation of frequencies approaching 100 MHz over distances of at least 5000 km (Refs. 6, 23) suggests that a second class of transequatorial propagation is needed. Furthermore, effective secant factors greater than four or five do not seem to be likely, leaving a requirement for unreasonably large plasma frequencies, that is, values approaching 20 MHz. There is little question, however, but that further ray-tracing studies through *measured* profiles are needed to establish the highest frequency that can propagate by normal refraction.

Most of the paths over which frequencies in excess of 50 to 55 MHz have been observed are less than 5000 km long. But on paths as long as 2600 km, the high signal strengths characteristic of the longer transequatorial paths have not been observed, even at the reasonably low frequency of 50 MHz (Ref. 12). It is suggested that paths capable of carrying the higher frequencies should have magnetically conjugate terminals that lie between about 2000 and 3000 km of the magnetic equator. We shall see further reasons for this choice.

4.2 Signal Characteristics

The signal characteristics for this second class of transequatorial propagation are a curious mixture of relatively large strength and severe spreading in both frequency and

time delay. Frequency spreads of 5 to 15 Hz are common, and the power spectral density of Figure 8(b) (plus the additional ones in Reference 23) indicates that many ray paths can be involved. While there is general agreement that the higher frequencies are characterized by high fade rates, little has been offered in the way of explanation. Observations for this class of signals are strictly nocturnal, with a pronounced maximum in rate of occurrence at the equinox (see Figure 2).

To contrast the signal strengths of transequatorial propagation with those of F scatter near the equator, typical and peak field strengths from various experiments are summarized in Table II. The tabulated values of transequatorial signal strengths are somewhat exaggerated, since they have been chosen for equinoctial months and for the most favorable time in the evening propagation period. Yet the differences in Table II are clear. While the 50-MHz data for the transequatorial paths may be explained by normal refraction, the higher frequencies appear to propagate by some partially coherent reflection process.

4.3 Spread-F

The role of spread-F in transequatorial propagation is enigmatic. Some authors[12] believe that the irregularities are nothing more than a veil of confusion - masking refraction, the principal means of ray reflection. Others believe that scatter is the vital mechanism, but it is not always possible to distinguish the generic use of the term from something more specific. Still other investigators employ some type of ray guidance to explain the reflection process.

From the available reports it is certain that, when the term spread-F is used generically, there is no close correlation with transequatorial VHF propagation[6, 12, 22]. That is, it is not a sufficient condition. But there is a closer association between VHF propagation and equatorial flutter fading. Finally, the author, in a separate paper[23], shows that the simultaneous reflection of 54, 72, and 90 MHz can be critically dependent upon large F-region irregularities moving along the magnetic equator.

4.4 Possible Mechanisms

In an attempt to explain the second class of signals, three mechanisms are examined: (i) reflections from overdense irregularities, in the manner of Class I signals but under spread conditions, (ii) weak scattering from underdense irregularities, and (iii) guidance along the same irregularities by means of gradients normal to their axis. From the arguments advanced earlier, and particularly from the off-path reflections obtained in Reference 23, the possibility of overdense reflections, at least at 90 MHz, seems remote. But let us first examine the possibility of ray guidance along field-aligned irregularities.

4.4 Guidance along Irregularities

The propagation of radio waves along field-aligned irregularities is normally placed in the province of the medium frequencies (0.3 to 3 MHz) and below. Several authors, however, have given the problem a sufficiently general treatment that the possibilities of HF and VHF propagation may also be considered[37-40]. In general, the requirements for guidance are: (i) that a suitable means exist for coupling energy into the region beneath (or between) the irregularity(ies) and (ii) that the ray curvature equal or exceed that of the local magnetic field.

The condition for coupling is likely to be one of obtaining the proper incidence angle at a height where the irregularities exist. Since the electron gyrofrequency is much greater than the electron collision frequency, we are assuming that the irregularities are aligned with the earth's magnetic field. If this is true, then a ray that is tangent to the magnetic field within the appropriate altitude and latitude range will be properly oriented. To locate these points of tangency, it is assumed that the magnetic

field can be represented by a centered, non-tilted magnetic dipole. The results, parametric over the latitudes and heights of interest, are plotted in Figure 9. The solid curves in the figure illustrate the latitude and altitude of tangency to the geomagnetic field of a ray path whose departure angle is Δ. Notice that at some terminal latitudes two points of tangency are possible[8]. For example, a terminal located at 20° geomagnetic latitude has points of tangency at 300 km at latitudes of 11° and 14° and at departure angles of 11° and 21°. The angle increments adjacent to the 200-km line indicate the variations if the ray is not tangent at H but intersects the field at ±5°. It can also be observed that, for a given terminal latitude, θ_{ter}, the "point" of tangency, θ_{tan}, is most widely distributed in latitude $(\partial\theta_{ter}/\partial\theta_{tan} = 0)$ when $\theta_{ter} = (5/3)\theta_{tan}$. (Correspondingly, $\Delta \simeq (5/4)\theta_{tan}$.)

The practical range of terminal latitudes most suited for the criterion of field tangency would be between about 16° and 30°. The upper limit is defined by the field lines whose apogees are excessive. The asterisks on the lines for H = 500, 600, and 700 km in Figure 9 indicate the value of θ_{tan} beyond which the apogee of the field line will exceed 1000 km. Thus the range of conjugate latitudes is similar to that of Figure 7.

To estimate the required electron density gradients in the irregularities, we refer to Gopal Rao and Booker[38]. From their Figure 6 a value of the fractional electron density gradient per unit curvature of the field can be obtained if values for the electron gyrofrequency, the plasma frequency, and the wave frequency are supplied. From an expression for the gyrofrequency f_H, we can obtain an expression for field curvature:

$$f_H = f_{H_{eq}} \left(\frac{R}{R+h}\right)^3 \left(1 + 3\sin^2\theta\right)^{\frac{1}{2}},$$

where

$f_{H_{eq}}$ = value at equator at the surface (0.88 MHz)

θ = geomagnetic latitude.

While the values from Gopal Rao and Booker assume curvature and gradients normal to the field line, for small values of θ (low latitudes) we may assume that the gradient is radial (that is, that $rd\theta << dr$). Thus the field curvature (K_F) is approximately

$$K_F = -\frac{1}{f_H}\nabla_r f_H = \frac{3}{r}.$$

On the basis of this expression, the necessary gradient of ionization normal to the field line for guidance of 54, 72, and 90 MHz is shown in Figure 10. Also shown in the figure are the electron density and gyrofrequency profiles used in the calculation. Notice that the percentage curves mirror the curve of electron density. This is the result of an almost constant value of ∇N as a function of altitude. These values are 0.25, 0.5, and 0.7 electrons/cm^3 per cm for 54, 72, and 90 MHz, respectively. For the lower ionospheric heights (< 500 km), these values are not unreasonably large, especially for the ionization peaks of the equatorial anomaly. The concept of guidance of this type has also been used by McCue[40].

Intuitively, it does not seem necessary for the guidance to depend upon only one irregularity, or even a few irregularities. One might draw an analogy to a flexible light tube whose transmission properties are enhanced by making it more fibrous or filimentary as opposed to using a single homogeneous cross-section.

4.5 Scatter

If it were not for the relatively large observed signal strengths, scatter would be an obvious postulate for the propagation mechanism at frequencies above 50 to 60 MHz. Even the rate of decrease in signal strength with frequency is indicative of scatter. But, since it is impossible to pursue the problem quantitatively without a knowledge of the common volume in the various experiments, only a brief comment on observed cross-sections can be made.

Without exception, the systems used in exploring transequatorial propagation have been of relatively low power. Because of this low power as well as the relatively nondirective antennas employed, the free-space field strength has usually been on the order of -70 dBm For a 5000-km path and an observed signal that is, for example, 20 dB below free space, the cross-section is about $10^{12}m^2$. If we consider cylindrical irregularities in which the electrons are perfectly coherent (10^{14} electrons/meter of cylinder length with no transverse coherence loss) over the first Fresnel zone (about 10 km at 70 MHz and a 500-km reflection height), about 10^4 such cylinders are required. If the overall collection of such small-scale irregularities forms an ensemble that is tens by hundreds of kilometers, that number of irregularities may be possible. In view of the assumption of coherence, however, it may be concluded that cross-sections of 10^9 to $10^{12}m^2$ are difficult to explain in these terms.

If, as indicated in Reference 23, the reflections at the higher frequencies are from moving irregularities near the magnetic equator, we are left with two rather untenable choices: that the number of partially coherent but weak scatterers within the large irregularities is sufficient to yield the observed cross-sections or that the irregularities are overdense to the transmitted frequency. For the latter to be a practical hypothesis, the background electron density would have to be at least 4×20^{12} electrons/m^3, with peak densities in the irregularities approaching 10^{13} electrons/m^3.

5. PATHS ASYMMETRIC TO THE MAGNETIC EQUATOR

While terminals symmetrically disposed about the magnetic equator have clear advantages, the effects of the equatorial F region are very evident on asymmetric paths. It appears, however, that the upper frequency limit on such paths is somewhat lower than that for the more symmetrical paths. Obviously, if a ray path has its reflection in the region of either of the low-latitude peaks of electron density, higher-than-normal oblique frequencies will result. During the post-sunset-to-midnight hours, maximum frequencies may exceed 55 to 60 MHz (Refs. 20, 33). Without the presence of irregularities, however, the upper limit is probably 10 to 15 MHz lower.

6. CONCLUSIONS

The above observations and reasoning suggest the following:

(i) Normal refraction from the large-scale horizontal gradients of the equatorial anomaly can explain propagation to frequencies approaching 50 MHz - occasionally perhaps even to 60 or 70 MHz, depending upon the position in the sunspot cycle and the relative path geometry. This type of propagation (F2F2) is dependent upon the correct density, height, and separation of the electron density peaks.

(ii) For frequencies greater than that possible by normal refraction, the radio wave can be guided along irregularities in electron density. For this guidance to occur, a certain electron density must exist prior to the commencement of irregularities occurring shortly after ionospheric sunset. The higher this density, the lower the percentage gradient required for guiding a given frequency and hence the greater the probability of that frequency propagating. The higher frequencies begin to propagate when both the irregularities and a given threshold

of electron density exist. They cease to propagate when either condition ceases to exist. The threshold of electron density is a function of the propagation path and the oblique frequency and may be necessary at one or more places along the path. This type of guidance applies only near the great-circle path.

(iii) Scatter propagation from field-aligned irregularities may be important at frequencies above 60 MHz, but current theory does not favor this conclusion. In general, observed signal strengths are too large to be accounted for by F scatter from underdense irregularities.

(iv) In light of the off-path reflection from large F-region irregularities it is not possible to eliminate reflection from overdense irregularities as an important mechanism. The reflection of frequencies as high as 95 MHz, however, places the required electron density at the upper limit of credible values. Certainly the off-path reflections at the higher frequencies are not easily pictured in the framework of rays guided along field-aligned irregularities.

(v) The VHF transequatorial propagation cannot be attributed solely to the presence of F-region irregularities. Either a more careful approach to the type of irregularities is required or other conditions, such as high background electron densities, are required. There is evidence that the particular irregularities associated with equatorial flutter fading may be important.

(vi) The pronounced seasonal and diurnal dependence of frequencies up to 50 to 60 MHz can probably be accounted for by a detailed analysis of the equatorial anomaly. The maximum electron densities, the heights, the separation of the peaks, and the symmetry with respect to the propagation path are important. The seasonal and diurnal dependence of the higher frequencies may be understood through a more complete knowledge of the F-region irregularities characteristic of the post-sunset-to-midnight period.

REFERENCES

1. Ferrell, O.P. — Nature, Vol. 167, 1951, pp. 811-812.
2. Tilton, E.P. — QST, Vol. 31 (10), 1947, pp. 56-57.
3. Tilton, E.P. — QST, Vol. 39 (12), 1955, pp. 99-101.
4. Cracknell, R.G. — QST, Vol. 43, Dec. 1959, pp. 11-17.
5. Southworth, M.P. — Journal of Geophysical Research, Vol. 65, 1960, pp. 601-607.
6. Kingan, S.G. — Private communication, 1968.
7. Villard, O.G. et al. — Journal of Geophysical Research, Vol. 62, 1957, pp. 399-412.
8. Obayashi, T. — Journal of the Radio Research Laboratory, Japan, Vol. 6, 1959, pp. 177-186.
9. Dueño, B. — Journal of Geophysical Research, Vol. 65, 1960, pp. 1691-1698.
10. Gallet, R. Utlaut, W.F. — Physics Review, Letters, Vol. 6, 1961, pp. 591-594.
11. Du Castel, F. — Comptes Rendus (Paris), Vol. 261 (10), 1965, pp. 1057-1060.
12. Cohen, R. Bowles, K. — Journal of Geophysical Research, Vol. 66, 1961, pp. 1081-1106.
13. Cohen, R. Bowles, K. — Journal of Geophysical Research, Vol. 68, 1963, pp. 2503-2525.
14. Cohen, R. Bowles, K. — Journal of Research, National Bureau of Standards, (US), Vol. 67D (5), 1963, pp. 459-479.
15. Smith, E.K. Finney, J.W. — Journal of Geophysical Research, Vol. 65, 1960, pp. 885-892.
16. Bateman, R. et al. — Journal of Geophysical Research, Vol. 64, 1959, pp. 403-405.
17. Carman, E.H. et al. — Australian Journal of Physics, Vol. 16, 1963, pp. 171-176.
18. Gibson-Wilde, B.C. Carman, E.H. — Journal of Atmospheric and Terrestrial Physics, Vol. 26, 1964, pp. 1231-1237.
19. Washburn, C.L. et al. — *Transequatorial F-Layer Propagation Study*. ITT Report, Project 4505, Task 450504, Contract AF 30 (602)-2506, 14 June 1963.
20. Nielson, D.L. — In *Spread F and Its Effects on Radiowave Propagation and Communication*. Agardograph 95, W. and J. Mackay, London, 1966, 467-490.
21. Bowen, E.D. et al. — Journal of Geophysical Research, Vol. 73, 1968, pp. 2469-2476.

22. Yamaoka, M. et al. — *Memorandum of the Antenna and Propagation Research Committee.* Radio Wave Research Institute (Japan), 28 October 1966 (in Japanese).

23. Nielson, D.L. — *The Importance of Horizontal F-Region Drifts to Trans-equatorial Propagation.* AGARD paper in this volume.

24. McCue, C.G. Fyfe, D.F. — Proceedings, Institute of Radio Engineers of Australia, Vol.26 (1), 1965.

25. Rastogi, R.G. — Journal of Geophysical Research, Vol.64, 1959, pp.727-732.

26. Rao, C.S.R. Malthotra, P.L. — Journal of Atmospheric and Terrestrial Physics, Vol.26, 1964, pp.1075-1085.

27. Lockwood, G.E.K. Nelms, G.L. — Journal of Atmospheric and Terrestrial Physics, Vol.26, 1964, pp.569-580.

28. Gibson-Wilde, B.C. — Journal of Atmospheric and Terrestrial Physics, Vol.29, 1967, pp.1269-1275.

29. Lyon, A.J. Thomas, L. — Journal of Atmospheric and Terrestrial Physics, Vol.25, 1963, pp.373-386.

30. Stein. S. — Journal of Geophysical Research, Vol 63 (1), 1958, pp.217-241.

31. Hanson, W.B. Moffett, R.J. — Journal of Geophysical Research, Vol.71, 1966, pp.5559 5572.

32. Ostrow, S.M. Stewart, F.G. — Journal of Atmospheric and Terrestrial Physics, Vol.29, 1957, pp.1005-1010.

33. — *Semi-Annual Report to Voice of America, Part B (Africa Ionosphere).* National Bureau of Standards (US), Report 7276, Dec.1961 - July 1962.

34. Wright, J.W. — Journal of Geophysical Research, Vol.64, 1959, pp.1931-1934.

35. Nielson, D.L — Radio Science, New Series, Vol.3 (1), 1968, pp.101-109.

36. Koster, J.R., — Journal of Geophysical Research, Vol.68 (9), May 1, 1963, pp.2571-2578.

37. Booker, H.G. — Journal of Geophysical Research, Vol.67, 1962, pp.4135-4162.

38. Gopal Rao, M.S.V. Booker, H.G. — Journal of Geophysical Research, Vol.68, 1963, pp.387-394.

39. Gothard, N. — Radio Science (New Series), Vol.3, 1968, pp.235-244.

40. McCue, C.G. — *Proposal of a New Theory of Transequatorial VHF Radio Wave Propagation Anomalies.* Weapons Research Establishment, Salisbury, South Australia, April 1965.

TABLE I

Distance Separating Peaks in MUF(ZERO)F2
(March 1967 Prediction) in Degrees of Latitude
(Underscored values indicate at least a 25% decrease in MUF(ZERO)F2 at equator)

0°W	–	–	28	28	27	25	25	24	22	–	
75°W		–	30	35	32	28	25	25	21	–	–
150°W	–	30	34	32	30	25	25	21	19	–	
225°W		–	27	33	34	30	25	25	22	20	–
	08	10	12	14	16	18	20	22	00	02	

Local Time at Indicated Meridian

TABLE II

Comparison of Observed Signal Powers
(Values in decibels below free-space level)

Reference	*Free-Space Level* (dBm)	*Normal Value* (dB)	*Peak Value* (dB)
50 MHz			
Cohen and Bowles[12] (1961)	-22	110	85
Smith and Finney[15] (1959)	-38	64	59
Washburn et al.[19] (1963)	-67	16	
Nielson[20](1966)	-53		< 10
Bowen et al.[21] (1966)	-72	38	18
Kingan[6] (1967)	-78 (est.)		< 10
Nielson[23]((1968)	-79	25	13
Yamaoka[22] (1966)	-66	< 10	> 0
70 MHz			
Yamaoka[22] (1966)	-64	< 18	< 8
Bowen et al.[21] (1966)	-73		42
Nielson[23] (1968)	-82		23
90 MHz			
Nielson[23] (1968)	-68		48

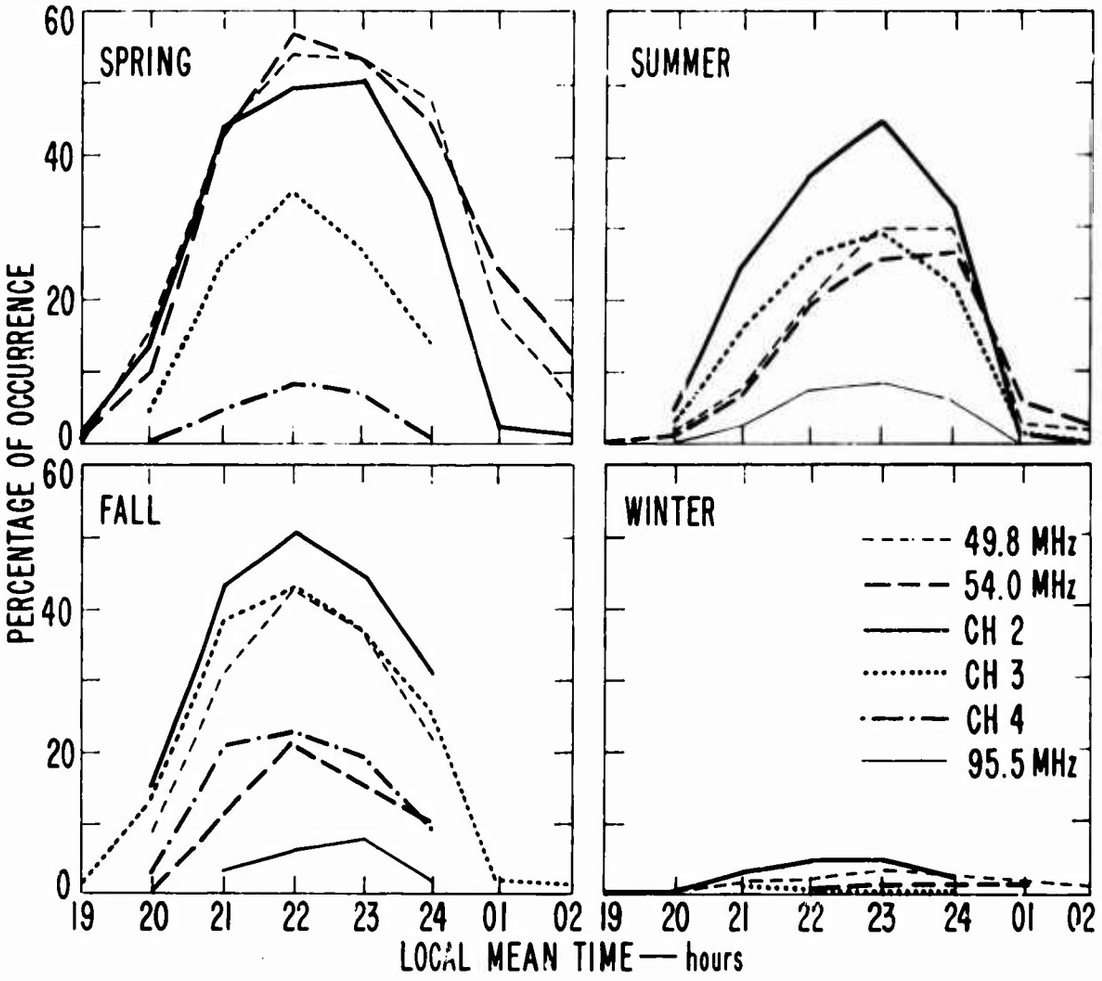


Fig. 1 Seasonal dependence and rate of occurrence of VHF propagation on the Hawaii-to-Rarotonga path. Seasons are defined for north latitude. (Courtesy Kingan[6]).

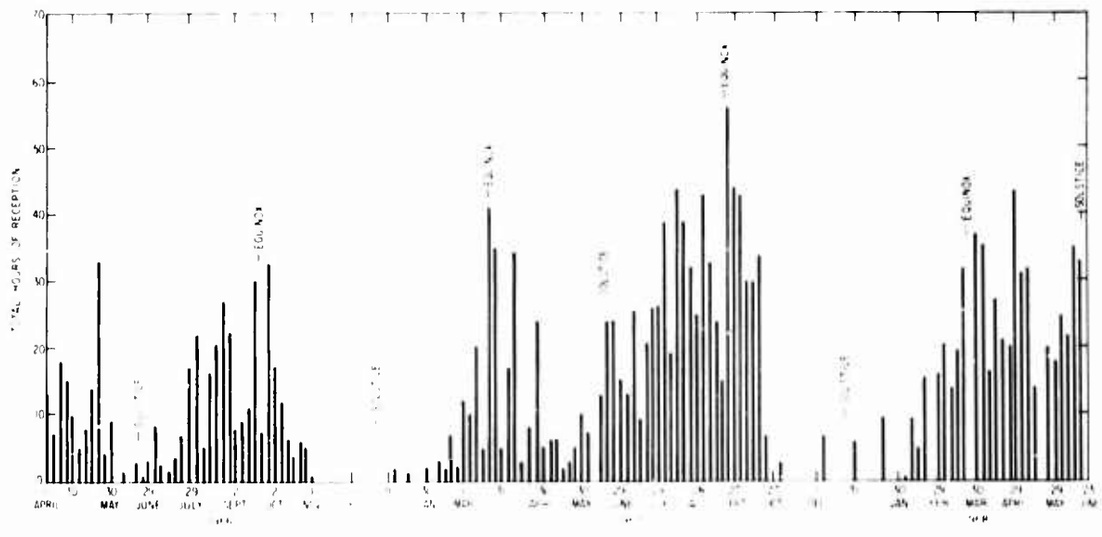


Fig. 2 Seasonal variation in VHF propagation for Hawaii-to-Rarotonga path for Television Channels 2, 3, and 4. (Courtesy Kingan[6])

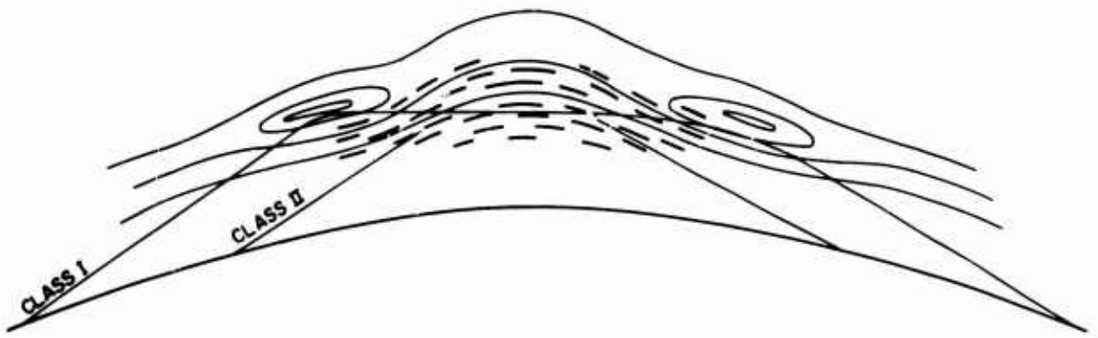


Fig. 3 Two possible classes of transequatorial propagation

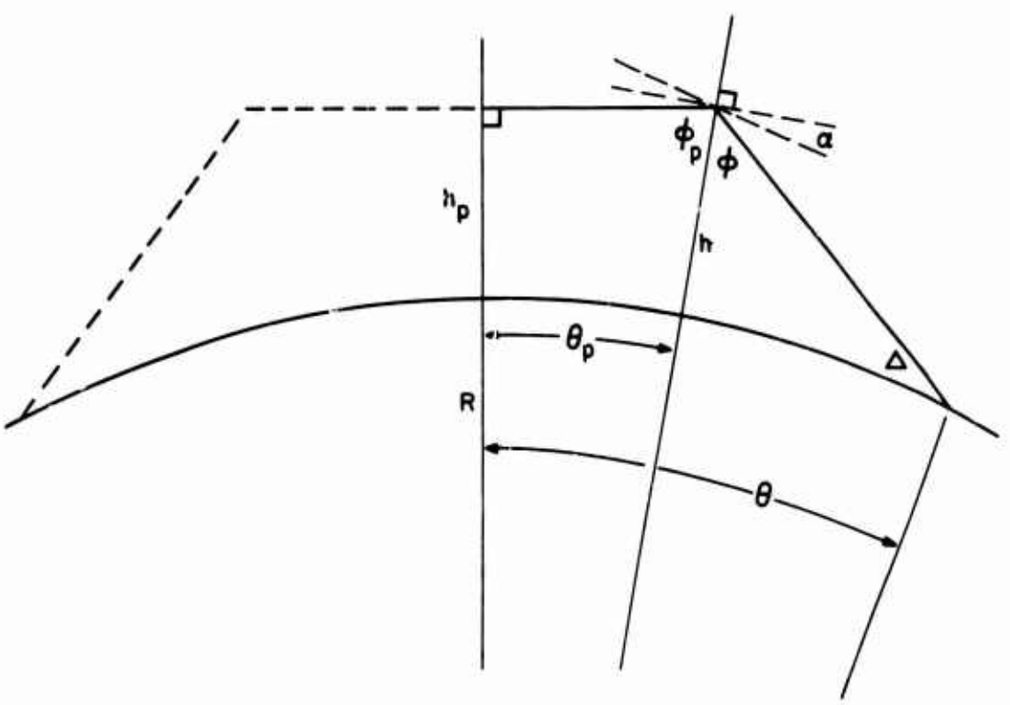


Fig. 4 Simple symmetric ray path for ionosphere-to-ionosphere (F2F2) reflections

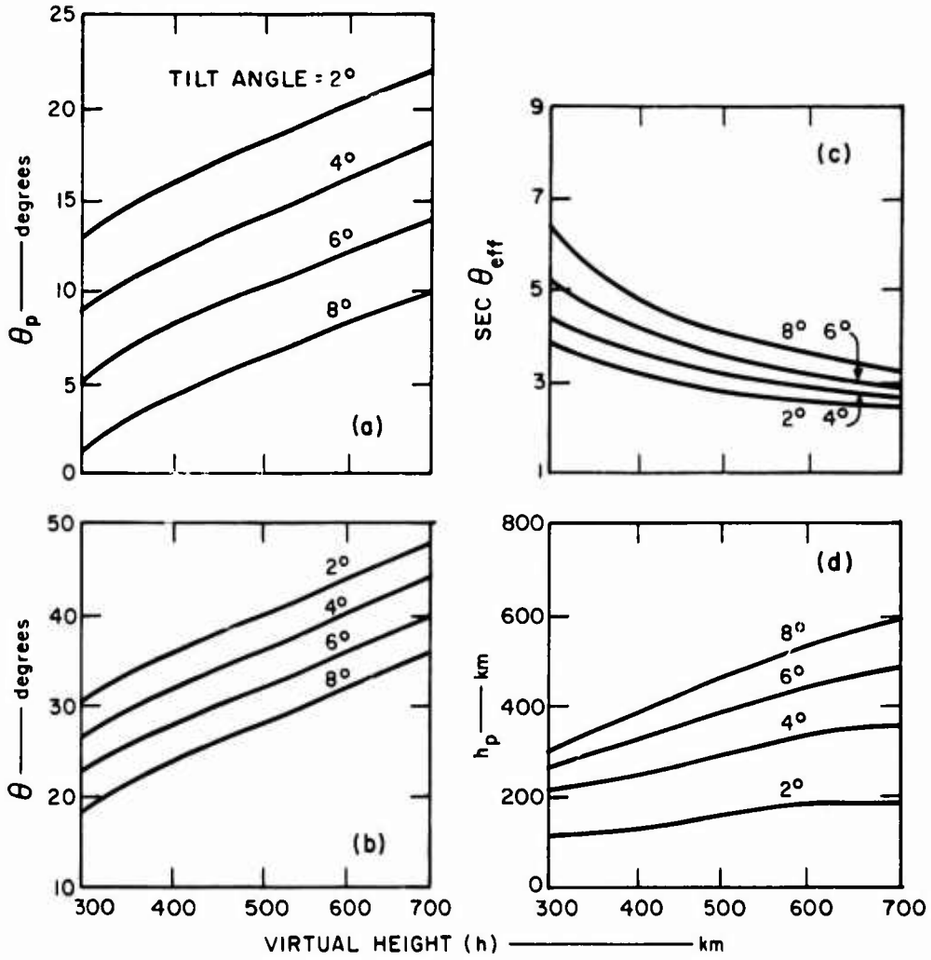


Fig. 5 Ray path and terminal locations that satisfy the conditions of Figure 4 for $\Delta = 0^{o}$

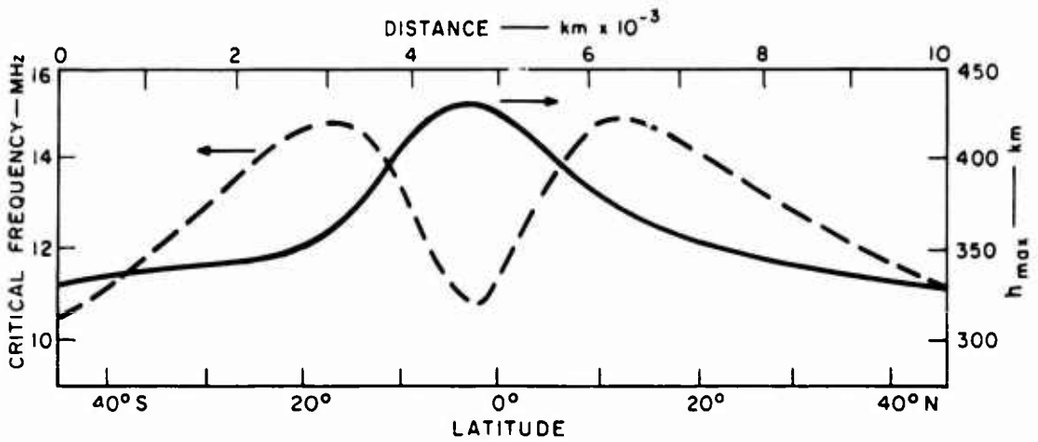


Fig. 6 Latitudinal profile of critical frequency and layer height (159°S, 1400 LMT, March 1968)

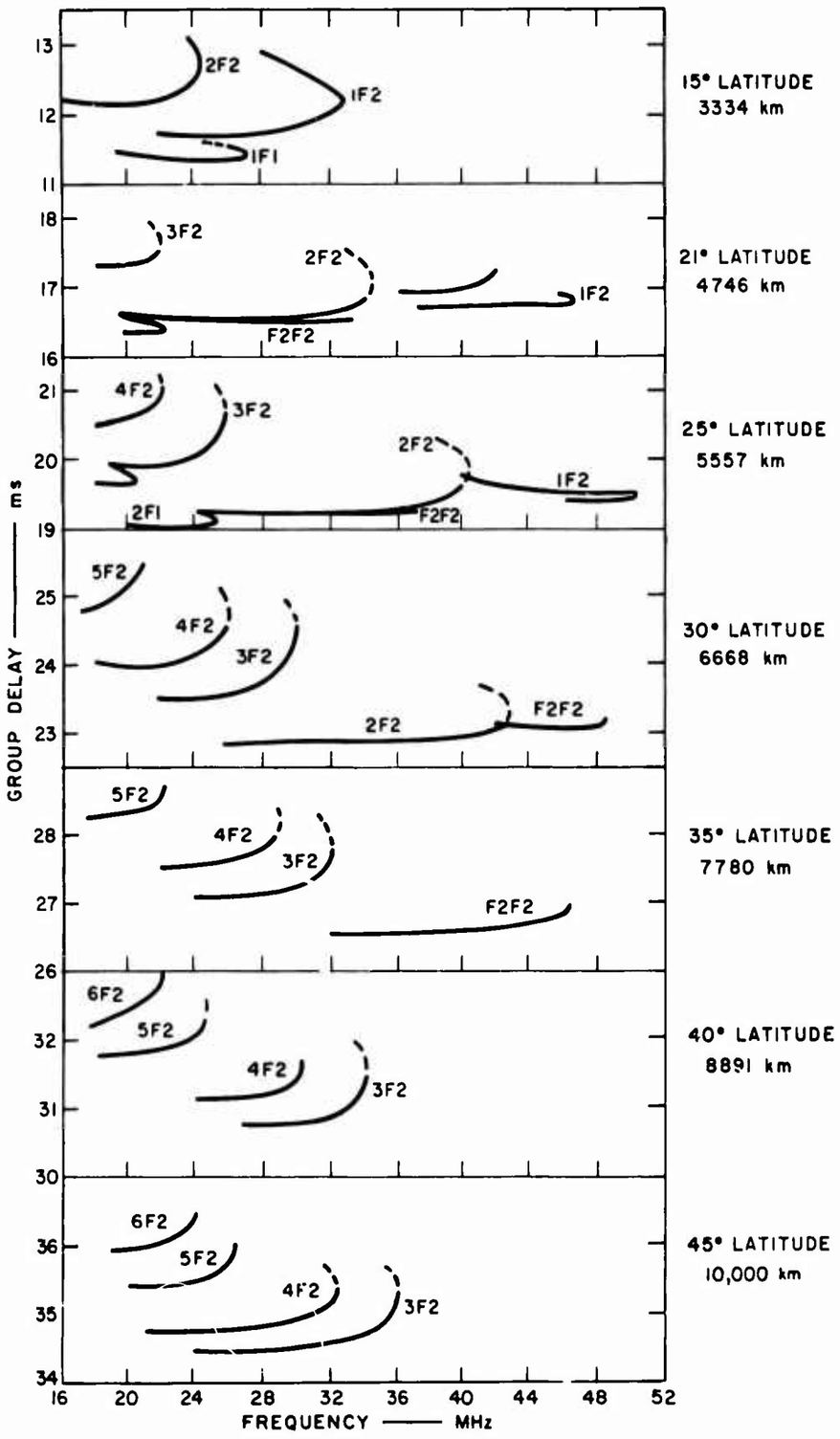


Fig. 7 Calculated ionograms using the profile of Figure 6

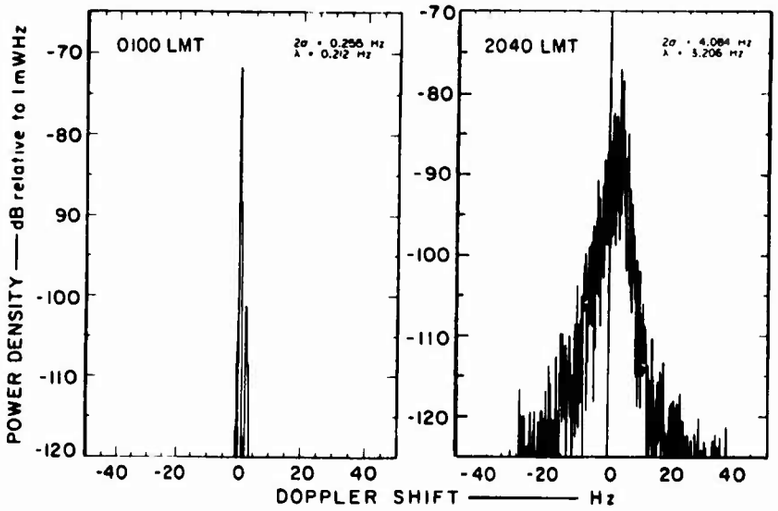


Fig.8 Examples of Doppler spectra at 54 MHz for the Rarotonga-Oahu path

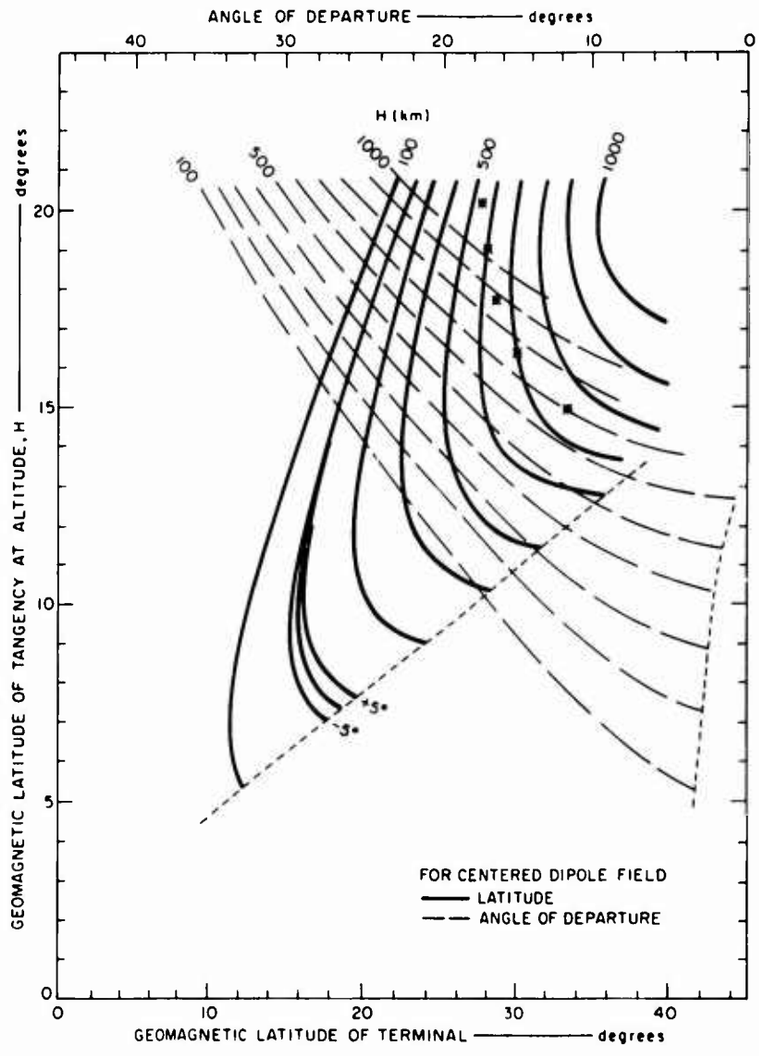


Fig.9 Terminal locations and departure angles for ray path tangency to geomagnetic field

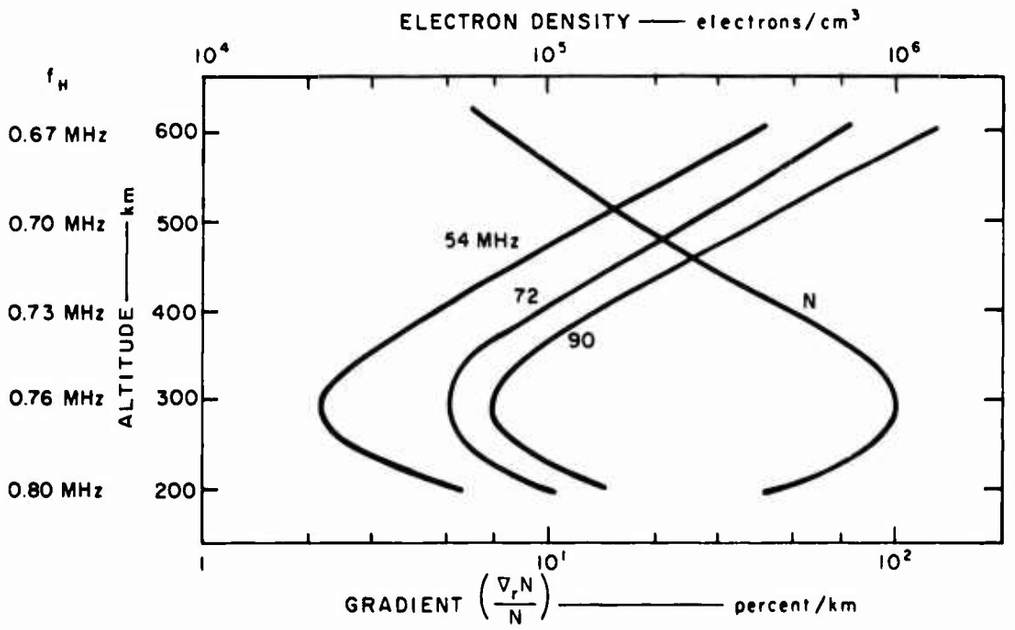


Fig. 10 Required electron density gradient for wave guidance

THE IMPORTANCE OF HORIZONTAL F-REGION DRIFTS TO TRANSEQUATORIAL VHF PROPAGATION

by

D.L. Nielson

Stanford Research Institute,
Menlo Park, California, 94025
USA

SUMMARY

Evidence is offered for oblique reflection from a moving F-region irregularity, at frequencies as high as 90 MHz. The velocity of the irregularity is 150 ms^{-1} in an east-west direction. Evidence is also presented showing the relative sensitivity of VHF propagation on a 5000-km transequatorial path to magnetic latitudinal and longitudinal variations.

NOTATION

Δ	Doppler shift
λ	free-space wavelength
v	velocity of irregularity
$P_{1,2}$	phase path length of oblique ray.

THE IMPORTANCE OF HORIZONTAL F-REGION DRIFTS TO TRANSEQUATORIAL VHF PROPAGATION

D.L.Nielson

1. INTRODUCTION

Our understanding of transequatorial propagation at frequencies above 50-60 MHz suffers from a lack of specific postulates or theories. The development of theories has been hampered by a lack of good diagnostic or experimental data. A mid-Pacific transequatorial propagation experiment carried on during the vernal equinox of 1968 has produced two important results that enhance our understanding of transequatorial VHF propagation. The 4800-km propagation path of this experiment, from Rarotonga in the Cook Islands to Oahu in the Hawaiian Islands, is highly symmetric to the geographic as well as the magnetic (dip) equator. A map of the path and surrounding islands is shown in Figure 1. In the experimental complement were CW transmitters and receivers on 36, 54, 72, 90, and 108 MHz. The transmissions were very coherent, making possible the spectral analysis of the complex received signal. Doppler spectra were produced by a Fourier analysis especially adapted for rapid computer calculation.

2. SIGNAL CHARACTERISTICS

2.1 Peak Signal Strength

While signal strengths showed great variability, the signal level tended to be quite high during the equinoctial month of March. Table I summarizes the peak median values for March. These peak values occurred between 2100 and 2200 local time.

TABLE I

Summary of Peak Signal Conditions for March
(Free-space loss = 145 dB)

Frequency (MHz)	*Free-Space Field Strength* (dBm)	*Peak Median Field Strength* (dBm)	*Corresponding Minimum Path Loss* (dB)
35	-86	-86	145
54	-79	-92	158
72	-82	-105	168
90	-68	-116	193
108	-81	Not observed	

2.2 Doppler Spectra

One of the important results of the experiment came from an analysis of the Doppler spectra. Each of these spectra was computed from 10 seconds of coherent CW signal. On

the two highest observed frequencies, and often on the three highest, the signal, while quite spread, appears as small Doppler segments moving from positive to negative Doppler frequency. A set of such records for each frequency is shown in Figure 2 for 25 March 1968. One apparent interrelationship is the linear variation of Doppler shift with frequency down to 54 MHz. The 36-MHz spectra seldom resemble those of the two highest observed frequencies, whereas the spectral characteristics of the 54-MHz data are often an admixture of the characteristics of 36, 72, and 90 MHz.

In an attempt to determine the meaning of these time-varying Doppler shifts, the normalized Doppler expression shown in Figure 3(a) was derived. For this expression, the existence of a north-south irregularity moving west to east along the magnetic equator was postulated.

Since

$$\frac{d(\lambda\Delta)}{dt} = \frac{-4v^2}{P_1} \text{ m Hz s}^{-1}, \quad \text{for} \quad P_1 >> 2vt = L,$$

the Doppler shift as a function of time may be used to calculate v directly. This elementary formulation, applied to the spectra of Figure 2, resulted in a surprisingly accurate fit. The observed and computed shifts are shown in Figure 3(b). The computed velocity is 150 m s^{-1}, a value that agrees with other equatorial F-region drift velocities[1]. The displacement of the reflection point at the equator was also computed; it is shown along the abscissa.

The fact that frequencies as high as 90 MHz can be reflected from these large irregularities adds a new dimension to the study of trans-equatorial VHF propagation. The measured signal strengths for 90, 72, and 54 MHz at 2220 LMT in Figure 2 are -116, -105, and - 85 dBm, respectively. These values correspond to scattering cross-sections of 10^9, 4×10^{11}, and 2×10^{13} m^2 - very large values.

2.3 Latitude and Longitude Variation

A three-month test of the spatial distribution of VHF signals was made during April, May, and June 1968 on the Islands of Rarotonga, Niue, and Manihiki (see Figure 1)[2]. The tests were for reception of Hawaiian television on Channels 2, 3, and 4 (55, 61, and 67 MHz).

Results to date show that the signals to Niue and those to Rarotonga had very similar occurrence statistics, although the reception periods were generally not concurrent. Since these stations are at approximately the same dip latitude, that result is not surprising. At Manihiki, however, the rate of occurrence was substantially lower: Channel 3 was heard briefly in only one instance, and Channel 4 was not heard at all. Yet at the same time Channels 3 and 4 were propagating well at the other stations. For example, at 2300 LMT, Channel 4 was received 31% of the time at Rarotonga and 42% at Niue.

The lack of signal on the shorter path has some important implications. First, for those signals propagated by normal refraction, the lack of signal might be caused by the southern terminal lying within the skip zone. Second, it appears that, if the propagation mechanism were largely weak scattering, there would be some non-equiangular scattering into the vicinity of the magnetic equator, while if the mechanism were ducting along F-region irregularities, a dead zone similar to that illustrated in Figure 4 would exist. The absence of certain frequencies at Manihiki would appear to exclude scattering as the mechanism. Finally, this reduction in signal occurrence illustrates the greater sensitivity of VHF propagation to magnetic latitudinal variations than to longitudinal variations.

3. CONCLUSIONS

The transequatorial propagation of frequencies as high as 90 MHz has been shown to be related to reflection from large F-region irregularities. These irregularities move east-west near the magnetic equator at a velocity of about 150 ms^{-1}. There is no reason to doubt that these irregularities are of the same type as those that have been observed by others at lower frequencies during the post-sunset to midnight period.

From a limited set of observations it appears that VHF propagation is substantially reduced when one terminal of a 4800-km symmetric path is moved 1200 km nearer the equator. But movement of the terminal along a line of constant dip by nearly the same distance does not change the VHF propagation characteristics.

REFERENCES

1. CALVERT, W. et al. — In *Proceedings of International Conference on the Ionosphere*, Physical Society, London, pp. 316-322, 1962.

2. SELBY, A. et al. — Private communication, July 1968.

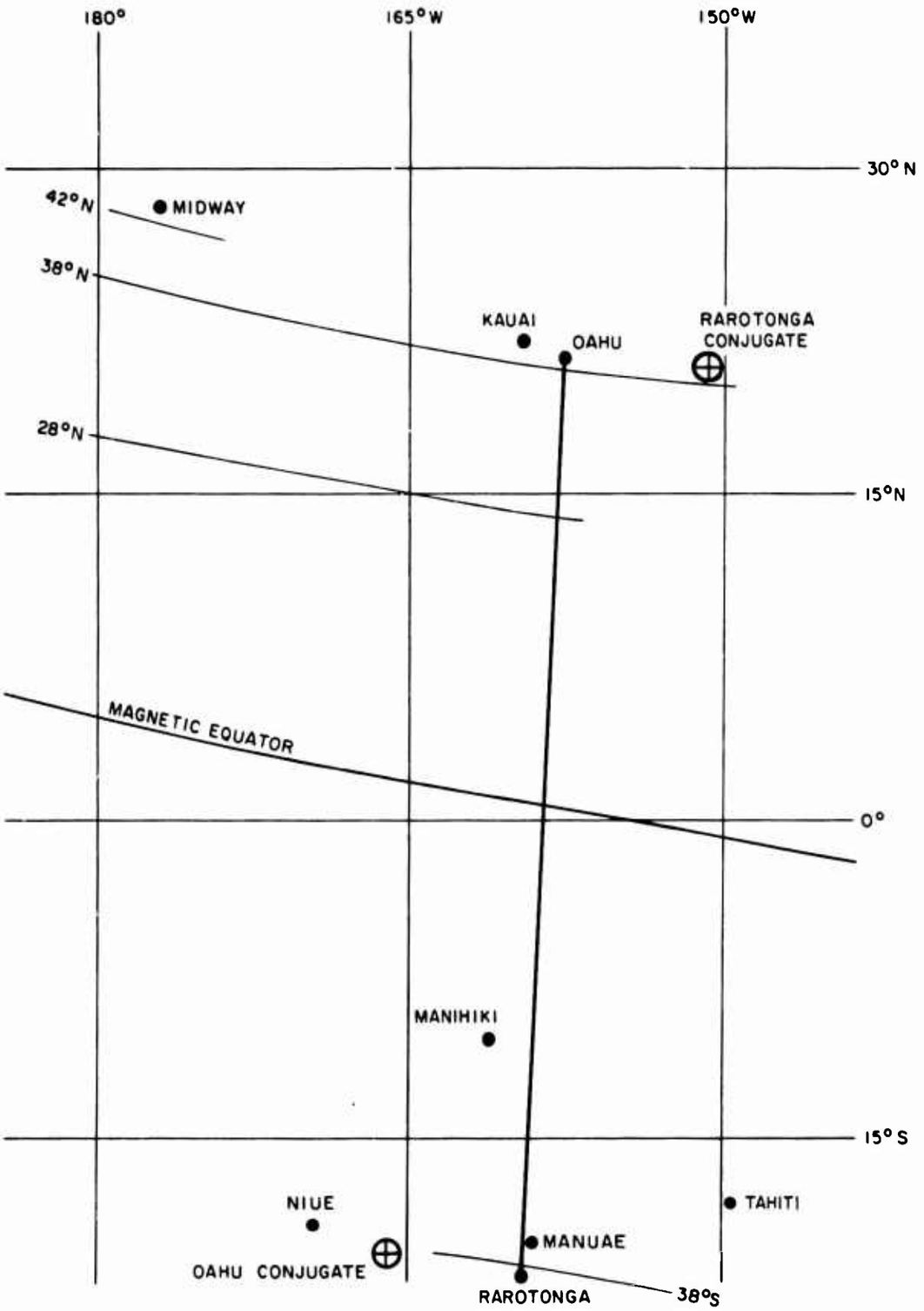


Fig. 1 Map of transequatorial propagation experiment

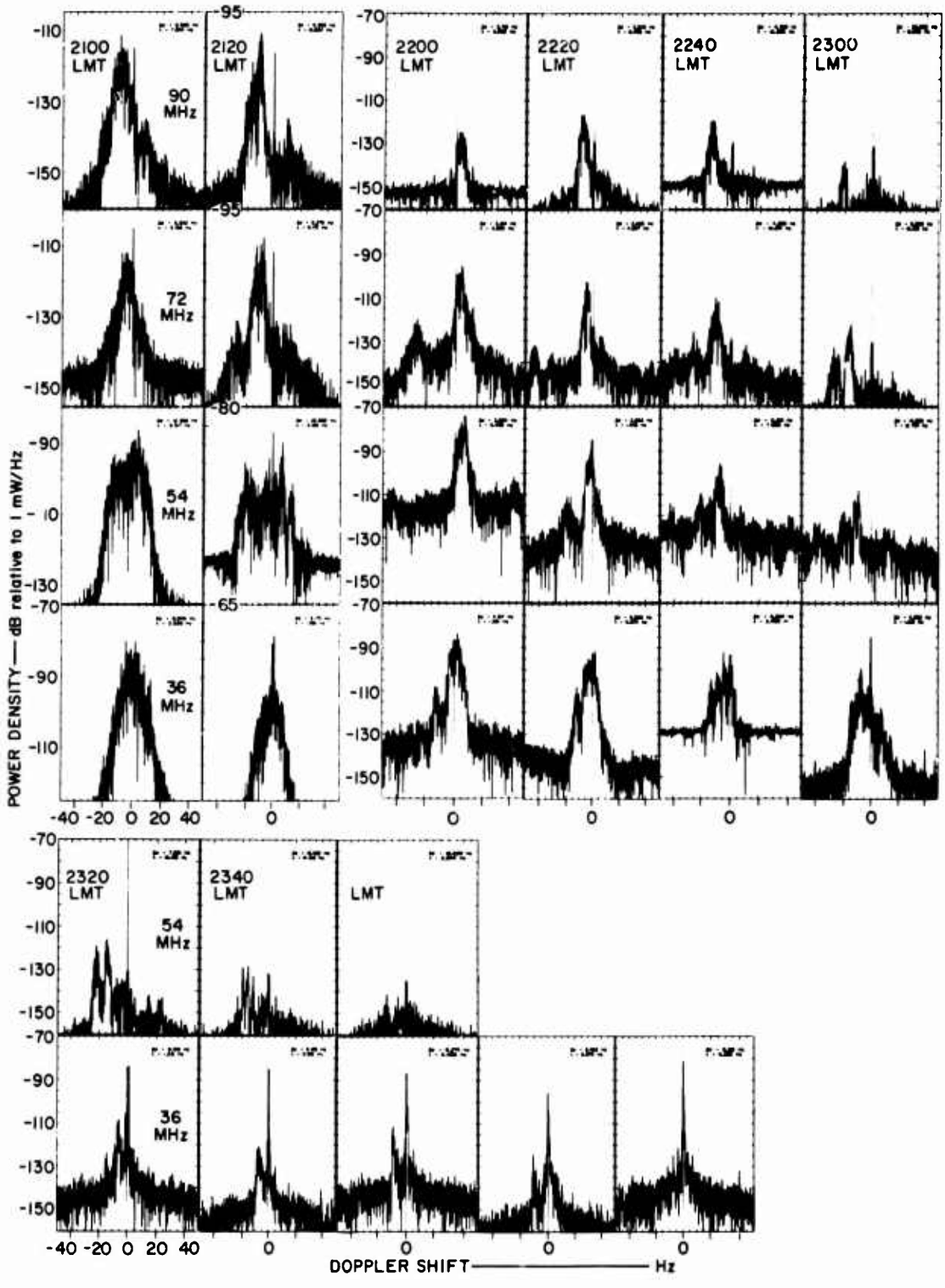


Fig.2 Doppler spectra for Rarotonga-to-Oahu path for 25 March 1968
(Ordinate scale varies prior to 2200 LMT)

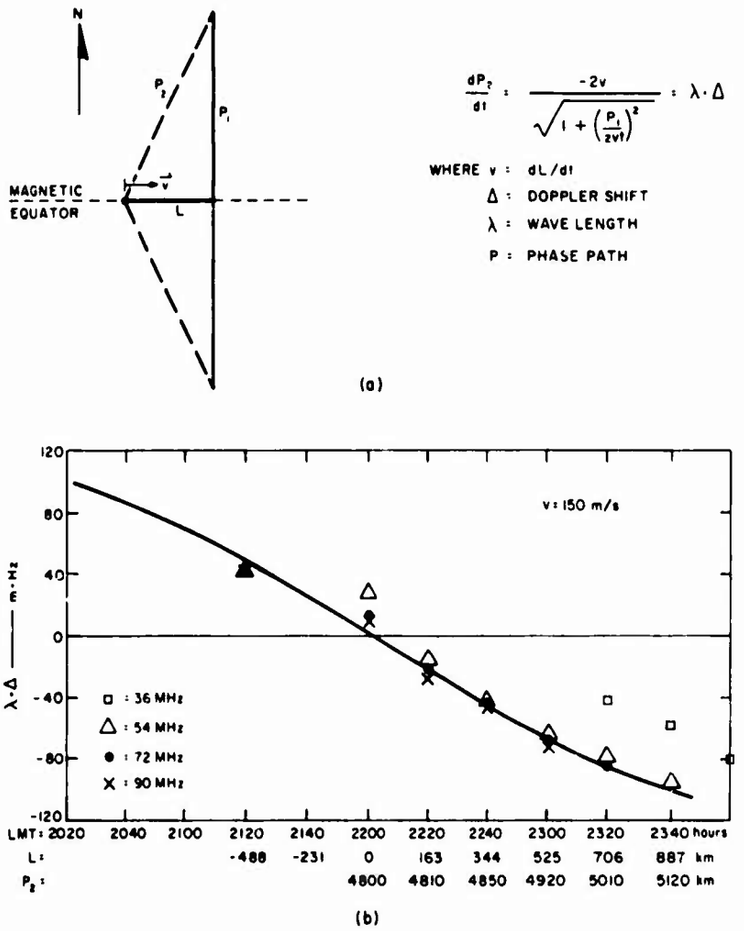


Fig.3 Test of Doppler shift for a moving irregularity

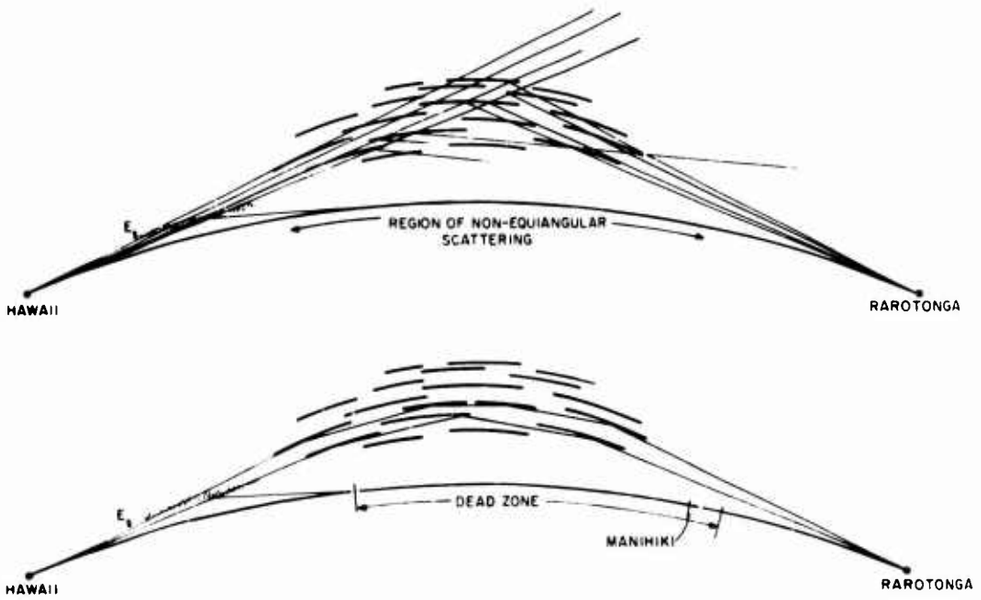


Fig.4 Example of difference in reception area with guidance along and with scatter from F-region irregularities

ETUDE D'UNE PROPAGATION TRANSEQUATORIALE EN DEHORS DU GRAND CERCLE EN PERIODE D'OCCURRENCE DE F DIFFUS

par

M. Crochet et P. Broche

Laboratoire de Physique de l'Exosphère
Faculté des Sciences de Paris, France

RESUME

Un type de propagation à très longue distance (16.000 km) en ondes décamétriques entre la France et Tahiti est étudié. Une propagation très stable en dehors du grand cercle a été mise en évidence. Son origine déterminée par les mesures des temps de transit des signaux et de leurs directions d'arrivée a été localisée dans la région de l'équateur magnétique.

Divers mécanismes possibles de production de ces signaux ont été considérés:

(a) réfraction par un gradient latéral,

(b) diffusion à la surface de la mer,

(c) diffusion dans la couche F associée à F diffus équatorial.

ETUDE D'UNE PROPAGATION TRANSEQUATORIALE EN DEHORS DU GRAND CERCLE EN PERIODE D'OCCURRENCE DE F DIFFUS

M. Crochet et P. Broche

1. INTRODUCTION

La propagation entre la France et le Pacifique Sud a été étudiée au cours de deux campagnes d'expérimentation en Juin 1965 et Juin 1967. Des phénomènes particuliers de propagation hors du grand cercle ont été mis en évidence en 1965 (Ref. 1) et confirmés en 1967.

2. RESULTATS EXPERIMENTAUX

Des impulsions de puissance de crête 100 kw émises dans deux directions à partir de Valensole au moyen d'un aérien large bande, directif (10^{o} à 3 dB à 10 MHz) ont été reçues à Tahiti (Fig. 1). La première direction qui est celle du grand cercle Valensole-Tahiti (azimut 315^{o}) présente les caractéristiques suivantes: elle est tangente à la zone aurorale dans laquelle l'énergie peut être fortement absorbée de nuit[2]. Pour une distance totale de 16.300 km, une partie de trajet d'environ 5000 km est terrestre et l'on peut s'attendre à 2 ou 3 reflexions sur le sol, alors que la caractéristique essentielle de la seconde direction (azimut 285^{o}), est d'être entièrement sur mer; elle ne traverse aucune zone d'absorption anormale et présente au contraire des conditions favorables de propagation longue distance par supermodes de 0400 à 0800 TU (Ref. 3).

En Juin 1965, on a constaté que le signal émis dans l'azimut 285^{o} était reçu à Tahiti avec une amplitude sensiblement égale à celle du signal émis dans le grand cercle. Un mode de fonctionnement de type balise-répondeuse à également permis de mettre en évidence une augmentation du temps de propagation aller-retour de 4,7 ms (Fig. 2). Une telle augmentation ne peut s'expliquer que par une trajectoire "brisée" suivant deux ou plusieurs arcs de grands cercles. Si l'on admet qu'il existe un mécanisme provoquant une déviation unique à une distance D de Valensole le long du grand cercle Valensole-Gambier, on peut calculer en fonction de D l'augmentation Δt du temps de propagation aller retour le long de ce chemin "brisé" par rapport à celui observé le long du grand cercle Valensole-Tahiti (Fig. 3). On voit ainsi que les résultats expérimentaux conduisent à adopter D = 12.500 km, la déviation qui se produit sensiblement à l'équateur magnétique, est de 23^{o}.

Ces résultats ont été confirmés en 1967 par des essais de goniométrie par cadre qui ont pu être effectués à Tahiti. Pour une émission à partir de Valensole dans l'azimut 285^{o} (grand cercle Valensole-Gambier) le signal est reçu à Tahiti dans une direction comprise entre 70 et 80^{o} (Fig. 4) c'est-à-dire en provenance de la région d'intersection de l'équateur magnétique et de la trajectoire Valensole-Gambier.

Cette méthode de goniométrie rudimentaire qui a été utilisée à titre exploratoire, ne permet d'obtenir des résultats que pour des ondes polarisées linéairement dans le plan vertical. Lorsque la polarisation est elliptique on peut encore observer des minima de signal assez nets si la polarisation n'est pas trop circulaire et les positions correspondantes du cadre n'ont en général aucun rapport avec la direction d'arrivée des ondes. Par ailleurs, la structure complexe du signal qui est très fluctuant, s'étale sur plusieurs millisecondes alors que l'impulsion émise ne dure qu'une milliseconde: il y aurait lieu

d'effectuer des mesures de goniométrie pour chaque partie du signal reçu mais ceci n'a pas été tenté en 1967. On a admis que l'observation d'un minimum net subsistant assez longtemps dans un secteur donné était une indication acceptable de direction d'arrivée pour la partie du signal comportant le plus d'énergie.

En 1967, un second ensemble récepteur-goniomètre était placé aux Gambier dans le but de détector des propagations en dehors du grand cercle pour des émissions faites à Valensole dans l'azimut 315°. Cette expérimentation n'a pas donné des résultats aussi nets qu'on l'escomptait pour les raisons suivantes:

- dans cette nouvelle configuration, un lobe secondaire de l'aérien de Valensole rayonne le long du grand cercle Valensole-Gambier (c'est-à-dire dans de très bonnes conditions de propagation), un signal résiduel d'amplitude égale ou supérieure à celle des signaux correspondants à l'autre direction;
- les différences de temps d'arrivée sont insuffisantes pour que les divers signaux ne se superposent pas au moins partiellement. Il a donc été très difficile de les distinguer;
- les mesures de goniométrie, déjà sujettes à réserves, ont été faites sur un site défavorable et il a été jugé préférable de ne pas se servir des résultats peu nets obtenus.

Cependant, les mesures relatives des champs reçus ont permis de calculer l'absorption aurorale moyenne et un coefficient caractéristique de l'efficacité du processus de déviation. Ces mesures ont été effectuées en fonctionnement en balise répondeuse à Valensole et à Tahiti en 1965 ainsi qu'à Valensole, Tahiti et aux Iles Gambier en 1967.

Avec les notations

P_{VT} = energie reçue à Tahiti par le grand cercle

P_{VG} = energie reçue aux Iles Gambier par le grand cercle

P_{ind} = energie reçue à Tahiti par la trajectoire brisée

on a les résultats

$$P_{ind} = P_{VT} + 3 \text{ dB} \quad (1)$$

$$P_{ind} = P_{VG} - 25 \text{ dB} , \quad (2)$$

soit

$$P_{VT} = P_{VG} - 28 \text{ dB} . \quad (3)$$

Trois causes contribuent à la différence d'énergie reçue:

- écart d'absorption non déviative voisine de 8 dB entre 03 00 et 06 00 TU (Fig.5),
- écart entre les pertes par réflexion sur terre et sur mer (des valeurs moyennes de R_{terre} (-3 dB) et R_{mer} (-0,3 dB) (Ref.4) conduisent dans le cas présent à une différence de 5 à 8 dB).
- perte par absorption aurorale.

On trouve ainsi une perte par absorption aurorale de 12 à 15 dB.

L'équation radar permet d'exprimer la puissance reçue indirectement sous la forme

$$P_{ind} = \frac{P_t G_t}{4\pi r_1^2} \frac{S\sigma}{4\pi r_2^2} A_r L_2 \ , \qquad (4)$$

avec les notations

P_t = puissance émise

G_t = gain à l'émission

A_r = surface de captation à la réception identique dans les 2 directions

r_1, r_2 = distances au point de diffusion

r = distance le long du grand cercle

S = surface responsable de la déviation

σ = coefficient rapporté à un élément rayonnant isotropiquement

L_1, L_2 = coefficients de pertes par réflexion, absorption, défocalisation.

Pour de grandes distances émetteur-récepteur et de faibles retards, la détermination de la surface efficace à l'aide des courbes isodistances[5] se simplifie et conduit à une surface illuminée large de 500 km et profonde d'environ 2000 km.

L'énergie reçue directement par le grand cercle s'exprime sous la forme

$$P_{VT} = \frac{P_t G_t}{4\pi r^2} A_r L_1 \ . \qquad (5)$$

Des expressions (4) et (5) nous déduisons le coefficient σ

$$\sigma = \frac{P_{ind}}{P_{VT}} \left(\frac{r_1}{r}\right)^2 \frac{4\pi r_2^2}{S} \frac{L_1}{L_2}$$

$$\sigma = 3 - 1{,}7 + 13{,}7 - 28 \text{ dB} \ ,$$

soit

$$\sigma \simeq - 13 \text{ dB} \ . \qquad (6)$$

Le processus de la déviation pour un angle de 23^0 est donc très efficace.

3. TENTATIVE D'INTERPRETATION

Trois mécanismes au moins peuvent être envisagés.

3.1 Réfraction dans la Couche

On peut remarquer qu'aux heures où les phénomènes sont observés (18.00 à 22.00 TML à l'endroit où se produit la déviation) l'ionosphère équatoriale est fortement perturbée. Alors que les prévisions CRPL n'indiquent pas de gradients Est-Ouest importants, des données fragmentaires[6] montrent que dans la région équatoriale la répartition des hauteurs de bas de couche est de forme conique (Fig.6). Aux heures qui nous intéressent, la trajectoire Valensole-Gambier traverse ce cône dans une région où le gradient latéral favorise une deviation vers l'Est. Un traitement sur calculateur a été effectué à l'aide d'un programme de tracé de rayons du National Bureau of Standards. On suppose que les lignes d'égale fréquence critique f_{c0} et d'égale hauteur de maximum h sont de révolution et que le profil vertical de la couche est un profil de Chapman

$$f_c^2 = f_{c0}^2 \left[1 + C\left\{\left(\theta - \frac{\pi}{2}\right)^2 + \phi^2\right\}^{1/2}\right] \quad (7)$$

$$h_{max} = h_{max\,0} + R_0 \frac{\pi}{180} E \{(\theta - \pi/2)^2 + \phi^2\}^{1/2} \quad (8)$$

avec les notations

C (rad^{-1}) = coefficient caractéristique du gradient de fréquence critique

E (deg) = gradient de hauteur.

Des valeurs moyennes extraites de l'article de Villard[6] et des prévisions CRPL sont les suivantes:

f_{c0} = 9 MHz, h_{max} = 450 km

C = - 3 rad^{-1} (diminution de 2 MHz pour 10^0 géocentrique)

E = - 3 deg (diminution de 50 km pour 10^0 géocentrique).

Le calcul a été effectué pour une fréquence de fonctionnement de 10 MHz pour différentes valeurs de l'élevation et différentes positions relatives de la trajectoire par rapport au cône. On constate (Tableau I) que les déviations azimutales par réfraction sont toujours faibles (en particulier pour les angles bas qui nous intéressent) et ne permettent pas d'interpréter une déviation de 23^0.

TABLEAU I

Angle d'incidence (degrés)	0	5	10	15	20	25	30	35	40
Déviation azimutale (degrés)	0,333	0,146	0,161	0,211	0,295	0,429	0,653	1,095	3,045

3.2 Energie Diffusée au Sol

La valeur du coefficient σ ($\simeq$ 13 dB) caractéristique de la déviation semble trop élevée pour avoir son origine dans une diffusion sur mer (les valeurs trouvées sur d'autres trajectoires[5] sont de l'ordre de - 22 dB). A cet argument s'ajoute le fait sur les zones à la surface du globe, déterminées à l'aide du retard dans le temps de transit et de la goniométrie, ne sont pas celles qui reçoivent le maximum d'énergie le long de la trajectoire d'émission. Des enregistrements systématiques en rétrodiffusion ont en effet, permis de montrer que le maximum d'énergie arrive au sol entre 14.000 et 16.000 km (Fig.4). Ce n'est donc pas la zone de rétrodiffusion au sol correspondant à cet écho qui joue un rôle. Cependant, la zone ionosphérique de contrôle correspondante, située entre 12.000 et 14.000 km, est dans la région d'anomalie équatoriale et il est donc tentant d'associer à ces propagations en dehors du grand cercle des particularités de l'ionosphère dans cette région. Les heures auxquelles les phénomènes sont observés (18.00 à 22.00 TML à l'endroit où se produit la déviation) sont celles où F diffus équatorial commence à se manifester. Ceci ne signifie pas cependant que la coïncidence horaire implique obligatoirement que F diffus soit la cause du phénomène car on peut remarquer qu'en dehors de ces heures c'est l'absorption non déviative qui empêche la réception (Fig.5).

3.3 Déviation par des Irrégularités dans la Couche F

Si on considère la diffusion par des irrégularités alignées le long du champ magnétique dont la fonction d'autocorrélation est de la forme[8]

$$\rho(x,y,z) = e^{-\frac{1}{2}\left(\frac{x^2}{T^2}+\frac{y^2}{T^2}+\frac{z^2}{L^2}\right)} \qquad (9)$$

La section efficace de diffusion dans la direction l_2 , m_2 , n_2 pour une onde incidente venant de la direction l_1 , m_1 , n_1 est de la forme

$$\sigma = Ke - (k^2/2)\{(l^2+m^2)\,T^2 + n^2L^2\} = Ke - k^2\,(T^2/2)\,(l^2+m^2+n^2Q^2)\,, \qquad (10)$$

dans un système où Oz est parallèle au champ magnétique, avec

$$l = l_2 - l_1$$

$$m = m_2 - m_1 \qquad A = l^2 + m^2 + n^2Q^2$$

$$n = n_2 - n_1 \qquad B = k^2T^2/2 = 2\pi^2\,(T/\lambda)^2\,.$$

$$Q = L/T$$

Le facteur A contient l'influence de la direction et de l'"excentricité" Q de l'irrégularité alors que la facteur B contient l'influence de la taille T de l'irrégularité et celle de la fréquence de l'onde diffractée. Le calcul a été effectué pour des déviations de – 80 degrés à + 80 degrés, par rapport à la direction incidente et pour des zones de récupération au sol distantes de 100 à 2000 km du point de diffusion. La station de Tahiti étant située à environ 4000 km de la zone de diffusion, on suppose que la propagation se fait en un bond et demi après diffusion.

Pour un angle entre la direction d'arrivée et le champ magnétique de 40^o et un angle de déviation de 23^o les atténuations ont été calculées pour $T/\lambda = 1$ (Tableau II).

TABLEAU II

Q	1	√(10)	10
Att(dB)	10	60	600

La valeur expérimentale de l'affaiblissement conduit à des modèles d'irrégularités d'une centaine de mètres de longueur.

4. CONCLUSION

Des déviations importantes observées au niveau de l'équateur magnétique sur des propagations transéquatoriales ne peuvent être interprétées ni par un mécanisme de déviation latérale par réfraction, ni par un mécanisme de diffusion à la surface de la mer. L'existence de F diffus équatorial aux heures où ces phénomènes sont observés rend plausible un mécanisme de diffusion par des irrégularités alignées dont la longueur serait de l'ordre de 100 mètres.

REMERCIEMENTS

Ce travail a été accompli dans le Cadre des Conventions 67-232 et 68-217 du Centre National d'Etudes Spatiales et des Conventions 66-342 et 174-68 de la Direction des Recherches et Moyens d'Essais.

REFERENCES

1. Crochet, M. Goutelard, C. — *Phénomènes de Propagation hors du Grand Cercle Observés sur des Liaisons à Grande Distance en Ondes Décametriques.* Comptes Rendus, Académie des Sciences, Paris, Vol. 264, 1967, pp. 348-351.

2. Yeh, K.C. Villard, O.G. — *Fading and Attenuation of High Frequency Radio Waves Propagated over Long Paths Crossing the Auroral, Temperate and Equatorial Zones.* Journal of Atmospheric and Terrestrial Physics, Vol. 17, 1960, pp. 255-270.

3. Crochet, M. Delloue, J. — *Sur La Variabilité des Propagations Anormales Longue Distance Observées par Rétrodiffusion.* Comptes Rendus, Académie des Sciences, Paris, Vol. 263, 1966, pp. 517-520.

4. Davies, K. — *Ionospheric Radio Propagation,* Dover Publications, 1965.

5. Crochet, M. — *A Study of Lateral Diffusion of HF Radio Waves by Means of a Bistatic Experiment and Simultaneous Backscatter Observations.* Paper in this volume.

6. Villard, O.G. et al. — Journal of Geophysical Research, No. 3 1957, p. 407.

7. Jones, R.M. — *A Three-Dimensional Ray Tracing Computer Program.* ESSA - Technical Report, 1966.

8. Ratcliffe. — *Some Aspects of Diffraction Theory and their Application to the Ionosphere. Report on Progress in Physics,* Vol. 19, 1956, p. 188.

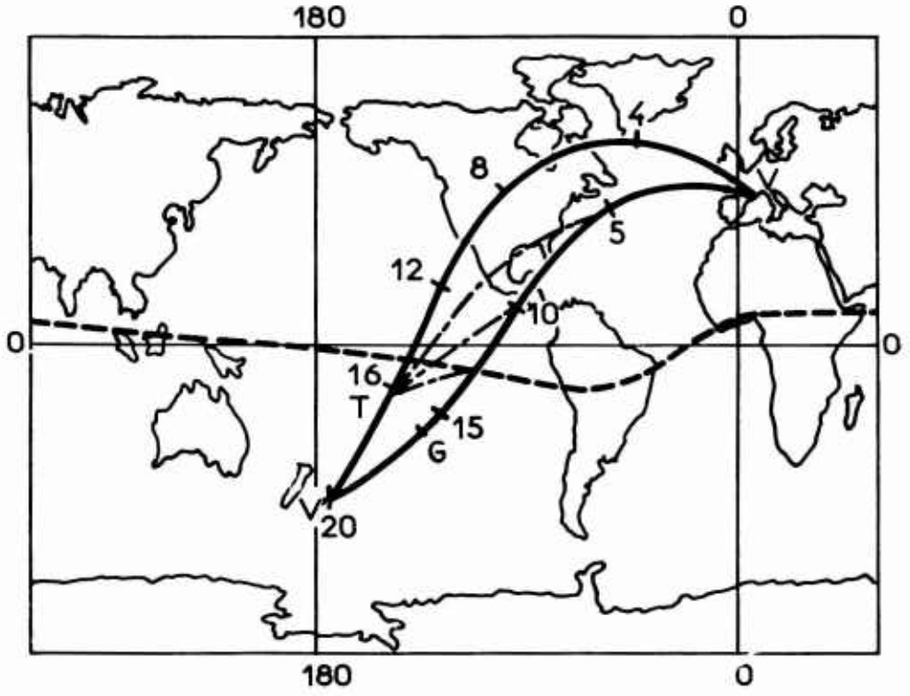


Fig. 1 Trajectoires

trajectoires

trajectoires déviées

équateur magnétique

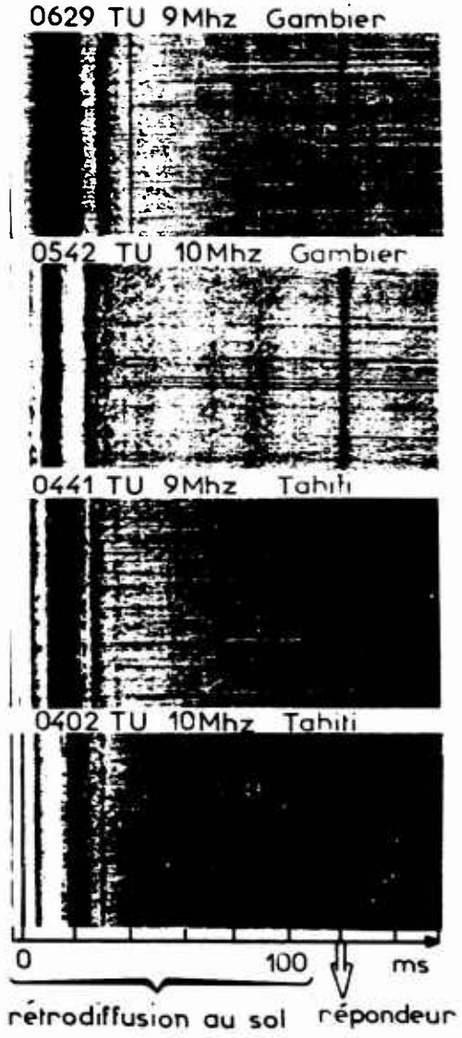


Fig. 2 Resultats experimentaux

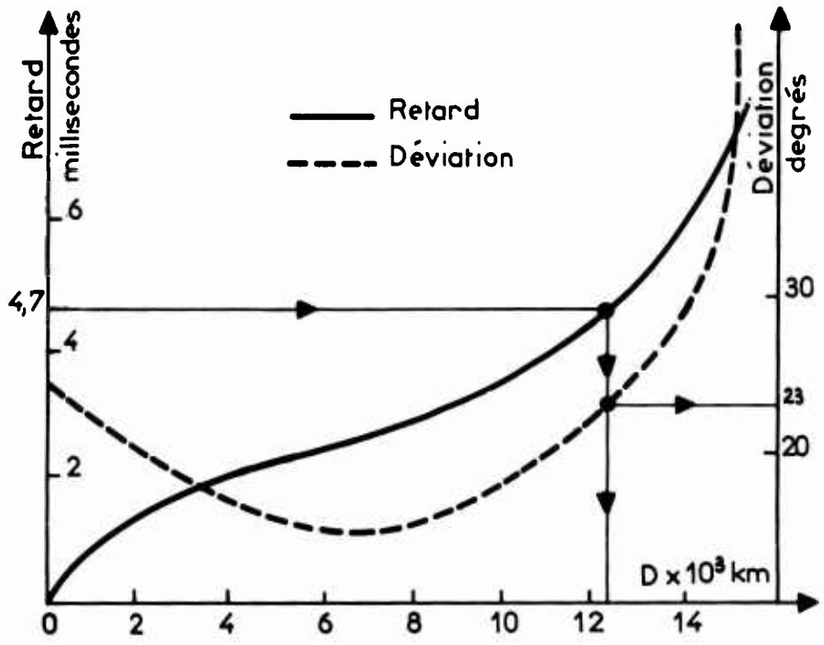


Fig. 3 Retards et deviation

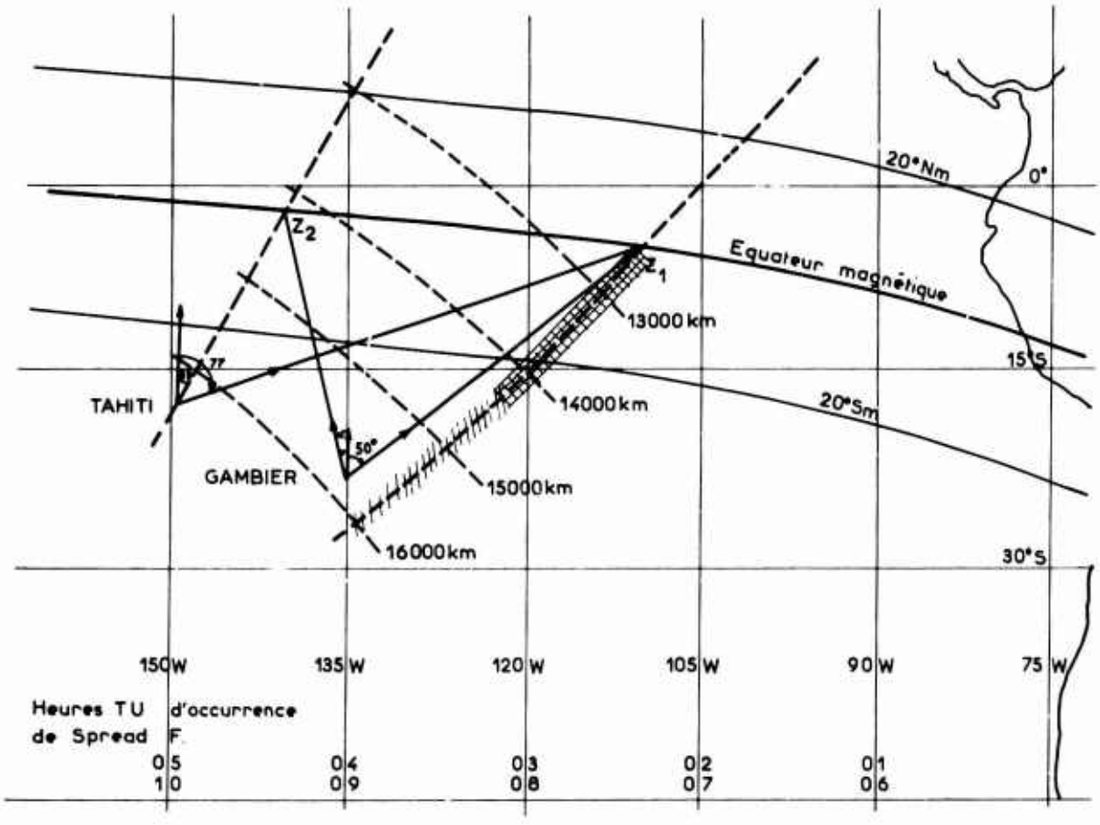


Fig. 4

zone de contrôle ionosphérique

zone de retour au sol

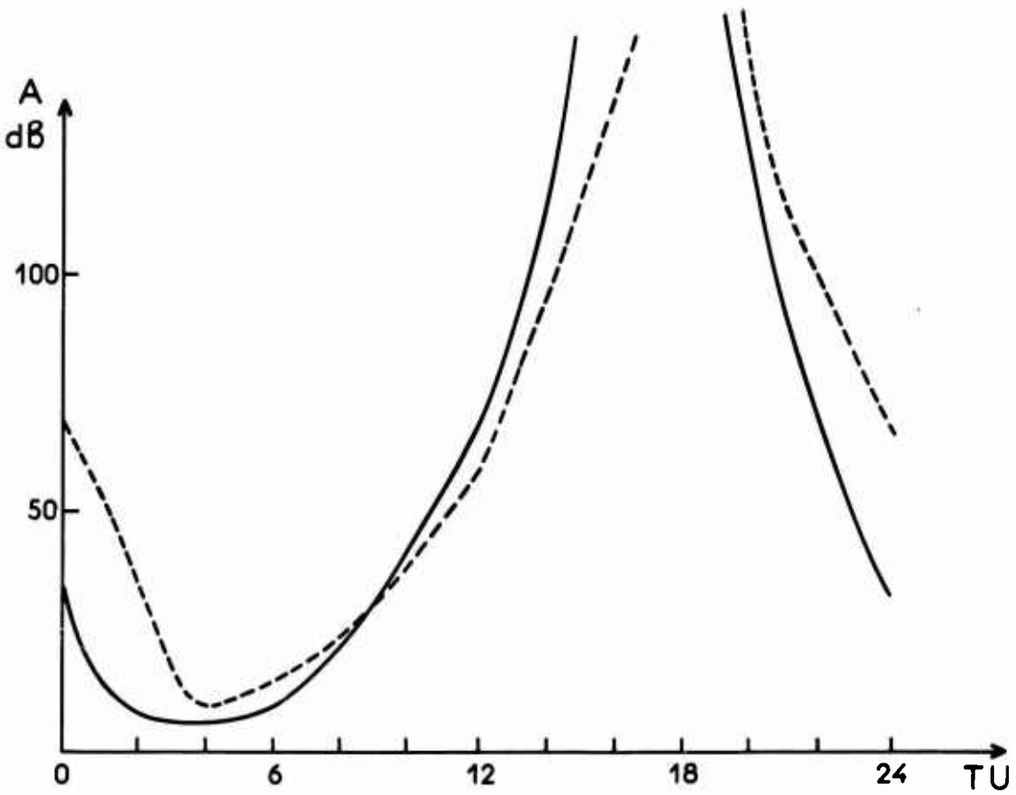


Fig. 5 ———— absorption non déviative sur Valensol-Gambier

- - - - - - - - - absorption non déviative sur Valensol-Tahiti

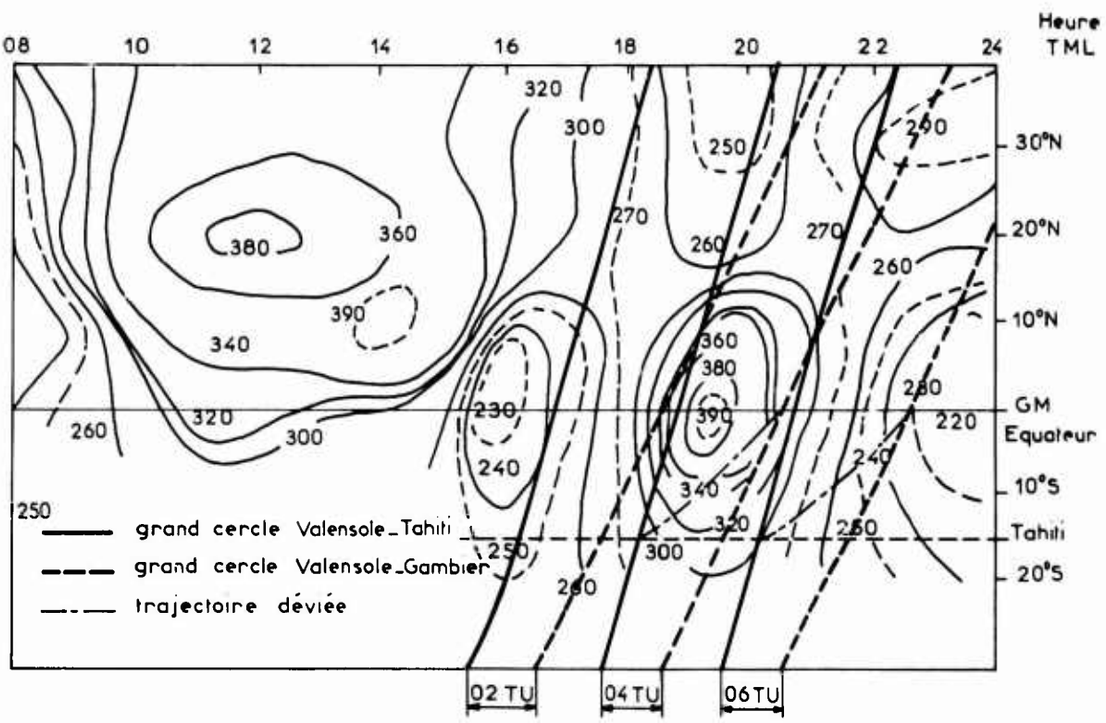


Fig. 6 Repartition des hauteurs de bas de couche

RAY TRACING OVER A TRANSEQUATORIAL PATH

by

N. C. Gerson

Syracuse University Research Corporation

SUMMARY

Ray-tracing procedures including the magnetic field were employed to clarify the mechanism of transequatorial propagation (i.e., the anomalous VHF propagation across the equator to distances of 6000 - 11,000 km without intervening ground reflection). The basic data employed were (a) 41 MHz backscatter soundings south from Mayaguez, Puerto Rico, and (b) vertical incidence observations along 75°W converted into electron density versus true height profiles. For the analysis, data from both sources obtained during the same ten-day interval were examined.

Insofar as rays refracted from the F-layer are concerned the usual effects were found: skip and horizon focusing, pre-dawn blackout (0200 - 0600 LST), escape of all rays launched above 18° irrespective of time of day, diurnal variation in Pedersen ray propagation distances, etc. Calculated rays attaining transequatorial echo (TE) distances (6000 - 11,000 km) occurred at 0800 LST, 1600 - 2000 LST and 2400 LST. Ray trapping to distances exceeding 11,000 km were present at 0800 LST and 1400 - 2400 LST.

Qualitative but not quantitative agreement between TE observations and TE calculated ray paths was found. While specific hours and distances did not correlate well, the general features of TE nevertheless were clarified. The calculations indicated that rays launched within 9° of the horizon southward across the (magnetic) equator were responsible for TE propagation. The half-range TE echo that precedes the evening full-range TE echo seems to arise from an extension of the Pedersen ray distance at this time. Signal flutter may then arise because of interference between the Pedersen and TE modes.

The primary mechanism responsible for TE seems to be a ducting or trapping condition in the ionosphere. For a ground-launched ray to propagate to TE distances, two requirements must be satisfied:

(a) vertical electron gradient propitious for duct formation,

(b) horizontal electron gradient allowing refraction of the ray into the duct.

TE seems to occur at 0800 LST because the latter condition rather quickly appears near 20°N geomagnetic latitude, probably because of the rapid increase in the post-sunrise electron density. The strong horizontal gradient disappears and does not reappear until late afternoon, possibly because of an atmospheric expansion.

A possible model allowing TE thus would be as follows. Between 0200 - 0600 LST, insufficient electron density occurs in the ionosphere to appreciably affect 41 MHz. At 0800 LST ionospheric trapping conditions have formed already. A sufficient horizontal gradient exists to allow a ground-launched ray to be refracted into the duct. After 1000 LST the horizontal gradient disappears, although trapping conditions still exist. During the late afternoon the horizontal gradient reforms, permitting TE.

The results imply that more TE would be observed at lower frequencies and with lower launch angles.

RAY TRACING OVER A TRANSEQUATORIAL PATH

N. C. Gerson

1. INTRODUCTION

This study was undertaken in an effort to better define the propagation mechanism responsible for transequatorial propagation. For this purpose a direct comparison was made between calculated ionospheric ray paths and backscatter observations. The basic data (e.g., (a) the vertical incidence soundings employed in the calculation, and (b) the oblique backscatter echoes) were obtained during the same time period and over the same geographic area.

The backscatter observations were made from Mayaguez, Puerto Rico, at 41 MHz (Ref. 1). The antenna provided an 80° horizontal beamwidth with a launch of about 5° above the horizon. The computations were based on a frequency of 40 MHz, and rays were traced at launch angles of 0°-19° at one-degree intervals. Thus, the elevation angles of the rays bracket all reasonable launch angles encountered in practice.

2. RAY-TRACING PROCEDURE

The ray-tracing program utilizes spherical coordinates with the origin at the center of an assumed spherical earth (Budden[2], Haselgrove[3]). In spherical coordinates the refractive index $\mu = \mu(r,\theta,\phi,\xi_r,\xi_\theta,\xi_\phi)$ where ξ_r, ξ_θ, ξ_ϕ are the direction cosines of the wave normal along the r, θ, ϕ directions.

The program utilized was that prepared by Langworthy[4], as summarized by Gerson and Geddes[5].

Hamilton's six equations provided only five independent relationships, since the sum of the squares of the direction cosines equals unity. In the computations all six equations were utilized because the sum of the squares of the direction cosines as calculated did *not* exactly equal unity. The procedure adopted summed these squares and then scaled each so that the sum of the squares with the scaled direction cosines equalled unity.

Inasmuch as the computations are made along a magnetic meridian the cyclotron frequency $\omega_H = \omega_H(r,\theta)$ and the electron density $n = n(r,\theta)$. Note that $\omega = 2\pi f$ = constant, since f = 40 MHz. The phase refractive index μ is obtained from the magnetoionic equation.

3. BACKSCATTER OBSERVATIONS

3.1 Distribution with Range

Backscatter results at 41 MHz during March 1958 are plotted in terms of the number of quarter-hours during which returns were obtained. The total possible number = 2976.

The distribution with range (Fig. 1) shows the expected peak of returns via the F2-layer between 2500-5200 km. A secondary peak between 6100-8000 km arises because of TE.

Maximum occurrence percentages are 27% between 3900-4000 km and 4% between 7100-7300 km. Of the total number of returns, those from the F2-layer constitute about 80%, from TE about 16% and from sporadic-E about 4%. The ratio of echoes via the F2-layer, TE, and sporadic-E thus is as 100/20/25.

3.2 Distribution with Azimuth

The number of quarter-hours containing returns versus geographical azimuth is displayed in Figure 2. Returns are categorized in five groupings; 01, 0-700 km; 02, 800 to 2400 km; 03, 2500 to 5200 km; 04, 5300 to 6000 km; 05, 6100 to 8000 km. These categories are considered to correspond, respectively, to returns arising via the propagation mechanisms of (a) tropospheric superrefraction; (b) sporadic-E; (c) F2-layer; (d) double-hop F2; and (e) transequatorial.

Figure 2 reveals that the great majority of echoes, as evidenced by the total curve, arises from southerly quadrants between 90°-180°-270°. Similar conclusions may be found for returns allowed by sporadic-E (category 02), the F2-layer (category 03), and TE category 05). Returns via meteorological superrefraction; important in other months, seem negligible in March. Those from double-hop F2-layer reflections are few and appear primarily from the East and West.

3.3 Diurnal Variations

The variation in number of quarter-hours containing returns versus time of day is portrayed in Figure 3. The characteristic behavior in the F2 returns is very evident: (a) the pre-dawn blackout (0200-0600 LST); (b) the maximum near noon; (c) the dip or bite-out caused by absorption (1300-1600 LST); (d) the secondary evening maximum (1700 LST); and (e) the general decrease in returns after sunset.

Echoes obtained via TE also are typical: (a) a minor maximum around 0800 LST; (b) a strong maximum between 1600-2300 LST; (c) the peak at 1800 LST followed by a decrease to insignificance by 2300 LST. As noted previously (Gerson and Geddes[6,5]) an afternoon minimum near 1400 LST followed by a rise to a maximum near 1700-1800 LST seems common to both the F2 and TE echoes. At 1700 LST, returns via TE are two-thirds those occurring via F2 reflections and at 2100 LST only slightly less.

3.4 Transequatorial Echo Backscatter during 22-31 March 1958

A summary of the echoes received via TE during 22-31 March 1958 is tabulated in Table I. The variation in percentage occurrence with local time is somewhat similar to that found for the entire month (Fig.3). However, a number of differences are present. The minor maximum at 0800 LST found in Figure 3 for the monthly data is not sharply evident although a semblance of a secondary maximum appears at 0900 LST.

Results for 22-31 March 1958 reveal a broad maximum exceeding 50% occurrence from 1100-2300 LST with a plateau of 70% occurrence from 1200-1700 LST. At 0900 LST the percentage also is 50%. The daily minimum (30% occurrence) exists from 0300-0800 LST. For the entire ten-day period, as a whole, the average occurrence was 50%. The F2 and TE returns obtained only during this ten-day interval will be compared with the ray tracings which were based on vertical incidence data obtained for the same period.

3.5 Summary of Backscatter Observations

All propagation modes display their individual peculiarities. TE reveals its marked predilection for the equinoctial evening, its abrupt termination near 2300 LST and its minor maximization near 0800-0900 LST. Echoes via the F2-layer attain a peak at 1300 LST and 1700 LST (with a valley between) and display the typical pre-dawn blackout between 0200-0600 LST. The afternoon decrease in occurrence that takes place for both the F2 and TE echoes may arise from the same cause (midday absorption) or may arise from different causes. However, the rise in number of echoes peaking near 1600-1700 LST for both almost suggests a single mechanism. In terms of range, the few sporadic-E returns seem mainly confined to 800-2400 km, F2-layer returns between 2500-5200 km and the TE returns between 6100-8000 km.

4. ELECTRON CONCENTRATION VERSUS ALTITUDE

Vertical incidence critical frequencies measured from eleven sites between 39°N-37°S near the 75°W meridian were utilized. The data were obtained during 22-31 March 1958, an ionospherically quiet period close to the maximum of the solar cycle. The vertical incidence soundings provide no information above the F2-layer maximum. Electron densities above this altitude were extrapolated in accordance with a standard model which agrees with available data on the topside F-region. From the hourly profiles along the meridian, average hourly electron densities along each 10 km level from 110-990 km, inclusive, were derived.

The overall behavior of the equatorial ionosphere (Wright[7]) is depicted in Figures 4 and 5 for the hours 0600-1200 LST and 1600-2200 LST, respectively. The graphs give the distribution of plasma frequency versus altitude and latitude.

The diagrams show a number of interesting details. First and perhaps most striking is the great height of the F2 peak electron density in the immediate vicinity of the geomagnetic equator. The altitude of the peak usually lies between 300-500 km but extensions to 600 km or more are not uncommon between 1400-2000 LST. The high altitudes are regularly attained between 0900-2000 LST at all seasons. Between 2200-2400-0500 LST the shape of the isopleth (for the maximum F2-layer electron density) differs from that found outside these hours. Between 0500-2200 LST this isopleth is higher over the geomagnetic equator and lower at other latitudes. However, from 2200-2400-0500 LST the reverse occurs: the isopleth (of F2 electron density maximum) is lower over the geomagnetic equator than elsewhere. Also, at 1900 LST, after the disappearance of the E-layer, a rapid rise takes place in the altitude of the F2-layer. An equally rapid descent in height occurs after 2100 LST.

Another remarkable aspect of the equatorial ionosphere is the high electron density which occurs spatially within geomagnetic latitudes ±15° between 1200-2400-0400 LST. Global ionospheric data reveal latitudinal maxima in electron densities north and south of the equator. Whether such symmetry was present in March 1958 is unknown, since no observations were available near 15° at this time. The asymmetry found in the figures near 15°S may be fictitious, although those at ±8° and ±25° (geomagnetic) seem real.

Ionospherically, the zone between ±15° geomagnetic latitude is of considerable interest. It contains the highest vertical incidence critical frequencies of any measured on the planet. A significant daily enhancement in electron density takes place at 15°N (near 1200 LST). The enhancement increases slowly with time but then quickly attains a diurnal maximum near 2000 LST. At this hour the equatorial F-region begins to fall rapidly. The enhanced ionization at 15°N decays slowly after 2000 LST but the maximum near 15°N still seems discernible at 0300 LST. This behavior of the F2-region with respect to that at other locations is anomalous. It undoubtedly arises because of the strong influence of the equatorial geomagnetic field whose direction is practically horizontal in this area.

5. CALCULATED RAY PATHS

5.1 Procedures

Ray paths for both the ordinary and extraordinary modes were computed for every two hours of the day and for each degree of elevation angle from 0° (horizontal launch) to 19° above the horizon. The corresponding rays are numbered 1 to 20, respectively. The graphs obtained (Gerson and Geddes[5]) provide a representation of rays launched from Mayaguez (latitude 18°N or colatitude 72°) south along 75° longitude. In all instances rays launched at 19° escaped through the ionosphere.

A number of distinct classes of ray paths may be noted on the graphs. For example, there are rays which (a) escape from the ionosphere after only relatively minor refraction; (b) refract from the F2-layer at least once and return to the ground; (c) become trapped on intruding into the F2-layer and propagate without intervening ground reflections over large latitudinal distances. Various combinations of these three basic types may appear; e.g., trapping after one ground reflection, escape from a trapped path, escape after one or more F2-layer and ground reflections, etc. All rays coming within 30 km of the ground are considered to be reflected from the ground.

Some studies (Grossi and Langworthy[8]) indicate that ground-launched rays can be trapped in the ionosphere only with difficulty. Chordal reflections require that a ray impinge on the ionosphere at an angle of incidence greater than 83°. Rays leaving the ground could hardly meet this geometric criterion unless some prior refraction occurs. The strong horizontal gradients of electron density found in equatorial or polar regions or within sporadic-E can provide the refraction needed.

5.2 Ray Paths

Computed ray paths for the ordinary ray at launch angles of 0°-19° inclusive in one-degree increments are illustrated in Figures 6 and 7 for hours of 0600-1200 LST and 1600-2200 LST respectively. When the rays attained an altitude of 500 km the computations were terminated, so that rays launched between 16°-18° above the horizon may have been somewhat more refracted than shown. Of these rays the only one whose path may be doubtful is the 17° ray at 1600-2000 LST.

The figures evince a number of interesting details, some of which may be quickly summarized. Elevation angles above which rays escape are tabulated in Table II. With a few exceptions ordinary and extraordinary rays behave similarly, but are by no means congruent. Although all comments apply to the ordinary ray, they usually also hold for the extraordinary.

The calculations for 40 MHz rays launched southwards from Mayaguez at elevation angles between 1° and 19° show the following features (note that one degree (latitude) = 111 km):

(a) Skip distance focusing is found in practically all cases.

(b) Horizon (low launch angle) focusing is found in practically all cases.

(c) All rays escape between 0200-0600 LST.

(d) Pederson rays occur on a fair number of occasions, e.g., at 1000, 1400, 1600, 2000 and 2200 LST. At 2000 LST the second hop of the ray launched at 10° becomes a Pederson ray.

(e) The ordinary ray seems more susceptible to changes in the electron density than does the extraordinary. The range of the Pederson or high-angle ray is more pronounced and the trajectory gyrations are greater. Occasionally (1800 LST) the ordinary ray shows a TE reflection whereas the extraordinary ray does not.

(f) Rays encountering a single reflection from the F2-layer reach the ground principally between distances of 2310-4840 km. Distances attained by the Pederson ray are about 4730-5500 km.

(g) A goodly number of rays escape after one F2-layer reflection (at 0800 LST and between 1400-2400 LST).

(h) A small number of rays escape after two F2-layer reflections (between 0800-1000 LST and at 1400 LST, 2000 LST and 2400 LST).

(i) Some rays portray unusual trajectories because of the peculiar combination of launch angle and existing electron density profiles (at 1000 LST and 1600-2000 LST).

(j) Some trapping (allowing rays to propagate to distances exceeding 11,000 km without intervening ground reflections) occurs (a) at 0800 LST and (b) between 1400-2400 LST. (Computations cease at 11,000 km south so that where the rays ultimately touched the ground, if at all, is not known (see (Table III).

(k) Trapping after a normal reflection from the F2-layer occurs to various degrees between 0800-2400 LST. To a much smaller extent trapping also is found after two reflections from the F2-layer.

(l) The diurnal variation of trapping shows a maximum occurrence at 1800-2000 LST. At these hours the number of trapped rays is a maximum.

(m) Trapped rays attaining TE distances (6100-8000 km or colatitudes of 128°-145°) without an intervening ground reflection occur at 0800 LST and possibly 1600-2000 LST and 2400 LST (see Table IV). These calculated time and range characteristics are very similar to those describing TE.

(n) The distance spanned by Pederson rays expands considerably at 1400 LST - 1600 LST, becoming 4600-4800 km (from about 2860-3000 km before and after these hours). Echoes from this mechanism seem remarkably similar to the half-range TE which often appears one to two hours prior to full-range TE propagation.

6 DISCUSSION

6.1 Comparison

The ray tracings depict the single-hop F2 reflections fairly well. Figure 1 (based upon backscatter returns for the entire month of March 1958) shows that most F2 returns occur between 2500-5000 km. Computed distances for this mode range between 2300-5500 km although at the greater ranges some contamination arises from double-hop F2 echoes. For example, at 0800 LST the computed separation between single-hop returns is about 1320 km, and at 1000 LST only about 220 km. It therefore would seem that the observed F2 returns between 2100-6000 km may be divided into single-hop returns (between 2100-3700 km) and mainly double-hop returns (between 4800-6000 km).

Table V summarizes TE predicted rays and the observed backscatter results. It reveals only fair agreement between the tracings and the TE backscatter observations. TE is predicted between 1600-2000 LST inclusive; percentage occurrences are 70-60% during this interval. However, TE was also predicted at 2400 LST and 0800 LST when observances are only 40% and 30% respectively. Furthermore, at 1200 LST and 1400 LST when occurrences are 70%, and at 2200 LST when occurrences are 60% no TE is predicted.

On an overall basis, the ray tracings are conservative. More TE echoes are observed than predicted. The discrepancy may, perhaps, stem from (a) the poor spatial resolution in the vertical incidence ionospheric data and (b) the neglect of probable East-West F2-layer ion gradients (tilts). Earlier analysis (Gerson and Geddes[6]) revealed the presence of F2-layer tilts whose magnitudes and orientations were a function of time of day. Obviously a strong East-West electron density gradient can markedly deflect a radio ray out of the great-circle plane.

Several comments may be made relative to the probably predicted TE return at 0800 LST. The observations (Tables I and II) indicate an actual occurrence of 30%. At 0900 LST, however, the actual occurrence was 50%, dropping to 40% at 1000 LST. Thus, there is qualitative agreement between observation and prediction in that a post-sunrise increase

in TE is predicted and observed. The duration of the predicted and observed increase in TE is one hour (0800 LST and 0900 LST, respectively). It is interesting to note that, during the more extensive analysis of 41 MHz backscatter returns, a minor increase in TE was found at 0800 LST (Gerson and Geddes[6]).

While the predictions are conservative they provide an insight into mechanisms probably responsible for TE. The North-South distance of 6100-8000 km at one hop arises because of ionospheric trapping, as shown in Figures 6 and 7. Trapping occurs most frequently during the evening hours, as summarized in Tables II and V. A trapped mode is not necessarily consistent with the trapezoidal or equatorial bulge model. It occurs when ionospheric ducting conditions are present, provided a refractivity discontinuity refracts the ray into the duct. Thus trapped modes may occur at many locations on the planet as noted by Gerson[9], Grossi and Smith[10] and others. There is an increasing amount of experimental evidence indicating their existence.

6.2 Mechanisms

Together with the ray tracings (Figs.6 and 7) the electron density versus altitude profiles (Figs.4 and 5) reveal the propagation mechanisms involved. They may be clarified as follows:

(a) 0200-0600 LST. The plasma frequency of the F2-layer is too low to refract the wave appreciably. A gradual increase in the horizontal gradient of plasma frequency occurs along 20°N geomagnetic. It is insufficient to affect 40 MHz but may affect a lower frequency.

(b) 0800 LST. The plasma frequency has increased sufficiently in the post-sunrise period and the horizontal electron density gradient has increased so that 40 MHz waves may be trapped.

(c) 1000-1600 LST. The plasma frequency at the maximum of the layer remains fairly constant near 14 MHz. The gradient, however, has weakened and is not as strong as it was at 0800 LST. Presumably the weakening of the gradient does not now permit refraction into a duct, if one exists.

(d) 1800-2400 LST. Plasma frequencies increase from 17 MHz at 1800 LST to 20 MHz at 2000 LST and then weaken to 15 MHz at 2400 LST. However, intense horizontal gradients develop, beginning at 1800 LST and becoming extreme at 2000-2400 LST. During this time period diurnal conditions are most optimum for deflection and trapping of the ray into an ionospheric duct.

The above analysis indicates that the marked horizontal gradients in electron density near 20°N geomagnetic probably are responsible for injecting a radio ray into an ionospheric duct. The gradients are most intense near 0800 LST and between 1800-2200 LST. For lower frequencies, correspondingly strong gradients are present for a greater number of hours of the day. These gradients are located about 10° south of the observing site - near 20°N geomagnetic or 8°N geographic. For a trapped ray to be ejected from the duct an appropriate electron density gradient would be needed between 28°S-55°S geographic.

The analysis reveals qualitative rather than quantitative agreement. The tracings indicate TE at 1600-2000 LST and 2400 LST. Observed occurrences are 60% or more from 1200-1800 LST and 2100-2200 LST. The appearance of the short range TE return (Dueno[1]) at 1400-1600 LST seems to result from the rather sudden, pronounced range extension of the Pederson ray at this time. The effect may be associated with the increase in altitude and electron density of the afternoon equatorial ionosphere.

The traces also show that trapping in ionospheric ducts to distances exceeding 11,000 km are predicted at 0800 LST and 1400-2400 LST (see Table III). It is interesting to note that these predicted ionospheric ducting conditions correlate with the observed TE

occurrences much better than do the predicted TE conditions. One explanation may be that TE is but one manifestation of a more widespread North-South ionospheric ducting condition that occurs across the geomagnetic equator because of the propitious equinoctial geometry. Secondly, the relatively poor spatial resolution in the electron density versus true height profiles may effectively "transform" TE rays into very long distance ducted rays. It is felt that the first suggestion is the more probable.

6.3 Launch Angles

The launch angle of the trapped rays is confined between 0°-9° (see Table III). At 1400 LST and 1600 LST the ray bundle comprises those launched between 5°-7°. The bundle increases its vertical beamwidth to 2°-9° at 1800 LST, after which it contracts rapidly and lowers to the horizon. At 2400 LST the ducted rays are at 0°-1°.

Several comments may be made relative to (a) the launch angle of the rays on the one hand and (b) TE and ionospheric ducting conditions on the other (Tables III and IV). In both latter instances, the long distance rays are launched close to the horizon - below 9°. It would seem that more TE and ionospheric trapping may be encountered in practice if the attenna launch angle is depressed and optimized to within 8°-9° of the horizon. Under these conditions more energy should be channelled into the ionospheric mechanisms, permitting TE and trapping.

It is also possible that a lower launch angle permits a greater range for a TE or ducted ray. In this connection, Gerson and Geddes[6] noted that TE ranges at 50 MHz were always greater than those at 41 MHz. During the experiment the launch angle at 50 MHz was several degrees lower than that at 41 MHz.

6.4 Altitude of Trapped Rays

Noticeable changes in the character of the calculated ray distributions occur after 1000 LST. Between 0200-0600 LST all rays escape, and at 0800 LST most rays still escape. From 1000 LST onwards more and more rays are multiply reflected between the surface and 280 km. Thus, the energy flux within this 280 km ground based stratum increases and becomes more uniform with altitude. It remains so until about 2200 LST for both the ordinary and extraordinary rays. There is little doubt that this condition becomes emphasized at lower frequencies - down to about 10 MHz. For some purposes (e.g., long range communications) this condition, which is controlled by the vertical antenna pattern, may be very useful.

The trapped rays, which occur at 0800 LST and 1400-2400 LST seem constrained between 70-250 km. They were found to propagate to distances of 11,000 km - the maximum range considered in the computations.

7. CONCLUSIONS

7.1 General

This investigation compares 40 MHz calculated ray paths and 41 MHz backscatter observations. For the former a ray-tracing program including the terrestrial magnetic field was utilized. The program employed as input hourly electron density versus true height profiles (to an altitude of 500 km) from about 20°N to 76°S. The original vertical incidence ionosonde data (from which the profiles were derived) were obtained during a ten-day period in March 1958. Comparison is made with backscatter sounding from Mayaguez, Puerto Rico, obtained during the same ten-day period.

Rays were traced southward at launch angles of 0°-19°, inclusive, in one-degree increments. Conclusions from the analysis are given in the following sections.

7.2 F2-Layer Effects

The normally expected F2-layer effects are very much in evidence;

(a) Skip distance focusing.

(b) Horizon (low launch angle) focusing.

(c) Numerous Pederson ray occurrences.

(d) Total ray escape (pre-dawn blackout between 0200-0600 LST).

(e) Maximum energy retention (between the F2-layer and ground) between 1200-1800 LST.

(f) Greater sensitivity of the ordinary than extraordinary ray to electron density variations.

(g) Escape of all rays irrespective of time of day emitted at launch angles of 18° or more.

(h) One-hop distances to 2310-4840 km.

(i) Pederson ray distances to 4730-5600 km.

(j) Marked expansion of Pederson ray distances at 1400-1600 LST.

7.3 Unusual Ray Paths

A number of unexpected, interesting ray trajectories occur after F2-layer reflection:

(a) Fairly frequent ray escape after one ground reflection (0800 LST; 1400-2400 LST).

(b) Some ray escape after two ground reflections.

7.4 Ray Trapping

The results show an unexpectedly high occurrence of ray trapping conditions;

(a) Unusual trajectories (1000 LST; 1600-2000 LST).

(b) Ray trapping to 11,000 km or greater (0800 LST; 1400-2400 LST).

(c) Ray trapping after one or more ground reflections (0800-2400 LST).

(d) Maximum trapping occurrence between 1800-2000 LST.

(e) Escape from a trapped mode at TE distance at 0800 LST; 1600-2000 LST and 2400 LST.

(f) Trapped rays constrained between 70-250 km.

7.5 Transequatorial Propagation

A number of rays exhibit the characteristics of TE rays, having the following features.

(a) Occurrences only at 0800 LST; 1600-2000 LST, and 2400 LST (see Table IV and Figures 6 and 7).

(b) First ground attainment at distances of 6100-8000 km (colatitudes 128°-145°).

(c) Suggestion of short range TE echo between 1400-1600 LST arising from a sudden expansion in the Pederson ray distance.

(d) Propagation constrained to two bundles below a launch angle of 8°; (a) horizon-launched, weakly-refracted ray, and (b) ionospherically trapped rays escaping to ground at TE distances.

(e) Propagation mechanisms analogous to that found in tropospheric propagation: (a) meteorological superrefraction and meteorological ducting (cf. 7.5(d) immediately above).

(f) Implication that TE may be merely one manifestation of a more generalized ionospheric ducting condition existing at this time.

(g) Implication that TE effects may be enhanced if low-launch-angle antennas are emphasized.

(h) TE trapped rays confined between 70-250 km.

7.6 Comparison of Computed and Observed F2-Layer Reflections

(a) The comparison between computed and observed F2-layer returns is fairly good, although discrepancies appear.

(b) Observed F2-layer returns occur between 2500-5000 km. Predicted distances are 2300-5500 km.

(c) Single-hop returns are mainly confined between 2100-3700 km and double-hop between 4800-6000 km.

7.7 Comparison of Computed and Observed Transequatorial Echo

(a) Only fair (quantitative) agreement exists between computed TE ray paths and TE observations (see Table V).

(b) TE observations exceed 50% of the time from 1100-2300 LST and 0900 LST. TE was predicted from 1600-2000 LST at 2400 LST and 0800 LST.

(c) Additional discrepancies include: No TE predicted at 2200 LST and TE predicted at 2400 LST and 0800 LST. Observed occurrences at these times were 60%, 40% and 30%.

(d) Qualitatively, agreement between TE predictions and observations is good. A maximum is predicted in the afternoon-evening and in the morning. Both are found, although displaced in time from the predictions.

(e) Fairly good agreement is found between predicted ionospheric trapping conditions (exceeding 11,000 km) and TE observations. The former are predicted at 0800 LST and 1400-2400 LST. The latter show maxima at 0900 LST and 1100-2300 LST.

(f) On a general basis, the ray tracings indicate a possibility of TE at 0800 LST. Occurrences at this time have been noted previously.

(g) The ray tracings indicate a better possibility of TE the lower the antenna launch angle. Previous reports showed that the lower the launch angle the greater the distance of TE echoes.

7.8 Deficiencies of Ray-Tracing Procedures

Discrepancies between the observations and the ray tracings may be ascribed to (a) deficiencies of the model, (b) limitations of the program, and (c) limitations of the computer. The first are probably by far the most serious The employ of Fermat's principle is basically sound.

The principle deficiency of the model is the poor spatial resolution in profiles of electron density versus true height. If observations are available for every point along the ray path, the tracing should provide the actual ray path. Unfortunately, the obtainment of the refractive index at every point of the ray path is impossible of fulfillment. It seems reasonable to assume, however, that the more precise the basic data (the better the resolution in time and space) the better the ray traces. However, unless a fairly accurate time rate of change of the model is available, rapid time variations of the electron density will always introduce considerable error. Undoubtedly improvement can be made in the interpolation procedures employed when utilizing ionospheric data.

Deficiencies in the computations may arise from a number of factors: too large an integration interval; neglect of double precision when necessary in the calculations; "lack of closure" when computing the three direction cosines, etc.

Perhaps the greatest value of ray-tracing procedures is to depict expected ray paths under various ideal ionospheric conditions. These may include expected median and extreme electron density spatial distributions over the path.

ACKNOWLEDGEMENT

The author wishes to express his deep appreciation to Dr Braulio Bueno, of the University of Puerto Rico, who not only supplied the original data, but also made invaluable comments during the analysis.

REFERENCES

1. Dueno, B. — *Peculiarities and Seasonal Variations of TE Backscatter Observed at Mayaguez, Puerto Rico.* Journal of Geophysical Research, Vol.65, 1960, pp.1691-1695.

2. Budden, K.G. — *Radio Waves in the Ionosphere.* Cambridge University Press, 1961, p.282.

3. Haselgrove, J. — *Ray Theory and a New Method for Ray Tracing.* Report of Conference on Physics of the Ionosphere, Physical Society, London, 1955, pp.355-365.

4. Langworthy, B.M. — *Hamiltonian Ray Tracing Digital Computer Program.* Report AFAL-TRgg-326, USAF Avionics Laboratory, Dayton, 1966.

5. Gerson, N.C.; Geddes, W.H. — *Propagation Data Analysis.* Technical Report No.25, Syracuse University Research Corporation, Syracuse, 1967.

6. Gerson, N.C.; Geddes, W.H. — *Propagation Data Analysis.* Third Quarterly Progress Report, Syracuse University Research Corporation, Syracuse, 1967.

7. Wright, J.W. — *Vertical Cross Sections of the Ionosphere Across the Geomagnetic Equator*. Technical Note 138, US National Bureau of Standards, Boulder, 1962.

8. Grossi, M.D. Langworthy, B.M. — *Geometric Optics Investigation of HF and VHF Guided Propagation in the Ionospheric Whispering Gallery Mode*. Radio Science, 1966, pp.877-886.

9. Gerson, N.C. — *Radio Wave Absorption in the Ionosphere*. Pergamon Press, London, 1962, p.123.

10. Grossi, M.D. Smith, B.M. — *Computer Simulation of HF and VHF Waveguidance Phenomena in the Lower Ionosphere*. Fall URSI, Hanover, 1965.

TABLE I

Hourly Reception of 41 MHz Long-Range Transequatorial Echoes (Mayaguez, Puerto Rico, 22-31 March 1958)

Date 1958	*Time (LST)*												*Reception Summary* (Hours, LST)
	00	02	04	06	08	10	12	14	16	18	20	22	24	
March 22														None
March 23														None
March 24						---	---	---	---	---	---	---		09-22
March 25						---	---	---	---	---	---	---		09-23
March 26	---	---	---	---	---	---	---	---	---	---	---	---	---	00-24
March 27	---	---					---	---	---	---				00-02; 12-18
March 28							---	---	---					11-16
March 29									---	---	---	---	---	17-23
March 30	---	---	---	---	---	---	---	---	---	---	---	---	---	00-24
March 31	---	---	---	---	---		---	---	---			---		00-09; 12-16; 21-23
Total Occurrences	4 4	4 3	3 3	3 3	3 5	4 5	7 7	7 7	7 7	6 5	5 6	6 5	4	00-24
Percentage Occurrence (%)	40 40	40 30	30 30	30 30	30 50	40 50	70 70	70 70	70 70	60 50	50 60	60 50	40	50

TABLE II

Calculated Angles Above which Rays Escape (Southwards from Mayaguez, Puerto Rico, 40 MHz, March 1958)

LST	*Ordinary Ray*			*Extraordinary Ray*		
	Initially	*After One F2 Reflection*	*After Two F2 Reflections*	*Initially*	*After One F2 Reflection*	*After Two F2 Reflections*
0200	0°	---	---	0°	---	---
0400	0°	---	---	0°	---	---
0600	0°	---	---	0°	---	---
0800	10°-19°	9°	4°-8°	11°-19°	9°	4°-8°; 10°
1000	15°-19°	---	11°-13°	15°-19°	---	11°-14°
1200	17°-19°	---	---	**	**	**
1400	18°-19°	0°; 15°-16°	1°	18°-19°	15°-16°	0°
1600	0°; 18°-19°	1°; 2°; 15°	---	18°-19°	0°-2°; 15°-16°	---
1800	17°-19°	0°; 14°-16°	---	13°-19°	14°-17°	---
2000	1°; 16°-19°	10°-15°	10°	1°; 17°-19°	11°-15°	---
2200	11°-19°	7°-10°	---	11°-19°	7°-10°	---
2400	10°-19°	5°-8°	9°	*	*	*

* Not Computed

** Computed only for angles between 0°-9°; no escape in this range.

TABLE III

Rays Trapped to Distances Exceeding 11,000 km with no Intervening Ground Reflection (Southwards from Mayaguez, Puerto Rico, 40 MHz, March 1958)

Time LST	*Ordinary Rays Trapped Launch Angle(°)*	*Comments*
0200	All rays escape	
0400	All rays escape	
0600	All rays escape	
0800	0° (?); 1°	**
1000	----------	
1200	----------	
1400	5°, 6°, 7°	
1600	5°, 6°, 7°	*
1800	2°-9°	*
2000	2°-5°	*
2200	1°, 2°	
2400	0°, 1°	

* Trapping to transequatorial propagation distances.
** Possible trapping to transequatorial propagation distances.

TABLE IV

Calculated Occurrence of Transequatorial Echoes South of Mayaguez, Puerto Rico (22-31 March 1958)

Time (LST)	*Ordinary Ray*			*Extraordinary Ray*		
	Launch Angle (°)	*Colatitude (°)*	*Distance (km)*	*Launch Angle (°)*	*Colatitude (°)*	*Distance (km)*
0200	All rays escape	----------	--------	All rays escape	----------	--------
0400	All rays escape	----------	--------	All rays escape	----------	--------
0600	All rays escape	----------	--------	All rays escape	----------	--------
0800	1°	140°P	7480	1°	140°P	7480
1000	----------	----------	--------	----------	----------	--------
1200	----------	----------	--------	----------	----------	--------
1400	----------	----------	--------	----------	----------	--------
1600	4° 7° 8°	124° 144° 148°	5720 7920 8360	7°	147°P	8250
1800	1°	143°	7810	?		
2000	0° 6° 7°	128° 138° 134°P	6160 7040 6820	0° 7°	127° 133°P	6050 6710
2200	----------	----------	--------	----------	----------	--------
2400	1°	143°	7810	*	*	*

* Not calculated
P = Possible
NOTE: Transequatorial echoes are considered to arise, without intervening ground reflections, between colatitudes of 128°-145°, corresponding to distances of 6100-8000 km south of Mayaguez.

TABLE V

Comparison of Observed and Predicted Transequatorial Echo Occurrences*

Time (LST)	*Predicted*** (Ray Launch Angles)	*Observed* (Percentage Occurrence)
0200	----------	40
0400	----------	30
0600	----------	30
0800	P (1°)	30
1000	----------	40
1200	----------	70
1400	----------	70
1600	(4°; 7°; 8°)	70
1800	(1°)	60
2000	(0°; 6°; 7°)	50
2200	----------	60
2400	(1°)	40

* On the basis of ray tracings south from Mayaguez.
** P = Possible

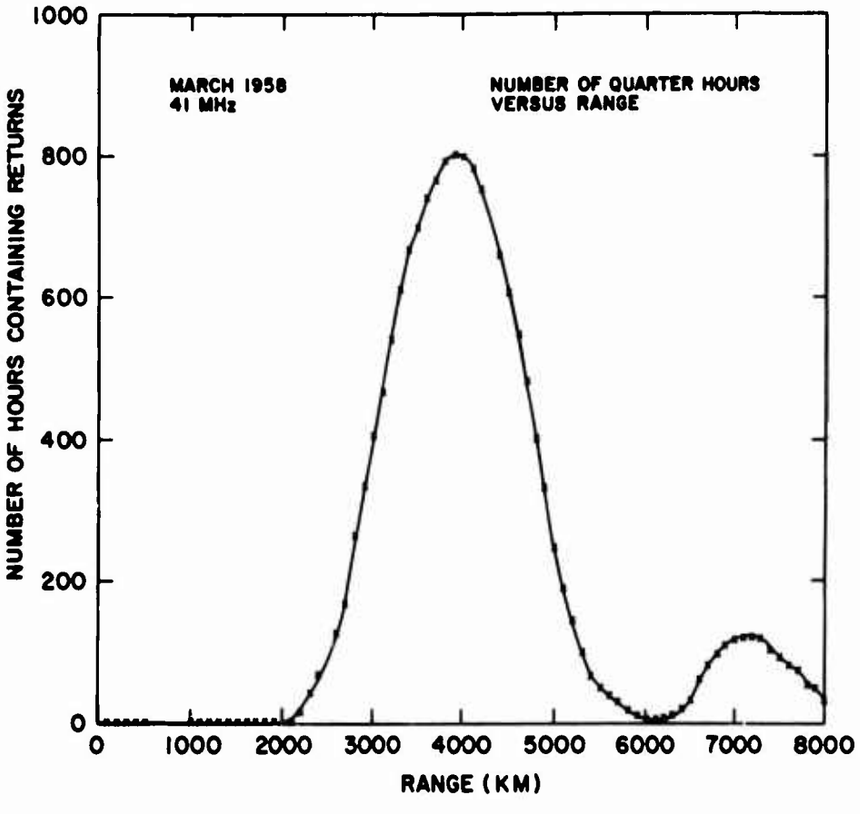


Fig. 1 Number of quarter hours containing 41 MHz backscatter returns versus range (Mayaguez, P.R., March 1958)

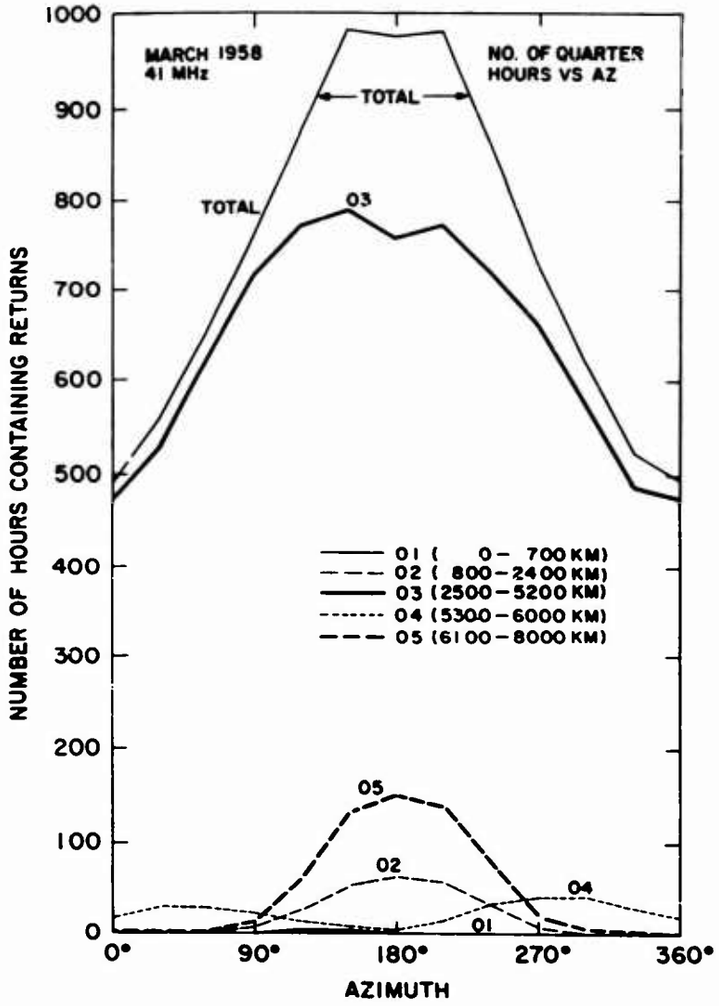


Fig. 2 Number of quarter-hours containing 41 MHz back-scatter returns versus geographic azimuth (Mayaguez, March 1958)

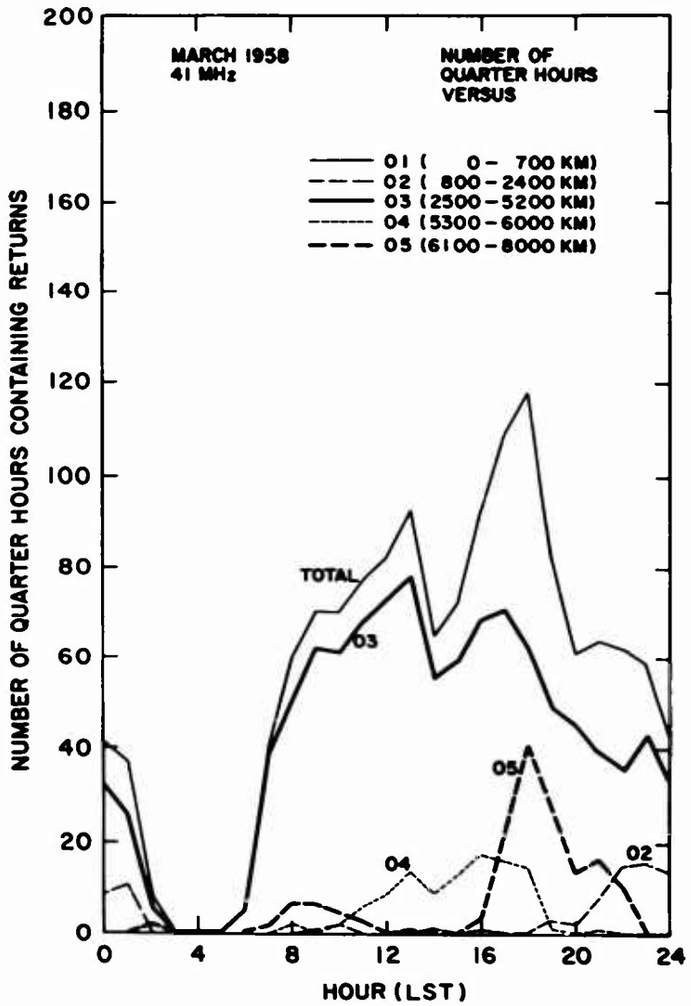
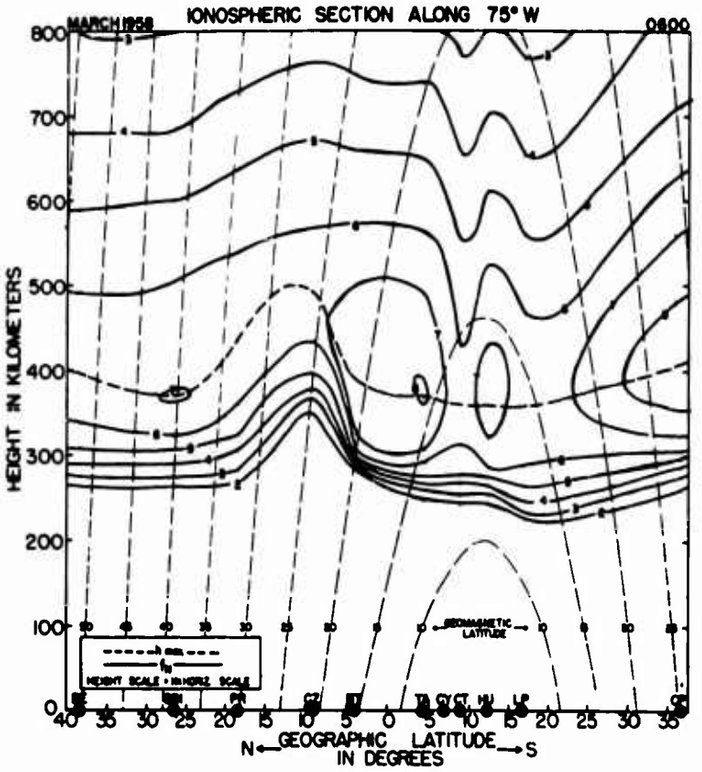


Fig. 3 Number of quarter-hours containing 41 MHz back-scatter returns versus time of day, LST (Mayaguez, March 1958)



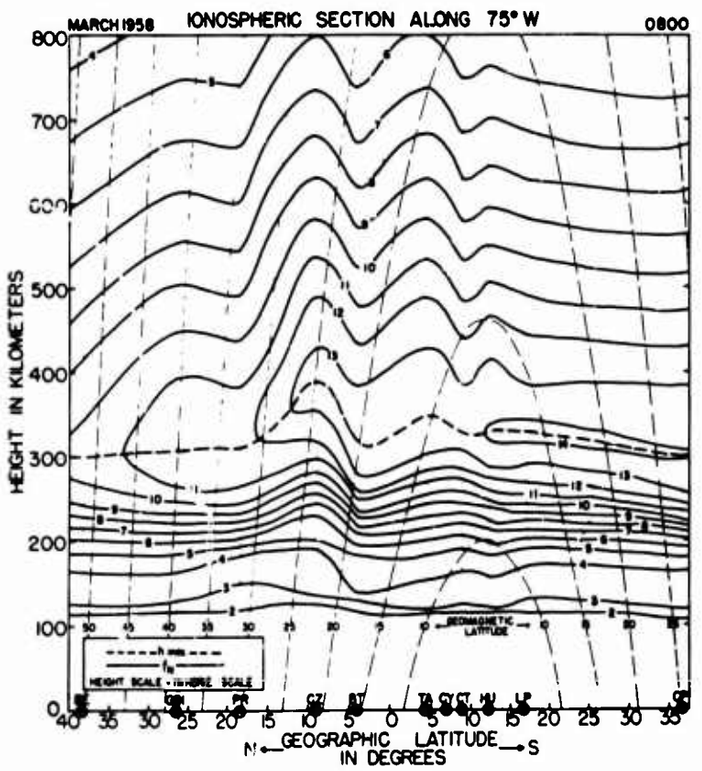
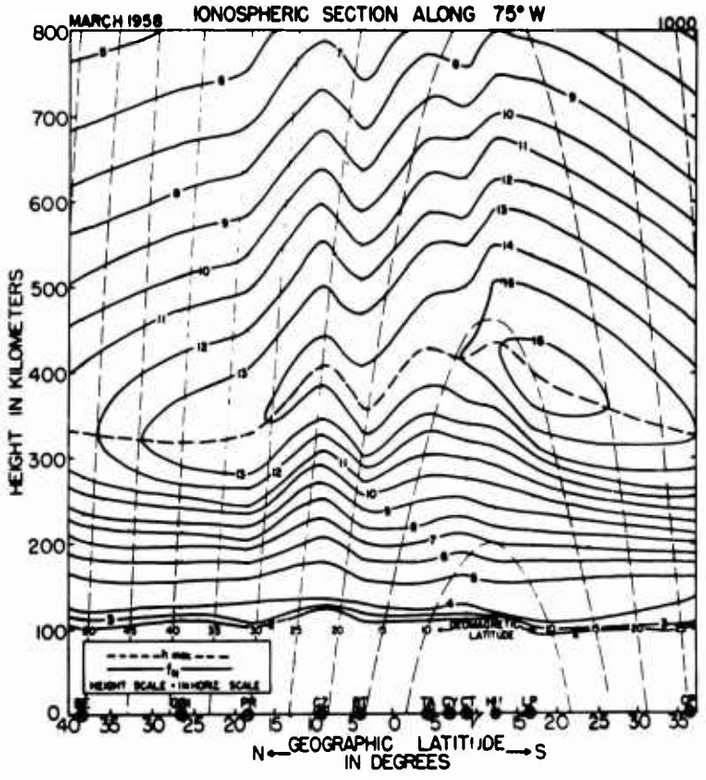


Fig. 4(a) Electron density versus true height profile along 75°W.
0600, 0800 LST



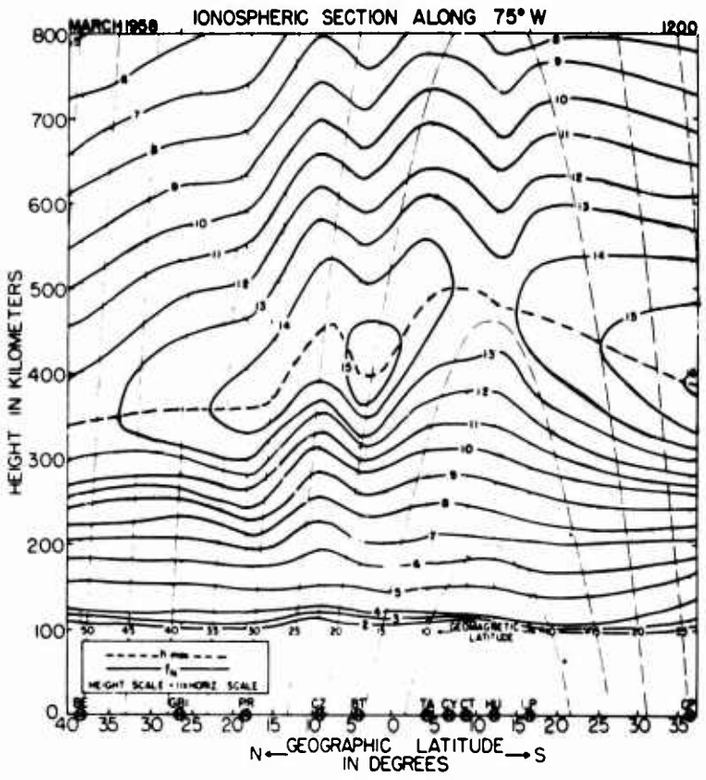
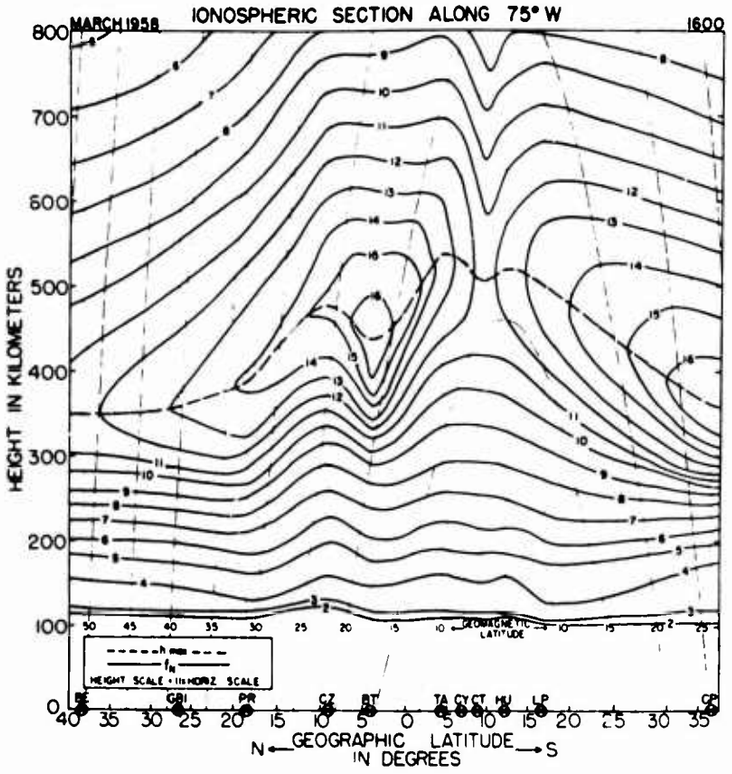


Fig. 4(b) Electron density versus true height profile along 75°W. 1000, 1200 LST



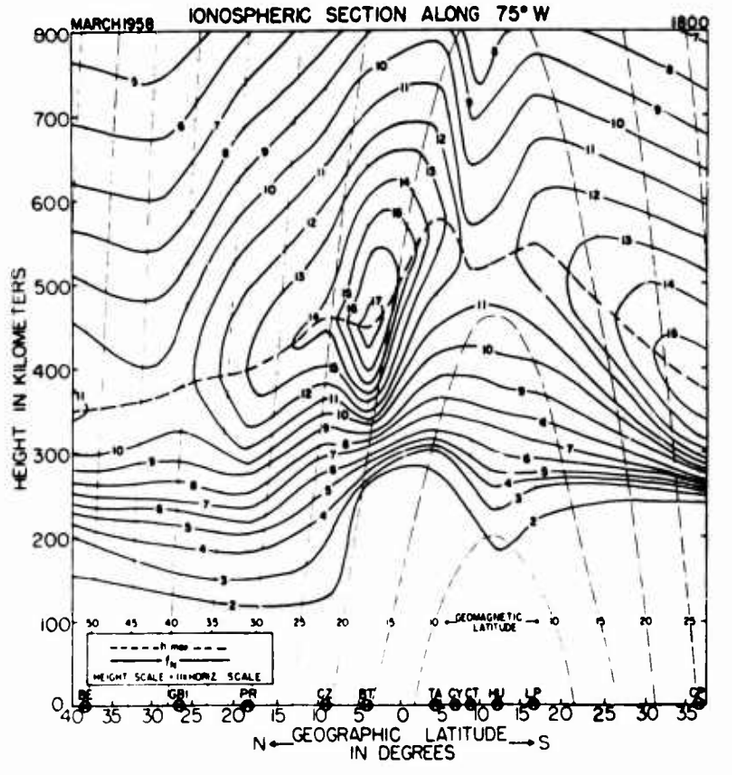
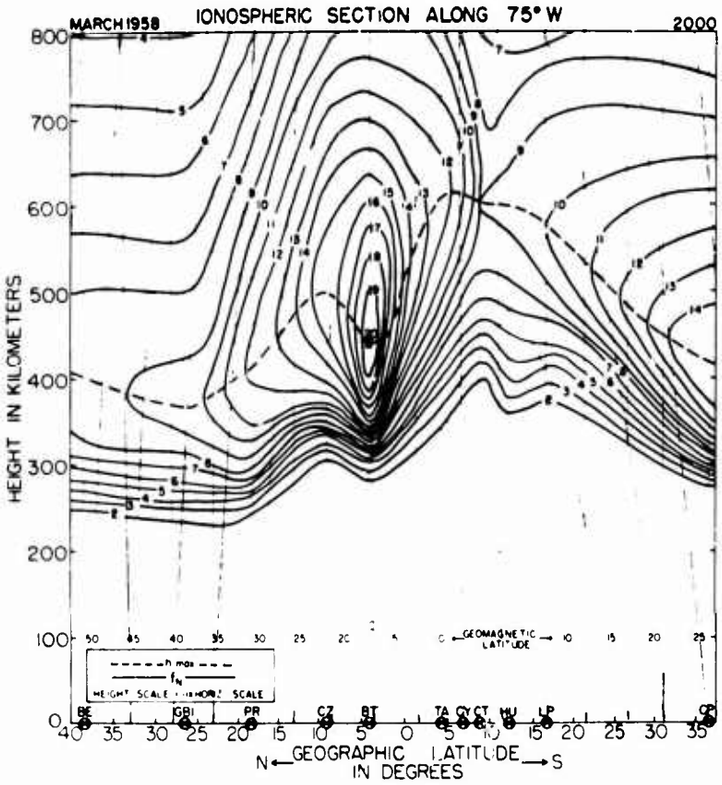


Fig. 5(a) Electron density versus true height profile along 75°W. 1600, 1800 LST



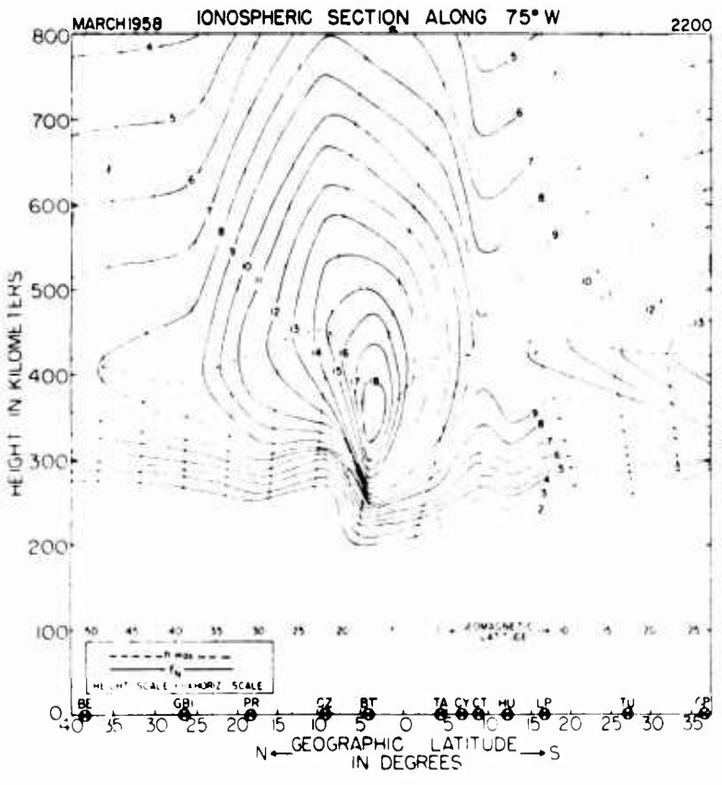


Fig. 5(b) Electron density versus true height profile along 75°W. 2000, 2200 LST

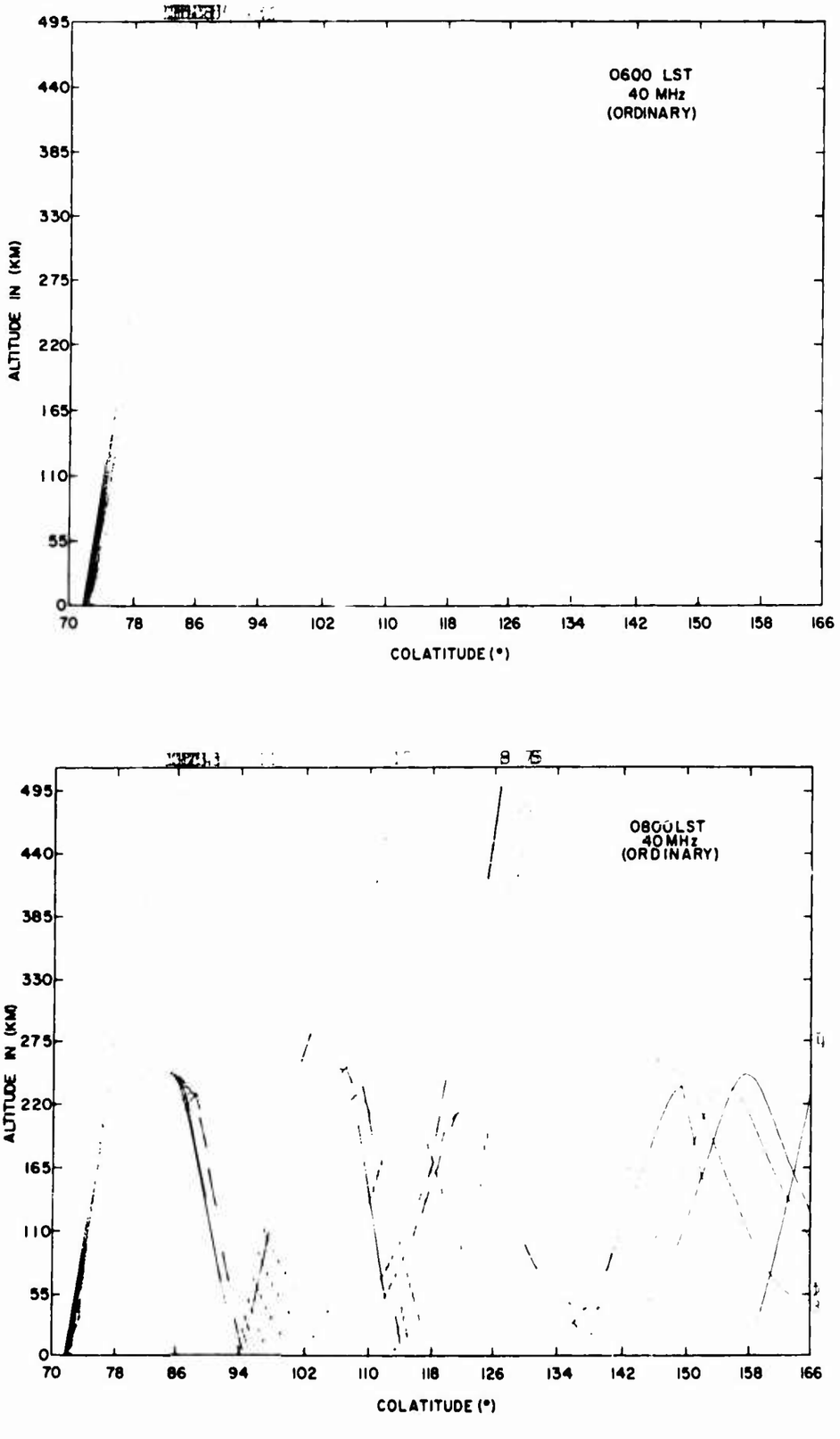


Fig. 6(a) Trace of ordinary rays launched southwards from Mayaguez at elevation angles of 0^{o}-19^{o}. 0600, 0800 LST

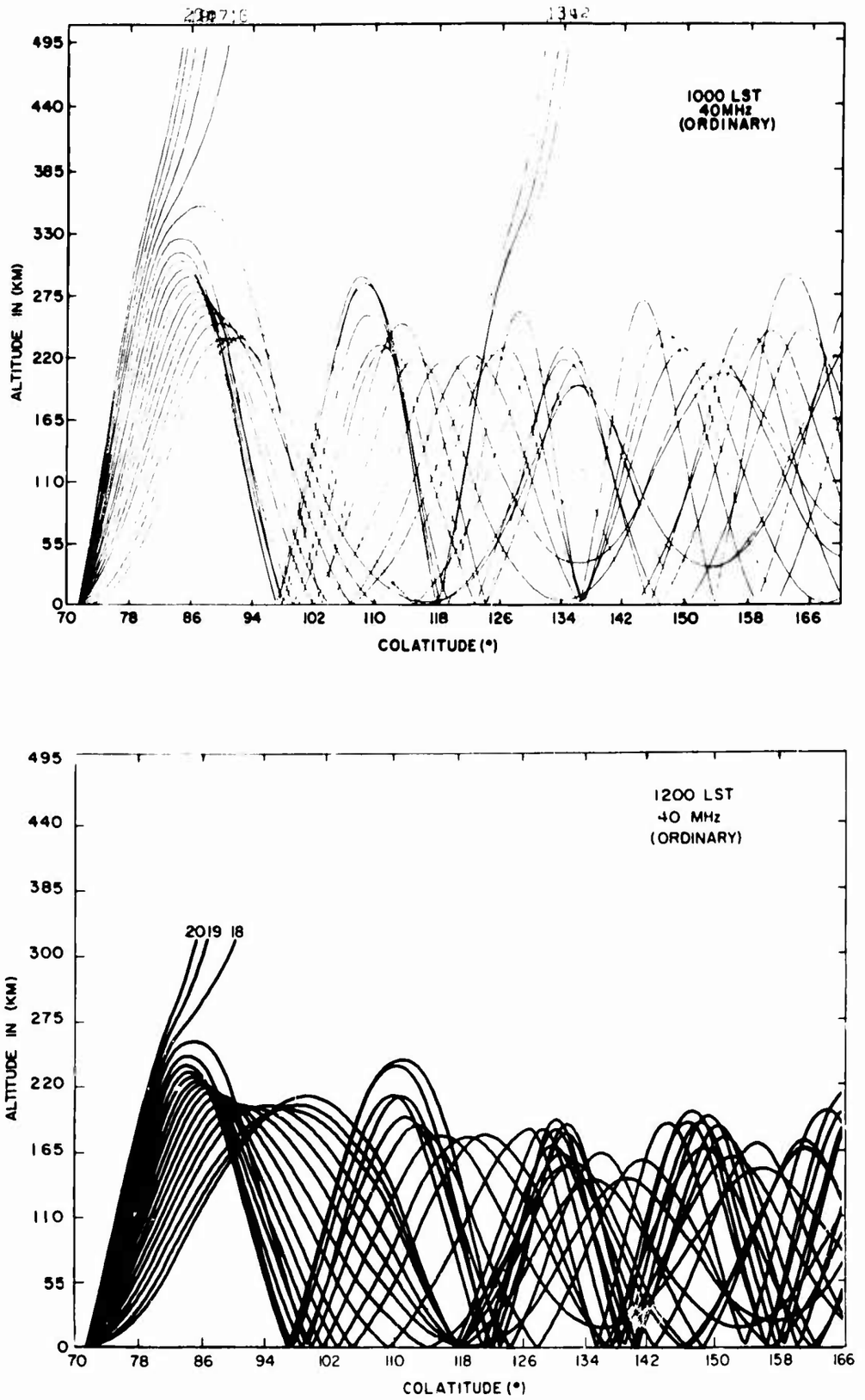
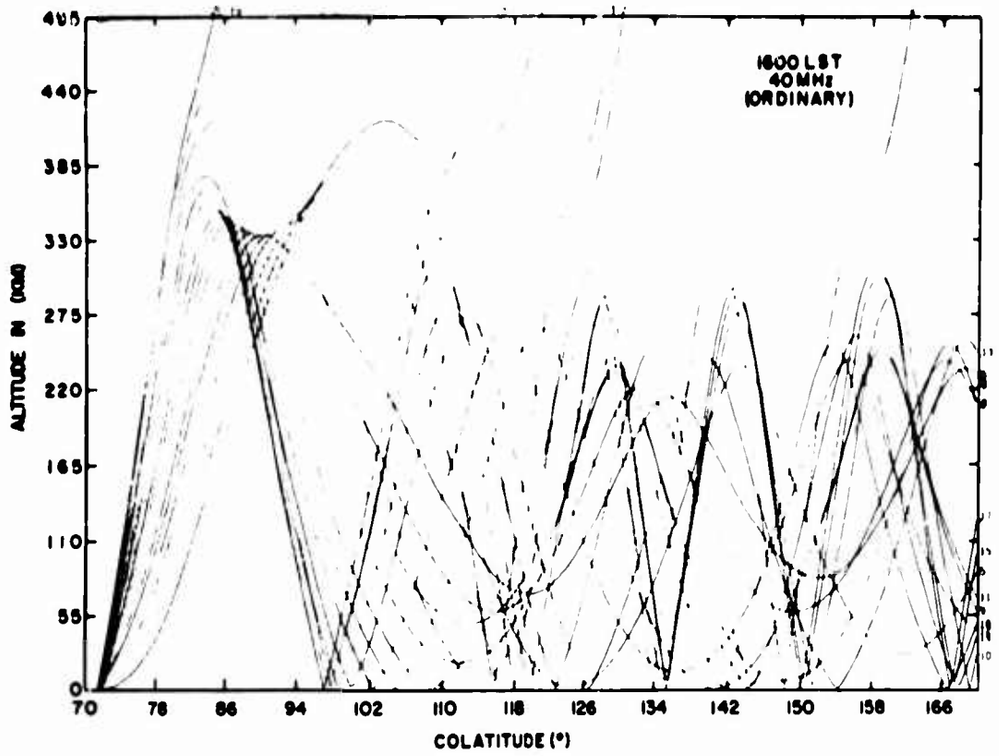


Fig. 6(b) Trace of ordinary rays launched southwards from Mayaguez at elevation angles of 0^{0}-19^{0}. 1000, 1200 LST



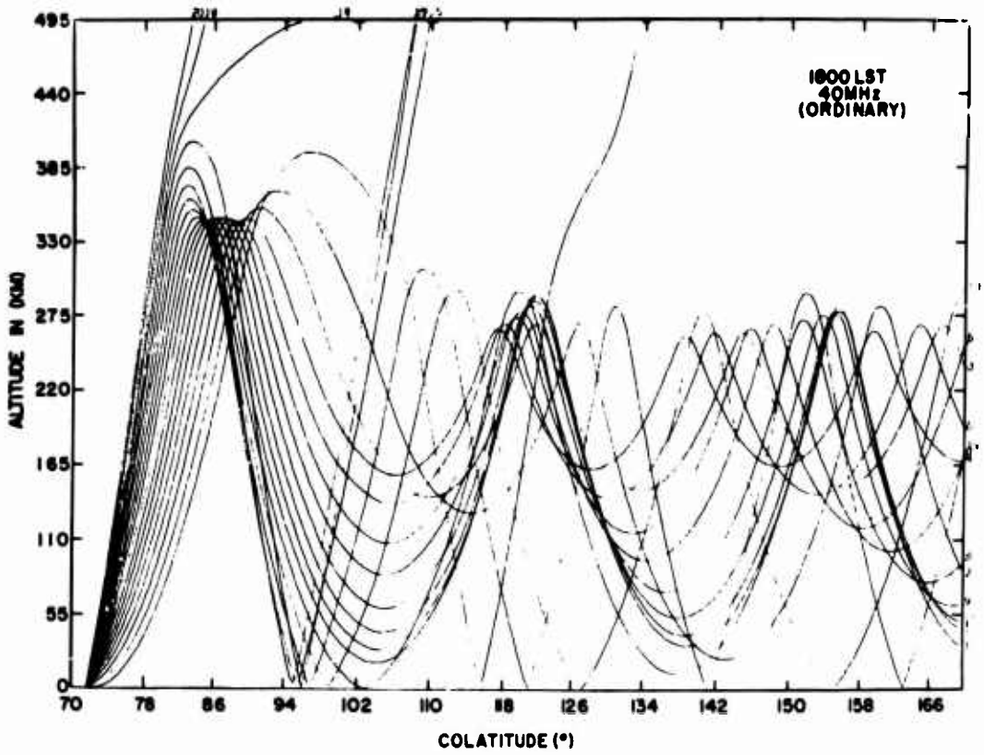


Fig.7(a) Trace of ordinary rays launched southwards from Mayaguez at elevation angles of 0^{o}-19^{o}. 1600, 1800 LST

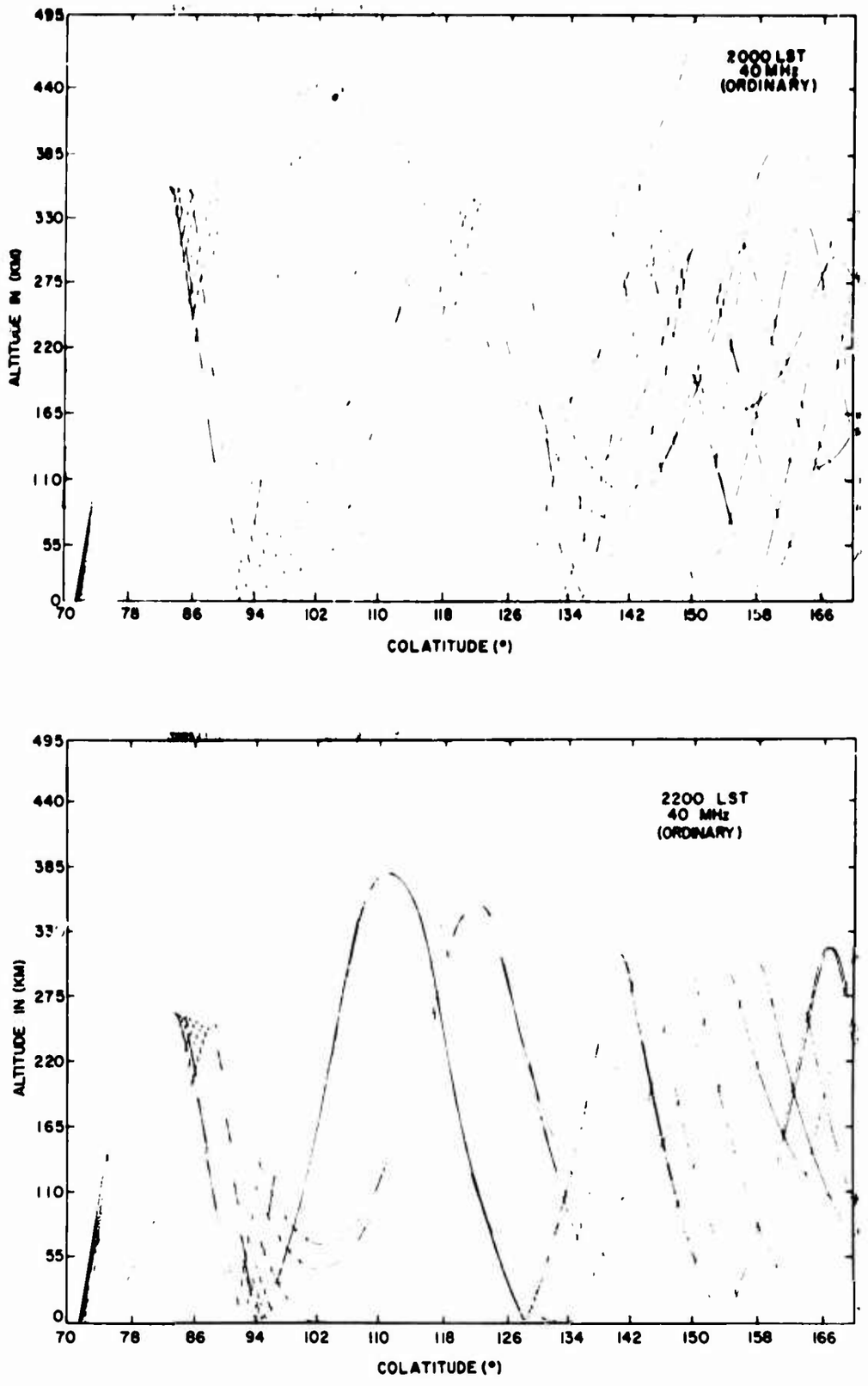


Fig. 7(b) Trace of ordinary rays launched southwards from Mayaguez at elevation angles of 0^{o} - 19^{o}. 2000, 2200 LST

TRANSEQUATORIAL PROPAGATION IMPLICATIONS OF EQUATORIAL VERTICAL DRIFT MEASUREMENTS

by

Robert Cohen* and
J.P. McClure†

*Aeronomy Laboratory, ESSA Research Laboratories
Boulder, Colorado 80302, USA.

†Jicamarca Radar Observatory, Apartado 3747, Lima, Perú

SUMMARY

In view of the successes of current theoretical developments leading toward a time-dependent theory of the transequatorial ionization distribution ("equatorial anomaly"), along with the recently developed ability to measure vertical drifts of the F-region plasma at the magnetic equator (that are an essential parameter for the theory), it appears that the application of these results should help clarify the transequatorial propagation phenomena. The status of theory and the status of experiment are discussed, along with the interrelation of theory and experiment, and a program of investigation is recommended involving radar observations from satellites and from the ground, radio propagation studies, airglow observations, ray-tracing, and theoretical analysis.

TRANSEQUATORIAL PROPAGATION IMPLICATIONS OF EQUATORIAL VERTICAL DRIFT MEASUREMENTS

Robert Cohen and J.P.McClure

1. INTRODUCTION

The so-called "equatorial anomaly" refers to a transequatorial distribution of ionization having peaks of enhanced electron concentration at latitudes north and south of the magnetic equator. The source of this distribution, as originally suggested by Martyn[1], is the upward drift and subsequent diffusion of F-region ionization near magnetic equator. This drift, according to Reference[1], is propelled by electrodynamic forces originating in the E-region and coupled via geomagnetic field lines. The phenomenon has been aptly described as the "fountain effect". The details of this process have been studied theoretically by many workers, and considerable amounts of experimental information have been obtained, as summarized in Reference[2].

From a propagation standpoint, there has been considerable unusual experience on HF and VHF paths traversing the magnetic equator. Much of this experience has been obtained by radio amateurs who found, for example, that VHF signals could be received over long distances at frequencies appreciably in excess of the predicted maximum usable frequency (MUF). They found "openings" for such propagation mainly during evening hours and in the equinoctial months. Subsequently experiments have been conducted suggesting that the peculiar transequatorial distribution of ionization supports this propagation via refraction. However, because of the "flutter fading" of the received signals, a scatter mechanism may also be involved. The experience to date in transequatorial propagation is summarized in Reference 2 and 3.

In recent months there have been some new developments, both experimentally and theoretically, that suggest that we should now be able to obtain a fuller understanding of the transequatorial propagation. It is the purpose of this paper to review these developments and discuss their implications for further, concerted and definitive experimentation and interpretation leading toward this goal. In particular, measurements of vertical drifts of the F-region plasma (along with measurements of other ionospheric parameters) at the magnetic equator in Peru, coupled with time-dependent theoretical developments now becoming available, promise to define the transequatorial distribution of ionization as a function of height, latitude and time. Concurrent propagation measurements, the results of which are compared with ray tracing through the known ionization distribution, should then prove decisive.

2. THEORETICAL STATUS

Quantitative theoretical treatments of the "equatorial anomaly" problem, following the suggestion of Martyn[1], seem to be quite satisfactory in their comparison with observations, to the point where it is probably obsolete parlance to continue referring to the transequatorial phenomenon as an anomaly. Similar theoretical treatments of the problem by Bramley and Peart[4], Moffett and Hanson[5], Hanson and Moffett[6], and Bramley and Young[7] have led to similar conclusions. All of these developments were toward a *steady-state* theory, whereas the ultimate goal is to obtain a *time-dependent* theory. Recently, a

first step toward a time-dependent theory has been published by Baxter and Kendall[8]. Progress is now being made by Hanson[9] on a more elaborate time-dependent theory.

Several of the theoretical developments[6,7] take into account meridional neutral wind components along the geomagnetic lines of force. Such winds would explain some of the observed asymmetries (about the magnetic equator) of the transequatorial ionization distribution, as discussed in the following section. Theoretical developments to date have not fully taken into account the height variation of electron temperature (T_e), of ion temperature (T_i), or of ion composition.

3. EXPERIMENTAL STATUS

Measurements increasingly pertinent to the transequatorial propagation problem are being made at the Jicamarca Radar Observatory (11.95°S, 76.87°W; Dip: 2°). Until 1968, these measurements included the determination of electron concentration (N_e) as a function of height and time[10] and the determination of T_e, T_i and ion composition as functions of height and time[11]. In addition, the incoherent scatter technique permitted the determination of neutral temperature T_n as a function of time at certain heights [12].

A significant development in 1968 at Jicamarca was that a technique was perfected [13] to directly monitor vertical drifts of the ionospheric plasma as functions of height and time. The height range for all of these measurements extends from about 150 or 200 km up to about 800 km. The ceiling for electron concentration measurements extends to about $L = 2$, and this may be extended to $L = 2.5$. It may also be possible to raise the present ceilings for the temperature observations.

An allied development was the ability to measure (somewhat less directly) electric fields in the equatorial electrojet, at a height of 105 km (Ref. 14). These measurements demonstrated the diurnal cycle of the dynamo (S_q) electric field, evidencing the field reversals near sunrise and sunset.

The observations of F-region ionization drifts were reported by McClure[15], while the related observations of E-region fields were reported by Balsley[16], who has also correlated such measurements with the apparent vertical motions of F-region ionization[17]. Based upon Balsley's interpretation of their measurements, Romero et al.[18] have obtained seasonal variations of the times of field reversal in the morning and evening. By employing simultaneous temperature, electron concentration and drift measurements, Peterson and McClure[19] have analyzed F-region electron motions through use of the continuity equation.

The F-region ionization drifts are obtained by measurement of the Doppler shift of the incoherent-scatter spectrum[13]. Each drift measurement is directly convertible into a measurement of the East-West electric field (E) propelling the vertical drift (v), since the magnitude (B) of the geomagnetic field vector (B) is known to within less than 1%. The magnitude (E) of that field component is proportional to B and to the magnitude (v) of the vertical drift, since $v = (E \times B)/B^2$; hence $v = E/B$, or $E = Bv$. For an F-region geomagnetic field strength of approximately 0.25 gauss, or 25,000 gammas, this means that a vertical drift of 20 m/s corresponds to an East-West electric field of 500 μV/m.

Some typical measurements[15] of F-region drift profiles are shown in Figure 1. It is apparent that the drifts can be measured to within an accuracy approaching 1 m/s over much of the height range, as discussed in Reference[13]. The example shown corresponds to a an integration period of 12 minutes. Such measurements can be obtained throughout the 24-hour period. However, at times when F-region ("spread F") "scattering" irregularities[20] are present, strong coherent scatter is obtained from the irregularities at heights where they are present. This signal swamps the incoherent scatter echo from the background plasma. Consequently, F-layer drifts can still be obtained at heights from which there are no such echoes, while the vertical drift of the irregularities is simultaneously observable at heights at which the irregularities occur.

In Figure 2 are presented the results of a series of drift profiles obtained over an eight-hour period. As the time of the electric field reversal approaches, we note that the monotonic height dependence of drift obtained during the afternoon evolves into a height profile with a maximum drift near 400 km. Such a surge often precedes the evening electric field reversal. Figure 3 presents the profiles of electron concentration obtained simultaneously with the drift profiles of Figure 2. Simultaneous information on electron temperature, ion temperature, neutral temperature and ion composition is typically available to complement the electron concentration and drift information.

Another characteristic of the equatorial ionosphere responsive to electric fields is the emission of F-region nightglow, according to the interpretation[21] of VanZandt and Peterson, who are obtaining nightglow measurements at Jicamarca. King[22] has used airglow measurements as an indicator for studies of the "equatorial anomaly". The F-region nightglow, except near the magnetic equator, is also an indicator of meridional neutral winds[21]. In particular, as suggested by Hanson[9], measurement of airglow from latitudes north and south of Jicamarca would give some indication of the integrated effect of steady neutral wind components along the geomagnetic lines of force. These neutral winds are an important factor in producing asymmetries in the "equatorial anomaly", as discussed by Thomas[23]. Since theoretical analyses leading to the transequatorial distribution of ionization must therefore include neutral wind information, some observation of the North-South neutral winds (such as the airglow measurement) is an important adjunct to the vertical drift observations.

4. INTERRELATION OF THEORY AND EXPERIMENT

The essential input ingredient for the current theoretical treatments of the transequatorial ionization distribution problem is the height profile of vertical drifts. A measure of the success of these treatments is that the experimentally measured upward drifts (ranging from 10 to 30 m/s) are about the magnitudes that were previously assumed by theorists, who then obtained realistic ionization distributions.

So far, however, theory and experiment do not take into account or measure, respectively, any East-West component of drift velocity that would be produced by vertical electric fields. Similary, theoretical developments do not take into account currents along the geomagnetic lines of force that would result from electric fields along these lines of force; nor is there yet any experimental measurement of such currents. In principle, both flows could be measured using the incoherent scatter technique, by employing vertical transmission from Jicamarca and appropriate installations to the north and east for oblique reception. However, the longitudinal electric fields are probably negligible, so that only the vertical fields would be worth investigating.

The theories require input information concerning the neutral wind components parallel to the geomagnetic lines of force in order to account for asymmetries in the transequatorial ionization distribution. Some of this information, as discussed in the previous section, is probably obtainable from airglow studies. It is also possible to observe effects of these winds on profiles of electron concentration[24]. Such observations are often characterized as resulting from "travelling ionospheric disturbances", but provide only the time-varying components of the neutral winds[9]. On the other hand, experimental input information for use by the theory is available regarding the height profiles and time variation of T_e, T_i, T_n and of ion composition, whereas theoretical developments have not yet been constructed that would employ this information.

From the standpoint of transequatorial propagation, the effects of the upward drifts seem to be manifest[25] on a time scale that might be expected, since the peak occurrence of this propagation phenomenon at VHF is at about the time when the upward drifts terminate. To a first approximation, the integrated effect of the upward drifts is the significant factor, and this would maximize at the time of electric field reversal.

5. PROPOSED PROGRAM OF INVESTIGATION

In view of the considerations discussed, it seems that the time is ripe to design experiments and analytical procedures that would provide definitive answers to the interrelations between theories of the transequatorial ionization distribution and experimental measurements of that distribution. By obtaining concurrent propagation experience, this could then be compared with the predictions of ray theory for the measured and/or predicted ionization distributions, leading to an understanding of the related transequatorial propagation problem. Some suggestions for such a program of investigation follow.

Propagation experiments would be designed to study both the amplitude and frequency characteristics of the received signals, employing several transmitted frequencies. Measurements would be made of the angle of arrival of the received signals. Pulse studies would be conducted over these paths; such studies during the IGY Ref.26 established, for example, that purely scatter propagation was involved over a fairly short (2580 km) transequatorial VHF circuit.

Observations at Jicamarca would provide input data for theories concerning drifts and other parameters, along with appropriate[27, 28] coherent scatter studies of F-region "scattering" irregularities. Such studies of irregularities would be useful in clarifying the role of scattering in the transequatorial propagation. Studies of patches of irregularities[29, 30] and their East-West motions could be conducted using the conventional ionosondes at Jicamarca and Huancayo. Supplementary reception from the east of Jicamarca signals would provide information on East-West plasma drifts, insofar as they are significant. Airglow studies with photometers at various locations would furnish data on neutral winds and regarding the latitudinal variation of vertical plasma motions.

Satellite "topside" ionosondes and the existing network of ground-based ionosondes would provide information concerning the transequatorial ionization distribution with which to check predictions of the theory, and through which to perform ray tracing. Such ray tracing is useful[31] for comparison with concurrent transequatorial propagation studies, insofar as the propagation can be accounted for, wholly or partly, by refraction mechanisms.

Ionosonde measurements are also useful[20, 32, 33] for studying duct irregularities, along with ground-based measurements of scintillations. Such scintillations are frequently observed near Jicamarca, especially when satellite telemetry signals are being monitored[34]. Transequatorial propagation may also involve guidance along such irregularities[3].

ACKNOWLEDGEMENTS

This research was partially supported by the National Aeronautics and Space Administration under Fund Transfer R-06-012-008.

REFERENCES

1. Martyn, D.F. — *Atmospheric Tides in the Ionosphere. I. Solar Tides in the F_2-Region.* Proc.Roy.Soc. A, Vol.189, 1947, pp.241-260.

2. Cohen, Robert — *The Equatorial Ionosphere.* pp.561-613 in "Physics of Geomagnetic Phenomena, edited by S. Matsushita and W.H. Campbell. Academic Press, 1967.

3. Nielson, Donald L. — *A Review of VHF Transequatorial Propagation.* Paper 45 in this volume.

4. Bramley, E.N. Peart, M. — *Diffusion and Electromagnetic Drift in the Equatorial F_2-Region.* Journal of Atmospheric and Terrestrial Physics, Vol.27, 1965, pp.1201-1211.

5. Moffett, R.J. Hanson, W.B. — *Effect of Ionization Transport on the Equatorial F-Region.* Nature, Vol.206, 1965, pp.705-706.

6. Hanson, W.B. Moffett, R.J. — *Ionization Transport Effects in the Equatorial F-Region.* Journal of Geophysical Research, Vol.71, 1966, pp.5559-5572.

7. Bramley, E.N. Young, Margaret. — *Winds and Electromagnetic Drifts in the Equatorial F_2-Region.* Journal of Atmospheric and Terrestrial Physics, Vol.30, 1968, pp.99-111.

8. Baxter, R.G. Kendall, P.C. — *A Theoretical Technique for Evuluating the Time-Dependent Effects of General Electrodynamic Drifts in the F_2-Layer of the Ionosphere.* Proc.Roy.Soc., A, Vol.304, 1968, pp.171-185.

9. Hanson, W.B. — Private Communication, 1968.

10. Farley, Donald,T. Jr., — *Observations of the Equatorial Ionosphere Using Incoherent Backscatter.* pp.446-449 in "Electron Density Profiles in Ionosphere and Exosphere", edited by Jon Frihagen. North-Holland, Publishing Company, 1966.

11. Farley, D.T. et al. — *Temperature and Composition of the Equatorial Ionosphere.* Journal of Geophysical Research, Vol.72, 1967, pp.5837 - 5851.

12. McClure, J.P. — *The Diurnal Variation of Neutral and Charged Particle Temperatures in the Equatorial F-Region.* To be published in the Journal of Geophysical Research.

13. Woodman, R.F. Hagfors, T. — *Methods for the Measurement of Vertical Ionospheric Motions near the Magnetic Equator by Incoherent Scattering.* To be published in the Journal of Geophysical Research.

14. Balsley, Ben B. — *Evidence for Plasma Turbulence in the Equatorial Electrojet. I, Observations.* Submitted to the Journal of Geophysical Research.

15. McClure, J.P. — *Observations of Vertical Drifts in the Ionosphere Near the Magnetic Equator.* Paper presented at Spring URSI Meeting, Washington, DC, 1968.

16. Balsley, B.B. — *A Comparison between Vertical Motions of the Equatorial F-Layer and E-Region Electric Fields during Nighttime Periods.* Paper presented at Spring URSI Meeting, Washington, DC, 1968.

17. Balsley, Ben B. — *On Nighttime Electric Fields and Vertical Ionospheric Drifts Near the Magnetic Equator.* Submitted to the Journal of Geophysical Research.

18. Romero, Carlos A. et al. — *VHF Ionospheric Scatter Propagation via the Equatorial Electrojet.* Paper 41 in this volume.

19. Peterson, V.L. McClure, J.P. — *Electron Drift in the Ionosphere Near the Dip Equator.* Paper presented at Fall URSI Meeting, Boston, Massachusetts, 1968.

20. Cohen, Robert. — *F-Region Scatter.* Paper 51 in this volume.

21. VanZandt, T.E. Peterson, V.L. — *Detailed Maps of Tropical 6300 Å Nightglow Enchancements and their Implications on the Ionospheric F_2-Layer.* Annales de Géophysique. 24 No.3 (1968).

22. King, J.W. — *Airglow Observations and the Decay of the Ionospheric Equatorial Anomaly.* Journal of Atmospheric and Terrestrial Physics, Vol.30, 1968, pp.391-402.

23. Thomas, L. — *The F_2-Region Equatorial Anomaly during Solstice Periods at Sunspot Maximum.* Journal of Atmospheric and Terrestrial Physics, Vol.30, 1968, pp.1631-1640.

24. Sterling, D.L. — *Traveling Disturbances Observed at Jicamarca.* Paper presented at Thomson Scatter Conference, University of Illinois Aeronomy Report 19, 1967.

25. Washburn, C.L. et al. — *Transequatorial F-Layer Propagation Study, Final Report.* ITT Federal Laboratores, Nutley, New Jersey, 224 pp; 1963.

26. Cohen, Robert. Bowles, Kenneth, L. — *On the Nature of Equatorial Spread-F.* Journal of Geophysical Research, Vol.66, 1961, pp.1081-1106.

27. Clemesha, B.R. — *An Investigation of the Irregularities in the F-Region Associated with Equatorial Type Spread-F.* Journal of Atmospheric and Terrestrial Physics, Vol.26, 1964, pp.91-112.

28. Cohen, Robert. — *Spectra of 50 Mlz Radar Echoes from Equatorial F-Region Irregularities as a Function of Direction of Observation. in the Equatorial Plane.* Paper presented at Spring URSI Meeting, Washington, DC, 1966.

29. Calvert, Wynne, Cohen, Robert. — *The Interpretation and Synthesis of Certain Spread-F Configurations Appearing on Equatorial Ionograms.* Journal of Geophysical Research, Vol.66, 1961, pp.3125-3140.

30. Cohen, Robert. — *Triangulation Measurements of Drifting Patches of Equatorial F-Region Irregularities.* pp.298-299 in "Report on Equatorial Aeronomy", edited by F. de Mendonça, São José dos Campos, Brazil, 1965.

31. Gerson, N.C. — *Comparison of Ray Tracings with Experiments over Transequatorial Paths.* Paper 48 in this volume.

32. Pitteway, M.L.V. Cohen, Robert. — *A Waveguide Interpretation of "Temperate-Latitude Spread-F" on Equatorial Ionograms.* Journal of Geophysical Research, Vol.66, 1961, pp.3141-3156.

33. Loftus, Brigid T. et al. — *Observations of Conjugate Ducting by the Fixed-Frequency Topside-Sounder Satellite.* Annales de Géophysique, Vol.22, 1966, pp.530-537.

34. Woodman, Ronald F. — *Irregular Refraction of Satellite Signals Observed at Ancón, Perú.* Unpublished manuscript privately communicated, 1961.

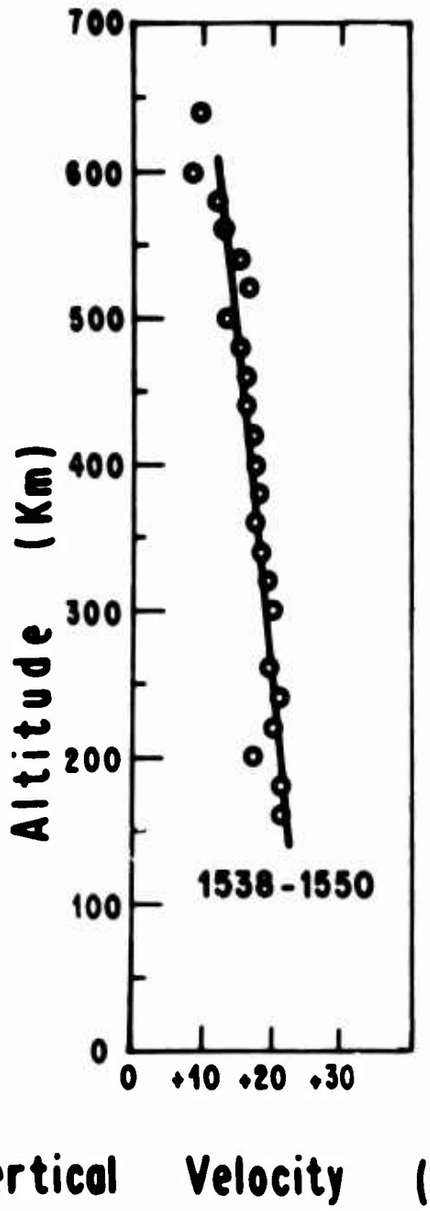


Fig. 1 Vertical profile of plasma drift velocities, obtained by integration from 1538 to 1550 hours local time (Jicamarca Radar Observatory, Perú, 75°W, 24 January 1968). A positive velocity corresponds to upward drift of the electrons.

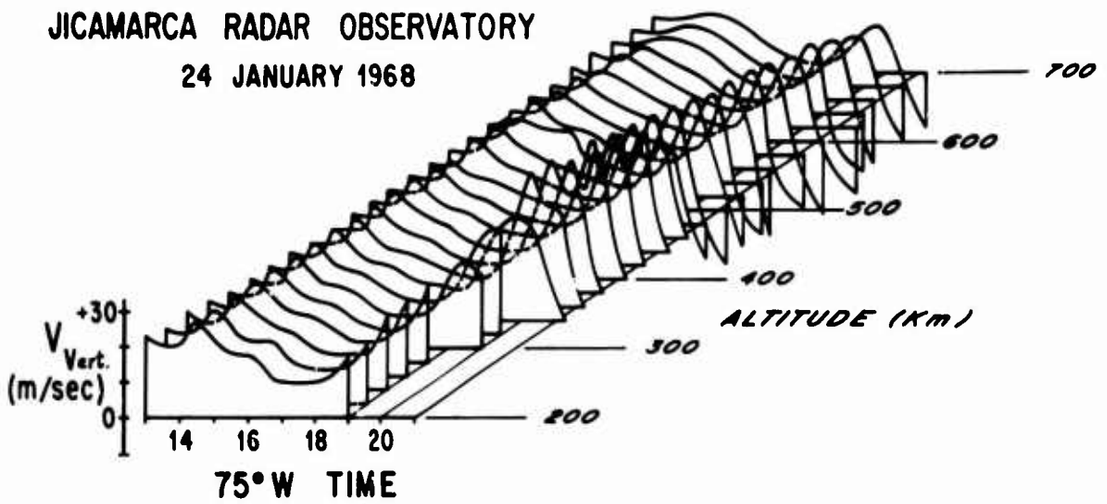


Fig. 2 A series of profiles of plasma drift velocities, plotted as the time variations of drift velocity for heights separated by 20-km intervals.

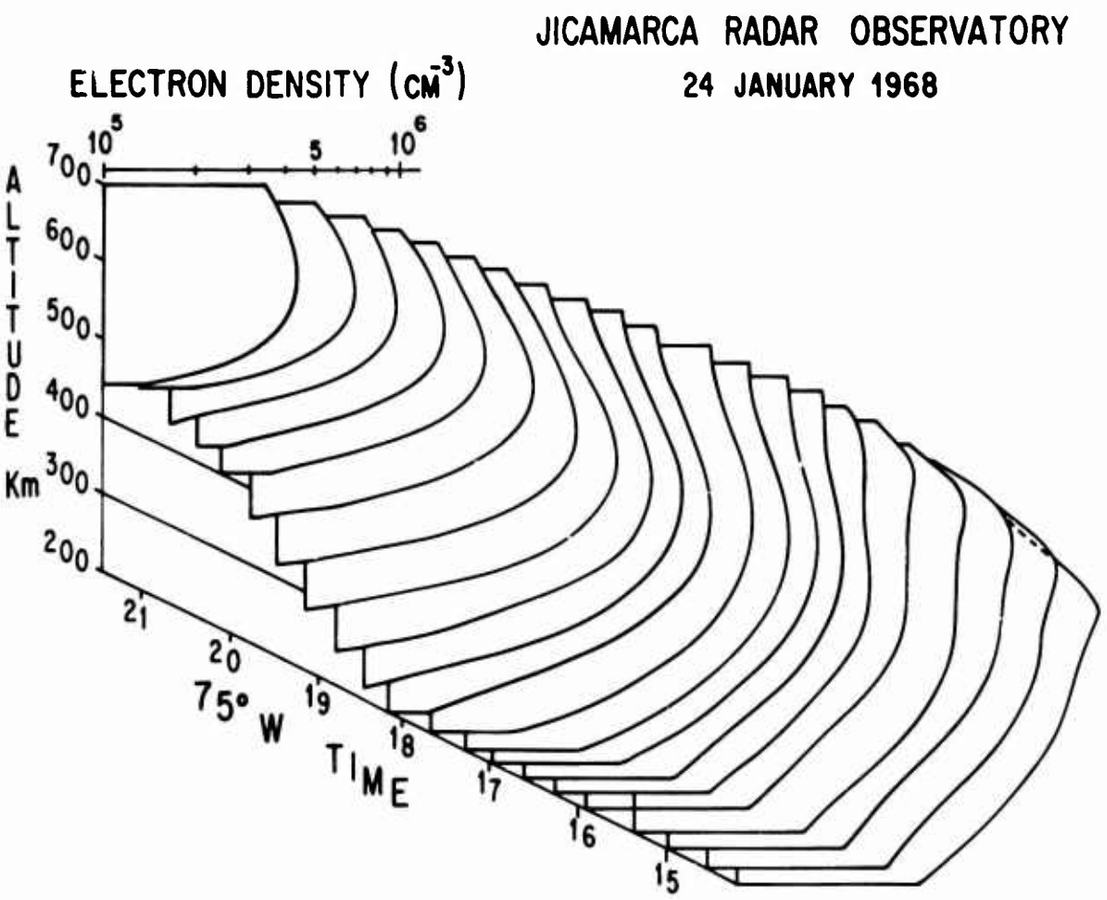


Fig. 3 A series of vertical profiles of electron concentration, as determined by the Faraday rotation of the incoherent scatter signals.

DISCUSSION ON THE PAPERS PRESENTED IN SESSION VI (TRANSEQUATORIAL PROPAGATION).

Discussion on Paper 45, "A review of VHF transequatorial propagation", by D.L.Nielson.

Dr C.R.Roberts: Would you, Dr Nielson, identify the values of propagation losses you have shown? Have you included the effect of antenna patterns and other parameters, so that the values are actual propagation losses? If so, there may indeed be an indication of actual focusing. I also have a question concerning the discussion of whether or not the propagating mode was FF or 1F2. To bolster the propagation time measurements, were there indications from elevation angle measurements (or angle sensitivity) that the mode was a 1FF or 1F2 mode?

Dr D.L.Nielson: The median minimum path losses for the mid-Pacific experiment are tabulated in the article on F-region drifts (Paper 46). They are propagation losses and therefore point to focusing of some type. With regard to your second question, since elevation angles are very difficult to measure at these frequencies, information is lacking. Bowen et al., Journal of Geophysical Research, Vol.73, 1968, p.2469, indicate a difference in elevation angle between a normal refracted ray and a spread ray. I do not choose to draw any such distinction, and certainly the elevation is mainly a function of station latitude. Absolute delay measurements indicate that these echoes are F-region echoes. Finally, I would expect inordinately long delays to be the result of lateral displacements.

Dr J.Ramasastry: Can you tell me what the changes in the signal characteristics are when the directivity at the transmitting site is varied?

Dr D.L.Nielson: Some evidence from Bowen et al. (see my paper) shows that path angles of the order of 40° with respect to the magnetic equator do not normally favour frequencies much above 50 MHz. Our results do not indicate noticeable changes in above-50 MHz signals over angles like $10\text{-}15^{\circ}$ with the magnetic meridian.

Dr K.Davies: What is the direct evidence for FF-type paths?

Dr D.Nielson: I believe the only "direct" evidence can come through simultaneous measurement of the transequatorial electron density profile and the employment of adequate ray-tracing techniques. I know of no such results that rule out such propagation and several results do show this ray path to be not only possible, but likely, in the presence of suitable manifestations of the equatorial anomaly. Measurements of pulse travel time also encourages this conclusion.

Dr N.C.Gerson: Some transequatorial results imply that, if the launch angle of the radio ray is decreased, the path length increases. For example, a launch angle of 8° at 41 MHz provided mean transequatorial ranges of 7000 km, but at 5° elevation at 50 MHz, transequatorial distances of 7500 km were obtained. How would your model clarify these results?

Dr D.L.Nielson: It would be inappropriate for me to comment on such specific quantities in an experiment about which I know nothing.

Discussion on Paper 48, "Comparison of ray tracing with experiments over transequatorial paths", by N.C.Gerson.

Dr J.Ramasastry: Don't you think, Dr Gerson, that the final results of the ray-tracing program are critically dependent upon whether or not you have included the types of mechanisms that are responsible for phenomena like the transequatorial propagation?

Dr N.C.Gerson: The model chosen for the ray-tracing computations is very critical. For example, the ray-tracing procedure utilized in my paper confined itself solely to ionospheric rays for the F2 layer plasma frequencies observed during a ten-day period. The ray-tracing procedure did not consider ray tracing along the exospheric ducts and therefore provides no information on the possibilities of this mechanism. Any ray-tracing technique can suffer from mathematical imprecision inherent in the computer program, from lack of spatial and time resolution in the basic refractivity data, etc. The great value of ray-tracing computations is to provide an indication of extreme conditions, which can provide limits on possible interpretations of specific propagation phenomena.

Dr C.R.Roberts: In your ray-tracing study, did you notice any focusing of the trapped rays providing the transequatorial propagation? In the data presented previously there appeared to be a good indication of focusing.

Dr N.C.Gerson: The 40 MHz ray tracings showed no indication of focusing to transequatorial distances (6100-11000 km). However, there were definite indications of focusing at 1-hop F2 or 2-hop F2 conditions.

Dr M.Crochet: En ce qui concerne les focalisations je desirerai faire remarquer que nous avons observé de nombreuses propagations longue distance a 9000-12,000-15,000 km et que généralement les échos recupérés par gradients geographiques sont focalises, alors que les échos recuperés par les gradients equatoriaux sont généralement diffus.

Dr K.Davies: In transequatorial ray tracing it is important to correct for the effect on the vertical incidence ionogram of the equatorial distortion of the ionosphere. (See Davies and Jones, Proceedings of the XIIth AGARD/EPC Symposium, Leicester 1966, in the press).

Professor E.D.R.Shearman: I would like to comment on Dr Davies's doubts that a chordal hop or "supermode" type of trajectory occurs. I would like to confirm Dr Gerson's remarks about the frequent observation, not only at equatorial latitudes, of 2-hop ground scatter persisting after 1-hop ground scatter has faded out. This seems to me to be the most striking evidence we now have that such long-hop modes exist. The observations are too frequent to be explained by M modes involving Es.

Dr I.Paghis: The interpretation of transequatorial propagation data requires not only adequate ray-tracing techniques, but also rather detailed information on vertical profiles of electron density and the associated horizontal gradients. Bottomside sounders are usually too far apart to provide sufficient detail on horizontal gradients. One should therefore make an effort to obtain additional data from other sources, and, in particular, I wish to draw your attention to the topside sounder data. Considerable topside data on equatorial anomalies and irregularities are now available and, of course, the observed electron density distributions do not terminate abruptly at the F2-maximum simply because the sounder data terminate there. One important feature of the topside sounder data is the availability of consecutive ionograms at relatively close horizontal spacings. This feature may be of considerable value to transequatorial propagation studies.

Dr D.L.Nielson: Alouette I and II data were obtained for the mid-Pacific experiment I mentioned. On one occasion 61 MHz was propagated point-to-point and Alouette records from overhead showed no irregularities. The problems encountered in the further analysis of these Alouette data were the failure of the virtual depth trace to show a clear critical frequency and the 11.5 MHz upper frequency limit of the satellite. The remarks in the review paper included some information from Alouette records.

Dr I.Paghis: I agree that the topside sounder data, like other experimental data, have severe limitations. In view of the fact that transequatorial propagation has now been studied for many years without producing reasonably certain interpretations, the time may be ripe for planning definite experiments. It is probably impractical to send up a satellite specifically for this purpose, but it is possible to forecast the probable future avail-

ability of specific topside sounder observations and to plan other ground based experiments of a complementary nature. I believe that such a program could yield very valuable results.

Discussion on Paper 49, "Transequatorial propagation implications of equatorial vertical drift measurements", by R.Cohen.

Dr E.N.Bramley: The detailed correlation shown between the vertical F-layer drift and the horizontal electrojet speeds, both at the magnetic equator, is very striking and perhaps more marked than would be expected, since the equatorial F-region is connected, by geomagnetic field lines, to parts of the E-region which are some distance north and south of the equator itself.

Dr R.Cohen: This correlation with time, which you noticed in an illustration not presented in the talk, is quite detailed in that instance, but such a good correlation is not always obtained. As you imply, a lack of correlation could be explained by invoking the fact that the electric fields at different field lines are not identical. On occasions such as the one to which you refer, the high correlation would indicate that there is a fairly uniform East-West electric field out to 1000 km north and south of the magnetic equator.

Dr D.L.Nielson: Some of the attempts to explain equatorial spread-F have called attention to the large and rapid virtual motion of the F-layer near sunset. Does this drift measurement, which is more direct than a virtual one, reveal a pronounced increase in drift at F-region sunset?

Dr R.Cohen: There is often a surge in the upward vertical drift velocity just before it moves rapidly toward zero, followed by the downward vertical drifts of the night-time period. This reversal occurs at about the time of F-region sunset.

F-REGION SCATTER

by

Robert Cohen

Aeronomy Laboratory, ESSA Research Laboratories
Boulder, Colorado 80302, USA

SUMMARY

Experience in F-region propagation attributable to scattering is reviewed. (Some facets of F-region scatter phenomena are discussed in greater detail in the review papers in this volume on incoherent scatter (Paper 31) and on transequatorial propagation (Paper 45).) The results of forward scatter (scintillation) and backscatter (radar) diagnostic studies of F-region irregularities are summarized. These results are related to their consequences and utility for F-region scatter propagation. The ionospheric observations of the waveguide and 'whispering-gallery' modes of propagation are summarized.

F-REGION SCATTER

Robert Cohen

1. INTRODUCTION

From a propagation standpoint, ionospheric scattering phenomena are of interest when they result in the transmission of radio signals from one point to another. In general, scattering is one method of solving the radio communication problem and refraction is the other. (Line-of-sight communication is a limiting case of the refraction mechanism.) However, scattering effects can be detrimental to radio propagation via refraction, so that we must give passing consideration to the occasional coexistence of the two propagation processes.

Ionospheric scatter-propagation can be studied both by so-called 'forward-scatter' circuits and by the use of radar techniques, or 'backscatter'. The radar techniques provide a valuable diagnostic tool in that they are conducted at a single location, or 'monostatically', as against the 'bistatic' forward-scatter measurements. The separation of transmitter and receiver in the bistatic case is logistically less convenient.

The conventional ground-based ionosonde, or swept-frequency 'vertical incidence' radar, is a source of considerable monostatic information concerning ionospheric scattering phenomena, even though it was not really designed for this application. Also, bistatic information on scattering is now obtainable from the more recently introduced oblique incidence swept-frequency ionospheric sounders. Ionosondes mounted in satellites are another recently available source of scattering data, and these remote sensors have the advantage of moving through the irregularities that are responsible for the scattering phenomena. The geographic distribution of irregularities has been studied both from the ground-based network of ionosondes and from the satellite ionosondes.

The ionospheric irregularities in the F-region and above tend to be oriented in a direction parallel to the geomagnetic lines of force, and are said to be 'field-aligned'. This feature leads to certain scattering characteristics often referred to as 'aspect sensitivity'. The field-alignment is best described in terms of an autocorrelation function of electron concentration and means that the longest dimension (defined in autocorrelation terms) of the irregularities is oriented along the geomagnetic field.

Besides the utilization of ground and satellite-based ionosondes to study the irregularities, specially designed radar and forward-scatter experiments have been employed to obtain range, height, and Doppler information. Such information is useful in understanding the possibilities and limitations of F-region scatter.

Perhaps the ultimate in reliability for employing F-region scatter propagation would be the utilization of so-called 'incoherent scatter' from F-region *electrons*, as opposed to 'coherent scatter' from F-region *irregularities*. Such scattering would be obtained as long as there were sufficient electrons in the F-region, which would usually be the case even through the night, which the F-layer commonly survives. The possibilities and experience in incoherent-scatter propagation are summarized in the paper by Peterson[1] in this volume.

The exploitation of F-region irregularities for ionospheric scatter propagation would usually be accomplished by utilizing their scattering properties in the dimensions (in an

autocorrelation sense) transverse to the geomagnetic field direction. However, for irregularities (i.e., ionization depletion regions) sufficiently thick (compared to the exploring wavelength) in the transverse dimension, it is possible to 'duct' electromagnetic radiation within the irregularities. This ducted propagation within 'waveguide' irregularities is included in the discussion of this paper, since it can be considered as a scatter-propagation phenomenon in the F-region.

It is likely that these same ducting irregularities are also the source of the scintillations produced during the course of the passage of HF and VHF radio signals through the ionosphere. In this case, the effects are purely detrimental from a propagation standpoint, and result from true 'forward scatter' imposed by irregularities that have dimensions large compared to the exploring wavelength.

Another example of the apparent coexistence of scattering and refractive phenomena is in the area of transequatorial propagation, especially at VHF. The mode of propagation in some cases is still a subject of some doubt, in that radio signals of considerable strength can be propagated, but with an associated distortion known as 'flutter fading'. It is apparent that scattering processes must be involved in producing this fading, but it is difficult to see how anything but refractive processes could result in the transmission of such strong signals. This seeming dilemma is treated in the review paper by Nielson[2] in this volume (Paper 45), while attention in what follows is limited to transequatorial and other F-region propagation phenomena that result solely from scattering processes.

The presentation below subdivides the F-region coherent scattering phenomena into two categories, those associated with 'thick' and with 'thin' irregularities. In each category, information regarding the physical characteristics and geographical distribution of the pertinent irregularities will be summarized, followed by a discussion of the resulting implications for propagation and a review of the propagation experience.

Before discussing these categories of scattering phenomena, we must first specify in what sense the terms 'thick' and 'thin' are defined. It is here that the concept of an 'autocorrelation function' of electron concentration is useful, by which is meant a certain spatial correlation function of electron concentrations at points in the medium that are separated by a specified distance, r. The normalized time average of this correlation is known as the autocorrelation function, $\rho(r)$, and a sometimes physically applicable function of this kind is the isotropic exponential autocorrelation function, $\rho(r) = \exp(-r/l)$. In this spherically symmetric case, l is referred to as the scale size of the irregularity, which corresponds to the distance in which the correlation diminishes by a factor e. A similar autocorrelation function could be defined for a cylindrical irregularity, in which separate exponential factors would contain transverse and longitudinal scale sizes, T and L, respectively. For lack of a better description of F-region irregularities, we shall use this concept of cylindrical distributions of ionization, with the cylinders oriented so that T is transverse to the geomagnetic field and L is aligned with the field.

Accordingly, in categorizing the scattering phenomena, 'thick' is intended to refer to transverse scale sizes T that are large compared to an exploring wavelength, while 'thin' refers to transverse scale sizes of order half the exploring wavelength. The longitudinal scale sizes L are in both cases one or more orders of magnitude greater than the transverse scale sizes. The 'axial ratio' of irregularities is defined as L/T.

2. SCATTERING PHENOMENA ASSOCIATED WITH THICK IRREGULARITIES

2.1 General

The presence of large ionospheric irregularities is often manifested by the 'scintillation' of radio stars and of satellite signals. The term 'scintillation' refers to fluctua-

tions with time of the amplitude, angle-of-arrival, and phase of the signals from such transmitters. These fluctuations, or scattering effects, are imposed by passage through ionospheric irregularities, and have been correlated[3], with the observation of 'spread-F' on ground-based ionosondes.

The term 'spread-F', in turn, refers to configuration of weak echoes on ionograms. Such configurations tend to appear mainly at night and in conjunction with the trace (which they sometimes obliterate) corresponding to the F-layer. The literature concerning this manifestation of F-region irregularities has been reviewed by Herman[4]. Some spread-F configurations seem to result from thick irregularities[5], some from thin irregularities[6], and some no doubt from both classes of irregularities, and it is not always readily apparent just how the configurations arise. Indeed, many workers have not attempted to resolve the confusing spread-F configurations on the ionograms that are obtained.

Inferences from scintillation studies regarding the characteristics of thick irregularities have been limited. For example, information pertaining to the height of irregularity occurrence is not readily obtainable from the scintillation data. However, the scintillations are usually imposed while the radio waves are traversing the vicinity of the height of maximum electron concentration (h_{max}). Scintillation measurements obtained with signals from satellite-borne transmitters in asynchronous orbits offer the possibility of determining the height of the scattering irregularities.

The scattering phenomena associated with the thick irregularities causing scintillations fall into two categories: (i) Detrimental effects imposed by forward scatter during ray passage through the ionosphere, and (ii) ducting of radio energy within irregularities that represent a depletion of electron concentration. The observations of scintillations provide a means for estimating the factors associated with the detrimental effects, while radar observations, especially from ionosondes in satellites, are presently the best source of information regarding the irregularity characteristics and their potentialities for ducted propagation.

2.2 Detrimental Effects on Space-Earth Communications

To summarize the results from scintillation measurements that are pertinent to detrimental effects on propagation, it is known that the irregularities occur mainly at night, and that they are aligned with the geomagnetic field lines. The transverse dimensions of the thick irregularities range from 100 m in the auroral zone[7] to 500 m at the magnetic equator[8], although values up to a kilometer have been reported at temperate latitudes[9]. The axial ratios reported from scintillation measurements range from 5 to 10 or more, but observations of conjugate ducts (see Section 2.3) suggest much larger values. The altitudes over which scintillations are obtained are from about 200 to 1500 km (Ref. 10).

From a knowledge of these characteristics of the irregularities, it is possible to deduce some implications for earth-space propagation. In particular, one would expect an 'aspect sensitivity' of the scintillations, by which is meant a dependence upon the propagation geometry. Scintillation perturbations of radio signals are thus most significant for ray geometries in which the earth-to-space or space-to-earth propagation paths are perpendicular to the irregularities. Also, scintillation effects are encountered for propagation paths in the equatorial plane, and for paths north of the vertical in the northern hemisphere, and south of the vertical in the southern hemisphere. The severity of the scintillations would be expected to be modulated by the seasonal and latitudinal variations of irregularity occurrence and intensities. The irregularities also tend to occur in patches. Experiments indicate that the regions of greatest severity are the auroral zone and, in the equatorial ionosphere, the vicinity of the magnetic equator.

Since amplitude scintillations on the space telemetry band (136-138 MHz) in the auroral zone can have peak-to-peak variations up to 12 dB or more, the deleterious effects can be quite serious. Inasmuch as the scintillation effects depend inversely on the radio frequency employed[11], it is evident that they can be substantially avoided by utilizing

sufficiently high frequencies. Alternatively, the use of space or frequency diversity for reception makes the application of lower frequencies more tenable.

2.3 Propagation in Ducts

The thick irregularities responsible for scintillations can have beneficial propagation properties, in that they can be used for duct or waveguide propagation. Ground-based studies of ducted propagation along the entirety of a geomagnetic field line are still in the realm of the controversial and inconclusive [12, 13]. However, the existence of ducted propagation in combination with refraction has been inferred from certain spread-F configurations on equatorial ionograms[5]. Subsequently, studies from ionosondes on satellites[13-15] have been a powerful tool for localizing the ducting irregularities and for demonstrating the occurrence of conjugate ducting (propagation along ducts extending between magnetically conjugate points in the ionosphere) and 'near-end' ducting (propagation along ducts extending downwards along geomagnetic lines). Also, the satellite studies reveal propagation resulting from the combination of ducting and refraction. The percentage occurrence of ducting found by Calvert and Schmid[15], as a function of local time and of geomagnetic latitude, is shown in Figure 1. Other occurrence patterns have been obtained by Hice and Frank[16] It would be expected that scintillation phenomena should vary in much the same fashion. The latitudinal variation of conjugate ducts observed from Explorer XX (Ref.13) is shown in Figure 2.

The possibility of practical utilization of ducted propagation, for example, between conjugate points on the earth's surface, is problematical[12, 13]. Also, the utility of ducted communications between the earth and a satellite, or between satellites, would seem to be extremely limited.

Another F-region 'scatter propagation' phenomenon of probably limited utility is the so-called 'whispering gallery' mode of propagation. This term refers to refractively guided, spherical paths about the earth, conceivably over long distances. Perhaps the antipodal propagation around the world that is sometimes experienced is attributable to this mode, which is named after an acoustical propagation phenomenon that has been noted, in particular, in the Whispering Gallery at St. Paul's in London. The reason that this mode qualifies for inclusion in the present review of F-region scatter is that such guided paths cannot be entered from the ground unless some scattering or refraction mechanism causes radio waves to attain the appropriate angle of incidence on the F-layer. A similar fortuitous mechanism is required for reentry to a reception point on the ground. It is likely that ducted propagation would be one reasonable method for fulfilling this requirement at one or both ends of a transmission path. Grossi and Langworthy[17] report maximum usable frequencies for such propagation reaching about twice those for the equivalent multi-hop paths, with reductions in attenuation as high as 30 dB. Their studies employed satellite-to-satellite transmissions, which are possible only infrequently.

3. SCATTERING PHENOMENA ASSOCIATED WITH THIN IRREGULARITIES

The subject of F-region scattering from thin irregularities turns out to be the most promising possibility (treated here) from the stand-point of utility for telecommunications. For many years there have been noted on ionograms certain manifestations of such scattering, known as 'spread-F'. The mechanism of scattering was first advanced as an explanation by Eckersley[18]. The worldwide network of ionosondes has, over the years, been a good source of data on scattering from thin irregularities, but this mode was not usually resolved from other modes of scattering.

Although multiple scattering from turbulence in the F-region has been invoked to account for spread-F configurations[19], it is clear that turbulence does not occur above about 100 km (Ref.20). However, even if turbulence did extend to F-region heights, it would be unlikely to produce multiple scattering, although ducted propagation[5] can be considered as being tantamount to multiple scattering. However, single scattering models such as Renau's[21] were a first step in accounting for some spread-F configurations arising from thin irregularities.

Because of the aspect sensitivity of F-region scatter from thin irregularities, it is essential to attain orthogonality between the radio wave propagation vector and the irregularities in order to obtain coherent echoes. One way of achieving this is by observing with a radar in appropriate northerly directions in the northern hemisphere, and in southerly directions in the southern hemisphere. In the vicinity of the magnetic equator, perpendicularity is achieved in the vertical, as well as in East-West directions, or in other words, throughout the vertical equatorial plane. Thus, radar studies near the magnetic equator achieve a certain geometric simplification, which is advantageous in studying this rather complex phenomenon.

Radar studies at HF of F-region irregularities have been conducted at temperate latitudes by various groups[22, 23], and at auroral latitudes[24]. In the study by Weaver[23], echoes were obtained at altitudes from 200 to 700 km. The feasibility of using F-region scatter from these irregularities for propagation at temperate and high latitudes is not clearly established. It is, in principle, possible to obtain a favorable geometry for such scatter propagation by directing transmitter and receiver beams toward irregularities in such a way that the plane of propagation is normal to the irregularities, and so that the angles of incidence and of scattering are equal; in other words, the requirement is the same as that for reflection from a hypothetical mirror aligned with the scattering irregularity.

Scatter propagation of this sort is more customarily reported from equatorial latitudes, where the geometrical requirement (as contrasted to the radar case) is simply met, and where there is usually an abundance of thin irregularities from which to scatter. Trans-equatorial scatter propagation is encountered both at HF and VHF (Refs. 25-27), but there can be an admixture of refractive effects that tend to confuse the issue, depending both upon the propagation frequency and the separation between transmitter and receiver. A review of the more complicated propagation, such as reported in References 25 and 26, has been presented by Nielson[2]. A summary of results from an apparently pure case of VHF transequatorial scatter[27] is presented below.

A global study of the distribution of thin irregularities giving rise to 'aspect-sensitive' scattering has been obtained from satellite ionograms[15], as shown in Figure 3, and by other workers[16]. Morphological results from ground-based ionosondes are also available[28, 29].

The thin irregularities at equatorial locations have been studied best, by fixed-frequency radar techniques[30], ionosondes[6], and VHF forward scatter[27, 31]. Several summaries are available of the characteristics of the thin, equatorial scattering irregularities [4, 32-34]. It might be useful in the following to review the equatorial scatter propagation results[27, 31], in view of the relative purity of the scattering and the uniqueness of the interpretation.

A VHF propagation path was established in South America during the International Geophysical Year to investigate the possibility of observing F-region scattering. A frequency near 50 MHz was employed. The transmitter-receiver separation was arranged with the midpoint at the magnetic equator, at which point the Huancayo, Peru, ionosonde was operating. The separation chosen represented an effort to avoid scattering from E-region irregularities, and was 2580 km, as shown in Figure 4. Scatter propagation identifiable as coming from irregularities in the F-region was observed to occur during evening hours, but to be some 20 dB weaker[31] than propagation during the same time over an E-region path with the same midpoint (cf. Figure 5). During the final month of observations, pulse measurements were obtained over the propagation path, and these, in conjunction with the Huancayo ionograms, made it clearly demonstrable[27] that the scattering was associated with a layer of irregularities observable in the F-region ionograms taken at the midpoint (cf. Figure 6). Based on these scatter propagation studies and the simplicity of the equatorial geometry, considerable insight was obtained into the mechanisms by which the spread-F configurations on equatorial ionograms were produced[5, 6], leading to the ability to interpret some sequences of ionograms in terms of drift velocities[6, 34].

Some similar VHF scatter-propagation studies were conducted in the Far East during the IGY (Refs. 35 and 36). These were at somewhat higher latitudes than those measurements just discussed. There is some indication that F-region scatter propagation may have occurred during evening hours, and such propagation would have involved the aspect sensitivity discussed earlier.

In the preceding discussions on ionosonde studies of morphology of F-region irregularities, either topside or ground-based sounders were employed. A recent study by Dyson[37], involving a simultaneous comparison of the two kinds of ionograms, indicates that irregularities are more usually observed in the topside ionosphere, extending below the height of maximum ionization only part of the time.

REFERENCES

1. Peterson, A.M., *Thomson Scatter as a Communication Mode.* Paper 31 in this volume.

2. Nielson, Donald L., *A Review of VHF Transequatorial Propagation.* Paper 45 in this volume.

3. Dagg, M., *Diurnal Variations of Radio-Star Scintillations, Spread-F, and Geomagnetic Activity.* Journal of Atmospheric and Terrestrial Physics, Vol. 10, 1957, pp. 204-214

4. Herman, John R., *Spread-F and Ionospheric F-Region Irregularities.* Reviews of Geophysics, Vol. 4, 1966, pp. 255-299.

5. Pitteway, M.L.V. Cohen, Robert, *A Waveguide Interpretation of 'Temperate-Latitude Spread-F' on Equatorial Ionograms.* Journal of Geophysical Research, Vol. 66, 1961, pp. 3141-3156.

6. Calvert, Wynne Cohen, Robert *The Interpretation and Synthesis of Certain Spread-F Configurations Appearing on Equatorial Ionograms.* Journal of Geophysical Research, Vol. 66, 1961, pp. 3125-3140.

7. Lawrence, J.D., Jr. Martin, J.D. *Diurnal, Seasonal, Latitudinal and Height Variations of Satellite Scintillations.* Journal of Geophysical Research, Vol. 69, 1964, pp. 1293-1300.

8. Kent, G.S., Koster, J.R., *Height of Night-Time F-Layer Irregularities at the Equator.* Nature, Vol. 191, 1961, pp. 1083-1084.

9. Jespersen, J.L., Kamas, George *Satellite Scintillation Observations at Boulder, Colorado.* Journal of Atmospheric and Terrestrial Physics, Vol. 26, 1964, pp. 457-473.

10. Little, C.G., et al *An Experimental Investigation of the Scintillation of Radio Stars Observed at Frequencies of 223 and 456 Mc/s from a Location Close to the Auroral Zone.* Journal of Geophysical Research, Vol. 67, 1962, pp. 1763-1784.

11. Lawrence, R.S. et al. — *A Survey of Ionospheric Effects upon Earth-Space Radio Propagation.* Proceedings, Institute of Electrical and Electronic Engineers, Vol.52, 1964, pp.4-27.

12. Booker, H.G. — *Guidance of Radio and Hydromagnetic Waves in the Magnetosphere.* Journal of Geophysical Research, Vol.67, 1962, pp.4135-4162.

13. Loftus, Brigid T. et al. — *Observations of Conjugate Ducting by the Fixed-Frequency Topside-Sounder Satellite.* Annales de Géophysique, Vol.22, 1966, pp.530-537.

14. Muldrew, D.B. — *Radio Propagation along Magnetic Field-Aligned Sheets of Ionization Observed by the Alouette Topside Sounder.* Journal of Geophysical Research, Vol.68, 1963, pp.5355-5370.

15. Calvert, Wynne Schmid, Charles W. — *Spread-F Observations by the Alouette Topside Sounder Satellite.* Journal of Geophysical Research, Vol.69, 1964, pp.1839-1852.

16. Hice, James D. Frank, Bernadine — *Occurrence Patterns of Topside Spread-F on Alouette Ionograms.* Journal of Geophysical Research, Vol.71, 1966, pp.3653-3664.

17. Grossi, M.D. Langworthy, B.M. — Reported in 'Communications Designer's Digest', p.24, April 1968.

18. Eckersley, T.L. — *Studies in Radio Transmission.* Institution of Electrical Engineers Journal, Vol.71, 1932, pp.405-459.

19. Bugnolo, Dimitri S. — *Spread-F and Multiple Scattering in the Ionosphere.* Journal of Geophysical Research, Vol.65, 1960, pp.3925-3929.

20. Hines, C.O. — *The Upper Atmosphere in Motion.* Quarterly Journal of the Royal Meteorological Society, Vol.89, 1963, pp.1-42.

21. Renau, Jacques — *Theory of Spread-F Based on Aspect-Sensitive Backscattered Echoes.* Journal of Geophysical Research, Vol.65, 1960 pp.2269-2277.

22. Peterson, A.M. et al. — *Regularly Observable Aspect-Sensitive Radio Reflections from Ionization Aligned with the Earth's Magnetic Field and Located Within the Ionospheric Layers at Middle Latitudes.* Journal of Geophysical Research, Vol.60, 1955, pp.497-512.

23. Weater, Paul F. — *Backscatter Echoes from Field-Aligned Irregularities in the F-Region.* Journal of Geophysical Research, Vol.70, 1965 pp.5425-5432.

24. Leadabrand, R.L. Peterson, A.M. — *Radio Echoes from Auroral Ionization Detected at Relatively Low Geomagnetic Latitudes.* Institute of Radio Engineers, Transactions, PGAP, Vol.6, 1958, pp.65-79.

25. Davies, K. Barghausen, A.F. — *The Effect of Spread-F on the Propagation of Radio Waves near the Equator.* pp.437-466 in 'Spread-F and its Effects Upon Radio-Wave Propagation and Communication.' edited by P. Newman, Agardograph 95, Technivision, Maidenhead, 1966.

26. Nielson, D. — *Oblique Sounding of a Transequatorial Path.* pp.467-490 in 'Spread-F and its Effects Upon Radio Wave Propagation and Communication', edited by P. Newman, Agardograph 95, Technivision, Maidenhead, 1966.

27. Cohen, Robert
Bowles, Kenneth L.
On the Nature of Equatorial Spread-F. Journal of Geophysical Research, Vol.66, 1961, pp.1081-1106.

28. Singleton, D.G.
The Geomorphology of Spread-F. Journal of Geophysical Research, Vol.65, 1960, pp.3615-3624.

29. Singleton, D.G.
The Morphology of Spread-F over Half a Sunspot Cycle. Journal of Geophysical Research, Vol.73, 1968, pp.295-308.

30. Clemesha, B.R.
An Investigation of the Irregularities in the F-Region Associated with Equatorial Type Spread-F. Journal of Atmospheric and Terrestrial Physics, Vol.26, 1964, pp.91-112.

31. Cohen, Robert
Bowles, Kenneth L.
Ionospheric VHF Scattering near the Magnetic Equator during the International Geophysical Year. Journal of Research, National Bureau of Standards, Vol.67D, 1963, pp.459-480.

32. Bowles, K.L.
Radio Wave Scattering in the Ionosphere. pp.55-176 in 'Advances in Electronics and Electron Physics', Vol.19, edited by L. and C. Marton, Academic Press, 1964.

33. Cohen, Robert
The Equatorial Ionosphere. pp.561-613 in 'Physics of Geomagnetic Phenomena', edited by S. Matsushita and W.H. Campbell, Academic Press, 1967.

34. Calvert, Wynne
Equatorial Spread-F. Technical Note 145, National Bureau of Standards, 1962.

35. Bateman, R.
et al.
IGY Observations of F-Layer Scatter in the Far East. Journal of Geophysical Research, Vol.64, 1959, pp.403-405.

36. Smith, Ernest K., Jr
Finney, James W.
Peculiarities of the Ionosphere in the Far East: A Report on IGY Observations of Sporadic-E and F-Region Scatter. Journal of Geophysical Research, Vol.65, 1960, pp.885-892.

37. Dyson, P.L.
Comparison of Irregular Features Appearing on Ionograms Recorded by Topside and Ground-Based Sounders. Journal of Atmospheric and Terrestrial Physics, Vol.29, 1967, pp.881-886.

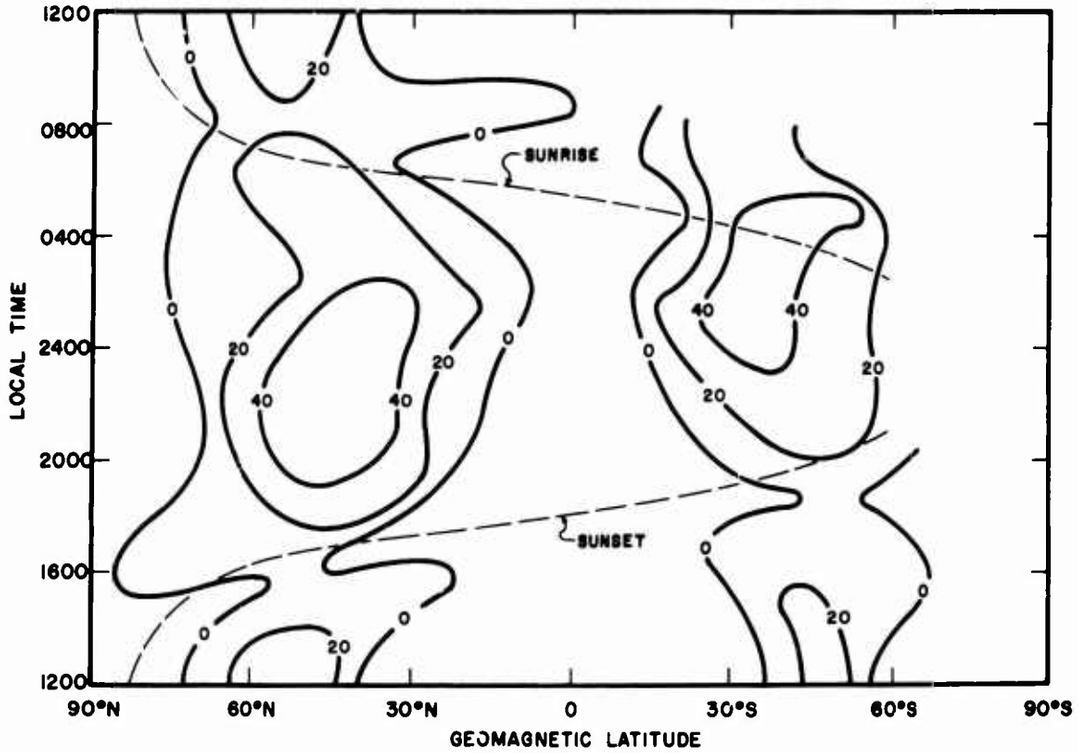


Fig. 1 The percentage occurrence of ducting spread-F on Alouette Ionograms. November 14 ground sunset and sunrise are shown. (From Calvert and Schmid (Ref. 15))

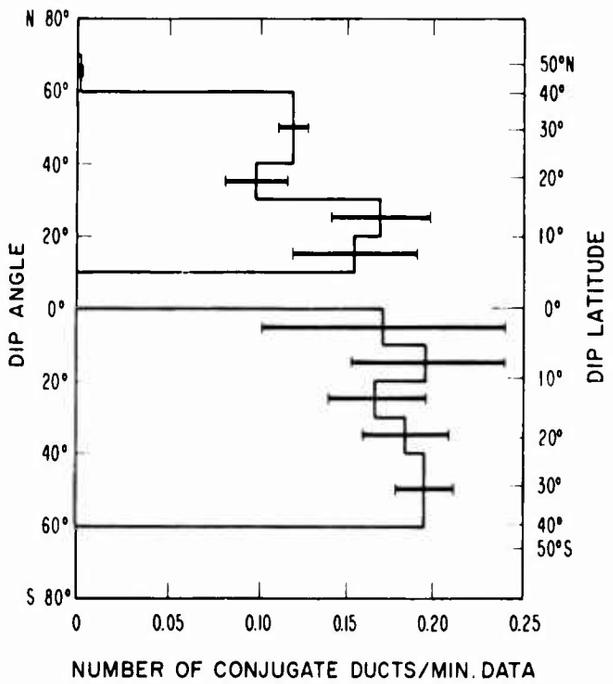


Fig. 2 The latitudinal variation of conjugate ducting over the Americas during the periods August-November 1964, and February-May 1965. The occurrence of conjugate ducting is expressed as the number of conjugate ducts observed per minute of data times the cosecant of I, the dip angle. (From Loftus, et al (Ref. 13))

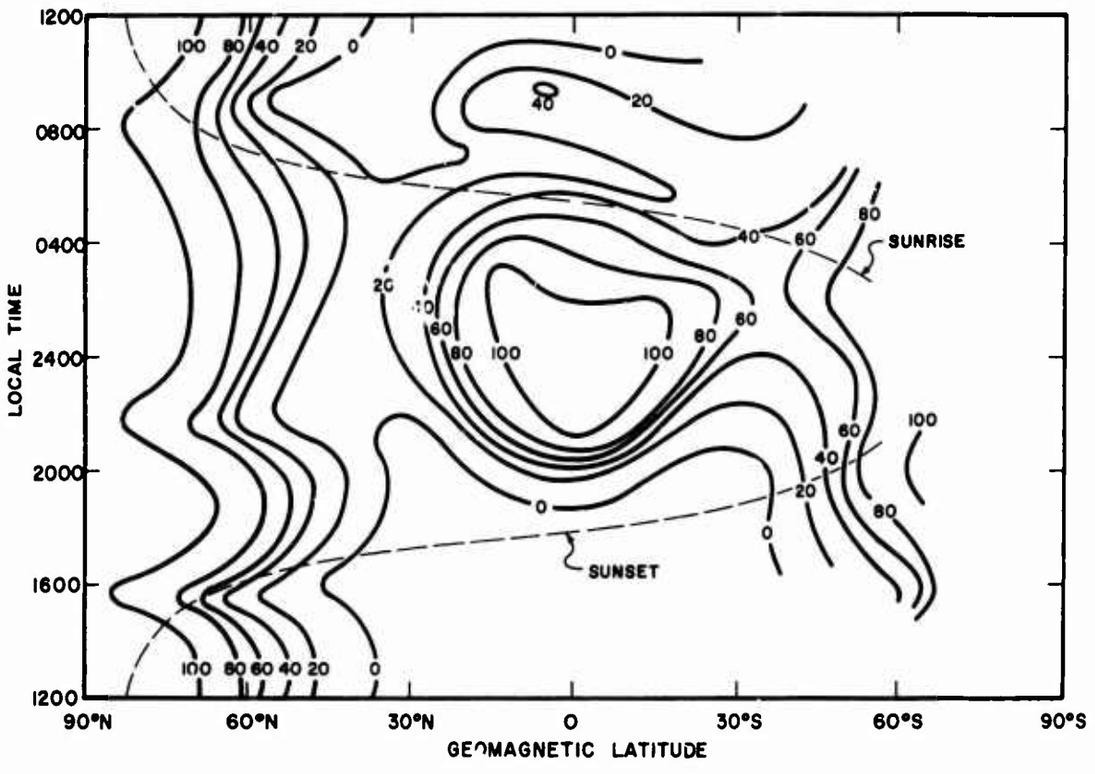


Fig. 3 The percentage occurrence of aspect-sensitive scattering observed by the Alouette topside sounder satellite. Ground sunset and sunrise for the middle of the observation period, November 14, is indicated (From Calvert and Schmid (Ref. 15))

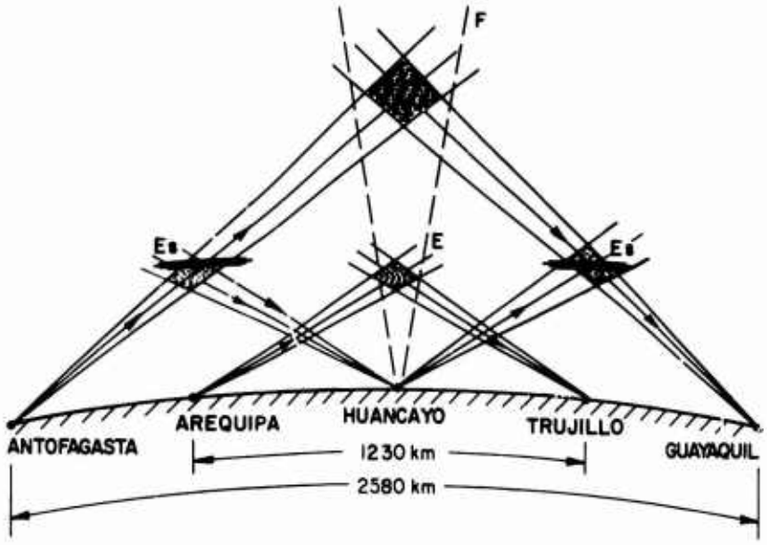


Fig.4(a) Vertical plane along the west coast of South America, showing the network of transmitting and receiving stations involved in the International Geophysical Year VHF forward-scatter experiment. (From Cohen and Bowles (Ref.31))

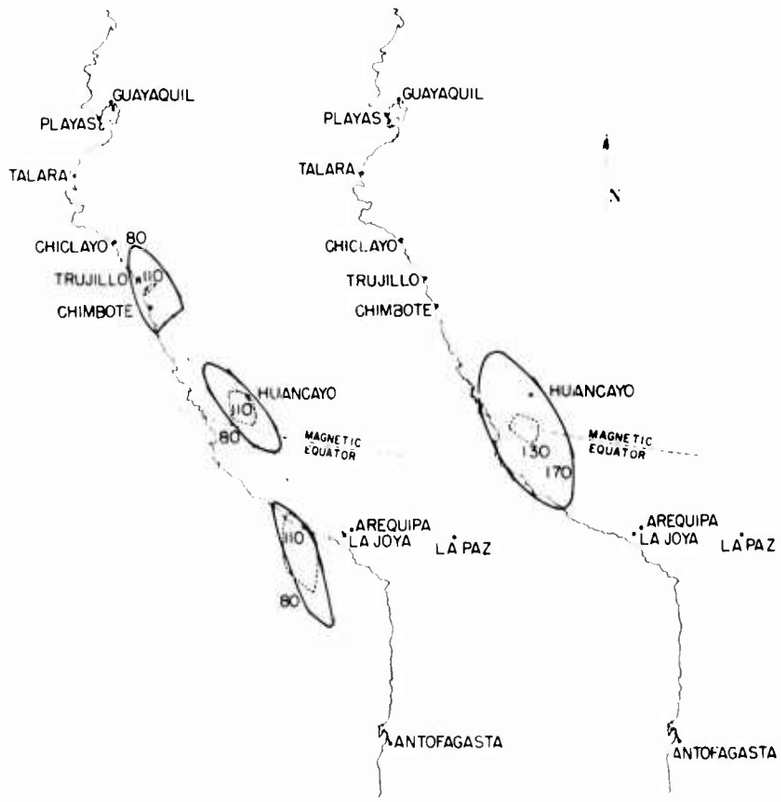


Fig.4(b) Antenna-beam intersections for the E-scatter and F-scatter circuits. The approximate loci are computed for the height (in kilometers) adjacent to each locus. The left-hand diagram is for the E paths, and the right-hand diagram is for the F path (prior to raising the antenna beams on that path). (From Cohen and Bowles (Ref.31))

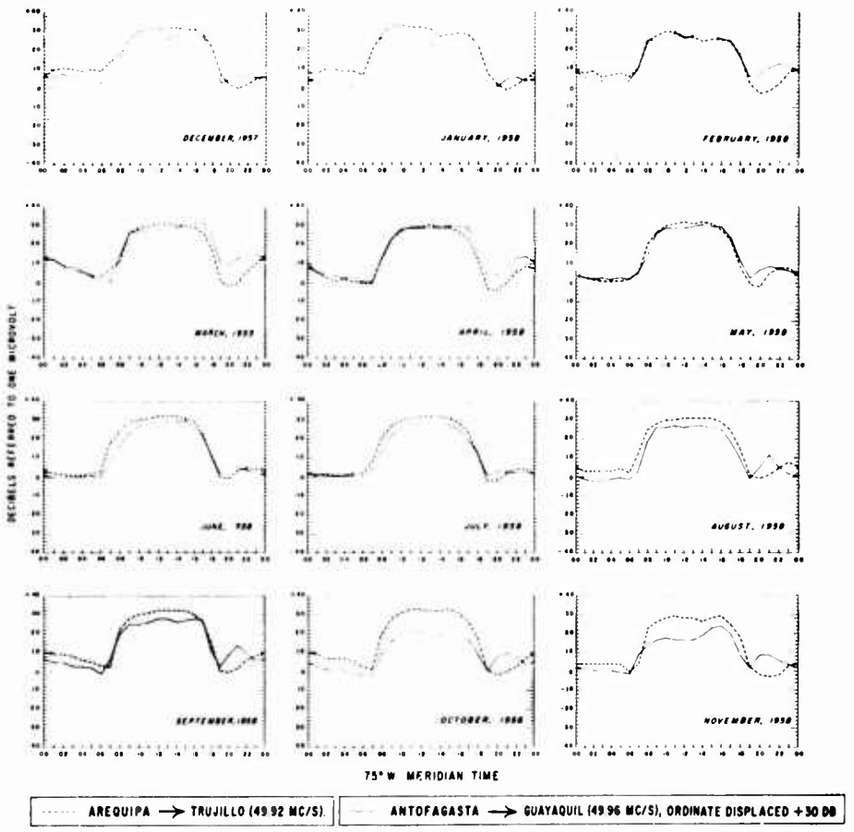


Fig.5 A monthly comparison of the diurnal variation of hourly median signal strengths over the long and short paths, with the long-path signal shifted +30 dB. (From Cohen and Bowles (Ref.31))

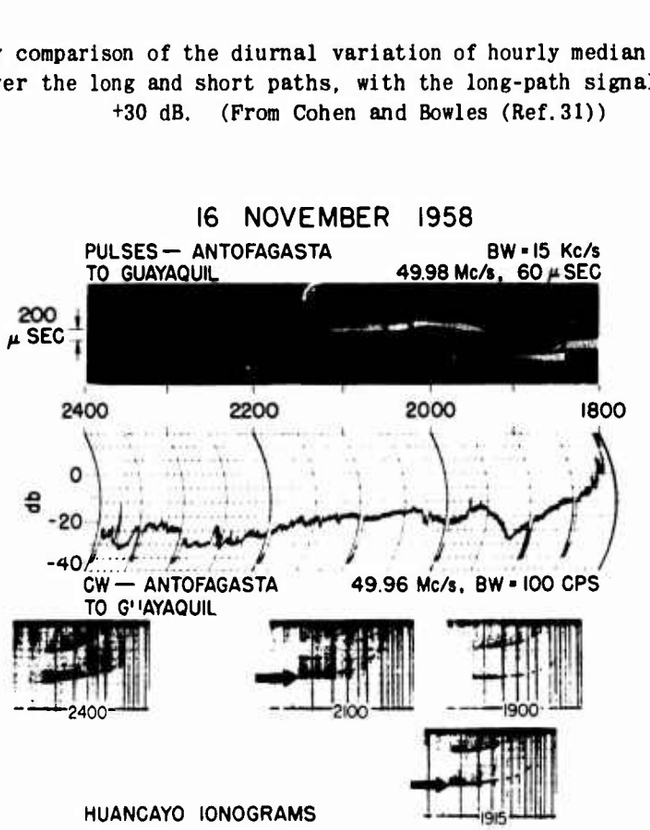


Fig.6 Simultaneous recordings on 1958 November 16 of pulse delay and signal strength over the Antofagasta to Guayaquil path, with selected Huancayo (midpoint) ionograms. (From Cohen and Bowles (Ref.27))

RADIO-DOPPLER OBSERVATIONS OF THE IONOSPHERE NEAR THE MAGNETIC EQUATOR

by

Kenneth Davies and Norman J.F.Chang

Space Disturbances Laboratory
Research Laboratories, ESSA
Boulder, Colorado 80302

SUMMARY

Radio observations of the ionosphere near the magnetic equator exhibit echoes with marked frequency scatter during evening hours. The mean frequency shift is predominantly positive but decays with time. A model is presented to explain this phenomenon in terms of asymmetric atmospheric waves propagating from West to East with velocities in the range 100 to 150 m/s. Statistical evidence is presented which shows that the duration of the echoes peaks around 60 min, the average period between the onset of successive echoes is also about 60 min and the occurrence of these echoes exhibits a pronounced minimum in the summer.

RADIO-DOPPLER OBSERVATIONS OF THE IONOSPHERE NEAR THE MAGNETIC EQUATOR

Kenneth Davies and Norman J.F.Chang

1. BACKGROUND

In this paper we propose a model of ionospheric motion to explain the Doppler shifts of high-frequency radio echoes observed after sunset near the magnetic equator. The technique and the type of records obtained have been described by Calvert et al.[1] and by Davies and Barghausen[2]. A sample record of the phenomenon being discussed is shown in Figure 1 and consists essentially of somewhat diffuse echoes with frequency decreasing with time towards the carrier frequency (given by the zero on the frequency scale). Any negative frequency deviations are relatively small. The appearence of these echoes is associated with the occurrence of equatorial spread-F and often with such radio phenomena as equatorial flutter fading[3].

Starting in 1961 Doppler recordings were made in Africa as part of a more general study of oblique radio propagation. The earliest observations were on the (3300 km) path Tripoli, Libya to Accra, Ghana and Calvert et al.[1] explained the observed frequency variation (positive Doppler shift decreasing with time) with a model of magnetic field-aligned ionospheric irregularities moving from West to East with velocities in the range 100 to 150 m/s. The fact that only positive frequency shifts were observed was explained by the aspect-sensitive geometry of the reflecting columns: the reflections would be very weak when the irregularities lay to the east of the path.

To check this model two circuits were set up near, and roughly parallel to, the magnetic dip equator, which eliminated the asymmetric geometry of the magnetic field over the Tripoli-Accra path. Transmitters were installed at Monrovia, Liberia and receivers at Accra, Ghana (1180 km) and at Natal, Brazil (2990 km). Frequencies near 10 MHz and 20 MHz were used and continuous observations were made over the period December 1962 through December 1965. Much to our surprise the same types of phenomena were observed on these paths as were seen on the Tripoli-Accra path. The Doppler shifts were predominantly positive, with only a slight negative shift, as in the example shown in Figure 1.

2. SOME STATISTICAL DATA

For lack of a better term we have given these descending frequency traces the name "swoopers". Some statistical data on these "swoopers" are given in Figure 2. In Figure 2(a) are shown the parameters used to describe the phenomenon, namely, the duration T and the interval Δt between successive echoes. Figure 2(b) shows that, on most nights when the phenomenon occurs, only a single swooper was present. Very few nights had as many as five of them. The duration T (Fig. 2(c)) varied from about half an hour to about two hours, the most frequently occurring duration being about one hour. Similarly the distribution of Δt given in Figure 2(d) appears to have a peak around one hour.

Data on the seasonal variations of occurrence of swoopers are shown in Figures 3(a) and (b) respectively. Both histograms exhibit a semi-annual periodicity, with peaks around February-March and October-November. There is a marked minimum during the summer months.

3. PROPOSED MODEL

The fact that sweepers are observed over West-East paths near the magnetic-dip equator makes the model of field-aligned irregularities untenable. We therefore propose an alternative model, which is illustrated in Figure 4(a). The surfaces of constant electron density are asymmetrical with a sharp leading (Eastern) edge and a slowly rising trailing edge. As the disturbance moves from West to East, radio echoes are obtained quite far to the west of the path midpoint, with relatively large Doppler shifts which will diminish to zero as the bottom of the irregularity approaches the path midpoint. When the point of reflection is to the east of the midpoint only small Doppler shifts are possible.

Using some reasonable numbers the model has been developed a little further. In Figure 4, two wave crests are shown at a height of 280 km moving with a speed of 113 m/s and separated by a distance (wavelength) of 400 km. These parameters give the $\Delta f(t)$ curve shown in Figure 4(b), which is the sort of record obtained in practice. Note that the position given by $X = 125$ km is arbitrary.

It may be relevant to note that such asymmetric waveforms can result from the interaction between an atmospheric gravity wave with the ambient electron density[4].

REFERENCES

1. Calvert, W. et al. — *Equatorial Spread-F Motions.* Proceedings of the International Conference on the Ionosphere, 1962. Chapman and Hall, London, 1963, pp. 316-322.

2. Davies, K. Barghausen, A.F. — *The Effect of Spread-F on the Propagation of Radio Waves near the Equator.* Chapter 2-13 of "Spread-F and its Effects on Radio-wave Propagation and Communications", edited by P. Newman, AGARDograph 95, Technivision, Maidenhead, 1966, pp. 437-466.

3. Osborne, B.W. — Journal of Atmospheric and Terrestrial Physics, Vol. 2, 1951, p. 66.

4. Hooke, W.H. — *Ionospheric Irregularities Produced by Internal Atmospheric Gravity Waves.* Journal of Atmospheric and Terrestrial Physics, Vol. 30, 1968 (in the press).

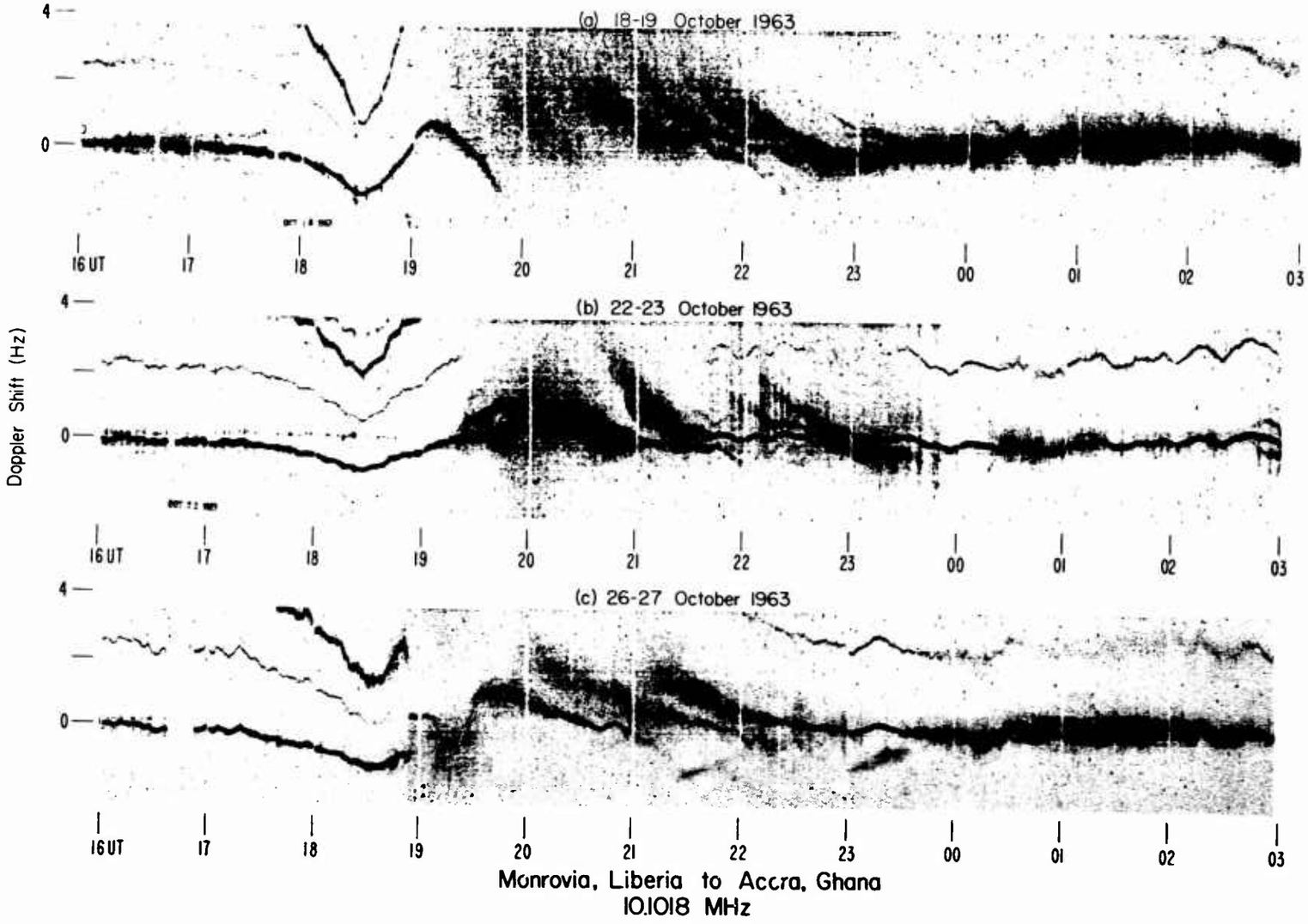


Fig. 1 Examples of swoopers, October 1963

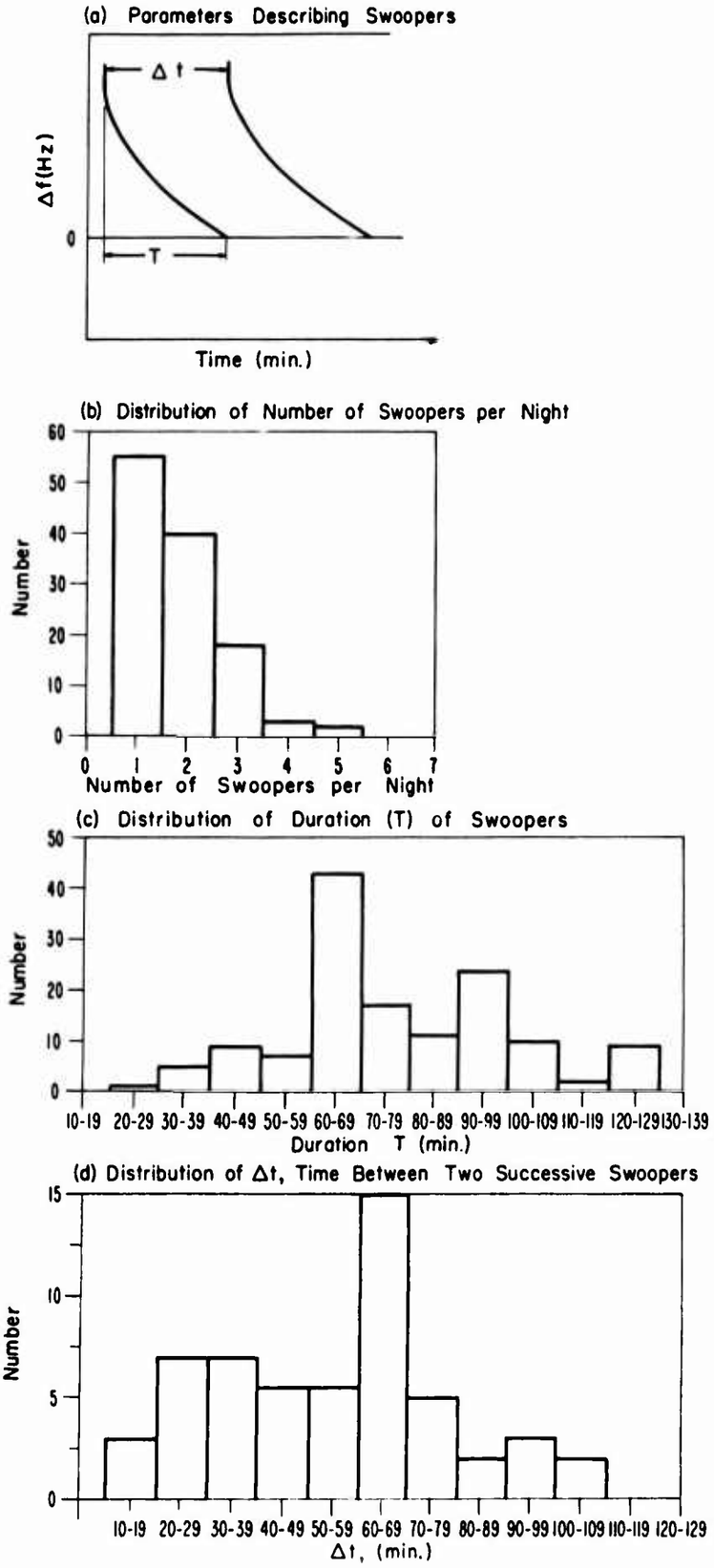


Fig. 2 Some statistical data on equatorial swoopers

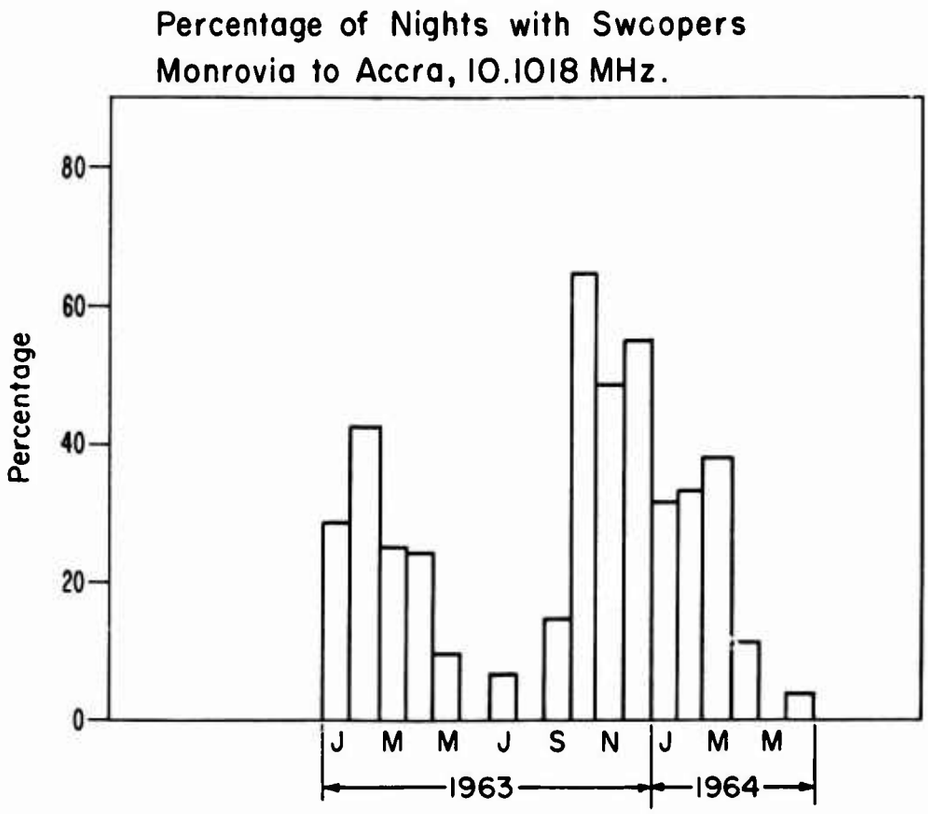


Fig. 3 Seasonal occurrence of swoopers

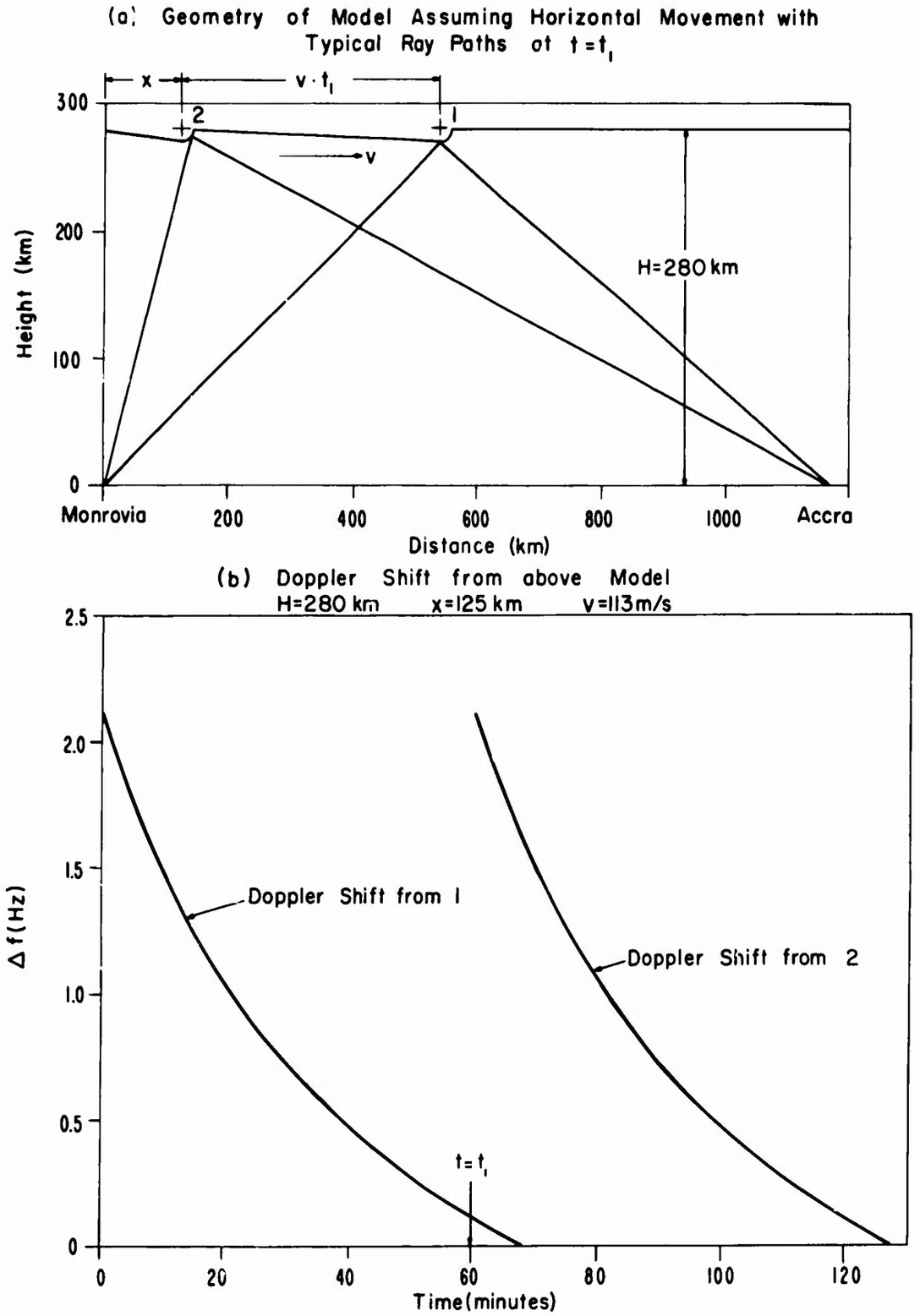


Fig. 4 Asymmetric ionospheric irregularities (a) suggested to explain frequency characteristics (b)

JOINT PROBABILITY DENSITY OF SIGNAL FADING AT SPACED RECEIVERS

by

T. J. Elkins

Air Force Cambridge Research Laboratories,
L. G. Hanscom Field,
Bedford, Mass., USA

SUMMARY

An attempt is made to apply the technique of spaced receiver measurements of fading signal propagation to include some cases in which the "drifting screen" analysis cannot be used successfully. One such case, commonly met in practice, is the presence of one or more periodic fading components, which distort the cross-correlation functions between separate fading records. It is suggested that, in these circumstances, the joint probability density of the signal fading at pairs of receivers may provide useful information about the properties of the irregular medium. A model is considered of a one-dimensional sinusoidal phase screen, modulated by a random phase component, and the joint probability density of the field strength at two spaced points beyond the screen is derived. It is suggested that, in situations where the model is valid, several interesting parameters of the medium may be estimated by comparing experimentally measured fading distributions with the derived ones. An attempt is made at such a comparison, using data obtained from measurements of geo-stationary satellite transmissions. Although the data used is not ideally suited for this purpose, there is some indication that this technique may prove of practical value.

JOINT PROBABILITY DENSITY OF SIGNAL FADING AT SPACED RECEIVERS

T. J. Elkins

1. INTRODUCTION

The method of the "drifting pattern", devised by Briggs et al.[1], is a well known technique for the remote analysis of the structure of an inhomogeneous medium. However, for a variety of reasons, this technique frequently breaks down in practice. Such failures usually stem from failure of the initial assumptions to be satisfied. When the fading signal is non-stationary, which is common in such instances, the conventional stochastic assumptions may no longer be applied, and the method becomes unreliable or impossible to apply. A signal which exhibits fading, due to transmission through an irregular medium, may be characterized by its probability density or, more generally, by the joint probability density at pairs of points in the scattered or diffracted field. The probability density is a stochastic function which is of substantial engineering importance, but has found little application, to date, in the study of the properties of the medium itself.

This paper is intended to point out the potential use of multi-dimensional probability densities in studies of irregular media. It appears to be easier to measure joint probability densities, rather than cross-correlation functions, as required by the method of the drifting pattern. Furthermore, it is not necessary to assume temporal coherence in the fading. In the conventional technique, when this assumption is not satisfied, the resulting random changes in the fading are usually characterized by a parameter, with the dimensions of velocity and usually denoted by V_c. It has not been found possible to ascribe any reliable physical meaning to this quantity. The proposed method, however, suffers from the disadvantage of being rather dependent on the type of model chosen to specify the inhomogeneous medium.

In this paper a model will be considered which appears to be appropriate to a type of fading frequently encountered in practice. Figure 1 shows a power spectrum, computed from an hour-long sample of fading data, taken from observations of transmissions from the geo-stationary satellite, Canary Bird, at 136 MHz. Several pronounced spectral features are apparent, with power densities exceeding the background "noise" by an order of magnitude - a figure which is often exceeded. Figure 2 shows the computed probability density for a sample of data which contained one dominant spectral peak. The form of this function is that of a Gaussian process, with a superimposed periodic component. Therefore, to illustrate the proposed technique, the joint probability density will be computed for fading produced by a model diffracting screen, incorporating both random and periodic components. The results of these computations will be compared with actual measurements, to the extent that available experimental data permit. For simplicity, a one-dimensional model will be assumed in the analysis. Such a model is appropriate, for example, to the case of a medium containing anisotropic or elongated irregularities, and there is considerable evidence in the literature to suggest that this situation is commonly found in the ionosphere.

2. ONE-DIMENSIONAL SCREEN

Let the plane $z = 0$ define the lower boundary of the ionosphere, and let the phase refractive index vary sinusoidally in the x-direction, so that the complex amplitude of a unit plane scaler wave, emerging downwards from the layer, is given by

$$E(x,0) = \exp\{i\phi \cos [bx + \theta(x)]\}, \tag{1}$$

where

$b = 2\pi/L$

L is the irregularity dimension

$\theta(x)$ is a random stochastic function which modulates the phase of the screen

ϕ is the magnitude of the maximum phase excursion on the screen.

For the case of a "thin" or "shallow" phase screen, $\phi < 1$, and (1) may be written approximately

$$E(x,0) \simeq 1 + i\phi \cos [bx + \theta(x)] \tag{2}$$

or

$$E(x,0) \simeq 1 + i\phi\, e(x,0), \tag{3}$$

where $e(x)$ represents a modulation component in quadrature with the unit unperturbed wave.

The spatial properties in the field will be determined by those of this modulation component. Viewed physically, this is a result of the fact that, since $\phi < 1$, the various components of the modulation term interfere only with the unit plane wave, while the interference between different modulation components, being of order ϕ^2, is negligible.

Let

$$e(x) = \cos [bx + \theta(x)] = X(x) \sin bx + Y(x) \cos bx\ ; \tag{4}$$

then

$$e(x + \xi) = X(x + \xi) \sin b(x + \xi) + Y(x + \xi) \cos b(x + \xi)\ . \tag{5}$$

Define the spatial frequency density as

$$g(ks) = \int_{-\infty}^{\infty} r(\xi) \cos k\xi\, d\xi\ , \tag{6}$$

where s is the sine of the angle between the incident propagation vector and an arbitrary point in the diffracted field, and $r(\xi)$ is the normalized auto-correlation function of $e(x)$.

Then

$$X^2(x) = Y^2(x) = \frac{1}{2\pi} \int_{-\infty}^{\infty} g(ks)\, d(ks) = 1 \tag{7}$$

$$\langle X(x)\, X(x + \xi)\rangle = \langle Y(x)\, Y(x + \xi)\rangle = \frac{1}{2\pi} \int_{-\infty}^{\infty} g(ks) \cos k\xi\, d\xi = r(\xi) \tag{8}$$

while, if $g(ks)$ is assumed to be symmetrical about the value $g(0)$,

$$\langle X(x)\, Y(x + \xi)\rangle = \langle X(x + \xi)\, Y(x)\rangle = \frac{1}{2\pi} \int_{-\infty}^{\infty} g(ks) \sin b\xi\, d\xi = 0\ . \tag{9}$$

Using (6), (7), and (8), it can be easily shown that

$$\langle e(x)\, e(x + \xi)\rangle = r(\xi) \cos b\xi, \tag{10}$$

where $\langle\ \rangle$ denotes spatial averaging.

Thus the spatial auto-correlation function in the field, immediately beyond the screen, is the product of a sinusoidal component, of period $b = 2\pi/L$, with the auto-correlation function of the random phase component.

The propagation of the wave beyond the screen (in the region $z > 0$) is described by the Fresnel – Kirchhoff integral

$$E(x,z) = \frac{1}{\lambda}\int_{-\infty}^{\infty}\int \exp\, i\{\phi \cos b\xi + ks(x-\xi) - kz\sqrt{(1-s^2)}\}\, d\xi ds \quad . \tag{11}$$

Again, using approximation (2), and noting that s is small ($s \lesssim \lambda/L$), the result is obtained that, for $z \lesssim L^2/\pi\lambda = z_R$,

$$E(x,z) = e^{-ikz}\left\{1 - \phi \sin\frac{\pi\lambda z}{L^2}\cos\,[bx + \theta(x)] + i\phi\cos\frac{\pi\lambda z}{L^2}\cos\,[bx+\theta(x)]\right\}. \tag{12}$$

Thus the spatial properties (phase and amplitude) of the diffracted field, within the Fresnel limit, are identical with those of the screen. The instantaneous power in the diffracted field exhibits a maximum value of

$$\begin{aligned} P_{max} &= E(x,z)E^{*}(x,z) \\ &\simeq 1 - 2\phi \sin\frac{z}{z_R} \end{aligned} \tag{13}$$

when $\cos[b + \theta(x)] = 1$.

If a stochastically stationary model is assumed, the relative power distribution in the fading signal may be simply written. Equation (37) is an example of the complexity which results when non-stationary models are considered.

3. RELATIVE POWER DISTRIBUTION IN THE FADING SIGNAL

The mean value of $E(x)$ is (neglecting the Z-dependence),

$$\bar{E}(x) = \phi\int_{-\infty}^{\infty}\cos\,(bx + \theta)\, p(\theta)\, d\theta \quad . \tag{14}$$

The power contained at spatial frequency b is

$$\begin{aligned} P_b &= \langle[\bar{E}(x)]^2\rangle \\ &= \phi^2\int_{-\infty}^{\infty}\int \langle\cos\,(bx + \theta_1)\cos\,(bx + \theta_2)\rangle\, p(\theta_1)p(\theta_2)\, d\theta_1 d\theta_2 \quad . \end{aligned} \tag{15}$$

In performing the spatial averaging, $d\theta/dx$ is assumed small compared to b,

$$\text{i.e.,}\quad P_b = \tfrac{1}{2}\phi^2\int_{-\infty}^{\infty}\int \cos\,(\theta_1 - \theta_2)\, p(\theta_1)p(\theta_2)\, d\theta_1 d\theta_2 \quad . \tag{16}$$

If θ is distributed symmetrically, as previously assumed,

$$P_b = \tfrac{1}{2}\phi^2\left\{\int_{-\infty}^{\infty}\cos\,\theta\, p(\theta)\, d\theta\right\}^2 \quad , \tag{17}$$

$$\text{e.g.,}\quad \text{if}\quad p(\theta) = \frac{1}{\sigma\sqrt{(2\pi)}}\exp -\left(\frac{\theta^2}{2\sigma^2}\right), \tag{18}$$

i.e., if the phase is normally distributed, then

$$P_b = \tfrac{1}{2}\phi^2 \frac{1}{2\pi\sigma^2}\left\{\int_{-\infty}^{\infty} \cos\,\theta \exp - \left(\frac{\theta^2}{2\sigma^2}\right) d\theta\right\}^2 \qquad (19)$$

$$= \tfrac{1}{2}\phi^2 e^{-\sigma^2} \quad .$$

Hence the ratio of the power contained in the random modulation to that contained in the sinusoidal component is $e^{\sigma^2} - 1$. If this ratio is denoted by R , then the variance of the phase deviation on the screen may be estimated from the power spectrum, using the relation

$$\sigma^2 = \log_e (1+R) \quad . \qquad (19a)$$

4. JOINT PROBABILITY DISTRIBUTION

It is required to determine the two-dimensional probability density, $p(E_1,E_2)$, in the diffracted field, where

$$E_1(x) = \cos\,[bx + \theta(x)] \qquad (20)$$

and

$$E_2(x) = E_1(x + \xi) \,, \qquad (21)$$

where $\theta(x)$ is now assumed to be a Gaussian process with zero mean.

In order to determine $p(E_1,E_2)$, it is convenient to first derive the two-dimensional characteristic function of the two random variables, E_1 and E_2 , which may be denoted by $\phi(\kappa_1,\kappa_2)$.

Thus, writing the phasors of E_1 and E_2 as

$$\delta_1 = bx + \theta(x) \qquad (22)$$

$$\delta_2 = b(x+\xi) + \theta(x+\xi) \quad , \qquad (23)$$

it follows that

$$\phi(\kappa_1,\kappa_2) = \int_{-\infty}^{\infty}\int_{-\infty}^{\infty} \exp\, i(\kappa_1 \cos\,\delta_1 + \kappa_2 \cos\,\delta_2)\, K(\delta_1,\delta_2)\, d\delta_1 d\delta_2 \quad . \qquad (24)$$

Here, the kernel, $K(\delta_1,\delta_2)$, is the joint probability density of the normally distributed variables δ_1 and δ_2 ;

$$\text{i.e.,}\quad K(\delta_1,\delta_2) = \frac{1}{2\pi\sigma^2\sqrt{(1-r^2(\xi))}} \exp\left\{-\frac{1}{2\sigma^2[1-r^2(\xi)]}\left[(\delta_1 - bx)^2 - \right.\right.$$

$$\left.\left. - 2r(\xi)(\delta_1 - bx)(\delta_2 - bx - b\xi) + (\delta_2 - bx - b\xi)^2\right]\right\}. \qquad (25)$$

The characteristic function of the density $K(\delta_1,\delta_2)$ is

$$H(j,m) = \exp\,[ijbx + imb(x+\xi) - \tfrac{1}{2}\sigma^2(j^2 + m^2 + 2jmr(\xi)] \quad . \qquad (26)$$

The required characteristic function $\phi(\kappa_1,\kappa_2)$ may then be found, in terms of $H(j,m)$, by using the expansion

$$\exp i\kappa\cos\delta = \sum_{n=-\infty}^{\infty} i^n J_n(\kappa) e^{in\delta} , \tag{27}$$

where $J_n(\kappa)$ is the Bessel function of order n.

Thus,

$$\phi(\kappa_1,\kappa_2) = \sum_{j=-\infty}^{\infty}\sum_{m=-\infty}^{\infty} i^{j+m} J_j(\kappa_1) J_m(\kappa_2) H(j,m) . \tag{28}$$

Then the required probability density, $p(E_1,E_2)$, is found by performing the inverse Fourier Transform

$$p(E_1,E_2) = \left(\frac{1}{2\pi}\right)^2 \int_{-\infty}^{\infty}\int_{-\infty}^{\infty} \exp -i(\kappa_1 E_1 + \kappa_2 E_2)\, \phi(\kappa_1,\kappa_2)\, d\kappa_1 d\kappa_2 . \tag{29}$$

Substituting (28) into (29) and reversing the order of integration and summation yields

$$p(E_1,E_2) = \frac{1}{(2\pi)^2} \sum_{j=-\infty}^{\infty}\sum_{m=-\infty}^{\infty} H(j,m)\Gamma_j(E_1)\Gamma_m(E_2) , \tag{30}$$

where

$$\Gamma_r(E) = i^r \int_{-\infty}^{\infty} J_r(\kappa) \exp(-i\kappa E)\, d\kappa . \tag{31}$$

It can be shown that

$$\Gamma_r(E) = \Gamma_{-r}(E) = \begin{cases} \dfrac{2T_r(E)}{\sqrt{(1-E^2)}} & \text{for } |E| < 1 \\ 0 & \text{for } |E| > 1 , \end{cases} \tag{32}$$

where $T_r(E)$ is the Tchebychev polynomial of the first kind, of order r.

In order to evaluate $p(E_1,E_2)$ in (30) explicitly, it is necessary to make use of the following property of characteristic functions, for a normal process[2]:

$$H(j,m) = H(j)H(m) \exp - [jm\sigma^2 r(\xi)] , \tag{33}$$

where $H(j)$ and $H(m)$ are the characteristic functions of the one-dimensional densities, $K(\delta_1,0)$ and $K(0,\delta_2)$, respectively.

Then, from (26) and (33),

$$H(j,m) = \exp i[jbx + mb(x+\xi)] \exp -\frac{\sigma^2}{2}(j^2+m^2) \exp -jm\sigma^2 r(\xi) . \tag{34}$$

Substituting into (30) gives

$$p(E_1,E_2) = \frac{1}{\pi^2} \sum_{j=-\infty}^{\infty}\sum_{m=-\infty}^{\infty} H(j,m) \frac{T_j(E_1)}{\sqrt{(1-E_1^2)}} \frac{T_m(E_2)}{\sqrt{(1-E_2^2)}} . \tag{35}$$

Noting the symmetry properties of the Tchebychev polynomials, the double summation may be written in the form represented by the following symbolic notation:

$$\sum_{j=-\infty}^{\infty}\sum_{m=-\infty}^{\infty}(S_{j,m}) = 4\sum_{j=1}^{\infty}\sum_{m=1}^{\infty} + 2S_{j=0}\sum_{m=1}^{\infty} + 2S_{m=0}\sum_{j=1}^{\infty} + S_{j=0}S_{m=0} \quad . \tag{36}$$

Under this summation, (34) and (35) together result in

$$p(E_1,E_2) = \frac{-1}{\pi^2\sqrt{(1-E_1^2)}\sqrt{(1-E_2^2)}} + \frac{p(E_1)}{\pi\sqrt{(1-E_2^2)}} + \frac{P(E_2)}{\pi\sqrt{(1-E_1^2)}} + \ldots\ldots$$

$$\ldots\ldots + \frac{4}{\pi^2\sqrt{(1-E_1^2)}\sqrt{(1-E_2^2)}}\sum_{j=1}^{\infty}\sum_{m=1}^{\infty}\left\{T_j(E_1)T_m(E_2)F(j,m)\exp -\frac{\sigma^2}{2}(j^2+m^2)\right\}, \tag{37}$$

where

$$F(j,m) = \cos jbx \cos mb(x+\xi)\cosh\left[jm\sigma^2 r(\xi)\right] + \ldots.$$

$$\ldots. + \sin jbx \sin mb(x+\xi)\sinh\left[jm\sigma^2 r(\xi)\right] \tag{38}$$

and $p(E_1)$, $p(E_2)$ are the one-dimensional probability densities of the variables E_1 and E_2;

$$\text{i.e.,}\quad p(E_1) = \frac{1}{\pi\sqrt{(1-E_1^2)}}\left\{1 + 2\sum_{j=1}^{\infty}T_j(E_1)\cos jbx \exp -\tfrac{1}{2}j^2\sigma^2\right\} \tag{39}$$

and

$$p(E_2) = \frac{1}{\pi\sqrt{(1-E_2^2)}}\left\{1 + 2\sum_{m=1}^{\infty}T_m(E_2)\cos mb(x+\xi)\exp -\tfrac{1}{2}m^2\sigma^2\right\} \quad . \tag{40}$$

The general solution for $p(E_1,E_2)$ is complicated, but (37) may be appreciably simplified, under certain conditions.

Thus, for $\sigma^2 r(\xi) \gg 1$, $F(j,m)$ in (38) may be approximated by

$$F(j,m) = \tfrac{1}{2}\exp\left[jm\sigma^2 r(\xi)\right]\cos\left[jbx - mb(x+\xi)\right] \quad , \tag{41}$$

so that

$$F(j,m)\exp -\frac{\sigma^2}{2}(j^2+\eta^2) \simeq \tfrac{1}{2}\exp -\left\{\frac{\sigma^2}{2}(j-m)^2 - jm\sigma^2\left[1-r(\xi)\right]\cos\left[jbx - mb(x+\xi)\right]\right\} \quad . \tag{42}$$

In performing the double summation in (37), it is permissible to consider only the first few terms, since the coefficients decrease rapidly with increasing j and m. Furthermore, by virtue of the negative exponent in (42), and because $\sigma^2 \gg 1$ (for $r(\xi)$ not too close to unity), it is only necessary to consider terms in which $j = m$. Finally, it is apparent that, for $\sigma^2 \gg 1$, $p(E_1)$ and $p(E_2)$ in (39) and (40) reduce to

$$p(E_1) \simeq \frac{1}{\pi\sqrt{(1-E_1^2)}} \tag{43}$$

$$p(E_2) \simeq \frac{1}{\pi\sqrt{(1-E_2^2)}} \quad . \tag{44}$$

Thus

$$p(E_1,E_2) \simeq \frac{1}{\pi^2\sqrt{(1-E_1^2)}\sqrt{(1-E_2^2)}}\left\{1 + 2\sum_{j=1}^{\infty} T_j(E_1)T_j(E_2)\exp\left[-j^2\sigma^2[1 - r(\xi)]\right]\cos jb\xi\right\}. \tag{45}$$

Note that, since the densities in (37), (39), and (40) contain the variable x, the one-dimensional and joint densities are non-stationary, in the general case. This is fundamentally, a result of the fact that the phase in (20) is not uniformly distributed. Since the assumption $\sigma^2 >> 1$ amounts to considering uniformly distributed phase, the densities in (43), (44) and (45) become stationary, and are consequently much easier to manipulate. Although, in practice, a fading signal may often be characterized by a stationary probability density, experience shows that such an assumption is frequently not justified. In such cases there is no alternative to the use of the more general densities in (37), (39), and (40).

Where the use of the stationary representation is valid, (45) may be further simplified by noting the following property of the Tchebychev polynomials:

$$T_j(E) = \cos j\delta \tag{46}$$

$$\text{where} \qquad E = \cos\delta \ . \tag{47}$$

Then (45) may be written

$$p(E_1,E_2) = \frac{1}{\pi^2 \sin\delta_1 \sin\delta_2}\left\{1 + \tfrac{1}{2}\sum_{q=1}^{4}\sum_{j=1}^{\infty}\cos ja_q \exp -j^2\sigma^2[1 - r(\xi)]\right\}, \tag{48}$$

$$\left.\begin{aligned} \text{where } a_1 &= \delta_1 - \delta_2 + b\xi \\ a_2 &= \delta_1 + \delta_2 + b\xi \\ a_3 &= \delta_1 - \delta_2 - b\xi \\ a_4 &= \delta_1 + \delta_2 - b\xi \ . \end{aligned}\right\} \tag{49}$$

The infinite series appearing in (48) has been summed numerically, using an IBM 7094 computer, and is illustrated in Figure 3. The series, however, is rapidly convergent under the assumed conditions and may, for many purposes, be well approximated by its first term (i.e., $j = 1$). When this is permissible, the density, after some reduction, degenerates to

$$p(E_1,E_2) \simeq \frac{2E_1E_2\cos b\xi\, e^{-\sigma^2[1 - r(\xi)]}}{\pi^2\sqrt{(1-E_1^2)}\sqrt{(1-E_2^2)}} \ . \tag{50}$$

Relations (45), (48), and (50) are valid for large phase variance, i.e., $\sigma^2 >> 1$, and for $r(\xi)$ not too close either to 0 or 1. It is of interest to consider now the limits approached when $r(\xi)$ tends to zero and unity respectively.

(i) When $r(\xi) \to 0$, E_1 and E_2 are nearly independent and

$$p(E_1,E_2) \to p(E_1)\ p(E_2)$$

$$= \frac{1}{\pi^2\sqrt{\{(1-E_1^2)\ (1-E_2^2)\}}} \ . \tag{51}$$

(ii) For $\sigma^2 \gg 1$ and $r(\xi) \simeq 1$, i.e., $\sigma^2[1-r(\xi)] \simeq 0$, the distribution reduces approximately to a family of ellipses,

$$E_1^2 + 4E_1E_2 \frac{\cos b\xi}{\pi^2 K} + E_2^2 = 2 , \qquad (52)$$

where K is a specified value of $p(E_1,E_2)$. The ratio of the axes is

$$\sqrt{\left\{\frac{K\pi^2 + 2\cos b\xi}{K\pi^2 - 2\cos b\xi}\right\}} .$$

5. COMPARISON WITH EXPERIMENT

Equations (10), (19a), (48), and (50) represent results which might be compared with suitable experimental data, under the conditions for which the initial assumptions are valid. Using a sufficient number of receivers, b, σ^2 and $r(\xi)$ might thus be estimated. The main limitation is the necessity for quasi-stationarity, represented by the requirement that the spatial rate of change of phase modulation be small compared to the spatial frequency. Clearly, this condition is not always met, so that some selection of data is necessary. From very limited experience, however, it appears that the results derived may be of some use, even when this requirement is not strongly satisfied. It should be noted that, since the form of the distribution (50) does not depend on the parameters of the medium, but only its amplitude, measurements at two locations will not, in general, be sufficient. This does not apply, however, to the limit represented by (52).

5.1 Experimental Details

The experimental arrangement which was available at the time of writing was not well suited for this comparison, since it was designed for another purpose. Nevertheless, several different baseline lengths were used simultaneously, so that some limited information has been gathered. The 136 MHz transmissions from the geo-stationary satellite ATS-3 were recorded continuously at a number of receiving locations, arranged as shown in Figure 4. Similar observations of the 136 MHz transmissions from the geo-stationary satellite, Canary Bird, were also recorded at two of these sites (150 ft dish and the lower Yagi) as well as at the locations shown in Figure 5. Note that the dimensions of the two arrays differ by roughly an order of magnitude. The detector characteristics were similar and approximately linear over most of the fading range but approached square-law at very low levels. No compensation for this low level behavior has been made in the subsequent analysis, although this would be necessary in a more precise study.

Data were recorded on multi-channel magnetic tape, at a central location, and converted to digital form. Selected samples of data were subjected to spectral analysis, and those displaying pronounced spectral features were analyzed to determine the appropriate probability densities. As a further selection criterion, only those records were chosen for which a reasonably confident estimate could be made of the drift velocity of the medium. This was done by applying the so-called "full correlation" analysis, and rejecting data which exhibited inconsistencies. Furthermore, only those records were selected which, while displaying a sinusoidal component, were immediately preceded and followed by periods with no such periodic component, and which gave consistent velocity estimates. Thus, in the attempt to ensure satisfaction of the initial assumptions, while still retaining reasonably reliable secondary information, the number of suitable data samples which resulted proved to be very small.

Figure 6 shows a short sample of the analog records of ATS-3 from two receivers, separated by 200 m, in the two upper traces. The lower trace shows the time variation of the cross-correlation coefficient, calculated by an analog computer, although the remainder of the results reported here were computed digitally. There is a well defined periodic component

present, with a period of approximately 17 seconds (note that the cross-correlation coefficient record, due to the method of computation, is symmetrical about its mid-point). Since the drift velocity at this time was approximately 65 m sec^{-1}, the parameter $L \simeq 1100$ m, which considerably exceeds the receiver baseline, if the sinusoidal component is presumed to move with the mean drift velocity. From (10), since b and ξ are known, the correlation coefficient of the random component, averaged over the time interval shown, is approximately 0.9. Thus, although the characteristic dimension associated with the random component cannot be accurately estimated from this single measurement, the approximation represented by (52) appears to be tolerably well satisfied. Figure 7 shows the computed joint probability density for a 15-minute data sample, incorporating the smaller sample of Figure 6. E_1 and E_2 are plotted in arbitrary units and are approximately normalized to the same scale. The contours are the loci of points of constant joint probability, and are seen to be of rather closely elliptical form, aligned in the direction shown by the straight line. This is the behavior expected if (52) is, in fact, valid. However, the value of σ^2 appropriate to this distribution is $\sigma^2 \simeq 4.5$, so that the requirement of large phase deviation is only poorly satisfied. Furthermore, the anisotropy of the ground pattern immediately before and after the period under discussion was approximately 1.8, so that the requirement for one-dimensional geometry is also poorly satisfied.

To examine the other limit represented by (51), a sample of Canary Bird data was analyzed, which showed characteristics, on the 120 m baseline, very similar to Figures 6 and 7. However, in this case, the data from the 10 km baseline were also available, and the joint density is shown in Figure 8. Clearly, there is no resemblance between this result and the predicted distribution (51). The square root terms in the denominator of (51) reflect critically the regularity of the peaks of the periodic component. It is apparent that these peaks, in the recorded data, are sufficiently poorly defined, and that there is sufficient amplitude variation along the long baseline, to wash out the sinusoidal characteristics in the probability distribution. What remains is simply the joint distribution of two effectively independent random variables.

An intermediate case, which might be supposed to correspond to (45) or (50), has been selected and its joint probability density is shown in Figure 9. In this sample, the computational resolution has been improved by a factor of 2 over the previous examples These data are from the 200 m baseline recordings of ATS-3, with $L \simeq 600$ m, and $r(\xi) \simeq 0.6$. The anisotropy of the ground pattern was approximately 2.0, and the "quasi-stationarity" requirement was not well satisfied, since the characteristic scale of the random component was of the same order as the periodic component. Figure 9, nevertheless, shows some tendency to conform to the distribution (45), especially in the lower left corner, where the bulk of the distribution lies. The effect of the square root factors, although distorted, is discernible. However, the distribution is asymmetrical, which is caused, at least partially, by the signal level frequently exceeding the dynamic range of the recording tape, owing to intense scintillation activity. Because of these limitations, no attempt has been made to fit the computed distribution to the data, since the effort involved would scarcely be warranted. However, a suitable procedure, if applied to data of good quality, could yield estimates of b and $\sigma^2[1 - r(\xi)]$. If σ^2 were independently estimated, for example from the considerations in Section 3, then $r(\xi)$ could be found, and eventually the characteristic scale size of the random components.

6. CONCLUSIONS

An attempt has been made to extend the application of spaced receiver measurements of fading propagation beyond the conventional drifting-screen technique. In particular, some allowance has been made for the presence of a periodic component in the fading, which seems to be encountered frequently in practice. Of necessity, since the approach is statistical, only quasi-stationary fading is considered. A model of a one-dimensional screen was postulated, containing both periodic and random components, and the propagation in the space beyond the screen was examined. The joint probability density of the signal fading at two points in the diffracted field was derived, and various limiting cases considered. In

addition, the distribution of fading power between the periodic and random components was derived. In order to test the validity of the derived results, a comparison was attempted with some available fading data of geo-stationary satellite transmissions, recorded at spaced receivers. Although the data available were far from ideal for this purpose, there is evidence that the proposed model may be appropriate under certain circumstances. In such cases it appears possible to estimate several parameters of interest, which relate to the characteristics of the fading medium.

REFERENCES

1. Briggs, B.H. et al. Proceedings of the Physical Society (London), Vol.63(B1), p.106.

2. Gnedenko, B.V. *The Theory of Probability*. Chelsea Publishing Company, New York, 1962.

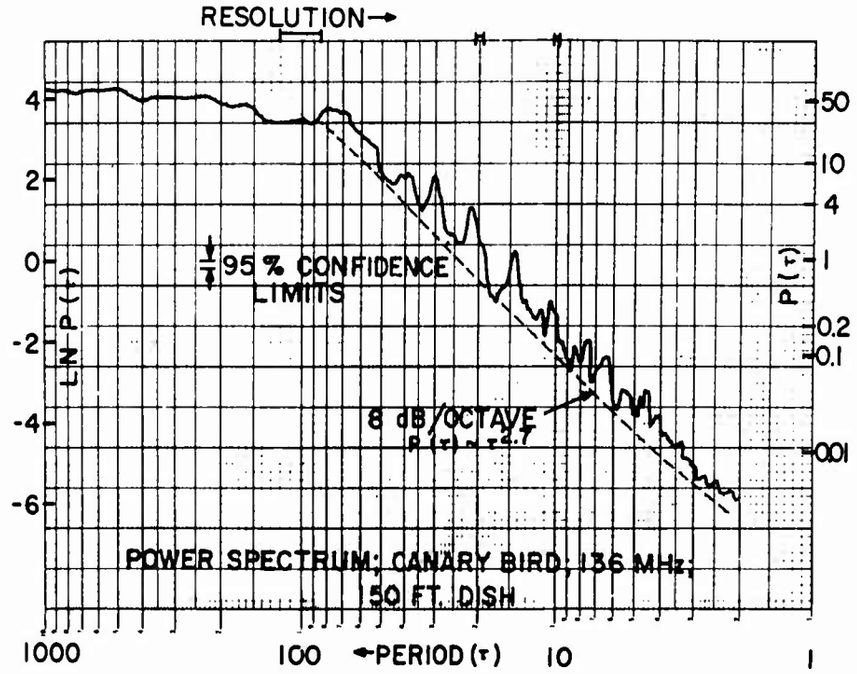


Fig. 1 Normalized power spectral density, for a one-hour sample of fading data, recorded at 136 MHz from the geo-stationary satellite, Canary Bird, using a 150 ft dish. The abscissa is fading period (seconds), while the ordinate represents power density (arbitrary units per Hz), on both logarithmic and linear scales

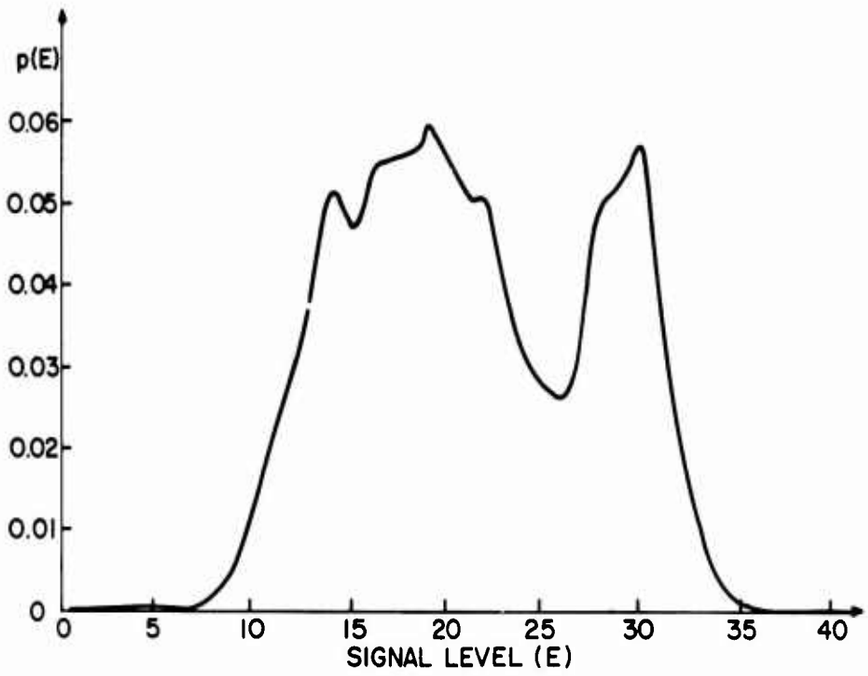


Fig. 2 Probability density computed from a data sample similar to that used in Figure 1, but exhibiting a single pronounced spectral feature. Abscissa represents signal level, in arbitrary units, while the ordinate represents the probability density per unit increment in signal level

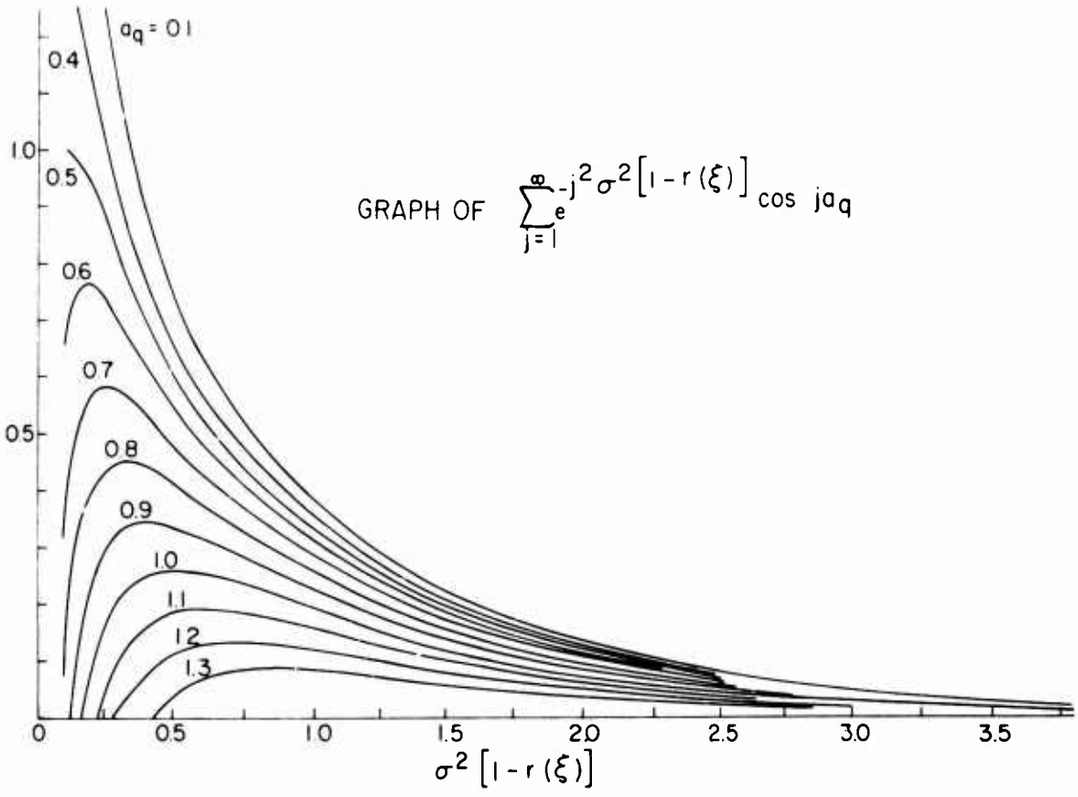


Fig.3 Computations of the infinite series appearing in Equation (48). The ordinate represents the value of the sum, while the parameters vary over the ranges indicated

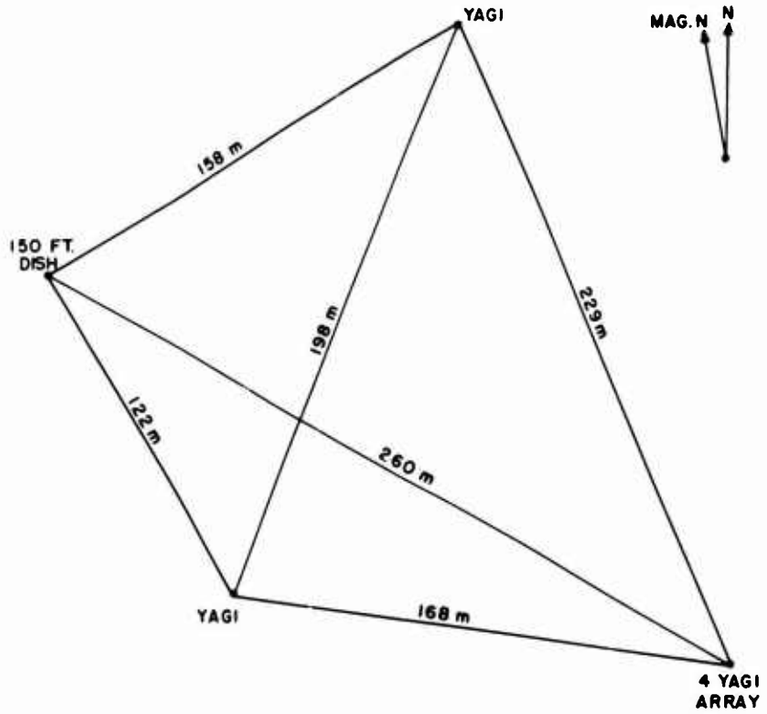


Fig.4 Short baseline receiver network used for satellite transmission reception

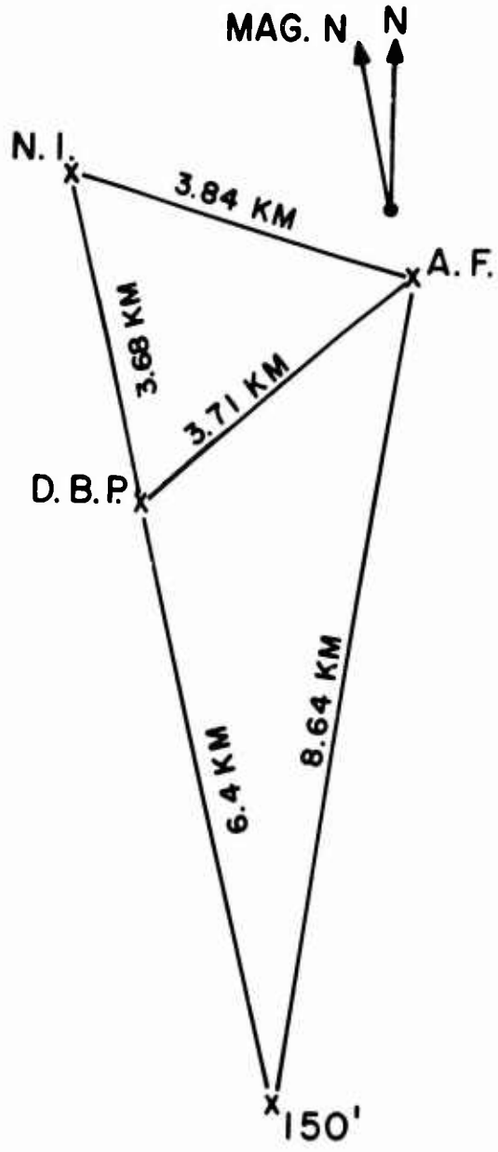


Fig.5 Long baseline receiver network

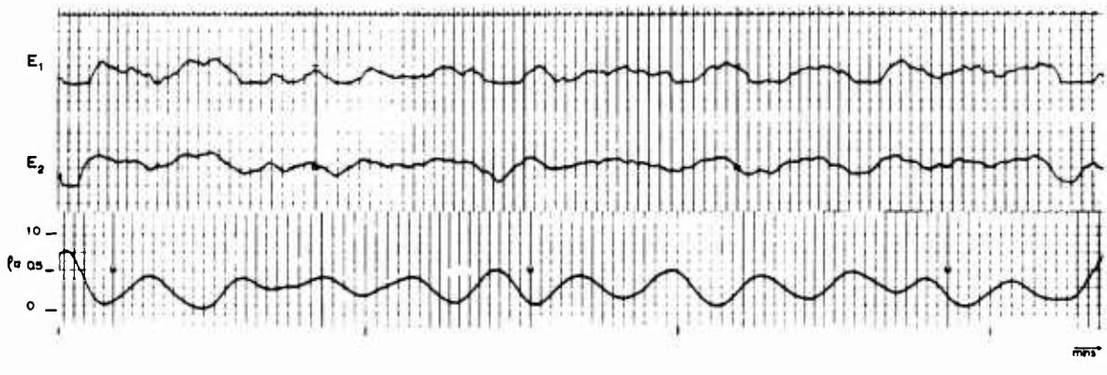
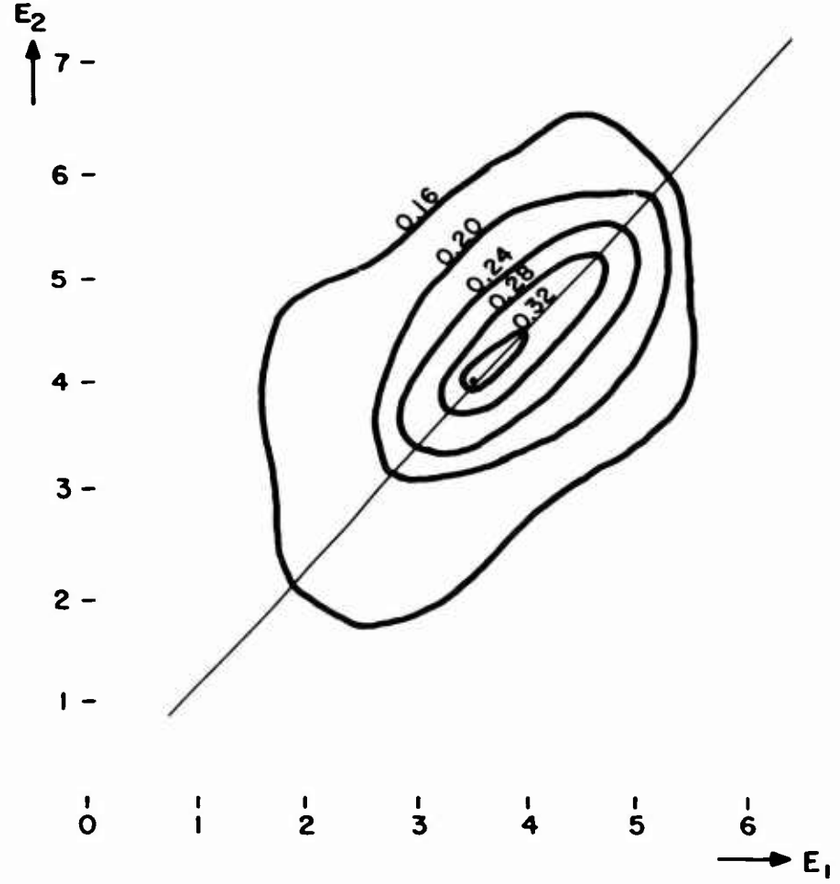
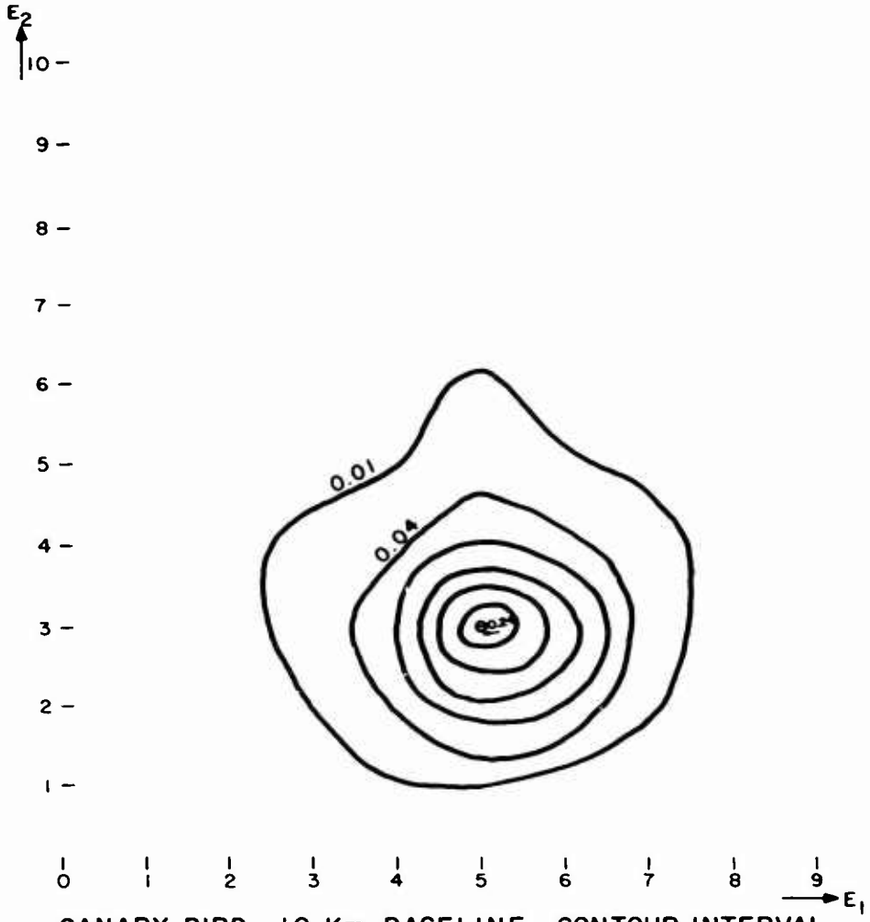


Fig.6 Short section of records from two receivers spaced 200 m apart (upper traces). Lower trace shows time variation of normalized cross-correlation coefficient. Minute marks are shown



ATS-3 200 METER BASELINE. CONTOUR INTERVAL = 0.04.

Fig.7 Joint p' 'ability density computed from two records which included the sample shown in Figure 6. Straight line shows approximate axis of distribution



CANARY BIRD 10 Km BASELINE. CONTOUR INTERVAL = 0.04.

Fig.8 Joint probability distribution from receivers spaced 10 km apart



Fig.9 Joint probability distribution from receivers 200 m apart, showing markedly different properties from Figure 7

SATELLITE SCINTILLATION AT HIGH LATITUDES

by

Jon Frihagen

Norwegian Defense Research Establishment,
Kjeller, Norway.

SUMMARY*

Results are presented of a study of satellite scintillation on 40 MHz as observed from a station on Spizbergen. There is a polar region of the ionosphere which gives rise to scintillation. This region has no observed poleward boundary, but has a southern boundary at $L \simeq 16$ during magnetically quiet days ($K_p = 0$). At night the boundary is out of range of the station ($L \leq 6$). During daytime the southern boundary is observed to be very K_p-dependent, moving out of range of the station for $K_p \geq 3$.

While the southern boundary has a diurnal motion and is K_p-dependent, the time of day or K_p does not seem to affect the depth of scintillation within the region producing scintillation.

The fading rate increases with increasing fading depth.

A model in which field-aligned irregularities are produced by soft particle precipitation is considered. Preliminary results of measurements of soft electrons have been published in References 2 and 3. Fluxes of the order of 10^{12} particles per (m^2 sec keV) at 1 keV have been observed to reach to high latitudes and they show large and rapid variation. If these variations are spatial, field-aligned irregularities must be produced. It is not yet clear whether such irregularities can account for the observed scintillation.

REFERENCES

1. Frihagen, J. — Journal of Atmospheric and Terrestrial Physics (in the press).

2. Burch, J.L. — Journal of Geophysical Research, Vol. 73, 1968, p. 11.

3. Hoffman, R.A.; Evans, D.S. — Goddard Space Flight Center Preprint X-611-67-592, 1967.

*The complete paper is published in Reference 1.

HF RADAR SIGNATURES OF TRAVELING IONOSPHERIC IRREGULARITIES

3D RAY-TRACING SIMULATION*

by

T.M.Georges and Judith J.Stephenson

Institute for Telecommunications Sciences
Environmental Science Services Administration
Boulder, Colorado 80302, USA

* A condensation of a paper to be submitted to Radio Science

SUMMARY

A technique is described for simulating a multitude of ground-backscatter displays using information supplied by three-dimensional computer ray tracing. Model ionospheres containing realistic wavelike traveling disturbances are used to produce representative displays and to correct some misconceptions about the interpretation of backscatter signatures.

HF RADAR SIGNATURES OF TRAVELING IONOSPHERIC IRREGULARITIES 3D RAY-TRACING SIMULATION

T. M. Georges and Judith J. Stephenson

1. INTRODUCTION

The usefulness of HF ground-backscatter radars in ionospheric mapping and surveillance systems depends on an ability to recognize and interpret radar echoes arising from focusing by natural ionospheric inhomogeneities. Although the first backscatter soundings of the ionosphere were made over two decades ago,[1,2] little progress towards understanding backscatter signatures in terms of ionospheric motions and structure has been evident, mostly because of the complexity of analyzing radio propagation in an irregular ionosphere. Defense applications of HF radar have stimulated renewed interest in the problem, and two recent developments hold the promise of significant progress in the future: the availability of a fast, accurate, three-dimensional ray-tracing computer program[3] and the development of some understanding of how atmospheric waves cause traveling irregularities in the ionosphere. Computer ray tracing permits rapid analysis of radio paths through arbitrary model ionospheres, while traveling disturbances have been found to play a major role in the dynamics of the ionospheric F-region and thus in modifying long-range radio paths through the ionosphere.

This paper shows how these two developments are used to create a technique for simulating and displaying on a digital computer the HF radar signatures of realistic traveling disturbances in virtually any radar-display mode. Some sample displays, constructed using model disturbances resembling atmospheric gravity waves, show features that are commonly observed, but also show that conventional interpretations of these signatures can lead to gross errors in estimating irregularity structures and motions. The simulation technique is not restricted to traveling disturbance models, but can be applied to any three-dimensional, time-varying ionosphere.

2. IMPLICIT ASSUMPTIONS

To simplify the interpretation of the results, as well as for economic reasons, the ground-backscatter process has been idealized by the following assumptions:

(a) The effects of the earth's magnetic field (anisotropy) and electronic collisions (absorption) are neglected.

(b) Backscatter takes place via two-way, one-hop propagation over the same ray path.

(c) The ground-scatter coefficient is uniform over the surface of the earth and varies only as $\cos^n\psi$, where ψ is the angle of incidence on the earth's surface, and n is an integer taken as unity in this paper.

(d) Radio waves illuminating the ground or backscattered to the radar over diverse paths add incoherently at least when a time average is considered.

This simplified picture hopefully retains the essential features of the backscatter process while eliminating complications that may obscure the results and add little to a basic understanding of the signatures.

3. EXTENSION OF THE BACKSCATTER-AMPLITUDE FORMULA TO THREE DIMENSIONS

Croft[4,5] has laid the foundations for synthesizing backscatter echoes using ray tracing. His work is directed mainly towards understanding sweep-frequency backscatter "ionograms" and considers only ionosphere models that vary in the direction of propagation, thus precluding lateral deviation of rays from great-circle paths. Extension of his backscatter-power formula[5] to the general three-dimensional case is relatively straightforward, however.

Using arguments and notation similar to Croft's[4] but leaving the areas A_1 and A_2 (A and A' in our notation) explicitly in the formulas, we obtain, for backscattered power density,

$$S_r = \left(\frac{P_0 G \Delta\beta \Delta\phi \cos\bar{\beta}}{4\pi}\right)\left(\frac{1}{A \sin\bar{\psi}}\right)\left(\frac{\sigma A \Delta\psi \Delta\xi \cos\bar{\psi}}{4\pi}\right)\left(\frac{1}{A' \sin\bar{\beta}}\right) \qquad (1)$$

The meaning of the symbols, including some new ones that are needed to generalize to three dimensions are shown in Figure 1: ψ and ξ are the elevation and azimuth of arrival of rays at the scattering region; β and ϕ are the elevation and azimuth of rays at the radar; θ is the azimuth of the ray landing point as viewed from the radar (different, in general, from ϕ). The antenna gain and radar power are G and P_0, and $\sigma(\bar{\psi})$ is the "dimensionless radar cross-section" per unit of ground area. Bars over the angle symbols indicate average values for the flux tubes. A is the area subtended on the ground by the outgoing flux tube, and A' is the area subtended at the radar by a similar returning flux tube.

Equation (1) is put together so it can be easily understood as follows: The first factor in parentheses is the power transmitted into the outgoing flux tube $\Delta\beta\Delta\phi \cos\bar{\beta}$ at the radar, and is therefore the power incident upon A. The first two factors give the power density at A. The first three factors given the power scattered into the returning flux tube $\Delta\psi\Delta\xi \cos\bar{\psi}$ and hence the power incident upon A'. All four factors give the power density at A', the radar.

Equation (1) involves three quantities, A', $\Delta\psi$, and $\Delta\xi$, that imply the necessity for calculating raypaths back to the radar from each ground-scattering region. These factors can be eliminated by applying the relationship

$$\frac{\Delta\beta\Delta\phi \cos\bar{\beta}}{A \sin\bar{\psi}} = \frac{\Delta\psi\Delta\xi \cos\bar{\psi}}{A' \sin\bar{\beta}} \qquad (2)$$

which is a statement of the reciprocity of flux-tube divergence. The backscattered power density then becomes

$$S_r = \left(\frac{\sigma P_0 G}{A}\right)\left(\frac{\Delta\beta\Delta\phi \cos\bar{\beta}}{4\pi \sin\bar{\psi}}\right)^2 \qquad (3)$$

which contains only quantities that are assumed given or are calculated in one-way ray tracing. (The reciprocity relation (2) is strictly true only if anisotropy in the ionosphere is neglected, but is known to be very nearly correct in the real ionosphere when times averages are considered.[6])

Whereas backscatter-amplitude calculations for two-dimensional ionospheres depend only on the incremental range per increment in takeoff angle (requiring only two raypath calculations), the three-dimensional problem requires the calculation of the elemental area subtended by a four-sided flux tube on the ground. Energy conservation applies to such a flux tube, so the power density on the ground (and thus the backscattered power) is inversely proportional to the ground area intercepted, as indicated by Equation (3).

Now suppose that we calculate raypaths for a "bundle" of rays launched at regularly and closely spaced elevation and azimuth angles. The landing points of the rays on the ground will form a grid, which, if connected by great circles, will form an array of spherical quadrilaterals that accurately represent the ground areas intercepted by the flux tubes formed by each set of four adjacent rays. The area of each quadrilateral can be calculated from the coordinates of its four corners (supplied in the raypath calculations) and, with angle-of-arrival information (also supplied) one can use Equation (3) to associate a backscatter power density with each flux tube. Since group path is also one of the quantities calculated in ray tracing, one now has all the necessary tools for simulating backscatter returns.

The accuracy of the approximation that the quadrilaterals have great circles for sides of course depends on the size of the angular increments of launch angles of adjacent rays. In practice these increments have to be so small that the quadrilaterals can be considered plane, and a simple formula for the area applied: If R_1, R_2, R_3, and R_4 are the ranges to four landing points (Fig. 1), and θ_1, θ_2, θ_3 and θ_4 are their azimuths,

$$A \simeq \frac{1}{2}\left|\frac{R_3 - R_1}{\sin\alpha}\right|\left|\frac{R_4 - R_2}{\sin\gamma}\right|\sin(\alpha+\gamma), \tag{4}$$

where

$$\alpha = \tan^{-1}\left|\frac{R_3 - R_1}{\theta_3 - \theta_1}\right|\left|\frac{2}{R_3 + R_1}\right|$$

$$\gamma = \tan^{-1}\left|\frac{R_4 - R_2}{\theta_4 - \theta_2}\right|\left|\frac{2}{R_4 + R_2}\right|.$$

This amounts to calculating the area of a quadrilateral by one half the product of its diagonals times the sine of the angle between them.

In practice, an idea of the errors involved can be obtained by plotting the landing points in the (R,θ) plane and connecting them with straight lines. If the points are sufficiently dense, the straight lines provide a reasonably smooth fit, and accuracy is good; if the points are more sparsely spaced, discontinuities become apparent, and accuracy is poor. For our purposes, accurate quantitative calculations are not of major interest, so occasional errors as large as perhaps 25% would be considered acceptable in view of the increased cost of improvement.

4. CORRECTION FOR PULSE SPREADING

The foregoing calculations strictly apply only to a CW radar and do not account for the possibility that, in a pulse radar, the echo amplitude may be diminished by time spreading. Consider a pulse traveling inside a single flux tube whose end points differ in group delay from the radar. The difference in travel times of parts of the pulse in different parts of the flux tube results in time spreading in the echo and, if the total pulse energy is to remain constant, an amplitude diminution must accompany time spreading. Figure 2 illustrates how this factor is calculated. If a pulse length τ is used, and a given flux tube intercepts an area with a group-delay spread ΔT, then the echo amplitude is diminished by a factor $(\tau/2\Delta T)$ if $2\Delta T > \tau$.

5. THE MODEL IONOSPHERIC IRREGULARITIES

The model ionospheres used in these simulation studies are analytical representations of traveling ionospheric disturbances based both on actual observations of such disturbances[7,8] and on the theory of internal atmospheric gravity waves[9]. Mathematically the model can be expressed by

$$N = N_0(1+\Delta)$$

$$\Delta = \delta \exp\{-[(R-R_0-z_0)/H']^2\} \cdot \cos 2\pi \left[t' + \left(\frac{\pi}{2}-\theta\right)\frac{R_0}{\lambda_x} + \frac{(R-R_0)}{\lambda_z}\right],$$

where

R, θ, ϕ are spherical, earth-centered polar coordinates (Δ is independent of ϕ),

R_0 is the radius of the earth,

$N_0(R,\theta,\phi)$ is any electron density model,

z_0 is the height of maximum wave amplitude,

H' is the wave-amplitude "scale height",

δ is the perturbation wave amplitude,

λ_x and λ_z are the horizontal and vertical wavelengths,

t' is the time in wave periods.

The wave parameters initially used are

z_0 = 250 km,

H' = 100 km,

δ = 0.1 (A), and 0.15 (B and C),

λ_z = 100 km,

λ_x = 100 km (A), 1000 km (B) and 300 km (C),

and N_0 is a single concentric α- Chapman layer representing a daytime F-layer and given mathematically by

$$f_N^2 = f_C^2 \exp\{\tfrac{1}{2}(1 - z - e^{-z})\}$$

$$z = (h - h_m)/H,$$

where

f_N is the plasma frequency,

f_C is the critical frequency and equals 6.5 MHz,

H is the scale height and equals 62 km,

h_m is the height of maximum electron density and equals 300 km.

The models are three-dimensional and time-varying such that the waves appear to originate at the earth's North pole and converge on the South pole as time progresses. Doppler-shift calculations are also possible in the ray-tracing program if $\partial N/\partial t$ is specified as well. Figure 3 shows North-South sections of the plasma-frequency contours for the three models presently in use. Model A is believed to represent a type of "medium-scale" wave motion that is commonly present in the F-region, model C represents a larger disturbance that is seen less frequently, and model B represents a "very large" traveling disturbance that usually accompanies large magnetic storms.

In these models we do not attempt to simulate the upward bending of the waveforms above the F-layer peak, such as has been recently observed by Thome[10], but this feature should have little effect on propagation entirely below the F-layer peak.

A modified wave model has been developed, where the wave "packet" is localized in latitude and longitude as well as in height, in contrast to the models shown here, where the waves cover the whole earth. This model will be used in future studies.

6. THREE-DIMENSIONAL FOCUSING EFFECTS

To illustrate the need for a three-dimensional ray treatment, Figure 4 shows the landing-point configuration of a bundle of rays launched within a 1° azimuth sector and at elevation angles from zero to penetration. The (R,θ) plane is a slightly distorted plan view of the earth's surface in the vicinity of where the ray bundle lands. The solid lines are contours of constant azimuth of transmission (ϕ), and the dashed lines are constant-elevation (β) contours. If the ionosphere were two-dimensional, the landing points would form a rectangular grid within the dashed lines indicating $\theta = 85^{\circ}$ and 86°.

Near the bottom of the figure, the usual "skip-distance" focusing effect is seen, where $\partial R/\partial\beta\big|_{\phi}$ passes through zero. However, along the skip-distance locus, we see that the azimuthal spread is greater than the 1° that would exist in the two-dimensional case; hence there is elevation focusing, but azimuthal *de*focusing at the skip distance.

Near the $\beta = 8^{\circ}$ locus we see an example of azimuthal focusing ($\partial\theta/\partial\phi\big|_{\beta}$ passes through zero) without elevation focusing. This occurs along $\beta = .^{\circ}$ locus as well. These calculations clearly indicate that both azimuthal and elevation focusing play important roles in determining the power distribution on the ground.

Some mention should be made of the use of ray theory in the vicinity of caustics such as those caused by azimuth or elevation focusing. Clearly, ray theory breaks down in these regions, and wave optics should strictly be used to avoid the possibility of infinite power densities. The problem is avoided in calculations using finite flux tubes, where the effect is to average the power density over the landing area. In the vicinity of caustics, the areas subtended become smaller and smaller, correctly predicting the behaviour of the power density. Occasionally, however, such an area lands right on a caustic and becomes "twisted" or "folded", and the quadrilateral-area formula gives an incorrect answer. Even more rarely, two rays of a flux tube could land at exactly the same point, predicting infinite power density. Such errors are simply ignored for the present, because complicated full-wave solutions would be required to obtain the correct fields in these regions. If a large number of flux tubes is used in a given problem, the relative number of such occurrences is so small that they can be ignored and, since high accuracy is not desired in the power-density calculations, such errors are believed to be acceptable.

7. COMPUTER SIMULATION PROCEDURE

First, raypaths are calculated for rays in a bundle of interest. (Let us generalize the term "bundle" to mean a set of rays launched at adjacent azimuth and elevation angles, as well as at successive radio frequencies or times.) Pertinent information about each raypath (e.g., landing point, apogee, group delay, direction of arrival, etc.) is punched onto a computer card called a "rayset"[4]. These cards are then processed by any of several "simulation" programs for producing the simulated backscatter displays. The rayset "data" to be processed by the simulation programs are determined by the particular rayset cards they are given. Thus are determined the effective "antenna beamwidths", "scan sectors", frequencies swept and times used. Since the computer time to calculate one raypath averages less than 2 seconds, it becomes economically feasible to compute the large number of raypaths required to produce these displays.

Most of the displays of interest have group delay as an ordinate. For these displays, the backscatter-intensity information is sorted into group-delay intervals of 200 μs, simply

adding intensities whenever two or more fall into the same interval. (Only pulse-length multiples of 200 μs are allowed because of resolution limitations of the plotting scheme.) If the abscissa is azimuth (or elevation), intensity is summed at each set of azimuth (elevation)-group-delay coordinates without regard to elevation (azimuth). For these plots only single values of frequency or time are used. If the abscissa is time (frequency), backscatter intensity is summed at each set of group-delay-time (frequency) coordinates without regard to the azimuth or elevation of transmission. (Again, the azimuth and elevation values are determined by the raysets used.)

Intensity can also be plotted in the elevation-azimuth plane for a single time and frequency. Here, intensity is summed over all group delays, giving, in effect, the total backscattered energy at each set of elevation-azimuth coordinated.

The simulated displays shown here have been drawn by a CDC 3800 computer and a CDC model 280 cathode-ray-tube-display system and are photographed on microfilm. The tonal gradations are achieved by means of a special Fortran plotting routine we have devised specifically for these simulations, but which is clearly applicable to plotting functions of any two-dimensional variable[11]. The appearance of tones of different densities is obtained by plotting arrays of small dots of variable size in a manner similar to the process of half-tone printing. The quantization of the plots into small rectangular blocks of dots is a result of using finite angular (frequency or time) increments in constructing the ray bundles, and is strictly an economic measure, not an inherent property of the plotting program.

In the simulation of radar displays, any location on the earth can be chosen for the "radar". In these examples, a latitude of 40°N was used.

8. RANGE-TIME DISPLAYS

Some of the early backscatter soundings were displayed in the "range-time" mode,[1,12,13] in which the radar antenna(s) is pointed at a fixed azimuth and the echoes are used to intensity-modulate a cathode-ray display which is recorded on slowly moving film. The result is a representation of the changes in the echo structure in the group-delay-versus-time plane. The reader is referred to the references cited for examples of experimental records of this type.

Figure 5 shows some simulated range-time displays for the ionosphere model B (disturbance with 1000 km horizontal wavelength). The four panels represent ray bundles launched at four azimuth angles (in degrees east of North). The effective antenna beamwidth (azimuth spread of raysets used) is 2°. The time interval shown is two (atmospheric) wave periods. That the simulated displays qualitatively resemble experimental range-time records can be seen by comparison with Figure 9 of Tveten[13].

Because of the East-West symmetry of the ionosphere model, azimuth angles can also be regarded as indicating degrees *West* of North. However, because of the North-South asymmetry, it is not possible to deduce the appearance of southward-looking displays from the northward-looking ones. This is evident from the asymmetrical appearance of the 90-92° display.

The conventional interpretation of range-time displays is that sloping traces indicate radial velocities of traveling disturbances, downward sloping (with time) indicating an approaching disturbance, and upward sloping indicating a receding one. It is clear from the simulated displays, however, that this simple interpretation is no longer tenable, for sloping traces appear in the case where no radial velocity component of the disturbance exists, namely, at 90° azimuth. (Recall that the disturbance wavefronts are oriented East-West and travel southward.) The explanation of the sloping traces must involve modification of the skip-distance echo by the passing disturbance, in addition to the focusing effects discussed by others[13,14]. The asymmetry in the 90-92° case is caused by the forward tilt of the wavefront, a well established characteristic of traveling disturbances.

9. RANGE-AZIMUTH DISPLAYS

When backscatter sounding is carried out with narrow-beam, steerable antennas, displays of echo intensity as a function of azimuth angle can be constructed. These are displayed either in polar or rectangular coordinates with group delay as ordinate (radius). Records of this type can be seen in the works of Valverde[15], Tveten[13] and Hunsucker and Tveten[16].

Two simulated range-azimuth displays are shown in Figure 6, representing rays traced through the time-varying ionosphere model at two times, one-half (disturbance) wave period apart. Again an East-West symmetry exists, so that azimuth can be regarded as being measured clockwise or counterclockwise from north.

The conventional interpretation of range-azimuth signatures[16] has been that the signatures can be transformed into the range-azimuth plane by simply regarding the signatures as representing the shapes of the irregularity structures located at one-fourth the range indicated by their group delays. That such an interpretation can lead to gross errors can be demonstrated by taking a portion of a simulated range-azimuth display (say the azimuth sector 90-140^{0} for T = 0), interpreting it in the conventional way, and comparing the deduced irregularity structure with the ionosphere model actually used.

Such a comparison is illustrated in Figure 7, where it is seen that the irregularity structure obtained by mapping the simulated range-azimuth display into polar coordinates bears little resemblance to the plane-wave model used in the simulation.

Figure 8 shows some examples of range-azimuth backscatter signatures obtained with the high-resolution, azimuth-scan antenna array at Boulder, Colorado. These signatures have been selected for their resemblance to the simulated display (for the same azimuth sector), reproduced again at the upper left of the figure. The similarity of the simulated and actual signatures suggests that the wavelike model disturbance is at least qualitatively realistic.

10. ELEVATION-AZIMUTH DISPLAYS

As yet, no experimental backscatter soundings have been made with pencil-beam antennas that would permit backscatter intensity to be mapped in the elevation-azimuth plane. Figure 9 shows how such a map should look in the presence of large traveling disturbances. As in the range-azimuth display, the two panels represent times separated by one-half wave period in the time-varying ionosphere model. It is in this type of display that the effects of changing the ground-scatter characteristics are most marked; echoes from low elevation angles are greatly enhanced by changing the ground-scatter cross-section from a cosine dependence on the angle of incidence to a constant, independent of angle.

Again, the East-West symmetry applies, while a marked North-South asymmetry is evident in the figure.

11. OTHER SIMULATED EFFECTS

Programs and representative displays for several other backscatter presentations have been completed, but at the deadline for completion of this paper, no figures have been prepared to show them.. They will be displayed in a paper in preparation.

Range-azimuth and range-time displays that have been constructed for the other two wave model disturbances show signatures that are similar in form to those shown here, except for a scaling down of the signatures, as would be expected. A few synthetic sweep frequency and range-elevation displays have been produced, and both show resemblances to actual records of each type. Finally, another program reproduces the backscatter echo shape in the "A-scan" format – power versus time.

Another possible display output is presently under development - a map of the distorted appearance of the ground in the elevation-azimuth plane; in effect, a picture of how the ground "looks" to the radar. All the information for such a display is contained in the backscatter raysets; only the mechanics of suitably displaying this information needs to be worked out. (The inverse process, mapping the (β,ϕ) plane onto the ground, has already been accomplished, as Figure 4 has shown.)

12. CONCLUSION

This has been a report on a technique for simulating ground-backscatter displays from information supplied by three-dimensional computer ray-tracing programs. Emphasis has been on methodology and some preliminary results that indicate errors in more simplified interpretations of backscatter signature of traveling disturbances. Although attention has thus far been confined to signatures of traveling disturbances, future work will explore the effects of concentric layers, gross tilts, and other anomalies of various kinds. The ultimate objective of this work is to compile a sufficiently large collection of signatures to permit actual backscatter data to be recognized and interpreted in terms of the structure and motions of ionospheric irregularities of all kinds.

Since direction-of-arrival information is also contained on the raysets produced for backscatter simulation, little additional effort is required to extract information on the bearing and elevation fluctuations characteristic of ionospheric motions and irregularities.

Subsequent papers will report progress towards these ends.

REFERENCES

1. Hartsfield, W.L. et al. — *Backscatter Observations by the Central Radio Propagation Laboratory.* August 1947 to March 1948. Journal of Research, National Bureau of Standards, Vol.44, 1950, pp.199-214.

2. Hartsfield, W.L. — *A Comparison of CW Field Intensity and Backscatter Delay.* Proceedings, Institute of Radio Engineers, Vol.40, 1952, pp. 1700-1706.

3. Jones, R.M. — *A Three-Dimensional Ray Tracing Computer Program.* ESSA Technical Report IER 17-ITSA 17, 1966.

4. Croft, T.A. — *Computation of HF Ground Backscatter Amplitude.* Radio Science, Vol.2 (New Series), 1967, pp.739-746.

5. Croft, T.A. — *The Influence of Ionospheric Irregularities on Sweep-Frequency Backscatter.* Journal of Atmospheric and Terrestrial Physics, Vol.30, 1968, pp.1051-1063.

6. Terman, F.E. — *Electronic and Radio Engineering.* McGraw-Hill, New York, 1955.

7. Munro, G.H. — *Travelling Ionospheric Disturbances in the F Region.* Australian Journal of Physics, Vol.11, 1958, pp.91-112.

8. Georges, T.M. — *Ionospheric Effects of Atmospheric Waves.* ESSA Technical Report IER-57/ITSA-54, US Government Printing Office, 1967.

9. Hines, C.O. — *Internal Atmospheric Gravity Waves at Ionospheric Heights.* Canadian Journal of Physics, Vol.38, 1960, pp.1441-1481.

10. Thome, G.D. — *Incoherent Scatter Observations of Traveling Ionospheric Disturbances.* Journal of Geophysical Research, Vol.69, 1964, pp.4047-4049.

11. Stephenson, J.J. — *A Tonal Plotting Routine for CRT Plotters Computer Facility.* ESSA Internal Memo, 1968.

12. Silberstein, R. — *A Long-Distance Pulse-Propagation Experiment on 20.1 Megacycles.* Journal o Geophysical Research, Vol.63, 1958, pp.445-466.

13. Tveten, L.H. — *Ionospheric Motions Observed with High-Frequency Backscatter Sounders.* Journal of Research, National Bureau of Standards, Vol.65D, 1961, pp.115-127.

14. Surtees, W.J. — *An Approximate Synthesis of HF Backscatter Considering Ionospheric Motions.* Radio Science, Vol.3 (New Series) 1957, pp.57-67.

15. Valverde, J.F. — *Motions of Large-Scale Traveling Disturbances Determined from High-Frequency Backscatter and Vertical Incidence Records.* Stanford Electronics Laboratories, Scientific Report, No.1, 1958.

16. Hunsucker, R.D. Tveten, L.H. — *Large Traveling Ionospheric Disturbances Observed at Midlatitude Utilizing the High-Resolution HF Backscatter Technique.* Journal of Atmospheric and Terrestrial Physics, Vol.29, 1967, pp.909-916.

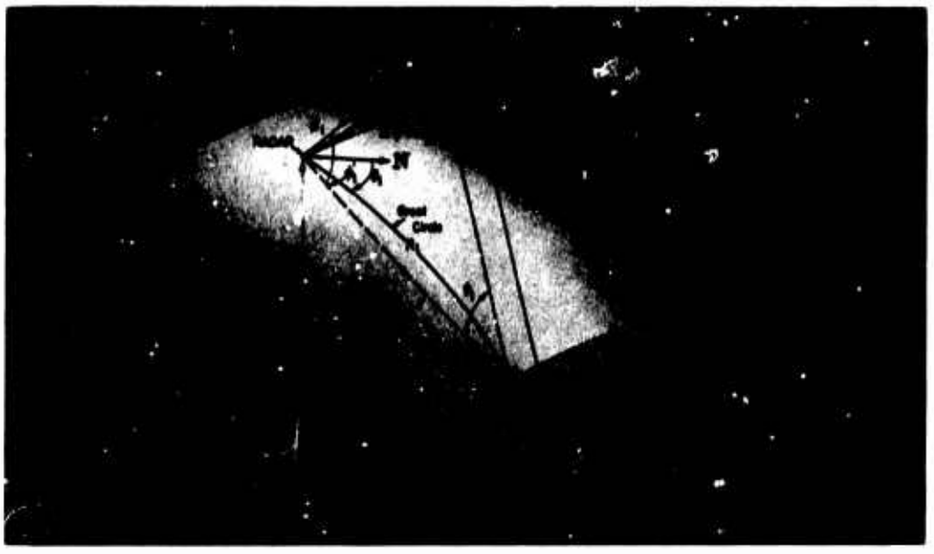


Fig. 1 Geometry of an outgoing flux tube bounded by four rays.

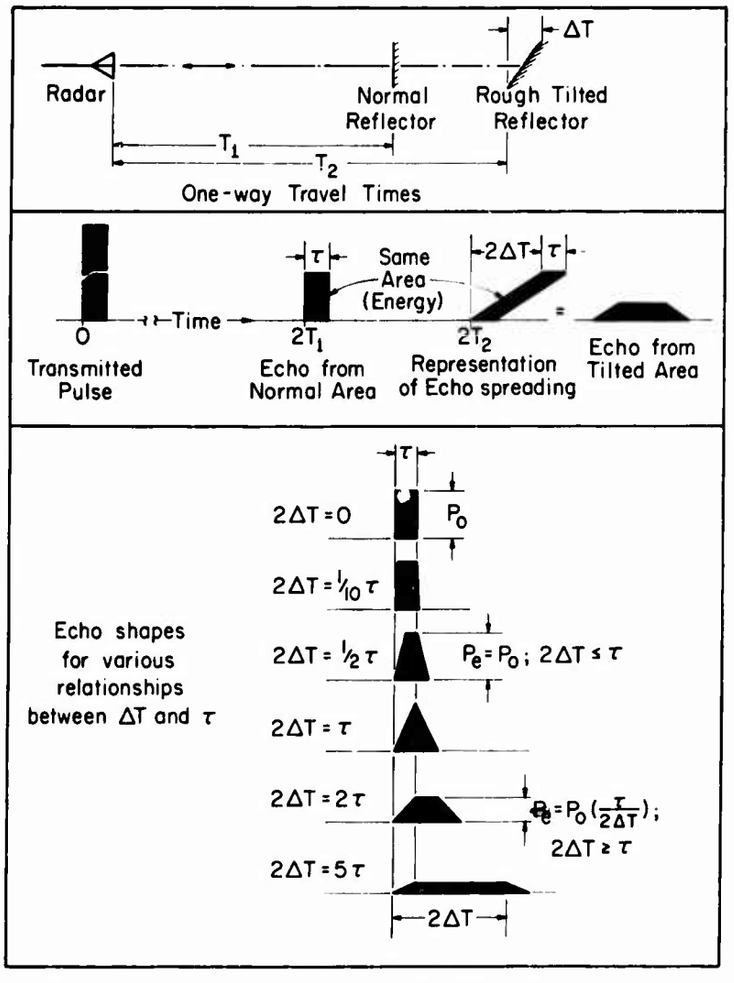
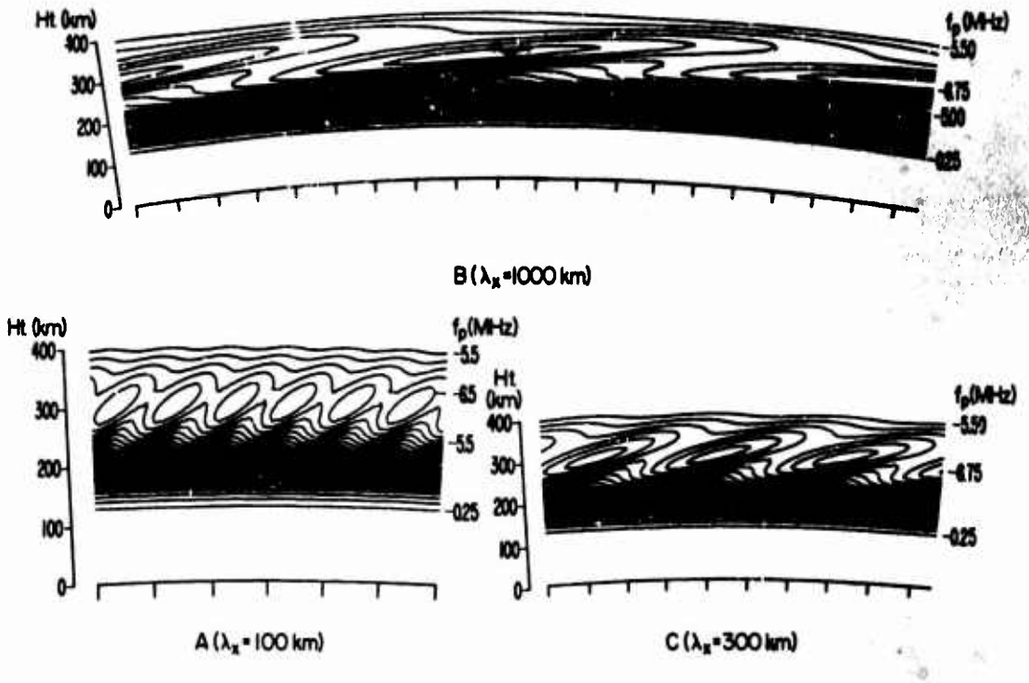


Fig. 2 Illustrating the calculation of the pulse-amplitude correction factor to account for group-delay spreading.



PLASMA-FREQUENCY CONTOURS FOR THREE MODEL IONOSPHERES
(Horizontal Scales: 100 km per Division)

Fig. 3 Idealized model ionospheric traveling disturbances. The plane of the figure is the North-South plane, and the pattern moves to the right with time

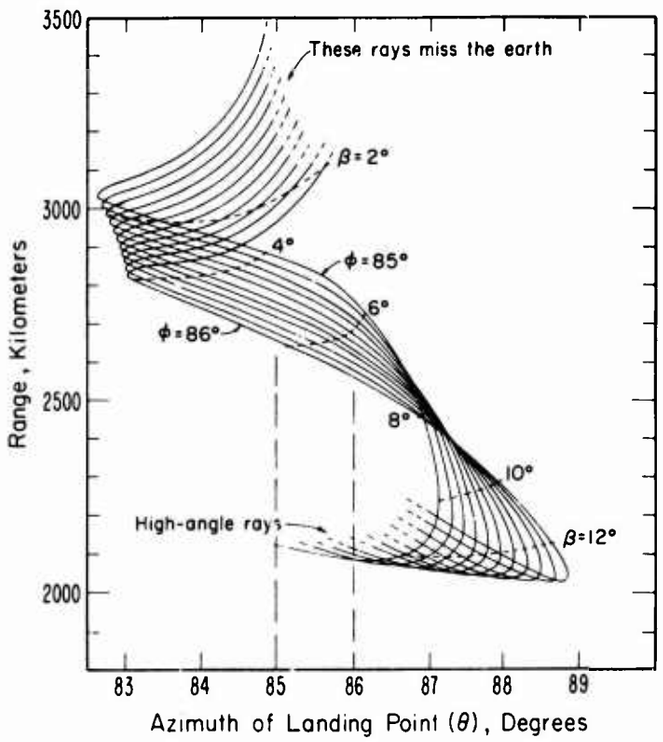
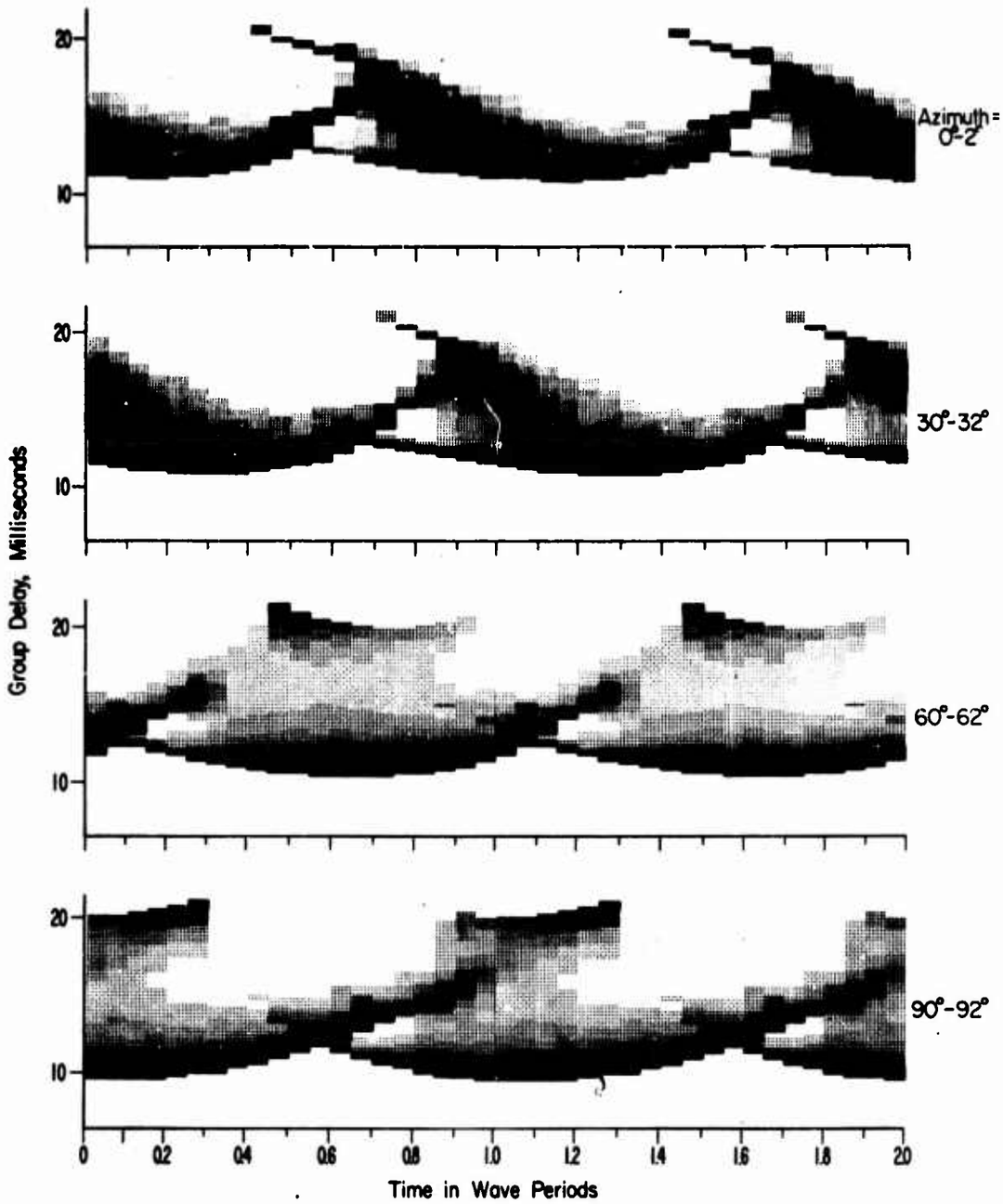
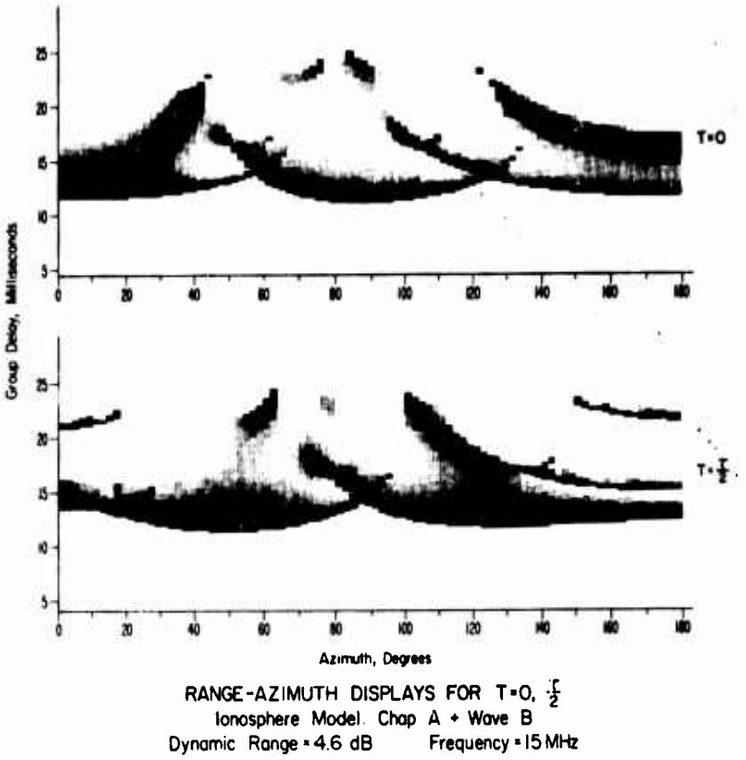


Fig. 4 Showing the distortion of a flux tube of rays as it intercepts the ground. The solid lines are constant ϕ contours; dashed lines, constant β.



RANGE-TIME DISPLAYS FOR FOUR AZIMUTHS OF TRANSMISSION
Ionosphere Model: Chap A + Wave B
Dynamic Range = 6 dB Frequency = 15 MHz

Fig. 5 Synthetic range-time backscatter



RANGE-AZIMUTH DISPLAYS FOR T=0, $\frac{T}{2}$
Ionosphere Model: Chap A + Wave B
Dynamic Range = 4.6 dB Frequency = 15 MHz

Fig.6 Synthetic range-azimuth backscatter

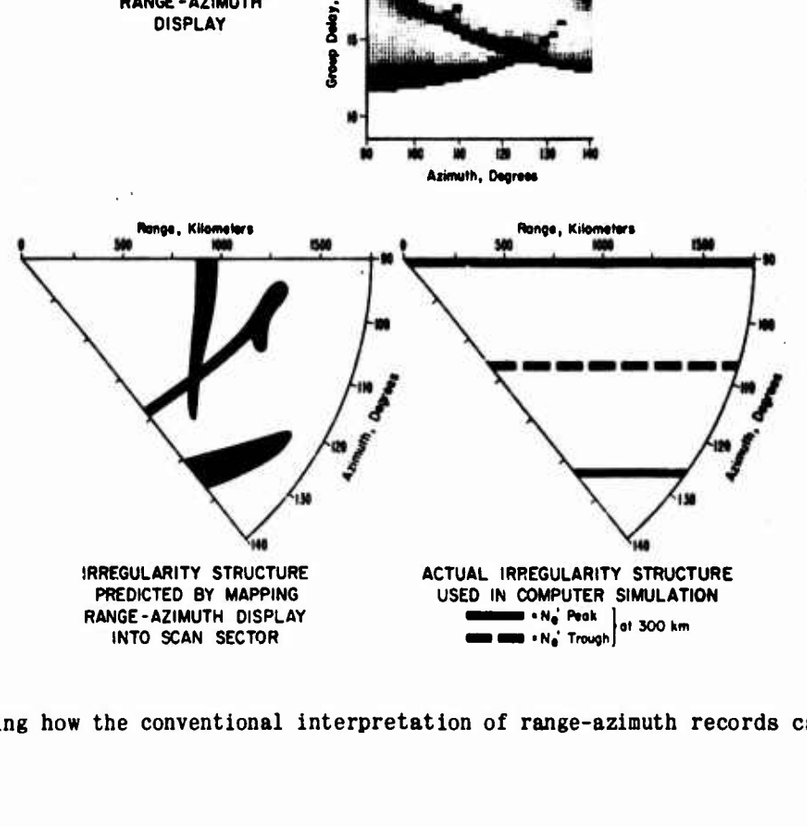


Fig.7 Showing how the conventional interpretation of range-azimuth records can be in error.

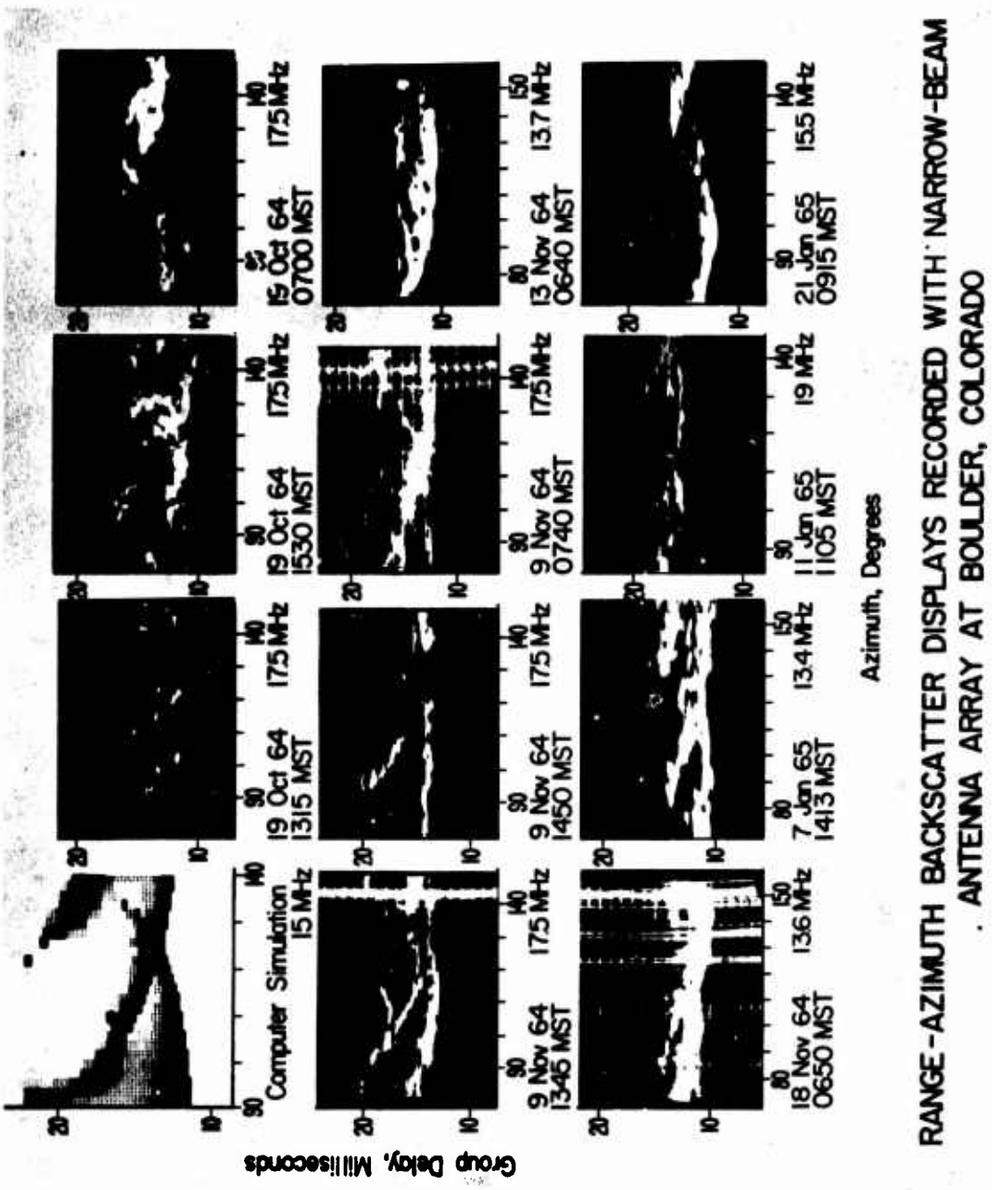
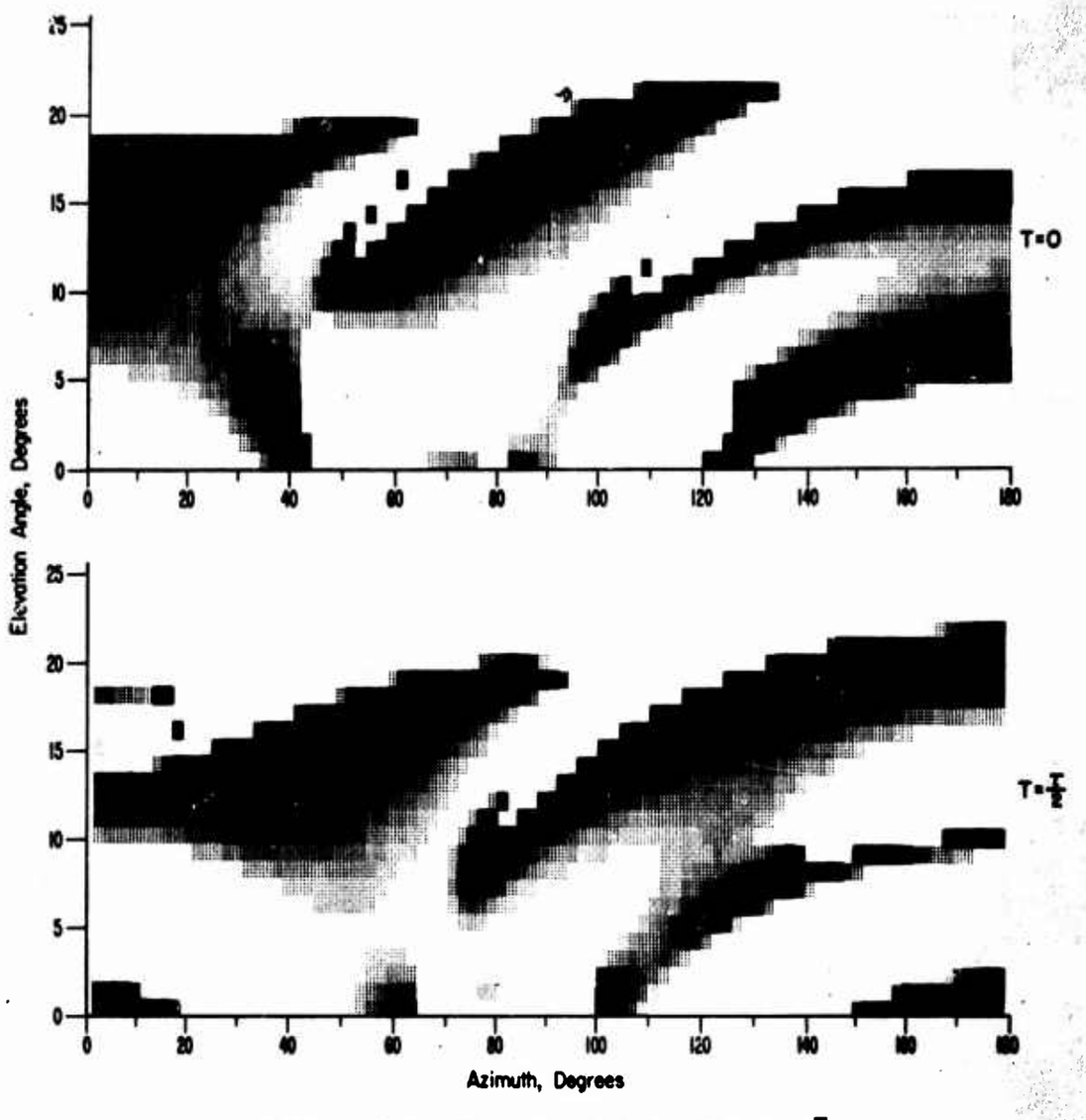


Fig. 8 Showing the resemblance of a sample simulated display to actual range-azimuth backscatter data



ELEVATION-AZIMUTH DISPLAYS FOR T=0, $\frac{T}{2}$
Ionosphere Model: Chap A + Wave B
Dynamic Range = 4.6 dB Frequency = 15 MHz

Fig. 9 Synthetic elevation-azimuth displays

NATURE OF F-REGION IRREGULARITIES INFERRED FROM OBLIQUE REFLECTION MEASUREMENTS

by

L.C.Humphrey*, C.R.Roberts* and R.Mather†

* General Electric Company,
Electronics Laboratory,
Syracuse, New York 13201

† EMASA, Rome Air Development Center,
Griffiss Air Force Base, Rome, New York 13440

SUMMARY

It is well known that the long-term fading statistics of ionospherically reflected radio waves are not Rayleigh distributed, as would be expected on the basis of interference from a collection of random scatterers. Measurements on a long-distance single-hop oblique forward ionospheric reflection path indicate that strong focusing effects associated with ionospheric irregularities upset stationarity for periods longer than a few minutes. The nature of the irregularities can be inferred from the characteristics of ionospherically reflected waves.

In this paper the data from two types of measurements are described which reveal the nature of both long-term and short-term irregularities, including traveling ionospheric disturbances. These measurements are the fading characteristics themselves, and the measurement of apparent azimuth of arrival on the long-distance path. The strength, curvature, and extent of the irregularities are deduced from the measurements.

NATURE OF F-REGION IRREGULARITIES INFERRED FROM OBLIQUE REFLECTION MEASUREMENTS

L.C.Humphrey, C.R.Roberts and R.Mather

1. INTRODUCTION

It has been known for some time that the fading characteristics of ionospherically reflected HF radio waves are not Rayleigh distributed, as would be expected on the basis of a superposition of a steady signal with small randomly phased components[1]; and, in fact, the statistics do not appear to be stationary for periods over ten minutes. In some measurements (independent from fading statistics) described in this report, it appears that the fading characteristics depend on interference between ionospherically focused radio waves. This conclusion may be reached by examining selected amplitude records which exhibit strong focusing gains and apparent azimuth of arrival records which exhibit properties of interference fields of focused components.

2. EXPERIMENTAL PROGRAM

The path on which the data described herein were measured is shown in Figure 1. It is essentially a 3760 km path oriented in a North-South direction with the transmitter in the Panama Canal Zone and the receiver in upstate New York. The total transmission loss in dB between transmitter and receiver was determined by accurately measuring power delivered to the antenna at the transmitter and the power delivered to the receiver, both in dBw, and subtracting. The antenna gain patterns, including line and foreground loss, were determined as a function of elevation angle of arrival. The elevation angle of arrival was estimated from the propagation time, so that the total propagation loss could be estimated by adding the total transmission loss to the antenna gain.

The transmitted pulses were coded to provide essentially 10-microsecond time resolution. This permitted separation of the various ionospherically reflected modes for examination. The modes were identified by comparison with oblique ionograms obtained on the same path. Received signal power for up to four modes was continuously recorded on a paper chart recorder.

A number of other measurements were carried out over this path, but the one with which we are concerned (in addition to loss) is the apparent azimuth of arrival. This made use of a gated phase detector which essentially measured the phase difference between two antennas lined up transverse to the path. This electrical phase difference for each mode was continuously recorded on a paper chart.

3. GEOMETRIC FOCUSING EFFECTS

An example of a signal anomaly which has been attributed to geometric focusing is shown in Figure 2. This figure shows the total power loss for a one-hop F reflection between that delivered to the transmitting antenna and that delivered by the receiving antenna with the free-space spreading loss (assuming unity gain antennas) subtracted. The striking feature here is the large negative value of this loss, which implies a gain above that which would be expected for reflection from a planar ionosphere. Some of this gain may be attributed to antenna gain. Since there is some uncertainty of elevation angle of arrival

under disturbed conditions, an upper bound of antenna gain is used which is the sum of the peak gains (in dB) of the transmitting and receiving antennas. This peak gain is shown in Figure 2 by the dotted line, and it is seen that there is about 7 dB signal gain above thi. Since there is also some expected ionospheric absorption, as shown by the dashed line, there appears to be some 15 dB signal gain over reflection from a flat surface. This effect, while not consistently present, did appear two to four days a month, usually around noon, with durations of one or two hours, as shown typically by Figure 2.

The high signal level was clearly evident on the record when compared with other modes (2 hop E, 2 hop F, etc.) and this, coupled with equipment tests, ruled out instrumental errors. Two natural explanations of the anomaly came to mind - guided modes and ionospheric focusing. The guided-mode hypothesis required well-defined ionospheric tilts at both ends of the path, which were considered more improbable than the frequency of occurrence would indicate. However, the focusing hypothesis would require only a slight change in ionospheric curvature since, with low-angle reception, the receiver is very near a focusing point for a concentric ionosphere. Figure 3 shows the caustic surface for reflection from the inside of a spherical surface representing the ionosphere. For horizontally transmitted waves ($\theta = 0$) at T, the focal point is at H and represents rays arriving horizontally. Unless antenna gain is compensated for, the effect of this focus is not normally observed because of the low gain of HF antennas in the horizontal direction. However, if the ionosphere is curved slightly more than the earth, the focused rays arrive at positive angles with respect to the horizon where antenna gains are higher, as shown in Figure 4. This is illustrated in Figure 5, which shows the equal gain contours in the vicinity of the horizon focusing cusp. For a concentric ionosphere, the high gain contours lie along the earth's surface where antenna gain is low. However, for increased ionospheric curvature, the contours are tilted so that high antenna gains are applicable. The fact that these disturbances occurred near noon may be attributed to the higher ionospheric height at the time, so that a positive arrival angle prevailed. When conditions were right for the higher ionospheric curvature, the high gains were observed.

4. AZIMUTH OF ARRIVAL EFFECTS

The apparent azimuth of arrival (AOA) is measured by means of a phase-detecting interferometer that essentially measures the phase difference of the signal arriving at the spaced antennas. A typical record of the phase difference for a one-hop F mode, along with the simultaneous amplitude record, is shown in Figure 6. The most striking feature is the rapid change in phase that occurs with some, but not all, the nulls in the amplitude record. There are a number of models that may account for this behavior, but the one we believe to be the simplest and most likely for this to be attributed to is illustrated in Figures 7 and 8.

Figure 7 shows the wavefronts that would be expected due to interference between a strongly focused disturbance and a uniform field. Two situations of relative phase are shown, one where the disturbance wavefronts are separated less than a half wavelength in front of the uniform field wavefront and one where it leads by more than a half wavelength. The directions of the resultant phase fronts are seen to change rapidly as the half-wavelength position is crossed. This may be seen in more detail in Figure 8, which shows the phasors in the region of the high-amplitude gradient of the disturbance. The resultant phasor is seen to vary very rapidly in direction in the vicinity of the null, even though the phase variation of the disturbance itself is small with respect to the undisturbed field. In addition, the gradient in amplitude provides a significant phase variation laterally, so that large shifts in apparent angle of arrival occur.

This mechanism accounts for the null that occurs simultaneously with rapid AOA variations. From the records examined to date, a null has occurred with every rapid AOA change. However, there are some nulls that occur without an AOA change, as may be seen in Figure 6. These may be attributed to other fading mechanisms, such as interference between magneto-ionic modes, defocusing effects, or interference between non-focused fields.

It should be noted that these effects will be emphasized for conditions where the interfering signals are of nearly the same amplitude, the maximum phase offset being approximately proportional to the ratio of the amplitude gradient to amplitude difference. The mechanism, then, tends to select those cases where the amplitudes of the interfering signals are nearly equal, but in these cases it should be noted that there are strong gradients of amplitudes, which implies focusing.

There are other mechanisms that can result in angle fluctuations that do not require the gradient hypothesis. One of these is described by Hayden[2], in which interference is observed between two rays at different azimuthal angles of arrival. With this type of interference, however, the severe fluctuations are in one direction at a time, rather than having the bidirectional characteristic shown here. Azimuth variations with these characteristics have also been observed with this experiment.

5. CONCLUSIONS AND REMARKS

On the basis of observations described, it appears that the ionospherically reflected field on an individual mode is actually a resultant of two or more components, some of which are subject to geometric focusing. The non-stationarity of the fading statistics can be attributed to long-term focusing effects, as can the non-Rayleigh statistic. It is suggested that future statistical analysis include the focusing effects described here. The effects described have also been observed on North and North Atlantic paths of similar distances, such as Central New York to Iceland and Thule.

ACKNOWLEDGEMENT

The work reported in this paper was performed under Air Force Contract AF 30(602)3946 with the Rome Air Development Center.

REFERENCES

1. Balser, et al. — *Some Statistical Properties of Pulsed Oblique HF Ionospheric Transmissions.* Journal of Research, National Bureau of Standards, D. Radio Propagation, Vol.66-D, No.6, November-December 1962, pp.721-730.

2. Hayden, E.C., — *Semi-Basic Problems in the Determination of the Angle of Arrival of Radio Waves.* PhD Dissertation, University of Illinois, September 1958.

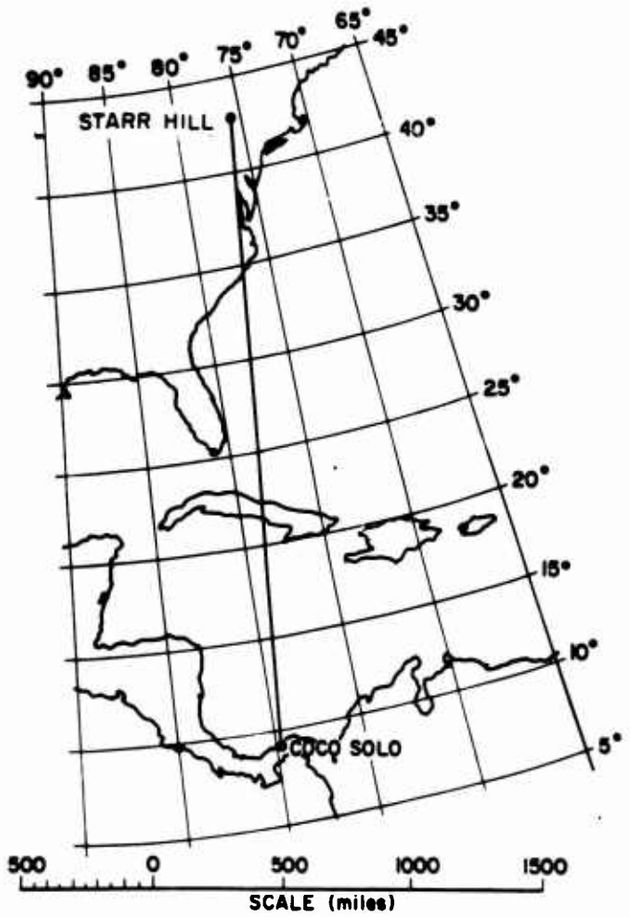


Fig. 1. Central New York-to-Panama propagation path

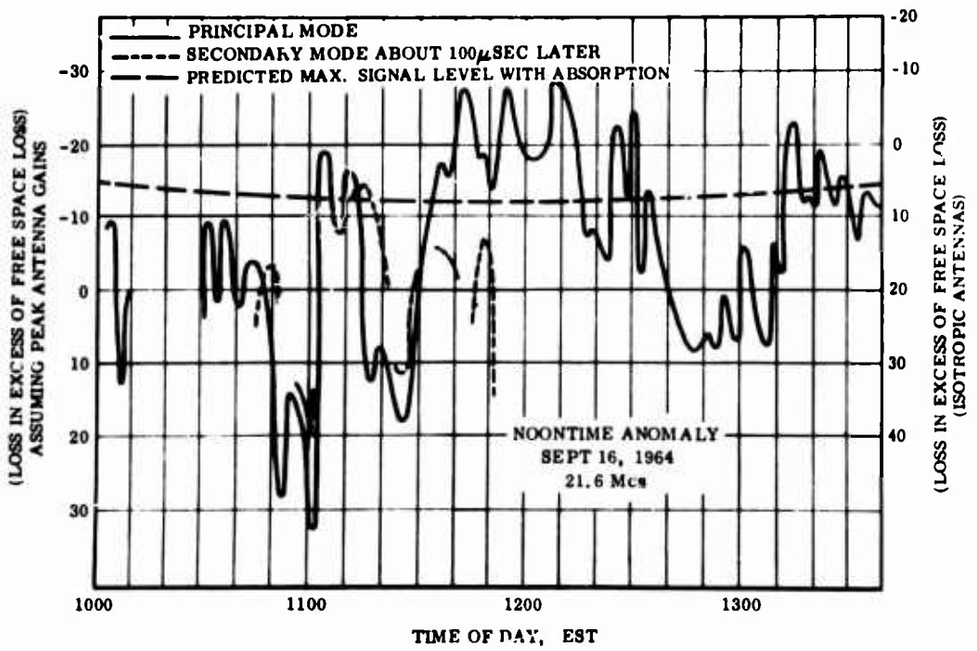


Fig. 2. Noontime anomaly showing geometric focusing

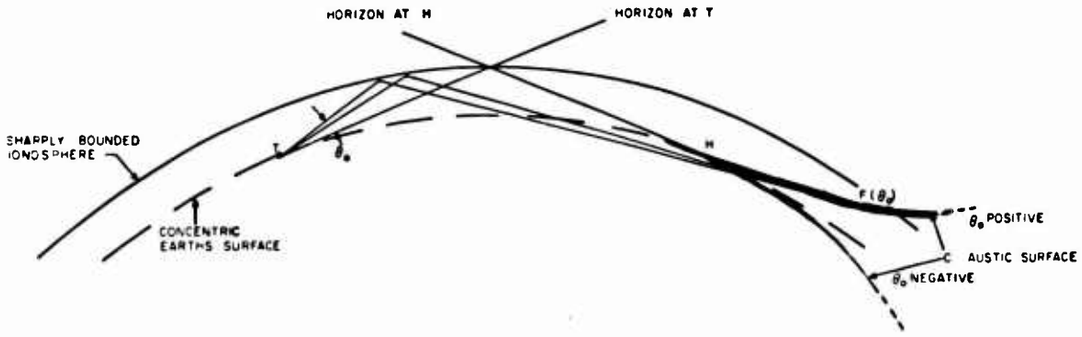


Fig.3. Caustic surface in diameter plane

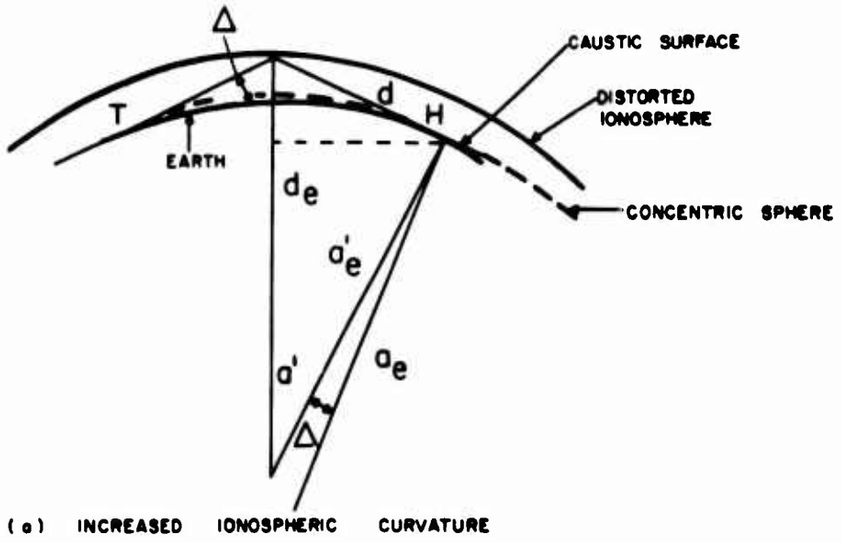


Fig.4. Ionospheric distortion required for high gain disturbance

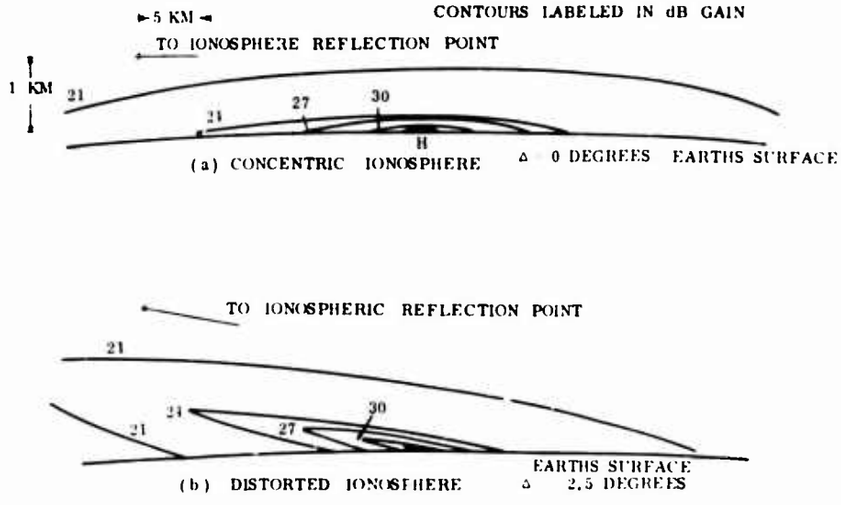


Fig.5. Effect of increased ionospheric curvature

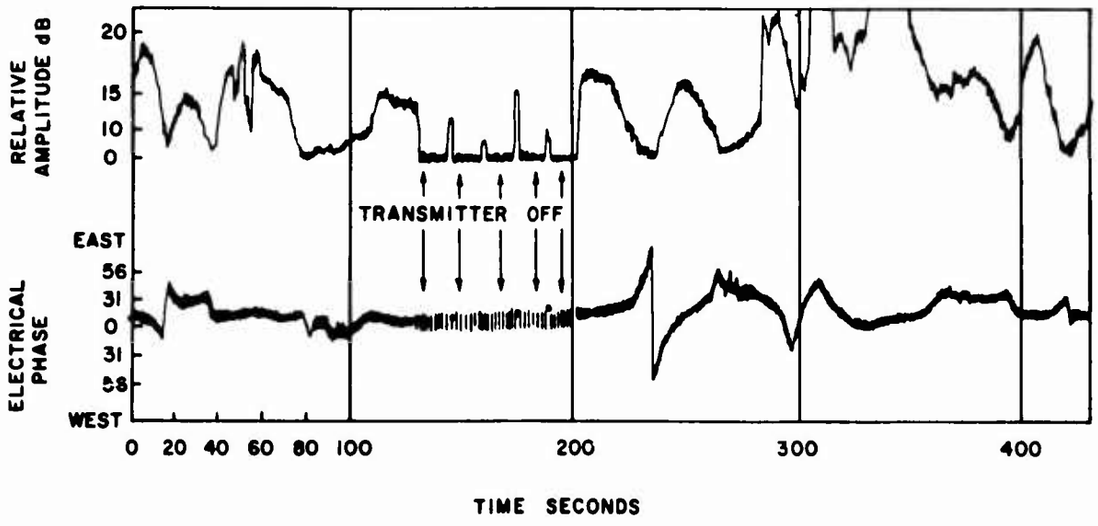


Fig.6. Phase (apparent angle of arrival) and amplitude measurements of the one-hop F mode

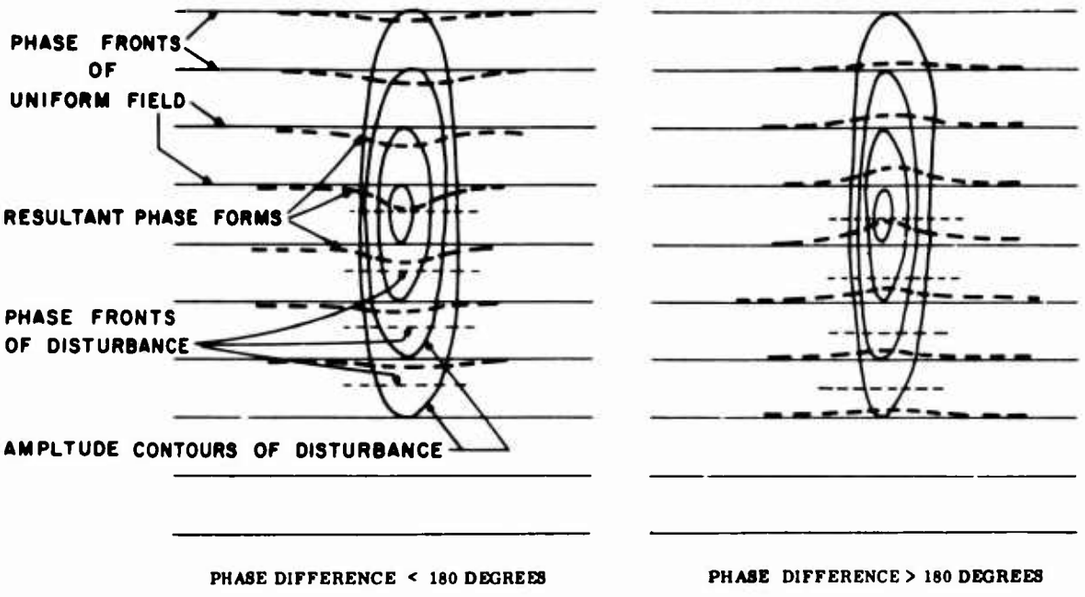


Fig.7. Wavefronts resulting from interference between a focused disturbance and a uniform field

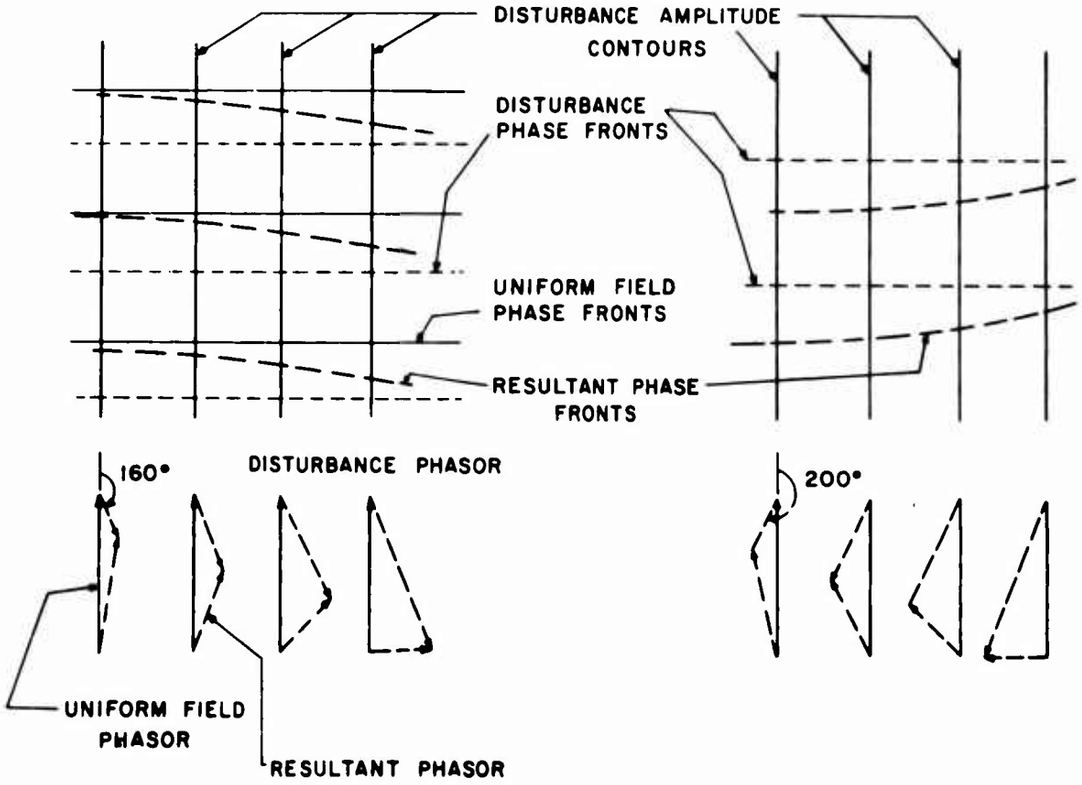


Fig.8. Phase diagram of disturbance effect

DISCUSSION ON THE PAPERS PRESENTED IN SESSION VI (F-REGION SCATTER).

Discussion on Paper 53, "Joint probability density of signal fading at spaced receivers", by T.J.Elkins.

Dr E.N.Bramley: What distance from the screen was assumed in your diffraction pattern calculations, Mr Elkins? The scale of the diffraction pattern does vary with distance from the screen, within the Fresnel zone, for both shallow and deeply modulated phase screens.

Mr T.J.Elkins: The distance was assumed to be smaller than the Fresnel distance, $Z_R = L^2/\pi\lambda$, and the model chosen was that of a shallow phase modulating screen. Under these conditions, the scale of the d ffraction pattern changes only very slowly until the distance from the screen approaches Z_R .

Discussion on Paper 55, "HF radar signatures of traveling ionospheric irregularities. 3D ray-tracing simulation", by T.M.Georges.

Dr R.Cohen: Dr Georges, do you have any feeling as to the uniqueness of the simulations; i.e., how sensitive are your agreements with the experimental results to your assumptions regarding variable parameters?

Dr T.M.Georges: Of course, the question of uniqueness always comes up in connection with experiment simulation. It is conceivable that other model ionospheres would yield similar simulated data, but I believe that one can feel comfortable about models that are both theoretically and observationally reasonable and at the same time produce simulated data that match real data. With regard to the effects of minor variations in the model parameters, this work largely remains to be done, and one should not at this point ascribe much significance to the exact values of the model parameters used here. However, I suspect that the essential properties of the simulated signatures will not change much as the model parameters are varied.

Dr C.Goutelard: Dr Georges pouvrait-il préciser si les modèles presentés étaient définis par des fonctions numériques ou purement analytiques, et dans ce cas quelle loi de variation a-t-elle été adoptée?

Dr T.M.Georges: The ionosphere models are analytically defined: the ambient height profile is a single Chapman layer: the model perturbation electron density varies sinusoidally with latitude, height and time. In addition there is a Gaussian wave amplitude variation with height.

Discussion on Paper 56, "Nature of F-region irregularities inferred from oblique reflection measurements", by L.C.Humphrey, C.R.Roberts and R.Mathers (presented by L.C.Humphrey).

Dr E.N.Bramley: Dr Humphrey, what is the estimated absolute accuracy of the signal strength measurements?

Dr L.C.Humphrey: The accuracy is of the order of ±3 dB. The antennas were calibrated by means of an instrumented aircraft.

BACKSCATTER OBSERVATIONS FROM DISTANT FIELD-ALIGNED IRREGULARITIES

by

H. Kopka and H. G. Möller,
Max-Planck-Institut für Aeronomie Lindau/Harz, Germany

and

W. Stoffregen,
Uppsala Ionospheric Observatory,
Research Institute of Swedish National Defence,
Stockholm 80, Sweden

SUMMARY

Reflections from distant field-aligned irregularities have been observed by backscatter observations and correlation with the occurrence of spread-F in the region from Uppsala and Juliusruh has been established. The relative magnitude of backscattered energy is calculated as a function of the relative electron density variation and the distance of the scattering irregularities. Comparison of topside spread-F observations and bottomside backscatter observations was made to find out whether the frequency of occurrence of spread-F is higher on the bottomside or on the topside of the ionosphere.

BACKSCATTER OBSERVATIONS FROM DISTANT FIELD-ALIGNED IRREGULARITIES

H. Kopka, H. G. Möller and W. Stoffregen

1. COMPARISON BETWEEN 1F-BACKSCATTER AND SPREAD-F OBSERVED AT BOTTOMSIDE VERTICAL SOUNDERS

In the Max-Planck-Institut für Aeronomie in Lindau sweep-frequency backscatter measurements have been made since 1962. The equipment used is almost the same as a vertical ionosonde, but with higher frequency range (2.8 – 45 MHz), higher power (200 kW), and antennas directed obliquely. Rhombic antennas pointed in 10 different directions, 36° apart, are used.

In the daytime we usually get records which are clearly due to ground backscatter. Sometimes the traces are so sharp that they split into the two magneto-ionic components[1].

During night time and especially in a northerly direction we get scatter signals (the so-called 1F-backscatter) whose delay time is about half of that for normal ground backscatter. The lower edge of the traces, i.e. the signals with shortest delay time, is usually sharply bounded. Figure 1 shows a typical example. Figure 2 shows the transition from daytime to night time. The distinct, nearly horizontal traces often merge during the early night hours but also often remain distinct all night. Figure 3 shows the frequency of occurrence of such traces for different group paths as a function of time. A similar distribution is shown for the occurrence of spread-F.

The correlation of spread-F in Uppsala with 1F-backscatter from the ionosphere around Uppsala observed at Lindau is given in Table I (November 1, 1965 – January 31, 1966).

TABLE I

		Spread-F at Uppsala	
		Yes	No
1F-backscatter ($P' \simeq 1000$ km)	yes	556	167
	no	269	195

The correlation of the two phenomena is somewhat indeterminate if only yes-no decisions are used. A quantitative comparison can be made by comparing the frequency interval of the spread-F, Δf_{sp}, with the signal-strength of the backscatter from the equivalent distance.

Since at Lindau only group-path frequency records are available the frequency range Δf for a fixed group-path interval (400 km $\leq P' \leq$ 550 km) was used as a rough measure for the strength of the scatter signals. This frequency range is plotted against Δf_{sp} at Juliusruh in Figure 4. For example, in half the cases in which, at Juliusruh, $\Delta f_{sp} = 0.3$ MHz, backscatter occurs in Lindau with a frequency range up to 0.9 MHz.

For these observations small Δf_{sp} (< 0.2 MHz) at Juliusruh is accompanied by weak scatter signals at Lindau. The maximum backscatter strength occurs when Δf_{sp} in Juliusruh is about 0.3 MHz.

It is surprising that, for larger values of Δf_{sp} at Juliusruh, the field strength of the backscatter signals decreases. This is seen more clearly if the observations after midnight are plotted separately, as shown in Figure 4(c).

Both 1F-backscatter and spread-F can be explained as scattering from ionospheric field-aligned irregularities. Renau[2] did this for spread-F and found good agreement at lower latitudes between calculation and observation, but worse agreement at higher latitudes. In other cases we often find spread-F records of higher latitudes (Uppsala) for which the agreement is much better (as an example, see Figure 5). Since the agreement differs at higher latitudes other factors are also responsible. (That means that, for a good correlation of 1F-backscatter coming from the ionosphere above Uppsala, one has to distinguish the type of the spread-F; this has not been done yet.) Here it is assumed that spread-F is caused by aspect-sensitive scattering on field-aligned irregularities.

An explanation of 1F-backscatter as scattering from field-aligned irregularities with a vertical earth's magnetic field has been given by Bates[3]. He showed that in this case the group path of the 1F-backscatter is half the group path of the normal ground backscatter. The principle is illustrated in Figure 6.

At middle latitudes the earth's magnetic field is inclined. In this case the slope of the 1F-backscatter trace on $P'(f)$ records is less steep, as shown by Möller. He calculated the backscatter trace as the envelope of all oblique ionograms (i.e. group path as a function of frequency) up to all magnetic field lines, until the corresponding rays reach the field line perpendicularly. A flat ionosphere above a curved earth was assumed in this calculation, but the calculation has now been improved, to include the case of a curved ionosphere. This is possible analytically, as is well known, by using the model of a quasi-parabolic layer:

$$N = N_{max}\left[1 - \left(\frac{r - r_m}{r_m - r_b}\right)^2 \left(\frac{r_b}{r}\right)^2\right] \quad \text{if} \quad r_b \leqslant r \leqslant \frac{r_m r_b}{2r_b - r_m}$$

$$N = 0 \quad \text{if} \quad r \leqslant r_b \ .$$

The new result, shown in Figure 7, differs only slightly from the results obtained with the assumption of a flat ionosphere.

The Lindau station is situated at a geographic latitude of 51.5° N . For the calculation, however, the backscatter station was taken as 49.5° N because with this assumption the dip angle of the dipole field fits the existing inclination better. The figures on the left of the calculated oblique frequency traces correspond to the latitude of the reflecting irregularity. The envelope of these traces corresponds to the leading edge observed on $P'(f)$ backscatter records. The height h_{MUF} indicates the height of reflection at leading edge. This height decreases with increasing frequency and has a minimum close to the highest frequency of the envelope.

Figure 8 shows envelopes calculated for different layer heights. At $h_0 < 220$ km, the highest frequency tends to infinity. This would also happen for $h_0 > 220$ km if the backscatter station had been moved farther south or if a slight deviation of the condition of perpendicular reflection had been admitted.

Backscatter observations made at Lindau gave good agreement with these calculations. Sometimes even the shape of the leading edge of the backscatter records resembled the shape of the envelope calculated for $h_0 = 220$ km and the highest observed frequency was 7 times the critical frequency at vertical incidence.

The good agreement between observation and calculation shows that the model of field-aligned scatter is physically real. But the model can be extended by an energy consideration. In the earlier papers it was always assumed that reflection was possible from the ionised columns along the magnetic field lines throughout the ionosphere, as if thin metal plates were fixed along the magnetic field.

The scattered energy from field-aligned irregularities will now be estimated. It will be assumed that, along the field lines, ionised columns exist so that, within the columns, the electron density is $N + \Delta N$ and in the background it is N, and that $\Delta N/N = \kappa = \text{constant}$. If the columns are much larger than the wavelength (as a rough estimate), the scattered energy is proportional to $(\Delta n/n)^2$. (A more exact estimate is very complicated (Liu[5])). For a parabolic layer this leads to

$$\left(\frac{\Delta n}{n}\right)^2 = \left[\sqrt{\left\{1 - \frac{\kappa(1-\phi^2)}{\rho^2 n^2}\right\}} - 1\right]^2$$

$$\rho = \frac{f}{f_c}, \quad \kappa = \frac{\Delta N}{N}, \quad \phi = \frac{z - z_m}{y_m}$$

$$\frac{\kappa(1-\phi^2)}{\rho^2 n^2} < 1, \quad \text{otherwise reflection occurs.}$$

On the other hand the field strength of the received scatter signal depends on the spatial attenuation δ of propagation. The spatial attenuation for a given ground distance and apex height is easily calculated for a flat ionosphere. The same values are valid for 1F-backscatter and a perpendicular magnetic field. The result is shown in the upper diagram of Figure 9. As is well known the energy decreases rapidly for the high-angle ray. In the middle diagram $(\Delta n/n)^2$ is plotted, as a function of frequency, and in the lower diagram the product $\delta(\Delta n/n)^2$, which gives the total effect of both parts on the received scatter signal. It shows that over a large frequency range the received scatter signals will come almost equally from the parts of ionosphere above and below the height of the MUF.

Figure 10 shows signal strength for different distances and electron density gradients $\Delta N/N$. It shows that for a higher gradient $\Delta N/N$ the height range of the ionosphere from which the received signals are scattered increases. But this means that less energy can be scattered at other distances, since more energy is scattered over a large height range of the ionosphere at that distance where $\Delta N/N$ is large. In other words, the farther regions are more shielded. This explains why, with higher Δf_{sp}, the 1F-backscatter signals have a shorter frequency range.

2. COMPARISON BETWEEN GROUND-BASED AND TOPSIDE OBSERVATIONS OF SPREAD-F

There are different hypotheses for the origin of spread-F. Dagg[6] suggested that turbulent electrostatic fields generated in the dynamo region of the ionosphere could be transferred to the F-region along the lines of the earth's magnetic field and may cause the formation of irregularities there. Axford and Hines[7] suggested that the turbulent electrostatic fields are generated in the magnetosphere and transferred downward. If it is assumed that only the greater turbulences can penetrate to the maximum of the F-layer and smaller ones do not, then the frequency of occurrence of spread-F should be higher on the bottomside, according to Dagg's suggestion, and vice versa, if the model of Axford and Hines is correct.

The occurrence frequency of spread-F as a function of time and latitude has been investigated by Singleton[8] using bottomside ionograms and by Calvert and Schmid[9] using Alouette I topside ionograms. A comparison of these investigations[9] yields the result that a greater frequency of occurrence of spread-F is found by topside sounder observations.

This finding would favour the model of Axford and Hines[7], if experimental differences could be excluded.

It could be that the interference level is high on the bottomside and therefore the lower sensitivity of the bottomside measurements would cause a lower rate of occurrence frequency of spread-F. To answer this question records produced by the fixed-frequency topside sounder Topsi were compared with bottomside records produced by the vertical and the backscatter sounder in Lindau.

The fixed frequency topside sounder uses five frequencies between 1.5 and 7.22 MHz. Occasionally it was found that spread-F was present only on the lower but not on higher frequencies, indicating that the inhomogeneities did not extend down to the maximum of the F-layer. To exclude those cases the highest possible frequency was always used for the above comparison. Calvert and Schmid[9] did not say that they made the same exclusion.

To get consistent results we used only those records for which the satellite passed the ground station at a horizontal distance < 700 km. As records were available only between January and July, 1965, not more than 31 observations could be reduced.

The comparison between these selected topside records and the vertical sounder yielded the following result (Table II):

TABLE II

		Topside spread-F	
		yes	no
Bottomside spread-F	yes	14	2
	no	3	12

Hence, spread-F was observed in 14 + 3 = 17 cases on the topside records, whereas 16 cases were observed at the bottomside records, or the occurrence frequency of spread-F observed on the topside exceeded the bottomside records by only 6%. 14 + 12 = 26 of 31 records gave the same answer, or agreement was found in 86% of the records compared.

For the comparison between topside records and bottomside backscatter it was necessary that the path of the satellite did not deviate too much from the direction of the main loop of the antenna pattern used at the ground station. Figure 11 shows the geography and the main antenna direction. The position of the satellite with respect to the ground station is given by the polar coordinates, distance D and angle α. If $\alpha = 0$ the satellite is in the main antenna direction.

Figure 12 shows a $P'(f)$ backscatter record and the simultaneous topside records, which show reflection on the lower frequencies 1.5 and 2.0 MHz. At the nearest approach to Lindau ($\alpha = 9C^{o}$) the trace of the x-component of the 1.5 MHz record shows strong distortions, whereas both components on the 2.0 MHz record are sharp lines, except at the distance D = 300 km where a short trace merges with the trace of the x-component. This trace resembles a combination mode as described by Muldrew[10] and Calvert and Schmid[9]. The vertical sounder at Lindau shows spread-F, and the backscatter sounder gives a faint indication of 1F-backscatter branching from the traces of the vertical incidence reflection. Between D = 300 km and D = 600 km all traces are sharp; no 1F-backscatter is detected. Beyond D = 600 km strong spread-F appears on the topside record. On the backscatter record strong 1F-backscatter starts at P' = 700 km, which corresponds to a horizontal distance of 650 km if a height of reflection h' = 250 km is assumed. The maximum range of the 1F-backscatter is P' = 1400 km or D = 1350 km.

Similar results are shown in Figure 13. Only one combination mode is merging with the x- and o-traces at D = 300 km . The vertical sounder shows faint spread-F. Up to D = 550 km both traces are clean. No 1F-backscatter is observed below P′ = 700 km . (The sharp heavy line at P′ = 600 km belongs to an oblique transmission from Sodankylä, Finland.) The spread-F on this topside record, as well as the backscatter traces, are slightly more structured than in Figure 12. The structure of the backscatter record is sketched at the bottom of the topside record. But it is hardly possible to identify the detailed structure of the different records.

On both records the apparent range of the x-component on 1.5 MHz was higher than on 2.0 MHz. The retardation is due to a gradient of electron density in the bottomside ionosphere. When this retardation decreases, spread-F appears. This same phenomenon was observed on 10 out of 12 paths during winter nights.

It can also be seen on records of the sweep-frequency topside sounder Alouette 1, as shown in Figure 14. On the first ionogram the x-mode is strongly retarded shortly above the x-mode cutoff frequency. In the subsequent ionograms this retardation diminishes and finally disappears when spread F becomes stronger.

In a way similar to that used for Figures 12 and 13, 23 observations were analysed. At fixed distances, in steps of 250 km, the agreement between bottomside and topside observations yielded the results shown in Table III.

TABLE III

Distance (km)	500	750	1000	1250	1500
Agreement: yes	16	16	15	16	11
no	2	6	8	4	7

At 500 km the frequency of occurrence of spread-F was equal for topside and backscatter records. At longer distances, however, the frequency of occurrence of spread-F was higher for the topside records. This is quite understandable, as the topside sounder does not change frequency with increasing distance. However, backscatter signals from larger distances have higher frequencies and it was shown in the previous section that, for higher frequencies, $\kappa = \Delta N/N$ has to be increased with increasing frequency to get the same scattered energy back to the receiver.

In conclusion, then, the frequency of occurrence of spread-F is equal for bottomside and topside observations if, for this comparison, only the highest frequency is used, so that the comparison is restricted to the vicinity of the maximum of the F-layer. Therefore, instrumental errors can be excluded for the comparison. As more spread-F is seen on the lower frequencies of the topside sounder, the total number of irregularities is higher on the topside of the ionosphere. This compares favourably with the model of Axford and Hines[7], which shows that a downward stream of turbulent electrostatic fields causes the irregularities in the F-region.

We are indebted to Dr Calvert for permission to use the Topsi records and to Dr King, who supplied the films recorded at Winkfield, England, and South Atlantic, UK.

REFERENCES

1. Stiewitt, H. — *Beobachtungen der magnetischen Aufspaltung bei Rückstreuversuchen mit variabler Frequenz*. Kleinheubacher Berichte, Band 11, pp.147-150.

2. Renau, J. — *Theory of Spread-F Based on Aspect-Sensitive Backscattered Echoes*. Journal of Geophysical Research., Vol.65, 1960, pp.2269-2277.

3. Bates, H.F. — *Direct HF Backscatter from the 1F Region*. Journal of Geophysical Research, Vol.65, 1960, pp.1993-2002.

4. Möller, H.G. — *Rückstreubeobachtungen mit variabler Frequenz in Lindau am Harz*. Gerlands Beiträge zur Geophysik, Vol.73, 1964, pp.81-92.

5. Liu, C.H. — *Wave Propagation in a Random Medium with Parabolic Background*. Radio Science, Vol.2, 1967, pp.961-977.

6. Dagg, M. — *The Origin of the Ionospheric Irregularities Responsible for Radio Star Scintillations and Spread-F. II, Turbulent Motion in the Dynamo Region*. Journal of Atmospheric and Terrestrial Physics, Vol.11, 1957, pp.139-150.

7. Axford, W.T.
Hines, C.O. — *A Unifying Theory of High-Latitude Geophysical Phenomena and Geomagnetic Storms*. Canadian Journal of Physics, Vol.39, 1961, pp.1433-1464.

8. Singleton, D.G. — *The Geomorphology of Spread-F*. Journal of Geophysical Research, Vol.65, 1960, pp.3615-3624.

9. Calvert, W.
Schmid, C.W. — *Spread-F Observations by Alouette Topside Sounder Satellite*. Journal of Geophysical Research, Vol.69, 1964, pp.1839-1852.

10. Muldrew, D.B. — *Radio Propagation Along Magnetic Field-Aligned Sheets of Ionization Observed by the Alouette Topside Sounder. 1F* Journal of Geophysical Research, Vol.68, 1963, pp.5355-5370.

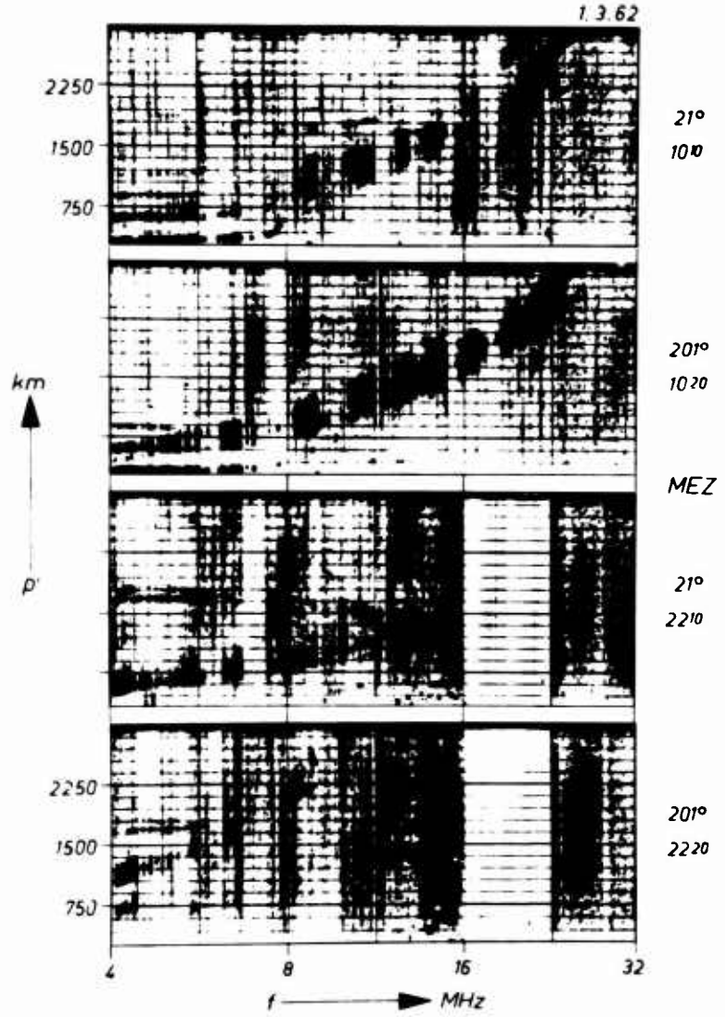


Fig. 1 Typical backscatter records from day and night in northern (21°) and southern (201°) direction

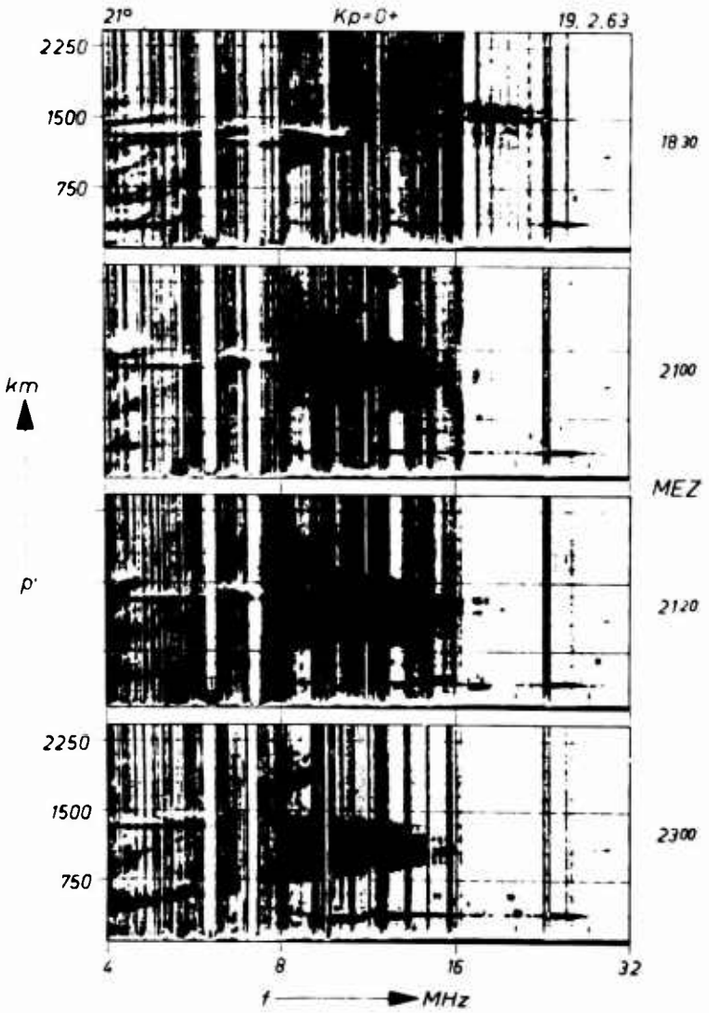


Fig. 2 Typical transition from daytime to night time in a northerly direction

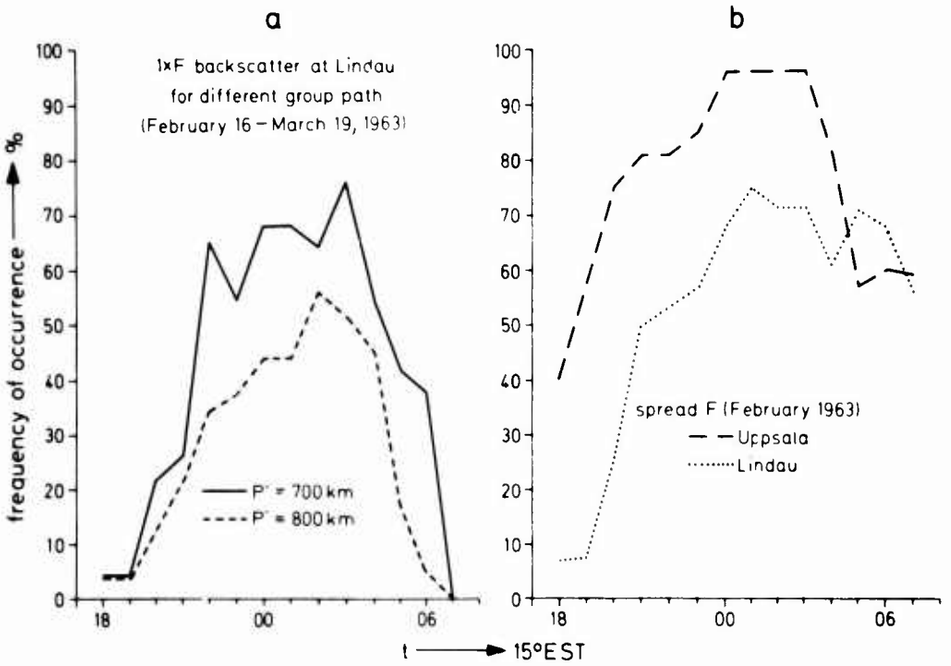


Fig.3 Frequency of occurrence of (a) 1F-backscatter and (b) spread-F as a function of time.

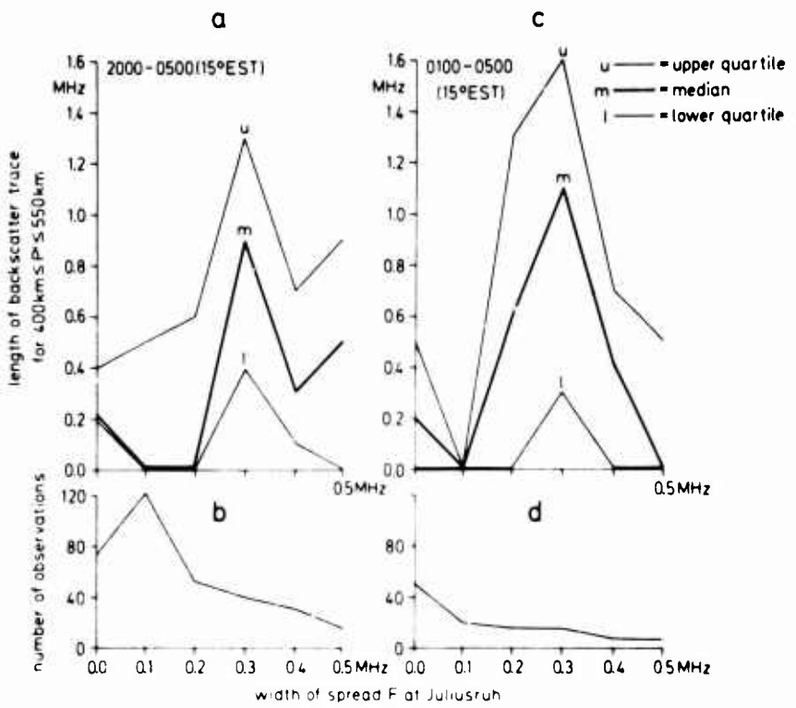


Fig.4 (a) and (c) Comparison of backscatter observed at Lindau with spread-F observed at Juliusruh.
(b) and (d) Number of observations of 60 nights during 1962/63

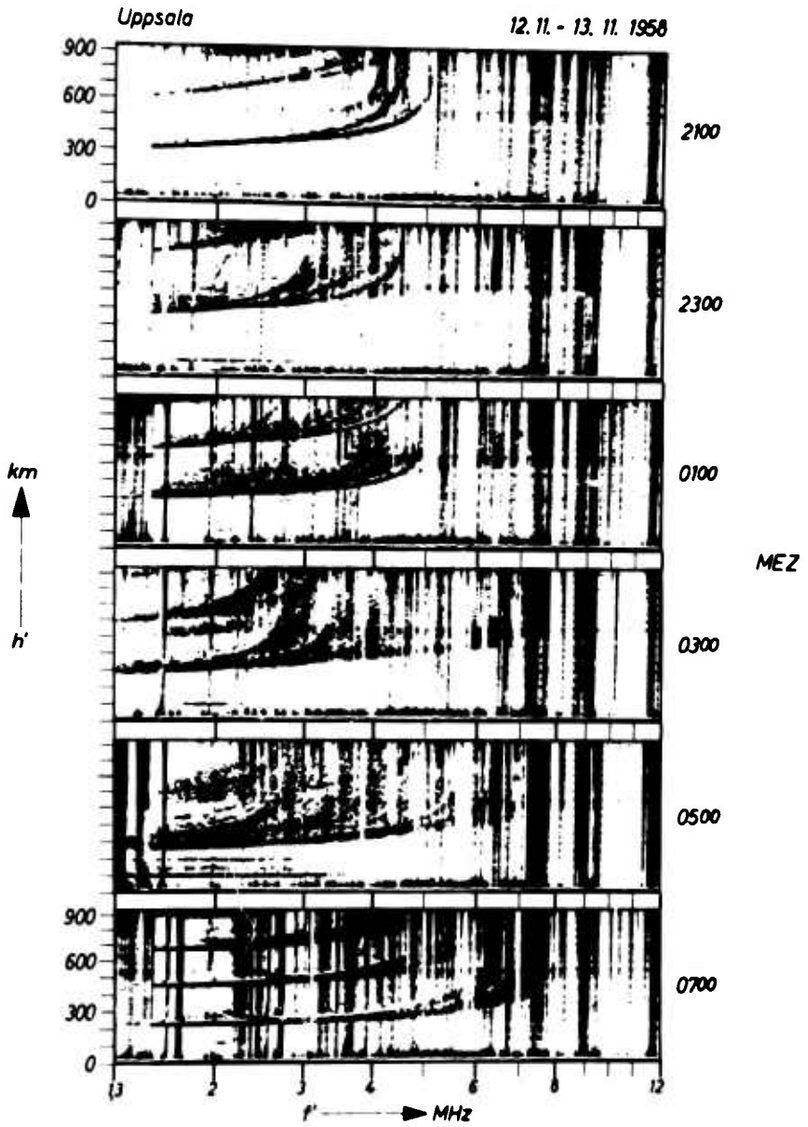


Fig. 5 Vertical ionograms from Uppsala with spread-F.

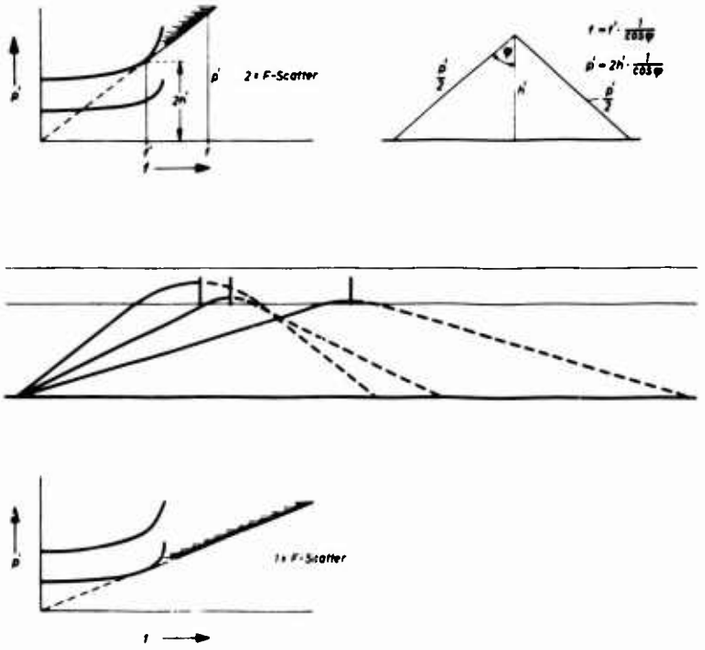


Fig.6 *Above:* P′(f) diagram for ground backscatter.
Middle: Transmission paths for a fixed frequency and different angles of transmission. The vertical dashes represent scattering irregularities in the F-layer.
Below: P′(f) diagram for backscatter from vertical irregularities in the F-layer

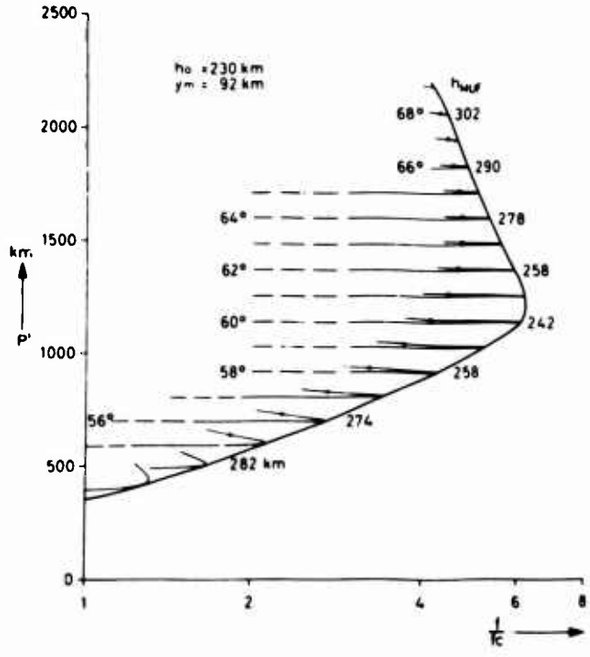


Fig.7 Oblique transmission path P′ as a function of normalised frequency, f/f_c, calculated for different irregularities; the figures on the left of the traces indicate the geographic latitude. The transmitter latitude is 49.5° north h_{MUF} is the reflection height of the highest frequency. The dots indicate the height of maximum electron density.

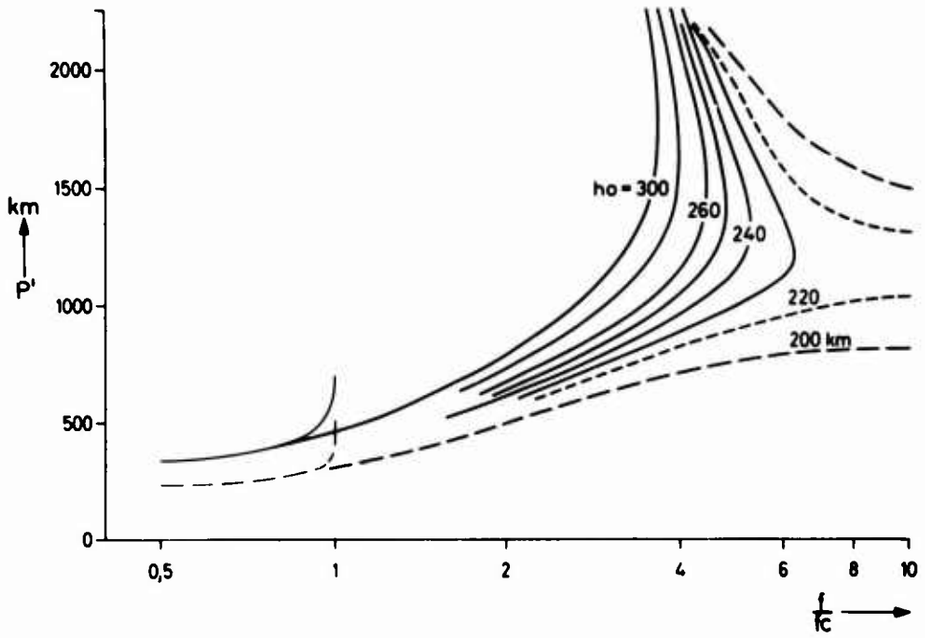


Fig.8 Envelopes of $P'(f)$ calculation as shown in Figure 7 for different layer height h_0.

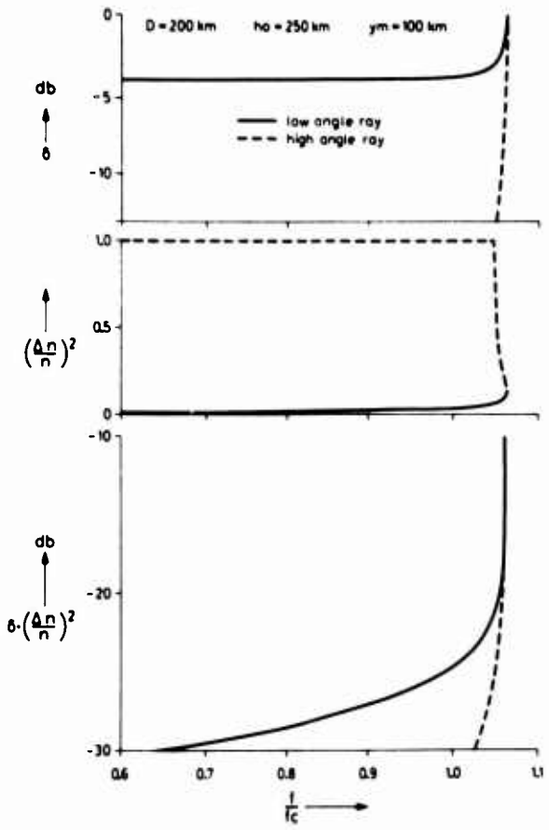


Fig.9 *Above:* Spatial attentuation δ.
Middle: Energy scattering coefficient $(\Delta n/n)^2$.
Below: Relative scattered energy $\delta(\Delta n/n)^2$ calculated as a function of frequency for an irregularity with a constant jump of relative electron density $\Delta N/N = \kappa = 0.1$

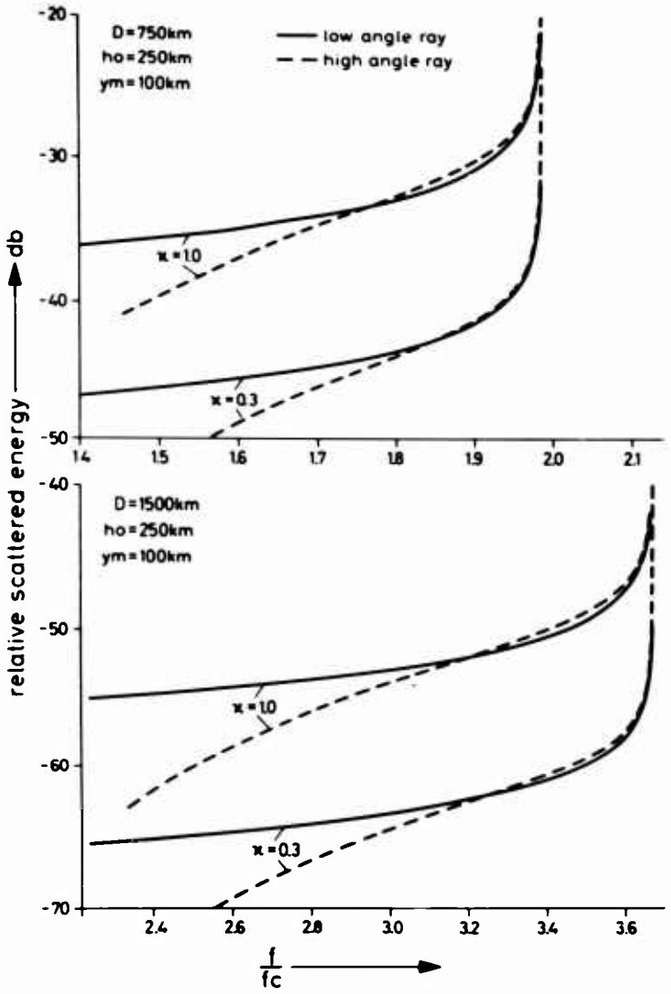


Fig. 10 As the lower diagram of Figure 9, for distances D = 750 km and D = 1500 km and κ = 0.3 and κ = 1.0

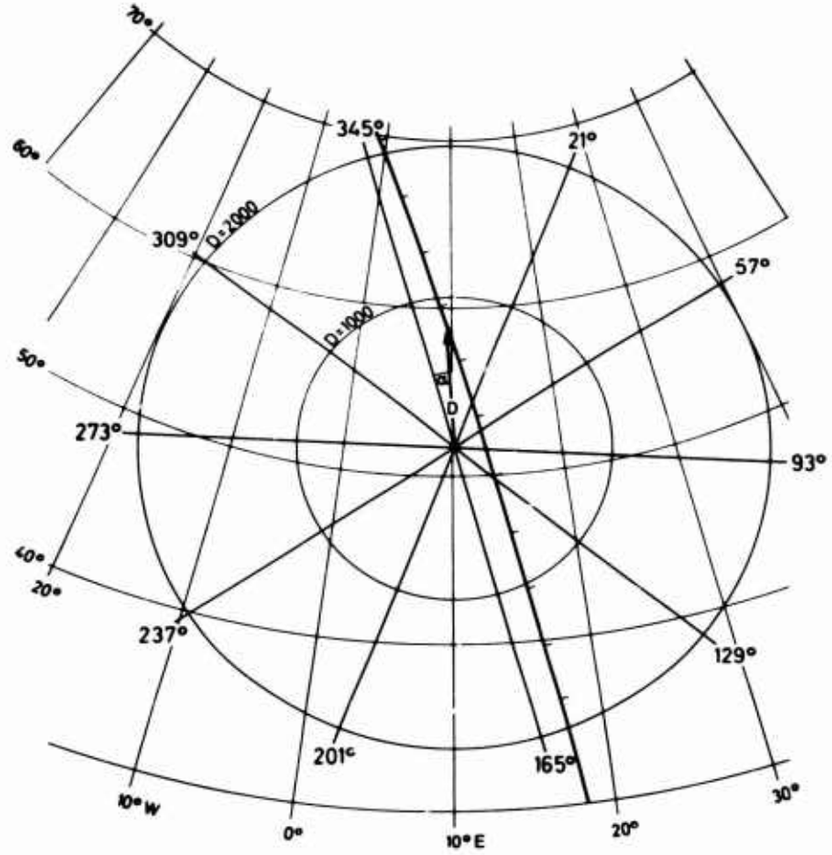


Fig. 11 Map showing the main antenna direction of the backscatter sounder and the path of the satellite. The position of the satellite with respect to the ground station is given in polar coordinates, distance D and angle α

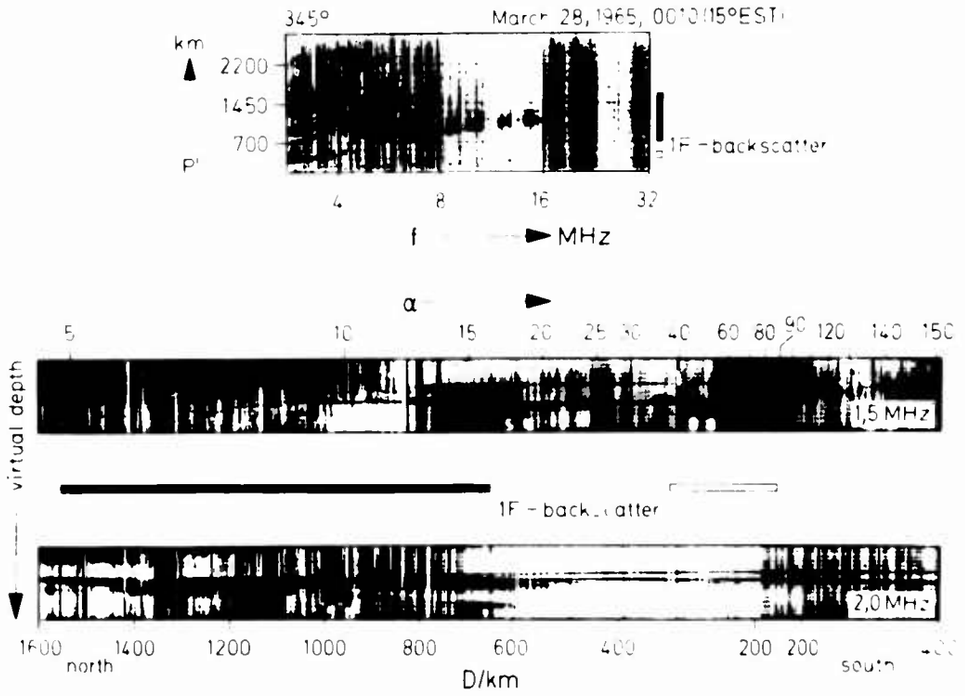


Fig. 12 Comparison of simultaneous observations of 1F-backscatter (upper diagram) and fixed frequency topside sounder 1.5 MHz and 2.0 MHz (lower diagram). The filled bar indicates strong 1F-backscatter and the open bar faint 1F-backscatter

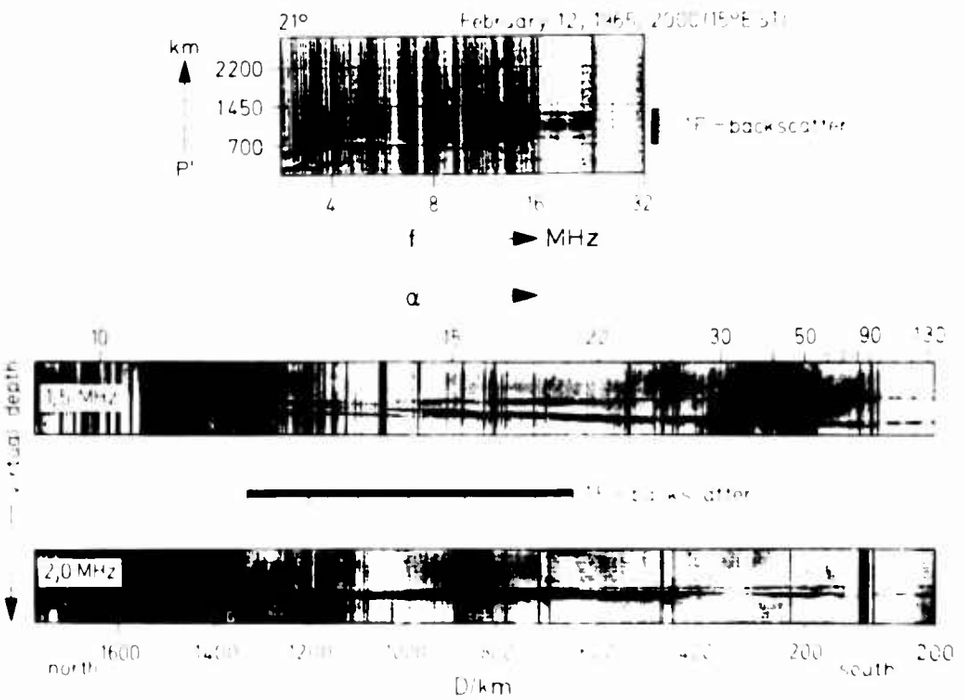


Fig. 13 Comparison of simultaneous observations of 1F-backscatter (upper diagram) and fixed frequency topside sounder 1.5 MHz and 2.0 MHz (lower diagram). The filled bar indicates strong 1F-backscatter and the open bar faint 1F-backscatter

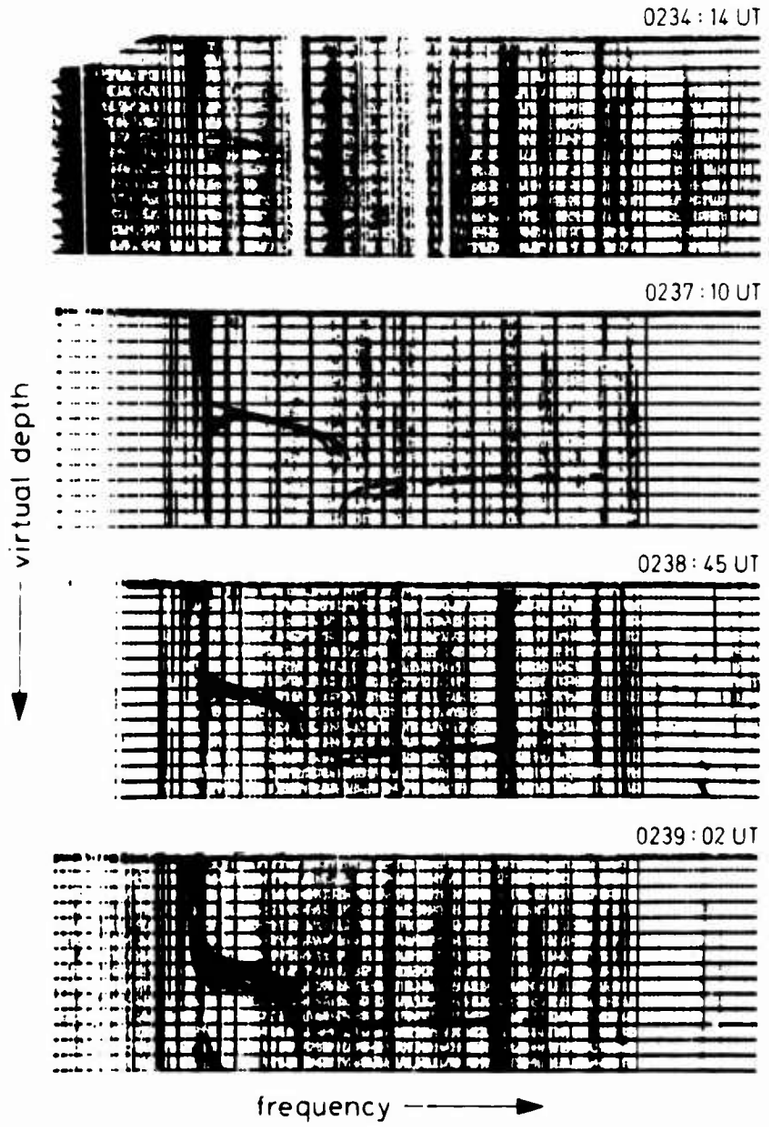


Fig. 14 Topside ionograms of Alouette 1 received in the South Atlantic.

RESEARCH ON FIELD-ALIGNED PROPAGATION OF HF RADIOWAVES USING ALOUETTE 2 TOPSIDE SOUNDER DATA AND DIGITAL RAY-TRACING TECHNIQUES

by

Jayaram Ramasastry*, Edward J. Walsh* and John R. Herman†

*Electronics Research Center/NASA
Cambridge, Mass. USA

†Lowell Technological Institute
Research Foundation
Lowell, Mass. USA

SUMMARY

The first part of this paper covers the study of guidance of HF radiowaves along field-aligned paths using the top-side sounder data from the Alouette 2 satellite. More than 100,000 Alouette 2 ionograms have been used in this analysis and an unusually high percentage of occurrence of conjugate echoes has been observed in the data of some equatorial stations. The maximum percentage of occurrence of conjugate traces around local midnight when the satellite is near the apogee (3000 km) throws some light on the diffusion mechanism responsible for the formation of field-aligned irregularities. The Singapore data (geomagnetic longitude $180^{o} \pm 30^{o}$) has shown higher occurrence of ducted echo traces (>10%) than the data from all other stations. This is rather a large percentage. The longitudinal preference may be conducted with the larger magnetic field strengths in that longitudinal range. Three interesting types of ionograms containing conjugate echo traces are presented. They are called the "double hook", the "triple hook" and the "equatorial" types. A self-consistent explanation based on the assumption of multiple reflections between conjugate points of the field line passing through the satellite is presented.

The second part of the paper covers the results of the digital ray-tracing study of the guidance of HF radiowaves along field-aligned ionization irregularities in the magnetosphere of the Earth. Various computer results are shown to illustrate the mechanism of guidance of radiowaves. Time-delay and trapping characteristics of the three types of conjugate echoes that are frequently observed in the Alouette 2 topside sounder records are simulated using the ray-tracing methods. Some of the optimum conditions for guidance of electromagnetic waves along a magnetic field line are discussed. The results reported here on the HF ducting phenomenon are directed primarily towards determining whether such a mechanism may be utilized to study the magnetospheric phenomena and whether it can be useful as a reliable communication link.

RESEARCH ON FIELD-ALIGNED PROPAGATION OF HF RADIOWAVES USING ALOUETTE 2 TOPSIDE SOUNDER DATA AND DIGITAL RAY-TRACING TECHNIQUES

Jayaram Ramasastry, Edward J. Walsh and John R. Herman

PART I

CONJUGATE ECHOES IN ALOUETTE 2 TOPSIDE SOUNDER DATA

1. INTRODUCTION

High frequency conjugate echoes were first observed on the Alouette 1 sweep frequency topside sounder data[1]. Conjugate signals have also been observed on the Explorer 20 fixed-frequency topside sounder ionograms[2]. Some occurrence statistics concerning the Alouette 2 ionograms have also been published[3]. However, the study of HF conjugate echoes on Alouette 2 ionograms has offered challenging problems and some exciting results. Three types of ionograms containing symmetric conjugate echo traces which appear frequently are presented and explained in terms of multiple reflections between the conjugate points of a field line passing through the satellite. Such symmetric traces have not been previously reported in the literature.

The Alouette 2 topside sounder is better suited to the study of conjugate echoes than that of Alouette 1 because of the lower frequency limit of the sounder. The transmitter and the receiver are tuned to the same frequency which is swept in time. The transmitter is pulsed once in 32 msec and the instrumentation provides a new zero time-reference each 32 msec, thus pulses returning with delays of 37, 69, or 101 msec will all be recorded as traces of 5 msec group delay on the same ionogram frame. More than 100,000 ionograms from eight stations (Quito, Fort Myers, Santiago, Johannesburg, Kano, Singapore, Winkfield, and Orroral Valley) have been examined by the authors and some of the observations of the HF ducting phenomena in the magnetosphere of the Earth have been very revealing. Various statistical results are presented and the occurrence characteristics of the conjugate echoes are discussed.

2. METHOD OF ANALYSIS

All the available ionograms from the eight stations were analyzed to identify the ionograms with conjugate traces. Muldrew[3] classified all the available ionograms into five groups depending on the value of f_{xs}, the frequency of the extraordinary wave which has zero refractive index at the satellite altitude. The reason given by the author for such a classification is that it gives a rough indication of the electron density at the satellite altitude. While it is a convenient method of classification, it does not provide any new physical insight into the guidance of HF radiowaves. Consequently, the authors have not adopted any method of classification of frames with conjugate echoes. The statistical data in the present analysis are restricted to those ionograms which exhibit conjugate echoes. Hence the percentage occurrence should be taken to mean that so many out of 100 ionograms with conjugate ducts occur at the indicated value of the parameter (altitude, local-time, or L value).

Since the argument that the perigee rotates only 1.89 deg/day, which is almost the same as the precession of the orbital plane with respect to the sun, the local time at perigee (or apogee) changes less than 3 hours/year. For the period of the data used in our analysis, the perigee occurs near local noon and the apogee near local midnight. Hence the satellite intersects the smaller L shells near noon and the larger L shells near midnight. As we shall see later, the percentage occurrence is rather large around local midnight, when the satellite is near the apogee.

3. CONJUGATE ECHOES AS A FUNCTION OF L VALUE

The percentage occurrence of conjugate echoes between 21 hours and 04 hours local time is plotted as a function of L in Figure 1. This period of local time is chosen to afford comparison with the results of Muldrew[3]. The results presented here are consistent with Muldrew's argument that the occurrence percentage is high and almost constant during this time period. The results for L values larger than 3.5 are not considered representative and hence may be deleted from discussion. Very few conjugates ducts are observed at these high L values because the receiver is no longer tuned to the frequency of echoes that arrive after the long delay required for propagation along a duct with an L value about 4 or greater. Such a conclusion agrees with our analysis of "triple hook" and "double hook" traces where the traces corresponding to multiple reflections between the conjugate point start fading out as the group delay exceeds 200 msec. The authors' results also show an apparent drop in occurrence for L less than about 1.35. It can also be agreed that such a rapid drop may not be real, since the data at such low L values are not representative because of the characteristics of the satellite orbit, i.e., the satellite intersects lower L shells during local noon where the percentage occurrence of conjugate echoes is almost zero[3]. One may say in this context that the Alouette 2 satellite was not designed originally to study conjugate ducting. Future experiments designed to study conjugate ducting should have the capability of receiving signals for longer periods of time at any one frequency; in addition, the orbital characteristics of the satellite should be such that the data are representative of guidance in field lines of both low- and high-L values.

4. CONJUGATE ECHOES AS A FUNCTION OF LOCAL TIME (1-HOUR AVERAGES)

The percentage occurrence of conjugate echoes as a function of local time is shown in Figure 2. The data were averaged in 1-hour intervals of local time. This averaging time interval is selected in view of the fact that the local time drift along the propagation path may be about an hour. It can be seen that the percentage occurrence of conjugate echoes is almost zero in the time interval 0600 to 1800 hours local time. There is a pronounced broad maximum between 2100 and 0400 hours local time. The post-midnight maximum in duct occurrence when the satellite altitude is near apogee brings forth the discrete characteristics of the field-aligned ionization irregularities. As may be noted, the ambient density during night time is considerably lower and any diffusion mechanism capable of channelling the particles along the field line creates larger gradients of electron density along the field line during the night time. Hence the increased efficiency in the guidance of radiowaves during night time can be anticipated.

5. CONJUGATE ECHOES AS A FUNCTION OF SATELLITE ALTITUDE

The percentage occurrence of conjugate echoes as a function of satellite altitude is shown in Figure 2. As mentioned before, the satellite is around the midnight meridian when it approaches the apogee of its orbit. Hence the high altitude maximum is consistent with the previous conclusions about midnight maximum . Conjugate echoes are rarely seen at altitudes less than 1200 km in the Alouette 2 data.

6. EXAMINATION OF CONJUGATE TRACES

In the Alouette 2 ionograms, the conjugate echoes generally appear as beautifully symmetric patterns of high intensity. When they appear, the normal traces in the ionogram are faded out because of the automatic gain control in the receiver. Figure 4 shows a series of evenly spaced "double hooks" separated by horizontal traces, while Figure 5 shows a pattern of symmetric "triple hooks." Figure 6 shows a pattern of "equatorial traces". The symmetry of these patterns is in sharp contrast to the types of conjugate traces reported by Muldrew[1] for Alouette 1 data. They are also in sharp contrast to the conjugate traces reported by Muldrew[3] for Alouette 2 data. The L values of the magnetic field lines passing through the satellite for these three examples (L = 1.53, 1.63, 1.45 respectively) are larger than the L values for the conjugate echo traces considered by Muldrew[1] for the Alouette 1 data. Hence, the major portions of the paths are in the regions of low electron densities for the cases considered here, N and S correspond to the north and south directions taken by the signal. Only the extraordinary wave traces of of conjugate echoes are observed. As the frequency of the radio waves increases, the medium behaves more like free space, tending to decrease the group delay. However, the rays penetrate deeper into the ionosphere at higher frequencies, giving rise to an increase in the group delay. If the two effects compensate each other, the group delay of the round trip trace (N + S) will be independent of frequency. Then, all the round trip traces (N + S, 2N + 2S, 3N + 3S,...) appear as horizontal traces in the ionograms. This condition is not always satisfied since round trip traces with group delays either increasing or decreasing with frequency are frequently observed.

The far-end echo from the satellite always heads along the field line away from the Earth towards the region of decreasing electron density, except at the equator where the path lengths and the characteristics are the same. Hence, reflections were not obtained from near the satellite as for the case of the near-end echo which follows the field line towards the Earth and towards the region of increasing electron density. This results in reflections from near the satellite. The subsequent symmetry of the N and S traces follows from the magneto-ionic properties of the ray path.

The ionogram in Figure 4 is a typical example of the frequently observed "double hook" patterns. It was recorded at Quito, Ecuador. Also shown in the figure are the proper relative positions of the various traces according to their actual time delays. The satellite position (geomagnetic latitude = 12.56^{0}) is such that the group delays of the near-end and far-end paths along the field line differ approximately by 32 msec and the North and South traces seem to intersect in real time. The geometry of the path length of the field line requires the round trip trace (N + S) to be positioned twice as far from the beginning of its own time frame as the apparent intersection point of the N and S traces. The (2N + 2S) trace should be twice as far from the beginning of its frame as the (N + S) trace is from the beginning of its own time frame. Similar geometric considerations can account for the uniform spacing of the traces in the ionogram. The (2N + S) and (3N + 2S) traces are shaped like the N trace, and the (N + 2S) and (2N + 3S) traces are shaped like the S trace. This is because the delay times for the round trip traces (N + S), (2N + 2S), (3N + 3S),..... are virtually independent of frequency. The direct consequence of such a situation is that all the "double hook" traces do have the same shape. The (3N + 3S) trace is extremely faint but is discernible on the microfilm.

Figure 5 shows the "triple hook" ionogram and its various characteristics. The reason that all the triple hooks in the ionogram of Figure 5 have the same shape is once again caused by the frequency-independent group-delay characteristics of the round trip traces. The figure also shows the various traces according to their respective time delays. The near-end trace is easily recognizable in both Figures 4 and 5 because it is the most intense trace which starts from zero group delay. This characteristic is caused by reflections from near the satellite due to the increasing electron density in that direction. In both the ionograms, the far-end trace was initially selected on the basis of its intensity and the mirror-image-like characteristic with respect to the near-end trace. Also, the L value of the field line corresponding to that frame gave the clue as to the approximate

group delay of the far-end echo. Digital ray tracing analyses have, since then, borne out these assumptions.

Figure 5 exhibits triple hooks instead of double hooks because the satellite is displayed from the magnetic equator (geomagnetic latitude = -19.53^{o}) so that the group delays of the near-end and far-end echo traces differ by more than 32 msec. The apexes of all the *triple hooks* occur at the frequency where the time delay of the near end (S) echo is exactly one frame time (32 msec). Then the N , N + S , and N + 2S echoes all have the same positions in their relative time frames at that frequency and will seem to intersect in the ionogram where all the time frames are superimposed.

There is one significant condition which determines whether the conjugate echoes form a triple hook pattern or a double hook pattern. Double hooks are observed when the group delays of the near-end and far-end echoes differ by approximately 32 msec. Triple hooks are observed when the group delays differ by more than 32 msec.

Figure 6 shows an example of "equatorial trace" pattern of conjugate echoes in which the difference in the group delays between the near-end and far-end echoes is much less than 32 msec (satellite latitude $\theta = -3.32^{o}$). In this case, the N and S traces do not intersect but are in the same time frame. The symmetry of the other multi-hop traces follows from the group delay characteristics of the path.

The traces representing the round trip paths are sometimes inclined to the horizontal. The slopes of (2N + 2S), (3N + 3S), (4N + 4S), and so forth, are exactly twice, thrice, four times, and so forth, the slope of the trace (N + S). This can be easily verified by adding up the various group delays. Such inclined round-trip traces appear when the near-end and far-end distances differ by a small amount.

One of the significant features observed in Figure 5 is that the (4N + 4S) trace had a delay time of 465 msec. But with the receiver bandwidth of 30 kHz and the sounder frequency-sweep rate of 0.15 MHz/sec the receiver is essentially detuned after 200 msec. This may mean that the faintness of the (4N + 4S) trace is not caused by the leakage and attenuation of the signal within the "magnetospheric wave guide." On the contrary, the signal, after traversing four complete round trips from one hemisphere to the other, covering a total path-length of about 60,000 km, must have been quite strong to have shown up at all in the detuned receiver.

The faint (3N + 3S) trace in the "double hook" case (Fig. 4) has a time delay of 316 msec and probably would have been more intense if the receiver had been properly tuned to receive it.

Figure 7 shows a conjugate echo frame corresponding to a high L value of 1.76. The satellite was at -19.05^{o} (magnetic latitude) and the total field-aligned path was 17,463 km, with the near-end and far-end distances being 6593 and 10,870 km, respectively.

Figure 8 shows a series of seven ionograms recorded at Quito on June 12, 1966, from 03:23:45 to 03:26:59 UT. As may be seen, the triple hooks prominently appear and disappear. Such a sequence is representative of an event when the satellite passes through a cluster of ionization irregularities with strong coupling of signals into ducts of various closely spaced L shells.

One may also emphasize in this context that the ionization irregularities transverse to the field lines responsible for such a wave guidance may be either enhanced or depleted columns of ionization. The nature of the irregularities is not discussed in the present paper.

7. DISCUSSION AND CONCLUSION

One must bear in mind that the Alouette 2 satellite topside sounder experiment was not originally designed for detecting such long time-delay echoes. The frequency sweep rates and bandwidths used are essentially sufficient to receive the signals normally incident on the topside ionosphere. The Explorer 20 satellite[7] had a fixed frequency topside sounder transmitting at seven different frequencies in sequence, each time the corresponding receiver being tuned for 15 msec. The next time the receiver could receive the signal at that frequency was 105 msec later. Since the satellite altitude was only 1000 km (circular orbit) like that of Alouette 1, the experiment was once again not suitable for the study of conjugate ducting. A suitably designed satellite propagation experiment, with its receiver being capable of receiving signals of larger time delays, may unravel all the mysteries about magnetospheric wave guidance.

The authors also propose an experiment in which a transmitter in a low orbiting satellite (preferably eccentric polar orbit) transmits at HF to a high-altitude satellite (altitude of apogee $\simeq$ 6000 km) whose receiver should have the capability of receiving the signals for longer periods of time. The now orbiting Radio Astronomy Satellite might have the desired receiving characteristics in the frequency range 1-10 MHz. Many monostatic and bistatic radar experiments of the past aimed at verifying the existence of ducts and shells in the magnetosphere and the consequent guidance of electromagnetic waves have been *inconclusive*. The stability and frequency of occurrence of the conjugate echoes, combined with the relatively loss-free multiple reflections between the conjugate points, of the signals observed in the Alouette 2 satellite data have created challenging opportunities. Thus a well designed experiment may provide conclusive answers to the question of whether or not this unique magnetospheric wave guide could be used as a reliable HF communication link between conjugate points or between two satellites over large transequatorial distances along a field-aligned path. Even if this propagation mode cannot be used as a communication link, its use to study the magnetospheric phenomena cannot be discounted.

PART II

DIGITAL RAY-TRACING STUDIES

1. INTRODUCTION

Some of the echo traces appearing at virtual ranges greater than those of the normal vertical incidence echo traces on the topside sounder ionograms have been explained in terms of field-aligned ionization irregularities[1]. The irregularities are assumed to have thicknesses greater than the radio wavelength and to act as wave guides or "ducts" to trap HF energy and produce the long-range echo traces. A complete review of the past theoretical and experimental work directed towards testing such a guidance mechanism has been published[4].

The guiding of rays along field lines requires irregularities with a certain minimum transverse ionization gradient. Propagation between magnetic conjugate points or "conjugate ducting" occurs when the transverse ionization gradient exceeds the minimum required for guidance at the apex of the magnetic line of force. The current interest in the HF ducting phenomenon is directed primarily towards determining whether such a mechanism may be utilized to study the magnetospheric phenomena and whether it can be useful as a reliable communication link. Here, we also examine the conditions under which the HF radiowaves may be guided along field-aligned ionization irregularities.

2. RAY-TRACING METHOD

The ray tracing method is based on Hamilton's system of equations[5] as derived in a spherical polar coordinate system by Haselgrove[6] and extended by Grossi and Langworthy[7] for the investigation of HF and VHF ionospheric propagation. The reader is referred to Reference 7 for a description of the basic ray-tracing program. Because of the high accuracy obtainable, the use of a high-speed digital computer is preferred to an analog machine for the integration of the ray equations. The Adams-Moulton variable step-size integration method[8] is adopted because of its greater flexibility due to an automatic error control which halves or doubles the step size to ensure the desired accuracy along all parts of the ray path.

3. MAGNETOSPHERIC MODELS

The electromagnetic properties of the magnetosphere are characterized by (i) the electron density distribution, (ii) the magnetic field distribution, and (iii) the electron collision-frequency distribution. The mathematical models for these three items are implemented in the form of subroutines and can therefore be modified as and when necessary.

4. MAGNETIC FIELD MODEL

To a first approximation, a dipole model is used for the magnetic field of the Earth. The magnetic field equation which defines the gyrofrequency f_H is given by

$$f_H(r,\theta) = C_{11}\left(\frac{a}{r}\right)^3 \sqrt{(1+3\cos^2\theta)}, \qquad (1)$$

where a is the radius of the Earth, and r and θ are the geocentric distance and colatitude of any point on the field line.

$$C_{11} = \frac{e}{2\pi m} B_0 \times 10^{-6} \simeq 0.9 , \qquad (2)$$

where B_0 is the magnetic field on the surface of the Earth at the equator, and e and m are the charge and mass of an electron. A value of 0.3142 gauss is used for B_0.

For ray tracing along high L value field lines, the 63-term spherical harmonic expansion of Cains et al[9]. is used.

5. COLLISION FREQUENCY MODEL

The collision frequency model is based on results published by F.S.Johnson[10] in the *Satellite Environment Handbook.*

6. ELECTRON DENSITY MODEL

The model for the electron density distribution incorporates those features that have a bearing on the high-frequency ducting problem. Thus, an ionization irregularity normal to the field line is superimposed on the normal radial distribution of electron density. In this model, the electron density is given by

$$N(r,\theta,\phi) = N_1(r,\theta)*N_2(r,\theta,\phi) , \qquad (3)$$

where θ is the colatitude and ϕ is the magnetic longitude. $N_1(r,\theta)$ represents the background density in the magnetic meridional plane and $N_2(r,\theta,\phi)$ represents the ionization in the field-aligned irregularities in both the meridional and azimuthal planes.

The background ionization is assumed to have the form

$$N_1(r,\theta) = N_F + N_X . \qquad (4)$$

Here N_F and N_X refer to the electron densities in the ionospheric F-region and the exosphere, respectively.

$$N_F = N_{max}*\exp\left[\frac{1}{2}\{1 - W - e^{-W}\}\right], \qquad (5)$$

where N_{max} is the peak electron density and

$$W = \frac{h - h_{max}}{H_F} , \qquad (6)$$

in which h_{max} is the altitude of the peak electron density, N_{max}, and H_F is the scale height. In our calculations, the maximum altitude h_{max} is assumed to be 350 km and H_F = 50 km.

The Angerami and Thomas diffusive equilibrium model[11] is used for the exospheric electron density distribution above 1000 km and below the plasma-pause which exists at a distance of from 3 to 4.5 Earth radii. The centrifugal force caused by the rotation of the Earth is neglected while applying the Angerami and Thomas model. With this model the electron density in the exosphere is given by

$$N_X = N_r*[1.659 \times 10^{-3}\theta + 1.662 \times 10^{4}] \qquad (7)$$

where θ is the colatitude in degrees. The terms within the brackets represent the latitudinal variation of exospheric electron density as derived by Thomas and Sadar[12] using Alouette 1 satellite data.

$$N_r(Z) = \left[\sum_i \beta_i \exp\left(-Z_X/H_i\right)\right]^{1/2} , \tag{8}$$

where Z_X is the geopotential altitude given by

$$Z_X = \frac{r_0}{r}\left(r - r_0\right) , \tag{9}$$

where r_0 is the reference radial distance and is equal to 6870 km in the model. The symbol i refers to each ion present in the exosphere. H_i and β_i refer to the scale height and the fractional density of the i^{th} ion at the reference level r_0. The scale height is given by

$$H_i = \frac{kT_i}{M_i g(r_0)} , \tag{10}$$

where k is the Boltzmann constant, T_i and M_i are the temperature and mass, respectively, of the i^{th} ion, and $g(r_0)$ is the acceleration due to gravity at the reference level r_0. A three-ion gas model consisting of oxygen (0^+), helium (He^+), and Hydrogen (H^+) ions is assumed. The various parameters in the density equation have the following values:

$$T = 1000^{o}K \text{ for both electrons and ions} \tag{11a}$$

$$\beta_{He} = \frac{0.2 \times 10^{-T/1000}}{\beta_e} = 1.96 \times 10^{-2} \tag{11b}$$

$$\beta_H = \frac{0.16 \times 10^{-T/500}}{\beta_e} = 1.6 \times 10^{-3} \tag{11c}$$

$$\beta_0 = \frac{1}{\beta_e} = 0.9788 \tag{11d}$$

$$\beta_e = 1 + 0.2 \times 10^{-T/1000} + 0.16 \times 10^{-T/500}$$

$$= 1.0216 . \tag{11e}$$

The technique suggested by Swayze[13] is used to join the exospheric profile smoothly with that of the F-layer between 350 and 1000 km. The expression for N_e is modulated by a factor

$$\exp\left[-\left(\frac{h - 1000}{500}\right)^2\right] , \tag{12}$$

where h is the altitude in kilometers.

The electron density as a function of altitude at various geomagnetic latitudes is shown in Figure 9.

7. MODEL FOR THE IONIZATION IRREGULARITIES

The following assumptions are made in the development of this model:

(i) The ionization in the irregularities is distributed in discrete columns or sheets separated in latitude and aligned with the magnetic field lines.

(ii) The transverse scale of the field aligned irregularities follows the transverse (meridional) dimensions of the tube of magnetic flux.

(iii) The peak enhancement varies inversely as the transverse dimensions of the tube of magnetic flux.

(iv) The variation of the density within the irregularity follows a Gaussian distribution transverse to the magnetic field. The Gaussian distribution satisfies the equations for the diffusion of charged particles across a field line.

Hence

$$N_2(r,\theta) = 1 + \frac{\Delta N_0}{N^*(t/t_0)} * \exp\left[-\left(\frac{\Delta Z}{(t/t_0)H_0}\right)^2\right] . \qquad (13)$$

N_0 is the peak ionization enhancement and H_0 is the scale size of the irregularity at the base of the field line.

$$\frac{t}{t_0} = \frac{\text{Meridional width at } (r,\theta)}{\text{Meridional width at } (r_0,\theta_0)}$$

$$= \frac{\sin^3\theta\ (4-3\sin^2\theta_0)^{1/2}}{\sin^3\theta_0\ (4-3\sin^2\theta)^{1/2}} . \qquad (14)$$

While specifying the initial coordinates of the starting point, the geographic latitude, λ_a, and the longitude, ϕ_a, are converted to geomagnetic coordinates λ_m and ϕ_m by using the following transformation equations:

$$\tan\lambda_m = -\tan(\lambda_a-\lambda_0)\sin x \sec(x+\phi_0) \qquad (15)$$

$$\tan\phi_m = -\cos\lambda_m \tan(x+\phi_0) , \qquad (16)$$

where

$$x = \arctan\{\cos(\lambda_a-\lambda_0)\cot\phi_a\} \qquad (17)$$

and

$$\phi_0 = +78.5^\circ \text{ and } \lambda_0 = +291.0^\circ$$

are the geographic coordinates of the geomagnetic pole.

RESULTS

Figures 10 through 14 show a few results of the ray tracing. Figures 10 through 13 simulate some of the conjugate echo paths observed in Alouette 2 ionograms. Parameters shown in the figures are defined as follows:

R_0 = the geocentric distance (km) of the initial signal position,

PKFRAC = the peak fractional ionization enhancement,

LAMBDA = the colatitude of the field line,

A_0 = the initial angle the ray makes with the local vertical,

B_0 = the initial angle the ray makes with the South vector,

PHI and THETA = the magnetic longitude and colatitude of the initial signal position.

The frequency of the signal is 1.0 MHz for the cases considered in Figures 10 through 13.

Each figure consists of two plots. The rectangular plot shows the distance of the ray from the field line versus the distance along the field line from the near end. The polar plot shows the actual ray path with reference to the surface of the Earth. The polar plots give a clear indication of the positions of the conjugate reflection points as well as the L value of the field line guiding the rays.

Figure 10 shows the L = 1.76 case using a peak electron density enhancement of 13.0% at the point the ray is launched. A peak enhancement of 13.0% at a geocentric distance of 10,022 km corresponds to a much smaller percentage at lower altitudes. The ray starts at about 12,500 km along the field line from the northern hemisphere. It gets reflected on its way towards the Earth and travels all the way back to the southern hemisphere where it is reflected again. The program was stopped deliberately when the ray was at 15,500 km along the field line. Otherwise it could have bounced back and forth indefinitely. The bowing of the pattern at the equator is caused by larger scale sizes near the equator so that the ray rides further out from the field line because the enhancement structure is wider.

The oscillatory nature of the ray path seen in the rectangular plot is caused by the ray being launched too far away where the electron density gradient is insufficient to bend the ray back towards the direction parallel to the field line. The ray essentially tends to continue in a straight line, but appears to fall in towards the field line since the field line is curved. When the ray gets close enough, the gradient is large enough to bend the ray away from the field line and the apparent inward motion stops in the rectangular plot. It follows that similar oscillations also occur if the ray is launched too close to the field line or at the wrong angle relative to its equilibrium position. A careful launching of the signal can eliminate all these initial oscillations, even though they may grow later when the ray crosses the equator or upon reflection.

In Figures 11 and 12, the rectangular plots show one reflection each for the cases L = 1.63 and L = 1.53 , respectively, while the corresponding polar plots show several round trips. For these two cases the peak enhancement is 6% at the point of launch.

Figure 13 shows how a small peak enhancement is sufficient (3.0%) to trap the rays if the signal is properly launched. The physical conditions are the same as for the case of Figure 10

Figure 14 relates to an L = 2 field line and shows the manner in which a ray typically escapes when the oscillations grow too large, even with sufficient peak enhancement. A frequency of 2.00 MHz is used for this case.

REFERENCES

1. Muldrew, D.B. — *Radio Propagation Along Magnetic Field-Aligned Sheets of Ionization Observed by the Alouette 1 Topside Sounder.* Journal of Geophysical Research, Vol.68, 1963, pp.5355-5370.

2. Loftus, B.T. et al. — *Observations of Conjugate Ducting by the Fixed-Frequency Topside-Sounder Satellite.* Annales de Géophysique, Vol.22, 1966, pp.530-537.

3. Muldrew, D.B. — *MF Conjugate Echoes Observed on Alouette 2 Topside-Sounder Data.* Canadian Journal of Physics. Vol.45, 1967, pp.3935-3944.

4. Ramasastry, J. — *Review of High-Frequency Radiowave Ducting in the Magnetosphere of the Earth.* NASA TMX-1457, 1967.

5. Hamilton, W.R. — *Geometrical Optics.* Vol.1 of the Mathematical Papers of Sir William Rowan Hamilton, (A.W.Conway and J.L.Synge, editors) Cambridge University Press, 1931.

6. Haselgrove, J. — *Ray Theory and a New Method of Ray-Tracing, The Physics of the Ionosphere.* The Physical Society, London, 1965, pp.355-364.

7. Grossi, M.D. Langworthy, B.M. — *Geometrical Optics Investigation of HF and VHF Guided Propagation in the Ionospheric Whispering Gallery.* Radio Science, Vol.1 (New Series), 1966, pp.877-886.

8. Barker, J.I. Grossi, M.D. — *HF and VHF Ionosphere Wave Guidance.* NAECON Proceedings, Dayton, Ohio, 1963.

9. Cain, J.C. et al. — *An Evaluation of the Main Geomagnetic Field.* Journal of Geophysical Research, Vol.70, 1965, p.3647.

10. Johnson, F.S. — *Satellite Environment Handbook.* Stanford University Press, California. pp.127-131.

11. Angerami, J.J. Thomas, J.P. — *The Distribution of Ions and Electrons in the Earth's Exosphere.* Journal of Geophysical Research. Vol.69, 1964, pp.4537-4560.

12. Thomas, J.O. Sadar, A.Y. — *Alouette 1 Topside Soundings Monitored at Stanford University.*, Stanford Electronic Laboratories, Technical Report 6, Stanford University, 1963.

13. Swayzee, D.W. — *Digital Ray-Tracing Investigation of HF Guided Propagation in the Magnetosphere.* Technical Memo 145, Philco-Ford Corporation, Palo Alto, California, June 1968.

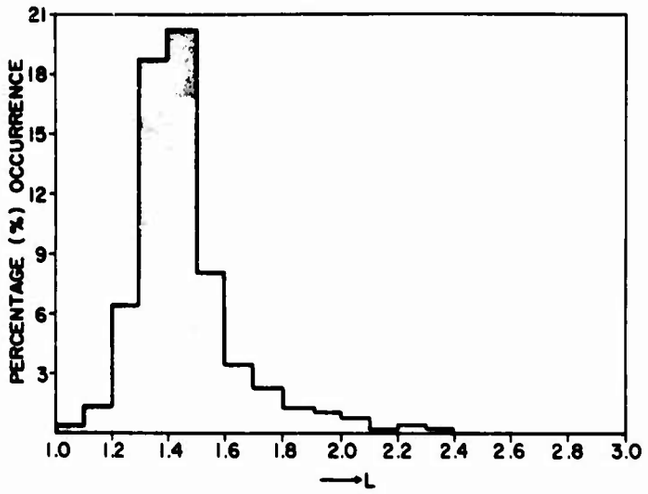


Fig. 1 Percentage occurrence of conjugate ducts as a function of L value

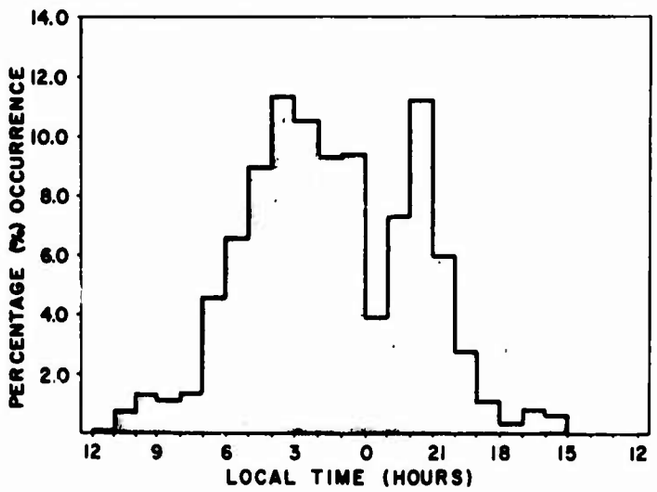


Fig. 2 Percentage occurrence of conjugate ducts as a function of local time (1-hour average)

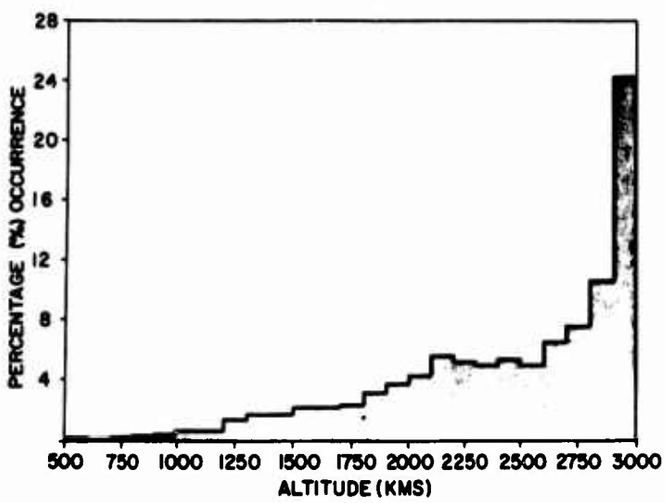
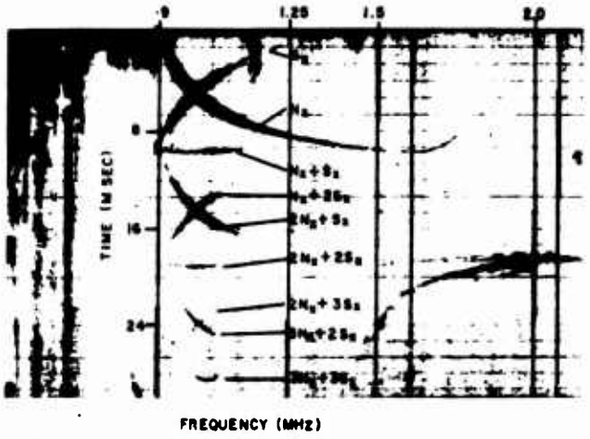


Fig. 3 Percentage occurrence of conjugate ducts as a function of altitude (100-km average)



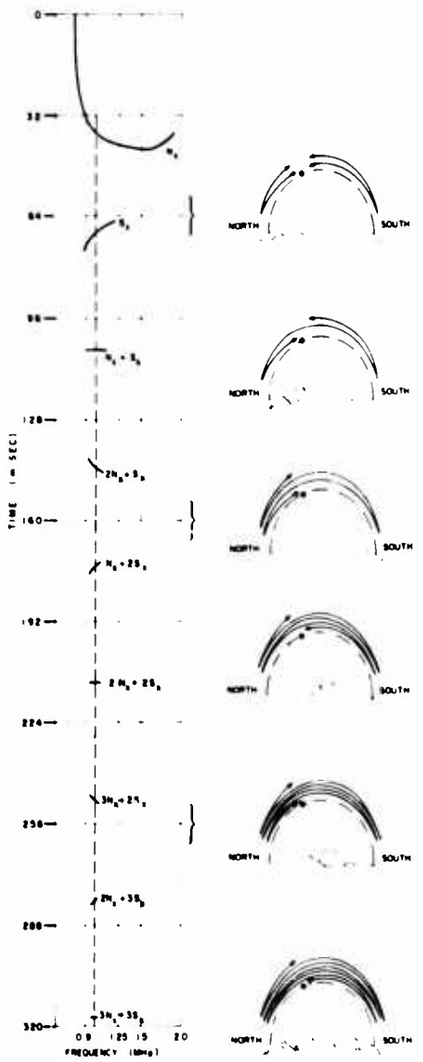


Fig. 4 The "double hook" pattern recorded at Quito, Ecuador, on August 18, 1966, at 08:00:05 GMT. (Local time = 02:07:46, geomagnetic latitude = 12.56°N, geomagnetic longitude = 18.22°W, L = 1.53)

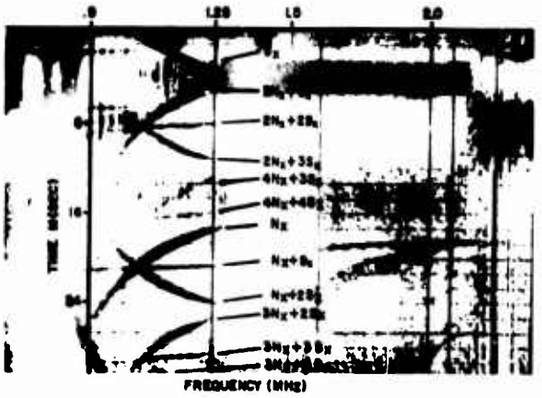




Fig. 5 The "triple hook" pattern recorded at Santiago, Chile, on April 22, 1966, at 09:01:48 GMT. (Local time = 04:38:41, geomagnetic latitude = 19.53°S, geomagnetic longitude = 2.54°E, L = 1.63)

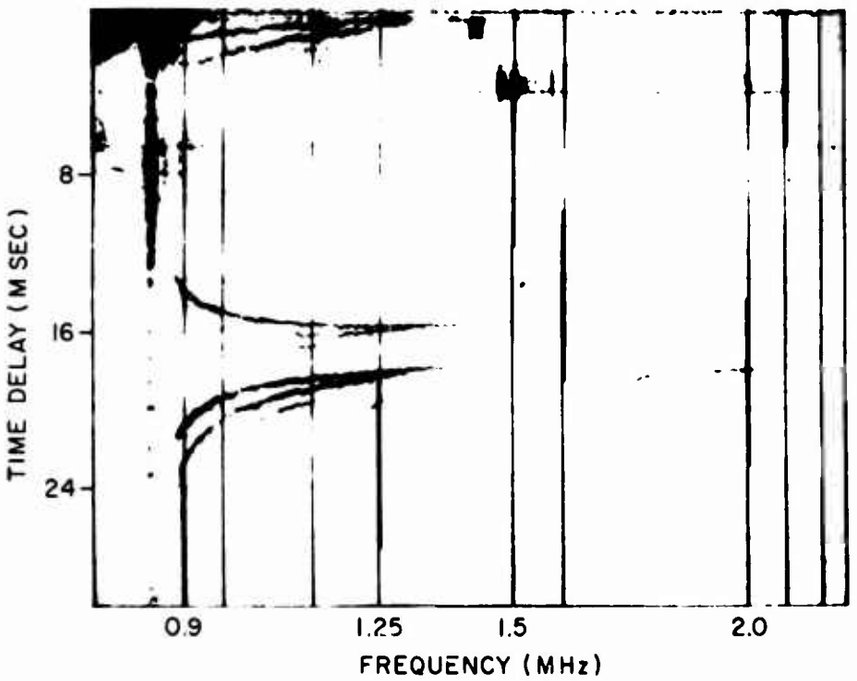


Fig. 6 The "Equatorial Trace" pattern recorded at Quito, Ecuador on April 22, 1966 at 08:55:03 GMT. (Local Time = 04:24:29, geomag. lat. = 3.32°S, geomag. long. = 1.05°E, L = 1.45)

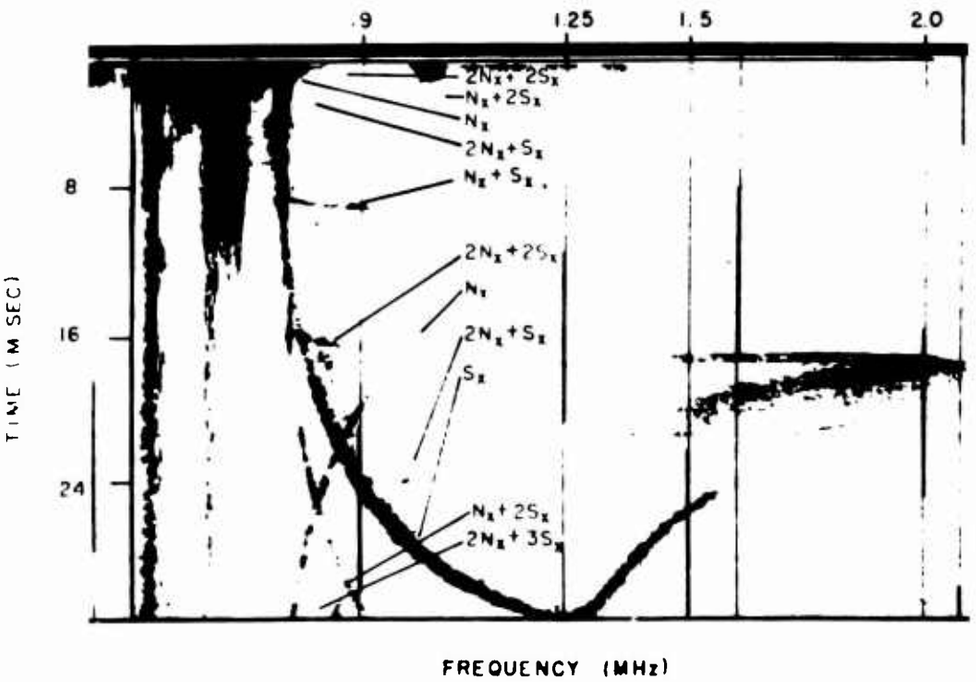


Fig. 7 Ionogram showing conjugate echoes for a high L value (L = 1.76) recorded at Johannesburg, South Africa, on August 12, 1966, at 02:02:54 GMT. (Local Time = 02:37:05, geomagnetic latitude = -19.05°S, geomagnetic longitude = 74.53°E)

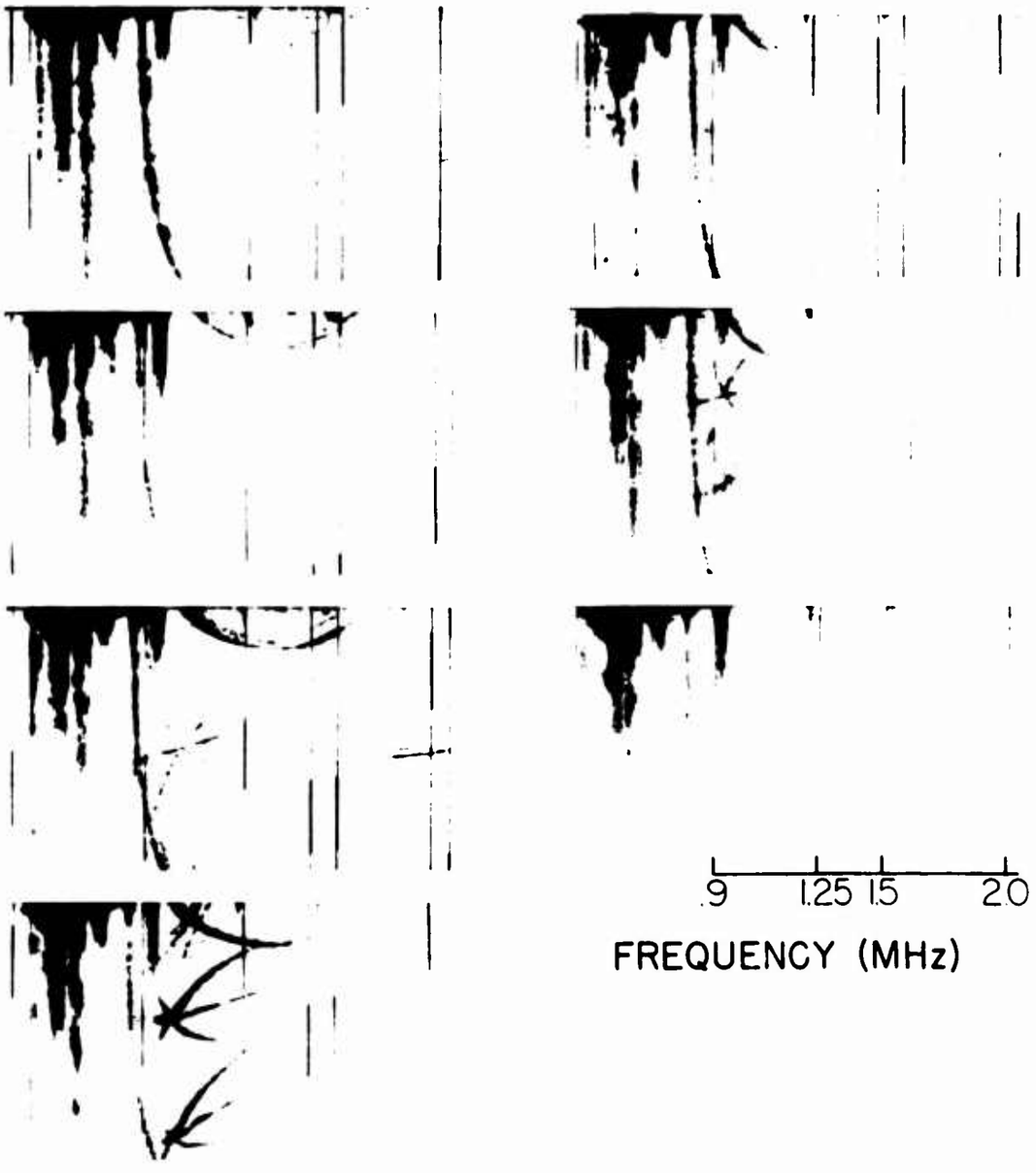


Fig. 8 A series of seven ionograms recorded at Quito, Ecuador, on June 12, 1966, from 03:23:45 to 03:26:59 GMT.

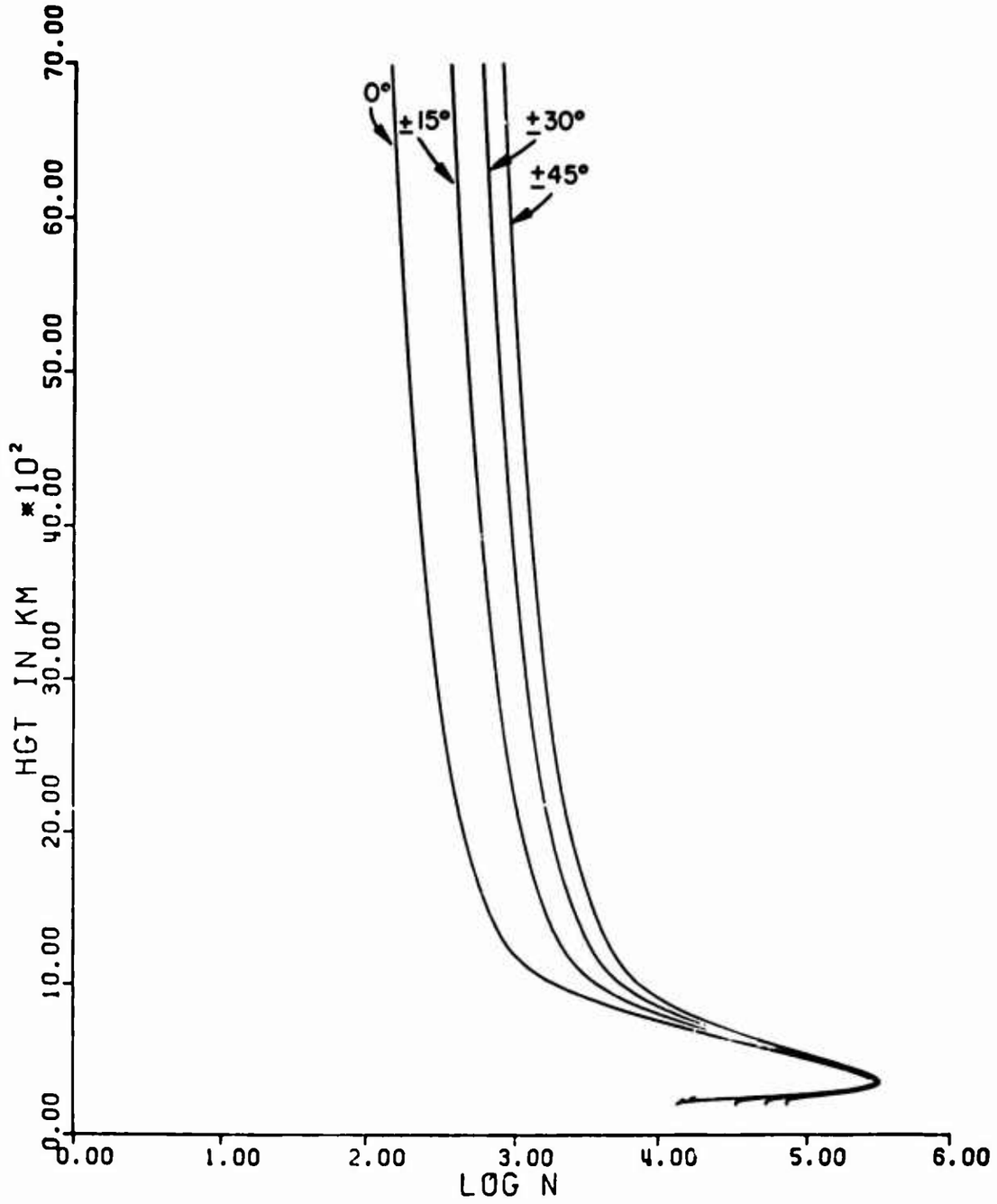
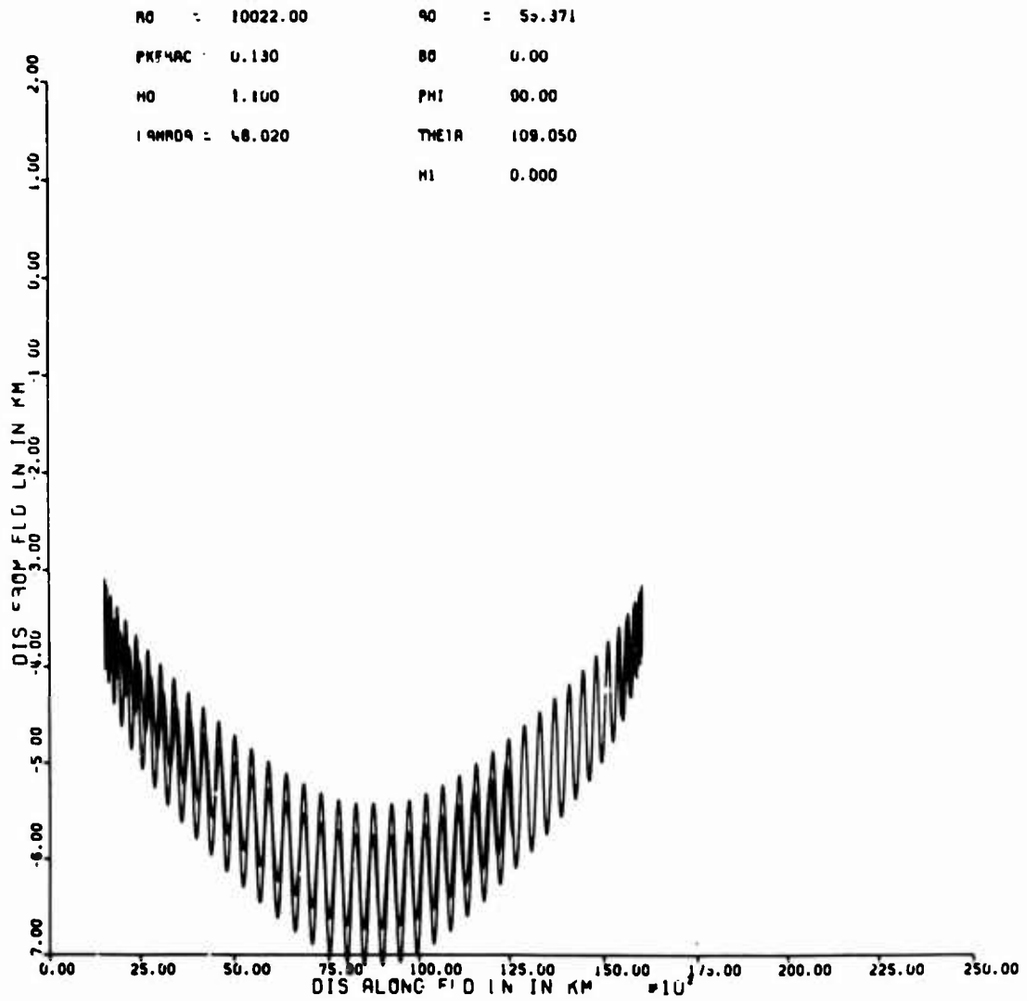


Fig.9 Electron density (cm^{-3}) versus altitude profile for geomagnetic latitude of 0^{o}, $\pm 15^{o}$, $\pm 30^{o}$, $\pm 45^{o}$



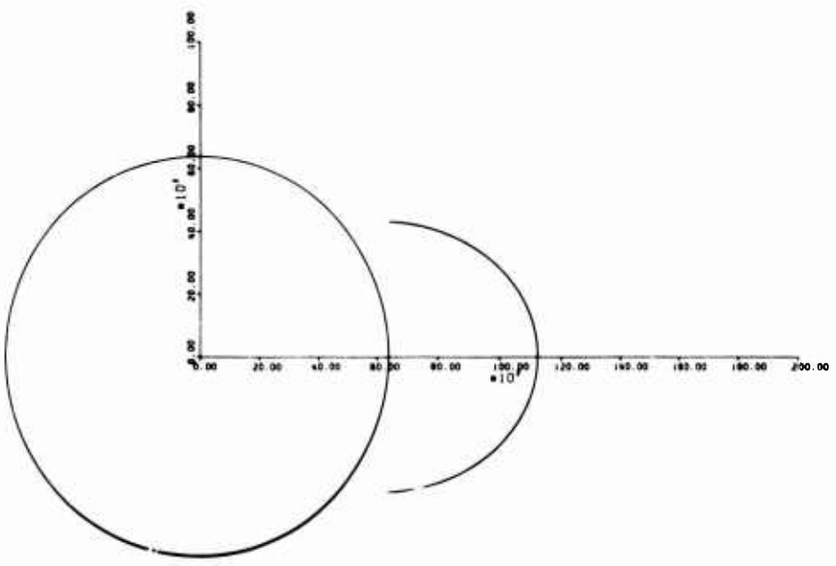
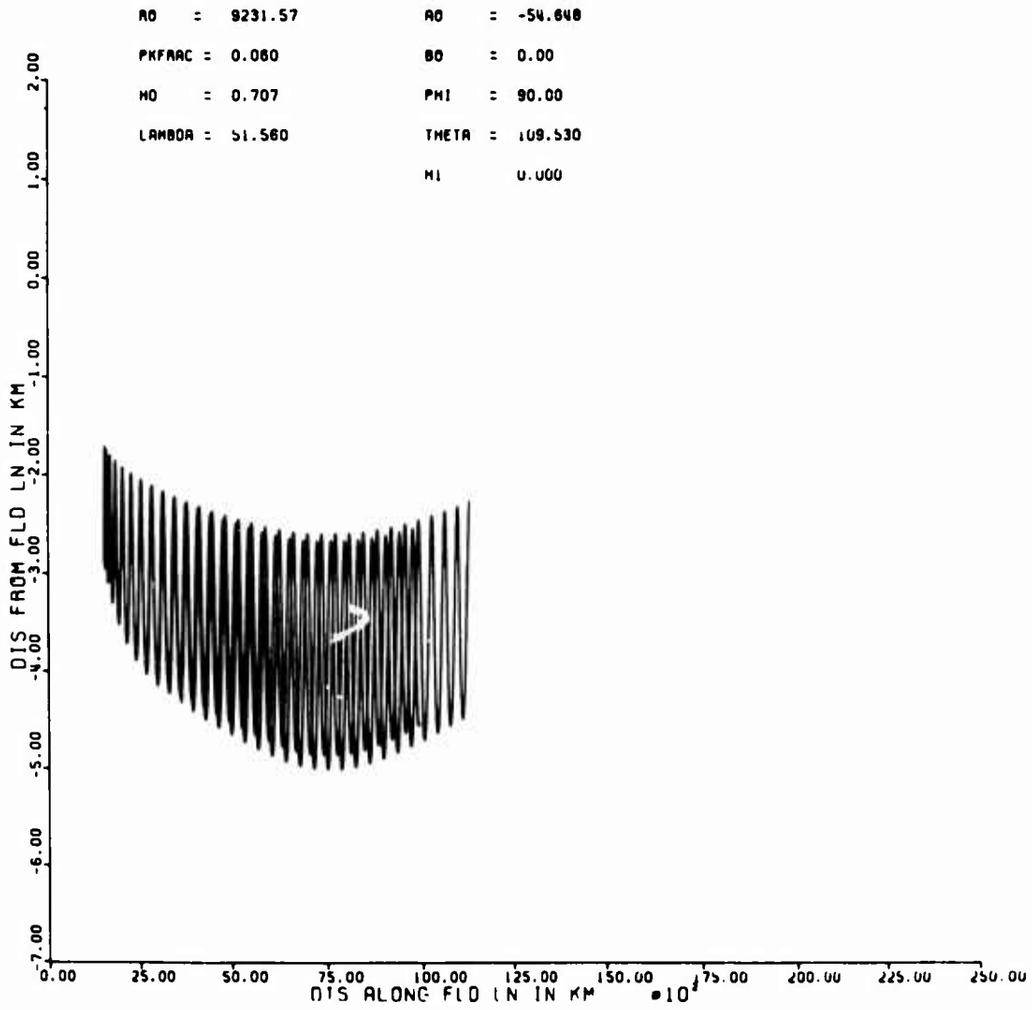


Fig. 10 Ray tracing showing multiple reflections along the L = 1.76 field line for 13.0% peak enhancement of electron density at a geocentric distance 10,022.00 km (frequency = 1 MHz, extraordinary wave)



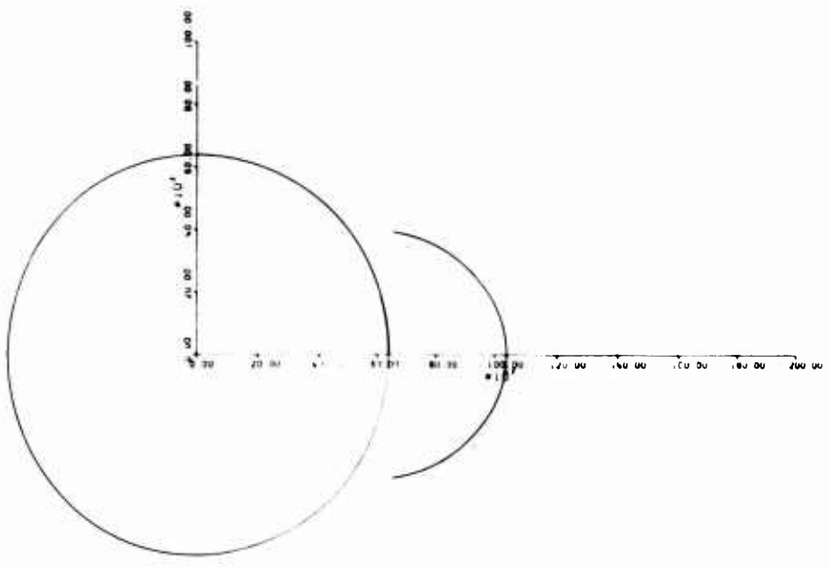


Fig. 11 Ray tracing along the L = 1.63 field line for 6.0% peak enhancement at a geocentric distance of 9231.57 km (frequency = 1 MHz, extraordinary wave)

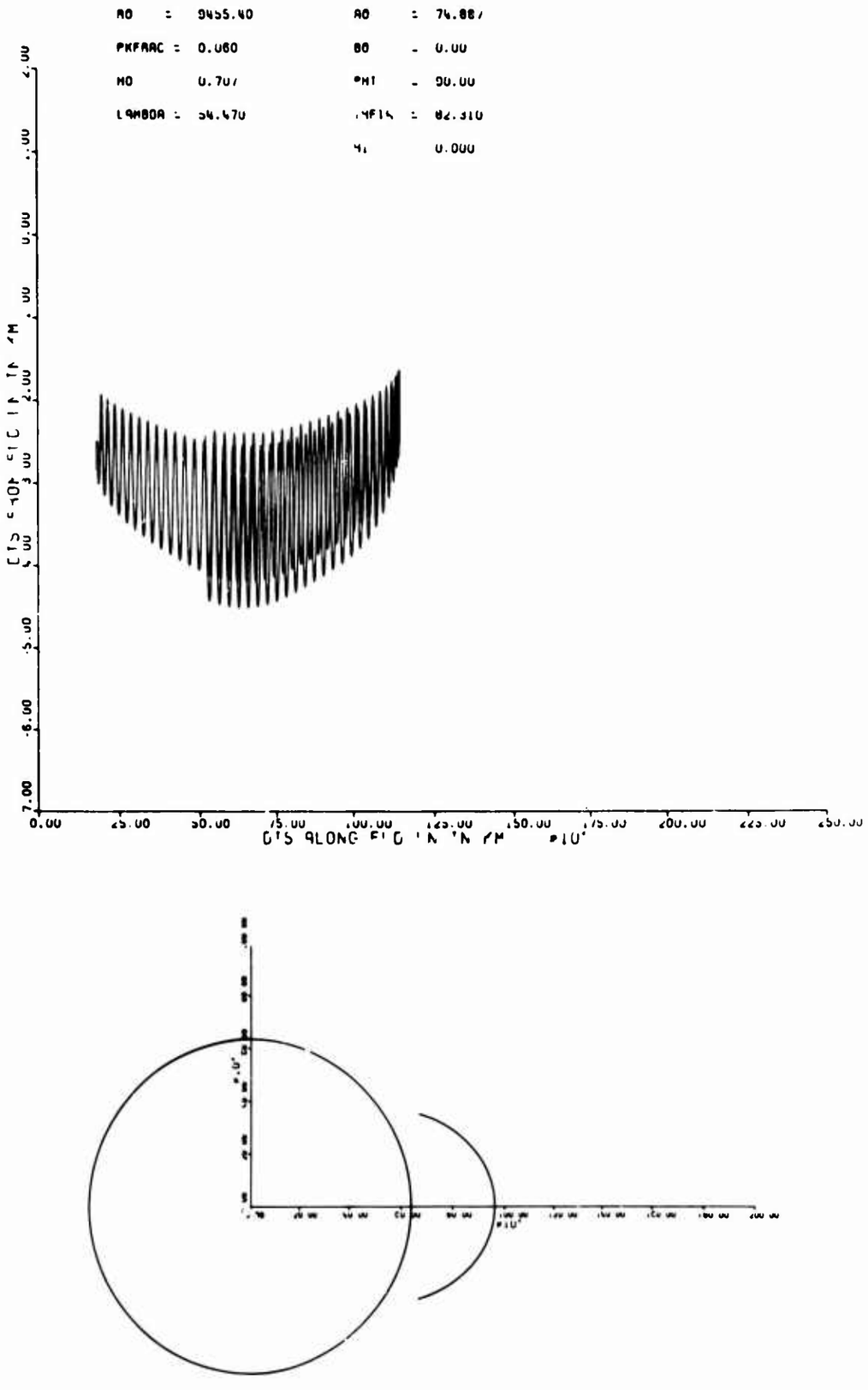


Fig. 12 Ray tracing along the L = 1.53 field line for 6.0% enhancement at a geocentric distance of 9455.50 km (frequency = 1 MHz, extraordinary wave)

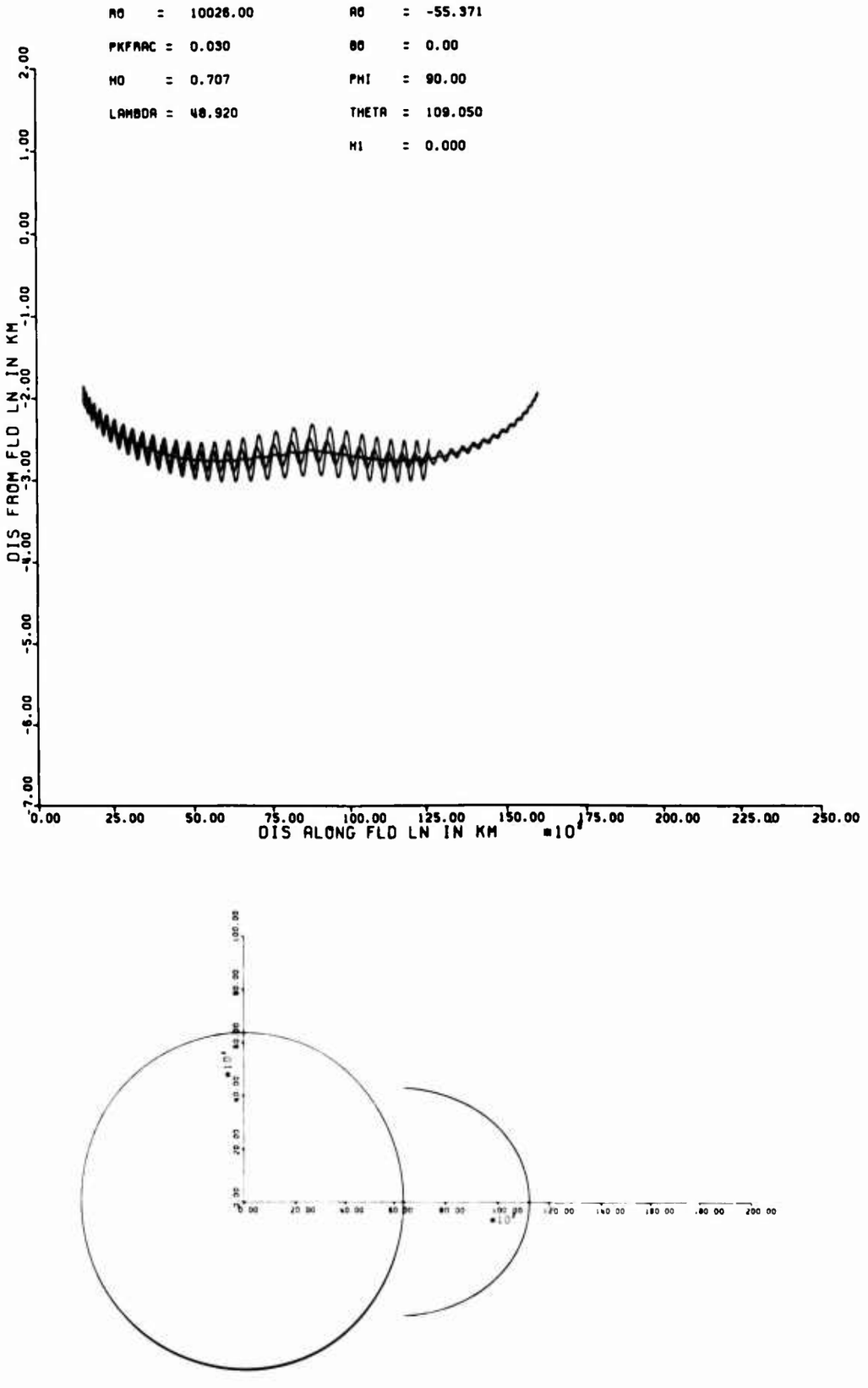


Fig. 13 Ray tracing along the L = 1.76 field line for only 3.0% peak enhancement of electron density at a geocentric distance of 10,026.00 km (frequency = 1 MHz)

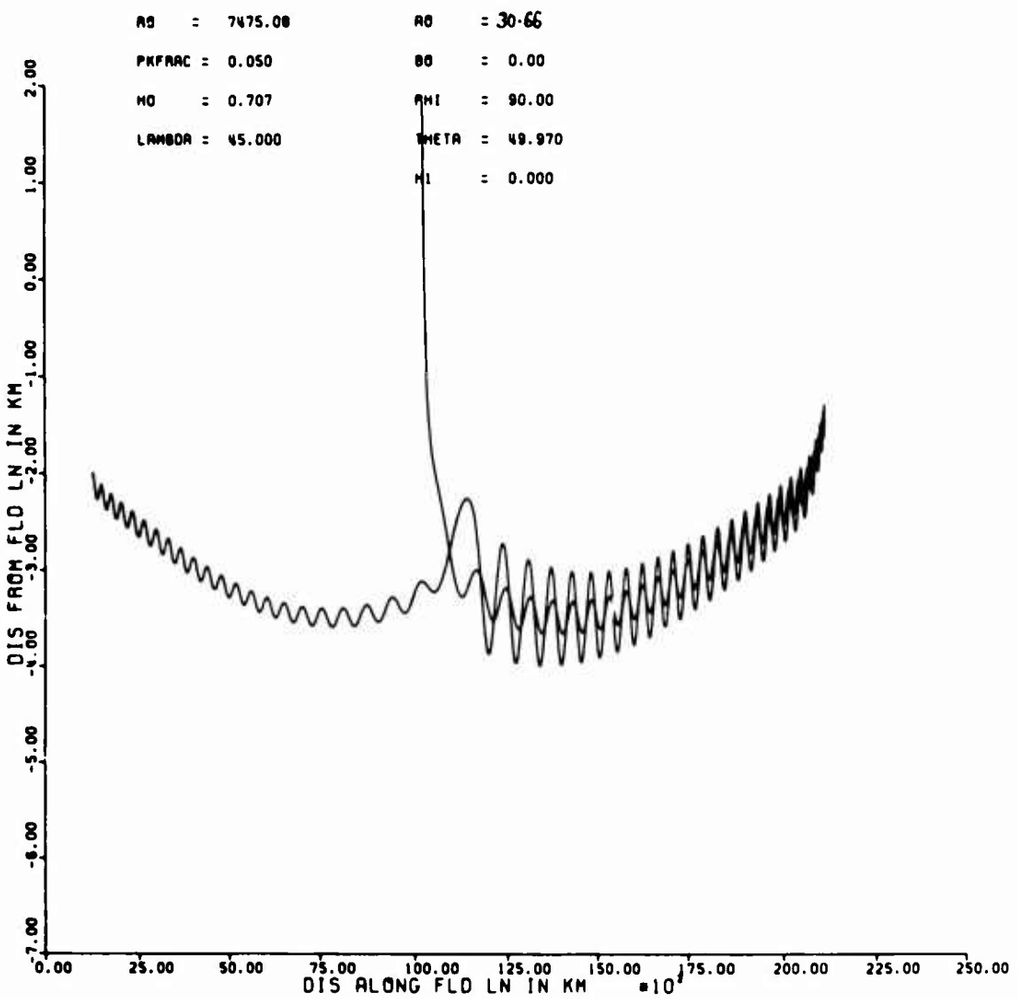


Fig. 14 Ray tracing along the L = 2.00 field line for 5.0% peak enhancement at a geocentric distance of 7475.08 km (frequency = 2.0 MHz) (The ray escapes on its trip from the conjugate point).

EVALUATION AND DISCUSSION

Four participants were asked by the Programme Chairman to give, after the last formal paper, their views and comments on the value of the symposium. After their summing up, which is recorded here, there was a general discussion.

A Review of the Tropospheric Scatter Session, by F.Eklund.

When I was asked to give some sort of review intended to point out the most important achievements of this meeting within the field of tropospheric scatter propagation, it seemed difficult for me to do so. This is the first AGARD-EPC meeting I have attended, and I am a member of a non-NATO country, so I did not really know what to expect from the meeting. Furthermore, there are many impressions that one gets at a meeting like this, so it is not easy to take an overall view, which is necessary in order to say which are the main advances, while one is still at the meeting.

Research work in the field of tropospheric scattering has been going on for almost two decades, so I think one should not expect any dramatic progress.

During past years it has successively become apparent that we need a more detailed picture of the troposphere for radiometeorological purposes than is usually required for ordinary meteorological work.

The fact that the irregular structure of the troposphere affects the propagation of radio waves gives us new tools for tropospheric investigations, in the sense that it should be possible to map tropospheric irregularities by analysing the radio field that is scattered by the irregularities.

If we become successful with this technique I am sure it will provide a background for very important progress in the understanding of meteorological processes near the earth.

There have been contributions here which, in a very convincing way, prove that scattered radio waves can be used to give a detailed picture of the distribution of turbulent irregularities and of their average movements.

When one wants to create a model for the tropospheric refractive index field, difficulties arise because one does not really know what the refractive index irregularities look like, and these are important for the propagation problem.

One important question is: Below which wavelength do ordered layer-, sheet-, facet-like structures play a dominant role and, on the other hand, above which wavelength is it sufficient to consider that incoherent scatter from turbulent fluctuations obey essentially the -5/3 law?

Results reported at this meeting have given some indications that at wavelengths longer than 30 cm, reflections in layer-like structures are of a great importance, and at wavelengths shorter than 10 cm scattering by quasi-homogeneous and approximately isotropic refractive index variations can account for most of the propagation phenomena observed in tropospheric forward scatter experiments.

When we have tried to find correlation between meteorological features and propagation characteristics we have, in the past, often used relatively long term average values of different quantities. However, work has been presented here which clearly shows that relevant structures of the tropospheric refractive index field move fast, and their properties change, within very short intervals of time. So the need for better spatial resolution and shorter integration time when performing radio propagation measurements together with meteorological measurements has been clearly demonstrated.

I should like to stress the need for continuous refinement of the theories of scatter propagation. There are many cases in troposcatter propagation where it is now only a guess that, for example, multiple scatter is of negligible importance. Reliable and practically applicable theories for multiple scattering that could change this guess into a well-founded statement are wanted. I think that the theoretical work presented here will be of some help in this respect.

The electronic technique has long ago become so advanced that, in many cases, the limits for the accuracy of different systems using free radio waves are not set by the equipment itself but by the way in which the propagation channel distorts the signal. I am thinking of precision distance or direction-finding equipment, especially in the microwave band, and extreme wide-band radio links.

In order to tell what the limits are, we need an almost unlimited number of detailed measurements of propagation characteristics in time, frequency and space domains.

Against this background I should personally have liked some more data presented here on the effect of scattering from refractive index irregularities over optical paths.

But something must be left for AGARD-EPC meetings to come. As a whole it has been a very stimulating meeting.

Recapitulation of Ground Scatter Session, by E.C.Hayden

I should like to underscore a number of Mr. Eklund's remarks, especially those relative to the need for more detailed knowledge - both theoretical and observational - of the mechanisms behind the various manifestations of signal scattering. This is in contrast to direct description of the scattered signal itself. While the latter may well be the ultimate goal, knowledge of the former is the best base from which to achieve the latter, especially when extrapolation beyond existing observation is required.

The need can be illustrated by the problem of the ground scatter coefficient in the HF portion of the spectrum. We do not yet know completely from observation how this parameter varies as a function of frequency, incidence angle, scattering angle, and terrain type. We can (perhaps) empirically devise mathematical models that fit what observational data we do have. However, we do not yet know how to translate physical terrain descriptions directly into mathematical models which reproduce the observed behaviour over its full range. Thus we cannot yet say that we *understand* the process, and we are not in a good position to extrapolate behavior to situations beyond those for which direct observational confirmation is available.

On a larger scale, and in a different area, similar need is illustrated by the problem of interpreting ground backscatter records such as, for example, those presented by Barclay and Muldrew. Here the ground scatter phenomenon enters only incidentally, making possible the observations, though its imprint is implicitly impressed on the records. While we can securely interpret many features on backscatter records that are due to regular ionospheric structure, the interpretation of irregular features is yet a highly speculative game. We are still at the stage in the game where we are trying to infer from the radio observations the nature and behavior of the atmospheric perturbations, or the sea state, and it turns out that the process for making that inference is distressingly complex. The odds have been greatly reduced by the development of good ray-tracing techniques, but unfortunately this process of synthesis-by-analysis offers no certainty of any solution, let alone a unique solution, for the cause of the irregular signal features. Ray tracing does, however, provide a secure cause-to-effect bridge.

Here a number of Mr.Eklund's comments on tropospheric problems have direct ionospheric counterparts. As in the case of propagation in the troposphere, we do not yet understand fully the *nature* of the atmospheric phenomena whose effects we are seeing in the radio

records (though I am sure we do have some good clues). Most particularly, we do not yet know the *sources* of these atmospheric disturbances with any significant degree of certainty. Information from other disciplines - global and regional meteorology, and auroral and magnetospheric studies, for example - is needed to supplement the radio data. Direct correlations between effect and suspected cause are sadly lacking. Once this cause-and-effect gap is closed, mutual benefit should certainly accrue to all related disciplines.

In these areas it seems important to promote more effective interaction between the theoretical and observational sides of the game. The problem is to delineate and understand existing physical systems, whose configuration we neither fully know nor can freely control or adjust. This problem is rather different from either analysis of the behavior of a fully specified system or synthesis of some system exhibiting a prescribed behavior within limits. Good observational information is essential, first to suggest theoretical models, and then to test the correspondence in behavior of such models to that of the physical world. Theoretical models are just as essential, because it is in terms of such that we can dare to say we "understand" what is going on.

In the review paper on ground scatter, four items were singled out that seemed to me to be troublesome. It is interesting that authors in this session have scored direct hits on three of the items, and a sort of oblique hit on the fourth.

The problem of improving the spatial resolution of antenna systems for use in backscatter radar systems was attacked by Shearman and Clarke (Paper 11). They described an aperture synthesis technique involving an ingenious and efficient optical data-processing method. If a full scale counterpart is put into operation, it will be quite interesting to see how effective it is in delineating the partially coherent, spatially extended, backscatter source.

The use of information in the backscatter signal in addition to signal amplitude was touched on by Goutelard, who related ionospheric variations to amplitude and spectral properties of the backscattered signal.

Three papers, those by Goutelard, Biggs and Rider (Papers 6, 2 and 10), were concerned with the ground scatter coefficient. The paper by Goutelard was of particular interest to HF practice. The treatment of scatter in all directions, including forward, for a variety of surface contour configurations provides useful new insight. Biggs presented information on the backscatter coefficient at microwaves of the ocean surface and of sea ice, and discussed the use of backscatter techniques in terrain investigation. Rider presented a treatment of the effects of ground forward scatter on microwave signal fading.

The interpretation of ground backscatter records was discussed by Barclay, Muldrew, Maliphant, and Georges (Papers 4, 8, 7 and 55). The first two authors presented backscatter records showing unusual signal configurations, and proposed interpretations in terms of ionospheric structure, ground scatter coefficient, or sea state. The last two authors showed methods for using ray tracing to aid in interpretation of backscatter records. In all of these, it becomes evident that focusing or diffraction effects are considerable, while the dynamic range of equipment is limited, leading to problems in recording and hence interpretation. This group of papers, and the discussion they engendered, serve to emphasize how primitive are the techniques we are yet using to interpret backscatter records. Except for the effects of the regular ionosphere, we are still not able to relate observed signal behavior to geophysical phenomena with a high degree of certainty.

In addition to the subjects already mentioned, observations on side-scatter transmission were contributed. Rice (Paper 9) described results over a path of rather short length, were the scatter region subtended a large angle at the receiver. Crochet (Paper 3) described results on a longer path, with perhaps several discrete scatter regions. Thus the two reports were complementary. Both contributed to understanding of the occurrence of this transmission mode and to the character of signals transmitted by it.

As a last observation, there is a strong need to gather together, and translate into engineering form, isolated scientific observations such as were presented at this meeting.

Such information would then be generally available for incorporating the effects of ground scatter into engineering and operational calculations. Until this is done, the job remains incomplete and academic.

Comments on the Symposium, by K.Davies.

Never having worked in the field of scatter propagation, I am a poor choice as a reviewer of this symposium. To an outsider this meeting is characterized as much by what it did not contain as by what it did contain. If this meeting had been held, say, ten years ago, the sessions on the ionosphere would have been completely dominated by very high frequency forward scatter from the D-region and by reflections from meteor trails. It is interesting to see that the only paper on D-region VHF forward scatter was the excellent (invited) review paper by R.C.Kirby (Paper 38). There were no papers on meteor propagation. Does this indicate the demise of research in these areas?

As far as the ionosphere is concerned there is a clear shift in emphasis from the lower (D and E) regions to the F-region. Even here a number of workers considered the ionosphere merely as a transmission medium for ground scattered signals rather than as a source of scattering. These workers have stressed the great importance of ray tracing in the interpretation of experimental results.

Yet another omission was the absence of an extensive discussion of the use of scatter signals. It was pointed out that in equatorial regions scatter signals are quite strong. Hence it should be possible to use these signals for communication purposes. It is my personal feeling that the experimentalists at the meeting failed to make the most of the theoreticians present (especially the aerodynamicists). This is largely due to the full program, which has tended to limit discussion.

Listening to the papers one gets the impression that *most* of the experiments on ionospheric scatter have been of an *ad hoc* nature. That is, a transmitter and receiver have been set up to measure signals, with relatively little regard to the overall picture. We are clearly at the stage where definitive experiments are required in which the frequencies, path lengths, and equipment characteristics are carefully controlled, in order to determine something about the nature of the scattering processes.

Comment on the Meeting, by P.A.Forsyth

The comments you have heard seem fairly to summarize the main impact of this meeting. I have only a few observations to add.

During the meeting I was struck by the fact that very little of the discussion seemed to involve consideration of the actual mechanism of scattering of electromagnetic waves. In contrast to the situation that prevailed a few years ago, there now seems to be general agreement regarding the various scattering mechanisms that can operate. The uncertainties now seem to be concentrated in the realm of geophysics. Most of our time was taken up in trying to arrive at adequate descriptions of the tropospheric or ionospheric (or aquatic) phenomena which gave rise to the observed scattering. This is a happy state, since it focuses our attention on the utility of scatter as a tool in the investigation of physical phenomena.

There was less optimism regarding the widespread utilization of the various scatter modes for efficient communications than was customary in the past. I am sure that this more realistic approach, due in part to the introduction of communication satellites, will be welcomed by the users, who will still need to turn from time to time to scatter modes to fulfil particular requirements.

I, too, would like to comment on the omission of meteor scatter from the conference. To me this omission seems justified, not because we know all we need to know about this unusual scatter mode but because the subject is in one of those periods of consolidation where one level of understanding is fairly complete and the next level has not been sufficiently penetrated to provide a profitable basis for discussion.

There are a few areas that were discussed - transequatorial, auroral and VHF scatter come to mind - on which there is still some lack of basic data from which to infer an acceptable model. In these cases it does seem that much assistance could be derived from measurements made by rocket or satellite, and these should be encouraged, but only under conditions that permit direct comparison with radio measurements.

For the future, clearly there are specific questions that need answering and I am sure that research already in progress will provide most of these answers. This meeting brought to my attention the uncertainty regarding the nature of the F-region irregularities responsible for scattering. This is a problem that likely will need a concentrated effort, using a wide variety of approaches, for its solution.

It would be too much to expect a universal recipe for the experimental approach to scattering but, in listening to the background papers covering the various scatter modes, I was struck by some common elements in the histories. Typically, the theorist is left floundering until he is presented with certain basic data and, once those data are presented, a satisfactory model emerges quickly. The data needed relates to the frequency dependence and angular dependence of the scattering, the frequency spectrum and the spatial characteristics of the scattered signal and, sometimes, the degree to which polarization is affected by the scattering process. These data are sometimes difficult to obtain but little can be done without them.

General discussion after Session VII.

Professor M.Z. von Krzywoblocki: I agree with Dr Eklund that multiple scattering should be explained theoretically. Turbulence fundamentals are not sufficiently developed. The paper presented by Professor Tchen has shown how much trouble we have in applying the theory of turbulence (any theory) to the scatter phenomenon. The scientists who argue about the fundamentals of the electromagnetic theory should be welcome and invited. The Maxwell equations were mostly guessed at and not rigorously derived on the basis of a set of axioms. One should argue and look for means of revising and remodeling the Maxwell equations. It is my impression that there have not been enough papers presented here dealing with mathematical models. The aerodynamicists should have been invited to attend and contribute to the present meeting of the EPC.

Professor C.M. Tchen: The term "scattering by turbulence" has often been used in this meeting. From the many experimental results, I do not see any confirmation of the presence of a turbulent medium with a turbulent structure. On the other hand, most theories of scattering by turbulence use the wave propagation equation with a stochastic refractive index coming from the random density fluctuations, and at the same time suggest the Kolmogorov spectral law for the density spectrum. This raises a paradox, because the scattering theories have not considered the velocity fluctuations, while the Kolmogorov theory deals strictly with the velocity fluctuations and not with the density fluctuations.

I agree with the previous speakers who would like to encourage participation by hydrodynamicists in future meetings on turbulent scattering.

Professor E.D.R. Shearman: The papers on backscatter, and M. Goutelard's contribution in particular, seem to me to underline the desirability to consider propagation modes in which the rays travel out and back by different routes. Dr Goutelard has shown that these rays can have comparable amplitude to those now considered. Such modes would be particularly important in summer daytime with F2, F1, E and Es propagation all present. This also indicates the desirability of measurements to find out the vertical angle at which the modes arrive.

Also I would like to throw out a provocative question. Is there any need to do research on HF communication at the present time when satellites appear to offer more reliable communication links for most of the present HF circuits? Are we doing research of the kind that was recently criticised by a commission in the UK - development of more efficient locomotive boilers shortly before the last steam locomotive was due to be phased out by British Rail?

Dr E.C.Hayden: One might appeal to the growth of population and Parkinson's law to get some idea of the potential future of HF radio. It seems to me that if there is a usable facility for communication, · use will be found for it. Having been interested in HF radio since my High School days, my one continuing impression is that the band has *always* been too crowded, and that it might be a good thing if satellites and other systems took up the load so that we could get down to using the HF band properly! Aside from the communication uses, I would note that this is still the part of the spectrum in which the greatest interaction exists between radio waves and the upper atmosphere. In this role HF, far from being obsolete, is probably near the beginning of an era of exploration of the dynamics of the upper atmosphere. It seems that the dynamic phenomena is that region may be more important than earlier meteorological models have indicated.

Dr J.Ramasastry: I am trying to defend HF research indirectly and from one point of view. It may be true that communications usage of the HF band may become obsolete in the present age. However, the use of HF to study geophysical phenomena cannot be ignored. I am, myself, planning to do a better designed satellite propagation experiment using HF band to uniquely establish the physical characteristics of field-aligned ducts of ionization irregularities, which are responsible for the guidance of HF waves in the magnetosphere.

Dr O.Holt: One aspect that we ought to be concerned with in this audience is the military application. Satellites may be rather vulnerable in wartime compared with HF communications. Also, I believe that HF communications for many circuits will compare favourably in price for many years yet.

Dr C.R.Roberts: There is a use of the ionosphere that has not been mentioned here, and that is its use as a mirror for radar signals. There is much yet to be learned about the ionosphere as far as this application is concerned, including the effects of ionospheric ducting, instabilities and irregularities as well as ground scatter.

On the measurements of ground scatter discussed during the meeting - the use of sporadic-E was mentioned. In collecting considerable data with a high resolution system we have found that, while the signal appears quite stable in azimuth of arrival, amplitude fluctuations can be severe, depending upon the type of sporadic-E used. This is a study in itself. In measuring ground scatter by use of sporadic-E, the accuracy will very much depend on taking the characteristics of the layer structure into account.

Dr A.Roederer: I should like to raise the following question: does the development of frequency-independent antennas bring any significant improvement in HF communications, and in particular in the study of backscattering?

Dr D.L.Nielson: Since frequency-independent antennas are invariably wide-beam devices, they have two disadvantages in backscatter work. First, due to low gain, the signal-to-noise ratio is reduced; but, more important, the directivity usually required in backscatter work is not available from such antennas unless they are arrayed together.

Information regarding the availability of further copies of AGARD publications may be obtained from

The Scientific Publications Officer,
Advisory Group for Aerospace Research and Development,
7, rue Ancelle,
92 Neuilly-sur-Seine,
France.



Printed by Technical Editing and Reproduction Ltd
Harford House, 7-9 Charlotte St. London, W.1.